

DRUG-DNA INTERACTIONS BY SPECTROSCOPIC AND MOLECULAR MODELING TECHNIQUES

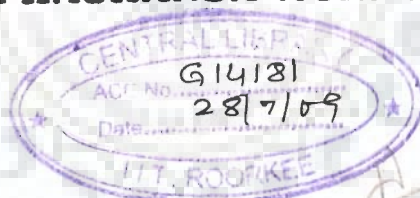
A THESIS

*Submitted in partial fulfilment of the
requirements for the award of the degree*

of
DOCTOR OF PHILOSOPHY
in
BIOTECHNOLOGY

by

PRASHANSA AGRAWAL



DEPARTMENT OF BIOTECHNOLOGY
INDIAN INSTITUTE OF TECHNOLOGY ROORKEE
ROORKEE-247 667 (INDIA)

DECEMBER, 2007



©INDIAN INSTITUTE OF TECHNOLOGY ROORKEE, ROORKEE, 2007
ALL RIGHTS RESERVED



INDIAN INSTITUTE OF TECHNOLOGY ROORKEE ROORKEE

CANDIDATE'S DECLARATION

I hereby certify that the work which is being presented in the thesis entitled, **DRUG-DNA INTERACTIONS BY SPECTROSCOPIC AND MOLECULAR MODELING TECHNIQUES** in partial fulfilment of the requirements for the award of the Degree of Doctor of Philosophy and submitted in the Department of Biotechnology of the Indian Institute of Technology Roorkee, Roorkee is an authentic record of my own work carried out during a period from March 2002 to December 2007 under the supervision of Prof. Ritu Barthwal, Department of Biotechnology and co-supervision of Late Dr. S. K. Barthwal, Department of Physics, Indian Institute of Technology Roorkee, Roorkee.

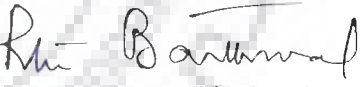
The matter presented in this thesis has not been submitted by me for the award of any other degree of this or any other Institute.

Dated: 24.12.07


(PRASHANSA AGRAWAL)

This is to certify that the above statement made by the candidate is correct to the best of my knowledge.

Dated: 24.12.07


(Ritu Barthwal)
Supervisor

The Ph.D. viva-voce examination of **Ms. Prashansa Agrawal**, Research Scholar has been held on

Signature of Supervisor

Signature of External Examiner

ACKNOWLEDGEMENTS

This thesis is a result of more than five years of research, at the Indian Institute of Technology Roorkee. It would not have been possible to complete this thesis without the help and guidance of numerous people and herein I would like to thank them all.

I would like to start thanking to almighty who has bestowed his blessings for the accomplishment of my thesis against all odds.

Vakratunda Mahakaya Surya-koti Samaprabha;

Nirvighnam Kuru Me Deva Sarva-Karyeshu Sarvada

I am also grateful to my supervisors, Professor Ritu Barthwal and Late Dr. S. K. Barthwal, for their guidance. I would also like to thank them for giving me the opportunity to discuss with so many famous NMR experts like Prof. G. Govil, Prof. R. V. Hosur, Prof. C. L. Khetrapal and Dr. Nagna Gowda who by their socratic questioning, brought me closer to the reality I had initially perceived, eventually enabling me to grasp its rich complexity. Their comments on research work are themselves a course in critical thought upon which I will always draw conclusion.

I am most grateful to all the members of FT-NMR National Facility at Tata Institute of Fundamental Research and Central NMR Facility at IIT ROORKEE for extending their cooperation and providing friendly atmosphere during my stay. I am thankful to the faculty of the department for help and valuable discussions during my stay.

I am thankful to my seniors Monica and Manpreet, for being such a good colleague and friend. I am also indebted to all the other people who had contributed in this thesis. Today I recall all the names: R. Durairaj, Santosh, Amit, Kushuma, Lata, Asif, Garima, Somashekhar whose timely help and suggestions will always be remembered. They always stood beside me through thin and thick.

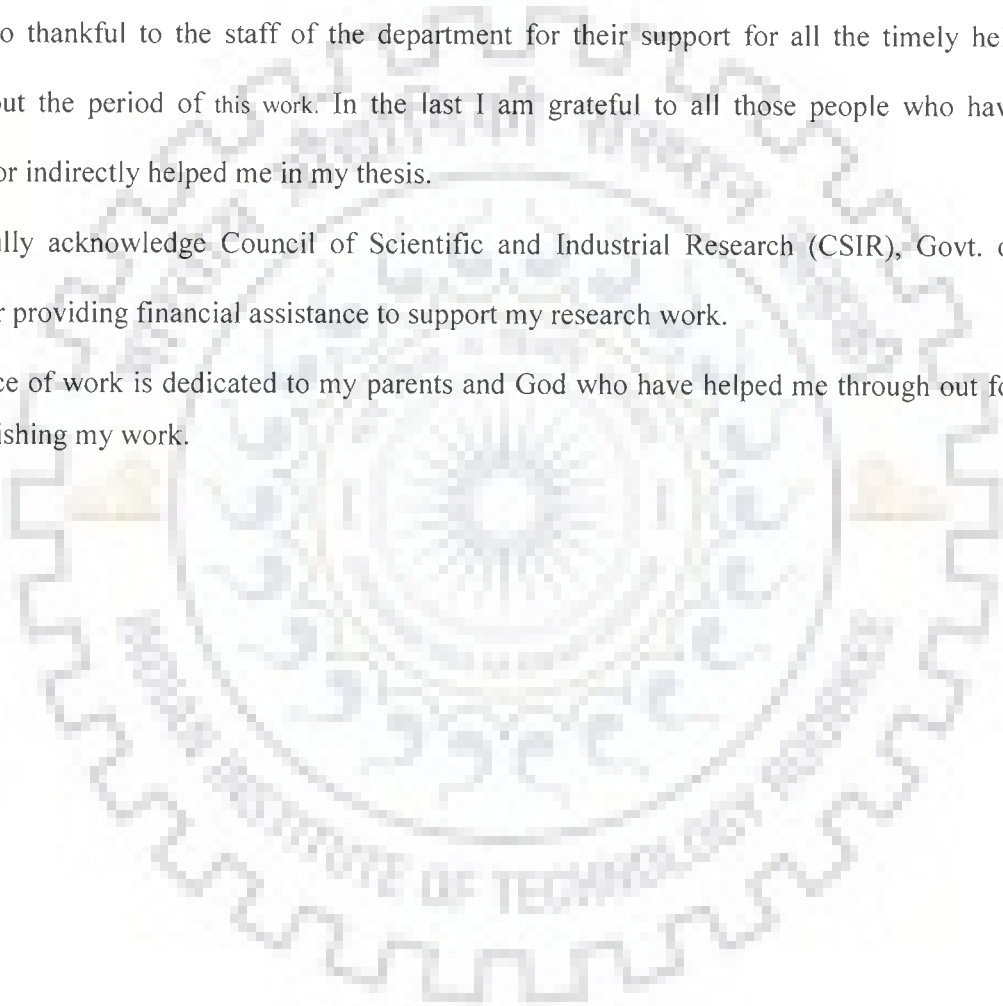
I am forever grateful to my parents whose foresight and values paved the way for a privileged education, and to my sister for supporting me with her gentle counsel. Their unconditional support at each turn of the road encouraged me to ameliorate my performance. Their faith on me has always inspired me in this venture.

I am very grateful to Dr. A.N. Tripathi whose timely and unconditional support paved the path for the submission of my thesis.

I am also thankful to the staff of the department for their support for all the timely help throughout the period of this work. In the last I am grateful to all those people who have directly or indirectly helped me in my thesis.

I gratefully acknowledge Council of Scientific and Industrial Research (CSIR), Govt. of India, for providing financial assistance to support my research work.

This piece of work is dedicated to my parents and God who have helped me through out for accomplishing my work.



CONTENTS

ABSTRACT

LIST OF PUBLICATIONS

		Page No.
CHAPTER 1	INTRODUCTION	1-58
1.1	General	1
1.2	Drug-DNA Interaction	2
1.3	Structure of Anthracycline Drugs	3
1.4	Classification of Anticancer Drugs	9
1.5	Structure of Nucleic Acids	11
1.6	General Phenomenon of Intercalation in DNA	20
1.7	Forces involved in Drug –DNA Interaction	22
1.8	NMR Spectroscopy, UV-Vis and Fluorescence Spectroscopy involved in drug –DNA Interaction	24
1.9	Molecular Modeling Study involved in Drug-DNA Interactions	26
2.0	Literature Review	27
2.1	Scope of Thesis	57
CHAPTER 2	MATERIALS AND METHODS	59-102
2.1	Materials	59
2.2	Sample Preparation for NMR	63
2.3	Methodology	66
2.4	Two Dimensional NMR Techniques	74
2.5	Experimental Parameters	84
2.6	Determination of Three-Dimensional Structure	84
2.7	Estimation of Interproton Distances	90
2.8	UV-Vis Spectroscopic Techniques	92
2.9	Restrained Molecular Dynamics and Simulated Annealing	93
3.0	Defining DNA Structure	97
3.1	Quantum Mechanical Calculations	101
3.2	Electron Spray Ionization Mass Spectrometry (ESI-MS)	102
CHAPTER 3	STRUCTURAL ELUCIDATION OF 4'-EPIADRIAMYCIN BY NUCLEAR MAGNETIC RESONANCE SPECTROSCOPY AND COMPARISON WITH ADRIAMYCIN AND DAUNOMYCIN USING QUANTUM MECHANICAL AND RESTRAINED MOLECULAR DYNAMICS APPROACH	103-144
3.1	Results and Discussion	105
A.	NMR Spectra of 4'-epiadriamycin	105
B.	Conformational studies of 4'-epiadriamycin, adriamycin and daunomycin using Restrained Molecular Dynamics	121
C.	Quantum Mechanical Calculations	129
D.	Flexibility of Sugar Ring	140
E.	Biological Relevance	141
F.	Structure-Activity Relationship	142
3.2	Summary and Conclusions	143
CHAPTER 4	STUDIES ON SELF-AGGREGATION OF ANTHRACYCLINE DRUGS BY RESTRAINED MOLECULAR DYNAMICS APPROACH USING NUCLEAR MAGNETIC RESONANCE SPECTROSCOPY SUPPORTED BY ABSORPTION, FLUORESCENCE, DIFFUSION ORDERED SPECTROSCOPY	145-198

	AND MASS SPECTROMETRY	
	4.1 Results and Discussion	145
	A. NMR Studies	145
	B. Restrained Molecular Dynamics (rMD) studies	178
	C. Absorption and Emission studies	180
	D. Diffusion Ordered Spectroscopy (DOSY) studies	185
	E. Electron Spray Ionization-Mass spectrometry Studies (ESI-MS)	190
	F. Biological Relevance	195
	4.2 Summary and Conclusions	198
CHAPTER 5	STUDIES ON COMPLEX OF ADRIAMYCIN WITH d-(TGATCA)₂ BY PHOSPHORUS-31 NUCLEAR MAGNETIC RESONANCE SPECTROSCOPY	199-232
	5.1 Results and Discussion	199
	A. d-(TGATCA) ₂	199
	B. Adriamycin-d-(TGATCA) ₂ Complex	205
	5.2 Summary and Conclusions	232
CHAPTER 6	STUDIES ON ADRIAMYCIN COMPLEXED WITH d-(TGATCA)₂ BY PROTON NUCLEAR MAGNETIC RESONANCE SPECTROSCOPY AND RESTRAINED MOLECULAR DYNAMICS	233-326
	6.1 Results and Discussion	234
	A. NMR studies on complex of adriamycin-d-(TGATCA) ₂	234
	B. TCSPC Analysis: Time-resolved fluorescence measurements	297
	C. Diffusion Ordered Spectroscopy (DOSY) studies on adriamycin-d-(TGATCA) ₂ complex	298
	D. Restrained Molecular Dynamics Studies	302
	6.2 Summary and Conclusions	325
CHAPTER 7	STUDIES ON COMPLEX OF 4'-EPIADRIAMYCIN WITH d-(CGATCG)₂ BY PHOSPHORUS-31 NUCLEAR MAGNETIC RESONANCE SPECTROSCOPY	327-362
	7.1 Results and Discussion	327
	A. d-(CGATCG) ₂	327
	B. 4'-Epiadriamycin-d-(CGATCG) ₂ Complex	333
	7.2 Summary and Conclusions	362
CHAPTER 8	STUDIES ON 4'-EPIADRIAMYCIN COMPLEXED WITH d-(CGATCG)₂ BY PROTON NUCLEAR MAGNETIC RESONANCE SPECTROSCOPY AND RESTRAINED MOLECULAR DYNAMICS	363-455
	8.1 Results and Discussion	364
	A. NMR studies on complex of 4'-epiadriamycin-d-(CGATCG) ₂	364
	B. TCSPC Analysis: Time-resolved fluorescence measurements	432
	C. Diffusion Ordered Spectroscopy (DOSY) studies on 4'-epiadriamycin-d-(CGATCG) ₂ complex	433
	D. Restrained Molecular Dynamics Studies	433
	8.2 Summary and Conclusions	454
References		i-xxiv

ABSTRACT

The natural products have been of considerable interest as potential anti cancer agents that bind to DNA, but with the common ability to act as potent inhibitors of DNA transcription and replication. Many synthetic compounds have been added to this list in the search for more potent drugs for use in chemotherapy in view of pronounced cytotoxicity of these drugs, resistance towards tumour cell lines and difference in their neoplastic potency. Structural tools such as X-ray crystallography and NMR spectroscopy, coupled with molecular modeling techniques have considerable impact in advancing our understanding of the microscopic structural homogeneity of DNA and the molecular basis for drug-DNA interactions. Besides above-mentioned techniques, theoretical studies using Density Functional method (DFT) by Gaussian 98 are done supported by Diffusion Ordered Spectroscopy (DOSY), Electron Spray Ionization Mass Spectrometry (ESIMS) and Fluorescence Life-Time Measurements Techniques. These studies help to understand the molecular basis for binding and identifying the preferred sequence specificity of many key drugs with DNA. The Ph.D. thesis work has been reported in the form of eight chapters.

Chapter 1 contains introduction to the subject, a comprehensive review of the literature and scope of thesis. **Chapter 2** deals with the materials and methods used. The detailed Nuclear Magnetic Resonance Spectroscopy- 1D NMR, DQF COSY, TOCSY, $^1\text{H} - ^1\text{H}$ NOESY for the proton assignment; HSQC ($^1\text{H} - ^{13}\text{C}$) and HMBC ($^1\text{H} - ^{13}\text{C}$) for the carbon assignment; $^1\text{H} - ^{31}\text{P}$ HMBC, $^{31}\text{P} - ^{31}\text{P}$ NOESY for the phosphorus assignment; UV-Visible and Fluorescence studies is for calculating the dimerization constant (K_{eq}); Diffusion Ordered Spectroscopy (DOSY) and Electron Spray Ionization Mass Spectrometry (ESIMS) studies are to see the self-aggregation; Fluorescence Life-Time Measurements methods are explained to know the intercalated complex formation. The strategies used for restrained energy minimization, molecular dynamics simulations and quantum mechanical calculations involving GIAO

method (for chemical shift calculation) and DFT method (for optimization) are also discussed. **Chapter 3** deals with the NMR spectral assignment of 4'-epiadriamycin and restrained Molecular Dynamics simulation and quantum mechanical calculations of 4'-epiadriamycin, adriamycin and daunomycin. In this chapter, the structural and electronic properties of 4'-epiadriamycin, adriamycin and daunomycin have been studied using Density Functional Theory (DFT) employing B3LYP exchange correlation. The chemical shift of ^1H and ^{13}C resonances in Nuclear Magnetic Resonance spectra have been calculated using Gauge-Invariant Atomic Orbital (GIAO) method as implemented in Gaussian 98 and compared with experimental NMR spectra recorded at 500 MHz. A restrained Molecular Dynamics approach was used to get the optimized solution structure of drugs using inter-proton distance constraints obtained from 2D NOESY spectra. The glycosidic angle C7-O7-C1'-C2' is found to show considerable flexibility by adopting $156\text{-}161^\circ$ (I), $142\text{-}143^\circ$ (II) and $38\text{-}78^\circ$ (III) conformations, of which the biological relevant structure appears to be the conformer (II). The observed different conformations of the three drugs are correlated to the differential anticancer activity exhibited by these drugs. **Chapter 4** deals with the studies on self-aggregation of 4'-epiadriamycin, adriamycin and daunomycin by restrained Molecular Dynamics approach using Nuclear Magnetic Resonance Spectroscopy supported by Absorption, Fluorescence, Diffusion Ordered Spectroscopy and Mass Spectrometry. Self association is a process which competes with binding to DNA and formation of hetero-complexes. The change in chemical shift shows the presence of stacked dimer in all the three drugs. The two-dimensional NOESY studies show several intra-molecular and inter-molecular inter-proton connectivities suggesting specific stacking patterns of aromatic chromophores in parallel and anti-parallel orientation. Absorption, emission and diffusion ordered spectroscopy demonstrate formation of self aggregates. Electron Spray Ionization Mass Spectrometry study also proves the presence of dimer and absence of higher aggregates.

Also there is cleavage of glycosidic bond in daunomycin and adriamycin but not in 4'-epiadriamycin which is a clear evidence of reduced cardiotoxicity by 4'-epiadriamycin, as compared to daunomycin and adriamycin. The restrained Molecular Dynamics simulations show structural differences between drugs which have been correlated to biological action.

Chapter 5 deals with Phosphorus-31 NMR studies on binding of adriamycin with DNA hexamer sequence d-(TGATCA)₂. Titration studies are performed by adding increasing amounts of drug to a fixed concentration of DNA at 275 K. Besides, the 5 phosphate group resonances observed in d-(TGATCA)₂, additional peaks are seen, which are in slow exchange with those in the uncomplexed DNA. 2D ³¹P NMR exchange spectrum give a direct proof of the existence of DNA bound to drug molecule. Presence of large downfield shift of ~ 1.3 ppm indicates that drug intercalates between the base pairs of DNA and induce opening of base pairs to 6.8 Å by change in backbone torsional angles. Besides this, linewidth and spin-lattice relaxation studies (T₁) are also done to see the change in the phosphodiester backbone of DNA. **Chapters 6** deals with a detailed proton NMR study of binding of adriamycin with DNA hexamer sequence d-(TGATCA)₂. Titration studies are performed upto drug to DNA duplex ratio of 2.0 at 275 K. 2D NOESY experiments on 1:1, 1.5:1 and 2.0:1 drug-DNA complexes yields several intra-molecular and inter-molecular contacts. The two sets of resonance protons of DNA for T4NH, G2NH, T1NH, T1CH₃ and T4CH₃ protons show that the bound complex is in slow exchange with uncomplexed DNA. The absence of sequential connectivities at the intercalation site, that is, T1pG2/C5pA6 base pairs steps, has been found. Along with it, the fluorescence life time measurement, Diffusion Ordered Spectroscopy (DOSY) studies are also done to see the formation of intercalated complex. The restrained Molecular Dynamics Studies of complex of adriamycin with DNA Hexamer Sequence d-(TGATCA)₂ is done using the inter-proton distance obtained from 2D NOESY spectra. The helical parameters and backbone torsional angles etc. have been analyzed using

CURVES software version 5.1. **Chapter 7** deals with Phosphorus-31 NMR studies on binding of 4'-epiadriamycin with DNA hexamer sequence d-(CGATCG)₂. Titration studies are performed by adding increasing amounts of drug to a fixed concentration of DNA at 275, 298 and 318 K. Besides, the 5 phosphate group resonances observed in d-(CGATCG)₂, additional peaks are seen, which are in slow exchange with those in the uncomplexed DNA at the low temperature on NMR time scale. 2D ³¹P NMR exchange spectrum give a direct proof of the existence of DNA bound to drug molecule. Presence of large downfield shift of ~ 1.7 ppm indicates that drug intercalates between the base pairs of DNA and induce opening of base pairs to 6.8 Å by change in backbone torsional angles. **Chapter 8** deals with a detailed proton NMR study of binding of 4'-epiadriamycin with DNA hexamer sequence d-(CGATCG)₂. Titration studies are performed upto drug to DNA duplex ratio of 2.0 at 275, 298, 318 K. 2D NOESY experiments on 1:1, 1.5:1 and 2.0:1 drug-DNA complexes yields several intra-molecular and inter-molecular contacts. The two sets of resonance protons of DNA for T4NH, G2NH, G6NH, and T4CH₃ protons show that the bound complex is in slow exchange with uncomplexed DNA. The drug is intercalated to the DNA and is placed close to C1pG2/C5pG6 base pairs. Intermolecular peaks of drug and DNA is present. Further, the fluorescence life time measurement, Diffusion Ordered Spectroscopy (DOSY) studies are also show the formation of intercalated complex. Besides this, the model is built using the inter-proton distance obtained from NMR by rMD simulations on complex of 4'-epiadriamycin complexed with d-(CGATCG)₂. Sequence dependent variations have been observed. The elucidations of the inter-proton distances obtained from NMR experiments and exchange of bound and free DNA by ³¹P NMR experiments, along with rMD simulations of the structure of drug-DNA complex show that these drugs intercalate between the base pairs of DNA and stabilize the complex. Deviation is found at the base pairs where the drug intercalates from the canonical B-DNA conformation. Finally the conclusion is summarized.

LIST OF PUBLICATIONS

1. Structural Elucidation of 4'-Epiadriamycin by Nuclear Magnetic Resonance Spectroscopy and Comparison with Adriamycin and Daunomycin using Quantum Mechanical and Restrained Molecular Dynamics Approach. Ritu Barthwal, Prashansa Agrawal, A. N. Tripathi, Uma Sharma, N. R. Jagannathan and Girjesh Govil. Communicated to FEBES Journal.
2. Studies on Self-aggregation of Anthracycline Drugs by Restrained Molecular Dynamics approach using Nuclear Magnetic Resonance Spectroscopy supported by Absorption, Fluorescence, Diffusion Ordered Spectroscopy and Mass Spectrometry. Prashansa Agrawal, Sudhir Kumar Barthwal and Ritu Barthwal. Communicated to European Journal of Medicinal Chemistry.
3. Comparative Studies of drug – DNA complexes, Adriamycin-d-(TGATCA)₂ and 4'-Epiadriamycin-d-(CGATCG)₂, by Phosphorus-31 Nuclear Magnetic Resonance Spectroscopy. Prashansa Agrawal, S. K. Barthwal, Girjesh Govil and Ritu Barthwal. Communicated to European Biophysics Journal.
4. Structure of Adriamycin complexed with d-(TGATCA)₂ by Proton Nuclear Magnetic Resonance Spectroscopy. Prashansa Agrawal, Girjesh Govil and Ritu Barthwal. Communicated to Journal of Biomolecular Structure & Dynamics.
5. Structure of 4'-Epiadriamycin complexed with d-(CGATCG)₂ by Proton Nuclear Magnetic Resonance Spectroscopy. Prashansa Agrawal, Girjesh Govil and Ritu Barthwal. Communicated to Biochemical and Biophysical research Communications.

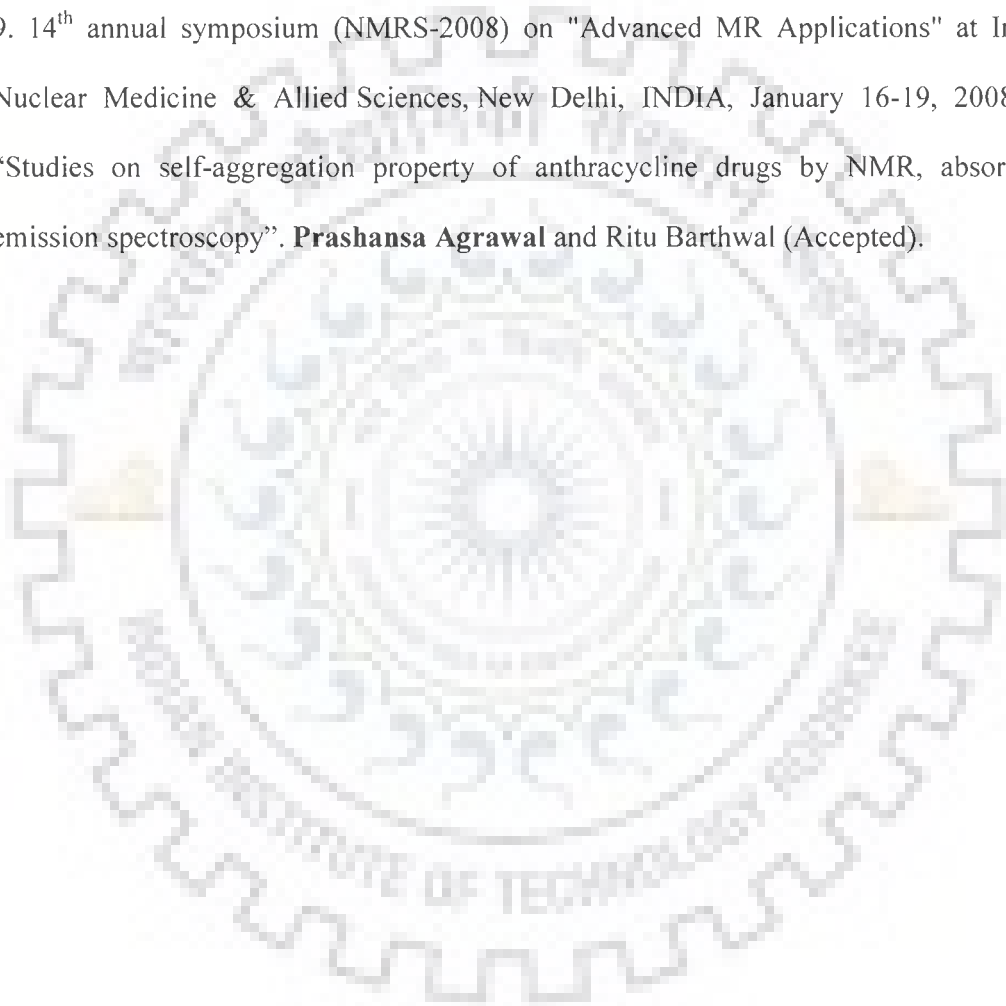
Conference/Symposium Presentation

1. National Symposium on Biophysics at Indian Institute of Technology Roorkee, (NSB-ECBB 2003) entitled "Spectroscopic Studies on Interaction of Mitoxantrone with Different base pairs Sequence of DNA" **Prashansa Agrawal**, S.K.Barthwal and Ritu Barthwal (2003).

2. National Symposium on Cellular and Molecular Biophysics, NIMHANS, Bangalore, (NSCMB-2004) entitled, “Studies on DNA binding of Camptothecin and /or its analog using Spectroscopy and Molecular Modeling Techniques” **Prashansa Agrawal**, Durairaj R. and Ritu Barthwal (2004).
3. National Symposium on Cellular and Molecular Biophysics, NIMHANS, Bangalore, (NSCMB-2004) entitled, “Direct DNA binding of Camptothecin Analog using molecular modeling Studies” Durairaj R, **Prashansa Agrawal** and Ritu Barthwal (2004).
4. XXI International Conference on Magnetic Resonance in Biological Systems, Hyderabad, Andhra Pradesh, INDIA (XXIst ICMRBS-2005) January 16 - 21, 2005, entitled “Structure of adriamycin complexed with d-TGATCA by Proton and Phosphorus-31 Nuclear Magnetic Resonance Spectroscopy” **P. Agrawal**, S. K. Barthwal, and R. Barthwal (2005).
5. XXI International Conference on Magnetic Resonance in Biological Systems, Hyderabad, Andhra Pradesh, INDIA (XXIst ICMRBS-2005) January 16 - 21, 2005, entitled “Structure of antitumor agent mitoxantrone with DNA hexamer d-(ATCGAT)₂ by ¹H and ³¹P NMR” R. Durairaj, **Prashansa Agrawal**, S. K. Barthwal, Ritu Barthwal (2005).
6. 13th Annual Symposium on “Current Trends in Solid State NMR Methodology and Practice” at National Chemical Laboratory, Pune, (NMRS-2007) February 05-08, 2007, entitled “Structure of 4'-epiadriamycin complexed with d-(CGATCG)₂ by proton and phosphorus-31 Nuclear Magnetic Resonance Spectroscopy” **Prashansa Agrawal**, Sudhir Kumar Barthwal and Ritu Barthwal (2007).
7. National symposium on Biophysics: Trends in Biomedical research” at New Delhi, India, February 13-15, 2007, entitled “Studies on Self Association of Anthracycline Drugs and their Interaction with Nucleic Acids by Absorption and Emission Spectroscopy” **Prashansa Agrawal**, Sudhir Kumar Barthwal and Ritu Barthwal. (2007).

8. Joint Meeting of the Biophysical Society 52nd Annual Meeting & 16th International Biophysics Congress at Long Beach, California, USA, February 2 – 6, 2008, entitled “³¹P and ¹H NMR Spectroscopy of Binding of Anticancer Drugs Mitoxantrone, Adriamycin and 4'-Epiadriamycin to DNA Hexamer Sequences - A Comparative Study of Intercalating and Non-intercalating (external binding) Drugs” Ritu Barthwal, Manpreet Kaur, **Prashansa Agrawal** and R. Durairaj (Accepted).

9. 14th annual symposium (NMRS-2008) on "Advanced MR Applications" at Institute of Nuclear Medicine & Allied Sciences, New Delhi, INDIA, January 16-19, 2008, entitled “Studies on self-aggregation property of anthracycline drugs by NMR, absorption and emission spectroscopy”. **Prashansa Agrawal** and Ritu Barthwal (Accepted).



Introduction

1.1 GENERAL

Mitosis is the process by which dividing cells control the separation of genetic material accurately into the two resulting daughter cells. Genes controlling mitosis in cancer and other proliferating cells are also the focus of cancer research. Proteins produced by gene targets interact with and regulate many aspects of the mitotic process; many interact with the mitotic spindle, which is the target of paclitaxel, the world's largest-selling cancer drug. These genes encode for many different classes of proteins such as enzymes, structural and scaffolding proteins, thereby increasing the likelihood of identifying new cancer targets amenable to small molecule drug development. The p53 gene, found on chromosome 17, is a tumor-suppressor gene. In the cell, the p53 protein binds DNA at specific locations and stimulates another gene to produce a protein called p21. In turn, p21 suppresses a division-stimulating protein (cdk2) to prevent the cell from passing through to the next stage of cell division. When p53 is mutated and can no longer bind DNA effectively, the p21 protein is not available to act as the “stop signal” for cell division. Thus cells may divide uncontrollably and form tumors. The p53 gene plays a key role in the pathogenesis or etiology of human cancers and clearly is an important component in a network of events that culminate in tumor formation. Mutations in p53 are found in most tumor types. Recent studies showed that the usage of anthracyclines (doxorubicin, epirubicin) along with the more recently discovered taxanes (docetaxel, paclitaxel), which are in phase III clinical trials, might be more effective in treatment of advanced metastatic breast cancer. Further steps toward optimizing the treatment schedules will include combining chemotherapy with the therapeutic principles of very different modes of action, such as target-specific antibodies against

cell surface receptors of growth factors or inhibitors of tyrosine kinases in pathways of signal transduction. Genetic factors would be included in breast cancer studies.

1.2 DRUG-DNA INTERACTION

DNA is an extremely important target for drug action, with a wide range of biological activities (anti-tumor, antiviral and antimicrobial) arising from the ability of compounds to bind sequence specifically to DNA and interfere with DNA topoisomerases or with transcription binding factor (Singh, et al., 1992). The mode of action of some drugs for the treatment of cancer, genetic disorders, and viral diseases is thought to be based on their binding to DNA and their modification of DNA activity. The activity of the drug is often linked to the binding geometry. Thus, the potential activity of a drug could be assessed by detecting the DNA binding location and fit of the drug candidate.

The design and evaluation of molecules that can recognize DNA in a sequence selective manner requires a multi-disciplinary approach to evaluate preferred binding sequences, a thermodynamic description of the interaction to measure complex stability, and high resolution structural data to define precisely the molecular basis for sequence recognition. In combination this data can be used predicatively in further rational design. The current research effort focuses on the application of a range of biophysical techniques, high resolution structural analysis by NMR spectroscopy, together with state-of-the-art computational methods to investigate the molecular basis for drug-DNA recognition, the role of solvent in mediating weak interactions, and cooperative interactions between adjacent binding sites. All this will lead to 'rational drug design'- a deterministic approach to combat disease or an infectious pathogen. For "rational" design, the first necessary step is the identification of a molecular target critical to a disease process or an infectious pathogen. Then the important prerequisite of "drug design" is the determination of the

molecular structure of target, which makes sense of the word "rational". Thus the mode of DNA/drug interaction could be important for the design of advanced drugs.

1.3 STRUCTURE OF ANTHRACYCLINE DRUGS

Anthracyclines are a class of compounds that are obtained from microorganisms (Fig.1.3a). They are well known for their ability to intercalate DNA and are potent chemotherapy agents. Intercalation is the insertion of planar molecules in between the bases of the DNA double helix. When this occurs, the helix unwinds partially.

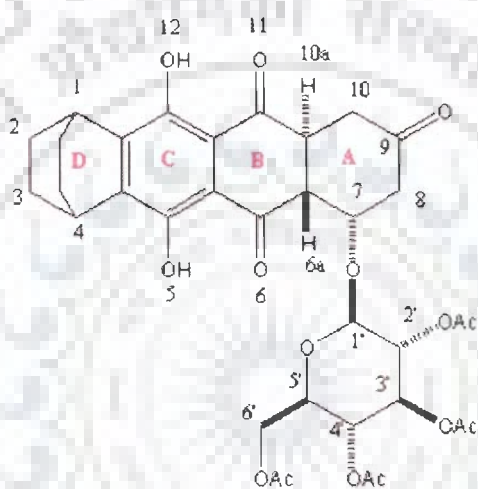


Fig. 1.3(a): Numbering System in Anthracyclines

This disturbs enzymatic mechanisms used in the transcription and translation of DNA. As a result, there are so many mistakes that cell replication is halted. Several mono-intercalating anthracyclines and groove binders have been well studied (Fig.1.3b). Crystal structure and kinetic data has been collected for the intercalation of DNA by these molecules. In close examination of these data, it was noticed that there was always a 2.0 drug/DNA ratio and that the orientation of the drug into the DNA molecule was always same. The idea of linking two drug molecules together to create a bisintercalator was conceived. The expected advantages of bisintercalator are enhanced binding affinity to DNA and increased biological activity. A few of

the intercalators are daunomycin, adriamycin, etc. The primary mode of action of daunomycin and adriamycin is believed to be their reversible binding to nucleolar DNA which causes inhibition of the replication process and hence death. The DNA base pairs buckle in order to accept the molecule; the aromatic D-ring enters first (at the major groove) and the substituted A-ring is at the minor groove. The anthracycline is at right angles to the direction of the DNA bases. The amino-sugar, attached to the A-ring, forms further H-bond with the DNA molecule via water molecules. There is π -bond formation above and below the aromatic rings in the complex. Nogalamycin, with its ring-D bicyclic sugar substituent actually intercalates with nucleic acids, and the DNA bases buckle even more. This has been proved by X-ray analysis of drug-DNA hexamers. Another mode of action of anthracyclines is via free radicals formation which attacks the DNA backbone, this is initialized by oxygen. Anthracyclines do not appear to form covalent bonds with DNA, although in the presence of formaldehyde this can occur.

Numerous biochemical studies including evidence from NMR spectroscopic and X-ray crystallographic studies have shown that daunomycin and adriamycin intercalate into the B-form of the DNA double stranded helix with cytosine-guanine d-(CpG) site-specific interactions. The base pairs above and below the drug 'buckle' in conformation to afford a distorted DNA helix thereby preventing association with the DNA helicase, DNA topoisomerase and polymerase families of enzymes to initiate DNA replication for RNA synthesis, protein formation and thereby cell division. The anthracycline is stabilized by electrostatic bond formation, hydrogen bond and stacking π -bond interactions between the electron-deficient quinone-based chromophore and the electron-rich purine-pyrimidine bases.

Hydrogen bonds play an important part in the stabilization of the complex assisted via several water molecules and a solvated sodium ion. Indeed, an anthracycline lacking the hydroxyl group

at C-9 on the right side of the ring-A is devoid of anticancer activity. Also, the hydrogen atom of the charged amino group is hydrogen bonded to O-2 of the thymine base (T10) and two water molecules. Replacing the C-13 hydrogen atom with a hydroxyl group as in adriamycin, creates additional hydrogen bond interactions involving solvent media around the substituent.

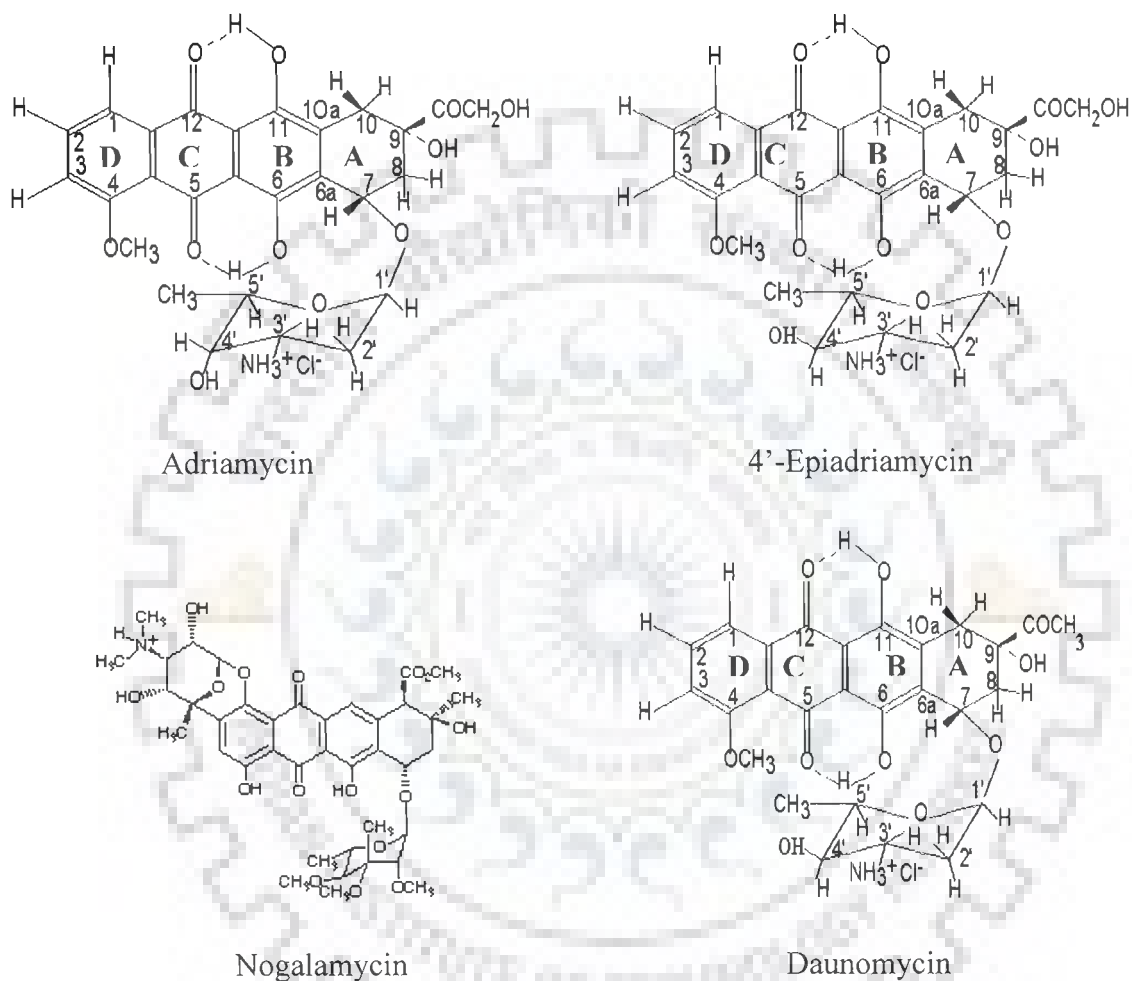


Fig. 1.3(b): Structures of a number of DNA Intercalators and Minor Groove Binders

This shows some possibility of the target ring-D modified anthracycline (R=H) intercalating with DNA and thereby test anticancer activity and intercalation theory. However, anthracyclines are also known to be enzymatically reduced to radical species that form hydroxyl radicals (in the presence of molecular oxygen) leading to strand breaks in DNA and thereby causing inhibition of the replication process. Adriamycin bearing the bridge on the A-ring could possess enhanced

anti-cancer effectiveness by intercalating with DNA and causing single strand breaks by forming the benzene biradical, in situ.

1.3.1 Mechanism of Action for some anthracycline antibiotics

Daunorubicin and its 14-hydroxy derivative, doxorubicin (Adriamycin), are anthracycline antitumor antibiotics produced as the fermentation product by the fungus *Streptomyces peucetius* var. *caesius*. These drugs are characterized by a tetrahydrotetracene quinone chromophore, which contains three flat, coplanar six-membered rings and has one additional non-planar six membered rings and daunosamine sugar moiety attached to ring A at C1' position through a glycosyl linkage. Ring A of adriamycin (doxorubicin) differs from that of daunomycin, that is, the 9COCH_3 group at position nine in daunomycin is replaced by the $9\text{COCH}_2\text{OH}$ group in adriamycin. Daunomycin and doxorubicin were first shown to have antitumor activity in the 1960. The two torsion angles defined as $\text{H1}'\text{-C1}'\text{-O7-C7}$ and $\text{C1}'\text{-O7-C7-H7}$, respectively describe the orientation of sugar moiety with respect to non-planar ring A (Fig.1.3b). These angles play an important role in the determination of the three-dimensional structure of the drug. Daunomycin is used mostly for the treatment of acute lymphocytic and myelogenous leukemias. Although it has some activity against pediatric solid tumors, it has little activity against adult solid malignancies. Daunorubicin damages DNA by intercalating between base pairs resulting in uncoiling of the helix, ultimately inhibiting DNA synthesis and DNA-dependent RNA synthesis. Daunorubicin may also act by inhibiting DNA topoisomerase II activity, affecting regulation of gene expression and generating free radicals. Cytotoxic activity is cell cycle phase-nonspecific, although it exerts maximal cytotoxic effects in the S-phase. Doxorubicin has the broadest spectrum of activity and is one of the most active agents in the treatment of breast cancer.

Doxorubicin has limited but demonstrable activity against thyroid cancer, ovarian cancer, and small cell lung cancer. Finally, it also has demonstrated activity against endometrial carcinoma, cancer of the testis, prostate, cervix, and head and neck, and multiple myeloma. Doxorubicin damages DNA by intercalation of the anthracycline portion, metal ion chelation, or by generation of free radicals.

4'-Epirubicin is a stereoisomer of doxorubicin in which the hydroxyl group in the C-4' position of the amino sugar is epimerized. Like other anthracyclines, the precise mechanism of action of epirubicin is unknown, but is primarily related to intercalation of the planar ring within DNA and subsequent inhibition of DNA and RNA synthesis. Epirubicin is cell cycle phase-nonspecific.

Binding Modes: Most drugs that bind to DNA do not involve covalent bond formation and, therefore, is an equilibrium process. The binding constant can be determined by measuring the free and bound forms of the drug. The thermodynamics are classically driven by electrostatic attractions, hydrophobic interactions, hydrogen bonding, and van der Waals forces. There are two key modes of non covalent drug interactions with the DNA, helix-groove binding and intercalation, as well as combinations of these modes and nonspecific binding. Polyamines, such as spermidine and spermine, are considered to be nonspecific binders with primary interactions being electrostatic binding to the anionic phosphate backbone. Cyanine dyes are known to exhibit a combination of the binding modes.

Groove Binders

Minor groove binding drugs are typically thin and crescent shaped to sterically fit into the narrow minor groove. Examples of minor groove binding ligands include distamycin, netropsin, Hoechst 33258, and chromomycin. They do not change the gross structure of DNA. There are fewer major groove binding drugs, although this is a very common binding mode for proteins to

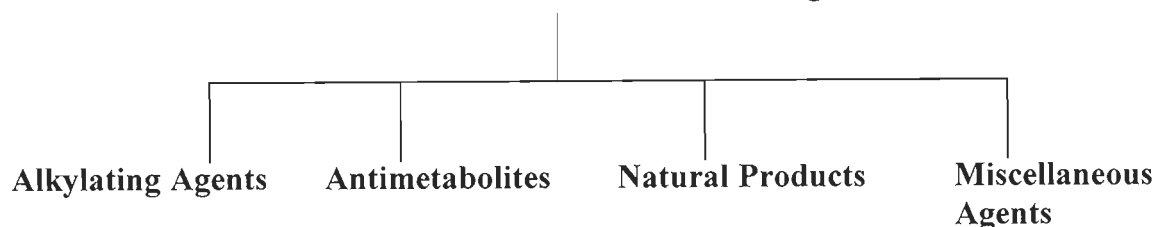
regulate gene expression. Few examples of major groove binders are cisplatin, alkylators, and mustards.

Intercalators

Intercalation occurs when a planar aromatic structure is inserted between the Watson-Crick basepairs which causes the DNA base pairs to separate and the overall strand to lengthen and slightly unwind. Compounds with two or three fused rings do not completely fill the space between the base pairs while four fused rings correspond in size to stack efficiently with the base pairs. Intercalators generally have a preferential binding between 5' pyrimidine-purine 3' steps. Examples of intercalators include ethidium, daunomycin, echinomycin, actinomycin, and quinacrine. Intercalators are effective drugs based on interruption of DNA replication, transcription and repair processes. Poly-intercalators are a class of intercalators in which multiple intercalating units are joined together with a linker compound. The chemical moieties, physical length, and rotational rigidity of linker compound have an important influence on the binding affinity and selectivity of the intercalator. In addition, distortion of the DNA occurs with some bis-intercalators the degree of which is dependent on the linker structure. Ditercalinium, ethidium and acridine are examples of bis-intercalators that have been shown to cause twice the DNA helical extension and unwinding of a mono-intercalator. Traditionally, the detection of intercalation has been based on a spectrophotometric shift which requires that the intercalating moieties are chromophores. Another indirect method of inferring intercalation has been based on the increase in DNA double helix stability resulting in decreased heat denaturation. NMR images of ligands intercalated with DNA have been acquired which help establish the structural position of the ligand binding. All anthracyclines produce cardiac damage that can result in serious and even life-threatening complications.

1.4 CLASSIFICATION OF ANTICANCER DRUGS

Classification of Anticancer Drugs



1.4.1 Alkylating agents: They are developed from nitrogen mustard war gases of World War I which were highly reactive vesicants and are the first chemicals used for cancer. They are not cell cycle specific, but still more active in dividing tissues. They are "Radiomimetic" - action on DNA resembles radiation. They are highly reactive and form covalent bonds. Also are strongly electrophilic - carbonium ion intermediates. Their adverse effects are that they are more toxic to bone marrow and gut than to liver and kidney, etc., and causes infertility to both males and females. They are Mutagenic and Carcinogenic. Also increases DNA repair systems. Their clinical use is of wide spectrum, Lymphoreticular tissue tumors and limited activity against sarcomas. Examples include Nitrogen mustards: Mechlorethamine, Cyclophosphamide, Melphalan, Chlorambucil.

1.4.2 Antimetabolites: They resemble normal substrates and mostly inhibit DNA synthesis. Some of them inhibit RNA synthesis and/or function. The Bone Marrow cell replication is profoundly inhibited by them. They are highly cell cycle specific and also "phase specific", e.g., S or M phase. Some examples are: Folic Acid Analogs- Methotrexate, (MTX), Pyrimidine analogs- Fluorouracil, (5-FU), Cytarabine, Purine analogs - 6-Mercaptopurine, (6-MP).

1.4.3 Natural products: Their uptake is by energy dependent carrier. Then they bind to tubulin in microtubules to cause their dissolution. The colchicine-like arrest in metaphase is seen and altered intracellular transport. There is no cross resistance between vincristine and vinblastine.

They cause constipation and abdominal pain, less hematologic effects than many other cytotoxic drugs. Uses: They are the drug of choice for childhood leukemias in combination with prednisone and also used for lymphoreticular neoplasms, carcinomas, and sarcomas.

Antitumor Antibiotics: They are obtained from *Streptomyces* spp. All interact with DNA and/or RNA, but may also interact with other cellular constituents. They are less "phase-specific" than antimetabolites. Tissue necrosis is only generalizable toxicity. e.g, Clinical indications include broad spectrum anti-cancer activity. Activity observed in bladder tumors, and carcinomas of prostate, thyroid, endometrium, head and neck, and other solid tumors. One of the examples is given below.

(1.) Doxorubicin (Adriamycin): It is rigid, tetracyclic structure substituted with sugar – daunosamine. It is **DNA topoisomerase II inhibitor** and crucial to DNA replication and transcription. It intercalates between base pairs of DNA and inhibits DNA-dependent RNA synthesis and generates free radicals that cause membrane damage and DNA strand breaks. Its resistance include: alterations in Topoisomerase II activity, increased inactivation of radicals- Increase in glutathione-dependent enzymes, e.g., glutathione-peroxidase, altered NADPH contents, increase drug efflux- multi-drug resistance (MDR) and P-glycoprotein (gP-170) pump is product of *mdr* gene. **Adverse effects:** Local Toxicity -Interaction of doxorubicin and radiation in some tissues to produce enhanced reactions. The reactions include: Skin: intensity from erythematic to ulceration and necrosis, Pulmonary: fibrosis and sloughing of esophageal mucosa, Heart, and intestinal mucosa may also be affected. To reduce incidence, Dexrazoxane- chelating agent for reducing the severity of cardiomyopathy from Doxorubicin is given.

Examples of Natural Products: Vinca alkaloids - Actually an Anthracenedione and lacks sugar moiety, Vincristine, Vinblastine, Etoposide, Taxol, **Antitumor antibiotics-** Anthracyclines-

Doxorubicin hydrochloride, (Adriamycin), 4'-Epiadriamycin, Daunorubicin, Idarubicin, Mitoxantrone, Actinomycin D, Mitomycin C.

1.4.4 Miscellaneous agents: They enter cells by passive diffusion. Then aquated Cl^- moieties react with N7 of guanine and other nucleophiles. They form Intrastrand (rapidly) and Interstrand (slowly) crosslinks in DNA and also DNA - protein crosslinks. They are Cell-cycle nonspecific, but may be most active in G1 phase of the cell cycle. They cause nausea, vomiting, anaphylactic-like reactions, neurotoxicity, myelosuppression- mild compared to alkylating agents. Examples include Cisplatin, Carboplatin, L-Asparaginase, Hydroxyurea, Mitotane and Corticosteroid.

1.5 STRUCTURE OF NUCLEIC ACIDS

Deoxyribonucleic acid (DNA) is the “polymer of life”. DNA is composed of units of purine and pyrimidine bases attached to a backbone of a 5-carbon sugar (deoxyribose) alternating with a phosphate group (Fig.1.5a and 1.5c). The purine bases- adenine (A) and guanine (G), and pyrimidine bases- thymine (T) and cytosine (C) are paired together A to T and G to C to allow replication of the DNA code. DNA is typically double stranded in a “spiral staircase” structure with the paired bases forming the “steps”. Base when combined with sugar is *nucleoside* and when a phosphate group is added to it, *nucleotide* is formed (Fig.1.5b). Nucleotides exist in activated forms, nucleotide diphosphates or triphosphates and the sugar is deoxyribose or ribose. The 5' carbon has an attached phosphate group, while the 3' carbon has a hydroxyl group. DNA can be found in three principal forms: A, B, and Z. A form occurs under anhydrous conditions (<75% relative humidity) and is found in bacterial spores. The A form has 11 base pairs per helical turn, a helical rise per base pair of 0.26nm, and a diameter of 2.6 nm. The B form is the most common form found under natural conditions. It has 10 base pairs per helical turn, a helical rise per base pair of 0.34 nm, and a diameter of 2.0 nm. Both the A and B forms are right-handed

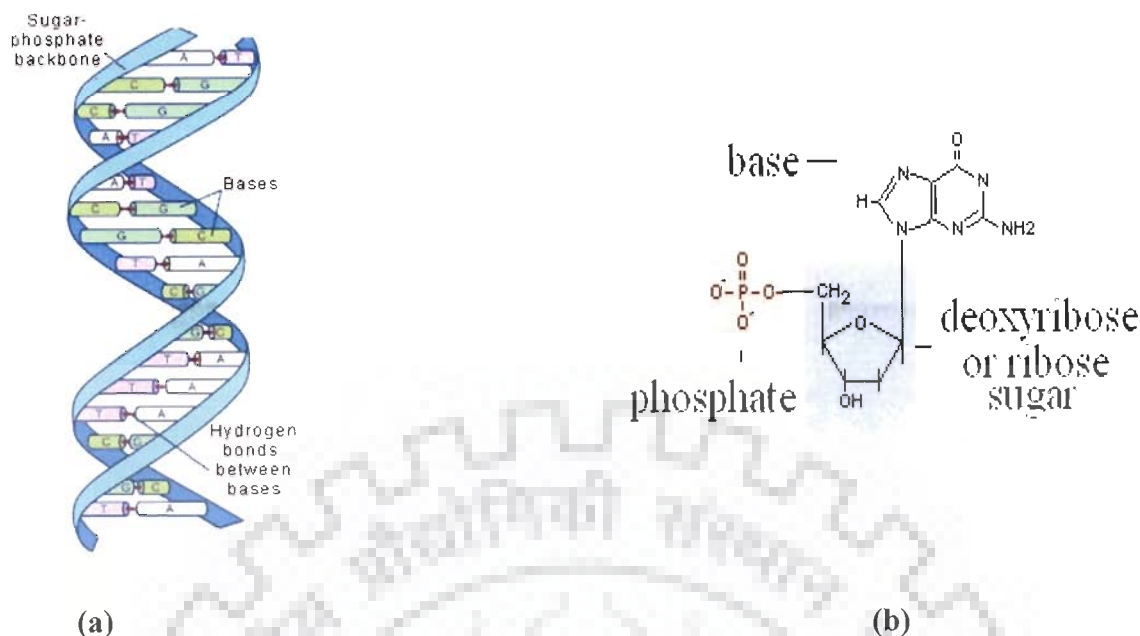


Fig. 1.5(a-b): Structure of Double-stranded B-DNA along with Basic Unit of Nucleotide

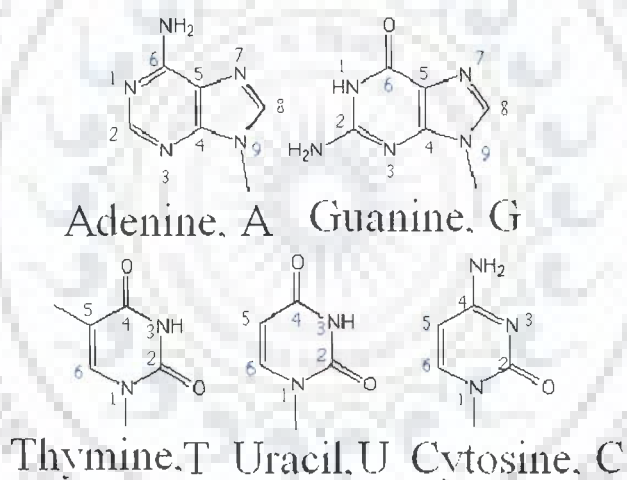


Fig. 1.5(c): Chemical Structures of purine and pyrimidine bases: (A) Adenine, (G) guanine, (T) thymine, (U) Uracil and (C) cytosine.

helices, however, the Z form is a left handed helix and is believed to serve as a genetic switch. The Z form has 12 base pairs per helical turn, a helical rise per base pair of 0.37 nm, and a diameter of 1.8nm.

1.5.1 Base Pairing and Double Stranded Nucleic Acids

Most DNA exists in the B form. The major force promoting formation of this helix is complementary base pairing: A's form hydrogen bonds with T's (or U's in RNA), and G's form hydrogen bonds with C's. If we mix two ATGC's together, the following duplex will form (Fig.1.5d).

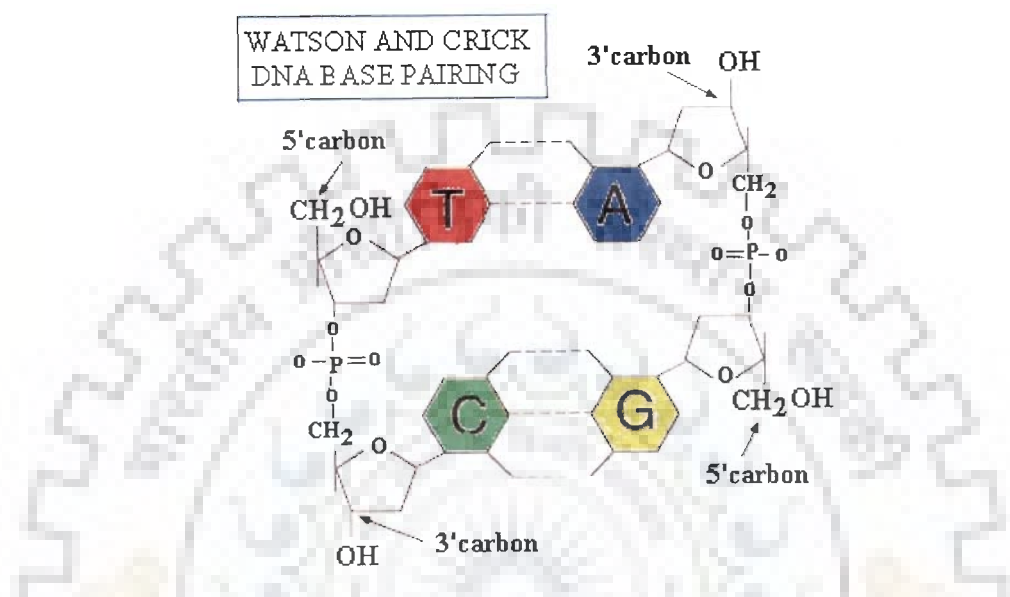


Fig. 1.5(d): Structural representation of DNA backbone and base pairs

A major and minor groove traversing the spiral structure is formed by the DNA backbone. The major and minor grooves differ not only in size, but also in polarity and chemistry. The chemistries present in the grooves are specific to the base pairs which can lead to sequence specific binding in the grooves. In the major groove A-T has a sequence of acceptor-donor-acceptor and G-C has a sequence of acceptor-acceptor-donor (Fig.1.5e). The major groove has more binding sites and exhibits directionality (e.g. AT vs. TA). DNA is a polyanion which attracts positively-charged counter ions such as calcium and magnesium ions in buffer solutions to shield the electrostatic charges. DNA is a fairly stiff molecule with a persistence length of about 50 nm. According to the IUPAC Compendium of Macromolecular Nomenclature,

persistence length is “the average projection of the end-to-end vector on the tangent to the chain contour at a chain end in the limit of infinite chain length”.

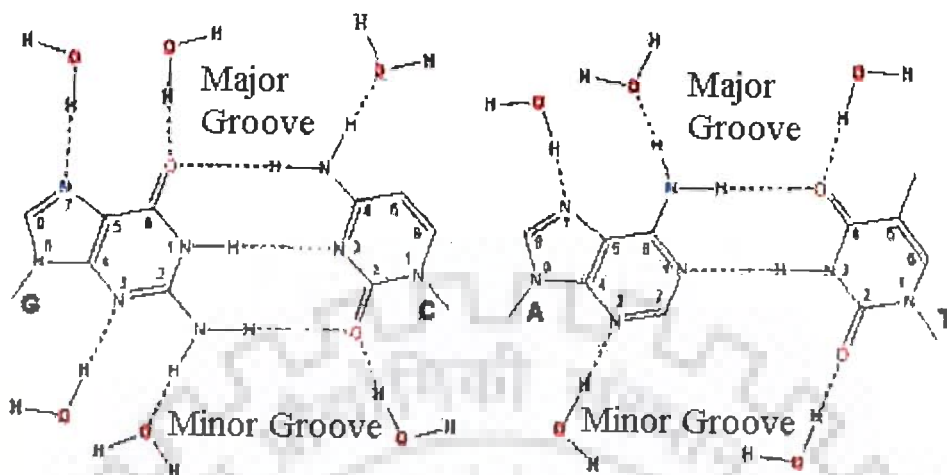


Fig. 1.5(e): Chemical structure of base pairs extending into major and minor grooves

1.5.2 Nucleic Acid Function

Deoxyribonucleic acid (DNA) and ribonucleic acid (RNA) are the informational molecules of all living organisms. Besides storing and transmitting information, RNA forms structural and functional parts of units such as the ribosome and in some system has a catalytic function as ribozymes. Both DNA and RNA are long polymers assembled for repeating subunits, the nucleotides. The sequence of nucleotides in information nucleic acids molecules (mainly DNA) makes up a code that stores and transmits the direction required for assembling all types of proteins. DNA serves two central roles. First, it maintains the genetic information and is replicated to pass this information to each new cell. Second, it contains the code which is translated into RNA which is then transcribed into proteins. This has become known as the central dogma of molecular biology (Fig.1.5f).

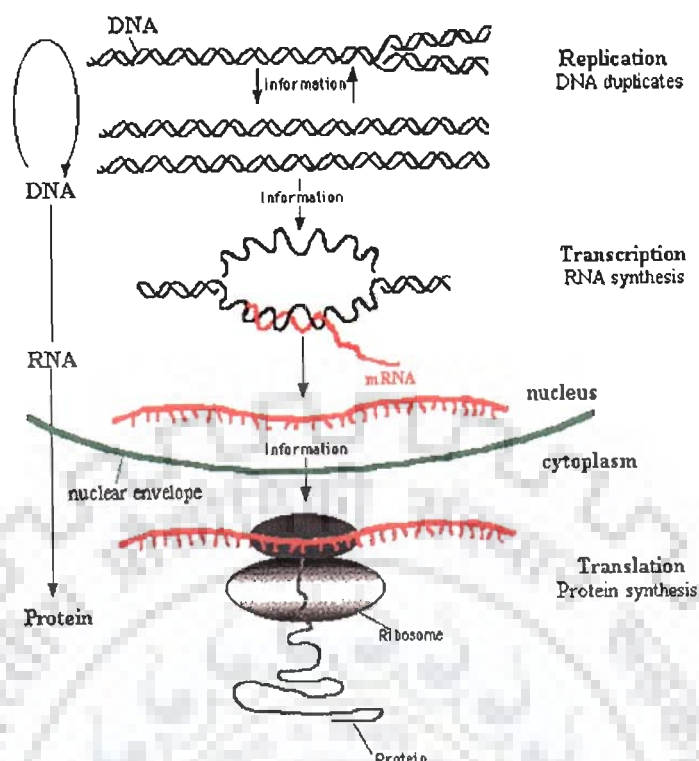


Fig. 1.5(f): The “Central Dogma of Molecular Biology” depicting the key cellular processes of DNA replication and translation

Individual nucleotides provide the building blocks of nucleic acids and carry out a variety of biological functions. Many nucleotides transport chemical energy in the form of phosphate groups or electrons from one reaction system to another. Others carry metabolites such as acetyl groups between reactions. Other nucleotides in cyclic form are important in cell regulation.

1.5.3 Conformation of sugar phosphate backbone and furanose sugar ring

The conformation of the sugar-phosphate backbone, following the sequential numbering of atoms P–O5'–C5'–C4' etc., is defined by torsional angles α , β , γ , δ , ϵ and ζ . Angles ν_0 , ν_1 , ν_2 , ν_3 and ν_4 decide the geometry of sugar ring (Fig. 1.5g and Fig. 1.5h). The different families of DNA structures are characterized by the values of these torsion angles.

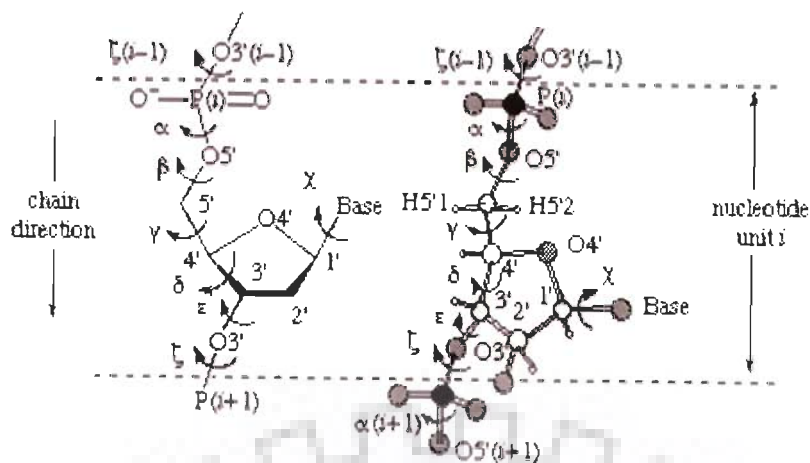


Fig. 1.5(g): Section of a polynucleotide backbone showing the atom numbering and the notation for torsion angles

The sugar ring occupies a pivotal position in the nucleotide unit because it is part of both the backbone and the side chain. In order to provide a complete description of the ring conformation, it is necessary to specify the endocyclic torsion angles for the ring as well as the bond lengths and bond angles. The ribose sugar geometry is defined by the following five endocyclic torsion angles: ν_0 - ν_4 are denoted by the symbols, respectively. The sequence of atoms used to define each backbone torsion angle is shown in e.g. $\nu_0, \nu_1, \nu_2, \nu_3, \nu_4$ refers to the torsion angle of the sequence of atoms C4'-O4'-C1'-C2', etc (Fig. 1.5h).

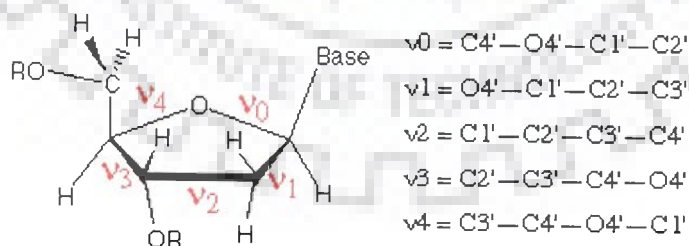


Fig. 1.5(h): Endocyclic torsional angles in the sugar ring

The magnitudes of such angles are all interrelated and, therefore, the geometry of the ribose ring can be defined from two parameters: the pseudorotation phase angle (P) and the pucker

amplitude. The ribose ring is not a planar and usually presents C2'-endo (South) or C3'-endo (North) conformation. For the sugar pucker conformation, homonuclear $^3J_{\text{H-H}}$ coupling constants serve as the most direct determinant. These constants can be measured in a qualitative way from 2D ^1H - ^1H TOCSY, 2D ^1H - ^{13}C TOCSY-HMQC or 2D ^1H - ^{13}C TOCSY-HSQC experiments:

- Very weak $J_{\text{H1}'\text{-H2}'}$ and strong $J_{\text{H3}'\text{-H4}'}$ cross-peaks correspond to *pure N-type conformation* (preferred conformation in RNA).
- Strong $J_{\text{H1}'\text{-H2}'}$ and weak $J_{\text{H3}'\text{-H4}'}$ cross-peaks correspond to *pure S-type conformation*.
- $J_{\text{H2}'\text{-H3}'}$ is similar in both states.
- Intermediate intensities indicate equilibrium between N and S states.

1.5.4 Sugar pucker

The five-membered ring is generally non planar and its conformation is designated as follows. If four atoms lie in the plane, this plane is chosen as reference plane and the conformation is designated as envelope (E) and if they do not, the reference plane is then that of the three atoms that are closest to the five-atom, least-squares plane, and the conformation is described as twist (T).

- The present *E* and *T* notations for puckered forms of the sugar ring conform to those recommended for the conformational nomenclature of five and six-membered rings of monosaccharide and their derivatives.
- The *E/T* notation has superseded the *endo/exo* description in which atoms now designated by superscripts were called *endo*, and those now designated by subscripts were called *exo*. They are shown by both systems of designation (Fig. 1.5i). Examples: C3'-*endo*/C2'-*exo* has become 3T_2 and C3'-*endo* has become 3E .

c) Symmetrical twist conformations, in which both atoms exhibit equal displacements with respect to the five-atom plane are denoted by placing the superscript and subscript on the same side of the letter T , e.g. ${}_2^3T$, ${}_4^3T$, etc.

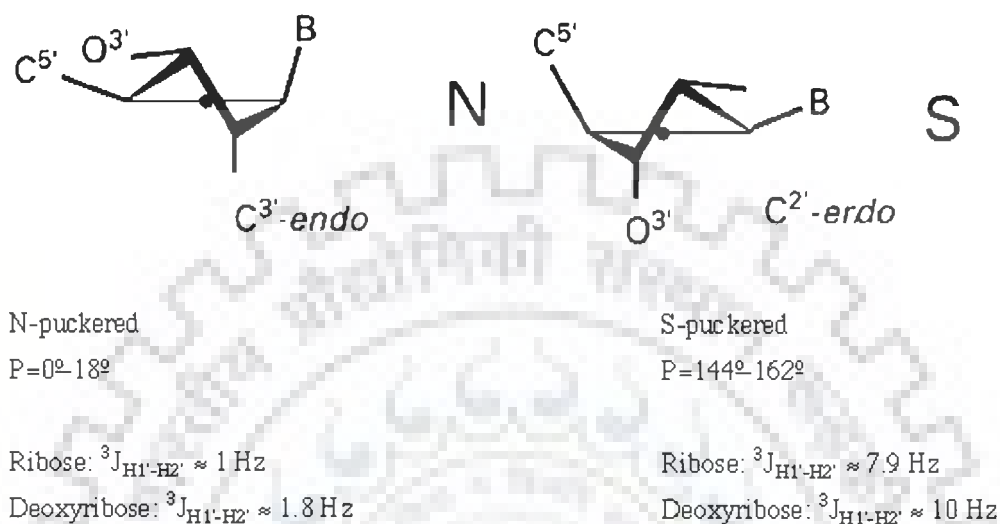


Fig. 1.5(i): Preferred conformation of sugar pucker C2' endo and C3' endo of sugar

1.5.5 Pseudo rotation cycle

Sugar conformation can only be approximately defined by sugar pucker if intermediate twist modes are considered and hence inadequate. In furanose ring maximum pucker rotates virtually without any potential energy barriers, giving rise to infinite number of conformations. Each conformation of the furanose ring can be unequivocally described by two pseudorotational

$$\tan P = \frac{(v_4 + v_1) - (v_3 + v_0)}{2v_2 (\sin 36^\circ + \sin 72^\circ)}$$

parameters: the phase angle of pseudorotation, P , and the degree of pucker, ψ_{\max} . In nucleotides, the pseudorotation phase angle P is calculated from the endocyclic sugar torsion angles according to Altona C. and Sundaralingam M.

Given the phase angle P , the five torsional angles are related by:

$$v_j = v_{\max} \cdot \cos(P + j \cdot \psi)$$

Where $j = 0$ to 4 and $\psi = 720^\circ / 5 = 144^\circ$. The maximum torsion angle, v_{\max} is derived by setting $j = 0$.

$$v_{\max} = v_0 / \cos P$$

At every phase angle P , the sum of the positive torsional angles is equal to the sum of the negative torsional angles, i.e. the sum of the five angles is zero.

$$v_0 + v_1 + v_2 + v_3 + v_4 = 0$$

Standard conformation ($P=0^\circ$) is defined with a maximally positive $C1'-C2'-C3'-C4'$ torsion angle [i.e. the symmetrical ${}_2^3T$ form], and P has value $0-360^\circ$ (Fig.1.5j). Conformations in the upper or northern half of the circle ($P = 0 \pm 90^\circ$) are denoted N and those in the southern half of the circle ($P = 180 \pm 90^\circ$) are denoted S conformation. It is seen that the symmetrical twist (T) conformations arise at even multiples of 18° of P and the symmetrical envelope (E) conformations arise at odd multiples of 18° of P . The symbols 'r' and 'd' represent the usual range of P values for N and S conformations of ribo- (r) and 2'-deoxyribo- (d) furanose rings of β -D-nucleosides and nucleotides. In B- DNA two ranges of pseudorotation phase angles are preferred $C3'$ – endo at $0^\circ \leq P \leq 36^\circ$ (N conformer) and $C2'$ endo at $144^\circ \leq P \leq 180^\circ$ (S- conformer).

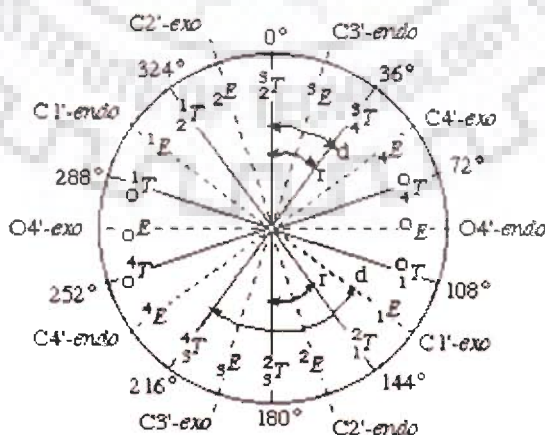


Fig. 1.5(j): Pseudorotation cycle of furanose ring in nucleosides (Altona and Sundarlingam)

1.5.6 N-Glycosidic Bond rotation (χ_{CN})

The torsion angle about the N-glycosidic bond (N-C1') that links the base to the sugar is denoted by the symbol χ_{CN} . The sequence of atoms chosen to define this angle is O4'-C1'-N9-C4 for purine and O4'-C1'-N1-C2 for pyrimidine derivatives. Thus when $\chi = 0^\circ$ the O4'-C1' bond is eclipsed with the N9-C4 bond for purine and the N1-C2 bond for pyrimidine derivatives. Relative to the sugar moiety, the base can adopt two main orientations, called anti and syn. In anti, the six membered rings in purines and O2 in pyrimidines is pointing away from the sugar, and in syn it is over or towards the sugar. High anti is a variant of anti, in which the bond C1'-C2' is nearly eclipsed with N1-C6 in pyrimidine or N9-C8 in purine nucleosides. The term high anti actually denotes a torsion angle lower than anti (Fig. 1.5k).

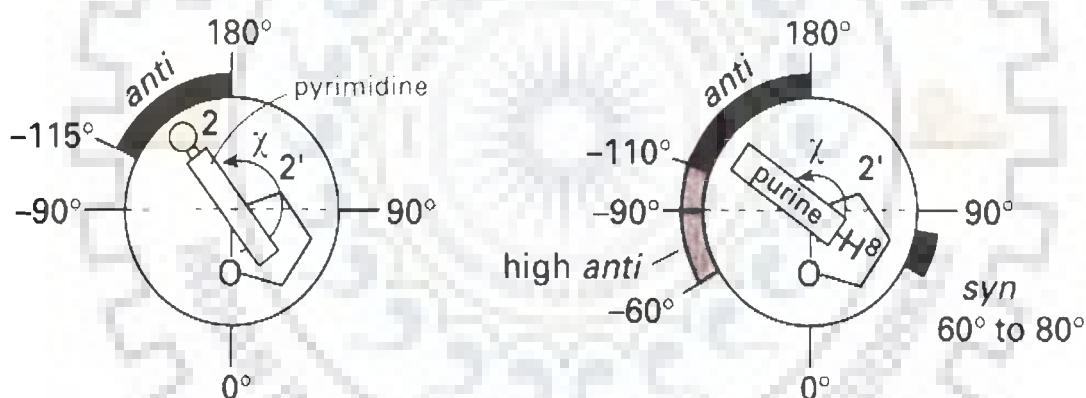


Fig. 1.5(k): Anti high, anti and syn orientations about the glycosidic bond

1.6 GENERAL PHENOMENON OF INTERCALATION IN DNA

1.6.1 Intercalation changes the physical properties of a double helix

Intercalation changes the physical properties of a double helix of DNA because base pairs must separate (unstack) vertically to allow the drug entry, the sugar phosphate bone is distorted and the regular helical structure is destroyed. According to such a model, the DNA must lengthen

with increasing amount of added drug. This is indeed observed by enhanced viscosity and the diminution of the sedimentation coefficient, effects which also suggest overall stiffening of the DNA duplex (Gabbay et al, 1976). A two stage, anti-cooperative process was established from non-linear scatchard plot and from the kinetics which is the characteristic of intercalating agents.

1.6.2 The Nearest-neighbor exclusion principle

This principle states that intercalators can at most bind at alternate possible base pair sites on DNA, giving a maximum one intercalator between every second site. The exclusion principle states that when an intercalator binds at one particular site, binding of another intercalator at adjacent site is inhibited probably because nucleotides flanking the intercalator are geometrically distorted. All spaces between base pairs are potential binding sites for a non-specific intercalator.

1.6.3 Intercalation causes DNA unwinding

The separation of base pairs makes room for the intercalator. This can be visualized as a combination of pulling along the B-DNA double helix axis and left handed unwinding in order to prevent breakage of sugar-phosphate backbone. Intercalation into the pyrimidine 3'-5' purine sequence is 7-13 Kcal/mole more favorable than purine 3'-5' pyrimidine intercalation because base overlap is more pronounced in former than latter. The intermolecular interaction is supported by intramolecular electrostatic forces rendering pyrimidine 3'-5' purine sequences more prone to intercalation.

1.6.4 Intercalation causes Sugar puckering

Usually all complexes have purine sugar at the 5' position in C3'-endo pucker. In most of them, the pyrimidine sugar at the 3' end is C2'-endo with only few cases of C3'-endo are found (Fig. 1.6). Upon intercalation both χ and β increase by over 50°, χ being pushed into high anti range.

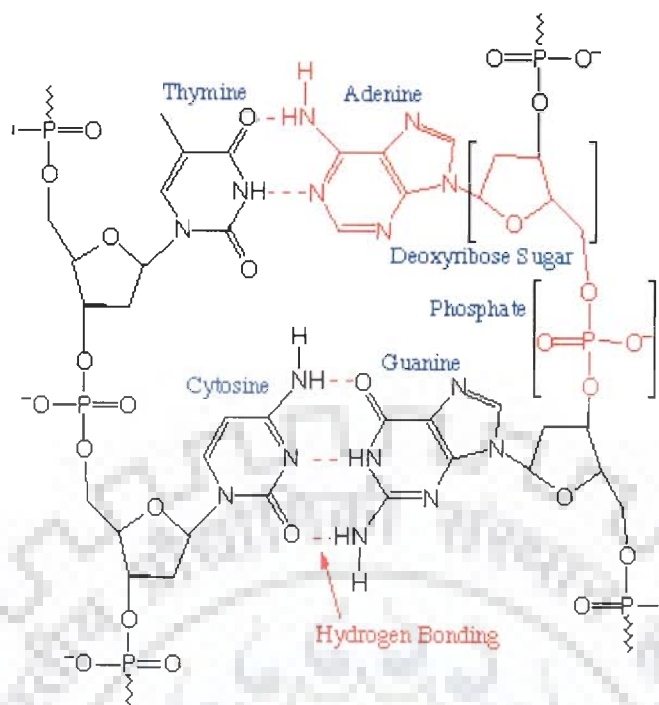


Fig. 1.6: Watson and Crick base pairs showing the hydrogen bonding arrangements in the double helical DNA

Model building studies suggested that the unwinding angle is dependent on a combination of small variations in the backbone torsion angles and base-pair geometry expressed as bend and twist, and not just on sugar pucker. It is clear that a correlation exists between unwinding angle and shape of intercalating agent.

1.7 FORCES INVOLVED IN DRUG –DNA INTERACTION

The binding of drug to DNA involves different energy contributions. These include energy from any conformational changes, from the entropic cost of forming a bimolecular complex, from the hydrophobic transfer process, from the polyelectrolyte effect, and from the formation of non-covalent molecular interactions (e.g. hydrogen bonds and van der Waals' interactions) within the complex. A few of these forces play an important role in stabilizing the intercalation of drug in drug-DNA complex are as follows:

(i) Hydrogen bonding

The phosphate group, sugar, bases in nucleic acids and hydrophilic groups in anthracycline drug participate in hydrogen bonding with water. Since all linear hydrogen bonds have similar free energies, they make little net contribution to the favorable free energy change when drug and nucleic acid interact in solution. In contrast, the formation of poorly aligned hydrogen bonds or absence of some of them on the complex formation carries a 4 KJ mol^{-1} free energy penalty. Thus hydrogen bonds are one of the most important means of making sequence specific interaction of nucleic acid with drug. For example in Adriamycin complex with DNA, two hydrogen bonds $9\text{OH}\dots\text{N3}$ and $9\text{O}\dots\text{N2H}$ between Adriamycin and the base G2 stabilize the conformation of ring A (Chen et al, 1986; Frederick et al, 1990; Moore et al, 1989; Nunn et al, 1991; Wang et al, 1987). The $9\text{OH}\dots\text{N3}$ hydrogen bond has been found to be necessary for the *in vivo* anti tumour activity of Adriamycin. There is additional hydrogen bonding interactions linking the C-14 hydroxyl of Adriamycin to DNA, which further stabilizes the complex (Frederick et al, 1990). The Daunomycin complex with $d\text{-(CGTACG)}_2$ (Wang et al, 1987) is stabilized by hydrogen bonding interactions involving hydroxyl and carbonyl groups at C9 of the Daunomycin chromophore, the hydroxyl group being essential for activity.

(ii) Electrostatic forces: salt bridges

Salt bridges are electrostatic interactions between groups of opposite charge. They typically provide about 40 KJ mol^{-1} of stabilization per salt bridge. In drug-DNA complex, they are formed between the ionized phosphates of nucleic acid and positively charged groups of drug. Salt bridges are influenced by the concentration of salt in the solution. Strength of salt bridge decreases with the increase in concentration of the salt. They are much stronger when there are

no water molecules between the ionized groups because water has a high dielectric constant. These are relatively long-range forces.

(iii) Entropic forces: the hydrophobic effect

The hydrophobic effect is due to the behavior of water at an interface. Any molecule in water creates a sharply curved interface and so orders a layer of water molecules around itself. When molecules aggregate, the ordered water molecules at the interface are released and become part of the disordered bulk water, thus stabilizing the aggregate by increasing the entropy of the system. Polar surfaces, where the enthalpy loss tends to offset the entropy gain or de-solvation are less likely to aggregate than non-polar ones. Molecules of water left at the interface between the drug and the nucleic acid obviously decrease the entropy of the system. Therefore the surface of the non-planar aromatic chromophore of drug tends to be exactly complementary so that no unnecessary water molecules remain when the complex forms.

(iv) Base stacking: dispersion forces

Base stacking is caused by two kinds of interaction: the hydrophobic effect mentioned above and dispersion forces. Molecules with no net dipole moment can attract each other by a transient dipole-induced dipole interaction. Such dispersion forces decreases with the inverse sixth power of the distance separating the two dipoles, and so are very sensitive to the thermal motion of the molecules involved. Despite their extreme distance dependence, dispersion forces are clearly important in maintaining the structure of double stranded nucleic acids because they help to cause base stacking. Besides they allow aromatic ring of the drug to intercalate between bases and stabilize it by base stacking.

1.8 NMR SPECTROSCOPY, UV-VIS AND FLUORESCENCE SPECTROSCOPY INVOLVED IN DRUG –DNA INTERACTION

NMR spectroscopy has enjoyed many advances recently, and the pace of development shows no signs of slowing. These advances are allowing NMR to help solve important problems in the widespread manner the field of drug discovery. NMR spectroscopy is now being used to determine protein structures, to monitor ligand-receptor binding, to study diffusion, to analyze mixtures using LC-NMR, to analyze solid-phase synthesis resins and to determine the structures of organic small molecules. Biomolecular NMR spectroscopy has expanded dramatically in recent years and is now a powerful tool for the study of structure, dynamics, and interactions of biomolecules. NMR spectroscopy is already well-established as an efficient method for ligand screening. A number of recently developed techniques show promise as aids in structure-based drug design. An advantage of the method is that all these interactions can be studied in solution-time-consuming crystallization is not necessary. Being in solution form, even structural and biochemical changes in intact cells (*in vivo* NMR) can be monitored. Nuclear Magnetic Resonance (NMR) spectroscopy uses radiation to induce nuclear spin state changes which are unique for different atoms and their local environment. From the 1D and 2D NMR spectrum acquired on solid or liquid samples, the structure of molecules can be deduced. NMR can observe static as well as dynamic interactions between molecules. It requires that the sample to be dissolved in a deuterated solvent. The most commonly used resonances in NMR studies are ^1H , ^{13}C , ^{31}P and ^{15}N . ^1H NMR gives rise to a series of absorption lines in the region 0-15 ppm. A larger spectral dispersion of chemical shifts is observed in ^{13}C NMR. In ^{15}N NMR, chemical shifts are sensitive to primary structure as well as molecular conformation. But it has low sensitivity due to low natural abundance (0.36%) which causes difficulties in its detection hence offers limited applications of ^{15}N NMR. ^{31}P NMR has developed as a powerful probe of the structure and dynamics of DNA due to existence of spin $\frac{1}{2}$, 100% natural abundance, moderate

relaxation times, wide range of chemical shifts and non-interference from solvent peaks. In ^{31}P NMR, chemical shifts are sensitive to molecular conformation of the phosphate group. Thus it becomes very informative in case of nucleic acid structure elucidation since backbone of DNA and RNA contains phosphorus nuclei. NMR spectroscopy can provide both qualitative and quantitative information. This information can benefit numerous disciplines in drug discovery, including natural products research, synthetic medicinal chemistry, metabolism studies, drug production, quality control, rational drug design and combinatorial chemistry. This focuses on how they might be of value in removing some of the current "bottlenecks" in structure-based drug discovery.

Fluorescence spectroscopy provides structural information on the basis of emission and excitation wavelength. The fluorophore has different emission and excitation wavelengths which gives different spectra ranging from 200-800nm. UV-Vis spectroscopy uses the wavelengths of light in the spectrum ranges of 120 to 800 nm. DNA typically absorbs in the region of 160 to 300 nm due to the electronic transitions regions of the bases. These techniques are conducted in solution and are simple to conduct, but average the results across molecules in different states.

1.9 MOLECULAR MODELING STUDY INVOLVED IN DRUG-DNA INTERACTIONS

Molecular modeling is a broad term that encompasses ab initio quantum mechanical calculations, semi-empirical calculations, and empirical calculations (charge-dependent molecular mechanics force fields). These techniques can be used to study the three-dimensional structure, dynamics, and properties of a molecule of interest. Molecular modeling can identify and define the possible key details of the molecular interaction and, using the graphics/computational approach, decide on optimal structural modifications likely to enhance either general binding affinity or recognition of a particular nucleotide-binding site. A number of studies have revealed the

converse, with the discovery that particular patterns of chemical modification on a given drug (e.g., doxorubicin) can result in both low biological activity and low-ranking interaction energy. The molecular modeling, particularly molecular mechanics and dynamics, are highly complementary to macromolecular NMR and X-ray crystallography. Molecular dynamics simulation can, in principle, provide a complete theoretical description of DNA structure and motions, and are thus a valuable independent means of developing models and interpreting experimental data. A combined approach is desirable and, where the parent experimental structure is available, the simulation can be partially validated by reproducing the structure, thus paving the way for 'rational drug-designing'. For "rational" drug design, choice of a target, the evaluation of a structure of that target, the pivotal questions to consider in choosing a method for drug lead discovery, and evaluation of the drug leads. The following figure (Fig.1.9) briefly shows the flowing of drug design.

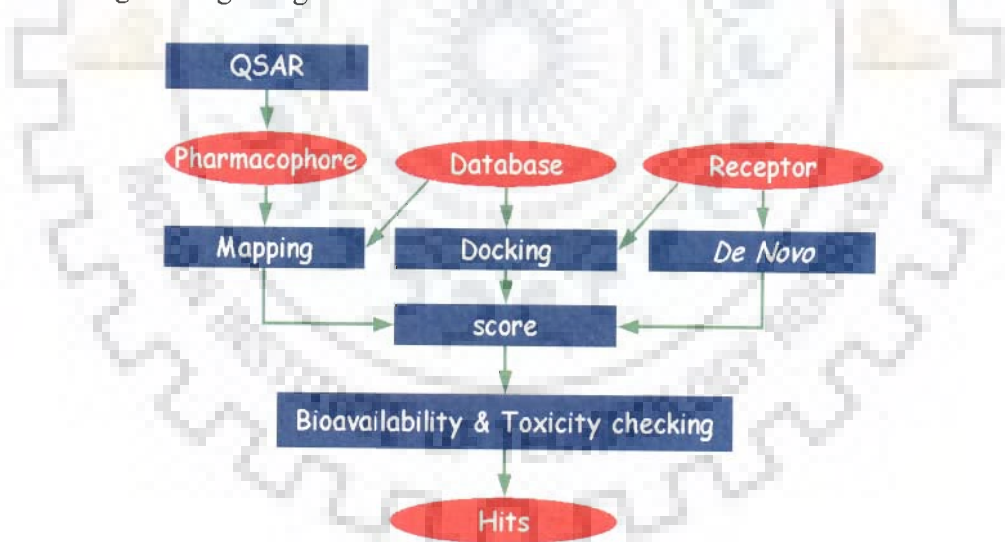


Fig.1.9: Flow chart for Drug-Designing

2.0 LITERATURE REVIEW

The first suggestion of the intercalation of planar aromatic molecules between and parallel to adjacent base pairs was made on the basis of hydrodynamic and X-ray fiber diffraction studies of

DNA in presence of acridine dyes. (Lerman et al, 1961). Anthracycline antibiotics typically possess a tetracyclic aglycon chromophore and an amino sugar. The crystal structure of anthracyclines, among them daunomycin (Anguilli et al, 1971; Coursielle et al, 1979) carminomycin (von dreele et al, 1977), nogalamycin (Arora, 1983) and steffimycin B (Arora, 1985) all show similar features. In these structures, the semi saturated ring A is in half chair conformation with C8 farthest out of plane of the ring. Daunomycin is most effective in the treatment of leukemia (Paciucci et al, 1997) and the closely related adriamycin is more effective in treatment of solid tumors (Di Marco et al, 1974). The intercalation of anthracyclines between base pairs of DNA produces the elongation and distortion of double helix, inducing the inhibition of topoisomerase II (Tewey et al, 1984). The positioning of the amino sugar in the minor groove and its additional substituent groups contributes to the inhibition of topoisomerase I (Pilch et al, 1997). Inactivation of both topoisomerase I and II prevents the replication and transcription of DNA. Calendi et al, 1965 suggested that daunomycin complexes with DNA through two bonds; the one at the chromophore and the other at the amino sugar. Kersten et al, 1974 noted that daunomycin and planar compounds such as the acridines have similar effect on DNA in solution and suggested that the chromophore of daunomycin intercalates between successive base pairs of DNA in the manner postulated by Lerman et al in 1961 for the DNA-proflavin complex. It has been demonstrated that to allow the intercalation, the size of cavity must be such that an intercalating molecule would fit in, that is, the distance between two base pairs along the helix axis within the cavity must be at least 6.8 Å.

2.0.1 UV-Visible, Fluorescence, Circular Dichroism, and other biophysical studies on drug - DNA complexes

High-resolution structural information is necessary, but by no means sufficient, for understanding how drugs bind specifically to DNA. Structural studies provide a static view of the final complex that forms, and inevitably focus attention on to the specific molecular interactions between the drug and the DNA. In order to completely understand the molecular forces that drive and stabilize complex formation, biochemical studies are needed to complement the structural studies.

The relation between the stereochemistry of anthracycline antibiotics and their ability to bind to DNA has been investigated (Zunino et al, 1972) using homologous series of derivatives of daunomycin. The quenching of fluorescence and high stability of DNA by 4-demethoxy daunomycin shows that 4-methoxy group does not interfere with chromophore/base pair stacking. However inverted configuration at position 7 and 9 decreases the binding to DNA. Complexes of calf thymus DNA with daunomycin, nogalamycin and carminomycin were studied by circular dichroism over a range of drug/DNA ratios (Dalglish et al, 1974). The existence of intercalative complex is predicted for daunomycin along with presence of free drug and DNA. Comparing the results with that obtained for 9-aminoacridine, which is believed to intercalate in DNA, it was observed that none of these antibiotics appeared to behave exactly as intercalating molecules. This was attributed to difference in chromophoric group present in antibiotics giving rise to transition dipoles in different directions and due to the difference in position of intercalation. Zunino et al, 1976 carried out spectroscopy, viscometry and thermal denaturation studies to investigate the interaction of daunomycin, adriamycin and its other derivatives with calf thymus DNA. It was observed that binding of daunomycin to DNA involves more than one class of sites. Adriamycin binds to DNA as strongly as daunomycin itself. The amino sugar residue plays an important role in the stabilization of the complex. Interaction specificity of

salmon sperm DNA with various derivatives of daunorubicin was looked into, using ^1H Nuclear Magnetic Resonance (NMR), flow dichorism, DNA template inhibition, rates of dissociation and circular dichroism techniques (Gabbay et al, 1976). Their studies indicated that daunorubicin, adriamycin, rubidazone form more intimate complexes with DNA and rate of dissociation of both daunomycin and adriamycin from DNA is same but greater than rubidazone. Their results were found to be consistent with an intercalative mode of binding of the anthracycline drugs. Their preliminary approach has been centered on the modification of the amino group of the sugar moiety of daunorubicin. The results are consistent with specific H-bonding of the amino group of the sugar moiety with DNA as has been suggested by Pigram et al in 1972.

The interaction of adriamycin with single stranded polydeoxyribonucleotides, double stranded DNA and double stranded ribonucleotide hybrids were investigated by Tsou et al, 1976. This work represented a model study about the period of stability of the complex in the circulatory system before it reaches the target tissue. The most important factor in determining the stability of the complex is the interaction of the complex with DNase I in serum. Adriamycin effectively inhibited DNase II more than DNase I. Change in fluorescence intensity accompanied by large increase in polarization was used as an indicator of intercalation. Poly (dT) and poly (U) have very little effect on fluorescence of adriamycin. Poly (A) and 5'd-GMP slightly quenched the fluorescence of adriamycin. Poly (dG) efficiently quenched the fluorescence of adriamycin suggesting interaction between Poly (dG) and adriamycin. It is the known fact that Poly (dG) forms multi-strands itself through hydrogen bonding of guanine bases and comparative studies of association constant of this complex with other complexes suggested that Poly (dG)-adriamycin complex could be thermodynamically less stable. Double stranded Poly (dA). Poly (dT), Poly (dA-dT), Poly (dA).poly (dT) quench the fluorescence of adriamycin. Double stranded poly (dG-

dC) complex of adriamycin has higher association constants and better adriamycin incorporation than calf thymus DNA. The rate of hydrolysis decreased in order poly(dA-dT) > calf thymus DNA > Poly(dG-dC) > Poly(dA).Poly(dT) > poly(dG).poly(dC) for DNase I and poly(dA).poly(dT) > calf thymus DNA > poly(dG-dC) > poly(dA).poly(dT) > poly(dG).poly(dC) for DNase II. On the other hand, intercalation of adriamycin to homodeoxynucleotide duplex poly (dA). (dT) and poly(dG).poly(dC) enhanced the DNase I hydrolysis. Adriamycin, daunomycin and their reduced forms bound intercalatively and completely relax supercoiled DNA. The results provide a possible rationale for the degradation of DNA, which accompanies anthracycline administration (Lown et al, 1977). Plumbridge et al (1977) investigated the changes in the visible absorption spectrum and the degree of fluorescence polarization of daunomycin and mepacrine on binding to DNA. The results have been compared with those shown by intercalating agent ethidium bromide. Ethidium bromide shows a reduction in extinction coefficient and bathochromic shift on binding to both DNA and poly (I.C) but interacts less avidly with poly (I.C) than with DNA. For daunomycin similar results were obtained with DNA but no isobestic point was observed with poly (I-C). Further the shift of λ_{\max} was less and extinction coefficient of bound daunomycin to poly (I-C) showed much smaller decrease with respect to free drug. When daunomycin binds to DNA, fluorescence was quenched but enhancement of fluorescence was observed with poly (I.C) therefore it was inferred that daunomycin does not intercalate into poly (I.C) and external ionic binding is the probable mode of intercalation. Mepacrine behaves similar to daunomycin and its fluorescence was also quenched on binding to DNA and the fluorescence polarization was increased significantly. Mepacrine is able to intercalate into DNA though it does not intercalate into poly (I.C) and electrostatic binding is the probable mechanism of its intercalation with poly (I.C). It was shown

that the interaction of daunomycin with t-RNA is different from that of daunomycin with viral ds-RNA (Shafer et al, 1977). By fluorescence, quenching, spectral titration and T_m studies, it was revealed that t-RNA interacts with daunomycin in a manner similar to DNA. These results are consistent, but not proof of intercalation of the drug in the double helical segments of t-RNA is found, as proposed for ethidium bromide.

Pachter et al, 1982 has published his results on the binding of anthracycline analogues - adriamycin, carminomycin, pyrromycin, Musettamycin, marcellomycin and aclacinomycin to calf thymus DNA and covalently to closed circular PM-2 DNA. Quenching of the fluorescence of marcellomycin occurs by increasing concentration of native and heat denatured calf thymus DNA. The ratio of heat denatured to native apparent association constant (K_{app}) demonstrated that the binding affinities of all the anthracyclines studied for heat denatured DNA were only 35-62% of the corresponding binding affinities for native DNA. This suggests the dependence on double strandedness of the DNA for binding. The significant increase in affinity for DNA was observed for adriamycin, carminomycin and marcellomycin as the ionic strength of reaction buffer decrease. The apparent number of binding sites per nucleotide (n_{app}) was also higher in low ionic strength buffer and this shows the importance of electrostatic forces in the interaction of these anthracycline with DNA. Viscometric studies indicated that under high ionic strength conditions, which negated electrostatic effects, all of the anthracyclines induced an unwinding-rewinding process of the close superhelical PM-2 DNA typically observed for DNA intercalators. The anthracycline exhibited unwinding angles that were approximately half that of ethidium bromide; that is, compared to an unwinding angle of 26° observed in ethidium bromide, anthracycline indicated unwinding angle of approximately 13° . Adriamycin and carminomycin induce greater extent of uncoiling while pyrromycin, musettamycin and marcellomycin exhibit

lower unwinding angles. With decrease in ionic strength, unwinding angles of adriamycin did not change significantly while that of carminomycin and marcellomycin slightly decreases and increases, respectively relative to ethidium bromide. Since the present study has shown that non intercalative binding contributes to the DNA binding of several anthracycline and ethidium bromide to similar extends, it is more likely that the lower unwinding angle of the anthracycline results from some other mechanism, such as a difference in the drug-DNA intercalation complex. Among other possibilities, the anthracycline may achieve only partial insertion between base pairs upon intercalation into DNA or the mechanism of intercalation of anthracycline may differ fundamentally from that in ethidium bromide. Structural differences in the intercalation complexes have also been proposed to explain the low unwinding angles of quinoline derivatives relative to that of ethidium bromide (Jones et al, 1980). The lack of change in the unwinding angle of pyrromycin with additional 2-deoxyfucose residues on the glycosidic side chain at higher ionic strength demonstrate that the presence of second and third sugars on the anthracycline side chain does not effect the drug ability to distort DNA upon intercalation. Thus, it is likely that these sugars do not sterically hinder the intercalation of anthracycline into DNA duplexes.

Chaires et al, 1982 studied the interaction of daunomycin with DNA by equilibrium dialysis, fluorescence and absorption titration techniques. The binding of daunomycin to DNA results in red shift and hypochromism. Ionic strength has no apparent effect on the extinction coefficient of the free or bound drug. In the presence of DNA, the fluorescence emission of daunomycin was quenched. Daunomycin binds tightly to DNA and shows negative cooperativity. Binding strength of daunomycin (intrinsic binding constant) drops as sodium ion concentration increases with the exclusion parameter, essentially constant at 3.25 ± 0.25 . Daunomycin binding is

exothermic with vant Hoff enthalpy of -12.8 Kcal/mol. The G+C rich DNAs bind more strongly to daunomycin and preferentially alter the bouyant density of G+C rich DNAs in CsCl density gradient. Daunomyin dramatically stabilizes the DNA as it increases T_m by about 30° C. The biphasic thermal denaturation seen at low r (where r is the number of moles of bound daunomycin per mole of DNA) values are similar to those observed by Patel and Caunel, 1978. Daunomycin, a potent anthracycline antibiotic self-associates in aqueous solution at concentrations greater than $10 \mu\text{M}$ (Chaires et al, 1982a). In this study they have carried out visible absorbance, sedimentation equilibrium and NMR experiments that characterize the self-association. Sedimentation studies show that daunomycin aggregates beyond a dimer. NMR data shows that the aromatic protons of daunomycin are most affected by aggregation, probably due to stacking of the anthracycline rings. Knowledge of the applicable model for the self-association process has enabled them to assess quantitatively the possible effects of drug aggregation on the interpretation of drug-DNA binding data. Mainfait et al, 1982 made an attempt to determine the nature of the interaction of the chromophore of adriamycin with nucleic acid by comparing of the resonance raman spectra of the free and bound drug in water solution at neutral pH. The spectral change shows that adriamycin is intercalated between GC sequences and hydrogen bonds are formed at intercalation site. Graves et al, 1983 studied the binding of antitumour agents by phase partition techniques. Both adriamycin and daunomycin exhibit positive cooperativity in their equilibrium binding to DNA as indicated by the positive slopes in the initial region of the binding isotherms under conditions of simulating physiological ionic strengths. Adriamycin exhibits a greater degree of positive cooperativity then daunorubicin. The dependence of the equilibrium-binding constant upon the ionic strength has been well established for a variety of drugs (Chaires et al, 1982). At ionic concentration of 0.01 M and 1M NaCl, both drugs have

been shown to interact with DNA in a non-cooperative manner. In an effort to examine the effects of base composition or sequence on the binding of adriamycin and daunomycin at low r (where r is the number of moles of bound daunomycin per mole of DNA) values, the alternating copolymers poly (dA-dT).poly (dA-dT), poly (dG-dC).poly (dG-dC) and poly (dA-dC).poly (dG-dT) were examined. Adriamycin exhibits a much greater degree of cooperativity with poly (dA-dT).poly (dA-dT) than daunorubicin under identical conditions. Conversely the binding to poly (dG-dC).poly (dG-dC) showed a marked decrease in this cooperative binding effect. The correlation of base sequence with the cooperative binding could be associated with the thermodynamic property of helix as for example stability of poly (dG-dC).poly (dG-dC) as compared with poly (dA-dT).poly (dA-dT) or the relative enthalpy of base pair stacking in the three polynucleotides studied.

Chen et al, 1983 reported the effects of adriamycin on B to Z transition of poly (dGm⁵dC).poly (dGm⁵dC) by using CD and ³¹P NMR data. Addition of adriamycin to poly (dGm⁵dC) in Z form resulted in its conversion to B form in presence as well as in absence of MgCl₂. The transition between Z and B forms was found to be cooperative. Further, it was observed by CD spectroscopy that high concentration of Mg²⁺ was required to induce B to Z transition in the presence of adriamycin. Thus, it was inferred that adriamycin inhibits B to Z transition and binds preferentially to B-DNA. The interaction of daunomycin with calf thymus DNA over a wide range of temperature and NaCl concentration was studied (Chaires et al, 1985a). High NaCl concentration or temperature decreases binding affinity. Daunomycin binding is exothermic. Favourable free energy of binding of drug to DNA arises primarily from the large negative enthalpy. Both enthalpy and entropy of the binding reaction are strongly dependent on the ionic strength but free energy is less dependent due to compensating changes in the enthalpy or

entropy. Hydrogen bonding at the intercalation site is the primary contributor to the observed thermodynamics parameters. The kinetics of the interaction of daunomycin with calf thymus DNA has been studied using (Chaires et al, 1985) stopped flow and temperature jump relaxation methods. A binding constant (K) = $7.0 \times 10^{-5} \text{ M}^{-1}$ and exclusion parameter (n) of 3.6 was obtained. Three relaxation times were observed, all of which were concentration dependent; the two slower relaxation approaches constant value at high reactant concentrations. Relaxation time over a wide range of concentrations was gathered, and data were fitted by a minimal mechanism in which a rapid bimolecular association step is followed by two sequential isomerization step. The six rate constants for this mechanism were extracted by relaxation analysis. The values determined for the six rate constants may be combined to calculate an overall equilibrium constant that is in excellent agreement with that obtained by independent equilibrium measurements. Additional stopped flow experiments, using first sodium dodecyl sulphate to dissociate bound drug and second pseudo first order conditions to study the first bimolecular step, provides independent verification of three of the six rate constants. The temperature dependence of four of the six rate constants was measured, allowing estimates of the activation energy of some of the steps to be made. They speculated that the three steps in the proposed mechanism may correspond to the rapid outside binding of daunomycin to DNA, followed by intercalation of the drug, followed by either conformational adjustment of the drug or DNA binding site or redistribution of bound drug at the preferred sites.

2.0.2 Footprinting studies: Sequence specificity for anthracycline drugs, clinical and Biochemical studies

Foot printing and binding experiments (Chaires et al, 1987) have shown that the preferred daunomycin triplet binding site contains adjacent G.C base pairs flanked by A.T base pairs.

Recent results from a high resolution DNase I foot printing titration procedure identified that the most strongly preferred daunomycin binding site is 5' A/TGC or 5' A/TCG, where notation A/T indicates that either A or T may occupy the position neighbouring the intercalation site. Most preferred site is 5'-ATCG (Chaires et al, 1990). Foot printing (Chaires et al 1987) and theoretical (Pullman et al, 1987) studies indicate that sequence specificity of the daunomycin-DNA interaction cannot be described in terms of the two base pairs comprising the intercalation site. A quantitative explanation can be obtained only by model in which a triplet of base pairs is regarded as the recognition sequence of the drug. The binding of adriamycin to DNA phosphate was investigated by infra-red spectroscopy and quantum chemical calculations (Pohle et al, 1987). The distinct absorption at 1070 cm^{-1} region corresponding to C14-OH of adriamycin was found to split in presence of DNA. The quantum chemical CNDO/2 calculations performed on those structural fragments of DNA and adriamycin involved in interaction, show diminution of both P-O bond distance and O-P-O bond angle of phosphate groups on complexation. These results corroborate the speculation about involvement of C14-OH group of adriamycin in binding to DNA phosphate during its interaction. Skorobogaty et al in 1988 investigated the DNA sequence specificity of daunomycin by DNase I footprinting and an E.Coli RNA polymerase transcription- inhibition assay. The 5'CA sequence was identified as being the highest affinity binding site although other modest affinity (5'GC, CG, CT, TC, AC) and poor affinity sites (5'AA, AT, TA) sites were also observed. The preference of daunomycin for 5'CA nucleotide sequence suggests that its biological activity may arise from association with the 5'CA containing sequences which are thought to be associated with genetic regulatory elements in eukaryotes. Xodo et al, 1988 explored the binding range of $r > 0.05$ (where r is ratio of bound drug to DNA base pairs). The intercalation of drug into the DNA proved to be anti-cooperative,

as indicated by the pronounced upward curvature of all scatchard plots obtained. Extinction coefficient of the bound daunomycin does not markedly depend upon the polynucleotide base composition but level of fluorescence quenching showed marked dependence on base composition of the intercalation site. Presence of a guanine residue at the intercalation site completely quenched fluorescence while AT, AU or IC base pairs at intercalation site cause only a partial fluorescence quenching. Calf thymus DNA quenches the daunomycin fluorescence in a way intermediate between poly (dG-dC):poly (dG-dC) and poly (dA-dT):poly (dA-dT) at low DNA/drug (P/D) ratios, but it tends to promote a nearly total quenching at very high DNA/drug (P/D) ratios. Intercalation of daunomycin with polynucleotides shows anti-cooperativity, which can be entropic or energetic in origin due to the neighbour exclusion effects or due to polyelectrolyte effects or due to the interactions between ligands. Data is fitted by applying the formalism of Friedman and Manning considering both limiting cases: model I FM-I (site size = 1 bp) and model FM-II (site size = 2 bp). As number of binding site (n) is integer in FM-II and not in FM-I, it is suggested that probably FM-II better reflects the physical nature of the system. The anti-cooperativity, which accompanies an intercalation process, is essentially poly-electrolytic in origin. The binding affinity shown by the drug for the different sites decreases in the order $G_m^5C > AT > AC-GT > IC > GC > AU$, indicating a stabilizing effect of the $-CH_3$ group of pyrimidines. Total quenching at high DNA/drug ratio suggests a rather complicated sequence specificity of this drug involving at least base triplets. At low DNA/drug ratios the drug binds to both classes of sites (i.e. with and without the 2-NH₂ purine group), but at a very high DNA/drug ratios, it binds mainly to the sites which quenched the fluorescence totally i.e. G containing sites. The influence of the temperature and the ionic strength on the free energy of drug intercalation into calf thymus DNA, poly (dG-dC):poly (dG-dC) and poly (dA-dC):poly (dG-dT) was

examined and discussed. Infra red spectroscopy shows the formation of hydrogen bond between the intercalated drug molecule and the PO_2^- moiety of DNA via the following terminal hydroxyl groups; C14OH for adriamycin and daunomycin and C4OH for both aclacinomycin A and vidamycin BI and more tentatively the external side chain OH of mitoxantrone (Pohle et al, 1990). By transcriptional footprinting (Cullinane et al, 1990) showed that the physical size of the drug induced blocking moiety comprising of a maximum of two base pairs and the same was observed at all the three GpC elements probed by RNA polymerase from both directions. Fe (III) enhanced the amount of transcriptional blockages by 12-15 folds. Remeta et al, 1991 determined the binding enthalpies of daunomycin with 10 polymeric DNA duplexes. It was found that daunomycin binding enthalpies exhibited small but significant dependence on Drug/Phosphate ratio (r). Binding enthalpies depend on the drug binding densities. Duplex dilution enthalpies in terms of influence of base composition sequence and conformation/hydration was also discussed. Pindur et al, 1993 have discussed structure dependent models of intercalation with DNA as well as with that base paired oligonucleotide for some cytostatic agents of the anthraquinones, compounds of carbazole series, actinomycin D, triostin A, the bleomycins and amasacrine. The results described are based on molecular spectroscopic data in combination with molecular modeling. The combinations of experimental and theoretical methods have actively promoted the rational development of cytostatic agents of the intercalator type in the last few years. Molecular permutations can now be performed with greater reliability and potentially useful compounds can be developed rapidly. Roche et al, 1994 analyzed whether there was multiple binding site of daunomycin to oligonucleotide and the effect of having the A tracts at the end of the molecule. The information so obtained is used to determine whether daunomycin binds preferentially to any particular sequence. CD spectra showed the oligonucleotide conformation is the summation

of the internal concentration which is presumed to be B form and the A tracts. Daunomycin exhibits affinity by two fold for CGATCG core sequence. The exothermic binding enthalpy for daunomycin with CGATCG core is twice as large as that for the TATATA sequence. Binding with dA₂₀.dT₂₀ is endothermic and for oligomers containing flanking A sequence less exothermic component can be detected in the binding curve. Affinity of daunomycin to CGATCG core sequence is slightly larger than that for other sequences. Stopped flow data indicates that the AG sequence does not have a relatively strong site for the drug and is least comparable in kinetic stability to that of CG sequence. Hairpin sequence containing CG shows weak binding possibly due to structural distortion. Relative binding of daunomycin and its analogs (differing in sugar moiety) was tested. Daunomycin has high affinity for each oligonucleotide tested relative to other analogs except for iodo substituent in the L-sugar. In general L-form of sugar elicits a more favourable interaction than the D-form and is naturally occurring isomer. The intercalative binding of drugs daunomycin, ethidium bromide, nogalamycin etc. has been verified by observing changes in the supercoiling of closed circular DNA, as revealed by changes in the sedimentation coefficient (Waring, 1970). Daunomycin causes a definite decrease in the sedimentation coefficient S_{20} of ϕ X174 RF, as expected for intercalative binding. The apparent unwinding angle has been calculated for all intercalating drugs by taking the unwinding angle of ethidium $\approx 12^\circ$ as a reference. Doxorubicin and idarubicin is a very well known topoisomerase II poisons. However, some of their disaccharide analogs have been shown to poison topoisomerase I. (Guano et al, 1999).

2.0.3 NMR Spectroscopic Studies

The Nuclear Magnetic Resonance studies are done on various drug-DNA complexes. Interaction of Iremycin (IM) and Daunomycin (DM) with DNA was studied by electric dichroism (Fritzsche

et al, 1982). The protonation of the sugar dimethylamino group of IM-HCl is expected to affect the NMR lines of the neighbouring nuclei with respect to the lines of the free base. The significant difference of the IM HCl ^1H NMR spectrum to the corresponding spectrum of the IM base dissolved in CDCl_3 is the strong downfield shift of the N-dimethyl signal, which may be attributed to the protonation of the nitrogen of the N-dimethyl group of IM HCl. The apparent increase in length of DNA by drug intercalation increases in the order $\text{DM} < \text{IM} < \text{IM-Cu (II)}$. The tilt (long axis) and twist (short axis) of the iremycin chromophore was $28 \pm 4^\circ$, whereas for daunomycin the long axis is perpendicular to the helix axis and the short axis is twisted by about 25° . Unwinding behaviour of iremycin and daunomycin is similar with respect to orientation of both drugs. It was observed that long axis of daunomycin was almost perpendicular to the helix axis whereas that of iremycin is 30° tipped away from perpendicularity. For the major short-axis transition both daunomycin and iremycin are nearly 25° tipped away from perpendicularity. It was inferred that cyclohexane ring and sugar residue must play an important role in the geometry of orientation. Patel et al, 1978 elucidated structural features of the intercalated complex of daunomycin and nucleic acids by high resolution NMR spectroscopy in aqueous solution. The proton NMR parameters for the nucleic acid and the antibiotic resonances for the daunomycin-poly (dA-dT) complex at various DNA/drug ratios were reported. Patel et al, 1979 studied the duplex to strand transition of the self-complementary sequence dG-dC-dG-dC by monitoring the exchangeable and the nonexchangeable protons and backbone phosphates. The complex formed between the antitumour anthracycline daunomycin and the dG-dC-dG-dC duplex was probed by the nucleic acid and the antibiotic resonances as a function of temperature.

Nuss et al, 1980 proposed a model consistent with the intercalation of daunomycin with different dinucleotides. This model was consistent with (1) the aromatic and methoxy proton resonances

being shifted upfield (2) small but significant upfield chemical shifts of the protons on the A ring and (3) down field shift of some of the daunosamine protons. Proton nuclear magnetic studies of the self complementary hexanucleotide d (TpA)₃ and its interaction with daunomycin was investigated by Philips and Roberts, 1980. Extensive fraying was observed at 5°C but the hexanucleotide duplex was stabilized on interaction with daunomycin at 21°C at a drug/nucleotide ratio of 0.063. Daunomycin was released cooperatively from d(TpA)₃-daunomycin complex on heating. The chemical shift of 5'CH₃ of dausoamine sugar was found to be independent of temperature. These results suggested that planar aromatic portion of drug (rings B and C) intercalates while ring D protrudes outside the helix and on opposite side of the sugar moiety.

Patel et al, 1981 have performed proton and ³¹P NMR investigations on complexes of daunomycin and its analogue 11-deoxydaunomycin with poly (dA-dT) respectively in H₂O. The 6-OH and 11-OH protons of ring B, C of daunomycin shift upfield by ≈ 1.6 ppm on complexation, which is characteristic of intercalation. One of the ³¹P signals presumably the one at intercalation site also shift downfield by ≈ 0.45 ppm on complexation. The 11H proton of 11-deoxydaunomycin was found to undergo large upfield shift of ≈ 1.42 ppm which shows that ring B, C intercalate between base pairs while ring D protrudes out. Neumann et al, 1985 studied interaction of daunomycin with B and Z helices of a self complementary DNA fragment d(CGm⁵CGCG). It was observed that with increase in daunomycin concentration, proportion of both B and Z free duplexes decreases and only duplex-daunomycin complex was detected. No signal corresponding to Z duplex-daunomycin complex was observed. It was shown that daunomycin binds exclusively to the B form of d(CGm⁵CGCG). The interaction of daunomycin with self complementary DNA fragment d(CGATCG) was studied by ³¹P NMR. Two molecules

of drug intercalate between d(CG) at both ends of the helix and evidence for deformation in backbone is given. Binding constants were calculated to be 2 ± 10^4 and $1.4 \pm 1.0 \times 10^4 \text{ M}^{-1}$ while dissociation constant is $1.5 \times 10^{-3} \text{ M}$ (Ragg et al, 1988). Gorenstein and Lai, 1989 studied ^{31}P to monitor phosphate ester backbone conformational changes upon binding of the intercalating drugs ethidium, quinacrine and daunomycin to sonicated poly (A).poly (U), to calf thymus DNA and RNA. A new ^{31}P signal arises from phosphates, which are in perturbed environments due to intercalation of the drug. Similar, though smaller deshielding of the ^{31}P signals was observed in sonicated poly (A).Poly (U)-quinacrine complexes as well as in daunomycin complexes. The effect of added ethidium ion, quinacrine and daunomycin on the ^{31}P spectra of sonicated calf thymus DNA is consistent with earlier study by Wilson and Jones, 1982. In these drug-DNA complexes, the drug produces a gradual downfield shift in the ^{31}P signal without the appearance of a separate downfield peak. These differences are attributed to differences in the rate of chemical exchange of the drug between free and bound duplex states (Wilson and Jones, 1982). Searle et al, 1990 the conformation of dynamics of the deoxyribose rings of (nogalamycin)₂-d(GCATGC)₂ complex have been determined from one-dimensional NMR spectra and from COSY and DQF-COSY. Structure of the 2:1 complex of antitumor drug 3'-(2-methoxy-4-methylphenyl) doxorubicin with d-CGATCG was solved (Odefey et al, 1992). The drug intercalates between CG base pairs. Eight intermolecular NOEs (nuclear Overhauser enhancement) were extracted from the spectra and were used in building a model of the complex. Their results show that insertion of the primary amino group of the daunosamine moiety of anthracycline into a morpholinyl ring increases the potency of the drug dramatically and can interact covalently with DNA to form adducts. Barthwal et al, 1994 investigated interaction of daunomycin with dCpG by two dimensional proton magnetic resonance techniques. The non-exchangeable base protons

of dCpG and the ring protons of the drug chromophore shift upfield upto 0.27 ppm on intercalation. Changes in chemical shift decreases with temperature and are attributed to stacking of drug chromophore between G.C and G.C base pairs. The sugar is predominantly in the S-conformation state for both cytosine and guanine residues in the right-handed helix of the d-CpG complex. The glycosyl angles are about $-120 \pm 20^\circ$ and $-90 \pm 20^\circ$ for C and G residues, respectively. The observed intermolecular NOEs- CH6-2H, 1H; CH6, CH5-4OCH₃; CH1'-2'axH and CH4'-9COCH₃ demonstrate the existence of specific conformation of the complex. Solution structure of d (CGTACG)₂ with 9-Amino anthracycline (SM-5887) with drug to DNA ratio 2:1 was solved by Igarashi et al, 1995. The cytosine residue shows that their chemical shift is affected by ring currents of drug, therefore it was inferred that the drug intercalates between two cytosine residues. Ring D of the anthracycline aglycon is sandwiched between C1 and C5 bases. In comparison to daunomycin and adriamycin, this model of the 2:1 d (CGTACG)₂-SM-5887 complex has its aglycon sliding toward the minor groove. The intercalation geometry of SM-5887 is a hybrid between those of adriamycin and nogalamycin. Mazzini et al, 1996 made an attempt to study the interaction (2S)-2-methoxymorpholino doxorubicin and morpholino doxorubicin with hexanucleotide d(CGATCG)₂ and d(CGTACG)₂ by 2D ¹H NMR and ³¹PNMR coupled with molecular dynamics techniques. The results of above study were compared with doxorubicin and daunorubicin. On intercalation of drug, deformation was noticed in DNA as torsional angle α and ξ changes from value of gauche gauche (as found in B-DNA) to gauche trans values. The change is associated with downfield shift of phosphorus. Different nucleotide sequences do not affect the dissociation rate constants of the drug from the DNA. As a consequence it appears that structural modifications at a level of ring A and amino sugar in the anthracycline molecule are important and the methoxymorpholino moiety plays a significant role

in stabilizing the complex. Many intermolecular NOEs indicates that aglycone moiety of drug is oriented in orthogonal position with respect to terminal base pairs. Ring D protrude out on a major groove and ring A is placed in front of G2 and G12 residues. Their work report that during complex formation, the B_{II} conformational state increases.

Robinson et al, 1997 has designed new class of bis-intercalating drug with lower cytotoxicity, higher activity for resistant cancer cells. Two daunorubicins symmetrically linked together via a p-xylenyl group, either at their N3' (WP631) or N4' sites (WP652). WP631 has high affinity towards DNA than WP652. In WP631-ACGTACGT complex, the aglycon chromophore has its D ring protruding into the major groove and two daunosamines plus the p-xylenyl ether moiety occupying the entire minor groove. WP652 binding is reminiscent that of the other bisintercalating antibiotics triostin A and echinomycin. The two aglycon rings of WP652 bracket two base pairs. Such drastically different binding models for WP631 and WP652 are due to the respective 3' and 4' sites of linkage for the tether. WP631 prefers CGTACG sequence while sequences like CGCG or more generally PyGCPu are required by WP652. Lam et al, 1997 studied the structure of eight self complementary DNA molecules d(CGXX'CG)₂ and d(CAXX''TG)₂ (where X=C, G, T or A and X' is complementary of X). Based on the structural data obtained in solution, a novel sequence dependent local structure function, Σ_{LS} , is composed of the sum of the contributions from the helix twist, Ω , base roll, ρ , base pair slide $\Delta\delta$ and propeller twist, ω is introduced to describe their sequence specific local structure. The results demonstrate that in addition to the inter-strand purine-purine clashes, the base morphology of the nearest neighbour base pair is also important in defining the local geometry of the base pairs. Their results also form the basis for using the trimer-tetramer model for the prediction of sequence specific local structures of deoxyribonucleic acid. Favier et al (2001) used 1D and 2D

homonuclear NMR spectroscopy combined with simulated annealing/rMD to characterize the interaction of 2-(pyrido[1.2-e]-purin-4-yl) with d-(CGATCG)₂. Intercalation occurs at the C1pG2 step. Pyridopurine derivative rings were not exactly perpendicular to the helix. C1 was not involved in the intercalation process and does not stack with its upper base G2. There was a weak, stacking interaction between the intercalated ligand and the DNA bases; however the drug/DNA affinity was enhanced by a hydrogen bond between the hydroxyl group at the end of the intercalator (drug) side chain and amide group of G6. The structure of the intercalated complex enabled insight into the structure activity relationship. The determination of the structural and thermo dynamical characteristics of the intercalative binding of aromatic drugs to defined DNA sequence by NMR spectroscopy is done by Kotovych, et al., 1986. It is well known that unspecific binding of protein to DNA leads to the formation of several types of complexes, each of them owing different contact points with low populations, generating undetectable NOEs. On the contrary, specific interaction only produces one type of complex where NOEs observation is expected. Such situations were observed in NOESY spectra of specific and unspecific complexes between the Lac Repressor headpiece and DNA for example (Lancelot , et al., 2003).

2.0.4 X-ray studies

The X-ray studies done by Pigram et al, 1972 stated that an intercalation model can be built in which the amino sugar of the daunomycin is in the large groove of the DNA and the hydrophobic faces of the base pairs and the drug overlap extensively. The amino sugar is at the side of the groove close to a sugar phosphate chain enabling the ionized amino group to interact strongly with the second DNA phosphate away from the intercalation. A possible additional intercalation would be a hydrogen bond between the first phosphate and the hydroxyl attached to the saturated

ring of the daunomycin chromophore. Molecular structure of daunomycin complexed to d-(CGTACG)₂ has been solved by Wang et al, 1987. In daunomycin the C9 atom is displaced by 0.59 Å in the same direction as the amino sugar relative to the plane of aglycon having O9 perpendicular or axial to the plane of the aglycone molecule. O7 is projected further away from A ring so that O7 and O9 atoms can no longer form an intramolecular hydrogen bond in contrast to those observed in other crystal structures of anthracycline antibiotics (Anguilli et al, 1971; Neidle and Taylor, 1977; von Dreele and Einck, 1977). DNA adopts a distorted right-handed double helical structure with modification in local area where it accommodates the drug molecule. The sugar pucker are mostly C2' endo while glycosyl for all other residues is high anti (-86°) except C1 which has a normal anti glycosyl torsion angle ($\chi = -154^\circ$). In overall conformation, daunomycin molecule intercalate their aglycone chromophore between the CpG sites at both ends of the hexamer duplex with drug amino sugar filling the minor groove of the duplex and ring D protruding into the minor groove. O9 of daunomycin forms hydrogen bond with N3 and N2 of G2 residue. Two bridging water molecules between the drug and DNA stabilize the complex in the minor groove. In the major groove, a hydrated sodium ion is coordinated to N7 of the terminal guanine and with O4 and O5 of daunomycin with a distorted octahedral geometry. The intercalator allows identifying three principal functional components of anthracycline antibiotics: the intercalator (rings B-D), the anchoring functions of ring A and the amino sugar. The structure-function relationships of daunomycin binding to DNA as well as other related anticancer drugs are discussed.

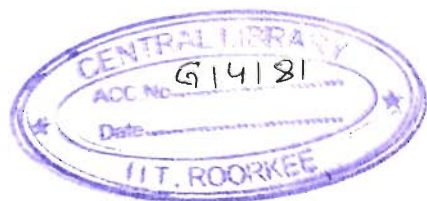
Holbrook et al, 1988 studied the local mobility of nucleic acids. The directions and amplitude of the local motion indicate that changes in the mobility of DNA due to daunomycin binding and is primarily limited to the residues forming the intercalation site. The intercalated daunomycin ring

system (aglycon) is rigidly fixed in the base stacks, apparently serving as an anchor for the amino sugar segment of the drug, which is one of the most mobile regions of the entire complex. This mobility implies that if the central AT base pair is switched to a CG base pair, there should be a low energy cost in avoiding the guanine amino group. The energy difference (for the sugar-binding preference) between $d(CGTACG)_2$ and $d(CGCGCG)_2$ could be considerably less than 20kcal/mol, a value proposed previously from computation. Moore et al, 1989 found out that the overall intercalation geometry in the daunomycin- $d(CGATCG)$ complex is similar to that observed in the same complexes by other workers (Quigley et al, 1980; Wang et al, 1991). The larger differences in backbone torsion angles, especially between those of the intercalation sites $d(C1pG2)$ and $d(C5pG6)$ indicate a somewhat more extreme asymmetric conformation adopted by $d(CGATCG)_2$ than by $d(CGTACG)_2$ on binding to daunomycin. The daunomycin aglycon chromophore is oriented at right angles to the long axis of the DNA base pairs. This head on intercalation is stabilized by hydrogen bonding interactions between the chromophore and its intercalation site base pairs. The cyclohexene ring and amino sugar substituent lie in the minor groove. The amino sugar N3' forms the hydrogen bond with O2 of the next neighbouring thymine. This electrostatic interaction helps to position the sugar in a way that results in extensive van der waal's contacts between the drug and the DNA. There is no interaction between daunosamine and the DNA sugar-phosphate backbone.

Structural comparison of anticancer drugs, adriamycin and daunomycin complexed with DNA sequence $d(CGATCG)_2$ was done by Frederick et al, 1990. In all the three complexes, that is, daunomycin- $d-(CGATCG)_2$, daunomycin- $d-(CGTACG)_2$ and adriamycin- $d-(CGATCG)$, the aglycon moiety intercalates at the GC base pair on either ends of the duplex. The orientation of the aglycon and conformation of ring A are highly conserved throughout the series. It appears

that neither the addition of a hydroxyl group nor the change in DNA sequence adjacent to the intercalation site has an effect on the position of the aglycon. In all three complexes, the one end is anchored by two direct hydrogen and indirect hydrogen bond and the other end is anchored by coordination to a solvent molecule that appears to be a sodium ion. Due to presence of extra hydroxyl group in adriamycin containing complex, there are bridging interactions to phosphate groups of the proximal DNA strand. While in daunomycin containing complexes, there are several water molecules interacting with minor groove edges of the terminal base pair. The amino sugar of it extends into the minor groove. In comparison with daunomycin-d(CGTACG)₂, the amino sugar in daunomycin-d(CGATCG)₂ and adriamycin-d(CGATCG)₂ form more favorable interactions with the DNA. Daunomycin and adriamycin complex with (dCGATCG)₂ has increased stability as N3' of amino sugar forms additional direct hydrogen bond and several van der waal's contact with the edges of base pair within the minor groove. The two hydrogen bonds from N3' to solvent molecules are conserved in all three complexes. In DNA at G2pA3 step and theC5pG6 steps, ξ values have been increased to trans conformation; while ϵ for C1 is reduced and χ adopts low anti conformation which causes base pair separation. The conformation and interactions in the complexes formed by 4'-epiadriamycin with d(CGATCG)₂ are consistent with the previously reported complex. A direct hydrogen bond from 4'OH group of amino sugar to N3 of A3 is formed due to inversion of stereochemistry at the 4' position of 4'-epiadriamycin. This bond is not formed in other complexes. Hydrogen bond is formed between 9-OH with N2 of G2. Solvent molecules form hydrogen bonds with O4, O5, N3 and O4' of drug chromophore and with N7 of G12, O2 of T4. A water mediated hydrogen bond is observed from the O13 of the A ring to the O2 of C1. Anthracycline sugar interacts more intimately with d(CGATCG)₂ than with d(CGTACG)₂ forming direct hydrogen bond to d(CGATCG)₂ but not to

d(CGTACG)₂. Spermine binds to major groove of the complex and its methylene and amino groups form van der waal's contact with both the DNA and drug. In daunomycin–CGATCG–spermine complex, the spermine molecule forms two direct hydrogen bonds and several indirect hydrogen bonds via mediating water molecule to the backbone of the DNA. Spermine molecule aligned roughly perpendicular to the helical axis. In epiadriamycin-CGATCG-spermine ternary complex, terminal amino group of spermine forms two hydrogen bonds with the phosphate oxygen of DNA (Williams et al, 1990). Nunn et al, 1991 studied the complexes of daunomycin with d(TGTACA) and d(TGATCA) referred to as TGT-daun and TGA-daun, respectively. Binding occurs via intercalation of the drug chromophore at d(TpG) step. Hydrogen bonding interactions involve the drug, DNA and solvent molecules. The torsion angles values for the oligonucleotide backbone and glycosyl bond for two complexes are similar to those observed in literature (Frederick et al, 1990; Moore et al, 1989; Wang et al, 1987). The TGT sugar puckering is close to that observed for d(CGTACG)-daunomycin complex (Frederick et al, 1990; Moore et al, 1989; Wang et al, 1987). Major deviations occur at intercalation site with significant buckling at T1.A12 base pair (10° for TGT-daun and 11° for TGA-daun). The G2.C11 at other side is buckled by 20° in opposite direction for both complexes. The position of chromophore is similar in both complexes but the orientation and conformation of sugar is however different. The daunomycin sugar is located in the minor groove of the DNA and is stabilized by hydrogen bond between the amino and functional groups of the sugar. The amino sugar of the d(TGATCA)₂ duplex interacts directly with the DNA sequence, while in the d(TGTACA)₂ duplex, interaction is via solvent molecules. In all the complexes analyzed, the distance from O9 to N3 is shorter than O9 to N2. In the four T/CGT/A-daunomycin complexes, a water molecule is bonded to the O13 of drug. This water further coordinates in all cases to O2 of T1 or C1 with



the exception of TGATCA-daunomycin complex. Sodium or water mediated interaction with ring D is absent only in TGT-daunomycin. For the sequences T/CGA there is direct hydrogen bonding with O2 (T10), O2 (C11), O4' (C11) and water. Their calculation predicts that an AT base pair at the center of the DNA is more stable than a GC base pair in this position. MAR 70, a synthetic derivative of the anticancer drug daunorubicin containing an additional sugar, attached to O4' of daunosamine was crystallized with the DNA hexamer d(CGTⁿACG), where ⁿA is 2-aminoadenine. In both complexes, two MAR 70 molecules are intercalated within the CpG steps. The ring A-D of MAR70 penetrates the DNA with ring D protruding in major groove and disaccharide of it lies in the minor groove of DNA. O9 of drug forms two hydrogen bonds with N2 and N3 of guanine G2. C13 of drug is bridged to O2 of C1 by water molecule; O7 of glycosyl linkage forms weak hydrogen bonds with NH₂ of G2. High buckle (18.4° for TⁿA complex and 17.8° for TA complex) and low unbending angle (-8.4° in TⁿA complex and 17.8° in TA complex) was observed. The cross-linking reaction by HCHO in the MAR 70 TⁿA complexes appear quite effective. Both sugars are in chair conformation and torsion angles C5'-C4'-O4'-C1'F (τ_1) and C4'-O4'-C1'F-C2'F (τ_2) (F is fucose) between two sugars are 268°, 160° for TA complex and 276°, 151° for TⁿA complex, respectively. The combination of τ_1 and τ_2 makes both sugars nearly perpendicular to each other. It was suggested that attaching certain functional groups (e.g. alkylating) at the N3' amino position of daunomycin/doxorubicin molecule is useful as they may be able to alkylate the N3 position of adenine very effectively, thereby increasing the therapeutic index.

The structure of the complex between d(TGATCA) and the anthracycline 4'-epiadrimycin has been determined by Langlois d' Estaintot et al, 1992. The overall structure is similar to that observed in the series of hexamer anthracycline complexes (Frederick et al, 1990; Leonard et al,

1992; Moore et al, 1989; Nunn et al, 1991; Williams et al 1990; Quigley et al, 1980). The crystal structure of morpholino derivative of adriamycin bound to d(CGTACG)₂ was studied by Cirilli et al, 1992. Chromophore ring interacts between CpG base pairs, with ring D in major groove and amino sugar in minor groove. Hydrogen bonds are formed between O9 of drug and N2, N3 of G2 and G8, respectively. Indirect hydrogen bond is formed from O13 of drug through water molecule to O2 of C1 and C7. On major groove side, the other end of aglycon is anchored by coordinating to a solvent molecule. This solvent forms direct hydrogen bonds to O4 and O5 of aglycon and N7 of G2 and G12. The binding site involves four base pairs and the absence of positive charge on the amino sugar appears to influence the hydration pattern on both grooves.

The structures of two hexanucleotide anthracycline complexes d(CGGCCG)/daunomycin and d(TGGCCA)/adriamycin have been determined using single crystal X-ray diffraction techniques (Leonard et al, 1993). In both cases the anthracycline molecule is bound to non-preferred d(YCG) base-pair triplet sites, daunomycin type anthracyclines lack affinity for d(YGG) and d(YGC) sites.

WP631, a bisintercalator, intercalates between CG base pair at both ends of d-(CGATCG)₂. DNA conformation is most conserved at the intercalation site and most disparate in the center of the complexes. The central AT base pair show significant positive buckle which is in contrast to the daunomycin-d-(CGATCG)₂ complex (Hu et al, 1997). Hydrogen bonds from 9-OH of daunomycin to N2 and N3 of G2 are conserved in WP631 complex. Minor groove binding of amino sugar is observed. In the daunomycin complex, the 3' amino nitrogen forms three hydrogen bonds with the DNA, but these hydrogen bonds are lost in the WP631 complex. In WP631 complex, there is absence of stabilization of van der waal's interactions between the amino sugar/linker and the minor groove of the DNA. The unfavorable oxygen-oxygen

interaction and deficiency of stabilizing interactions of the linker/amino sugar with DNA are evidenced of the linker getting strained. The DNA binding of WP631 is ultra tight. The study by Saminadin et al, 2000 was conducted on N-cyanomethyl-N-(2-methoxyethyl)-daunomycin (CMDA), a synthetic analogue of cyanomorpholino-daunomycin complexed with d-(CGATCG)₂. Crystal structure shows that the chromophore is intercalated at each extremity of the duplex. The amino sugar moiety is in the minor groove while the chromophore ring D protrudes in the major groove. The long axis of the chromophore is roughly perpendicular to the flanking base pairs. Numerous van der waal's interactions between the methoxy ethyl chain, A9 and T10 are observed. The observed densities indicate the formation of N-hydroxymethyl-N-(2-methoxyethyl)-daunomycin (HMDA) with the release of cyano moiety without DNA alkylation. The formation of this degradation compound is discussed in relation with other drugs modifications when they bind to DNA. The comparison of the two different drug-DNA crystal structures show a correlation between a slight change in DNA conformation and nature of the amino sugar substituent at the N3' position located in the minor groove. The binding of macrocyclic bisacridine and ametantrone to CGATCG was studied (Yang et al, 2000). Only one acridine of the bisacridine drugs binds at C5pG6 step of DNA, while the other acridine plus both linkers are completely disordered. Surprisingly both terminal G.C base pairs are unreveted. The C1 nucleotide is disordered and the G2 base is bridged to its own phosphate through a hydrate Co⁺ ion, G2 swing towards the minor groove with its base stacked over the backbone. The C7 nucleotide is flipped away from the duplex part and base pair to a two-fold symmetry related to G6. An unusual intercalation platform is formed by bridging four complexes together such that the intercalator cavity is flanked by two sets of G.C base pairs (i.e., C5G8 and G6C7) on each side, joined together by G6.G8 tertiary base pair interaction. NMR titration of the bisacridine to

AACGATCGTT suggests that the bisacridine prefers to bridge more than one DNA duplex by intercalating each acridine to different duplexes. The results are relevant in knowing binding of certain intercalators to DNA structure associated with the quadruplet helix and holiday junction.

2.0.5 Theoretical studies

Miller's technique AGNAS was used to determine possible intercalation site geometries in B-DNA (Miller et al, 1982). Nuss et al, 1979 carried out empirical potential function calculations on a base paired dinucleotide GpC and CpG and its complex with proflavin, ethidium bromide and 9-aminoacridine and their calculations were able to reproduce and rationalize the pyrimidine-3'-5'-purine specificity of these intercalators. Islam et al, 1985 deduced that the best intercalator was 1, 5 disubstituted compound while 1, 6 disubstituted was the weakest. The antiproliferative effects were in agreement with the ranking 1, 5 > 1, 4 > 1, 8 > 1-6. The flexibility of daunomycin about the chromophore-sugar linkages, defined by $\phi_1 = \text{C8-C7-O7-C1}'$ and $\phi_2 = \text{C7-O7-C1}'\text{-O5}'$ have been explored using semi empirical energy calculations (Neidle and Taylor, 1979). The minimum energy conformation is close to the N-bromo acetyl derivative, which does not have intermolecular O7...O9 hydrogen bond. The conformational analysis of both the neutral (NH_2) and charged (NH_3^+) forms of doxorubicin has been carried out by metric energy minimization method (Nakata and Hopfinger, 1980). Three energy minima were observed for the neutral molecule and the conformer having $\phi_1 = 250^\circ$, $\phi_2 = 260^\circ$ was the most stable one than the other two conformers. It was observed that the stable conformation for both doxorubicin and daunomycin were different from their crystal structure. The intercalation of doxorubicin with dinucleotide dimer sequences d-CpG and d-TpC has been modeled using molecular mechanics calculations (Nakata and Hopfinger, 1980a). Minor groove intercalation was preferred. The conformation was characterized by the anthraquinone ring aligned nearly

perpendicular to the long axis of CpG base pairs having alternate C3'-endo 3'-5' C2'-endo sugar ring puckering. The energy preference for the minor groove intercalation decreased for the ionized form of doxorubicin. The conformational preference was not found for intercalation with TpC/ApG dimer. Miller and Newlin, 1982 results were used to form three and four fused ring systems that can bind in an optimum manner to form ideal intercalators. Chen et al, 1985 performed theoretical computations on the energy and the structural factors involved in sequence selective binding of daunomycin to six self-complementary hexanucleotides including d (CGTACG)₂ sequence. The analysis of interaction of individual constituents of daunomycin, namely daunosamine side chain, its two 9-hydroxyl substituents and 9-acetoxy substituent and the chromophore ring revealed that the overall sequence preference found was a result of intricate interplay of intrinsic sequence preferences. Theoretical computations were performed on the structural and energy factors involved in sequence binding of adriamycin to five self-complementary hexanucleotides (Chen et al, 1986).

The model adopted for computation was similar to the one used in a previous study on daunomycin (Chen et al, 1985). The analysis here revealed overall preference of adriamycin for mixed oligomeric sequence d (CGTACG)₂. The 14-OH of adriamycin participated in additional hydrogen bonding with O1' oxygen of deoxyribose linked to base on 3' strand. There was an overall parallelism in the sequence selectivity of adriamycin with that of daunomycin. Cieplak et al, 1990 has performed free energy perturbation studies showed the preferences of acridine and daunomycin to bind to a specific base sequence in the DNA. It was observed that daunomycin prefers GC as second base pair and TA as third base pair, which was consistent with studies done earlier (Chen et al, 1985; Wang et al, 1987). Structural properties and intercalator-DNA interactions were investigated in daunomycin bound to 14-mer DNA duplex using molecular

modeling technique (Treib et al, 2004). They had revealed that at each site of intercalation, the phosphorus in Ist strand was in the B_I state and the phosphorus directly lying on the opposite strand was in B_{II} state which were not subjected to fluctuations but stable during the course of simulations. Thus daunomycin induces and stabilizes a distinct pattern of the phosphates of the DNA backbone. It was suggested that daunomycin intercalation increases the population of B_{II} conformation of DNA. Amino sugar is flexible at the glycosidic bond angle which allows the sugar to switch in different conformations and is very important for anchoring the intercalator in the minor groove. Ammonium group of the drug imparts sequence specificity. For the glycosidic angle of amino sugar, 3 conformations were found, out of these two conformations i.e. 155° to 162° and 135° to 138° was also represented by X-ray. The third conformation shows a dihedral angle value of 57° to 61°. It was inferred that rise alone is not sufficient to accommodate daunomycin and an additional buckle of the concerned base pair is also necessary coupled by high unwinding of DNA at intercalation step. It is also seen that intercalation causes widening of major groove. The deformations occur on DNA backbone upon binding of drug is shown by Monte Carlo simulations (Rohs et al, 2005). Intercalation requires a major deformation owing to the formation of a binding cavity, in contrast to minor-groove binding that does not require major conformational changes of the DNA. They have shown DNA sequence specificity of the drug through ab initio drug docking to DNA through Monte Carlo simulations. They have proved the mode of binding is also DNA sequence dependant. Besides this, it was seen that the anthracycline drugs show self-association. The self-association affinity was more for the adriamycin than for the daunomycin as shown by Evstigneev, et al, 2006a and 2006b. There was existence of two antibiotic daunomycin structures in solution. The mutual orientation of the chromophores was parallel in one structure and anti-parallel in the other.

2.1 SCOPE OF THESIS

Interactions of small molecules with DNA have been studied extensively in the hope of learning design principles for the targeting of specific DNA sequences in order to control gene expression. Many small molecules that bind to DNA are clinically proven as therapeutic agents although their exact mode of action remains incompletely defined. There is a renewed focus on the use of small molecules as therapeutic agents in the biotechnology industry. Several physico-chemical techniques like absorbance, fluorescence, circular dichroism, etc., were used for the drug-DNA interaction studies, binding specificity and kinetics of daunomycin and adriamycin on interaction with calf-thymus DNA and certain polydeoxyribonucleotide sequences till year 1980. The 5'-3'd-CpG /d-TpG sequence is the preferred sequence for daunomycin, adriamycin and 4'-epiadriamycin. X-ray, NMR and theoretical computation studies were also performed on daunomycin, adriamycin and 4'-epiadriamycin.

Therefore, these studies are aimed in particular at the development of new anticancer drugs whose anti-tumor efficacy is associated with their interactions with DNA, i.e. for which DNA is the main target inside tumor cells. Understanding structure-function directed macromolecule-target interactions of anticancer drugs, and further rational design of improved anticancer agents are the long-term research goals of our laboratory. The facilities of this laboratory make it possible to understand drug-DNA interactions, which are needed for design and synthesis of new cytostatics and suggestions for structure-pharmacological activity. This thesis deals with (i) the typical procedure for obtaining the structure of the anthracycline drugs and their self-aggregation property using Nuclear Magnetic Resonance (NMR), Restrained Molecular Dynamics approach along with the quantum mechanical calculations (ii) structure elucidation of the anticancer drug complexed with hexanucleotide (iii) to investigate the relationship between the structure and

biological activity of the drug (iv) suggesting the functional groups of drug which may be modified to get the drug with better anticancer activity and less side effects. The Ph.D thesis work has been reported in the form of eight chapters. Chapter 1 contains introduction of the subject as well as highlights the work carried out in literature. Chapter 2 deals with the materials and methods used. Chapters 3 deal with NMR, restrained Molecular Dynamics and quantum mechanical calculations studies of the 4'-Epiadriamycin and its comparison with Adriamycin and Daunomycin. Chapter 4 deals with the studies on self-aggregation of anthracycline drugs by restrained Molecular Dynamics approach using Nuclear Magnetic Resonance Spectroscopy supported by Absorption, Fluorescence, Diffusion Ordered Spectroscopy and Mass Spectrometry. In chapter 5 and Chapter 6, we have discussed the results of ^{31}P and ^1H NMR studies of Adriamycin- d-(TGATCA)₂ complex respectively. Chapter 7 and 8 deals with ^{31}P and ^1H NMR of 4'-Epiadriamycin complexed with d-(CGATCG)₂ and elucidating the torsional angles and inter-proton distances obtained from proton NMR experiments and exchange of bound and free drug by ^{31}P NMR experiments, along with the Restrained Molecular Dynamics of it. The helical parameters and backbone torsional angles etc. have been analyzed using CURVES software version 5.1. Sequence dependent variations have been observed. Besides this, fluorescence life-time measurement studies and Diffusion Ordered Spectroscopy (DOSY) studies are also done to see the formation of the complex. All these studies can be used as a strategy of regulation of the medico-biological activity of aromatic drugs in clinical practice, e.g., in reduction of the consequences of drugs' overdosing during chemotherapy or in production of anti-mutagenic effects in vivo.

Materials and Methods

2.1 MATERIALS

The deoxyribonucleic sequence d-(CGATCG)₂ and d-(TGATCA)₂ was purchased from Microsynth, Switzerland. Deuterium Oxide (D₂O), with isotopic purity 99.96%, daunomycin and adriamycin were purchased from Sigma Chemical Co., USA and 4'-Epiadriamycin was purchased from Calbiochem, USA. Sodium 2, 2-dimethyl-2-silapentane-5-sulphonate (DSS), an internal NMR reference was purchased from Merck Sharp Dohme Ltd. All other chemicals like Na₂HPO₄ and NaH₂PO₄, etc. used for phosphate buffer preparation were purchased from Sigma Chemical Co., USA. All HPLC grade reagents like water, triethyl amine, acetonitrile, glacial acetic acid, etc. were from Qualigens, Ltd. Drug samples were used without further purification but nucleotide sample was purified using benzoylated dialysis tubing from Sigma-Aldrich Co.

Further, d-(CGATCG)₂ and d-(TGATCA)₂ samples were also synthesized for routine 1D NMR experiments and absorption studies. Synthesis was carried out on 0.2 μM, 1 μM and 10 μM scale on Applied Biosystems DNA Synthesizer (model 392 A) using cyanoethyl phosphoramidite chemistry. The starting material was a solid support derivatized with a nucleoside, which will become the 3'-hydroxyl end of the oligonucleotide. The 5'-hydroxyl end was blocked with a dimethoxytrityl (DMT) group. The steps of the DNA synthesis cycle are as follows:

(i) Detritylation: DMT is the blocking group on 5'-OH. The treatment of derivatized solid support with acid removes the DMT group and thus frees the 5'-hydroxyl for the next base to be added during coupling reaction (Fig. 2.1a).

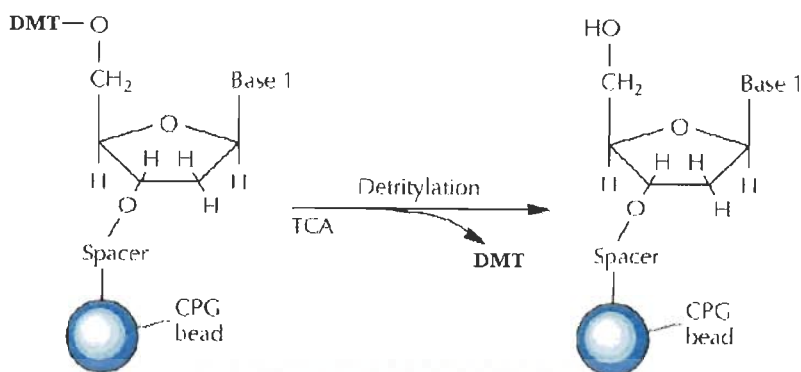


Fig. 2.1(a): Detritylation Step of the DNA Synthesis cycle

(ii) Activation and Coupling: Synthesizer introduces next phosphoramidite and activating reagent. An activated intermediate is created simultaneously adding the monomer and tetrazole, a weak acid, to the reaction column. The intermediate is so reactive that addition is complete within 30 seconds. The blocking group on 3'PO₄ is lost and linking is done to 5'OH of previous phosphoramidite (Fig. 2.1b).

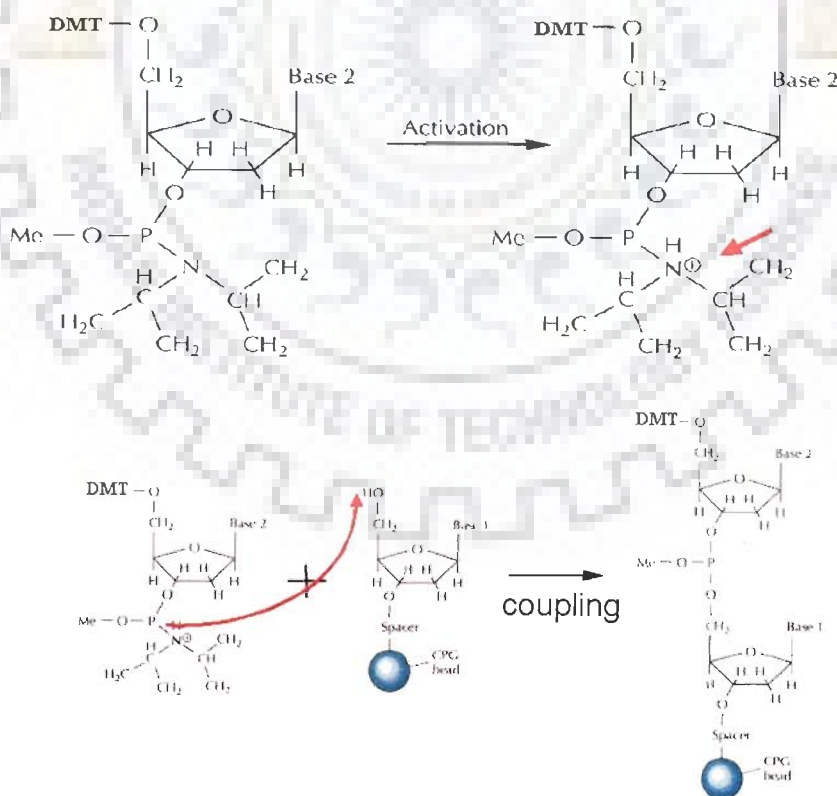


Fig. 2.1(b): Activation and Coupling Step of the DNA Synthesis cycle

(iii) Capping: It is required to prevent uncoupled nucleotides from linking in next addition cycle. Capping is done with acetic anhydride and 1-methylimidazole. Capping minimizes the length of the impurities otherwise oligonucleotide sequence will be altered and thus facilitates their separation from the final product (Fig. 2.1c).

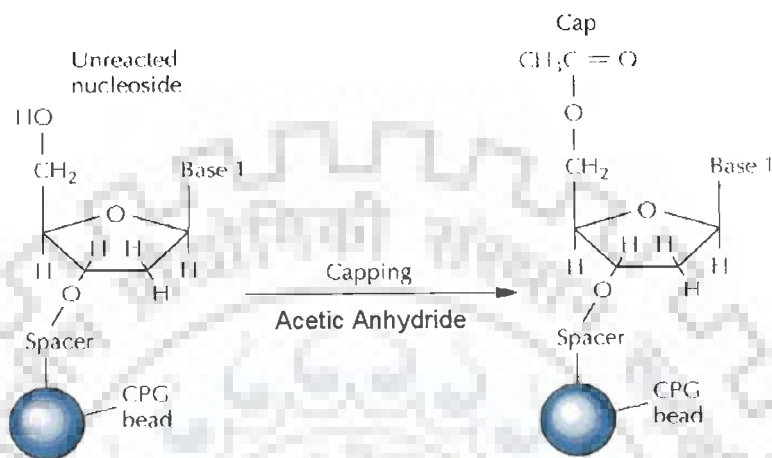


Fig. 2.1(c): Capping Step of the DNA Synthesis cycle

(iv) Oxidation: During the last step of oxidation, the internucleotide linkage is converted from the phosphate, reactive grouping coupling reaction, to the more stable phosphotriester. Hence oxidizes P from +3 to +5 valence. Iodine is used as an oxidizing agent and water as oxygen donor. The reaction gets completed in less than 30 seconds (Fig. 2.1d).

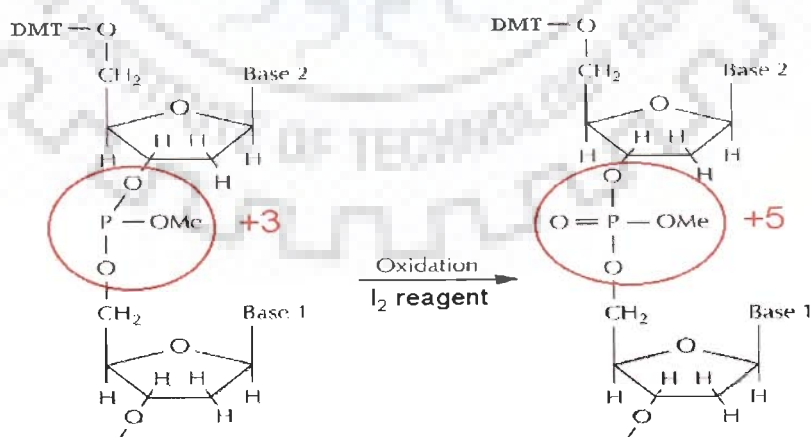


Fig. 2.1(d): Oxidation Step of the DNA Synthesis cycle

After oxidation, the DMT group was removed with trichloroacetic acid. The cycle was repeated until chain elongation was complete (Fig. 2.1e). Treatment with concentrated ammonium hydroxide for 1 hour removes β -cyanoethyl protecting groups and also cleaves the oligonucleotide from the support. At 5' end, PO_4 group is replaced by $-\text{OH}$ group. The benzoyl and isobutyryl base protecting groups were removed by giving ammonia treatment, i.e., heating at room temperature in ammonia for 8-15 hours.

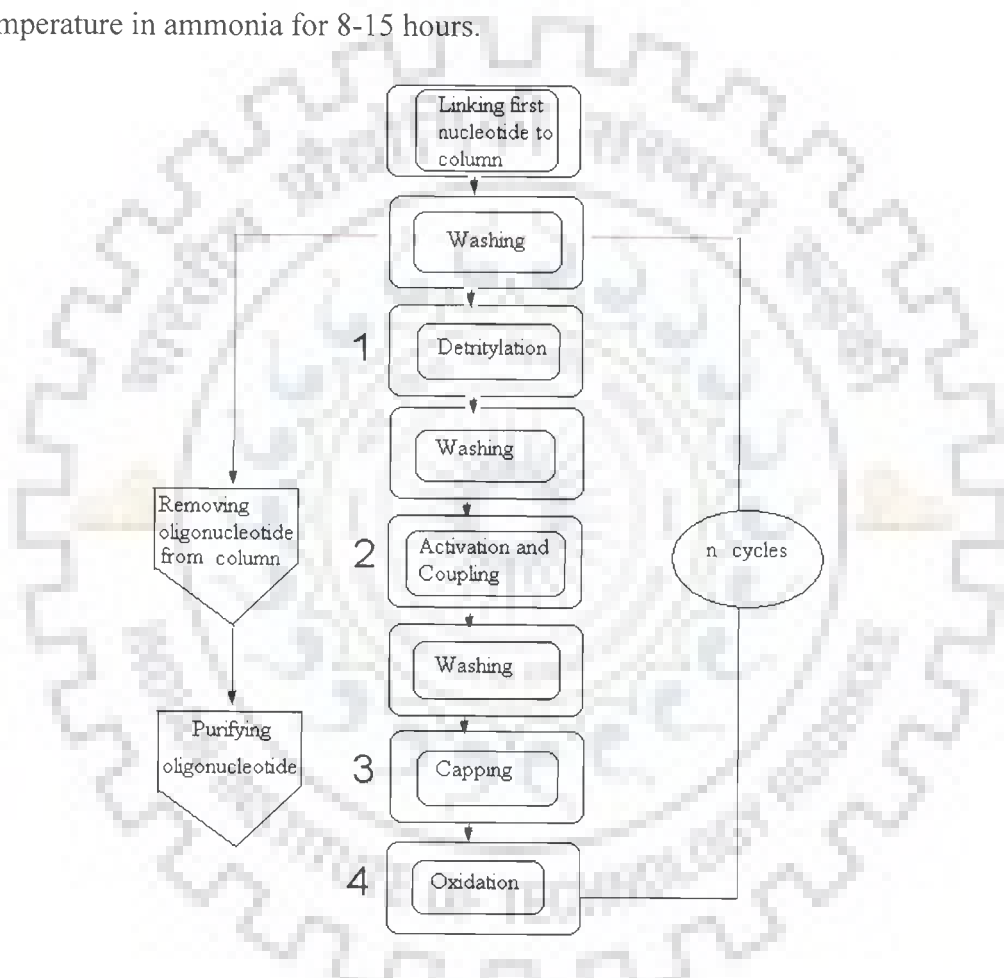


Fig. 2.1(e): Flow Chart for Chemical Synthesis of DNA

2.1.1 Purification by dialysis

The sample was further purified by dialysis using benzoylated dialysis tubing. The tube of 6 cm length was cut and activated by boiling it in large volume of 2% (w/v) sodium bicarbonate and 1 mM EDTA (pH = 8.0) for 10 minutes followed through rinsing in distilled water. Dialysis

membrane was then again boiled for 10 minutes in 1 mM EDTA (pH = 8.0). The sample was then put into the tubing, sealed with holders and dialysed against 4 M NaCl for 12 hours followed by dialysis against distilled water for 12 hours twice. Sample was then taken out lyophilized and dissolved in phosphate buffer. The purified oligonucleotide was annealed by heating it in a computer aided Cary 100 Bio Spectrophotometer equipped with a thermoelectric control unit (peltier unit) upto 80°C at the rate of 1°C per minute with hold time of 10 minutes and then slowly cooled it to the room temperature to get oligonucleotide in duplex state (Fig. 2.1f).

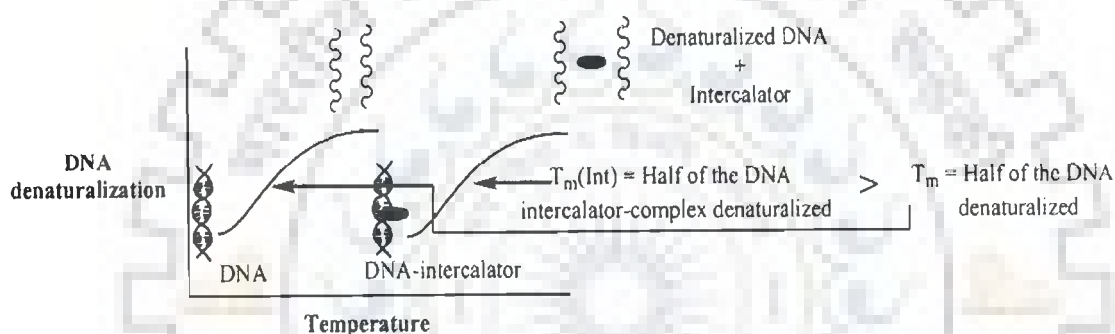


Fig. 2.1(f): Denaturation and Renaturation of DNA and drug-DNA complex showing the extra stabilization in the melting temperature on the complex formation

2.2 SAMPLE PREPARATION FOR NMR

Solution of Adriamycin (20.49 mM) was prepared by dissolving a known quantity of sample in 20mM Phosphate buffer having 70mM NaCl concentration. The final concentration was checked by absorbance measurements at wavelength of 480 nm using Cary 100 Bio Spectrophotometer. The extinction coefficient (ϵ) value used for adriamycin was $\epsilon = 11500 \text{ M}^{-1} \text{ cm}^{-1}$. Similarly the solution of 4'-Epiadriamycin (88.33 mM) was also prepared. Solution of deoxyoligonucleotide, d-(TGATCA)₂ (3.42 mM duplex concentration) and d-(CGATCG)₂ (4.62 mM duplex concentration) were prepared by dissolving a known quantity of sample in 90% water and 10%

D₂O phosphate buffer (20 mM) of pH = 7.0 having 70 mM Na salt and their concentrations were determined by absorbance measurements at 260 nm using the extinction coefficient (ϵ) value, 61400 M⁻¹cm⁻¹ for d-(TGATCA)₂ and 57200 M⁻¹cm⁻¹ for d-(CGATCG)₂. Ethylene diamine tetra acetic acid (EDTA), 0.1 mM, was added to suppress paramagnetic impurity, which may cause line broadening during NMR measurements. Typically 1 μ l of 0.1 M solution of DSS was added to the complex of d-(TGATCA)₂ and adriamycin as an internal reference as well as to the d-(CGATCG)₂ and 4'-Epiadriamycin complex.

2.2.1 Preparation of complex

(i) d-(TGATCA)₂ and adriamycin complex: A complex of d-(TGATCA)₂ and adriamycin was prepared by titration. 180 μ l of 20.49 mM adriamycin was added in steps of 10 μ l to 0.6 ml of 3.42 mM d-(TGATCA)₂ sample during titration in order to make 2:1 complex of adriamycin: d-(TGATCA)₂. The concentration of d-(TGATCA)₂ (N₁) in total volume of 0.61 ml is determined as follows:

$$N_1V_1 = N_2V_2$$

$$N_1 \times 0.61 = 3.42 \times 0.6$$

$$N_1 = 3.36 \text{ mM}$$

The concentration of adriamycin in this solution is determined as follows:

$$N_3V_3 = N_4V_4$$

$$N_3 \times 0.61 = 20.49 \text{ mM} \times 0.01$$

$$N_3 = 0.34 \text{ mM}$$

Like wise other adriamycin-d (TGATCA)₂ complexes of different drug/ nucleotide (D/N) ratios were prepared. The concentration of adriamycin (D), d-(TGATCA)₂ (N) and drug/ nucleotide (D/N) ratio are shown in Table 2.1A.

Table 2.1A: Various concentration ratios (D/N) for the complex formed between Adriamycin and d-(TGATCA)₂

Nucleotide Concentration (mM) = N	Drug Concentration (mM) = D	D/N
3.42	0.00	-
3.36	0.34	0.1
3.31	0.66	0.2
3.25	0.98	0.3
3.20	1.28	0.4
3.15	1.58	0.5
3.11	1.86	0.6
3.06	2.14	0.7
2.97	2.67	0.9
2.93	2.93	1.0
2.89	3.17	1.1
2.85	3.42	1.2
2.81	3.65	1.3
2.77	3.88	1.4
2.73	4.10	1.5
2.70	4.31	1.6
2.63	4.73	1.8
2.56	5.12	2.0

(iii) d-(CGATCG)₂ and 4'-Epiadriamycin complex: 4.62 mM d-(CGATCG)₂ and 88.33 mM 4'-Epiadriamycin samples were taken as a stock solution for preparation of complex. A complex of d-(CGATCG)₂ and 4'-Epiadriamycin was prepared by titration. 65 μ l of 88.33 mM 4'-Epiadriamycin was added in steps of 5 μ l to 0.6 ml of 4.62 mM d-(CGATCG)₂ sample during titration in order to make 2:1 complex of 4'-Epiadriamycin: d-(CGATCG)₂. The calculations for this complex are same as done above. Like wise other 4'-Epiadriamycin-d (CGATCG)₂ complexes of different drug/ nucleotide (D/N) ratios were prepared. The concentration of 4'-Epiadriamycin (D), d-(CGATCG)₂ (N) and drug/ nucleotide (D/N) ratio are shown in Table 2.1B.

Table 2.1B: Various concentration ratios (D/N) for the complex formed between 4'-Epiadriamycin and d-(CGATCG)₂

Nucleotide Concentration (mM) = N	Drug Concentration (mM) = D	D/N
4.62	0.00	-
4.58	0.73	0.16
4.54	1.45	0.32
4.51	2.16	0.48
4.47	2.85	0.64
4.44	3.53	0.80
4.40	4.21	0.96
4.37	4.87	1.11
4.33	5.52	1.27
4.30	6.16	1.43
4.26	6.80	1.60
4.23	7.42	1.75
4.20	8.03	1.91
4.17	8.63	2.03

2.3 METHODOLOGY

2.3.1 NMR Spectroscopy- Technique for biological structure determination

NMR is a powerful spectroscopic technique that provides information about the structural and chemical properties of molecules and probes the biological systems and processes. Modern NMR Spectroscopy includes: High resolution mode on homogenous solutions; high power mode on highly relaxing nuclei which exhibit very broad lines, or polymers etc.; the study of solids using Magic angle spinning techniques; NMR 3D imaging to resolutions of ~ 1 mm.

The types of information accessible *via* high resolution NMR include: Functional group analysis (chemical shifts); Bonding connectivity and orientation (J coupling); through space connectivity (Overhauser effect); Molecular Conformations, DNA, peptide and enzyme sequence and structure; Chemical dynamics (Line shapes, relaxation phenomena). As ¹H, ¹³C, ¹⁵N and ³¹P are all present in nucleic acids; their signals report on structure, dynamics and the effect of ligand binding. Thus it has proved to be a valuable tool in the determination of structure and dynamics

of biological macromolecules in aqueous solution, under conditions similar to those in real systems.

2.3.1.1 The phenomenon

A spinning charge generates a magnetic field. The resulting spin-magnet has a magnetic moment (μ) proportional to the spin. In the presence of an external magnetic field (B_0), two spin states exist, $+1/2$ and $-1/2$. The magnetic moment of the lower energy $+1/2$ state is aligned with the external field, but that of the higher energy $-1/2$ spin state is opposed to the external field (Fig. 2.3a). Note that the arrow representing the external field points north. The difference in energy between the two spin states is dependent on the external magnetic field strength, and is always very small. The following diagram illustrates that the two spin states have the same energy when the external field is zero, but diverge as the field increases.

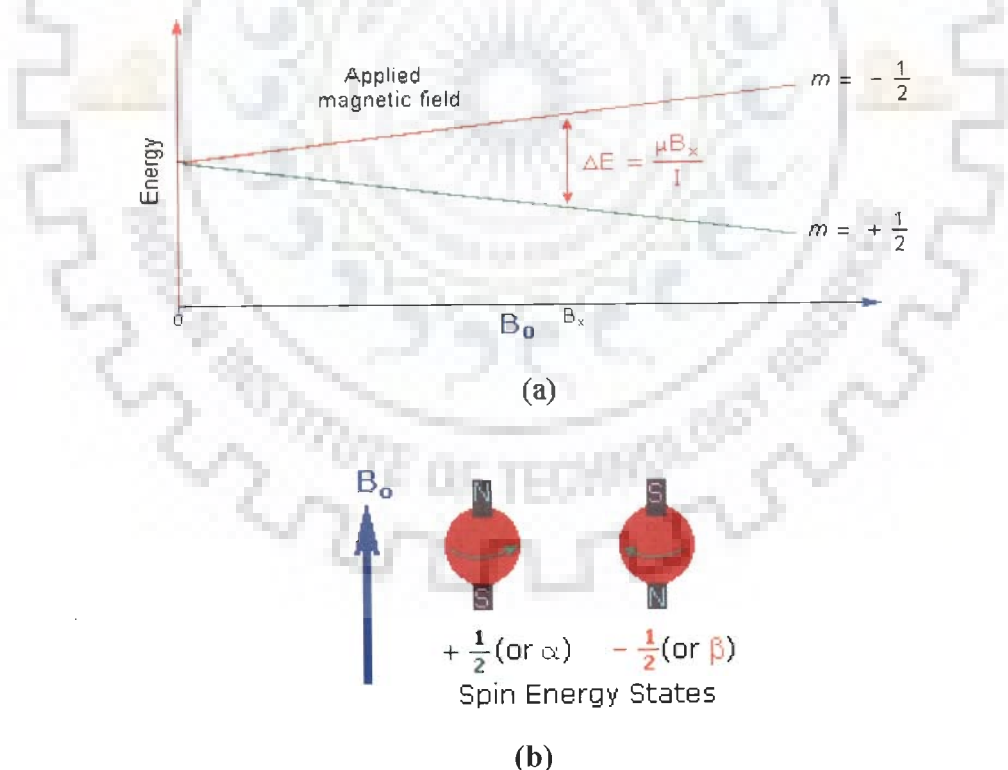


Fig. 2.3: (a) Energy levels for a nucleus with spin quantum number $\frac{1}{2}$ (b) Spin Energy States of the nuclei in the presence of magnetic field.

At a field equal to B_0 , a formula for the energy difference is given ($I = 1/2$ and μ is the magnetic moment of the nucleus in the field).

$$\Delta E = h \gamma B_0$$

Even with these high fields, the energy difference between the two spin states is less than 0.1 cal/mole. For NMR purposes, this small energy difference (ΔE) is usually given as a frequency in units of MHz (10^6 Hz), ranging from 20 to 900 MHz, depending on the magnetic field strength and the specific nucleus being studied. Irradiation of a sample with radio frequency (rf) energy corresponding exactly to the spin state separation of a specific set of nuclei will cause excitation of those nuclei in the $+1/2$ state to the higher $-1/2$ spin state (Fig. 2.3b). These spins are capable of interacting with a beam of electromagnetic radiations. These energy levels correspond to the spins aligned along and against the applied magnetic field, B_0 . The spin oriented to oppose B_0 has higher energy. These spin do not align perfectly along B_0 and this give rise to a permanent torque. The nucleus also has the property of angular momentum because of its spin and thus as a result the nuclei precesses (Fig. 2.3c), with frequency of precession given by:

$$\omega_0 = \gamma B_0$$

Where, γ is proportionality constant, ω_0 is the resonant or Larmor frequency in radians/second and B_0 is the magnitude of the applied magnetic field. When the frequency of the beam is same as that of precessing spin then absorption of energy takes place, which causes the nuclei to flip from a lower energy state to a higher energy state by a process termed resonance (Fig 2.3d). In an NMR sample there are many molecules, each with its spin precessing about B_0 at same frequency and result in a net magnetization of M_z oriented along the Z-axis. On application of a rotational radio frequency field with frequency at or near $\omega_0 = \gamma B_0$, the spin resonate giving rise to net M_{xy} component which is phase coherent. NMR spectroscopy is therefore the energetically

mildest probe used to examine the structure of molecules. For spin 1/2 nuclei the energy difference between the two spin states at a given magnetic field strength will be proportional to their magnetic moments. For the three common nuclei noted above the magnetic moments are:

$${}^1\text{H } \mu = 2.7927, {}^{31}\text{P } \mu = 1.1305 \text{ \& } {}^{13}\text{C } \mu = 0.7022.$$

The following are the spectral parameters in NMR:

2.3.1.2 Chemical Shift

The bonding electrons always produce a shielding effect. The magnetic field at the nucleus is not equal to the applied magnetic field, B_0 ; electrons around the nucleus shield it from the applied field. The difference between the applied magnetic field and the field at the nucleus is termed the

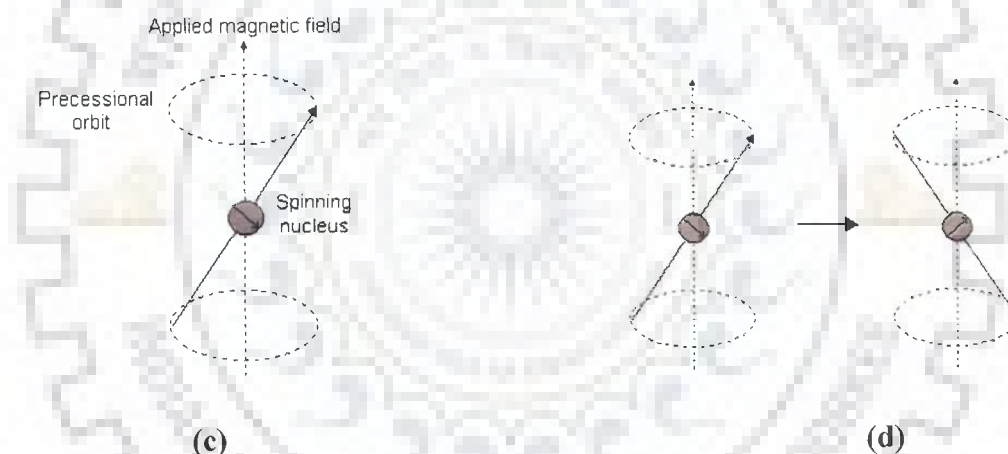


Fig. 2.3: (c) Precessional motion by the nucleus spinning on its axis in presence of the external magnetic field (d) Flipping of the magnetic moment on absorption of the radiations

nuclear shielding. The induced field is directly proportional to B_0 . This is represented by the equation:

$$B_{\text{eff}} = B_0 (1 - \sigma)$$

where, σ is the shielding constant which depends on the nature of electrons around the nucleus.

Chemical shift is a function of the nucleus and its environment. It is measured relative to a

reference compound. For ^1H NMR, the reference is usually tetramethylsilane, $\text{Si}(\text{CH}_3)_4$.

Chemical shift is expressed in parts per million (ppm) is given as:

$$\delta = 10^6 \times \left(\frac{\delta_{\text{obs}} - \delta_{\text{ref}}}{\delta_{\text{ref}}} \right)$$

Where, δ_{ref} is the position observed for a reference compound and δ_{obs} is the position of the signal of interest. There are, however, some effects which can actually produce a magnetic field that reinforces B_0 . One of these effects is a ring current. The primary shielding effect comes from the electron's inherent magnetic field. However, a moving charge (current) can also produce a magnetic field by virtue of its motion. Organic compounds containing π -systems permit this type of electron "motion". Because the benzene ring is the classic example of this type of system, this electron "motion" is termed a ring current (Fig.2.3e). As in the case of an individual electron, the magnetic field generated by this ring current opposes the externally applied magnetic field, B_0 . The aryl hydrogens, however, are located in the "return" portion of the ring current magnetic field and experience a magnetic field which reinforces B_0 . Ring currents strongly deshield the aryl hydrogens as they are along the plane of the aromatic ring and the circulation of the electrons in the aromatic orbital creates a magnetic field at the hydrogen nuclei which enhances the B_0 field. This phenomenon is called deshielding. (towards higher ppm) while the protons above and below the plane are shielded (towards lower ppm).

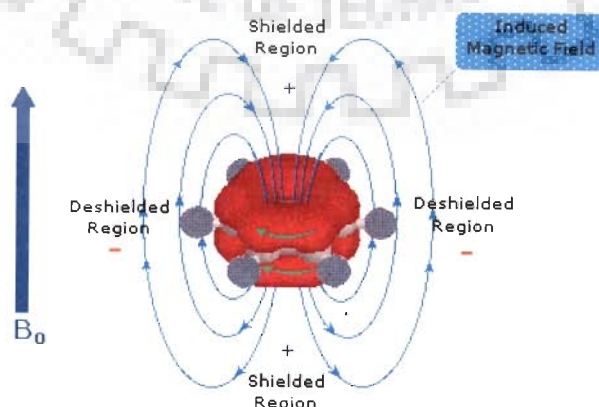


Fig. 2.3(e): Ring current effect on the benzene ring

2.3.1.3 Spin-spin coupling constant (J)

Nuclei experiencing the same chemical environment or chemical shift are called equivalent. Those nuclei experiencing different environment or having different shifts are non-equivalent. Nuclei, which are close to one another, exert an influence on each other's effective magnetic field. This effect shows up in the NMR spectrum when the nuclei are non-equivalent. If the distance between non-equivalent nuclei is less than or equal to three bond lengths, this effect is observable. This effect is called spin-spin coupling or J coupling and is expressed in Hertz. This coupling causes splitting of lines as shown below (Fig. 2.3f).

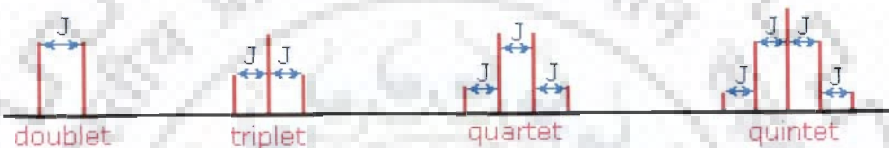


Fig. 2.3(f): Splitting of lines due to coupling

The appearance of multiple peak patterns depends on relative magnitude of δ and J for coupled nuclei. Vicinal Coupling (3J) is mediated by the interaction of orbital within the bond framework. It is therefore dependent upon overlap, and hence upon dihedral angle. The relationship between the dihedral angle and the vicinal coupling constant 3J (as observed from ^1H NMR spectra) is given theoretically by the Karplus equations:

$$^3J_{ab} = J^0 \cos^2 f - 0.28 \quad (0^\circ < f < 90^\circ) \quad \text{and} \quad ^3J_{ab} = J^{180} \cos^2 f - 0.28 \quad (90^\circ < f < 180^\circ)$$

Where $J^0 = 8.5$ and $J^{180} = 9.5$ are constants which depend upon the substituents on the carbon atoms and f is the dihedral angle. In some cases the axial-axial coupling constant for an antiperiplanar 180° H-C-C-H configuration may be more than 9.5 Hz e.g., rigid cyclohexanes it is around 9-13 Hz, because the dihedral angle is close to 180° , where the orbitals overlap most efficiently. The dihedral angle and an approximate calculated relationship (ignoring the small

constant of 0.28 in this graph) between the dihedral angle and the coupling constant is shown in Fig. 2.3g.

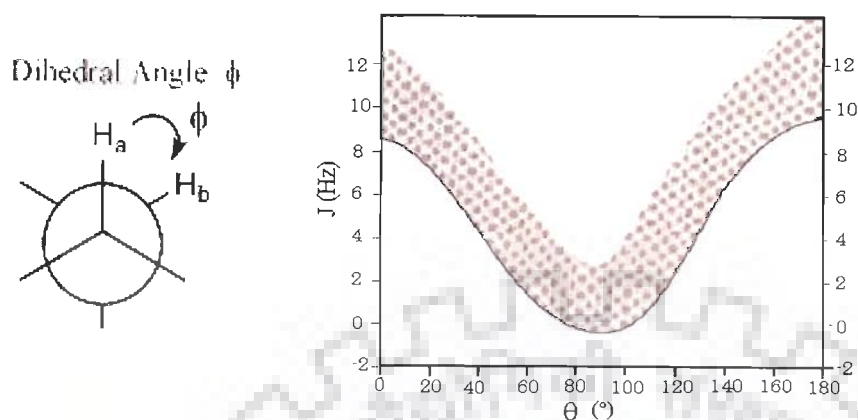
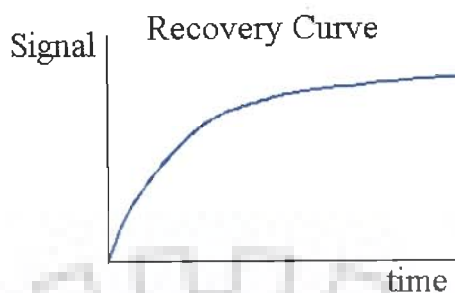


Fig. 2.3(g): Definition of the dihedral angle and Karplus Curve showing relationship between J couplings and dihedral angle

2.3.1.4 T1 and T2 Relaxation process

The magnetization does not precess infinitely in the transverse plane but turns back to the equilibrium state. This process is called relaxation. Two different time-constants describe this behavior. The importance of these phenomena is in the Nuclear Overhauser Effect (NOE), which can be used to probe inter-nuclear distances in a molecule. There are two major relaxation processes namely, Spin-Lattice (longitudinal) relaxation (T_1) and Spin-Spin (transverse) relaxation (T_2). The relaxation time T_1 represents the "lifetime" of the first order rate process that returns the magnetization to the Boltzman equilibrium along the +Z axis. The components of the lattice field can interact with nuclei in the higher energy state, and cause them to loose energy (returning to the lower state). The energy that a nucleus loses increases the amount of vibration and rotation within the lattice. The relaxation time, T_1 depends on the motion of the molecule. As mobility increases, the vibrational and rotational frequency also increases, making it more likely

for a component of the lattice field to be able to interact with excited nuclei. T_1 spin-lattice relaxation rate is then measured by plotting M as a function of τ :

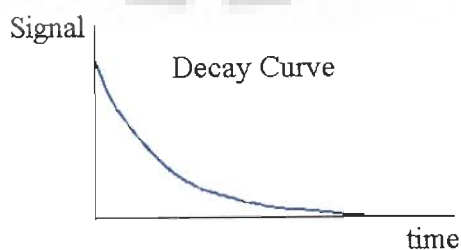


$$M(\tau) = M_0 [1 - 2\exp(-\tau / T_1)]$$

T_2 represents the lifetime of the signal in the transverse plane (XY plane) and it is this relaxation time that is responsible for the line width. In Solution NMR, very often T_2 and T_1 are equal. The very fast spin-spin relaxation time provides very broad signals. The transverse relaxation constant T_2 is related to the line width of the signals. The width of the signal at half height is given by:

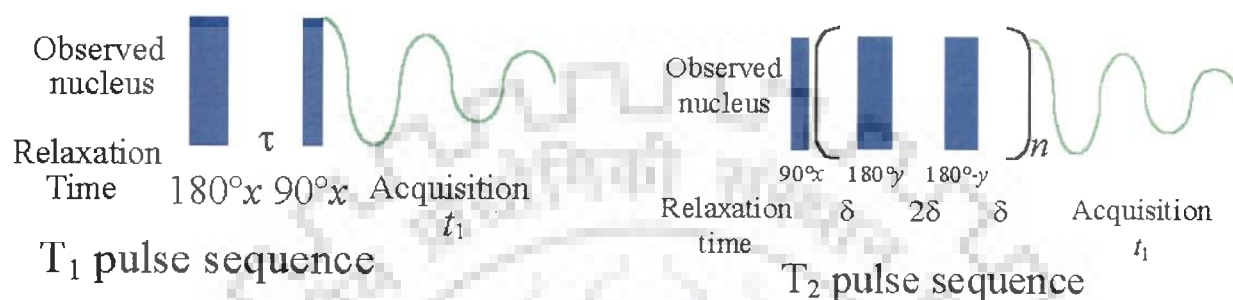
$$(\Delta\omega)_{1/2} = 1 / \pi T_2$$

Fast decay leads to broad signals and slow decay to sharp signals. The transverse relaxation constant T_2 of spin $I=1/2$ nuclei is mainly governed by the homogeneity of the magnetic field and the strength of the dipolar interaction with other $I=1/2$ nuclei depending on the number and the distance of neighboring nuclei the overall tumbling time of the molecule which is related to its size. Transverse relaxation (T_2) is faster than longitudinal relaxation. T_2 spin-spin relaxation rate is measured by plotting M as a function of τ (tau):



$$M(\tau) = M_0 [\exp(-\tau/T_2)]$$

where τ is the total evolution time ($4n\delta$) and the value of delta (δ) in the pulse sequence should be much shorter than $1/J$ but long enough that the sample should not heat up significantly. A delta (δ) of 10 ms is usually appropriate. If the sample is very concentrated then the relaxation time will appear shorter than it really is due to saturation.



2.4 TWO-DIMENSIONAL (2D) NMR TECHNIQUES

In one-dimensional pulsed Fourier transform NMR the signal is recorded as a function of one time variable and then Fourier transformed to give a spectrum, which is a function of one frequency variable. In two-dimensional NMR the signal is recorded as a function of two time variables, t_1 and t_2 , and the resulting data Fourier transformed twice to yield a spectrum, which is a function of two frequency variables. The two-dimensional signal is recorded in the following way. First, t_1 is set to zero, the pulse sequence is executed and the resulting free induction decay recorded. Then the nuclear spins are allowed to return to equilibrium, t_1 is then set to $\Delta 1$, the sampling interval in t_1 , the sequence is repeated and free induction decay is recorded and stored separately from the first. Again the spins are allowed to equilibrate, t_1 is set to $2\Delta 1$, the pulse sequence repeated and free induction decay recorded and stored. The whole process is repeated again for $t_1 = 3\Delta 1, 4\Delta 1$ and so on until sufficient data is recorded, typically 50 to 500 increments of t_1 . Thus recording a two-dimensional data set involves repeating a pulse sequence for

increasing values of t_1 and recording free induction decay as a function of t_2 for each value of t_1 . The general scheme for two-dimensional spectroscopy is shown in Fig. 2.4.

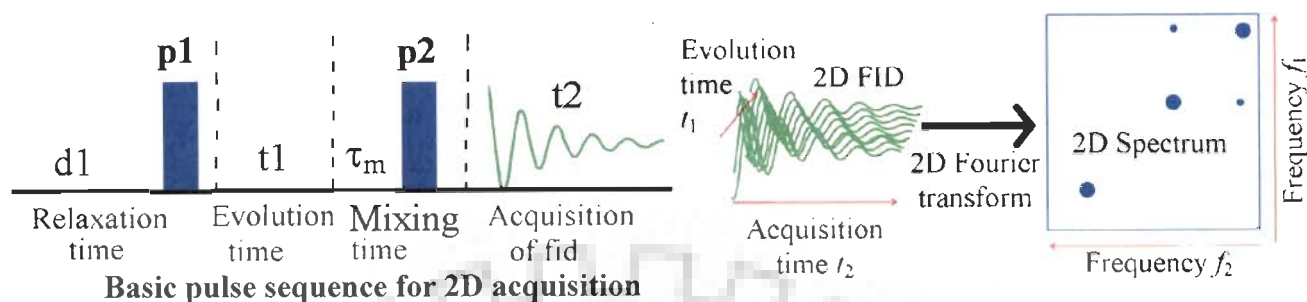


Fig. 2.4: Four different time segments of a 2D NMR experiment namely (i) Relaxation (Preparation) Period (ii) Evolution Period (t_1) (iii) Mixing Period (τ_m) (iv) Detection (Acquisition) Period (t_2)

Preparation time: The sample is excited by one or more pulse. This consists of a delay time or a sequence of pulses separated by fixed time intervals saturation sequences. Thermal equilibrium is attained during this period.

Evolution Period (t_1): The resulting magnetization is allowed to evolve for the first time period, t_1 . The evolution period is the pulse sequence element that enables frequency labeling in the indirect dimension. Further, one or several radiofrequency pulses may be applied to create coherence.

Mixing time (τ_m): During this period coherence is transferred between spins. Mixing sequences utilize two mechanisms for magnetization transfer: scalar coupling or dipolar interaction (NOE). After the mixing period the signal is recorded as a function of the second time variable, t_2 . This sequence of events is called a pulse sequence.

Detection Period: The signal is recorded during the time t_2 at the end of the sequence, detection, often called direct evolution time; during this time the magnetization is labeled with the chemical shift of the second nucleus. The data is recorded at regularly spaced intervals in both t_1 and t_2 .

Gradient enhanced NMR is a method for obtaining high resolution NMR spectra without the need for *phase cycling*. Gradient methodology is used extensively for two purposes, either rephasing (selection) or dephasing (elimination) of a particular magnetization transfer pathway. It includes the application of magnetic field gradient pulses to select specific coherences. By using actively shielded gradients, a gradient pulse is applied during the evolution period of the selected coherence to dephase the transverse magnetization and another gradient pulse refocuses the desired coherences remaining during the acquisition period.

2.4.1 Two-dimensional correlation spectroscopy (2D-COSY)

The COSY experiment is used in determining which atoms are connected through bonds. The basis of COSY experiment whose pulse sequence is shown in Fig. 2.4a is the classical Jeener sequence (Jeener, 1971). After the preparation period of 90° pulse constitutes brief mixing period whose effect is to mix single quantum coherence into a whole range of orders of coherence. However, only the single quantum coherence will give rise to any measurable signal during the detection period. The mixing process interchanges orders of coherence, mixes coherence among the transitions associated with a given spin and exchanges coherence between spins having a mutual scalar coupling. Thus a magnetization, initially associated with the A spin of an A-X spin system, may be transferred to spin X through the scalar coupling, J_{ax} . Therefore the A magnetization in the X-Y plane will also depend upon the Larmor frequency ω_x and the 2D COSY will show signals with frequency coordinates (ω_A, ω_X) and (ω_X, ω_A) as well as (ω_A, ω_A) . The former are the characteristic cross peaks of COSY spectrum and the latter, the diagonal peaks, which corresponds to 1D spectrum. The phase sensitive COSY spectra have cross peaks in anti phase. The antiphase multiplet structure of a cross peak only occurs in the active coupling giving rise to cross peak. Extra splitting present in multiplet but which do not give rise to cross

peaks are called passive couplings and appear in phase. Thus, the advantage of phase sensitive COSY is that the phase relation between peaks can be used for accurate assignment and calculation of coupling constants.

2.4.2 Phase sensitive COSY: Double quantum filtered COSY (DQF-COSY)

The experiment uses a pulse sequence $90_{\phi}-t_1-90_{\phi}-90_{\zeta}-t_2$ where ϕ , ϕ and ζ are the appropriate phase cycles (Piantini et al, 1982). In double quantum filter COSY experiment, Fig. 2.4a, the resonance from a COSY experiment is passed through a double quantum filter, thereby removing methyl and other singlets from the final spectrum. The short delays, Δ , immediately before and after the final pulse, are of order of microseconds. Twice as many transients are needed in these experiments to achieve the same signal to noise ratio than in conventional COSY. Another advantage of DQF COSY is that it converts the phase of COSY diagonal signals from dispersive antiphase to absorptive antiphase. These signals then do not interfere with the cross peaks. So, the cross peaks lying close to diagonal can be observed in double quantum filtered phase-sensitive COSY. Double filter COSY can be used to determine the coupling constants (Celda et al, 1989; Gochin et al, 1990).

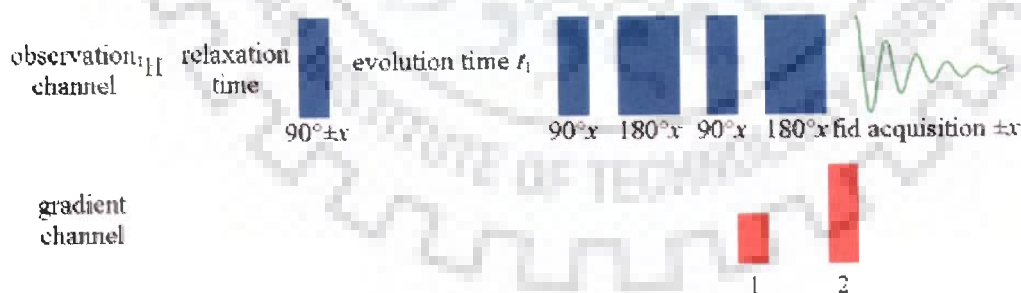


Fig. 2.4(a): Pulse sequence for gradient DQF-COSY

2.4.3 Total Correlated Spectroscopy (TOCSY)

During this pulse sequence, after the evolution period t_1 , the magnetization is spin-locked. During this mixing time, the magnetization exchange is through scalar coupling. During this

spin-lock period, the magnetization behaves as a strongly coupled spin system and evolves under the influence of a "collective spin-mode". In that collective mode, coherence transfer is possible between all coupled nuclei in a spin system, (even if they are not directly coupled). This essentially gives the same information as that of COSY, except that COSY gives information only on the directly coupled spins, whereas TOCSY gives the complete spin-coupling network, Fig. 2.4b.

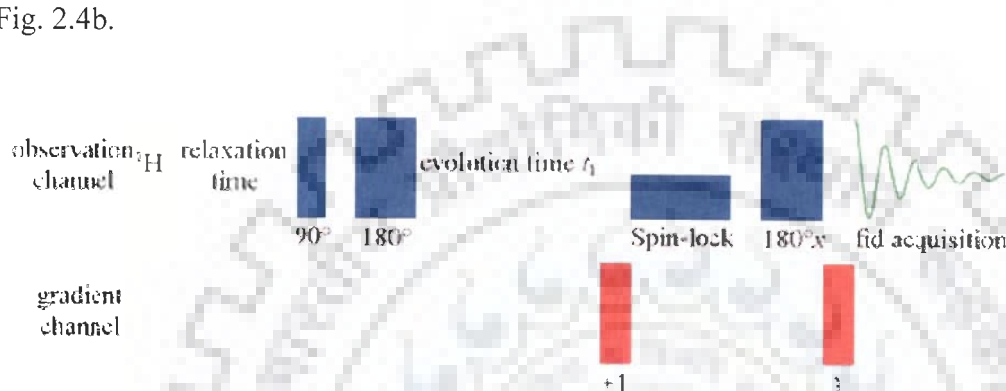


Fig. 2.4(b): Pulse sequence for gradient TOCSY

2.4.4 Nuclear Overhauser Effect Spectroscopy (NOESY)

NOE-type Experiments for nucleic acids: The nomenclature used for describing the through-space interactions in nucleic acids is $d_x(l;r)$ where l corresponds to the proton in the 5'-nucleotide unit, r to the proton in the 3'-nucleotide unit, and x is the type of interaction. Thus, several types of through-space interactions can be detected in polynucleotides by NMR: (1) **Intra-nucleotide interactions** giving information about sugar puckering and glycosidic torsion angle. (2) **Inter-nucleotide sequential interactions** giving information about base stacking. (3) **Inter-nucleotide cross-stand interactions** giving information about base pair formation. The inter-nuclear distance can be derived from the cross-peak intensities in NOESY-type experiments recorded in D_2O and /or H_2O (for exchangeable protons). Thus, in general we can distinguish the intense cross-peak for short distances between 1.8-3.0 Å, medium cross-peak for distances between 3.0-

4.0 Å, weak cross-peak for distances between 4.0-5.0 Å and absence of cross-peak for distance larger than 5 Å. Three-dimensional structures of oligonucleotides are usually generated by distance geometry and molecular dynamics calculations using distance and torsion angle constraints derived from NMR experiments.

NOESY is one of the most useful techniques as it allows correlating nuclei through space (distance smaller than 5 Å). By measuring cross peak intensity, distance information can be extracted. The pulse sequence starts as usual with a 90° pulse followed by an evolution time t_1 (Fig. 2.4c). This delay is varied systematically as usual to provide chemical shift information in the F1 domain. Then 90° pulse transmits some of the magnetization to the Z-axis and during the following mixing period, the non-equilibrium Z component will exchange magnetization through relaxation (dipole-dipole mechanism). This exchange of magnetization is known as NOE (Nuclear Overhauser Effect). After some time (shorter than the relaxation time T_1), the transverse magnetization is restored and detected. If relaxation exchange (or chemical exchange) has taken place during the mixing time, cross peaks will be observed in the spectra. The phase cycling ensures proper detection of NOESY signal, Fig. 2.4c.

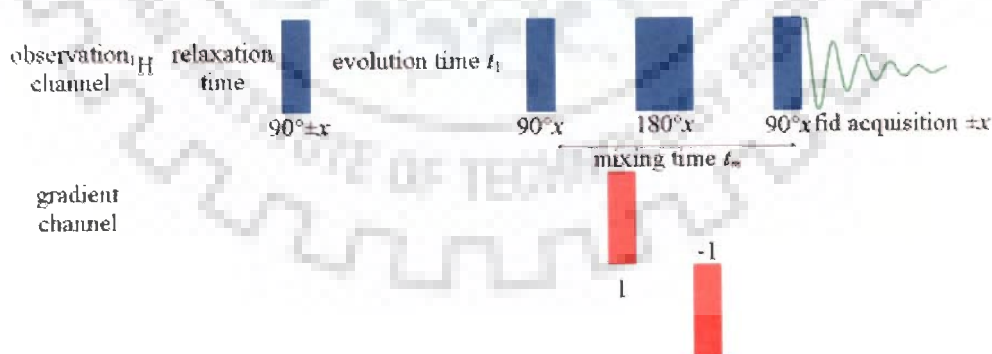


Fig. 2.4(c): Pulse sequence for gradient NOESY

2.4.5 Rotating frame Overhauser Effect Spectroscopy (ROESY or CAMELSPIN):

The aim of the dipolar correlation experiments in two dimensions is to take advantage of the vicinity in space of some nuclei. The result of this kind of experiment is a 2D map in which the signals outside the diagonal arise from the Overhauser enhancement effect between two space coupled nuclei. In this case, we apply a spin-lock on to the y axis. The correlation peaks arising from the ROE effect are on the opposite sign compared to the diagonal one and their intensity is different from 0. However, the correlation peaks coming from a chemical exchange are of the same sign than the cross peaks arising from ROE effect. The ROESY experiment allows by this way the separation of the contributions coming from the exchange and those coming from the dipolar interactions. The ROESY sequence is thus complementary of the NOESY one and it is more often used for the structural determination of the small molecules, Fig. 2.4d.

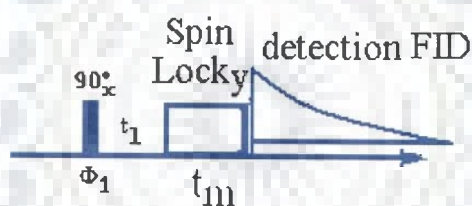


Fig. 2.4(d): Pulse sequence for ROESY

2.4.6 ^1H - ^{13}C Hetero-nuclear correlation emphasizing one-bond couplings (HSQC) and multiple-bonds coupling (HMQC)

Hetero-nuclear coupling (such as from ^1H to ^{13}C) is used to assign the spectrum of another nucleus once the spectrum of one nucleus is known. It may also be of help in assigning the spectra of both nuclei even when a partial assignment of one or both is available. Such an experiment may also provide chemical information which the spectra of neither nucleus can provide alone.

The most common experiment is that for large couplings which usually arise from one bond interactions, e.g. H-C or H-N. There are three common pulse sequences for this experiment that

are best suited for different conditions: HMBC (Heteronuclear Multiple Quantum Coherence), HSQC (Heteronuclear Single Quantum Coherence) (Fig. 2.4e) and HSQCSI (Heteronuclear Single Quantum Coherence Sensitivity Improved). ^1H - ^1H coupling reduces the resolution of HMQC spectra but HMQC is intrinsically more sensitive. HSQC is better when T_2 is much shorter than T_1 . HSQCSI is theoretically 41% more sensitive than HSQC with sensitivity similar to that of HMQC but for most regular samples it increases sensitivity by about 30% over HSQC. However, when the lines are broad, it actually reduces sensitivity. For signals with line-width less than 8 Hz, use HSQCSI, up to 20 Hz use HSQC. Above 20 Hz, use HSQC if the broadening is due to slow molecular tumbling or HMQC if it is due to para-magnetism. The peaks are pure in phase and positive for these three experiments. Δ should be $1/(4J_{AX})$ where J_{AX} is the coupling constant. The spectrum should be in phase, however, the precise phase of each peak is sensitive to the coupling constant so some phase distortion is to be expected. The correlation experiment does not contain a diagonal. Each proton signal is correlated with a carbon signal. Those signals in the 1D spectrum that do not correlate do not appear in the 2D spectrum.

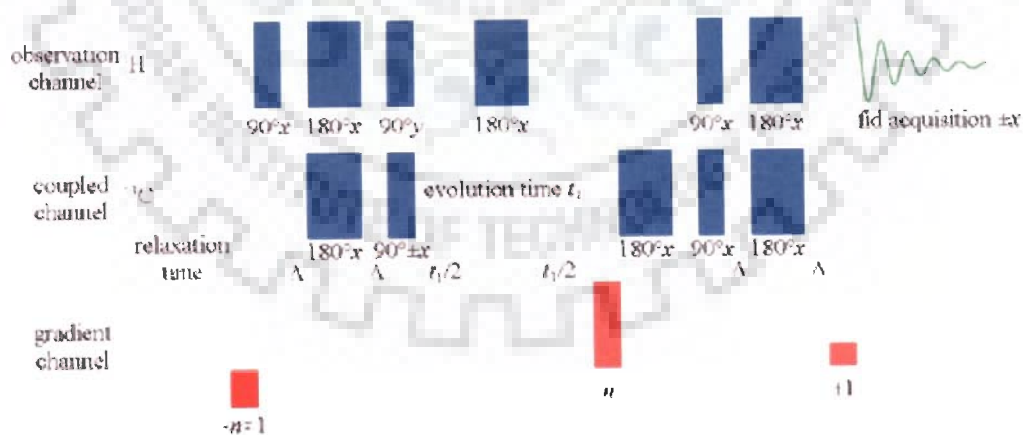


Fig. 2.4(e): Pulse sequence for HSQC

The gradient ratios (n) and coupling constants (J_{AX}) for HSQC and HSQCSI

Nucleus bound to H n J_{AX}

^{13}C	3.98	145 Hz
^{31}P	2.47	7 Hz (2 bond)

The hetero-nuclear correlation experiments suffer from t1 noise artifacts that appear as vertical streaks in the spectrum. This can be useful when there is strong overlap in the proton spectrum allowing advantage to be taken of the dispersion of the ^{13}C chemical shift. The ^1H - ^{13}C coupling constant can be measured by not using coupling. This has the advantage over the 1D carbon coupled spectrum in that the doublets do not overlap.

2.4.7 Hetero-nuclear correlation emphasizing long range couplings - HMBC

Long-range hetero-nuclear correlation can yield signals for these nuclei while suppressing one-bond correlations. The most common application of this technique is for ^1H - ^{13}C and ^1H - ^{31}P . $\Delta 1$ is set to $1/(2J \text{ one-bond})$ and $\Delta 2$ to $1/(2J \text{ long-range})$. The phase is strongly dependent on the long range and homo-nuclear proton coupling constant so each multiplet peak pattern has a different phase with an extreme first order component. The correlation experiment does not contain a diagonal. Each proton signal may be correlated with one or more carbon signals. Those signals in the 1D spectrum that do not correlate with carbons do not appear in the 2D spectrum, Fig. 2.4f.

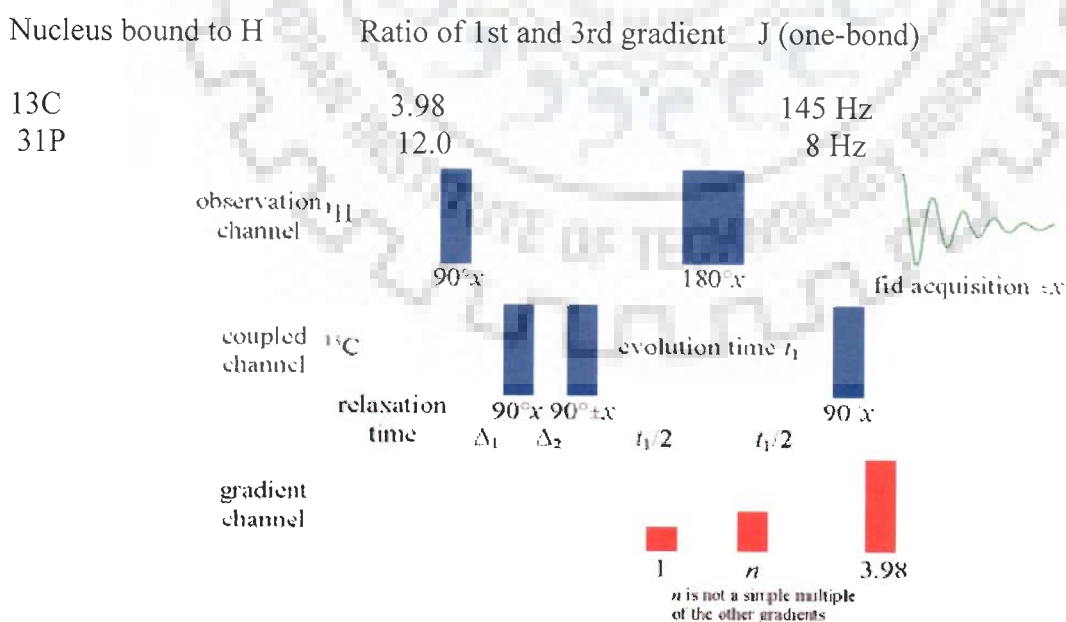


Fig. 2.4(f): Pulse sequence for HMBC

2.4.8 Diffusion Ordered Spectroscopy (DOSY)

The DOSY experiment is the measure of diffusion coefficients by NMR. In DOSY spectra, chemical shift is detected along the F2 axis and diffusion coefficient is along the F1 axis. We have used the method developed by Stejskal and Tanner (1965) which relies on two gradient pulses surrounding the 180° pulse in the spin echo. The first gradient dephases the transverse magnetization in a spatially dependent manner along the z-axis and the second gradient then rephases the magnetization. The relation between translational self-diffusion and the measurable NMR parameters (Stejskal and Tanner, 1965) is:

$$A/A_0 = -\exp [D_t \gamma_H^2 \delta^2 G_z^2 (\Delta - \delta/3)]$$

where A is the measured peak intensity (or volume), A_0 is the maximum peak intensity, D_t is the translational diffusion constant (in cm^2/s), γ_H is the gyromagnetic ratio of a proton ($2.675197 \times 10^4 \text{ G}^{-1} \text{ s}^{-1}$), δ is the duration of the gradient, Δ is the time between gradients and G_z is the strength of the gradient (in G/cm). Data can be plotted as $-\ln (A/A_0)$ versus $\gamma_H^2 \delta^2 G_z^2 (\Delta - \delta/3)$. The slope of the line gives the value of D_t . The pulse program used is Pulsed gradient spin echo (stimulated echo sequence incorporating bipolar gradients) sequence modified with binomial water suppression. The gradient strengths were incremented as a square dependence in the range from 1 to 32 G cm^{-1} . The diffusion time (Δ) and the duration of the magnetic field gradients (δ) were 100 ms and 6 ms, respectively. Other parameters include a sweep width of 6000 Hz, 32 K data points, 1024 transients and an acquisition time of 2.7 s and relaxation delay of 2.0 s. It has been developed in order to facilitate the complex mixture analysis without physical separation. This experiment will monitor any modification of the solvent or of the solutes, and molecular events such as molecular interactions or associations.

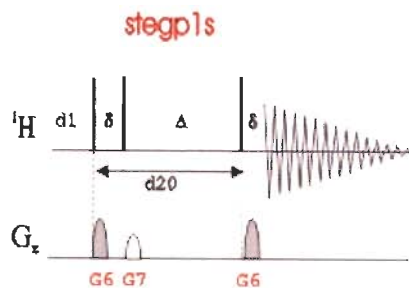


Fig: 2.4(g) Pulse sequence for DOSY

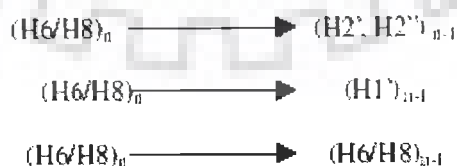
2.5 EXPERIMENTAL PARAMETERS

All NMR experiments were recorded on Bruker Avance 500 MHz FT-NMR spectrometer equipped with Topspin 1.3 version at Central NMR Facility located at Indian Institute of Technology Roorkee, Roorkee. Typical parameters for one-dimensional NMR experiments are pulse width = 7.5-14.5 μs (90° pulse); number of data points = 32-64 K; spectral width = 10,000 Hz; number of scans = 64-128 and FID resolution = 0.25-0.5 Hz/point. Receiver gain was optimized in each instance to obtain the best signal to noise ratio. Homonuclear ^1H 2D phase-sensitive DQF-COSY and NOESY experiments on d-(TGATCA)₂ and its complex with adriamycin, d-(CGATCG)₂ and its complex with 4'-epiadriamycin were carried out at 275 K in H₂O. However 2D NOESY experiments were recorded with variable mixing times (τ_m) 100, 200 and 300 ms at 500 MHz. Also, HMBC, HSQC, TOCSY, NOESY, DQFCOSY and ROESY of 4'-epiadriamycin is recorded at 298 K. Typical parameters for 2D experiments at 500 MHz were: 1024-2048 data points along t_2 dimension; 512 free induction decays in t_1 dimension; pulse width \approx 7.5-14.5 μs (500 MHz); spectral width \approx 10,000 Hz (500 MHz); no. of scans = 64-128 (500 MHz); FID resolution 2.30 – 4.60 Hz/point and relaxation delay \approx 2.0 sec and ssb 2, 2. Since the solvent used is water, so the water suppression using excitation sculpting with gradients is done.

2.6 DETERMINATION OF THREE-DIMENSIONAL STRUCTURE

2.6.1 Resonance assignments in nucleic acids

Resonance assignment is the first endeavor in the structural determination of DNA. The protons can be grouped into four categories: (i) exchangeable OH, NH and NH₂ protons of the bases (ii) non-exchangeable base protons between 7.0-15.0 ppm (iii) non-exchangeable sugar protons between 2.0-6.5 ppm (iv) methyl protons of thymine between 0.5-2.0 ppm. In order to observe OH, NH and NH₂ protons, experiments have been carried out in water whereas the other protons were observed in D₂O solution. The strategy for resonance assignment consists of two steps. In the first stage, the J correlated spectra are used to identify network of coupled spins. In the second stage, the spin systems so identified are assigned to particular nucleotides along the sequence of the molecule by making use of the NOESY spectrum as described below. The sugar protons H1', H2', H2'', H3', H4', H5' and H5'' form a complex J correlated network (Fig. 2.6a). The various cross peaks observed in the 2D J-correlated between these protons was used in identification of spin system within individual nucleotide units. The H1' proton shows a cross peak with H2', H2'' sugar protons. The H2' and H2'' protons are further coupled to H3' proton. We have used phase sensitive DQF-COSY spectra to identify the various J-coupled cross peaks. In the second phase, sequential assignment is carried out using NOESY spectrum. Short inter-nucleotide distances between adjacent nucleotide units are used as shown in Figure 2.6b. In right handed DNA with sugars in C3'-endo/C2'-endo/O1'-endo pucker and glycosidic angle in anti domain, a convenient strategy for sequential assignment is



Where, n stands for nth residue in 5'-3' oligonucleotide sequence. In case of Z-DNA, the repeating unit is a dinucleotide. The inter-nucleotide pathway is Base (2n-1) H5' (2n-1) Base (2n) H1' (2n) H2' (2n) and H2'' (2n) ... Base (2n+1).

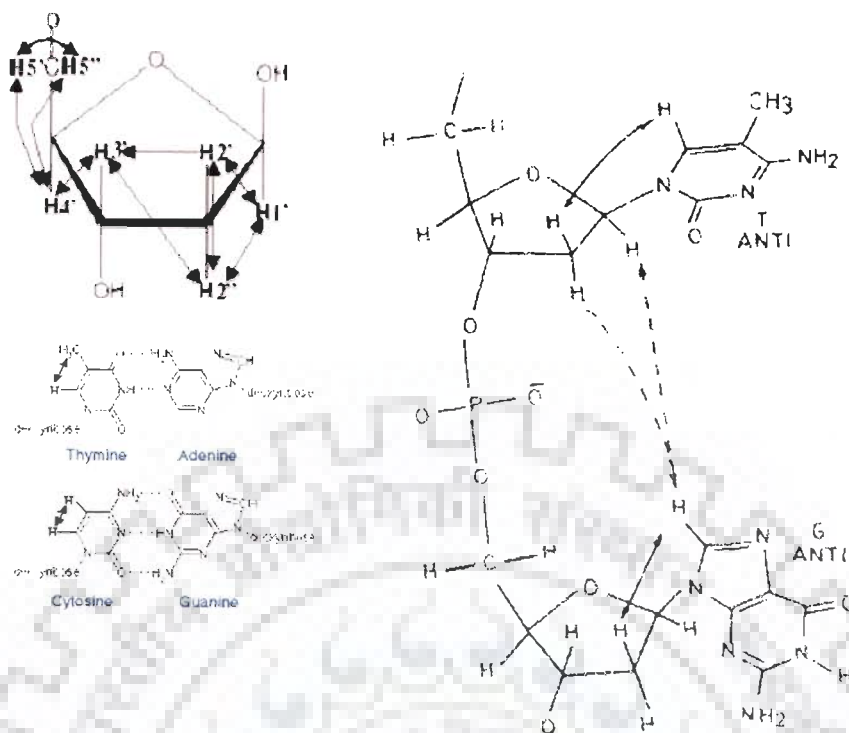


Fig. 2.6(a): Schematic representation of through bond J connectivity (\leftrightarrow) and short inter-proton distances between adjacent nucleotides units in right handed DNA bases

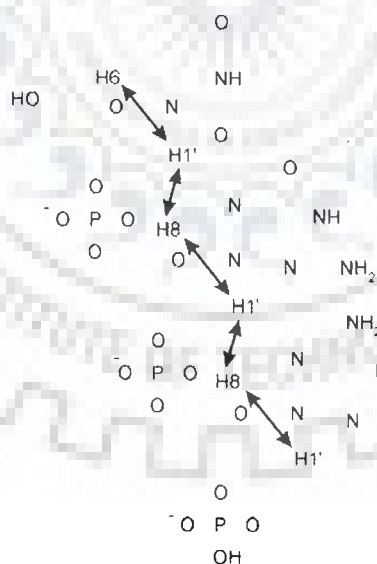


Fig. 2.6(b): Schematic representation of the H6/H8-H1' assignment pathway starting at 5'-terminal end of a DNA oligomer.

2.6.2 Pseudorotation

The glycosidic and sugar pucker conformations can be assessed qualitatively on the basis of the relative magnitudes of the intra-nucleotide sugar-base NOEs. The flexible five-membered sugar ring plays a pivotal role in nucleic acid structure and dynamic behaviour. In B-DNA family sugar responds to its surroundings (e.g. base stacking pattern) by an appropriate adaptation of its geometry. X-ray studies have now shown that P values occur in two distinct ranges. In a conformational wheel (Fig. 1.5j of Chapter 1) one range of form occupies the “Northern” half of the circle (N-type, $P_N 0^\circ \pm 90^\circ$); the second range occupies the “Southern” hemisphere (S-type, $P_S 180 \pm 90^\circ$). To a good approximation (0.4-0.7°) the torsion angles can be reproduced by a two-parameter pseudorotation equation:

$$v_j = \phi_m \cos [P + 0.8\pi (j-2)]$$

for j equals 0-4 and ϕ_m is amplitude of pucker. In crystal structures nucleotides usually a single pure N- or S-type conformer is found, but not necessarily the one that is predominant in aqueous solution. In some cases both N and S forms reside side by side in the same unit cell. Statistical analyses of X-ray data make it clear that details of sugar geometry of monomers are influenced by anisotropic crystal packing forces. The situation appears to be different in the helical oligomers, where stacking forces may play a more predominant role. NMR investigations in solution have demonstrated that N (C3'-endo) and S (C2'-endo) type conformations are in rapid equilibrium. If the inter-conversion rate between conformers is sufficiently rapid then observed couplings represent weighted average of couplings in individual conformers. Generally, in deoxyribose sugar, a trend to a larger proportions of C2'-endo pucker sugar is observed.

A phase sensitive DQF-COSY spectrum allows J-coupling patterns to be delineated from the well-resolved cross peaks. In general, the relation between 3J and φ takes the form of the semi-empirical Karplus equation: ${}^3J = A \cos^2(\varphi) + B \cos(\varphi) + C$

The constants A, B and C have to be determined from 3J values measured for compounds for which the value of φ , in solution, is known. There are five 3J values in deoxyribose sugar, $H1'-H2'$, $H1'-H2''$, $H2'-H3'$, $H2''-H3'$ and $H3'-H4'$, which are related to the relevant H-C-C-H dihedral angle, φ , according to the relation: $J = 10.2 \cos^2\varphi - 0.8 \cos \varphi$

The above dihedral angles are inter-dependent and their values can be calculated in terms of the two pseudorotation parameters, P and φ_m . φ_m is a constant for deoxyribose and thus various geometries can be expressed in terms of P. Fig 2.6c (Hosur et al, 1986) shows the plots of five coupling constants in a deoxyribose ring as a function of P, ($T_m = 38^\circ$). It is clear from the curves that the value of coupling constants ${}^3J(H1'-H2'')$ and ${}^3J(H2'-H3')$ vary within a narrow range of 6-10 Hz and are comparatively insensitive to the sugar geometry. On the other hand, the values of ${}^3J(H2''-H3')$, ${}^3J(H3'-H4')$ and ${}^3J(H1'-H2')$ coupling constant vary in the range 0-10 Hz and can be utilized with greater advantage in fixing the domains of sugar geometry. ${}^2J(H2'-H2'')$ is a geminal coupling which does not show significant conformational dependent variation. Rest five i.e. ${}^3J(H1'-H2')$, ${}^3J(H1'-H2'')$, ${}^3J(H2'-H3')$, ${}^3J(H2''-H3')$ and ${}^3J(H3'-H4')$ are vicinal coupling which show a strong dependence on the conformation of the deoxyribose ring (Hosur et al, 1986). The approach used for determination of sugar geometry is based on interpretation of intra-sugar proton-proton distances.

2.6.3 Conformation about the glycosidic bond

A large body of crystallographic data for nucleotides clearly establishes that the torsional angle, χ_{CN} , defining the orientation of base ring falls into two relatively narrow ranges designated as syn and anti conformation (Sundaraligham, 1969).

$$\chi \begin{cases} O4'-C1'-N9-C4 \text{ (Purines)} \\ O4'-C1'-N1-C2 \text{ (Pyrimidines)} \end{cases}$$

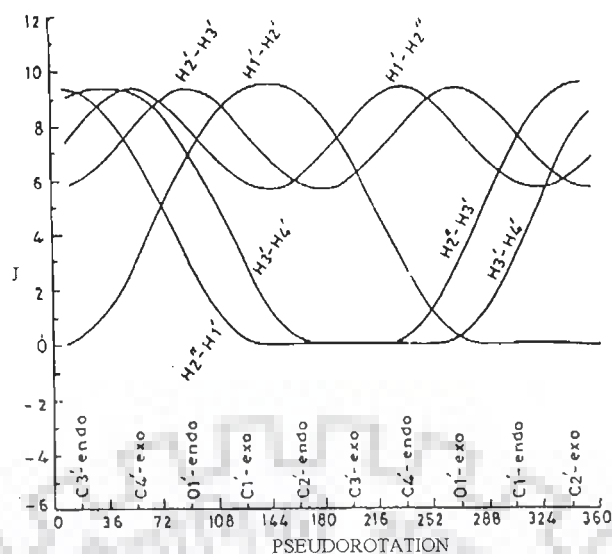


Figure 2.6(c): Variation of the vicinal coupling constants in the deoxyribose ring as a function of the ring geometry

The relative magnitudes of the intra-nucleotide and inter-nucleotide (H8/H6)-H1' and (H8/H6)-(H2', H2'') cross peaks in NOESY spectra at different mixing times can be used to establish the domains of glycosidic dihedral angles of individual nucleotide unit (Hosur et al, 1985; Roche et al, 1994). The intensity patterns for the above mentioned cross peaks for different glycosidic dihedral angles are given below:

1. For the syn conformation, a strong NOE between base H8/H6 and H1' protons should be observed. At the same time, the NOEs from base to H2' and H2'' protons will be relatively weak and will have different intensities.
2. In the anti conformation, the NOE from base H8/H6 to H2' is stronger than the NOE from base H8/H6 to H2''. Also, for right handed structures the H2'' proton shows a stronger NOE to the base proton of the next nucleotide.
3. In the high anti conformation, the (H8/H6)-H2' and (H8/H6)-H2'' NOEs will have similar intensities for C2'-endo geometry.

The (H8/H6)-H1' distance depends only on χ while, other distances depend on both P and χ . Iso-distance contours have been calculated by Wuthrich (Wuthrich, 1986) in (P, χ) space for H8/H6-H2', H2'', H3', H4' and H5' distances.

2.7 ESTIMATION OF INTERPROTON DISTANCES

If one resonance A is irradiated, an increase (positive NOE) or decrease (negative NOE) of signal intensity of other resonances such as resonance C is observed when spin C is close to spin A in space. This phenomenon is called Nuclear Overhauser Effect or NOE. The NOE effect is the method for elucidation of 3D structural features and stereochemistry using NMR together with information from scalar spin-spin couplings. The most important quantity derived from NOE cross peaks is the cross-relaxation rate between protons i and j. The cross relaxation rate σ_{ij} between two protons spin i and j is related to the distance between protons i and j in the following way:

$$\sigma_{ij} = \langle d_{ij}^{-6} \rangle f(\tau_{ij}) \quad (1)$$

$\langle d_{ij}^{-6} \rangle$ denotes an ensemble average of molecular structures inter-converting in thermal equilibrium where $f(\tau_{ij})$ is a function of correlation time τ_{ij} for the vector connecting the two spins. The cross relaxation rates can be measured from buildup rates of cross peaks in 2D NOE spectra at several mixing times. According to equation (1), the measured cross relaxation rates are a function of the ensemble average properties, which are dependent on the configuration space accessible to the molecular system at the temperature and time scale. If the inter-conversion between conformational equilibrium in the oligonucleotide is fast on NMR time scale, NOEs from several equilibrium conformations will be observed simultaneously. This means that the derived set of distance constraints does not necessarily represent the average structure, and there may be no single conformation that is consistent with the data set. Initially the intensity of the cross peak in equation (1) varies linearly with mixing time, and therefore this

condition is referred to as “linear regime”, but on higher mixing times, this condition does not exist due to multispin relaxation. Interproton distances can be estimated by measuring the intensities of cross peaks in the “linear regime”. Two-spin approximation is used in NOE distance measurements in which only the rate of dipolar magnetization transfer between proximal spins i and j is monitored and all other spins are ignored. For two spin approximation, the intensity I_{ij} can be written as:

$$I_{ij} = \frac{\gamma^4 \hbar^2 \tau_c \tau_m}{10r_{ij}^{-6}} \quad \text{when } \omega \tau_c \gg 1$$

where γ is gyromagnetic ratio and \hbar , is Planck’s constant divided by 2π . In order to determine the accurate value of τ_m for estimation of interproton distances, NOE build up curves should be obtained as a function of τ_m for several cross peaks, since spin diffusion can be different for different protons. Correlation times, τ_c , can be obtained from T_2 and T_1 measurements, according to the equation:

$$\tau_c = 2\omega^{-1}(3T_2/T_1)^{-1/2} \quad \text{which holds good for } \omega\tau_c \gg 1$$

If protons i, j, k, l have similar τ_c values and if r_{ij} is a known distance, then the unknown distance r_{kl} can be calculated by comparing the intensities I_{ij} and I_{kl} in a single spectrum.

$$\frac{I_{ij}}{I_{kl}} = \frac{r_{kl}^6}{r_{ij}^6}$$

The choice of known distance is important in the light of the mobility associated with different atoms in the nucleic acid. The thymidine (H6-CH₃) distance of 3.0 Å can be used as reference for all NOEs involving CH₃ protons, the sugar H2’-H2” protons and for the rest, cytidine H5-H6 distance of 2.45 Å can be used. The characteristics of NMR data can be summarized as below:

1. The exact distances cannot be calculated from NOEs, that is, NOEs give only a number of approximate upper limits (e.g., 3.0 Å, 4.0 Å and 5.0 Å for strong, medium and weak NOEs).

Sometimes it is not possible to make this division and only one single upper limit is used. For some proton pairs, corrections have to be applied to the upper limit value. This may arise due to stereo-specific assignments (e.g., methyl group of thymine) or because of dynamic effects such as rotation of hydrogen in a methyl group and flipping of the aromatic rings.

2. Translating NOEs into reliable lower limit constraints is difficult, and it is preferable to take the sum of van der Waals radii as a lower limit to the distance. The absence of NOEs between two assigned protons may be translated into a minimum distance of proton pair.
3. NMR data contain contributions from different molecular conformations. Not all distance constraints need to be consistent with the single conformation.
4. NOE information is limited to short distance relative to the size of the drug-DNA complex.

2.8.1 UV-Vis Spectroscopic Techniques: The concentration of oligonucleotides d-(CGATCG)₂ and d-(TGATCA)₂ were determined by using the standard value of the molar extinction coefficients i.e. 57200 M⁻¹cm⁻¹ and 61400 M⁻¹cm⁻¹ respectively by Cary 100Bio UV-Visible Spectrophotometer. The double – stranded nature of the oligonucleotides were confirmed by their thermal denaturation transitions (measured in 70 mM NaCl, 20mM phosphate buffer). The concentration of adriamycin, daunomycin and 4'-Epiadriamycin in buffer solution were determined spectrophotometrically at the λ_{max} of 480nm ($E_i = 11,500 \text{ M}^{-1}\text{cm}^{-1}$). All experiments were performed in the standard buffer containing 70mM NaCl, 20mM phosphate buffer, pH= 7.0 at 25°C. The buffer was filtered through 0.45 μm pore Millex Millipore filters. The oligonucleotide synthesis was done on DNA synthesizer (ABI Machine). The absorbance versus concentration as well as relative fluorescence versus concentration study is made to find whether the self association of the drugs exists.

2.8.2 Life Time Measurement using Fluorescence Spectroscopy: Time-Correlated Single-Photon counting on the Spectrofluorometer (model FluoroLog[®]-TCSPC, make HORIBA Jobin Yvon Spex[®]) is used for the life time measurement study. This is an ultra compact fluorescence lifetime spectrometer based on time correlated single photon counting (TCSPC) and ready to perform time-domain lifetime spectroscopy building up a histogram of the sample's fluorescence decay. This instrument has sub-ns pulsed LED. For our study, we used fixed-wavelength NanoLED of 470 nm. Standard optical pulse durations are <1.5 ns for LEDs. Resolution 0.2 nm, accuracy ± 0.5 nm, speed 150 nm/s, range 0-1300 nm, TAC range given is 50 nm, excitation wavelength is 470 nm and emission wavelength is 600 nm for the experiment.

2.9 RESTRAINED MOLECULAR DYNAMICS AND SIMULATED ANNEALING

When restrained energy minimization methods are used, inevitable local energy minima are encountered which can lead to inaccurate structures. To circumvent this, restrained molecular dynamics (rMD) are usually employed. This involves including NMR restraints in one of the many molecular dynamics simulation programs. Molecular dynamics solve Newton's equation of motion,

$$F_i = m_i a_i \quad (1)$$

Where F_i is the force, m_i is the mass and a_i is the acceleration of atom i . The force on atom i can be computed directly from the derivative of the potential energy V with respect to the coordinates r_i . The energy can be expressed in an explicitly differentiable form:

$$dV/dr_i = m_i d^2 r_i/d t^2 \quad (2)$$

Therefore, with an adequate expression for the potential energy and the known masses, this differential equation can be solved for future positions in time t_i . In general, this can be solved only approximately, since V is usually a complex function of the coordinates of all (or many) of

the atoms (i.e. $V = V(r_1, r_2, r_3 \dots r_N)$). The temperature can be calculated from the atomic velocities

$$3N/2 k_B T = \sum_{i=1}^N 1/2 m_i v_i^2 \quad (3)$$

Where, k_B is Boltzmann's constant, m_i and v_i are the mass and velocity of atom i , and N is the number of atoms (and $3N$ is the number of degrees of freedom). For a simulation at constant energy, the temperature fluctuates due to the inter-conversion of kinetic and potential energy. For constant temperature, the atomic velocities are adjusted accordingly. If the pressure is held constant, the volume is allowed to fluctuate by rescaling the inter-atomic distances. The total potential energy V_{total} is usually defined as the sum of a number of terms:

$$V_{\text{total}} = V_{\text{bond}} + V_{\text{angle}} + V_{\text{dihedr}} + V_{\text{vdw}} + V_{\text{coulomb}} + V_{\text{NMR}} \quad (4)$$

where, V_{bond} , V_{angle} and V_{dihedr} keep bond lengths, angles, and dihedral angles at their equilibrium values. The first five terms are empirical energy terms describing the physical interactions between the atoms, and the last term includes only the NMR information. They can be summarized as follows:

$$V_{\text{bond}} = \sum_{\text{bond}} 1/2 K_b (b - b_0)^2 \quad (5)$$

$$V_{\text{angle}} = \sum_{\text{angles}} 1/2 K_0 (\theta - \theta_0)^2 \quad (6)$$

$$V_{\text{dihedr}} = \sum_{\text{dihedr}} K \phi (1 + \cos(n\phi - \delta)) \quad (7)$$

These are pseudo-harmonic potentials that constrain bond lengths (b), bond angles (θ), and the rotamer angles (ϕ , δ) for staggered and eclipsed conformations, and K is a constant. The van der Waals and electrostatic interactions are described by V_{vdw} and V_{coulomb} :

$$V_{\text{vdw}} = \sum_{\text{pairs}(ij)} [C_{12}/r_{ij}^{12} - C_6/r_{ij}^6] \quad (8)$$

$$V_{\text{coulomb}} = \sum_{\text{pairs}(ij)} q_i q_j / 4\pi\epsilon_0\epsilon_r r_{ij} \quad (9)$$

where equation (8) is the Lennard-Jones potential, containing repulsive and attractive terms (C is a constant), and equation (9) describes the columbic interactions between two charged particles (i, j) with partial charges q that are at a distance r_{ij} apart in a dielectric medium described by $\epsilon_0\epsilon_r$ term. The potential V_{NMR} contains the NMR restraints, and has the effect of pulling the protons that show an NOE interaction closer to the measured distance r_{ij} . Similarly, these potentials are also pseudo-harmonic functions of similar forms to equations (5)-(7). Distance constraints which can be reasonably accurately determined may therefore be defined as follows:

$$V_{\text{NOE}} = \begin{cases} K_1 (r_{ij} - r_{ij}^0)^2 & \text{if } r_{ij} > r_{ij}^0 \\ K_2 (r_{ij} - r_{ij}^0)^2 & \text{if } r_{ij} < r_{ij}^0 \end{cases} \quad (10)$$

where, r_{ij} and r_{ij}^0 are the calculated and experimental interproton distances, respectively, and K_1 and K_2 are force constants given by:

$$K_1 = k_B T S / [2(\Delta_{ij}^+)^2] \text{ and } K_2 = k_B T S / [2(\Delta_{ij}^-)^2] \quad (11)$$

Where k_B is Boltzmann's constant, T , absolute temperature of the simulation, S a scale factor, and Δ_{ij}^+ and Δ_{ij}^- are the positive and negative error estimates, respectively, of r_{ij} . If, however, only ranges of distances can be specified, then the distance restraints are incorporated into a pseudo-square-well potential of the form:

$$V_{\text{NOE}} = \begin{cases} K_{\text{NOE}} (r_{ij} - r_{ij}^u)^2 & \text{if } r_{ij} > r_{ij}^u \\ 0 & \text{if } r_{ij} \leq r_{ij}^u \\ K_{\text{NOE}} (r_{ij} - r_{ij}^l)^2 & \text{if } r_{ij} < r_{ij}^l \end{cases} \quad (12)$$

where r_{ij}^u and r_{ij}^l are the upper and lower limits, respectively, of the target distances obtained from the experimental, and K_{NOE} is the force constant, which is typically chosen to be the order of $1000 \text{ kJ mol}^{-1} \text{ nm}^{-1}$.

To ensure that the experimental restraints are the dominating factor in determining the conformation of the molecule, it is very important that the force constants for the restraints are set sufficiently high that the experimental data are satisfied within the precision of the measurements. Thus convergence on the structure is guided by the requirement to minimize NOE or other restraint violations. The number of distance restraint violations N_{viol} is counted when, for example, $r_{ij} \geq r_{ij}^0 + 1$, which would be for 1 Å fluctuations. Other parameters which can be minimized in addition to N_{viol} is the sum of the distances in excess of the constraints $\sum \Delta r_{\text{viol}}$, which is defined as:

$$\sum \Delta r_{\text{viol}} = \sum_{K=1}^{N_{\text{viol}}} (r_{ij})_k - [(r_{ij}^0)_k + 1] \quad (13)$$

where the sum runs over all those interproton (or pseudoatom) distances for which N_{viol} is defined. The rMD approach requires a relatively large amount of computation time compared to distance geometry methods. This problem can be overcome by using a simplified potential energy function, where all non-bonded contact interactions are described by a single van der waals repulsion term. Simulated annealing involves raising temperature of the system followed by slow cooling in order to overcome local minima and locate the global minimum region of the target function. It is computationally more efficient than rMD and yield structures of similar quality. The potentials are very similar to rMD and again Newton's laws of motion are solved as a function of time. However, in implementations found in commercial programs, the non-bonded interaction potential is modified so that there is a simple van der waals repulsion term with a variable force constant K_{rep} :

$$V_{\text{repel}} = \begin{cases} 0 & \text{if } r \geq s \cdot r_{\text{min}} \\ K_{\text{rep}} \left(\frac{s \cdot r_{\text{min}}}{r} - 1 \right)^2 & \text{if } r < s \cdot r_{\text{min}} \end{cases} \quad (14)$$

The values of r_{\min} are given by the sum of the standard values of the van der Waals radii between two atoms as represented by the Lennard-Jones potential.

3.0 DEFINING DNA STRUCTURE

The structure of DNA can be described by a number of parameters that define the helix (Dickerson et al, 1989) termed as Helical Parameters. The output from helix analysis program CURVES 5.1 version of Richard Lavery (Lavery and Sklenar, 1988), includes “global helical parameters” defined relative to a global helix axis, that is, it depends on all the atoms in the structure and “local helical parameters” defined relative to local helix axis at each base pair, that is, arises if only a subset of neighboring atoms is used to determine that quantity. The helicoidal parameters are classified into three categories: 1. Global base pair-axis parameters 2. Intra-base pair or global base-base parameters 3. Inter-base pair or base pair-step parameters.

The global as well as the local inter-base pair parameters are related to particular base pair steps. These parameters are vector quantities, which have a defined location in 3-dimensional space and with respect to the nucleic acid sequence. In contrast, the average inter-base pair parameters are scalar values that are not related to any part of the structure. They characterize properties of the whole structure. Intra-base pair or global base-base parameters comprises of the translational components as stagger, stretch and shear, and the rotational components are propeller twist, buckle, opening. Propeller twist refers to the angle between the planes of two paired bases. A base pair is rarely a perfect flat plane with each aromatic base in the same plane. Rather, each base has a slightly different roll angle with respect to the other base. This makes two bases look like an aeroplane propeller. Twist or rotation per residue refers to the angle between two adjacent base pairs. Each step from one plate to the next can be described as a combination of a translational and a rotational movement.

The translational and the rotational displacements are three-dimensional vectors, which can be split into three orthogonal components. In inter-base pair or base pair-step parameters the three translational components are rise, shift and slide. Twist, roll and tilt are the three rotational components. Rise is the distance between adjacent planar bases in the DNA double helix i.e. it is a translation in the direction of the helical axis (z-axis), and shift is orthogonal to the helical axis and directs to the major groove side. Twist is a rotation about the helical axis (z-axis). Base pair roll refers to the angle of deflection of the base pair with respect to the helix axis along a line drawn between two adjacent base pairs relative to a line drawn perpendicular to the helix axis. A positive roll indicates that there is a cleft between two stacked base pairs, which opens towards the minor groove. A negative roll is related to an opening towards the major groove. Base pair tilt refers to the angle of the planer bases with respect to the helical axis. In the B-form DNA the bases are tilted by only -6° . In the A-form DNA the base pairs are significantly tilted at an angle of 20° . The sense of the base-pair tilt is associated with sugar pucker. In double helical polynucleotide, the normal to the base pair are not exactly parallel to the helix axis but inclined to it by up to 20° . The sense of tilt is positive in A-type and negative in B-type of helices, and hence is correlated with sugar pucker. Base tilt angle is correlated with rise per residue. If the bases in base pairs were coplanar and the base pairs exactly perpendicular to the helix axis, the axial rise per nucleotide should correspond to the van der Waal's distance, 3.4 \AA .

Global base pair-axis parameters: x- and y- displacement refers to the shift of bases in positive or negative x and y direction with respect to each other, besides this tip and inclination are also there (Fig.3.0a).

Inter-base parameters (Base pair step parameters): The helical parameters are derived from the spatial location of the bases, while the sugar phosphate backbone is not taken into account.

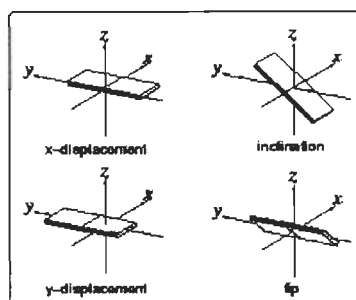


Fig. 3.0(a): Pictorial representation of global base pair-axis parameters

The six inter base pairs parameters (*rise, twist, shift, roll, tilt, slide*) describe the local conformation of a double helix at every base pair step (Fig. 3.0b). In the below figure the base pairs are shown as planar plates. In a regular helix such planar elements are stacked on each other. Each step from one plate to the next can be described as a combination of a translational and a rotational movement. The translational and the rotational displacements are 3-dimensional vectors, which can be split into three orthogonal components. The three translational components are **rise, shift and slide**. **Rise** is a translation component in the direction of the helical axis (z -axis) and **shift** is orthogonal to the helical axis and directs to the major groove side. **Twist, roll**

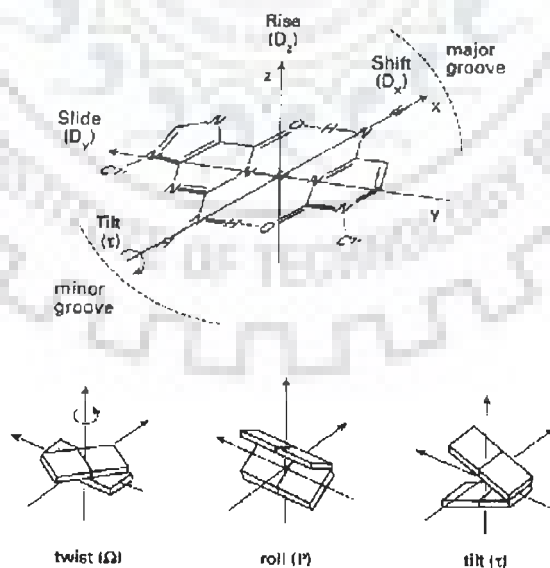


Fig. 3.0(b): Six inter-base pair parameters of DNA

and tilt are the three rotational components. **Twist** is a rotation about the helical axis (z-axis). A **positive roll** indicates that there is a cleft between two stacked base pairs which opens towards the minor groove. A **negative roll** is related to an opening towards the major groove. The definitions of the six inter base pair parameters are rigorous but the Cambridge convention does not define how to establish the reference coordinate system. The decomposition of the total translational and rotational movement into orthogonal components depends crucially on the reference system used. Several different algorithms and programs exist for calculating the helical parameters. The algorithms differ mainly in the methods used to derive the reference coordinate systems.

Intra-base pair step parameters (Base pair parameters): The base pairs in nucleic acid structures are not really planar. For example, the propeller twist of AT base pairs in B-DNA is usually in the range of -15° to -20° . If the base pairs are not planar, the six inter base pair parameters will give only a rough model of the helix. A more detailed picture is obtained if also the intra base pair parameters are taken into account. The Cambridge convention defines six base pair parameters which describe the deviation from planarity within a base pair. These six parameters describe the translational and rotational displacement between the two bases of a base pair. Again, the translational and rotational displacement is divided into orthogonal components. The translational components are *stagger*, *stretch* and *shear*, and the rotational components are *propeller twist*, *buckle*, *opening* (Fig. 3.0c). Instead of determining the (intra) base pair parameters, it is also possible to calculate the inter base pair separately for each strand.

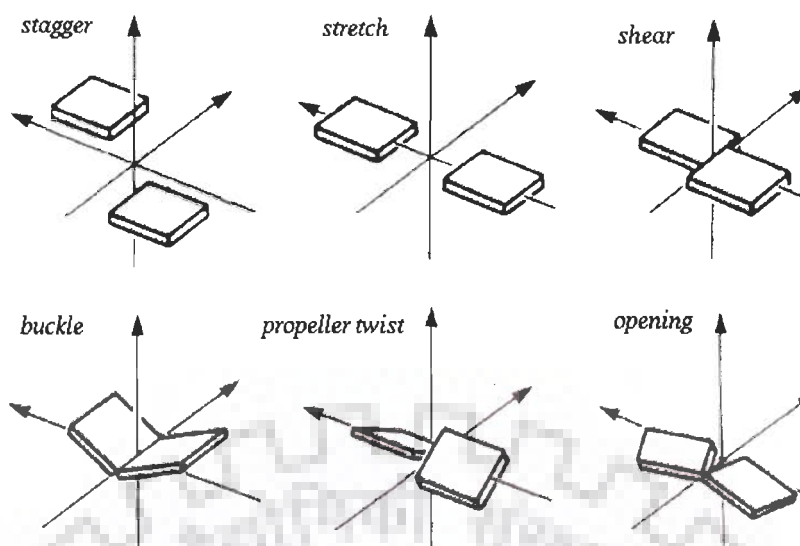


Fig. 3.0(c): Six Intra-base pair step parameters of DNA

3.1 QUANTUM MECHANICAL CALCULATIONS

The popularity of density functional methods and their applications to a broad range of problems and biochemical interest has been growing rapidly each year (Parr et al, 1989, Labauowski et al, 1991, Kohn et al, 1996). Therefore the calculations are carried out using a Density Functional Theory (DFT). Along with it, Hartree-Fock wave function (HF) with self-consistent field (SCF) calculation is used for the comparison. The DFT method used is as follows: Hybrid B3LYP based on Becke's three parameters functional (Lee et al, 1988) and the correlation functional provided by LYP (Becke et al, 1993).

In all of these calculations, Cartesian Gaussian type orbitals (GTO's) are used as basis function for the molecular orbital. Although the capability of the basis functions to describe bonding deformations of the electronic density can be enhanced by increasing the number of basis functions for each orbital or including higher angular functions, yet as a thumb rule it should be able to yield results which are comparable with larger basis set while remaining computationally

manageable, and thus at least a basis set of the split- valence type with polarization function should be employed.

All calculations presented are done using the Gaussian 98 program package (Marek et al, 2003). Full unconstrained geometry optimizations were performed using the density function as well as Hartree-Fock wavefunction as outlined above. For each of these density functional methods several basis sets like STO-3G, 6-31G, 6-31G**, 6-311G, 6-311G** are used for optimizing the geometry. All the molecular properties and chemical shifts are computed using the optimized structure of the molecule. The chemical shifts were also calculated using the same Gaussian package with the Gauge Independent Atomic Orbital (GIAO) approach. This approach allows the computation of the absolute chemical shielding due to the electronic environment of the individual nuclei. On the ground of variational theory, the quality of wave functions has been traditionally determined by the total energy which is the average of the Hamiltonian over the wave function. The lower the energy, the better the quality and we retain this concept despite the fact that for properties other than the total energy it may not be acceptable. In view of this, the calculations for structural properties and chemical shifts only using B3LYP method are reported.

3.2 ELECTRON SPRAY IONIZATION MASS SPECTROMETRY (ESI-MS)

Positive-ion ESI-MS spectra are obtained on Esquire 4000 (Bruker Daltonics, Germany) with the normal ESI source. The 5 μM concentration solutions of drugs are prepared in the water: acetic acid in the ratio of 90:10. This concentration is taken to see if the drugs show the phenomenon of self-association. The solutions are infused directly into the mass spectrometer at the rate of 240 $\mu\text{l/hr}$. In the cone voltage was set to 4.0 kV and the nebulizer pressure is 15 psi. Dry gas flow is 8 l/min. The capillary temperature was 100 $^{\circ}\text{C}$. Data is collected for approximately 10 scans. The maximum accumulation time is 200 ms and scan range is 400-1700 m/z.

Structural Elucidation of 4'-Epiadriamycin by Nuclear Magnetic Resonance Spectroscopy and Comparison with Adriamycin and Daunomycin using Quantum Mechanical and Restrained Molecular Dynamics Approach

In order to have stronger biological activity and lower toxicity, new anthracycline analogues are synthesized which can bind to DNA. For the structure based design of new ligands the knowledge of exact conformational behaviour is necessary. The aim of this study is to understand conformational behaviour of the three drugs, 4'-epiadriamycin (EPIADM), adriamycin (ADM) and daunomycin (DNM) (Fig. 1a-c) having different biological actions. The following is presented in this chapter:

- One- and two-dimensional NMR of 5.5 mM 4'-epiadriamycin, that is, 1D, DQF COSY, TOCSY, NOESY, HSQC (^1H - ^{13}C) and HMBC (^1H - ^{13}C) in D_2O at 298 K and proton 1D NMR spectra of all drugs at concentration of 0.01 mM in $\text{H}_2\text{O}/\text{D}_2\text{O}$ (90 : 10 v/v) at 275 K.
- Restrained Molecular Dynamics (rMD) simulations of 4'-epiadriamycin using NOE interproton distance constraints from 2D NOESY spectra and of adriamycin and daunomycin using NMR restraint data obtained earlier (Barthwal et al., 1994; Barthwal et al., 1996).
- Structural and electronic properties of all the three drugs using Density Functional Theory (DFT) employing B3LYP exchange correlation at different levels of basis sets and calculation of chemical shift of ^1H and ^{13}C resonances in Nuclear Magnetic Resonance (NMR) spectra of these molecules using the Gauge-Invariant Atomic Orbital (GIAO) method as implemented in Gaussian 98. The spin-spin coupling constant (J) has also been calculated from B3LYP/6-31G** using GAUSSIAN 03 version for all the three drugs. Besides this, B3LYP and HF method with 6-31G** basis set has been employed to compute the bond length, bond angle and dihedral angles.

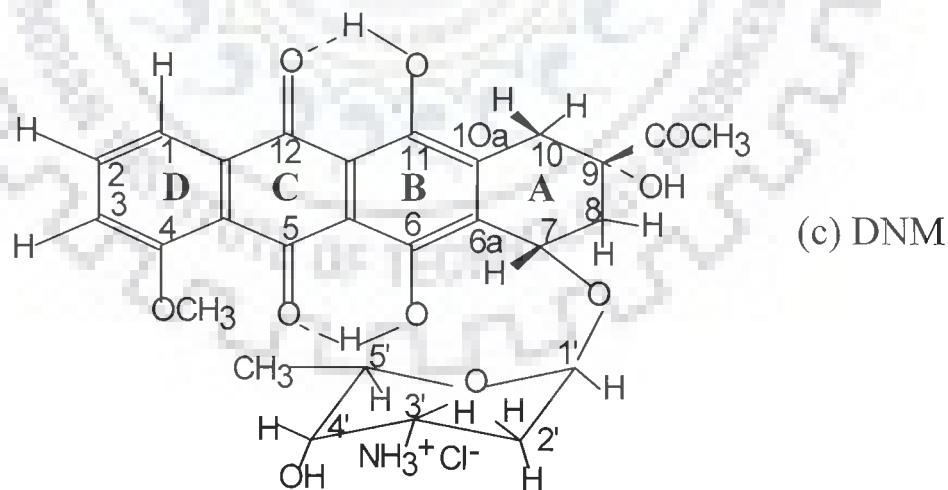
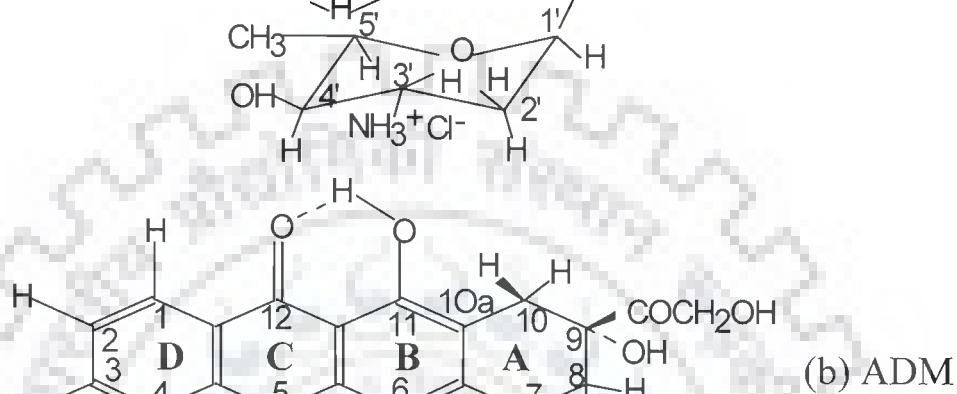
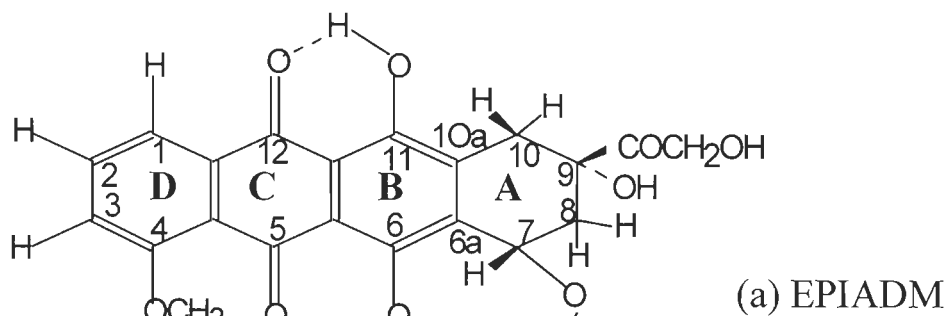


Fig. 1: Chemical Structure of (a) 4'-epiadriamycin (b) adriamycin (c) daunomycin

3.1 Results and Discussion

A. NMR Spectra of 4'-epiadriamycin

The proton NMR spectrum of 5.5 mM 4'-epiadriamycin in D₂O at 298 K and H₂O/D₂O (90:10 v/v) at 275 K is shown in Fig. 2(a-b). Expansions of specific regions of two dimensional dQF COSY and TOCSY spectra are shown in Fig. 3(a-e). Positions of NOESY spectra showing specific NOE connectivities are given in Fig. 4(a-b). The drug protons are assigned unambiguously following strategies adopted earlier for similar drugs, adriamycin (Barthwal et al., 1994) and daunomycin (Barthwal et al., 1996). The 6OH, 4'OH, 3NH₃⁺ and 11OH are observed in 1D NMR spectra at 275 K because of slow exchange with the water molecule, 5'CH₃ and 4OCH₃ peaks are easily recognized in the 1D NMR spectra of 298 K. The 2H, 1H and 3H protons are assigned on the basis of multiplicity pattern in 1D NMR spectra and their relative distance from 4OCH₃ protons in NOESY spectra. The daunosamine sugar protons get assigned by the connectivities in the dQF COSY, TOCSY and NOESY spectra. The pairs of doublets (8axH, 8eqH; 10axH, 10eqH) showing large geminal couplings in the region 2-3 ppm are assigned through their connectivities to 7H and 9CH₂OH protons. The chemical shifts of all protons thus obtained are listed in Table 1. To the best of our knowledge, the present NMR study is first characterization of 4'-epiadriamycin in literature. It is noted that the proton chemical shifts of 5.5 mM 4'-epiadriamycin are close to that observed in literature (Barthwal et al., 1996; Barthwal et al., 1994, Mondelli et al., 1987) for similar drugs, daunomycin and adriamycin. The differences in resonance positions are attributed to the slight variation in structure- conformation of the molecules.

The spin-spin coupling constant (J) has been estimated (Table 2) from splitting in 1D NMR spectra and cross peak patterns in dQF COSY spectra without carrying out spectral simulations. The couplings 5'H-4'H and 4'H-3'H, could not be estimated due to overlapping

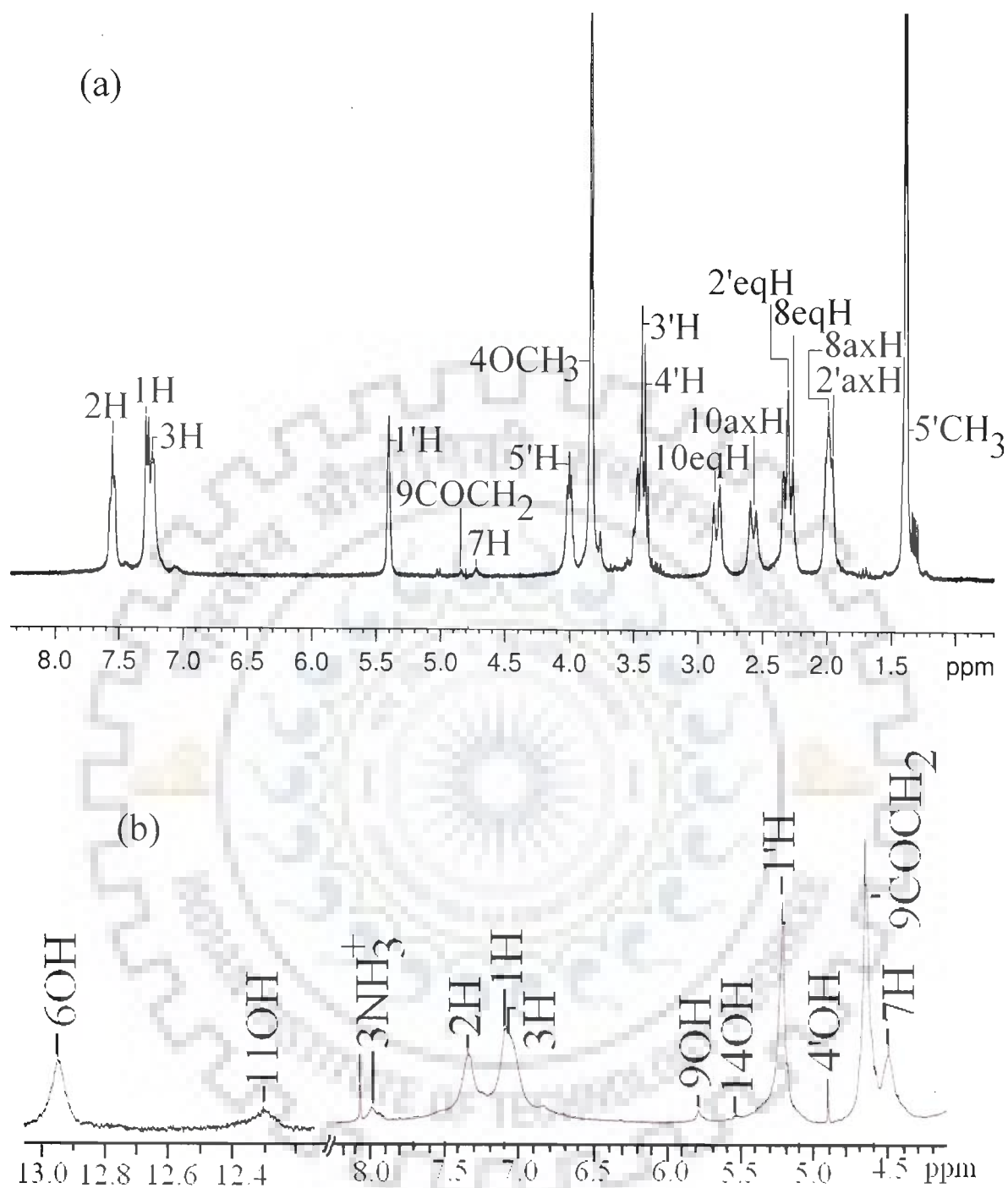
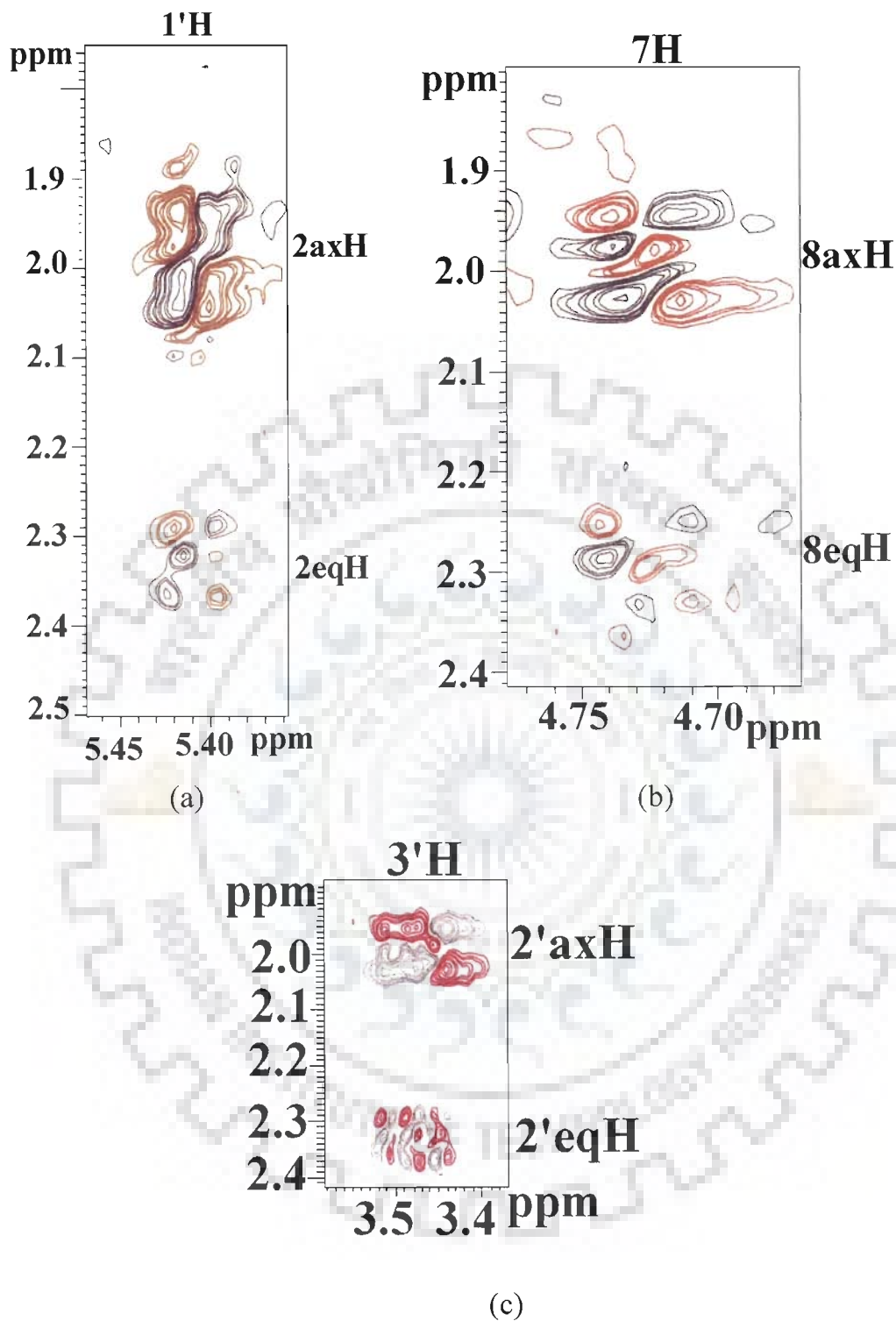


Fig. 2: 500 MHz 1D-Proton NMR spectra of 5.5 mM 4'-epiadriamycin in D_2O at (a) 298 K and (b) 275 K (pH=7.0).



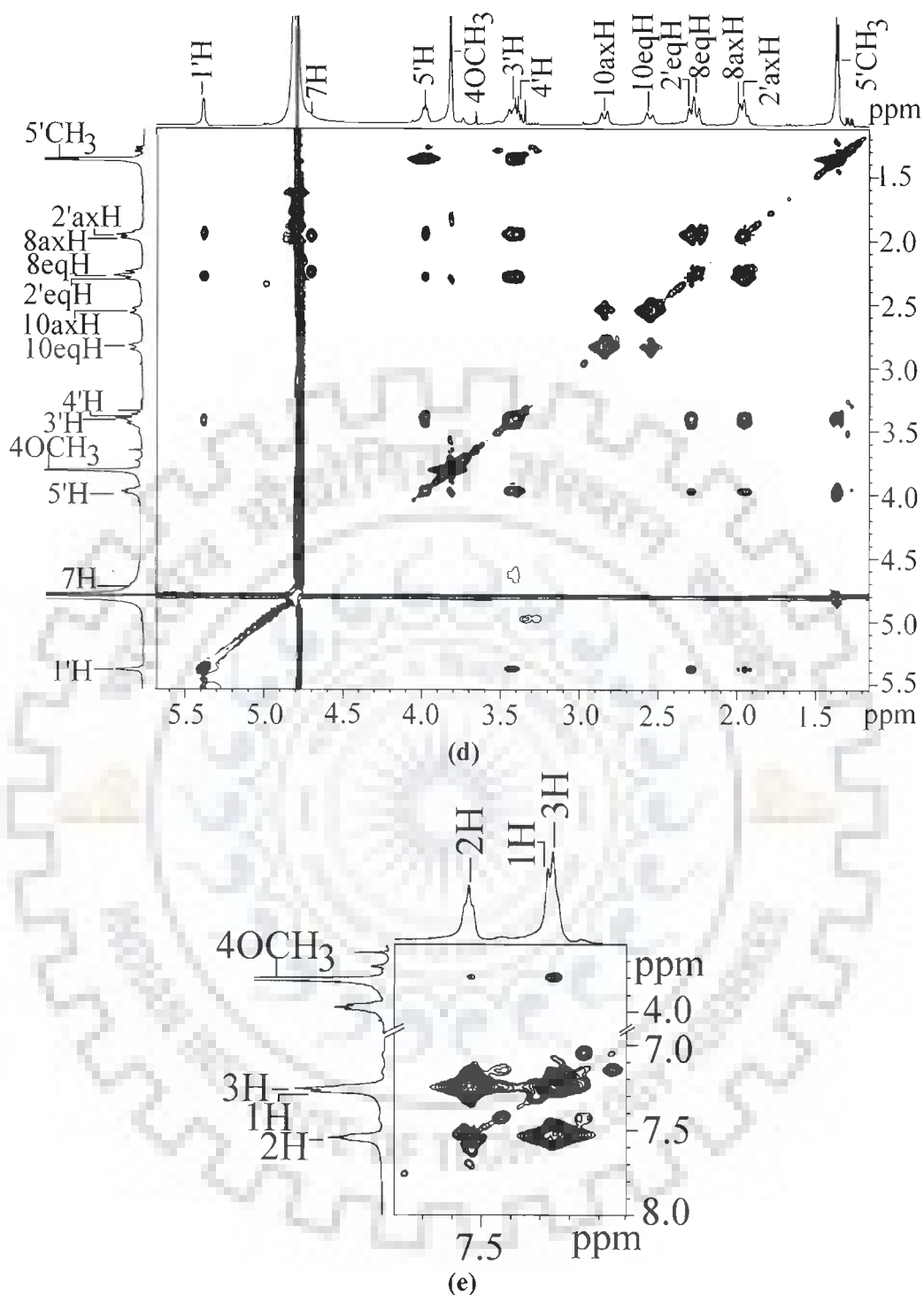
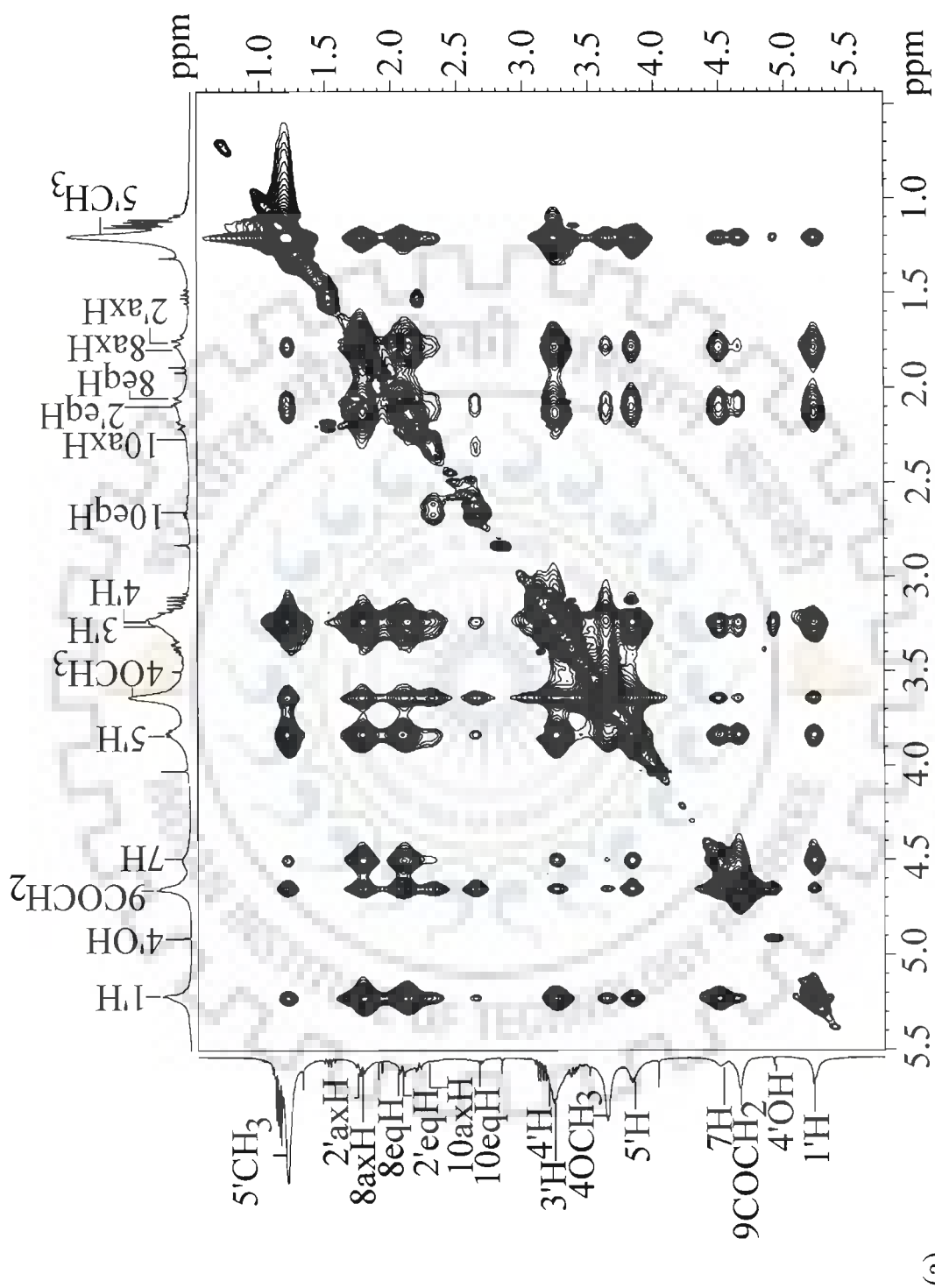
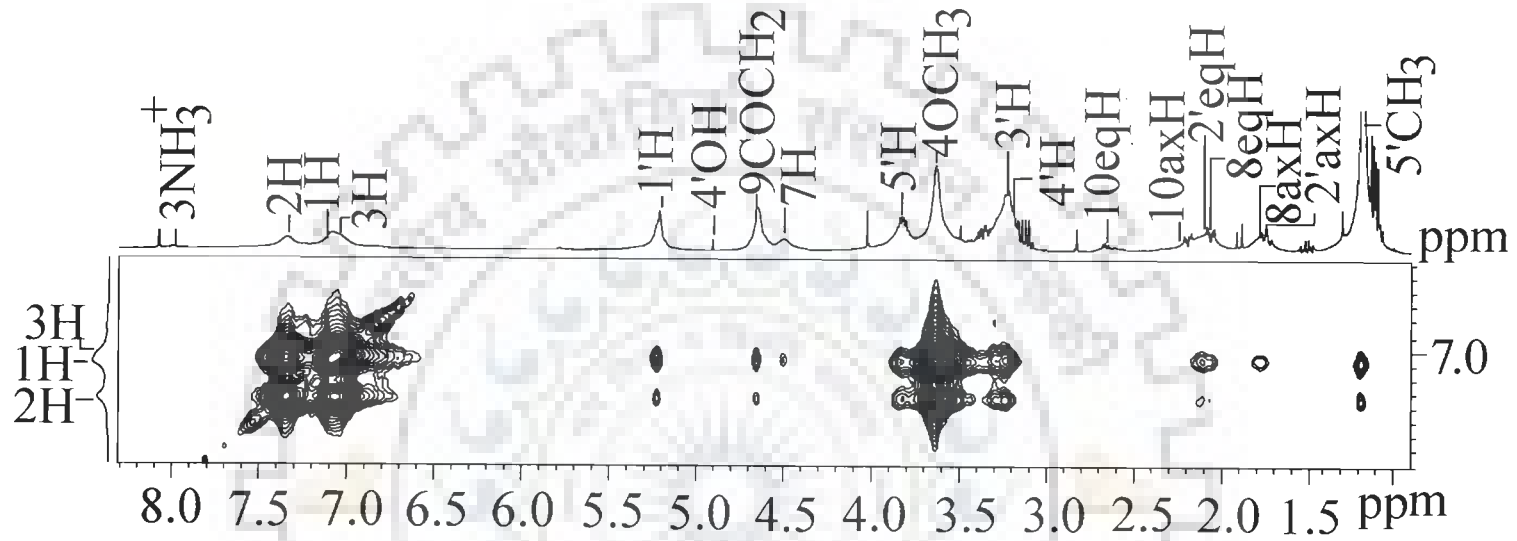


Fig. 3: Expansion of selected regions of 400 MHz dQF COSY spectrum of 5.5 mM 4'-epiadriamycin in D₂O at 298 K showing specific J-couplings correlations (a) 1'H with 2axH & 2eqH (b) 7'H with 8axH & 8eqH (c) 3'H with 2axH & 2eqH (d-e) Expansions of selected regions of 500 MHz TOCSY spectrum of 5.5 mM 4'-epiadriamycin in D₂O at 298 K





(b)

Fig. 4a-b: Expansion of selected portions of 500 MHz phase sensitive NOESY of 5.5 mM 4'-epiadriamycin in D₂O at 298 K showing specific through space correlations at $\tau_m = 400$ ms (a) 1'H, 7H, 5'CH₃ with 2axH, 2eqH, 8axH, 8eqH, 3'H, 4'H, 5'H protons (b) 1H, 2H, 3H, 7H, 1'H, 3'H, 4'H, 5'H, 2axH, 2eqH, 8axH, 8eqH, 10axH, 10eqH, 5' CH₃ with 3'H, 5'H, 1'H, 7H.

Table 1: NMR chemical shift values (in ppm) of 5.5 mM 4'-epiadriamycin (EPIADM) at 298 K and those reported in literature (Barthwal et al., 1996; Barthwal et al., 1994; Mondelli et al., 1987) for similar drugs, daunomycin (DNM) and adriamycin (ADM).

S.No.	Protons	EPIADM	ADM (Barthwal et al., 1994)	DNM (Barthwal et al., 1996)	ADM (Mondelli et al., 1987)	DNM (Mondelli et al., 1987)
1	1H	7.17	7.34	7.37	7.45	7.53
2	2H	7.51	7.61	7.62	7.66	7.71
3	3H	7.24	7.34	7.34	7.37	7.43
4	7H	4.70	4.80	4.80	4.82	4.82
5	8eqH	2.28	2.28	2.25	2.28	2.22
6	8axH	1.98	2.04	2.08	2.06	2.10
7	10eqH	2.83	2.93	2.89	2.95	2.92
8	10axH	2.55	2.60	2.65	2.68	2.67
9	1'H	5.40	5.48	5.48	5.43	5.48
10	2'eqH	2.33	2.04	2.04	1.98	1.96
11	2'axH	1.99	2.04	2.04	2.03	2.00
12	3'H	3.46	3.76	3.69	3.68	3.66
13	4'H	3.45	3.88	3.86	3.83	3.81
14	5'H	4.00	4.27	4.29	4.21	4.26
15	5'CH ₃	1.39	1.34	1.34	1.29	1.28
16	4OCH ₃	3.56	3.88	3.89	3.90	3.93
17	9COCH ₂ /9COCH ₃	4.70	4.80	2.46	4.79	2.43
18	*6OH	13.06				
19	*11OH	12.40				
20	*3NH ₃ ⁺	8.21				
21	*4'OH	3.53				

*observed at 275 K only

Table 2: Observed ^1H - ^1H coupling constants, (J in Hertz), and corresponding torsional angles, θ , in 4'-epiadriamycin, and those reported in literature (Barthwal et al., 1996; Barthwal et al., 1994; Mondelli et al., 1987) for similar drugs along with those obtained from DFT using B3LYP/6-31G**.

S.No.		EPIADM (Present work)			ADM (Barthwal et al., 1994)			DNM (Barthwal et al., 1996)			DNM (Mondelli et al., 1987)	ADM (Mondelli et al., 1987)
		J (B3LYP/6-31G**)	J (NMR)	θ	J (B3LYP/6-31G**)	J (NMR)	θ	J (B3LYP/6-31G**)	J (NMR)	θ	J	J
1.	7H-8axH	3.3	8.8	130.0	3.3	5.4	34.0	3.3	7.1	135.0	5.0	5.1
2.	7H-8eqH	3.2	6.6	26/36	3.2	w	60-100	3.2	w	60-100	2.4	2.5
3.	8eqH-8axH	16.1	14.1	156.0	16.0	15.6	-	16.0	12.5	-	15.0	15.0
4.	10eqH-10axH	18.6	18.0	-	18.6	18.5	-	18.9	18.6	-	18.0	18.6
5.	8eqH-10eqH	0.8	-	-	0.7	5.4	-	0.8	5.3	-	2.0	2.0
6.	1'H-2eqH	2.1	4.0	45/52	2.0	4.7	40.0	2.0	5.0	39.0	1.3	1.2
7.	1'H-2axH	2.5	8.0	0	2.9	7.3	14.8	2.9	6.1	29.0	3.9	3.8
8.	2eqH-2axH	12.7	14.0	15.5	12.5	13.4	-	12.5	14.0	-	13.1	13.0
9.	2axH-3'H	10.3	12.5	158-180	10.1	11.3	180.0	10.1	13.2	180.0	13.0	13.0
10.	2eqH-3'H	2.9	4.4	42.6/50	3.2	6.3	131.6	3.1	7.9	144.0	4.7	4.8
11.	5'H-4'H	7.0	-	-	2.0	5.4	35.0	2.0	6.7	20.0	1.4	1.3
12.	4'H-3'H	8.9	-	-	3.1	3.3	50.0	3.1	-	-	2.8	2.7
13.	5'H-5'CH ₃	5.7	6.3	38.0	6.0	13.6	180.0	6.0	13.3	180.0	-	-
14.	1H-2H	7.6	8.0	0	7.5	8.0	0	7.5	7.7	0	-	-
15.	2H-3H	8.2	8.2	0	8.3	8.7	0	8.3	8.5	0	-	-

of peaks in this region of spectra. The inter-proton distances were calculated from the NOESY spectra Fig. 4(a-b) recorded at $\tau_m = 400$ ms by integrating the volume of each cross peak. The distance between two protons 1H and 2H protons, $r(1H-2H) = 2.36 \text{ \AA}$, is used as an internal reference (Barthwal et al., 1994). Pseudo atom corrections were used for methyl and other equivalent protons. The inter-proton distance restraints for 4'-epiadriamycin, adriamycin and daunomycin are given. These restraints are compared with the results obtained earlier by X-ray (Neidle et al., 1977) and NMR spectroscopy techniques (Mondelli et al., 1987; Iwamoto et al., 1968; Cirilli et al., 1991; Barthwal et al., 1996; Barthwal et al., 1994) on similar drugs (Table 3). It is observed that within the ring A, the distances 10eqH-8axH, 10eqH-8eqH and 10axH-8eqH are higher in solid-state structure of daunomycin. Also inter-proton distances within daunosamine sugar, 1'H-3'H, 3'H-2'axH, 1'H-5'H are different from the corresponding distances in X-ray crystal structure. The 7H and 8axH protons are closer to 4'H/5'H and 5'CH₃ protons in solution structure of 4'-epiadriamycin. Some of the observed inter-proton distances in the 4'-epiadriamycin are different from the corresponding distances in the solution structure of other drugs. The notable differences in 1'H-4'H, 1'H-5'H, 7H-4'H, 7H-5'H, 8axH-5'CH₃ and 8'eqH-5'CH₃ distances show that conformation of daunosamine sugar and proximity of ring A to the sugar ring are not identical in these drugs. The proton NMR spectra of 4'-epiadriamycin and its analogues are also recorded at low concentration (0.01 mM) at which practically no self-association is expected. The chemical shifts are listed in Table 4.

The ¹H-¹³C Hetero-nuclear Single Quantum Coherence (HSQC) spectrum (Fig. 5a-c) of 4'-epiadriamycin shows the coupling of 14 carbon atoms to protons which are directly bonded through a single bond. The other 8 carbon atoms are easily assigned with the help of Hetero-nuclear Multiple Bond Correlation (HMBC) spectra (Fig. 6a-b). The observed carbon chemical shifts in all drugs and carbon-proton bond correlations in 4'-epiadriamycin are listed in Tables 5 and 6, respectively. Similar data has been obtained for adriamycin and

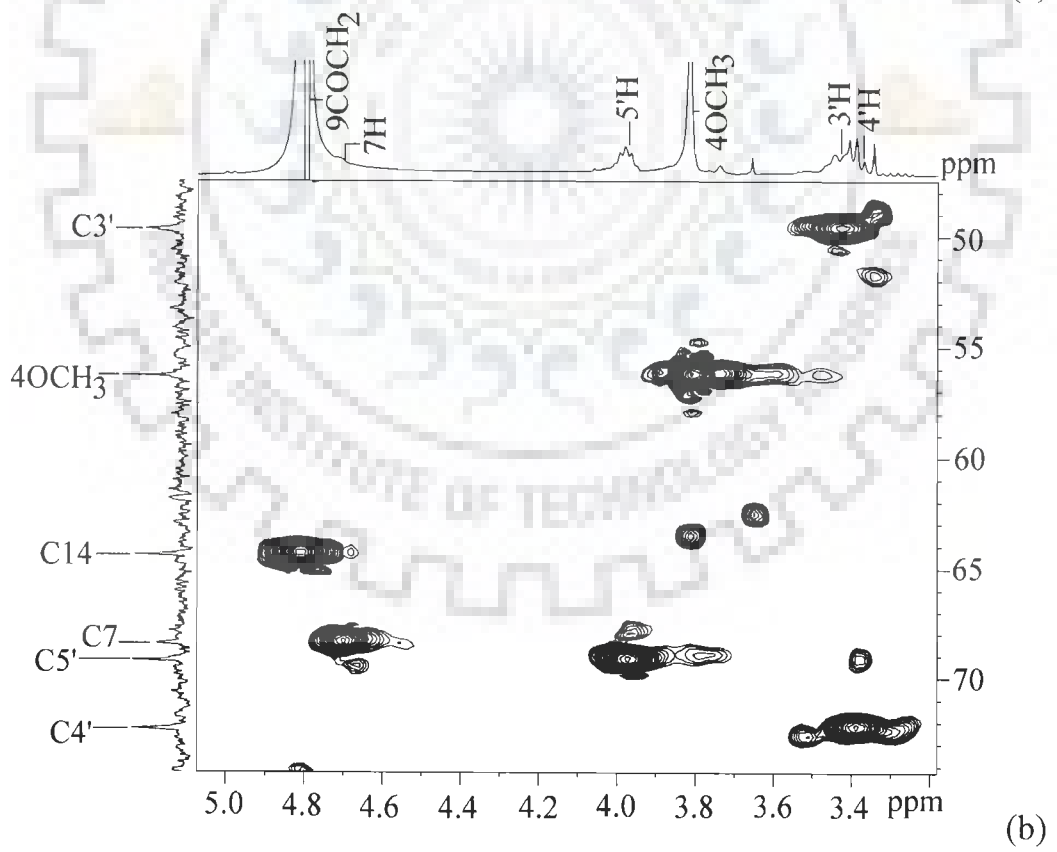
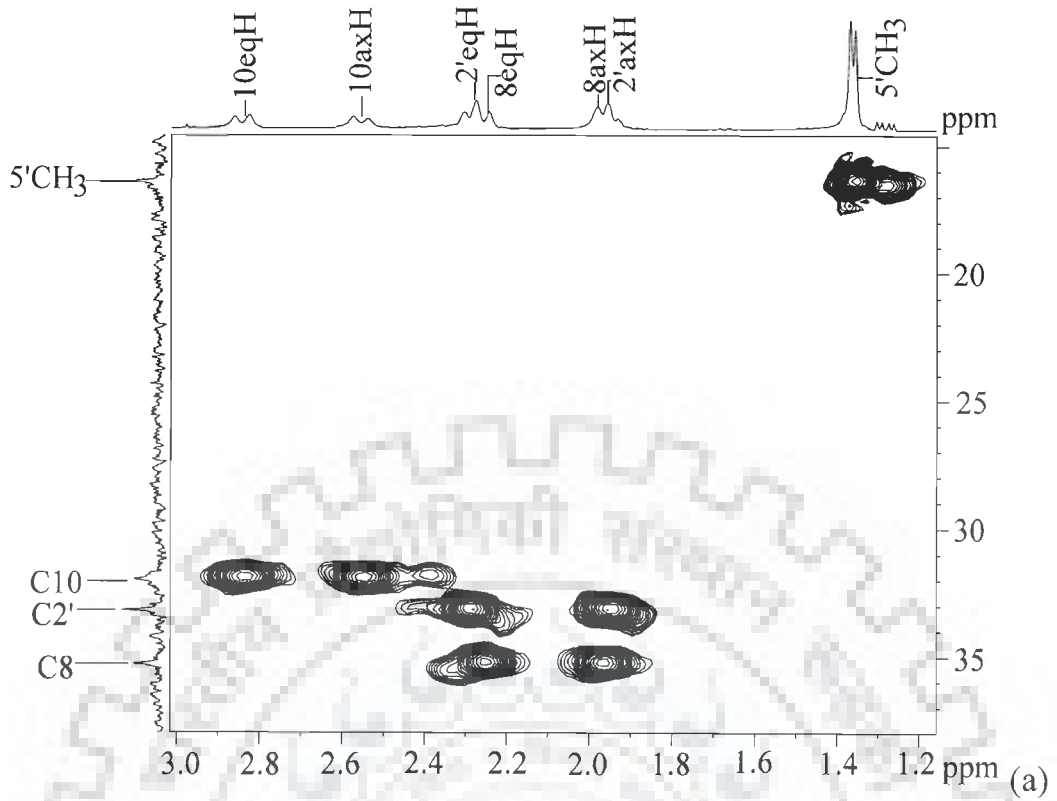
Table 3: The observed interproton distances (in Å) in 4'-epiadriamycin and those reported in literature for similar drugs using NMR (Barthwal et al., 1996; Barthwal et al., 1994; Mondelli et al., 1987) and X-ray Diffraction (Neidle et al., 1977; Courseille et al., 1979) techniques.

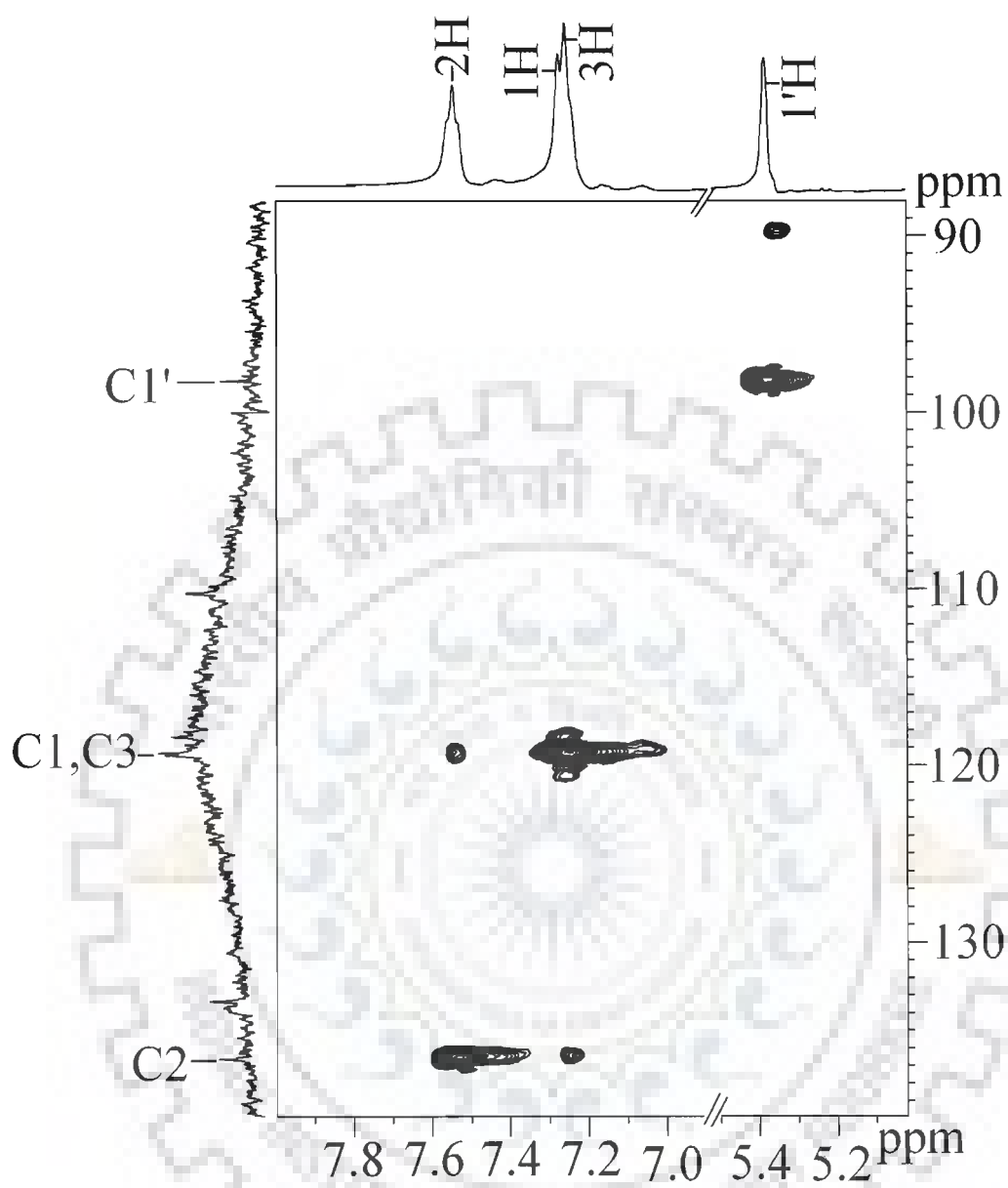
Connectivities	EPIAD M	ADM (Barthwal et al., 1994)	DNM (Barthwal et al., 1996)	n-acetyl DNM (Mondelli et al., 1987)	DNM-butanol (Courseille et al., 1979)	DNM (Neidle et al., 1977)
WITHIN RING D						
1H-2H	2.36	2.36	2.36		-	2.36
3H-2H	2.35	2.12	2.12			-
3H-4OCH ₃	2.32	2.05	2.08			-
2H-4OCH ₃	3.94	2.96	3.46			-
WITHIN RING A						
7H-8axH	2.49	3.30	3.46/2.30	2.30	2.33	2.36
7H-8eqH	2.46	W	W/2.45	2.45	2.42	2.40
10axH-10eqH	1.80	1.92	1.76			1.77
8axH-8eqH	o					
10eqH-8axH	3.12	3.01	2.71			3.71
10eqH-8eqH	3.06	2.96	2.98			4.25
10axH-8eqH	3.24	2.75	2.85			3.86
10axH-8axH	3.00	2.82	2.50			2.64
7H-10axH	3.63	-	-			-
7H-10eqH	3.71	-	-			-
9 CH ₂ OH-8axH	3.60	-	-			-
9 CH ₂ OH-8eqH	3.43	-	-			-
9 CH ₂ OH-10axH	3.73	-	-			-
9 CH ₂ OH-10eqH	3.62	-	-	-		
WITHIN SUGAR						
1'H-2'axH	2.39	2.31	2.31	2.21	2.34	2.56
1'H-2'eqH	2.45	2.28	2.29	2.35	2.39	2.53
1'H-4'H	3.12	3.22	4.58			4.90
1'H-3'H	3.12	3.30	3.40			3.76
4'H-5'H	2.40	2.16	2.27/2.35	2.35	2.33	2.45
5'H-5'CH ₃	2.65	-	-			-
3'H-2'axH	2.64	3.07	3.21			3.89
3'H-2'eqH	2.64	2.33	2.44			2.95
4'H-5'CH ₃	2.53	2.59	2.73			2.40
2'axH-2'eqH	o	-	-			-
1'H-5'H	4.17	3.69	3.54			3.66
RING A TO SUGAR PROTONS						
7H-1'H	2.89	3.24	2.88/2.17	2.19	2.20	2.22
7H-4'H	3.66	2.70	2.44			5.78
7H-5'H	3.62	3.02	2.70			3.65
8axH-5'H	2.87	2.50	2.63			4.35
8axH-5'CH ₃	3.75	2.60	2.87			4.75
8eqH-5'H	2.64	2.40	2.44/2.40	2.40	2.59	2.61
8eqH-5'CH ₃	3.27	2.84	3.75			3.28
9 CH ₂ OH-5'H	4.03	-	-			-
9 CH ₂ OH-4'H	4.17	-	-	-		

Table 4: Comparison of NMR Proton chemical shifts (ppm) with calculated chemical shifts (ppm) by GIAO method using B3LYP and HF methods and 6-31G** wavefunction for various drugs.

Proton	CALCULATED						NMR		
	HF/6-31G**			B3LYP /6-31G**			(Conc. 0.01mM in D ₂ O)		
	EPIADM	ADM	DNM	EPIADM	ADM	DNM	EPIADM	ADM	DNM
1H	8.640	8.558	8.608	8.473	8.461	8.465	7.810	7.860	7.770
2H	8.518	8.407	8.496	8.136	8.136	8.117	7.850	7.870	7.820
3H	7.372	7.330	7.364	7.282	7.292	7.278	7.550	7.580	7.550
7H	4.897	4.561	4.909	5.404	5.449	5.430	4.600	4.690	5.000
8eqH	2.196	2.137	2.129	2.337	2.342	2.358	2.180	2.280	2.210
8axH	1.656	1.510	1.652	1.996	1.984	1.903	2.130	2.160	2.140
10axH	2.803	2.790	2.729	2.801	2.767	2.687	2.920	2.900	2.880
10eqH	3.002	2.887	2.958	3.466	3.460	3.628	3.100	3.160	3.030
9OH	3.653	3.323	3.650	4.759	4.793	4.797	-	-	-
[#] 9COCH ₂ /9COCH ₃	4.461	4.455	2.455	5.042	5.030	2.560	4.860	4.770	2.350
14OH	2.236	2.254	-	2.604	2.601	-	-	-	-
[#] 4OCH ₃	3.932	3.890	3.926	4.124	4.138	4.127	3.950	4.020	4.000
1'H	4.941	4.975	5.002	5.519	5.602	5.609	5.460	5.540	5.500
2'axH	1.248	1.827	1.940	1.560	2.251	2.240	1.870	1.880	1.860
2'eqH	3.311	2.525	3.100	3.898	3.698	3.708	2.310	1.880	1.860
3'H	3.364	4.238	3.318	3.641	3.668	3.677	3.310	3.580	3.370
4'H	2.820	3.097	2.880	3.261	3.492	3.494	3.130	3.760	3.660
5'H	3.319	3.421	3.224	4.023	4.036	4.057	4.010	4.260	4.210
[#] 5'CH ₃	1.347	1.439	1.338	1.324	1.295	1.296	1.330	1.250	1.230

[#]Pseudoatoms





(c)

Fig. 5(a-c): HSQC spectra of 4'-epiadriamycin in D₂O showing ¹H-¹³C single bond correlations

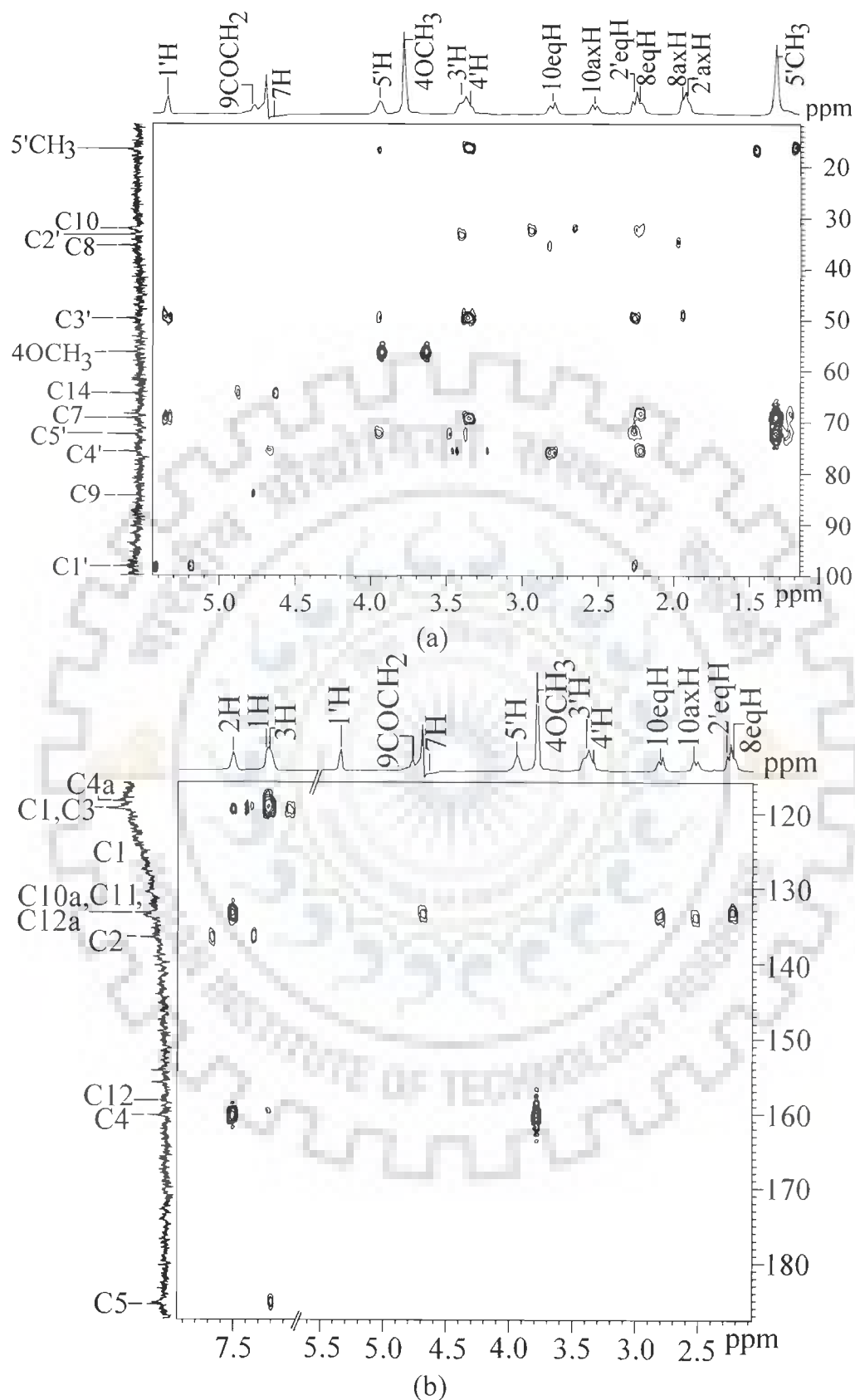


Fig. 6(a-b): Expansions of specific regions of HMBC spectra of 4'-epiadriamycin in D₂O showing ¹H - ¹³C multiple bond correlations

Table 5: Comparison of NMR Carbon chemical shifts (ppm) with calculated chemical shifts (ppm) by GIAO method using B3LYP and HF methods and 6-31G** wavefunction for various drugs.

Carbon	CALCULATED						NMR		
	HF/6-31G**			B3LYP /6-31G**			(D ₂ O)		
	EPIADM	ADM	DNM	EPIADM	ADM	DNM	EPIADM	ADM	DNM
C1	119.441	118.779	119.364	120.360	120.341	120.263	119.210	119.020	119.360
C2	143.504	141.630	143.193	136.110	136.137	135.964	136.440	136.290	136.510
C3	112.465	112.552	112.458	112.550	112.624	112.436	119.210	119.020	119.360
C4	159.359	159.350	159.106	157.500	157.439	157.303	160.500	160.320	160.320
C5	194.255	189.472	193.964	188.150	188.042	188.039	185.500	185.400	185.400
C6	145.564	148.954	145.428	149.760	149.561	149.481	-	-	-
C7	60.540	60.778	60.676	70.700	70.656	70.837	68.290	68.400	68.500
C8	30.977	29.506	31.388	36.200	36.409	36.216	35.230	34.920	34.880
C9	69.500	69.026	69.769	80.190	80.267	81.052	84.000	83.500	85.000
C10	31.296	31.506	31.749	36.090	36.115	36.095	31.380	31.650	31.220
C11	147.870	145.849	147.884	147.720	147.698	147.880	134.000	134.000	134.300
C12	173.341	174.675	173.622	173.420	173.361	173.423	160.000	160.000	160.000
C12a	141.263	140.858	141.296	132.930	132.865	132.927	133.000	133.000	134.100
C4a	116.347	116.701	116.519	117.210	117.163	117.211	118.000	118.000	118.000
C5a	117.326	115.813	116.890	115.440	115.356	115.128	-	-	-
C11a	118.836	122.410	118.273	113.740	113.454	113.131	-	-	-
C6a	128.443	124.899	128.837	126.050	126.429	126.598	-	-	-
C10a	135.578	135.122	136.469	133.590	133.728	135.423	133.000	133.000	133.500
9COCH ₂ /9COCH ₃	59.724	59.685	25.333	66.450	66.452	26.252	64.280	63.900	24.300
4OCH ₃	50.188	49.892	50.172	54.810	54.855	54.801	56.120	56.000	56.500
C1'	82.975	81.719	83.434	96.550	97.382	97.382	98.140	98.670	99.000
C2'	30.666	25.504	25.995	35.190	29.413	29.441	33.150	30.530	30.680
C3'	51.520	52.382	50.604	58.260	58.158	58.141	49.500	46.500	46.700
C4'	65.266	60.692	62.518	74.160	71.517	71.544	72.200	71.200	71.400
C5'	63.112	59.188	60.254	73.610	70.489	70.466	69.080	66.000	66.500
5'CH ₃	17.555	16.164	16.078	17.800	15.944	15.956	16.460	15.610	15.610

Table 6: Observed correlation of carbon atoms with specific protons in HSQC and HMBC spectra of 4'-Epiadriamycin

Carbon	HSQC	HMBC		
		ss	m	w
C1	1H	1H, 3H	-	2H
C2	2H	2H	-	-
C3	3H	3H, 1H	-	2H
C4	-	4OCH ₃₁ , 4OCH ₃₂ , 4OCH ₃₃	2H	-
C5	-	-	-	3H
C7	7H	5'CH ₃₁ , 5'CH ₃₂ , 5'CH ₃₃	8eqH	3'H, 4'H
C8	8axH, 8eqH	-	10eqH	8axH, 8eqH
C9	-	-	-	9COCH ₂₁ , 9COCH ₂₂
C10	10axH, 10eqH	-	-	10axH, 10eqH, 8eqH
C11	-	-	10axH, 10eqH	-
C12	-	2H	1H	-
C12a	-	2H	-	-
C4a	-	-	1H, 3H	-
C10a	-	2H	-	-
9COCH ₂	9COCH ₂₁ , 9COCH ₂₂	-	9COCH ₂₁ , 9COCH ₂₂	-
4OCH ₃	4OCH ₃₁ , 4OCH ₃₂ , 4OCH ₃₃	4OCH ₃₁ , 4OCH ₃₂ , 4OCH ₃₃	-	5'H
C1'	1'H	-	2'eqH	-
C2'	2'axH, 2'eqH	-	-	3'H, 2'axH, 2'eqH
C3'	3'H	3'H	1'H, 2'eqH, 4'H	2'axH, 5'H
C4'	4'H	5'CH ₃₁ , 5'CH ₃₂ , 5'CH ₃₃	2'eqH, 5'H	3'H
C5'	5'H	5'CH ₃₁ , 5'CH ₃₂ , 5'CH ₃₃	2'eqH, 4'H, 3'H	1'H
5'CH ₃	5'CH ₃₁ , 5'CH ₃₂ , 5'CH ₃₃	5'CH ₃₁ , 5'CH ₃₂ , 5'CH ₃₃	3'H, 4'H	5'H

ss- Very intense, m- Fairly intense, w- Weak intense

daunomycin (spectra not shown here). The carbon chemical shifts of these drugs have been assigned for the first time in the present study.

B. Conformational studies of 4'-epiadriamycin, adriamycin and daunomycin using Restrained Molecular Dynamics

Restrained molecular dynamics permits the system to undergo conformational and momentum changes so that different parts of the phase space accessible to the molecule can be explored and stable conformations are identified by energy minimization. The initial structure of 4'-epiadriamycin, adriamycin and daunomycin was built using builder module in MOE. In the present case, simulations are carried out for 25 ps. The structure obtained with and without NMR constraints are found to be quite different. This confirms that the structure is indeed defined by experimental restraints and not by the refinement procedure or variables used. During the final equilibrium stage, there is no significant change in either the potential energy or restraint deviation energy. The various structures at these time intervals differed only marginally from each other and hence indicate that the structure obtained is a minimum energy conformer. In all, 25 structures are saved at the regular interval of 1 ps out of which, only the minimum energy conformer is used for the analysis. In all the drug molecules, the root mean square deviation between any of the rMD structures and their starting structures is quite large but among various final structures it is very low. This is generally taken as an indication that the convergence has been achieved. Table 7 indicates an assessment of refined structures in terms of energetics including restraint violation energies with respect to the atomic coordinates, e.g., for daunomycin, the total potential energy of final structures is lower ($137 \text{ Kcal mole}^{-1}$) than that for the corresponding starting structure ($156 \text{ Kcal mole}^{-1}$). The forcing potential, which indicates contribution to potential energy due to violation of both experimental distance and torsional angle data, exhibit much lower values for all the final structures ($40\text{-}89 \text{ Kcal mole}^{-1}$) in comparison to that in their starting structures ($383\text{-}861 \text{ Kcal}$

Table 7: Energy terms (Kcal mol⁻¹) for starting model and final rMD structure.

Energies	EPIADM		ADM		DNM	
	Initial	Final	Initial	Final	Initial	Final
Total	144	136	211	188	156	137
Bond	15	16	25	23	22	23
Angle	36	28	65	53	42	38
Dihedral	15	35	13	24	16	22
Van der Waal	75	72	92	83	70	65
Repulsion	181	175	270	264	236	227
Dispersive	-106	-103	-178	-181	-166	-162
Electrostatic	4	-17	14	-0.8	4	-14
Restraint violation	-76	-70	-90	-77.2	-68	-62

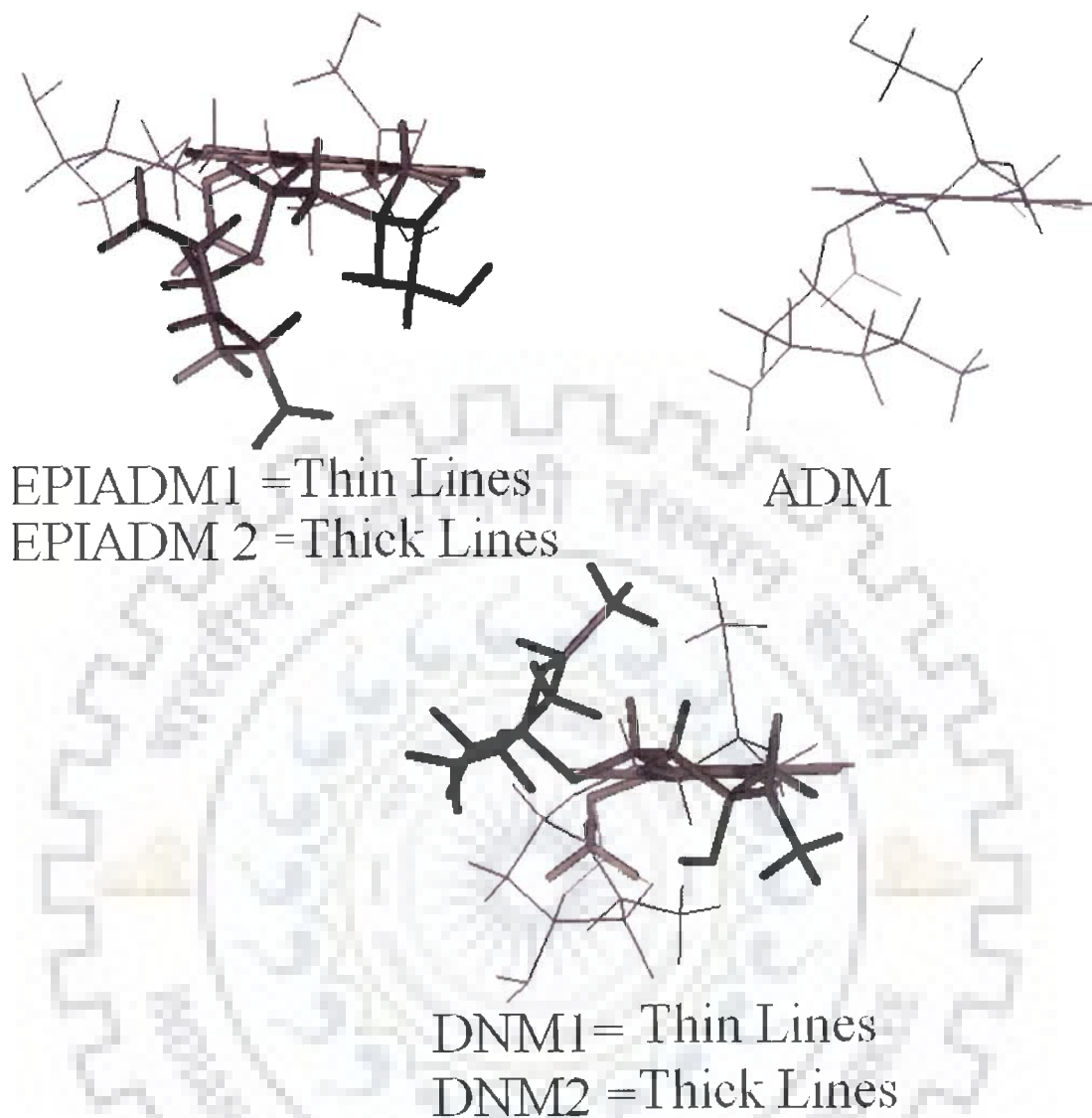


Fig. 7: Side view of different conformations of the drugs, EPIADM1=thin lines, EPIADM2=thick line, DNM1=thin line, DNM2=thick line, ADM

mole⁻¹). The energy gradient with respect to atomic coordinates is 0.1-0.2 Kcal mole⁻¹Å⁻¹. The side view of the superimposed conformers of all the three drugs obtained in rMD simulations is shown in Fig. 7.

To gain insight into the structural details, we have examined the trajectory (Fig. 8 a-c) of various torsional angles during the course of rMD simulations upto 25 ps. Within Ring A, the torsional angle C10-C10a-C6a-C7 is close to 0° and fluctuates within a small range of angles, being attached to the aromatic moiety, the ring BCD. The torsional angles C9-C10-C10a-C6a and C10a-C6a-C7-C8 also show variations within a small range of angles. The other three torsional angles within the cyclohexane ring A, show larger variations and adopt gauche⁺ or gauche⁻ conformations so that the atom C8 or C9 often is not coplanar with C7, C6a, C10a and C10 atom (Fig. 9). It is observed that in 4'-epiadriamycin, the conformer 1-11 have torsional angle C7-C8-C9-C10 as gauche⁺ and then adopts gauche⁻ conformation (conformer 12-25) during the course of simulations. The corresponding angle, C6a-C7-C8-C9 and C8-C9-C10-C10a also changes from one torsional value to another. Apparently the drug can adopt two distinct conformations and it flips from one conformational state to other with time. The glycosyl angle measured as C8-C7-O7-C1' or C6a-C7-O7-C1' remain the same but C7-O7-C1'-O5' or C7-O7-C1'-C2' decrease by about 30° with time. The torsional angles within the daunosamine sugar show similar behavior during the course of the simulations. Thus there are two conformational states one in 1-11 ps and other in 12-25 ps (Fig. 10). The two distinct conformations of 4'-epiadriamycin are referred to as epiadm 1 and epiadm 2 and the various torsional angles observed are listed in Table 8. The results on adriamycin show that the various torsional angles within ring A, glycosyl linkage and amino sugar do not vary significantly. The molecule appears to be confined in a single preferred conformational state. The torsional angles within ring A and glycosyl linkage in adriamycin are close to that

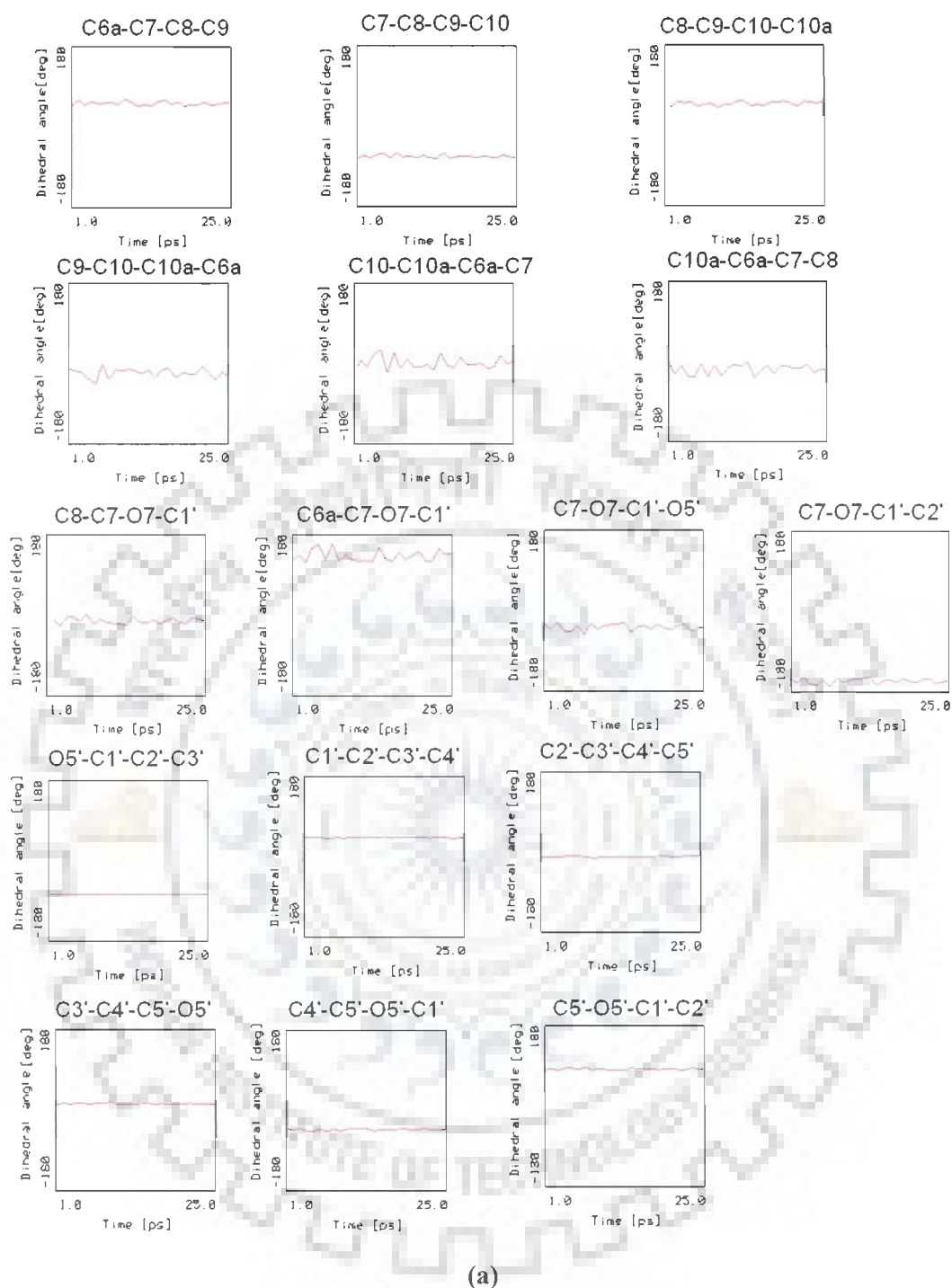
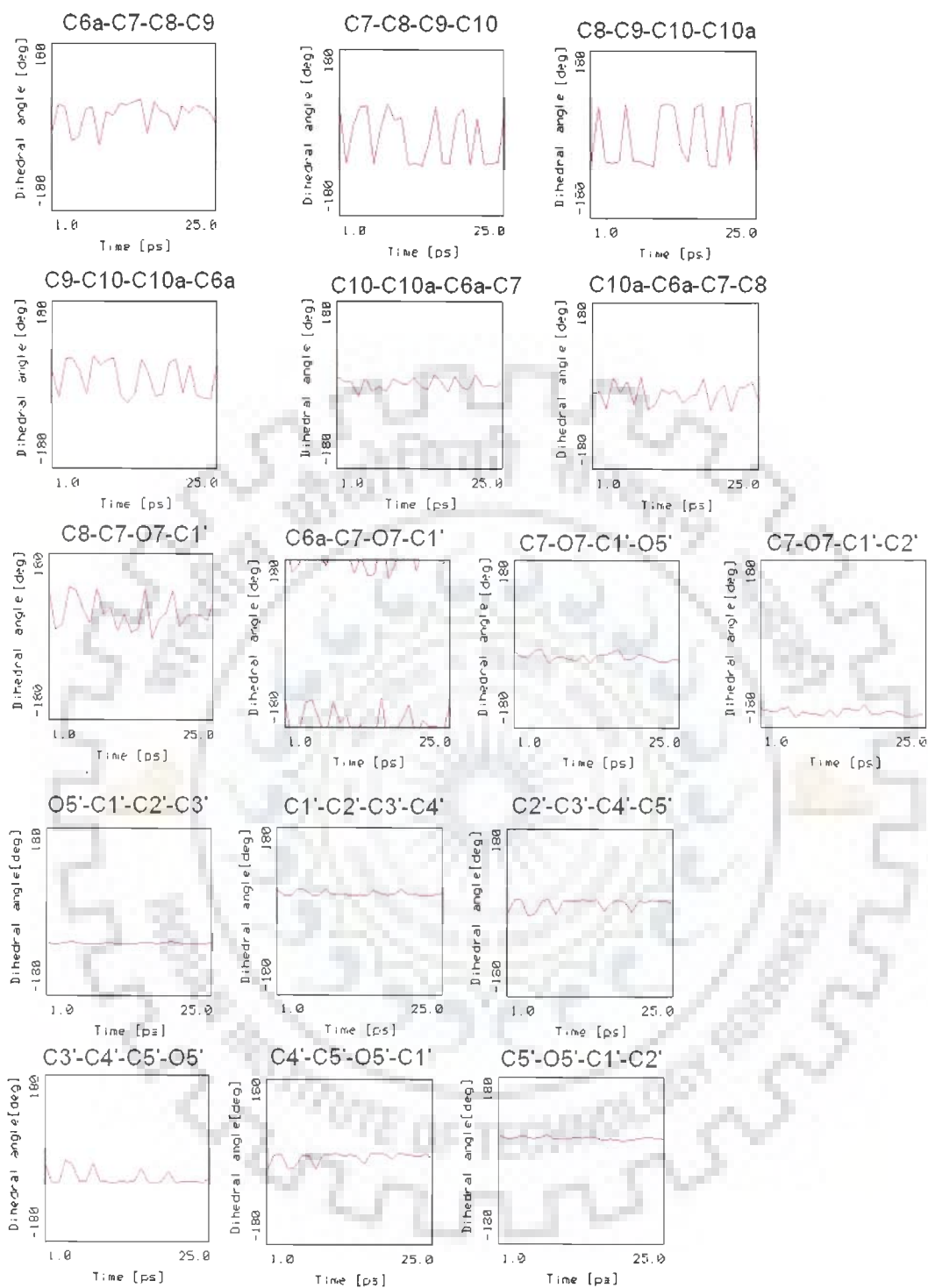
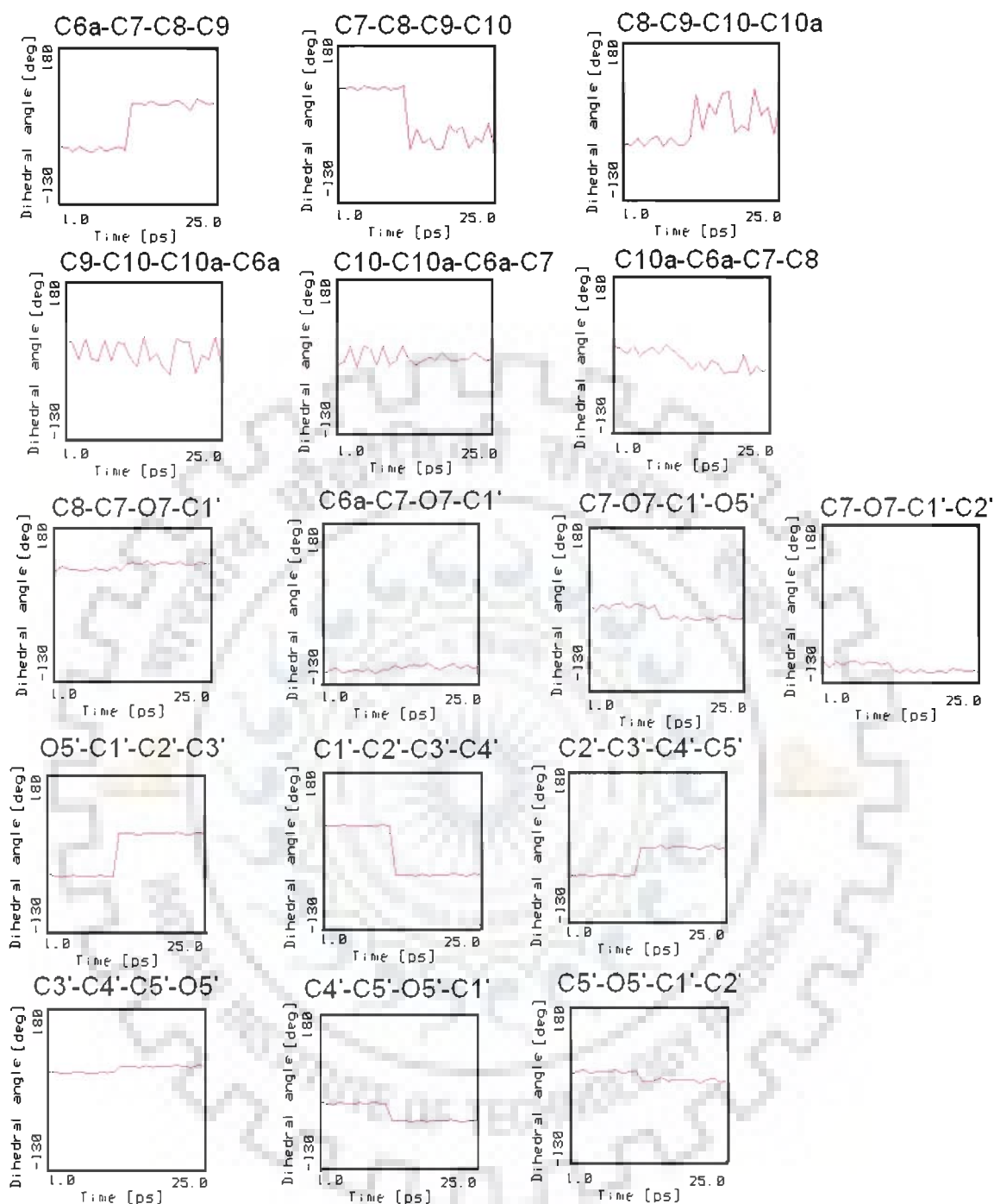


Fig. 8(a-c): Trajectory analysis of 25 ps restrained molecular dynamics simulations in all three drugs showing variations in ring A, glycosyl linkage and amino sugar of (a) adrimycin (b) daunomycin (c) 4'-epidriamycin



(b)



(c)

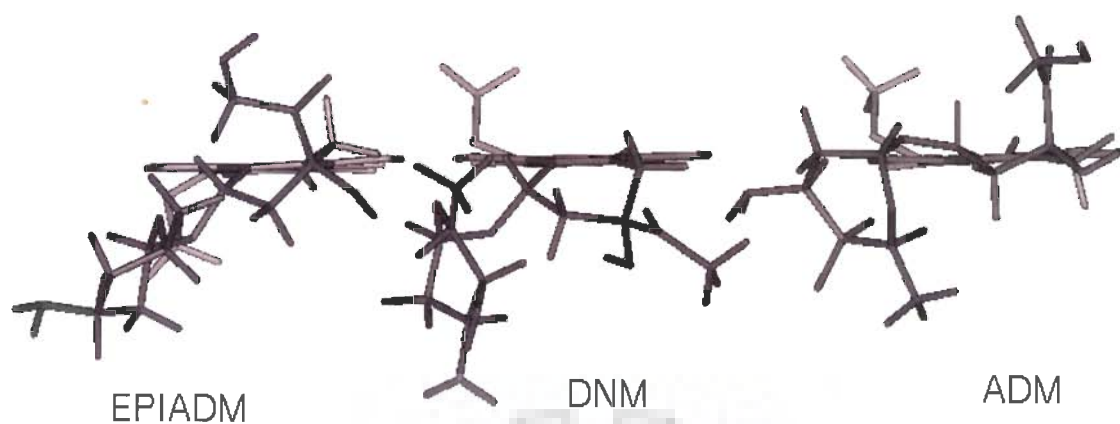


Fig. 9: Orientation of ring A and amino sugars in different conformations superimposed over each other in 4'-epiadriamycin, adriamycin and daunomycin

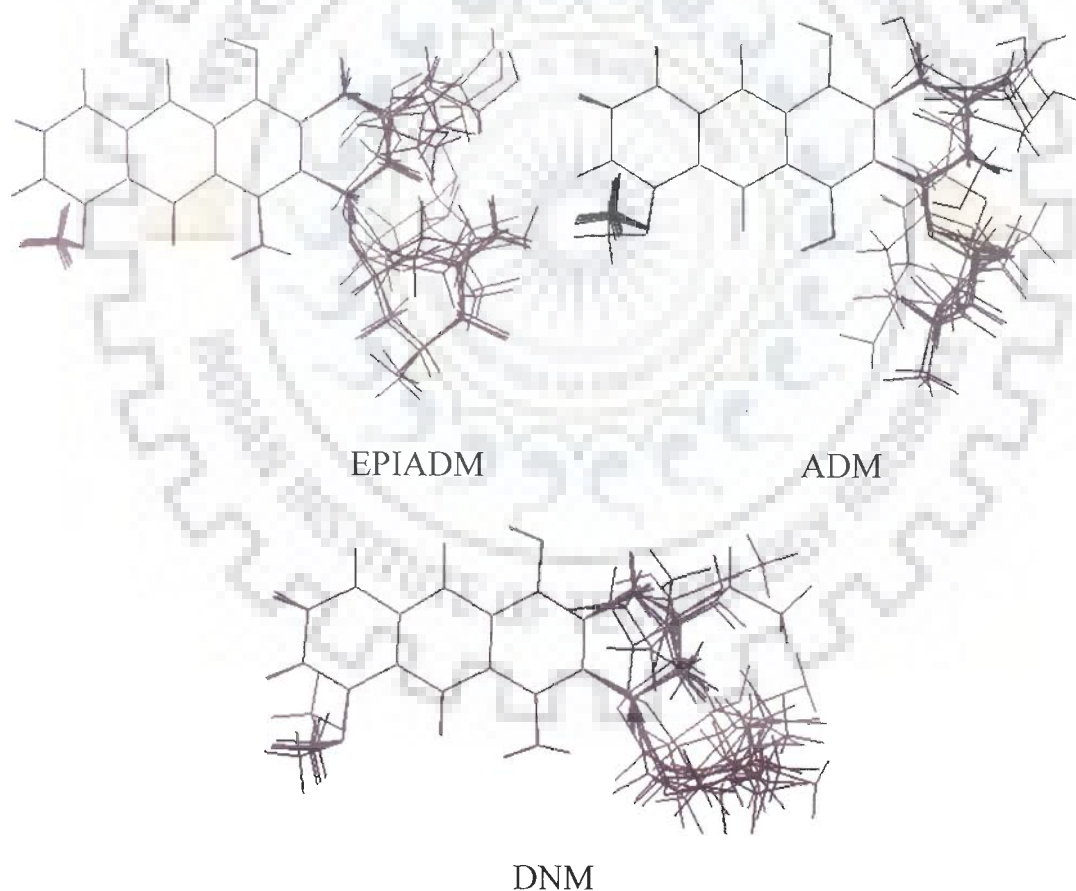


Fig. 10: Superimposition of 6 conformers obtained after carrying out rMD simulations for 1, 5, 10, 15, 20 and 25 ps in 4'-epiadriamycin, adriamycin and daunomycin

observed in epiadm 2 conformer but those within daunosamine sugar are closer to the corresponding torsional angles in epiadm 1 conformer (Table 8). The observed results of rMD simulations in daunomycin are different from that of adriamycin and 4'-epiadriamycin. The daunomycin molecule shows frequent transition from one conformational state to another throughout the course of rMD simulations. The torsional angle C10-C10a-C6a-C7, as expected shows minimum variation, being close to 0°. The torsional angle C7-C8-C9-C10 shows maximum flexibility and flips between gauche⁺ and gauche⁻ conformations. The torsional angles in two observed conformations (referred to as dnm 1 and dnm 2) are listed in Table 8. In daunomycin the glycosyl linkage C7-O7-C1'-O5' remain same in both conformers in contrast to that in 4'-epiadriamycin, in which the angle adopts two different conformations, but the glycosyl linkage C8-C7-O7-C1' or C6a-C7-O7-C1' remains unchanged. The difference in torsional angles within the daunosamine sugar is comparatively smaller in the daunomycin molecule. Table 9 shows the connectivities and inter-proton distances (Å) from NOESY spectra of the drugs and the corresponding distances obtained from optimized rMD structures. It is seen that the distances obtained from the rMD structures show only slight NOE violations.

C. Quantum Mechanical Calculations

Structural Parameters

In the present work, B3LYP functional with 6-31G** basis set has been employed to compute the bond length, bond angle and dihedral angles for the drugs along with HF calculations with the same basis set (Table 10a-c). It is noted that there is a great scatter of both DFT and HF results predicted with smaller basis sets (not shown here) but as we move towards better basis set, the difference between the calculated and experimental results narrows down. It is believed that polarization function at least must be used. Further, the presence of diffuse functions may improve the results, particularly for charged species. Unfortunately calculations using such functions are very expensive and time consuming and

Table 8: Observed values of torsional angles (θ) obtained after restrained molecular dynamics simulations and those observed in literature (Von Dreele et al., 1977; Anguilli et al., 1971; Neidle et al., 1977; Mondelli et al., 1987; Nakata et al., 1980).

	Carminomycin I Hydrochloride (Von Dreele et al., 1977)	N-Br-acetyl DNM (Anguilli et al., 1971)	DNM (Neidle et al., 1977)	n-acetyl DNM (Mondelli et al., 1987)	EPIADM		DNM		ADM	ADM-NH ₂ (Nakata et al., 1980)		ADM NH ₃ ⁺ (Nakata et al., 1980)		DNM-NH ₂ (Nakata et al., 1980)		DNM NH ₃ ⁺ (Nakata et al., 1980)		
					EPIAD M1	EPIA DM2	DNM 1	DNM 2		Con1	Con2	Con1	Con2	Con1	Con2	Con1	Con2	
RING A																		
C6a-C7-C8-C9	-48	-43	-48		-48	53	-21	47	47									
C7-C8-C9-C10	62	62	58		66	-70	57	-67	-73									
C8-C9-C10-C10a	-45	-61	-38		-65	45	-61	57	55									
C9-C10-C10a-C6a	18	39	14		48	-20	26	-30	-12									
C10-C10a-C6a-C7	-5	-25	-5		-24	24	-4	12	-18									
C10a-C6a-C7-C8	20	29	20		24	-20	-19	-50	-18									
GLYCOSYL																		
H1'-C1'-O7-C7				40							Con1	Con2	Con1	Con2	Con1	Con2	Con1	Con2
C8-C7-O7-C1'	117	102	125	125	79	79	103	15	-21	-101	77	-101	77	-102	79	-102	79	
C6a-C7-O7-C1'	-120	-120	-114	115	-157	-157	-119	150	130									
C7-O7-C1'-O5'	-70	-89	-68		-2	-35	-17	-17	-31	-103	-72	-103	-72	-103	-71	-103	-72	
C7-O7-C1'-C2'	167	162	167	170	-161	-143	-158	-142	-156	138	158	138	158	138	158	138	158	
AMINO SUGAR																		
C1'O7-C7-H7				0														
O5'-C1'-C2'-C3'	-50	-55	-54	-54	-46	49	-68	-68	-77									
C1'-C2'-C3'-C4'	50	62	56	55	59	-52	41	41	41									
C2'-C3'-C4'-C5'	-55	-65	-61	-60	-64	0	0	24	-10									
C3'-C4'-C5'-O5'	59	63	61	61	43	58	-10	-52	9									
C4'-C5'-O5'-C1'	-61	-65	-59	-58	-25	-66	-18	14	-43									
C5'-O5'-C1'-C2'	55	60	57	60	29	-12	56	56	71									

are abandoned owing to memory limitations. The results for HF and DFT calculations on these compounds differ. For example, DFT predicts results which compare better with our experimental as well as X-ray results (Neidle et al, 1977). For 4'-epiadriamycin molecule, we found that all the calculated bond lengths are very close to the present solution structure based on NMR experimental data and also compare reasonably well with the X-ray measurements reported in literature; the difference lies within a few hundredth of an angstrom. A similar trend is also seen for the bond angles.

The maximum variation in the calculated and measured values is less than 5° except those angles which are related to $4OCH_3$ group position, for example, the angles $C3'-C4'-C5'$ and $C3'-C4'-4'O$ have a difference of about $\sim 10^\circ$ and 11° , respectively. From the analysis of bond lengths and bond angles, we notice that such differences between calculated and measured values arise due to the fact that structurally the molecule is in dynamic state in solution phase (i.e. cyclohexyl ring A, daunosamine sugar and glycosidic bond) as compared to the gas phase optimized structure of the molecule. Somewhat similar results have been observed for adriamycin and daunomycin but with the slight variation. For example, $C6a-C7-O7$ and $C7-O7-C1'$ angles have a difference of about $\sim 20^\circ$ and 5° , respectively. It is seen that the daunosamine sugar moiety of the three drugs adopts syn conformation, thus forming hydrogen bond between $6OH$ and $9OH$ of the chromophore with $3NH_3^+$, $O7$ and $O5'$ of the daunosamine sugar moiety (Fig. 11a). Thus these structures are different from what we obtained through rMD simulations (Fig. 11b) where the daunosamine sugar moiety has anti conformation.

Chemical Shift

All the 1H and ^{13}C chemical shifts were referenced to those of tetra methyl silane (TMS). The absolute 1H and ^{13}C shielding of TMS based on the B3LYP and HF were calculated at the same level basis set used in the calculation to which they refer. In this way we compute

Table 9: Interproton distances (Å) from NOESY spectra of 4'-Epiadriamycin, Adriamycin (Barthwal et al., 1994) and Daunomycin (Barthwal et al., 1996). The corresponding distances obtained from optimized rMD structure are also shown. 'W' denotes very weakly intense NOE cross peak corresponding to distance ~ 4-5 Å.

Connectivities	NMR			rMD		
	EPIADM	ADM (Barthwal et al., 1994)	DNM (Barthwal et al., 1996)	EPIA DM	ADM	DNM
WITHIN RING D						
1H-2H	2.36	2.36	2.36	2.49	2.52	2.50
3H-2H	2.35	2.12	2.12	2.39	2.52	2.56
3H-4OCH ₃	2.32	2.05	2.08	2.36	2.41	2.66
2H-4OCH ₃	3.94	2.96	3.46	3.87	3.62	3.87
WITHIN RING A						
7H-8axH	2.49	3.30	3.46	2.50	3.13	2.89
7H-8eqH	2.46	W	W	2.32	2.67	2.08
10axH-10eqH	1.80	1.92	1.76	1.84	1.79	1.80
8axH-8eqH	1.80	1.79	1.80	1.77	1.75	1.78
10eqH-8axH	o	3.01	2.71	3.52	3.53	3.53
10eqH-8eqH	o	2.96	2.98	2.94	3.28	2.92
10axH-8eqH	o	2.75	2.85	3.66	3.61	3.58
10axH-8axH	o	2.82	2.50	3.15	2.26	3.16
7H-10axH	3.63	-	-	3.76	4.13	3.92
7H-10eqH	3.71	-	-	3.93	4.20	2.49
9 CH ₂ OH/9COCH ₃ -8axH	3.60	-	-	3.56	5.92	3.85
9 CH ₂ OH/9COCH ₃ -8eqH	3.93	-	-	4.05	3.94	3.50
9 CH ₂ OH/9COCH ₃ -10axH	3.73	-	-	3.76	3.97	4.09
9 CH ₂ OH/9COCH ₃ -10eqH	3.62	-	-	4.89	4.85	4.87
WITHIN SUGAR						
1'H-2'axH	2.39	2.31	2.31	2.34	2.46	2.41
1'H-2'eqH	2.45	2.28	2.29	2.57	2.62	2.48
1'H-4'H	3.12	3.22	4.58	3.37	3.89	4.10
1'H-3'H	3.12	3.3	3.4	3.28	3.39	3.57
4'H-5'H	2.50	2.16	2.35	2.71	1.73	2.61
5'H-5'CH ₃	2.35	-	-	2.30	2.22	2.28
3'H-2'axH	2.34	3.07	3.21	2.40	2.31	2.31
3'H-2'eqH	2.54	2.33	2.44	3.00	2.99	2.97
4'H-5'CH ₃	2.53	2.59	2.73	2.56	3.61	3.29
2'axH-2'eqH	o	-	-	1.80	1.81	1.79
1'H-5'H	4.17	3.69	3.54	4.15	3.38	3.50
RING A TO SUGAR PROTONS						
7H-1'H	2.89	3.24	2.88	2.90	3.15	2.54
7H-4'H	3.66	2.7	2.44	3.47	3.56	3.62
7H-5'H	3.62	3.02	2.7	3.58	3.20	4.04
8axH-5'H	2.87	2.5	2.63	2.95	1.82	3.80
8axH-5'CH ₃	3.75	2.6	2.87	3.88	3.11	3.66
8eqH-5'H	2.64	2.4	2.44	2.80	2.87	3.52
8eqH-5'CH ₃	3.27	2.84	3.75	3.15	3.40	2.42

Table 10a: Comparison of bond lengths in optimized NMR based rMD structure and that calculated by B3LYP and HF methods and 6-31G** wavefunction. The corresponding data from X-ray crystal structure available in literature is also shown (Neidle et al., 1977).

Bond Length (Å)	HF/6-31G**			B3LYP/6-31G**			NMR			X-ray
	EPIADM	ADM	DNM	EPIADM	ADM	DNM	EPIADM	ADM	DNM	DNM
C4-O4	1.331	1.331	1.331	1.347	1.347	1.347	1.410	1.380	1.380	1.310
C7-C8	1.522	1.525	1.522	1.526	1.527	1.526	1.550	1.550	1.560	1.490
C7-C6a	1.518	1.514	1.518	1.515	1.516	1.516	1.560	1.560	1.560	1.580
C7-O7	1.436	1.432	1.437	1.470	1.469	1.470	1.440	1.430	1.450	1.470
C7-7H	1.081	1.083	1.081	1.093	1.093	1.093	1.090	1.060	1.080	-
C8-C9	1.536	1.533	1.536	1.545	1.545	1.545	1.540	1.530	1.530	1.510
C9-C10	1.535	1.532	1.536	1.547	1.547	1.547	1.530	1.540	1.520	1.580
C13-13O	1.194	1.194	1.193	1.220	1.220	1.216	1.550	1.230	1.230	1.220
C10-C10a	1.516	1.516	1.516	1.513	1.513	1.512	1.560	1.540	1.530	1.440
O7-C1'	1.400	1.397	1.402	1.429	1.433	1.432	1.450	1.460	1.470	1.420
C14-O14	1.382	1.383	-	1.397	1.397	-	1.440	1.440	-	-
C14- C13	1.514	1.514	1.506	1.514	1.514	1.507	1.530	1.540	1.560	1.530
O14-14H	0.946	0.946	-	0.972	0.972	-	0.970	0.960	-	-
C9-O9	1.399	1.400	1.400	1.419	1.419	1.419	1.440	1.430	1.440	1.450
C1'-C2'	1.532	1.528	1.527	1.544	1.538	1.538	1.540	1.530	1.540	1.420
C1'-O5'	1.382	1.380	1.381	1.401	1.398	1.399	1.490	1.430	1.450	1.480
C2'-C3'	1.521	1.522	1.524	1.523	1.527	1.527	1.530	1.530	1.540	1.540
C3'-C4'	1.519	1.526	1.523	1.525	1.528	1.528	1.550	1.540	1.540	1.540
C3'-N3	1.506	1.512	1.507	1.520	1.523	1.522	1.480	1.480	1.480	1.540
C4'-C5'	1.538	1.535	1.540	1.548	1.551	1.552	1.510	1.520	1.500	1.510
C4'-O4'	1.400	1.402	1.400	1.424	1.420	1.420	1.430	1.440	1.440	1.470
C5'-O5'	1.416	1.409	1.412	1.442	1.437	1.437	1.470	1.410	1.440	1.520
C5'-5'H	1.085	1.086	1.086	1.097	1.099	1.099	1.090	1.090	1.010	-

Table 10b: Comparison of bond angles in optimized NMR based rMD structure and that calculated by B3LYP and HF methods and 6-31G** wavefunction. The corresponding data from X-ray crystal structure available in literature is also shown (Neidle et al., 1977).

BOND ANGLES (°)	HF/6-31G**			B3LYP/6-31G**			NMR			X-ray
	EPIADM	ADM	DNM	EPIADM	ADM	DNM	EPIADM	ADM	DNM	DNM
C8-C7-C6a	112.616	112.845	112.497	112.821	112.649	112.604	114.520	113.560	114.220	112.000
C8-C7-O7	109.719	110.540	109.653	109.345	109.088	109.209	107.950	112.720	115.110	113.000
C6a-C7-O7	105.285	106.809	105.510	104.802	105.239	105.208	110.680	126.400	121.140	102.000
C7-C8-C9	112.052	111.884	112.263	111.709	111.652	111.938	110.230	110.520	115.380	114.000
C8-C9-C10	110.267	109.439	110.211	110.090	110.105	110.045	102.860	102.960	102.200	111.000
C8-C9-9O	111.934	111.958	111.726	111.625	111.618	111.467	109.560	108.720	108.920	112.000
C10-C9-9O	110.609	110.852	110.402	111.173	111.075	111.147	107.690	108.180	111.840	108.000
C4-4O-4CH ₃	120.640	120.736	120.634	119.213	119.248	119.257	115.060	108.870	108.890	118.000
C7-O7-C1'	121.798	118.227	121.597	120.494	120.214	120.178	116.710	123.380	115.010	115.000
C14-14O-14H	109.385	109.331	-	106.453	106.465	-	108.920	109.160	-	-
O7-C1'-C2'	110.779	110.311	110.914	110.995	111.018	111.061	108.410	110.230	113.290	111.000
O7-C1'-O5'	107.886	108.796	108.007	107.463	107.662	107.740	114.360	117.020	109.820	109.000
C2'-C1'-O5'	109.697	110.093	109.406	110.607	110.365	110.239	116.630	103.720	108.360	113.000
C1'-C2'-C3'	105.740	107.605	106.449	106.018	106.743	106.680	107.100	103.950	108.450	110.000
C2'-C3'-C4'	109.477	111.230	109.711	109.677	109.628	109.666	109.760	114.630	116.330	109.000
C4'-C3'-N3	110.234	107.804	109.864	109.579	110.075	110.129	113.900	117.740	117.020	107.000
N3-C3'-3'H	103.921	106.542	105.436	103.955	105.538	105.548	109.480	110.880	110.460	109.000
C3'-C4'-C5'	107.477	109.019	108.604	107.736	108.725	108.676	117.220	117.500	109.550	107.000
C3'-C4'-4'O	106.000	104.625	105.037	105.538	104.868	104.909	116.100	116.380	111.000	107.000
C5'-C4'-4'O	113.174	114.997	115.703	113.446	115.866	115.887	114.820	116.690	116.070	116.000
C4'-C5'-5'O	109.777	111.421	112.575	109.972	113.053	113.051	109.920	115.330	122.260	107.000
C1'-5'O-C5'	117.841	116.968	117.497	116.444	116.400	116.367	122.920	108.400	114.000	113.000

Table 10c: Comparison of dihedral angles in optimized NMR based rMD structure and that calculated by B3LYP and HF methods and 6-31G** wavefunction. The corresponding data from X-ray crystal structure available in literature is also shown (Neidle et al., 1977).

DIHEDRAL ANGLES	HF/6-31G**			B3LYP/6-31G**			NMR			X-ray
	EPIADM	ADM	DNM	EPIADM	ADM	DNM	EPIADM	ADM	DNM	DNM
C6a-C7-C8-C9	-49.402	-47.493	-50.006	-50.404	-51.028	-51.204	-48.380	47.360	-21.400	-48.000
C7-C8-C9-C10	57.662	60.326	57.114	57.294	57.320	56.663	-70.470	-73.610	56.720	58.000
C8-C9-C10-C10a	-41.193	-43.134	-40.119	-40.338	-39.889	-38.853	-54.090	55.850	-71.440	-38.000
C9-C10-C10a-C6a	18.435	14.989	17.952	17.754	17.452	16.819	21.420	-27.640	45.420	14.000
C10-C10a-C6a-C7	-10.202	-10.653	-10.767	-10.532	-10.875	-10.930	10.900	7.750	10.660	-5.000
C10a-C6a-C7-C8	25.607	17.958	26.646	26.892	27.682	28.086	11.910	-19.920	-35.830	20.000
C6a-C7-O7-C1'	-134.254	-150.876	-131.756	-131.719	-128.450	-128.024	-156.620	-130.840	-149.610	-114.000
C8-C7-O7-C1'	104.317	86.011	106.860	107.088	110.444	110.878	79.320	-21.050	103.040	125.000
C7-O7-C1'-C2'	80.172	87.921	80.999	76.596	78.400	78.191	-143.560	-156.970	-158.050	167.000
C7-O7-C1'-O5'	-159.746	-151.220	-159.119	-162.344	-160.697	-160.986	-34.560	-30.830	-16.740	-68.000
C1'-C2'-C3'-C4'	62.846	57.128	62.304	62.289	62.489	62.612	56.980	39.940	34.730	56.000
C2'-C3'-C4'-C5'	-60.682	-53.474	-55.631	-60.942	-56.250	-56.247	-58.320	-9.330	14.980	-61.000
C3'-C4'-C5'-O5'	53.483	50.036	48.089	54.222	48.459	48.444	40.530	10.060	-40.150	61.000
C4'-C5'-O5'-C1'	-55.762	-56.088	-52.054	-55.364	-50.710	-50.844	-29.010	-45.250	8.500	-59.000
C5'-O5'-C1'-C2'	59.003	60.128	58.629	58.149	56.946	57.152	35.120	81.070	46.400	57.000
O5'-C1'-C2'-C3'	-59.248	-58.082	-61.495	-58.967	-61.303	-61.463	-47.230	-76.230	-67.630	-54.000
H1'-C1'-O7-C7	-43.534	-34.707	-42.846	-46.965	-45.220	-45.479	103.580	81.530	84.180	-
C1'O7-C7-H7	-15.959	-33.813	-13.394	-13.613	-10.101	-9.737	-23.200	-131.980	-19.610	-
Total Energy(a.u.)	-1917.703	-1917.702	-1842.849	-1928.969	-1928.965	-1853.756	-	-	-	-
μ (D)	16.906	19.382	14.317	16.741	15.954	13.870	-	-	-	-

chemical shifts to values in ppm, by subtracting the absolute shielding of each atom (^1H and ^{13}C) from the reference value for TMS. The chemical shifts are calculated from STO-3G to 6-31G** with GIAO method. Tables 4 and 5 show the calculated chemical shift using B3LYP/HF method with 6-31G** basis set for the three drugs along with the present experimental results. A quick look tells us that calculated chemical shift range for ^1H are more sensitive to the variation of basis sets compared to that of ^{13}C . Also, the carbon chemical shifts obtained by B3LYP/6-31G** are in very good agreement to that obtained by our NMR measurements, thus ascertaining the reliability of the assignment. This can be rationalized by the fact that ^1H atoms being the smallest of all atoms and being mostly localized on periphery of the molecules, would be more susceptible to intermolecular interactions in the aqueous solutions compared to heavier atoms. The observed percentage variation of the difference between measured data and calculated results for proton and carbon are 3.3 % and 2.8 %, respectively.

Considering the fact that NMR chemical shifts are affected by the chemical environment i.e. molecular conformation and interaction with the solvent molecules, it is seen that the overall agreement between the calculated and measured values both for ^1H and ^{13}C chemical shifts is satisfactory. It is of interest, however to see, how good the correlation between experimental and calculated results is? We therefore plot our experimental NMR results versus theoretical calculations obtained with B3LYP and HF method using 6-31G** basis set (Tables 4 and 5) for the 4'-epiadriamycin. A linear correlation between theoretical and experimental results, both for carbon and proton chemical shifts, is clearly seen in Fig. 12 with correlation coefficient r equal to 0.988 and 0.973, respectively i.e. very close to 1. Further we also see that largest difference between the calculated carbon chemical shifts of 4'-epiadriamycin and its analogues are at the position of C11, C12a and C12 which may be due to the solvent effect as the optimization is

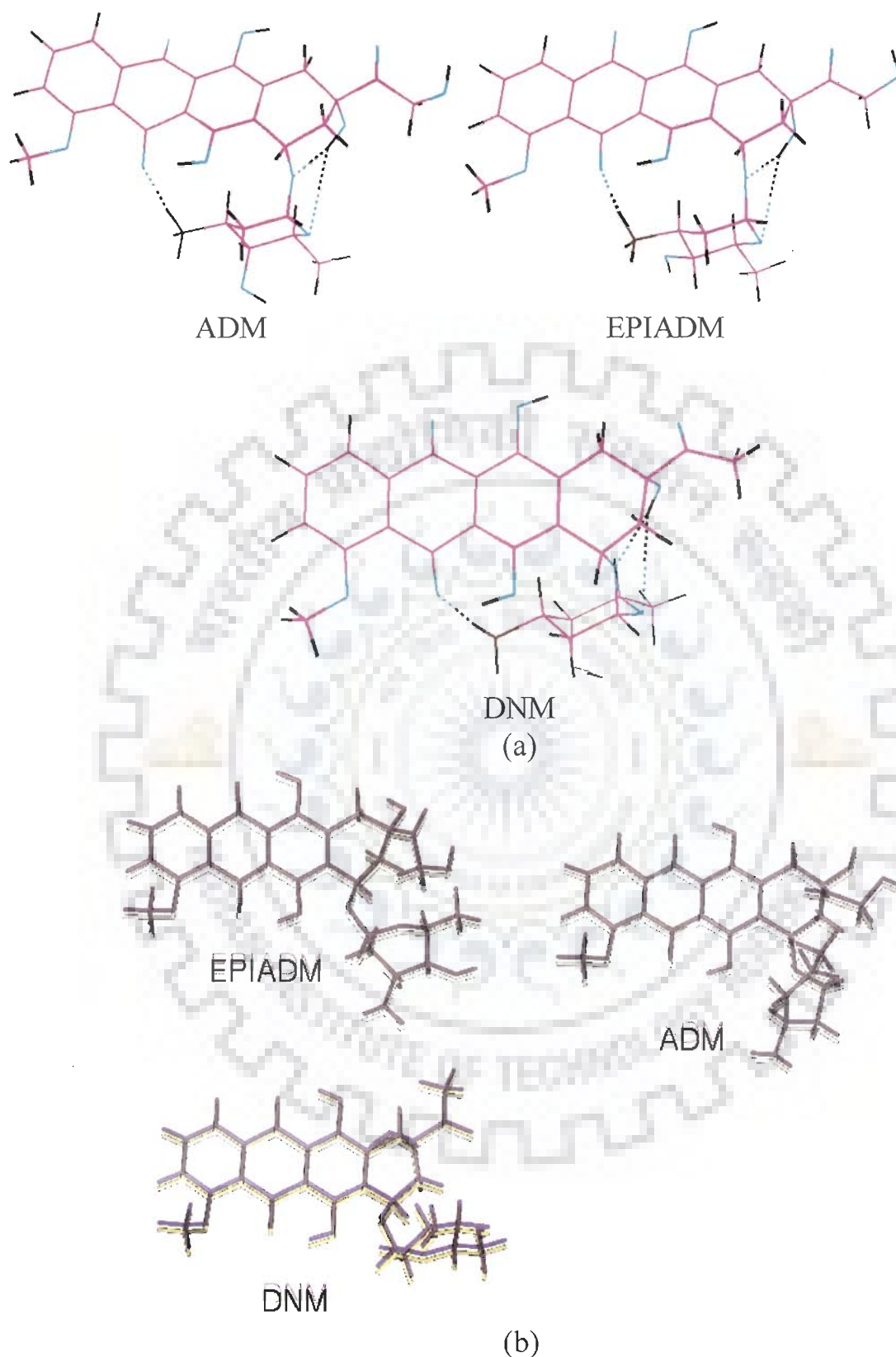


Fig. 11: (a) Gaussian Optimized structure of 4'-epiadriamycin, adriamycin and daunomycin using B3LYP/6-31G (b) Minimized solution structure of 4'-epiadriamycin, adriamycin and daunomycin using rMD**

done in gaseous phase. On the whole good correlation demonstrates that in general 6-31G** basis set with B3LYP method predicts the best NMR parameters in comparison to 6-31G** basis set with HF method. The chemical shifts, obtained from quantum mechanical calculations, which are similar to that obtained from NMR solution structures would therefore mean that the chemical shifts are not very dependent on conformation. This may possibly be due to the large ring current shifts expected for these structures. Further, the spin-spin coupling constant (J) has also been calculated from B3LYP/6-31G** using GAUSSIAN 03 version for all the three drugs. The values obtained from B3LYP/6-31G** follow that obtained from 1D NMR and DQF COSY except for certain violations at some positions of the atoms where either the pseudoatoms are present or overlapping of the peaks takes place, for example, 5'H-5'CH₃ and 5'H-4'H (Table 2). The difference in chemical structure of 4'-epiadriamycin and adriamycin exists only at the substituent H and OH placed differently at C4' position. This gets reflected in the difference in chemical shifts of 2'eqH, 2'axH, 3'H, 4'H, 5'H (Table 1). The chemical shifts in adriamycin and daunomycin are quiet close to each other except for 9COCH₃ and 9COCH₂OH groups which is expected and may give rise to alteration in geometry of ring A as observed in dihedral angle C7-C8-C9-C10. The value is 57° in daunomycin whereas in adriamycin and 4'-epiadriamycin, -73 and -70°, respectively (Table 8). The difference in spin-spin coupling constant (J^3) between 4'-epiadriamycin and adriamycin eg. 2'eqH-3'H, 5'H-5'CH₃ and inter-proton distances 2'H-3'H, 2'H-5'H indicates a difference in conformation of daunosamine sugar in these drugs. The chemical shift difference at 4'OH position also gets reflected in ¹³C chemical shift of C4' of 4'-epiadriamycin and adriamycin. These are expected to contribute to different sugar conformations in the two epimers.

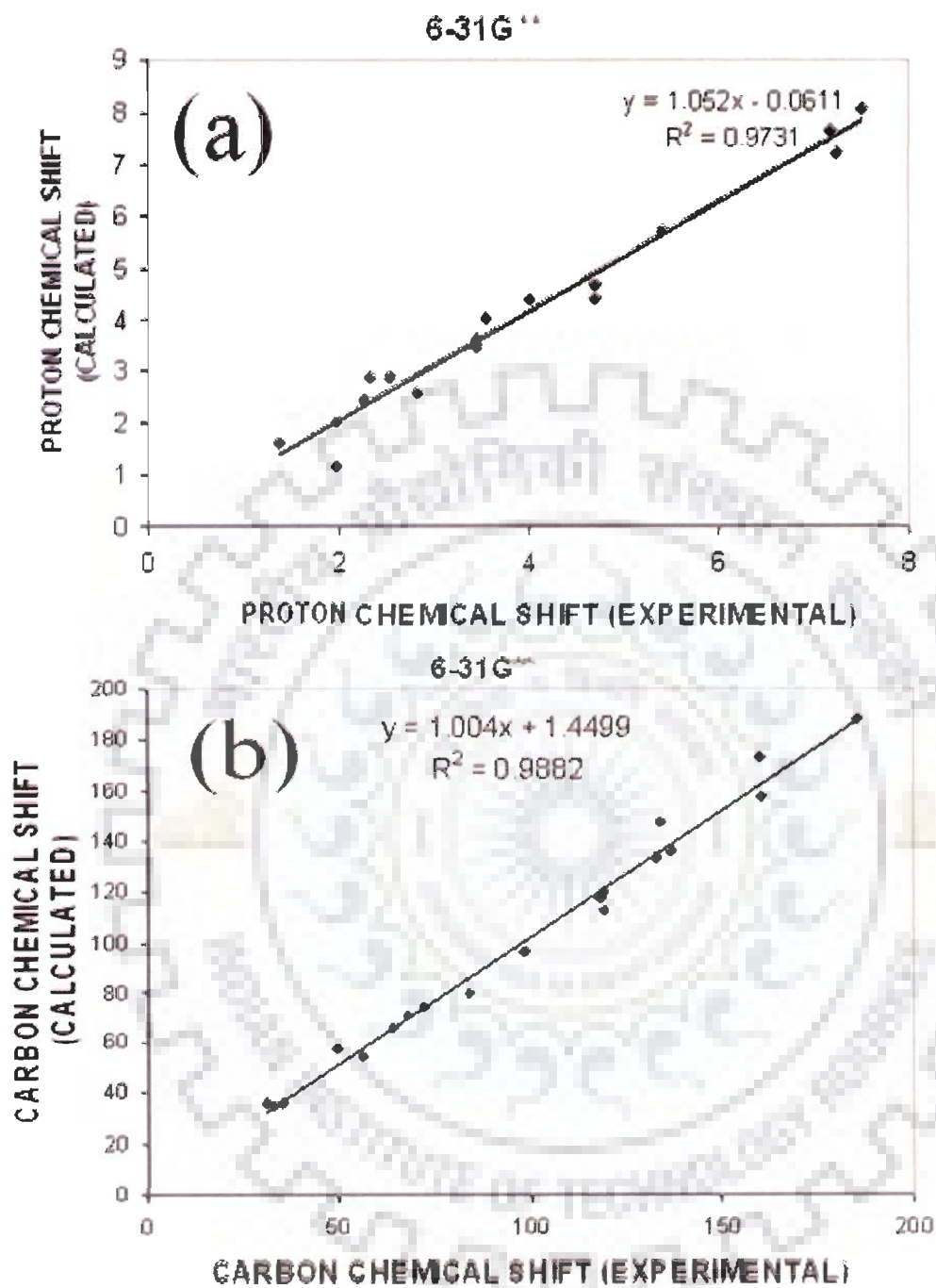


Fig. 12: Correlation of experimental and calculated (a) proton and (b) carbon NMR chemical shifts of 4'-epiadriamycin with B3LYP/6-31G**/GIAO method

D. Flexibility of Sugar Ring

Sugar - chromophore system is characterized by the bond rotations C8-C7-O7-C1' and C7-O7-C1'-C2' (Table 10c). An interesting feature of these drugs is the flexibility in the sugar rings. We have compared the dihedral angle formed by atoms C7-O7-C1'-C2', the glycosidic linkage, in various solution structures derived by using NMR restraints. In 4'-epiadriamycin, it adopts two conformational states, that is, 161° (I) and 143° (II). The 143° conformer (II) is 29 Kcal/mol lower in energy than the 161° conformer (I). Adriamycin which differs from it in the orientation of H and OH at 4' position of sugar moiety adopts only one conformational state, that is, 156° (I). The daunomycin has sugar moiety similar to that of adriamycin and differs from adriamycin in the substituent group attached at 9CO position only, that is, 9COCH₃ in daunomycin and 9COCH₂OH in adriamycin. The glycosidic linkage in daunomycin adopts two angles 158° (I) and 142° (II) of which 142° conformer (II) is lower in energy by 25 Kcal/mol. The corresponding observed values in x-ray crystallographic structures of these drugs, e.g., N-bromo-acetyl daunomycin, carminomycin-I-hydrochloride monohydrate, daunomycin (Neidle et al., 1977; Von Dreele et al., 1977; Anguilli et al., 1971) are found to be 161-167°, that is, they correspond to conformation I only.

The Gaussian optimized structure of all the three drugs shows glycosyl angle 76-78° (III), (Table 10c) which is neither observed in our NMR based solution structure nor in x-ray crystal structures (Moore et al., 1989; Nunn et al., 1991; Wang et al., 1987). However using semi-empirical energy calculations, Nakata and Hopfinger (Nakata et al., 1980) have shown earlier that the drugs and their several analogues adopt glycosidic linkage 158° (I), 138° (II) and 38° (III) of which the conformer 138° (II) is the global energy minimum conformation. Conformer 138° (II) is lower than the corresponding conformer 158° (I) by 3 Kcal/mol. On the other hand,

conformer 38° (III) is > 9.5 Kcal/mol higher than the global minima. Apparently in solution, both conformation $156-161^\circ$ (I) and $142-143^\circ$ (II) are being stabilized. Energetically conformer II is preferred over conformer I. However, $38-78^\circ$ conformer (III) obtained by theoretical computations having much higher energy is not observed experimentally.

E. Biological Relevance

The glycosidic linkage is involved in anchoring of intercalator in minor groove of DNA and building stabilizing contacts to the DNA through its charged NH_3^+ group. This contributes to the sequence specificity and the binding affinity of the drugs. The three different conformations, that is, $156-167^\circ$ (I), $127-144^\circ$ (II) and $38-78^\circ$ (III) orient NH_3^+ moiety differently in the minor groove and hence lead to a significant difference in interaction of the 3 N-H bonds to oxygen atoms of bases in hexamer sequence, d-CGATCG (Trieb et al., 2004). In the conformer 138° (II), there are 2 hydrogen bonds of NH with (a) O4' of cytosine (distance 3.2 Å) and (b) O2' of thymine (distance 3.0 Å). In the conformer 158° (I), these two distance increase to (a) 5.5 Å and (b) 5.1 Å, respectively. The third hydrogen bond of NH with (c) O4' of thymine (distance 3.2 Å) also exists. On the other hand in the 59° conformer (III), there are 3 hydrogen bonds of NH with (a) O4' of guanine (distance 3.4 Å), (b) O5' of guanine (distance 3.0 Å) and (c) hydroxyl group attached to daunosamine moiety of drug with O1P of guanine (distance 3.0 Å). The x-ray crystal structure of daunomycin / adriamycin complexed with hexamer sequence d-CGATCG, d-TGATCA, d-TGTACA (Moore et al., 1989; Nunn et al., 1991; Wang et al., 1987) show presence of $127-144^\circ$ conformer (II). Our recent results on binding of adriamycin with d-TGATCA (unpublished) by using NMR also show presence of 133° conformer (II).

It is noteworthy that x-ray structure shows that $159-166^\circ$ conformer (I) in uncomplexed drug changes to $127-144^\circ$ conformer (II) in drug-DNA complex while in solution both

conformers I and II were coexisting in uncomplexed drug (except in adriamycin) but on binding, 133° conformer (II) got stabilized. Thus it appears that 127-144 ° conformer (II) is perhaps the one which provides biological activity.

F. Structure-Activity Relationship

The difference in chemical structure between the three drugs, adriamycin, 4'-epiadriamycin and daunomycin, resulted in distinctly different conformations in rMD structures (Table 8 and 10c). This difference in conformation of three drugs is expected to lead to difference in their molecular basis of anticancer action.

It is well known that 4'-epiadriamycin is better tolerated, active against a variety of solid tumors with reduced cytotoxicity and lesser side effects. Daunomycin is used for acute lymphocytic and myelogenous leukaemia which inhibits *in vitro* growth of both normal and cancer cell lines and adriamycin is used for the treatment of solid tumors and acute leukemia that are distinct from those against which daunomycin is active. These drugs are localized in the nucleus and show cytotoxic and anti-mitotic activity. Large differences have been observed in the conformation of aglycone ring A and daunosamine sugar moiety on complexation with DNA. Orientation of the functional groups attached at C-9 position on ring A was found to be different in these complexes. The 4'-OH of daunosamine sugar formed additional hydrogen bonds as compared to that in daunomycin (Moore et al., 1989; Nunn et al., 1991; Wang et al., 1987) and adriamycin (Frederick et al., 1990) complexes. The role of drug-DNA covalent bonding in cells was also investigated with synthetic epidoxorubicin-formaldehyde (Epidoxoform) and synthetic daunorubicin-formaldehyde (daunoform) conjugate. It was observed that the fluorophore of daunoform appeared more rapidly in cells and was released more rapidly from cells than the fluorophore of epidoxoform. Epidoxoform was found to be 3- fold more toxic to MCF-7 human

breast cancer cells and greater than 120-fold more toxic to MCF-7/ adriamycin resistant cells than that for epidoxorubicin (Podell et al., 1999; Taatzes et al., 1999).

The active conformation happens to be 127-144 ° conformer (II) which is observed in drug-DNA complexes and is biologically the relevant one. A flexibility of adopting two conformers, 158 ° conformer (I) and 138 ° conformer (II) in 4'-epiadriamycin makes the molecule easily adjustable to the receptor site and maximizes the binding energy. On the other hand, existence of only one 156 ° conformer (I) in adriamycin may reduce relative binding. The efficacy of daunomycin, which adopts both conformers I and II is comparatively reduced due to lack of hydrogen bonding from 9COCH₃ (which replaces 9COCH₂OH group of adriamycin and 4'-epiadriamycin). Accordingly the specific structure-conformation of each drug molecule leads to a biological activity at cellular level, the anticancer action, which is unique for these drugs. Comparison of solution structure of these three drugs with different DNA sequences is expected to provide further knowledge on sequence specificity. Some of these experiments are in progress in our laboratory.

3.2 Summary and Conclusions

We present here a complete analysis of proton NMR spectra of anticancer drug, 4'-epiadriamycin, an analogue of adriamycin, using 1D and 2D NMR techniques. The NMR spectra of daunomycin and adriamycin has earlier been reported by us (Barthwal et al., 1996; Barthwal et al., 1994). ¹³C NMR assignments of the three drugs have been made using HMBC, HSQC and GIAO methods. To the best of our knowledge this is the first report on ¹H NMR of 4'-epiadriamycin and ¹³C NMR of these three drugs. Theoretical investigations using B3LYP Density Functional Theory (DFT) and HF (SCF) methods are carried out for all drugs in gaseous phase. All the geometries for the molecules studied were fully optimized with all the basis sets.

A variety of basis sets like STO-3G, 6-31G, 6-311G, 6-31G** were also used with B3LYP and HF methods (data not given here). The effect of increasing size of the basis set slows down the calculation but does not necessarily approach the experimental results always. B3LYP/6-31G** functional has shown to produce best results for geometries, energies, and all other NMR parameters. An optimized solution structure has been obtained by restrained Molecular Dynamics simulations using NOE restraints for all the three drugs. These structures are compared with that obtained from quantum mechanical calculations. It is observed that the daunosamine sugar moiety of the drug in rMD structure is near 9OH of the chromophore and away from 4OCH₃, while in case of quantum mechanical calculations, just the reverse is happening, that is, the sugar moiety is near 4OCH₃ and away from 9OH. This implies that the hydrogen bond formation between 6OH and 3NH₃⁺ stabilizes structure more in quantum mechanical calculations than that obtained by rMD. Three conformations of glycosidic bond angle C7-O7-C1'-C2' that is, 156-161 ° (I), 142-143 ° (II) and 38-78 ° conformer (III) have been obtained of which conformer II is the minimum energy conformation. Experimentally observed solution NMR and x-ray crystal structures (Nakata et al., 1980; Trieb et al., 2004) show presence of conformer I, II and conformer I, respectively. On binding to DNA, conformer II is stabilized in both solution NMR (unpublished) and x-ray crystal structures (Moore et al., 1989; Nunn et al., 1991; Wang et al., 1987). A variation in flexibility of adopting different conformations in these three drugs may be related to a differential efficacy in biological activity and hence anticancer action.

Studies on Self-aggregation of Anthracycline Drugs by Restrained Molecular Dynamics approach using Nuclear Magnetic Resonance Spectroscopy supported by Absorption, Fluorescence, Diffusion Ordered Spectroscopy and Mass Spectrometry

Anthracycline drugs are known to show the property of self association in solution by stacking of their conjugated anthracycline rings. Prior to the determination of the structural and thermodynamical characteristics of the intercalative binding of aromatic drugs to defined DNA sequences by NMR spectroscopy, it is necessary to determine the self-association of the drugs in solution. In this chapter, we present the following:

- Proton 1D NMR spectra as a function of concentration (0.01-8.00 mM) at 298 K and of 8 mM concentration as a function of temperature (275-355 K) in D₂O for the three drugs, 4'-epiadriamycin, adriamycin and daunomycin.
- Restrained molecular dynamics simulations of the dimer model of 4'-epiadriamycin, daunomycin and adriamycin using inter-proton distances calculated from 2D NOESY spectra at 355 K ($\tau_m = 400$ ms).
- Absorption and fluorescence spectral studies of drugs as a function of concentration.
- Calculation of diffusion coefficient from proton DOSY experiment for all the three drugs.
- Electron-Spray Ionization Mass Spectra (ESI-MS) studies of the anthracycline drugs.

4.1 Results and Discussion

A. NMR Studies

Fig. 1-3 shows the proton NMR spectra of 4'-epiadriamycin, adriamycin and daunomycin at 298K in D₂O in various concentrations. The variation in chemical shifts is shown in Fig. 4-6 and

the values are given in Table 1a-c. An increase in concentration from 0.01 to 8.00 mM leads to upfield shift in aromatic ring D protons, 1H, 2H, 3H, 4OCH₃ up to $\Delta\delta = 0.52$ ppm (Table 1d). The ring A protons 10axH, 10eqH, 8axH, 8eqH, also show significant upfield shifts up to 0.68 ppm. These are in accord with earlier observations on daunomycin reported in literature (Chaires et al., 1982; Barthwal et al., 1994; Barthwal et al., 1996; Evstigneev et al., 2006) and have been attributed to stacking of aromatic rings forming self aggregates. No such studies have been carried out so far for adriamycin and 4'-epiadriamycin to the best of our knowledge. The 4'-epiadriamycin and adriamycin differ in their structure only by an inversion of the substituents H and OH at C4' position of sugar moiety. We observe that there are substantial differences in $\Delta\delta$ values (0.21-0.46 ppm) of ring A protons, 8eqH, 10axH, 10eqH, 7H, 9COCH₂ due to stacking. The difference is evident (0.09-0.16 ppm) in 3'H, 4'H, 5'H and 4OCH₃ protons as well. This indicates that the self associated structures in 4'-epiadriamycin are different from that of adriamycin.

We have also examined the NMR spectra of drugs at 8 mM concentration as a function of temperature (Fig. 7-9). We observe considerable differences among the three drugs (Table 2a-d). The ring D protons 1H, 2H, 3H, reflect large downfield shifts up to 1.59 ppm with temperature (Fig. 10-12) which may be due to de-stacking in self aggregated structures. However there are other factors such as change in (i) monomer-dimer equilibrium (ii) hydrogen bonding if present and (iii) structural changes, which contribute towards change in chemical shift with temperature. It is noteworthy that there are significant differences in $\Delta\delta_{355-275\text{ K}}$ of 7H, 10eqH, 9COCH₂, 3'H, 1H, 2H and 3H protons in 4'-epiadriamycin and adriamycin. The 4'OH, 9OH, 6OH, 11OH, and 3NH₃⁺ are observed in NMR spectra of 4'-epiadriamycin but not in that of adriamycin and daunomycin. Apparently these protons are immobilized in stacked / self aggregated structure of

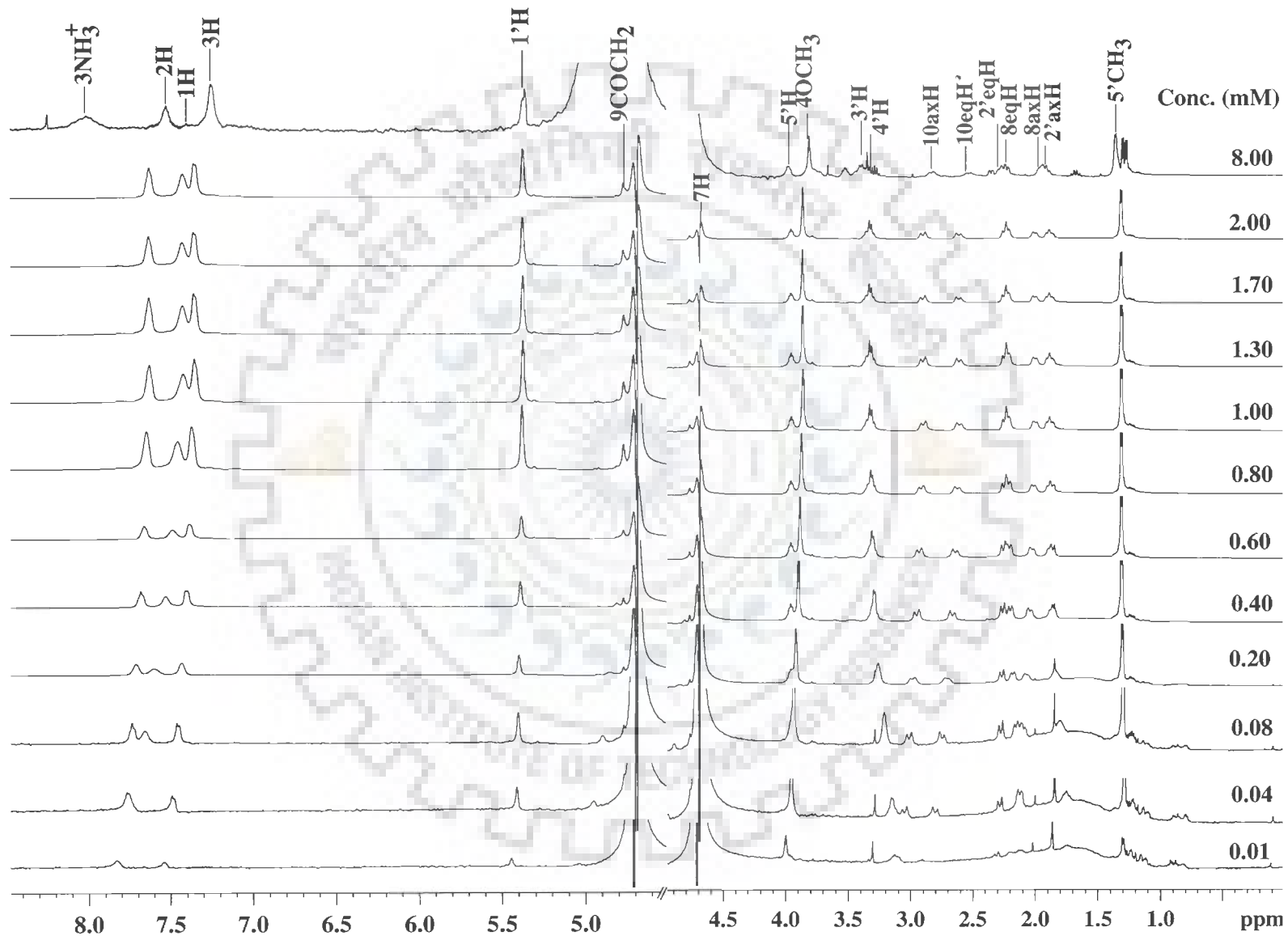


Fig. 1: One-dimensional proton NMR spectra of 4'-epiadriamycin in D_2O as a function of concentration at 298 K

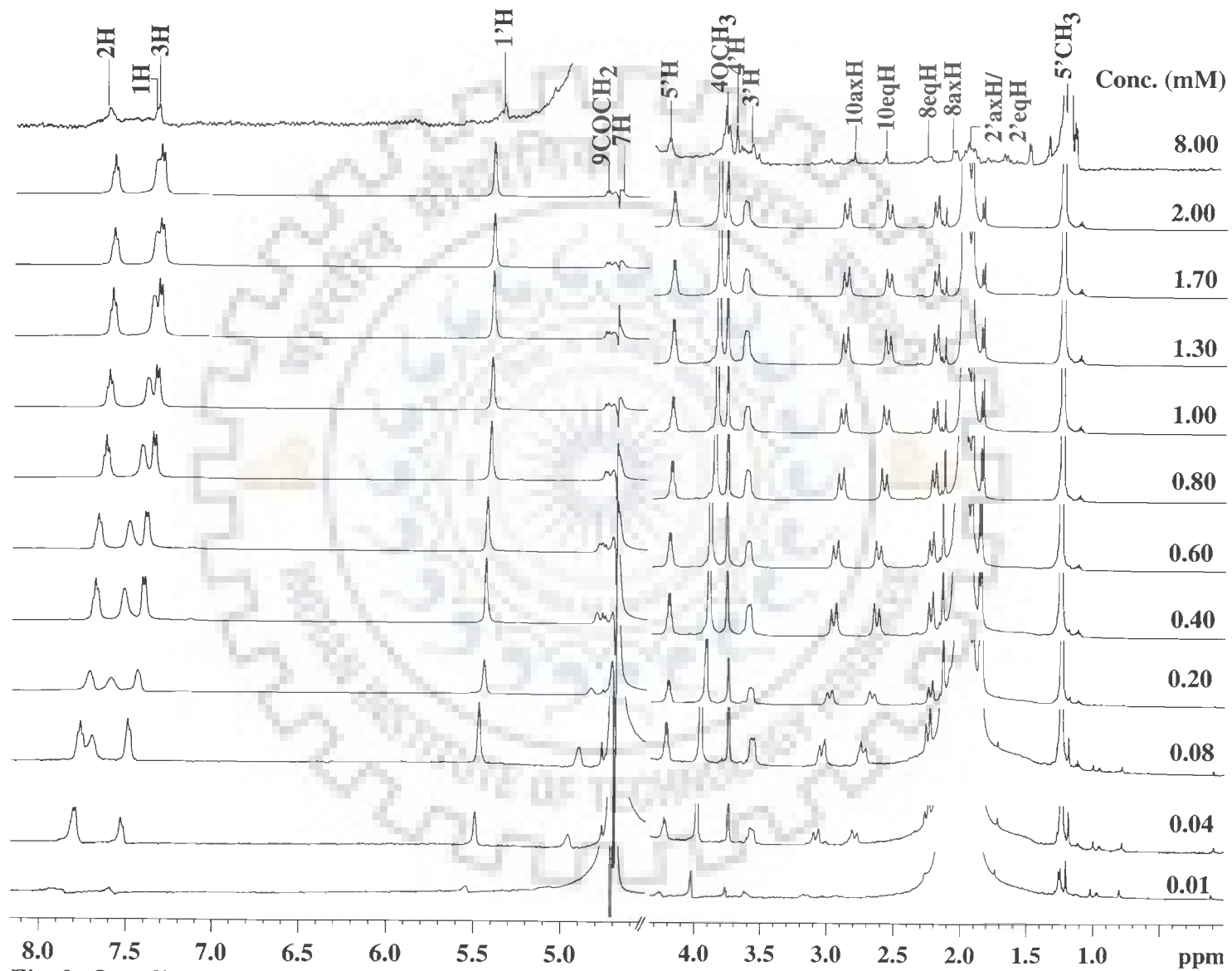


Fig. 2: One-dimensional proton NMR spectra of adriamycin in D_2O as a function of concentration at 298 K

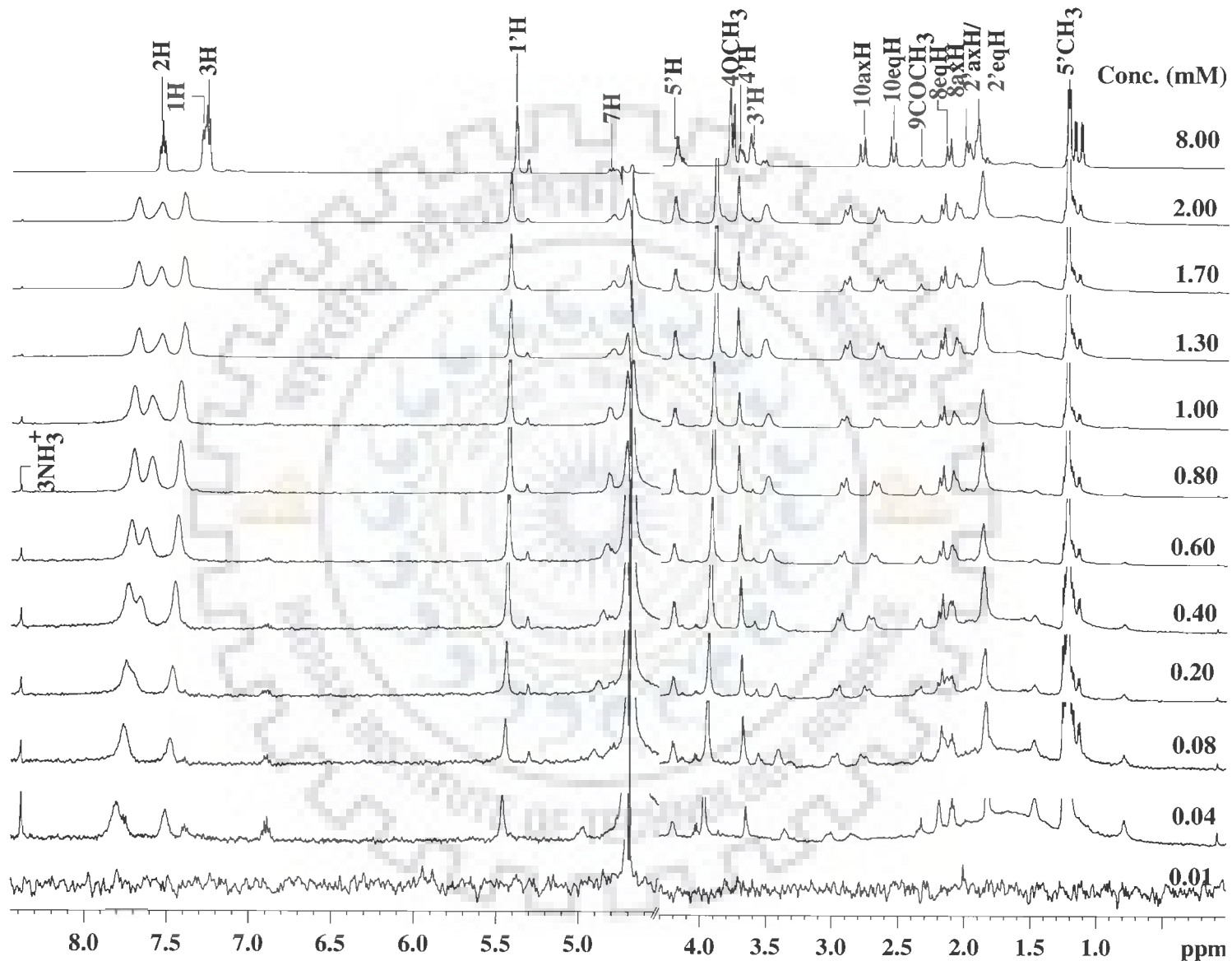


Fig. 3: One-dimensional proton NMR spectra of daunomycin in D_2O as a function of concentration at 298 K

Table: 1a Proton chemical shifts of 4'-epiadriamycin in D₂O as a function of concentration at 298 K. $\Delta\delta = \delta_{8\text{ mM}} - \delta_{0.01\text{ mM}}$ indicates total change in chemical shift due to self association.

Conc. (mM)	5'CH ₃	2'axH	8axH	8eqH	2'eqH	10axH	10eqH	4'H	3'H
0.01	1.33	1.87	2.13	2.18	2.31	2.92	3.10	3.13	3.31
0.04	1.33	1.87	2.13	2.18	2.31	2.83	3.07	3.17	3.31
0.08	1.33	1.87	2.12	2.18	2.30	2.77	3.04	3.22	3.31
0.20	1.33	1.87	2.09	2.18	2.30	2.72	3.01	3.26	3.31
0.40	1.33	1.88	2.07	2.22	2.28	2.69	2.97	3.29	3.33
0.60	1.33	1.88	2.05	2.22	2.26	2.68	2.95	3.29	3.34
0.80	1.33	1.90	2.04	2.22	2.26	2.66	2.94	3.32	3.36
1.00	1.33	1.90	2.03	2.22	2.26	2.64	2.92	3.32	3.36
1.30	1.33	1.90	2.03	2.22	2.26	2.64	2.92	3.32	3.36
1.70	1.33	1.91	2.03	2.22	2.26	2.64	2.92	3.32	3.36
2.00	1.33	1.91	2.02	2.22	2.26	2.64	2.92	3.33	3.37
8.00	1.34	1.91	1.95	2.22	2.26	2.52	2.82	3.33	3.50
$\Delta\delta$	+0.01	+0.04	-0.18	+0.04	-0.05	-0.40	-0.28	+0.20	+0.19
Conc. (mM)	4OCH ₃	5'H	7H	9COCH ₂	1'H	3H	1H	2H	
0.01	3.95	4.01	4.60	4.86	5.46	7.55	7.81	7.85	
0.04	3.94	3.99	4.65	4.82	5.44	7.51	7.77	7.81	
0.08	3.94	3.98	4.65	4.80	5.43	7.49	7.69	7.77	
0.20	3.94	3.98	4.66	4.80	5.43	7.46	7.62	7.74	
0.40	3.93	3.98	4.67	4.80	5.42	7.43	7.55	7.71	
0.60	3.91	3.98	4.67	4.80	5.41	7.41	7.51	7.69	
0.80	3.90	3.98	4.68	4.79	5.41	7.40	7.48	7.67	
1.00	3.88	3.98	4.68	4.79	5.40	7.38	7.45	7.66	
1.30	3.88	3.98	4.68	4.79	5.40	7.38	7.45	7.66	
1.70	3.88	3.98	4.69	4.79	5.40	7.38	7.45	7.66	
2.00	3.88	3.98	4.69	4.79	5.40	7.38	7.45	7.66	
8.00	3.79	3.97	4.97	4.78	5.35	7.24	7.25	7.52	
$\Delta\delta$	-0.16	-0.04	+0.37	-0.08	-0.11	-0.31	-0.56	-0.33	

Downfield shift is +ve

upfield shift is -ve

Table: 1b Proton chemical shifts of adriamycin in D₂O as a function of concentration at 298 K.
 $\Delta\delta = \delta_{8 \text{ mM}} - \delta_{0.01 \text{ mM}}$ indicates total change in chemical shift due to self association.

Conc. (mM)	5'CH ₃	2'axH/2'eqH	8axH	8eqH	10axH	10eqH	3'H	4'H
0.01	1.25	1.88	2.16	2.28	2.90	3.16	3.58	3.76
0.04	1.26	1.88	2.16	2.27	2.81	3.10	3.58	3.76
0.08	1.26	1.88	2.16	2.27	2.75	3.06	3.58	3.76
0.20	1.26	1.88	2.16	2.25	2.69	3.01	3.61	3.77
0.40	1.27	1.88	2.16	2.25	2.66	2.98	3.62	3.78
0.60	1.27	1.88	2.16	2.25	2.64	2.97	3.63	3.79
0.80	1.27	1.87	2.15	2.23	2.61	2.93	3.65	3.79
1.00	1.27	1.87	2.15	2.23	2.60	2.92	3.65	3.79
1.30	1.27	1.87	2.15	2.23	2.58	2.91	3.66	3.79
1.70	1.27	1.87	2.15	2.23	2.58	2.90	3.66	3.80
2.00	1.27	1.87	2.15	2.23	2.58	2.90	3.66	3.80
8.00	1.27	1.87	1.92	2.00	2.22	2.67	3.68	3.80
$\Delta\delta$	+0.02	-0.01	-0.24	-0.28	-0.68	-0.49	+0.10	+0.04
Conc. (mM)	4OCH ₃	5'H	7H	9COCH ₂	1'H	3H	1H	2H
0.01	4.02	4.26	4.69	4.77	5.54	7.58	7.86	7.87
0.04	4.00	4.24	4.69	4.77	5.51	7.54	7.81	7.82
0.08	3.98	4.23	4.69	4.77	5.49	7.50	7.71	7.78
0.20	3.94	4.22	4.69	4.77	5.46	7.45	7.61	7.73
0.40	3.92	4.22	4.69	4.77	5.45	7.42	7.54	7.70
0.60	3.91	4.22	4.69	4.77	5.45	7.41	7.51	7.69
0.80	3.88	4.20	4.69	4.77	5.43	7.37	7.44	7.65
1.00	3.87	4.20	4.69	4.77	5.42	7.35	7.41	7.63
1.30	3.86	4.20	4.69	4.77	5.42	7.34	7.38	7.61
1.70	3.85	4.20	4.69	4.77	5.42	7.33	7.36	7.61
2.00	3.85	4.20	4.70	4.77	5.42	7.33	7.36	7.61
8.00	3.72	4.09	4.7	5.31	5.42	7.30	7.34	7.50
$\Delta\delta$	-0.30	-0.17	+0.01	+0.54	-0.12	-0.28	-0.52	-0.37

Downfield shift is +ve
 upfield shift is -ve

Table: 1c Proton chemical shifts of daunomycin in D₂O as a function of concentration at 298 K. $\Delta\delta = \delta_{8\text{ mM}} - \delta_{0.01\text{ mM}}$ indicates total change in chemical shift due to self association.

Conc. (mM)	5'CH ₃	4'OH	2'axH/ 2'eqH	8axH	8eqH	9COCH ₃	10axH	10eqH	3'H
0.01	1.23	1.49	1.86	2.14	2.21	2.35	2.88	3.03	3.37
0.04	1.23	1.49	1.86	2.11	2.21	2.35	2.87	3.03	3.38
0.08	1.23	1.49	1.86	2.12	2.21	2.35	2.78	3.00	3.43
0.20	1.24	1.49	1.87	2.12	2.21	2.35	2.76	2.99	3.45
0.40	1.24	1.49	1.88	2.12	2.21	2.35	2.73	2.97	3.47
0.60	1.24	1.49	1.89	2.12	2.21	2.37	2.71	2.95	3.49
0.80	1.25	1.49	1.90	2.12	2.21	2.37	2.69	2.94	3.51
1.00	1.25	1.49	1.90	2.12	2.21	2.37	2.69	2.94	3.51
1.30	1.26	1.50	1.91	2.09	2.21	2.37	2.67	2.92	3.54
1.70	1.26	1.50	1.91	2.09	2.21	2.37	2.67	2.92	3.54
2.00	1.26	1.50	1.91	2.09	2.21	2.37	2.67	2.92	3.54
8.00	1.18	1.51	1.91	1.88	1.94	2.37	2.50	2.73	3.58
$\Delta\delta$	-0.05	+0.02	+0.05	-0.26	-0.27	+0.02	-0.38	-0.30	+0.21
Conc. (mM)	4'H	4OCH ₃	5'H	7H	1'H	3H	1H	2H	3NH ₃ ⁺
0.01	3.66	4.00	4.21	5.00	5.50	7.55	7.77	7.82	8.41
0.04	3.67	3.99	4.22	4.98	5.48	7.53	7.77	7.82	8.41
0.08	3.69	3.97	4.22	4.93	5.46	7.49	7.76	7.78	8.41
0.20	3.70	3.95	4.22	4.90	5.46	7.48	7.71	7.76	8.41
0.40	3.71	3.94	4.22	4.87	5.45	7.46	7.68	7.75	8.41
0.60	3.73	3.94	4.23	4.86	5.45	7.45	7.64	7.73	8.41
0.80	3.74	3.93	4.23	4.84	5.45	7.44	7.61	7.72	8.41
1.00	3.74	3.93	4.23	4.84	5.45	7.44	7.61	7.72	8.41
1.30	3.74	3.91	4.22	4.81	5.44	7.42	7.55	7.70	8.41
1.70	3.74	3.91	4.22	4.81	5.44	7.42	7.56	7.70	8.41
2.00	3.74	3.91	4.22	4.81	5.44	7.42	7.56	7.70	8.41
8.00	3.74	3.76	4.23	4.64	5.34	7.21	7.23	7.48	8.41
$\Delta\delta$	+0.08	-0.24	+0.02	-0.36	-0.16	-0.34	-0.54	-0.34	0.00

Downfield shift is +ve

upfield shift is -ve

Table: 1d Changes in chemical shift $\Delta\delta$ (in ppm) as a function of concentration of various drug protons in D₂O and its comparison with literature

	Present Work			Evstigneev et al., 2006	Chaires et al., 1982	
	$\Delta\delta = \delta_{8.00} - \delta_{0.01 \text{ mM}}$ 298 K			$\Delta\delta = \delta_{3.5} - \delta_{0.1 \text{ mM}}$ 303 K	$\Delta\delta = \delta_{7.0} - \delta_{0.5 \text{ mM}}$ 298 K	$\Delta\delta = \delta_{7.0} - \delta_{0.5 \text{ mM}}$ 323 K
	4'-Epiadriamycin	Adriamycin	Daunomycin	Daunomycin	Daunomycin	Daunomycin
5'CH ₃	+0.01	+0.02	-0.05	-	-	-
2'axH	+0.04	-0.01	+0.05	-	-	-
8axH	-0.18	-0.24	-0.26	-	-	-
8eqH	+0.04	-0.28	-0.27	0.05	-	-
2'eqH	-0.05	-0.01	+0.05	-	-	-
10axH	-0.40	-0.68	-0.38	0.16	-	-
10eqH	-0.28	-0.49	-0.30	0.19	-	-
4'H	+0.20	+0.04	+0.08	-	-	-
3'H	+0.19	+0.10	+0.21	-	-	-
4OCH ₃	-0.16	-0.30	-0.24	0.17	-0.32	-0.22
5'H	-0.04	-0.17	+0.02	-	-	-
7H	+0.37	+0.01	-0.36	-	0.00	0.00
9COCH ₂ / 9COCH ₃	-0.08	+0.54	+0.02	0.01	-	-
1'H	-0.11	-0.12	-0.16	0.08	-	-
3H	-0.31	-0.28	-0.34	0.24	-0.26	-0.23
1H	-0.56	-0.52	-0.54	0.43	-0.38	-0.37
2H	-0.33	-0.37	-0.34	0.25	-0.21	-0.20

Downfield shift is +ve; upfield shift is -ve

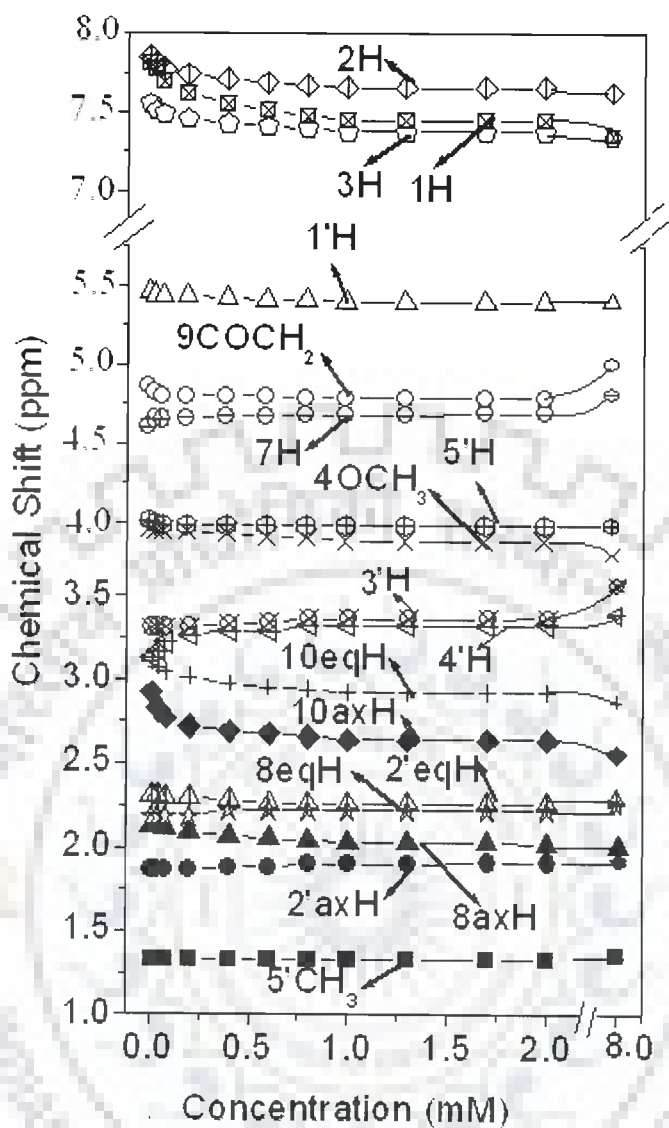


Fig. 4: Proton chemical shifts of 4'-epiadriamycin as a function of concentration at 298 K

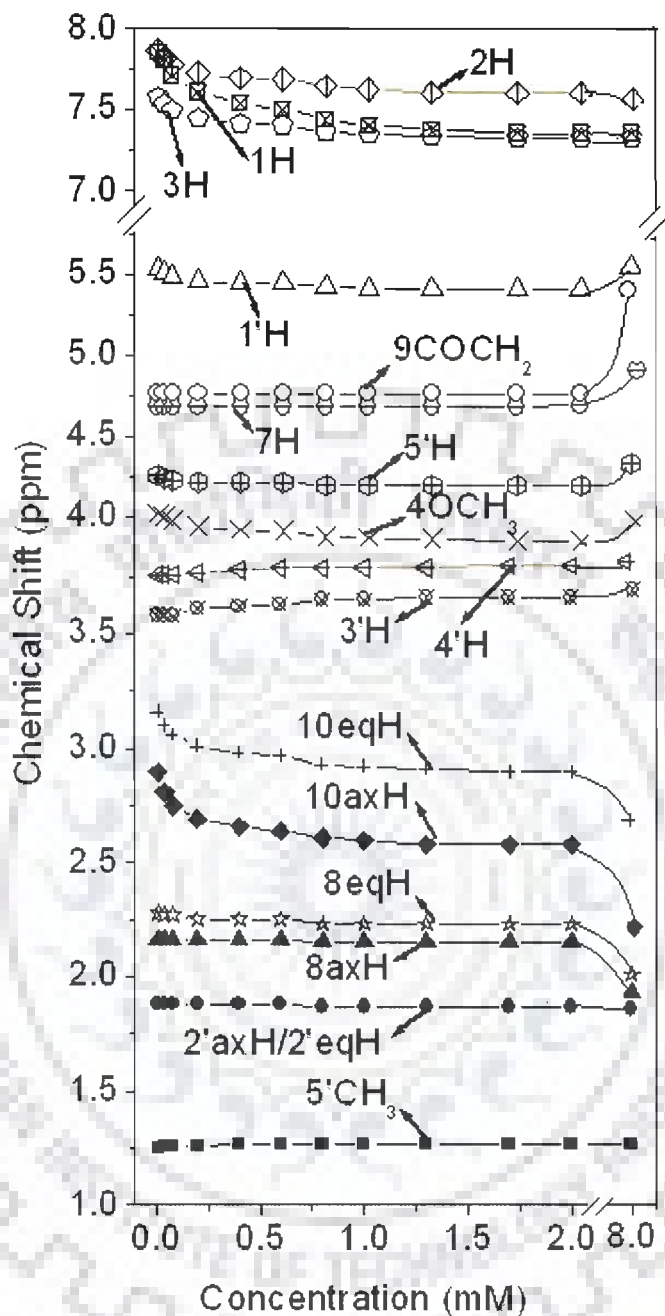


Fig. 5: Proton chemical shifts of adriamycin as a function of concentration at 298 K

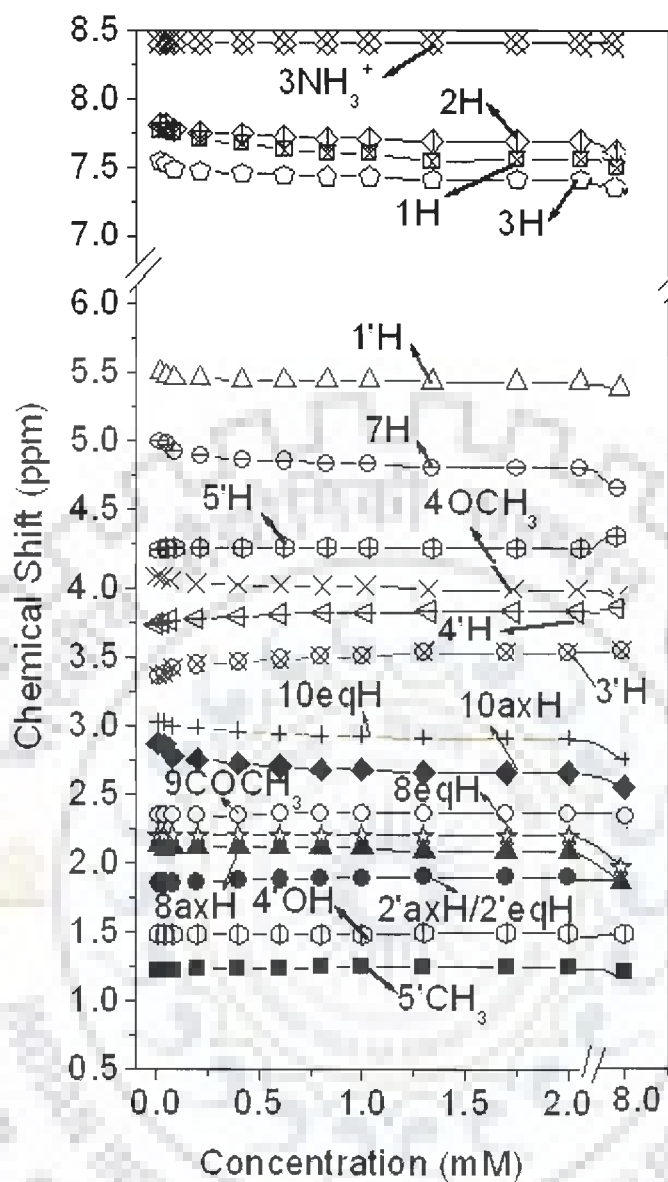


Fig. 6: Proton chemical shifts of daunomycin as a function of concentration at 298 K

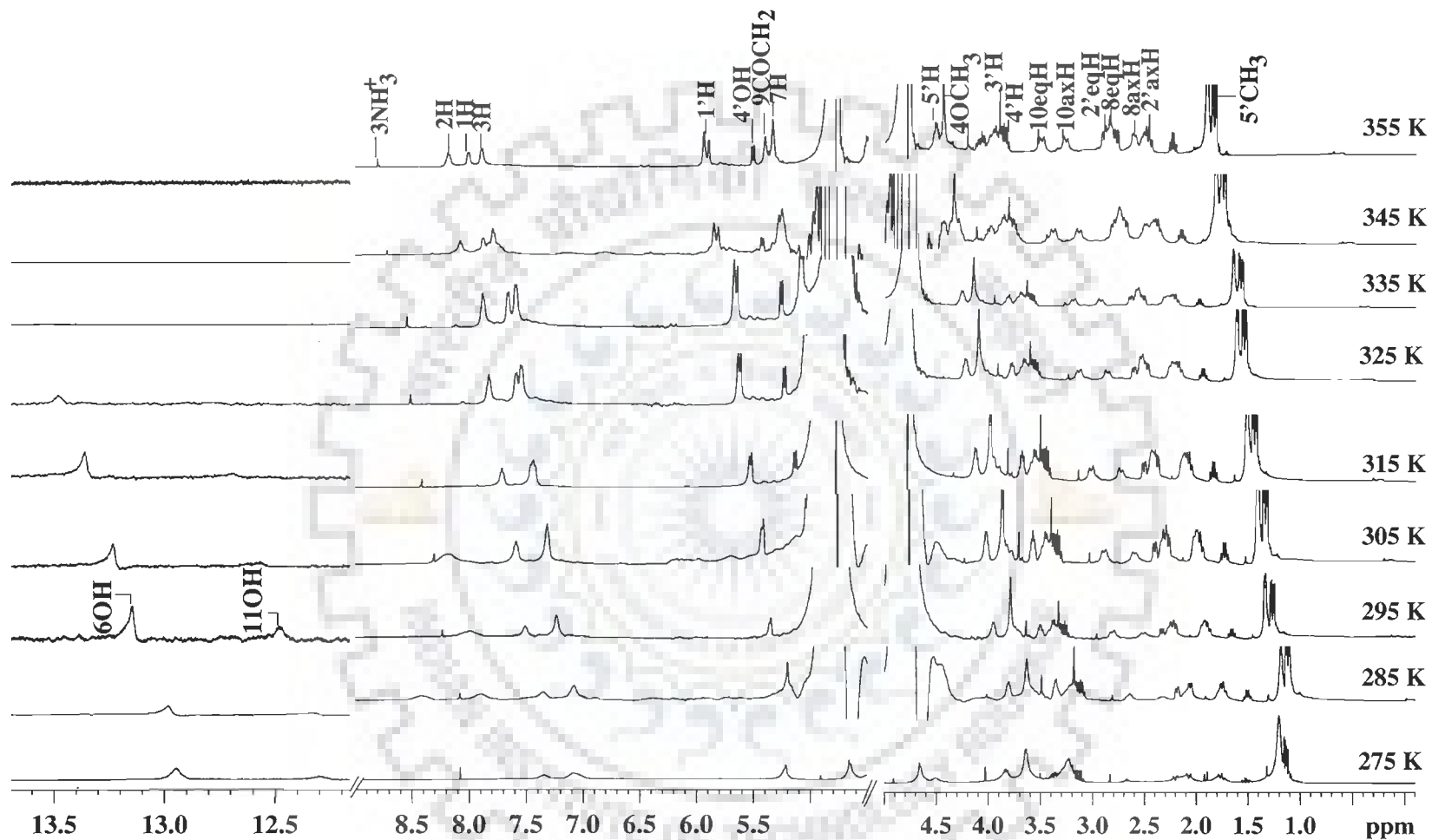


Fig. 7: One-dimensional proton NMR spectra of 8 mM 4'-epiadriamycin in D₂O as a function of temperature

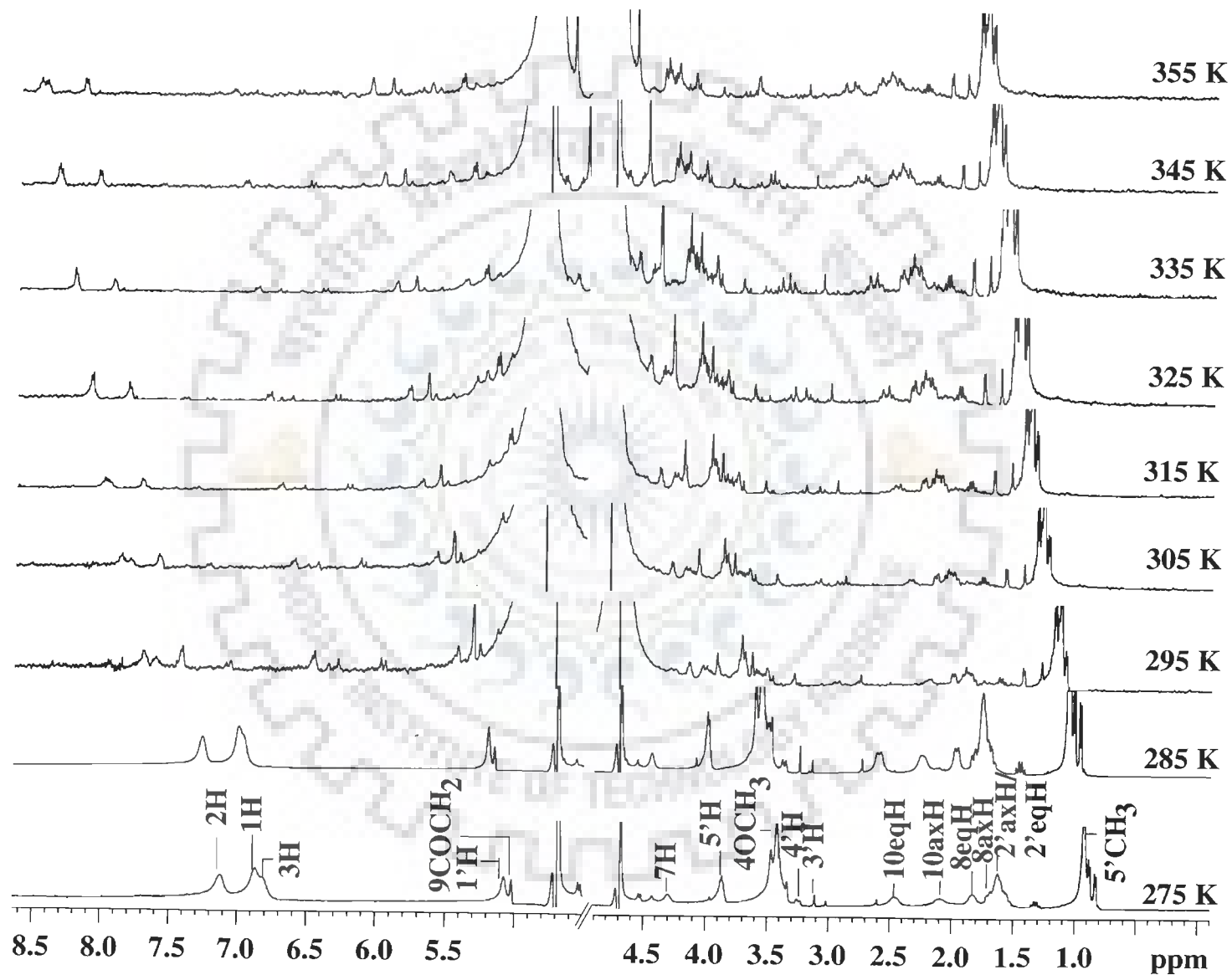


Fig. 8: One-dimensional proton NMR spectra of 8 mM adriamycin in D₂O as a function of temperature

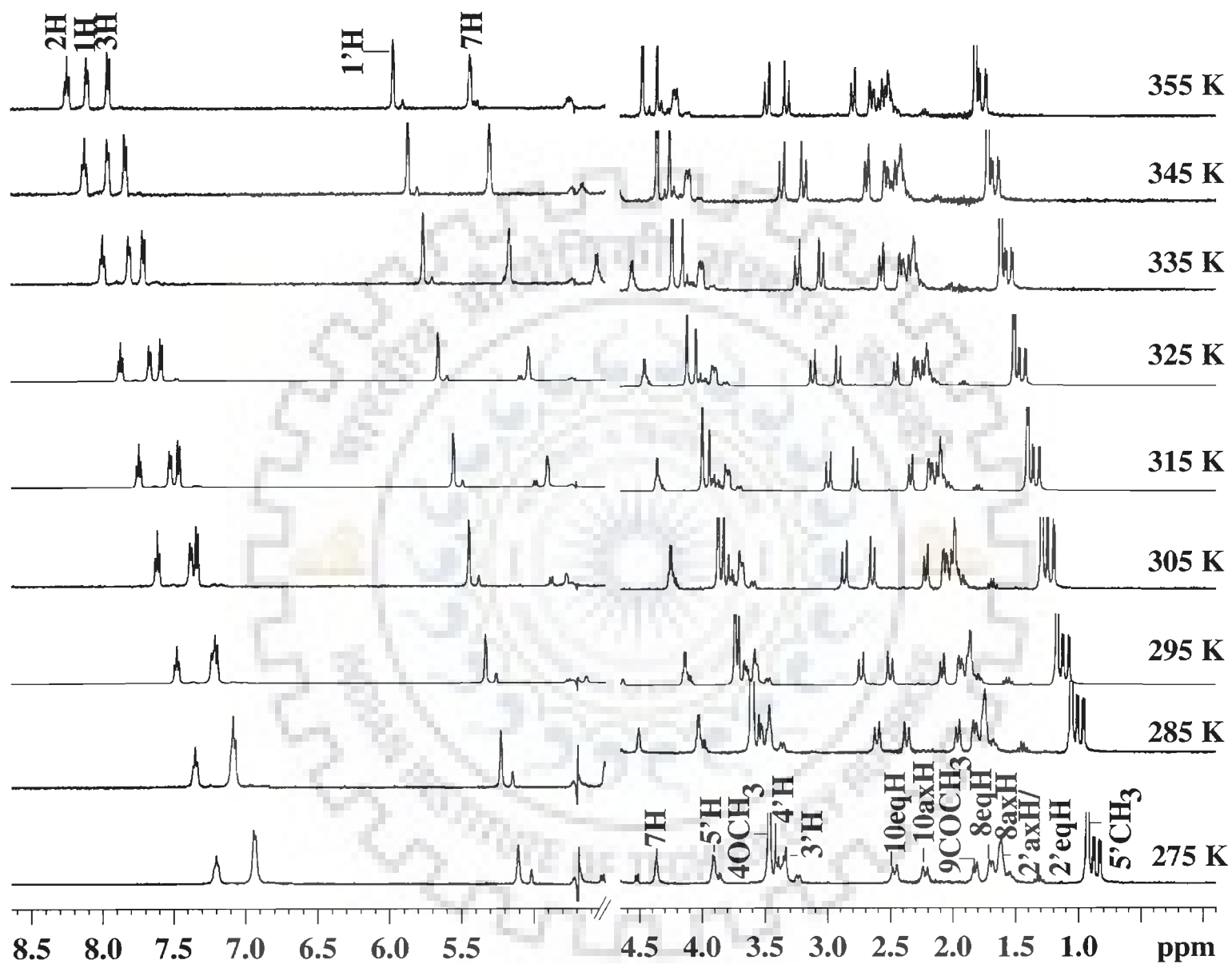


Fig. 9: One-dimensional proton NMR spectra of 8 mM daunomycin in D₂O as a function of temperature

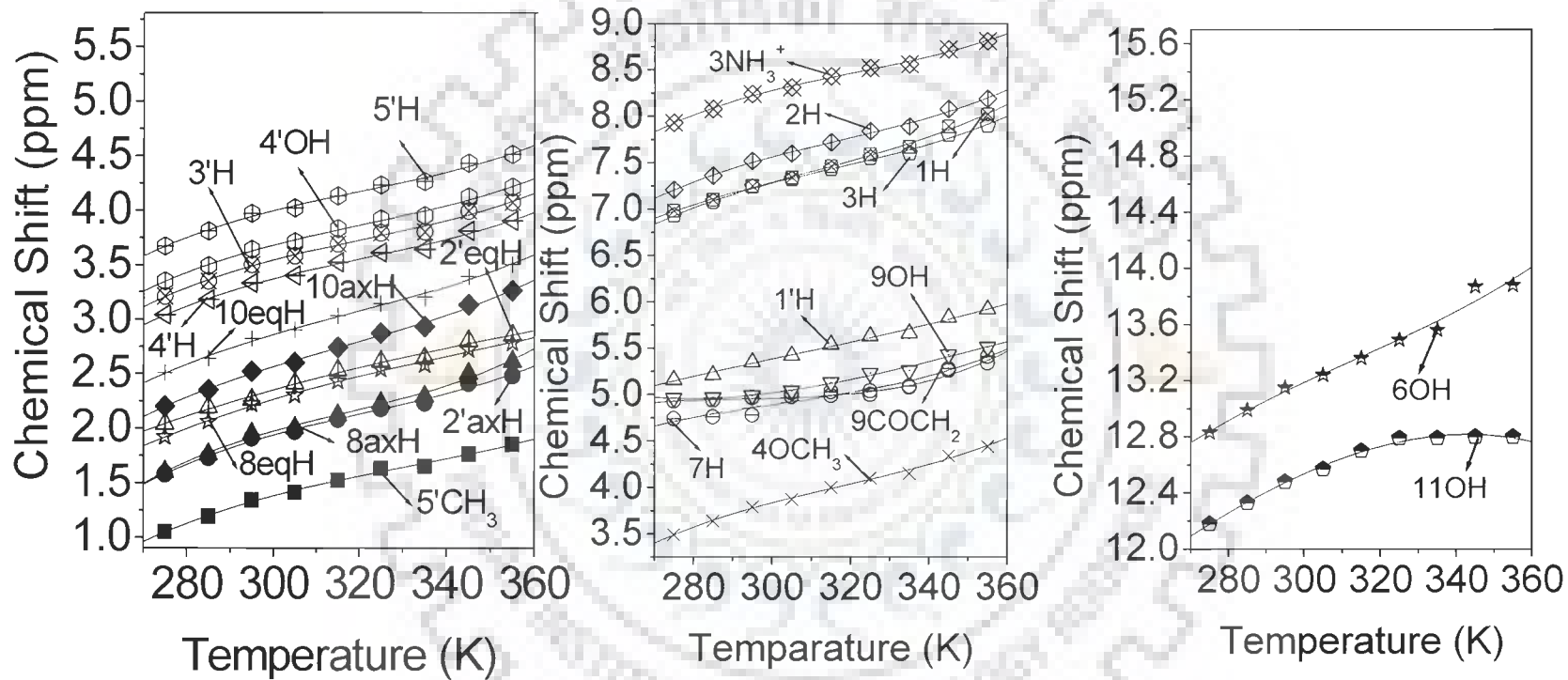


Fig. 10: Proton chemical shift of 8 mM 4'-epiadriamycin as a function of Temperature

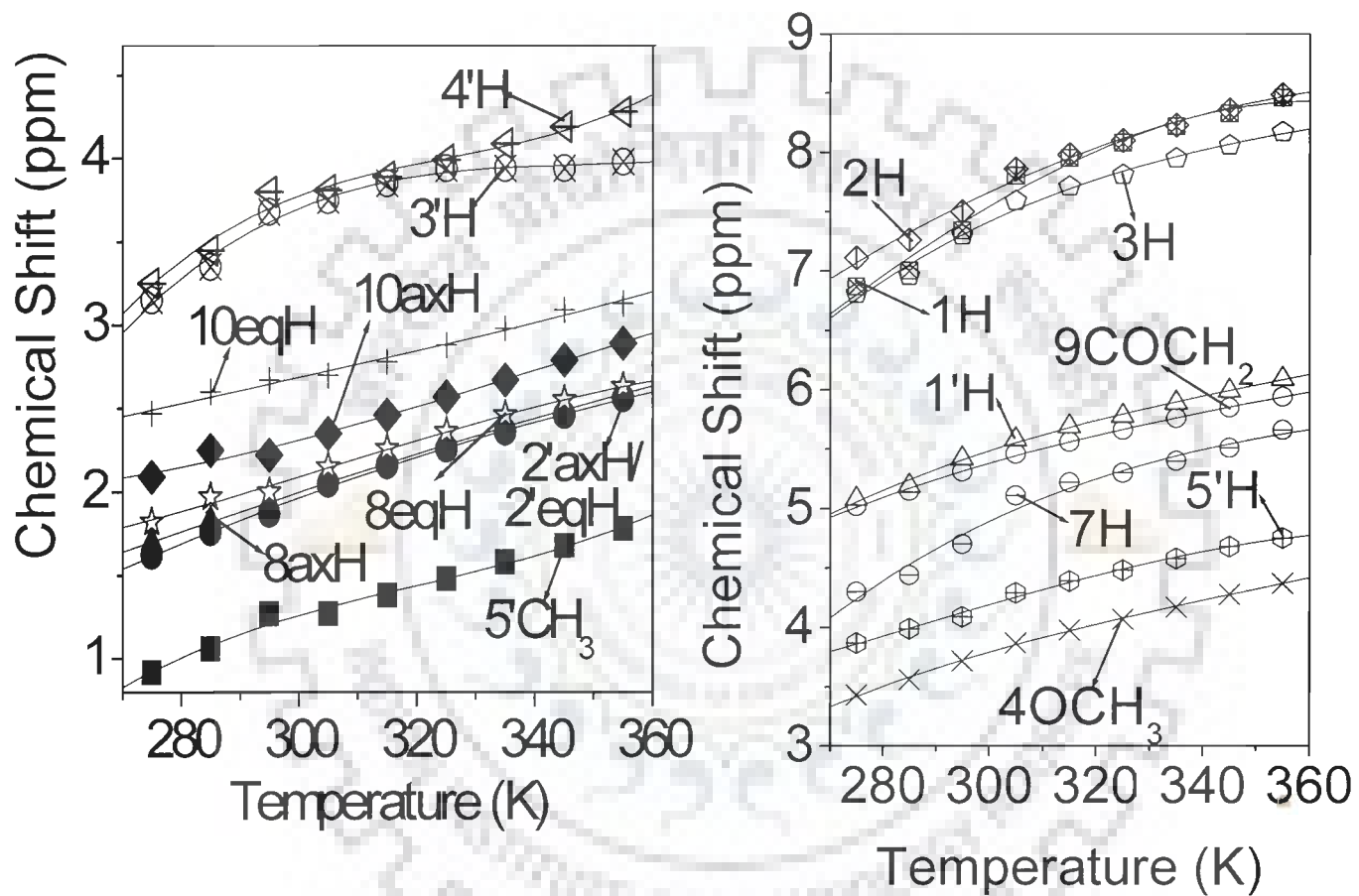


Fig. 11: Proton chemical shift of 8 mM adriamycin as a function of Temperature

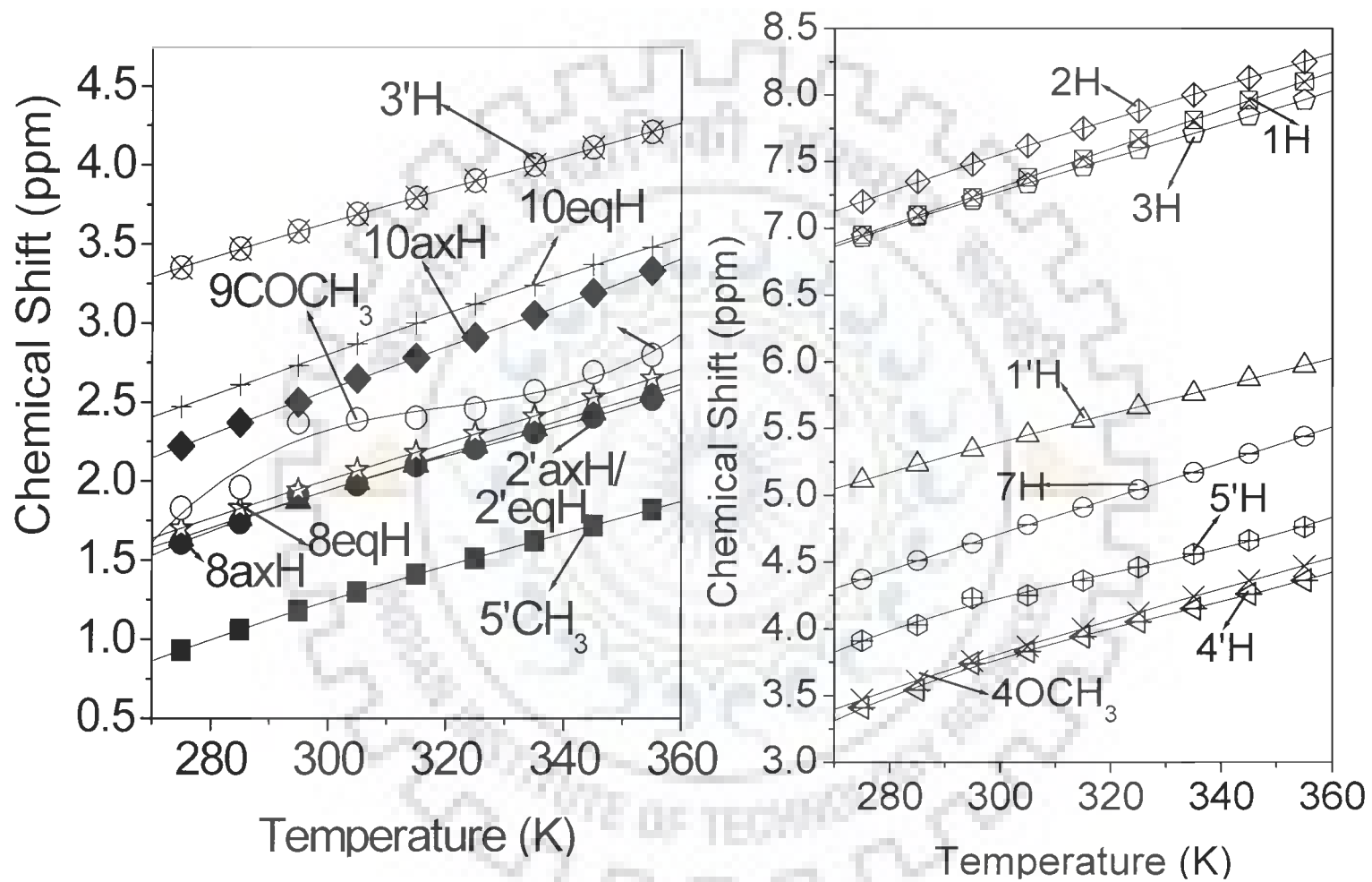


Fig. 12: Proton chemical shift of 8 mM daunomycin as a function of Temperature

Table: 2a Proton chemical shift of 8 mM 4'-epiadriamycin in D₂O as a function of Temperature. $\Delta\delta = \delta_{355\text{ K}} - \delta_{275\text{ K}}$ indicates total change in chemical shift due to self association.

Temp. (K)	5'CH ₃	2'axH	8axH	8eqH	2'eqH	10axH	10eqH	4'H	3'H	4'OH	5'H
275	1.05	1.58	1.60	1.92	2.04	2.20	2.51	3.04	3.21	3.35	3.67
285	1.19	1.73	1.76	2.06	2.19	2.35	2.64	3.18	3.35	3.49	3.81
295	1.34	1.91	1.95	2.22	2.26	2.52	2.82	3.33	3.50	3.64	3.97
305	1.41	1.97	2.00	2.30	2.41	2.60	2.90	3.40	3.58	3.71	4.02
315	1.52	2.08	2.12	2.43	2.53	2.74	3.03	3.52	3.69	3.83	4.13
325	1.63	2.18	2.23	2.54	2.61	2.87	3.14	3.61	3.79	3.92	4.23
335	1.65	2.23	2.29	2.58	2.64	2.93	3.20	3.64	3.80	3.95	4.26
345	1.76	2.41	2.50	2.72	2.80	3.13	3.39	3.81	3.99	4.12	4.43
355	1.85	2.48	2.61	2.78	2.85	3.26	3.50	3.90	4.07	4.21	4.51
$\Delta\delta$	+0.80	+0.90	+1.01	+0.86	+0.81	+1.06	+0.99	+0.86	+0.86	+0.86	+0.84
Temp. (K)	9COCH ₂	7H	9OH	1'H	3H	1H	2H	6OH	11OH	3NH ₃ ⁺	4OCH ₃
275	4.93	4.74	4.96	5.16	6.93	6.98	7.21	12.83	12.18	7.93	3.49
285	4.94	4.76	4.97	5.21	7.08	7.10	7.36	12.99	12.33	8.08	3.64
295	4.97	4.78	4.99	5.35	7.24	7.25	7.52	13.15	12.48	8.24	3.79
305	4.98	5.02	5.04	5.42	7.32	7.34	7.60	13.24	12.57	8.31	3.87
315	4.99	5.03	5.13	5.54	7.43	7.46	7.72	13.36	12.70	8.43	4.00
325	5.00	5.04	5.23	5.63	7.55	7.59	7.84	13.49	12.79	8.52	4.10
335	5.08	5.09	5.26	5.66	7.60	7.67	7.89	13.56	12.79	8.56	4.15
345	5.26	5.28	5.43	5.83	7.80	7.89	8.08	13.87	12.80	8.72	4.34
355	5.34	5.41	5.51	5.92	7.90	8.02	8.19	13.88	12.80	8.81	4.44
$\Delta\delta$	+0.41	+0.67	+0.55	+0.76	+0.97	+1.04	+0.98	+1.05	+0.62	+0.88	+0.95

Downfield shift is +ve
upfield shift is -ve

Table: 2b Proton chemical shift of 8 mM adriamycin in D₂O as a function of Temperature. $\Delta\delta = \delta_{355\text{ K}} - \delta_{275\text{ K}}$ indicates total change in chemical shift due to self association.

Temp. (K)	5'CH ₃	2'axH/ 2'eqH	8axH	8eqH	10axH	10eqH	3'H	4'H	4OCH ₃
275	0.92	1.62	1.70	1.82	2.09	2.47	3.15	3.25	3.43
285	1.06	1.76	1.83	1.97	2.25	2.60	3.35	3.45	3.56
295	1.27	1.87	1.92	2.00	2.22	2.67	3.68	3.80	3.72
305	1.27	2.05	2.06	2.15	2.35	2.70	3.75	3.81	3.87
315	1.38	2.16	2.18	2.26	2.46	2.78	3.85	3.89	3.98
325	1.48	2.26	2.28	2.36	2.57	2.88	3.94	3.99	4.07
335	1.58	2.36	2.38	2.46	2.67	2.98	3.94	4.09	4.17
345	1.68	2.46	2.49	2.55	2.79	3.09	3.94	4.19	4.28
355	1.78	2.56	2.59	2.63	2.89	3.13	3.98	4.28	4.37
$\Delta\delta$	+0.86	+0.94	+0.89	+0.81	+0.80	+0.66	+0.83	+1.03	+0.94
Temp. (K)	5'H	7H	9COCH ₂	1'H	3H	1H	2H	6OH	11OH
275	3.87	4.30	5.02	5.08	6.81	6.87	7.11	13.10	12.51
285	3.99	4.44	5.15	5.19	6.96	7.00	7.26	-	-
295	4.09	4.70	5.31	5.42	7.30	7.34	7.50	-	-
305	4.29	5.11	5.46	5.58	7.59	7.80	7.86	-	-
315	4.39	5.22	5.56	5.69	7.71	7.95	7.98	-	-
325	4.48	5.30	5.66	5.78	7.81	8.08	8.10	-	-
335	4.58	5.40	5.76	5.89	7.95	8.22	8.23	-	-
345	4.68	5.51	5.85	5.99	8.06	8.33	8.36	-	-
355	4.75	5.66	5.94	6.09	8.17	8.46	8.49	-	-
$\Delta\delta$	+0.88	+1.36	+0.92	+1.01	+1.36	+1.59	+1.38	-	-

Downfield shift is +ve
upfield shift is -ve

Table: 2c Proton chemical shift of 8 mM daunomycin in D₂O as a function of Temperature. $\Delta\delta = \delta_{355\text{ K}} - \delta_{275\text{ K}}$ indicates total change in chemical shift due to self association.

Temp. (K)	5'CH ₃	2'axH/2'eqH	8axH	8eqH	9COCH ₃	10axH	10eqH	3'H
275	0.93	1.61	1.64	1.70	1.83	2.22	2.47	3.35
285	1.06	1.74	1.77	1.83	1.96	2.37	2.61	3.47
295	1.18	1.91	1.88	1.94	2.37	2.50	2.73	3.58
305	1.30	1.98	2.00	2.07	2.39	2.65	2.87	3.69
315	1.41	2.10	2.11	2.18	2.40	2.78	3.00	3.79
325	1.51	2.21	2.23	2.30	2.46	2.91	3.12	3.90
335	1.62	2.31	2.34	2.41	2.57	3.05	3.24	4.00
345	1.72	2.41	2.44	2.53	2.69	3.19	3.37	4.11
355	1.82	2.52	2.56	2.65	2.80	3.33	3.48	4.21
$\Delta\delta$	+0.89	+0.91	+0.92	+0.95	+0.97	+1.11	+1.01	+0.86
Temp. (K)	4'H	4OCH ₃	5'H	7H	1'H	3H	1H	2H
275	3.41	3.47	3.91	4.37	5.11	6.93	6.95	7.20
285	3.54	3.61	4.03	4.51	5.23	7.09	7.10	7.35
295	3.74	3.76	4.23	4.64	5.34	7.21	7.23	7.48
305	3.83	3.87	4.25	4.78	5.45	7.33	7.38	7.62
315	3.94	4.00	4.36	4.91	5.56	7.46	7.52	7.75
325	4.05	4.12	4.46	5.04	5.66	7.59	7.67	7.88
335	4.15	4.24	4.56	5.17	5.76	7.71	7.81	8.00
345	4.26	4.36	4.66	5.31	5.87	7.84	7.96	8.13
355	4.36	4.47	4.76	5.44	5.97	7.96	8.10	8.25
$\Delta\delta$	+0.95	+1.00	+0.85	+1.07	+0.86	+1.03	+1.15	+1.05

Downfield shift is +ve
upfield shift is -ve

Table: 2d Changes in chemical shift $\Delta\delta$ (in ppm) as a function of temperature of various drug protons in D₂O and its comparison with literature.

	Present Work			Evstigneev et al., 2006	Chaires et al., 1982	Barthwal et al., 1994		Barthwal et al., 1996
	$\Delta\delta = \delta_{355} - \delta_{275\text{K}}$ 8.0 mM			$\Delta\delta = \delta_{335} - \delta_{278\text{K}}$ 1.6 mM	$\Delta\delta = \delta_{348} - \delta_{283\text{K}}$ 7.0 mM	$\Delta\delta = \delta_{355} - \delta_{277\text{K}}$ 11.5 mM	$\Delta\delta = \delta_{355} - \delta_{277\text{K}}$ 11.5 mM	$\Delta\delta = \delta_{350} - \delta_{277\text{K}}$ 4.95 mM
	4'-Epiadriamycin	Adriamycin	Daunomycin	Daunomycin	Daunomycin	Adriamycin	Daunomycin	Daunomycin
5'CH ₃	+0.80	+0.86	+0.89	-	-	+0.19	+0.18	-0.01
2'axH	+0.90	+0.94	+0.91	-	-	+0.20	+0.15	+0.01
8axH	+1.01	+0.89	+0.92	-	-	+0.26	+0.27	0.08
8eqH	+0.86	+0.81	+0.95	-	-	+0.29	+0.27	0.09
2'eqH	+0.81	+0.94	+0.91	-	-	+0.20	+0.15	+0.04
10axH	+1.06	+0.80	+1.11	-	-	+0.45	+0.46	+0.16
10eqH	+0.99	+0.66	+1.01	+0.13	-	+0.31	+0.33	+0.12
4'H	+0.86	+1.03	+0.95	-	-	+0.21	+0.17	-0.01
3'H	+0.86	+0.83	+0.86	-	-	+0.16	+0.13	-0.07
4OCH ₃	+0.95	+0.94	+1.00	-	+0.18	+0.28	+0.32	+0.11
5'H	+0.84	+0.88	+0.85	-0.02	-	+0.16	+0.14	-0.03
7H	+0.67	+1.36	+1.07	-	-	+0.15	+0.41	+0.14
9COCH ₂ / 9COCH ₃	+0.41	+0.92	+0.97	-	0.00	+0.41	-	0.00
1'H	+0.76	+1.01	+0.86	-	-	+0.17	+0.16	-0.02
3H	+0.97	+1.36	+1.03	-	+0.33	+0.30	+0.34	+0.17
1H	+1.04	+1.59	+1.15	-	+0.26	+0.44	+0.52	+0.20
2H	+0.98	+1.38	+1.05	+0.17	+0.20	+0.34	+0.38	+0.15

Downfield shift is +ve
upfield shift is -ve

4'-epiadriamycin. They are free and may be exchanging with solvent rapidly in daunomycin and adriamycin and therefore are not observable in their NMR spectra. These observations clearly are indicative of the fact that stacked structure in 4'-epiadriamycin is different from those of adriamycin and daunomycin. Analysis of 2D NOESY spectra at 355 K (Fig. 13a-b, 14a-b and 15a-b) shows presence of several inter-proton contacts (Table 3), for which the distances have been calculated. The corresponding distances in the rMD simulated structures are close to experimental restraints (Table 3) and hence are true representative of the experimental results. Several NOE connectivities, e.g. 5'CH₃-1'H, 8eqH-10axH, 8eqH-1'H, etc. (Table 3) show proximity of protons within daunosamine sugar, within ring A, within ring D as well as proximity of ring A protons to daunosamine sugar (Barthwal et al., 1994). These intramolecular connectivities characterize specific conformation of ring A and daunosamine sugar in each drug. Several NOE contacts such as 2H-10eqH / 10axH / 9COCH₂ / 7H / 8axH / 5'CH₃; 4OCH₃-10axH / 10eqH / 8axH / 8eqH / 9COCH₂ / 7H; 1H / 3H- 8axH / 10axH / 10eqH / 9COCH₂ / 7H in adriamycin are possible only if aromatic chromophores of two drug molecules overlap in a stacked structure forming dimer in which ring A lies above ring D, hence in an anti-parallel orientation (Table 3). Several other NOE connectivities e.g. 5'CH₃-10axH / 10eqH, 1'H-10eqH / 9COCH₂, 3'H-9COCH₂ / 10axH also refer to intermolecular contacts but in parallel orientation of aromatic chromophores in which ring A is stacked over ring A itself. Evidence of such dimer structures in parallel and antiparallel orientations were found for the first time by Evstigneev et al. (Evstigneev et al., 2006) in daunomycin molecule at 303 K. However, since 7H-10axH / 10eqH cross peak is observed in parallel mode of orientation, the ring A is stacked over ring A but is inverted. This is also evident from the orientation of 4OCH₃ moiety, which is lying in opposite sense in the two stacked molecules in the structure obtained after rMD simulations (Fig. 16-18).

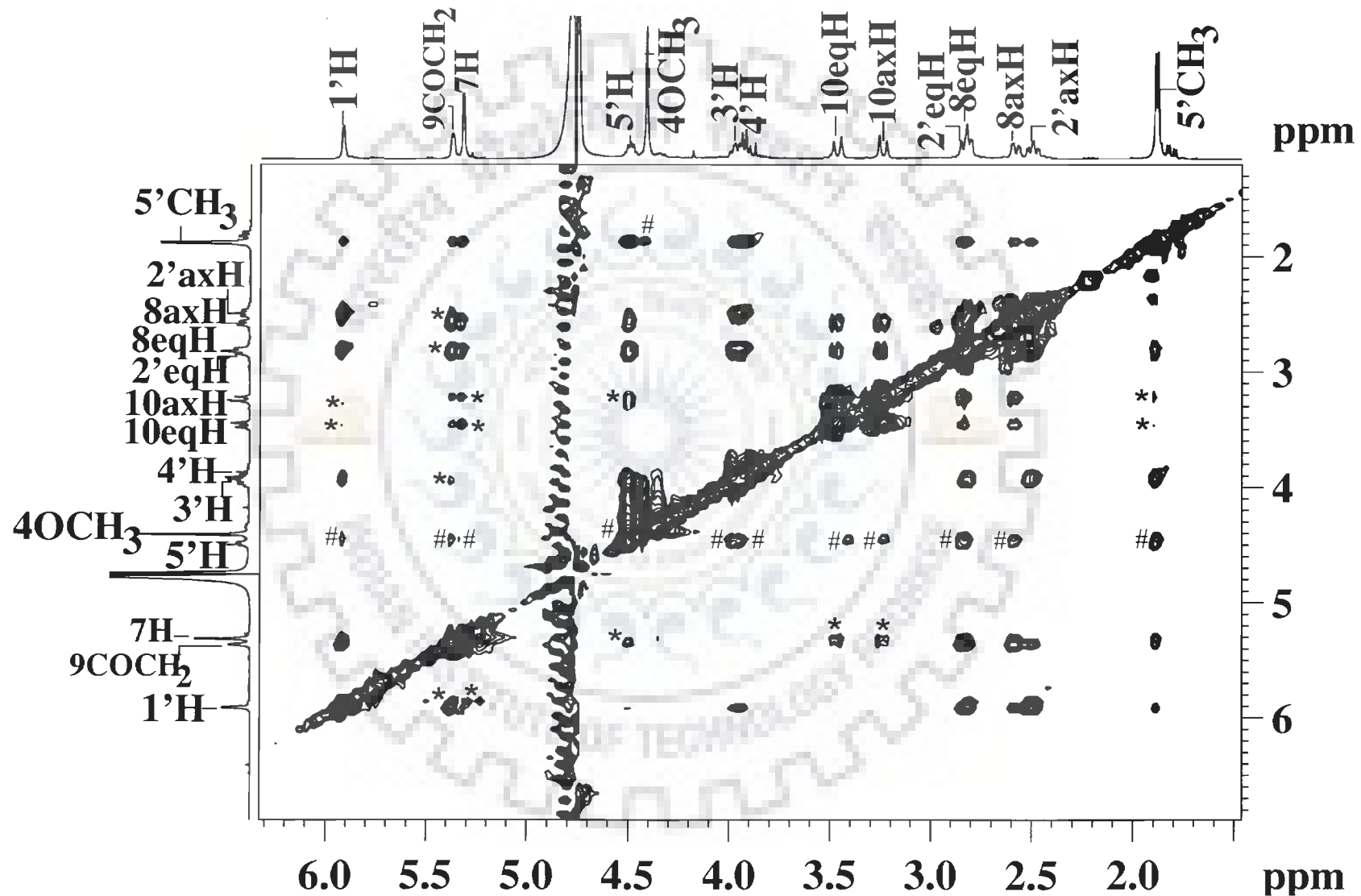


Fig. 13a: 2D NOESY spectra of 8 mM 4'-epiadriamycin in D₂O at 355 K at 500 MHz. The figure shows expansions of specific regions to highlight connectivities (* indicating parallel and # anti-parallel mode of orientation).

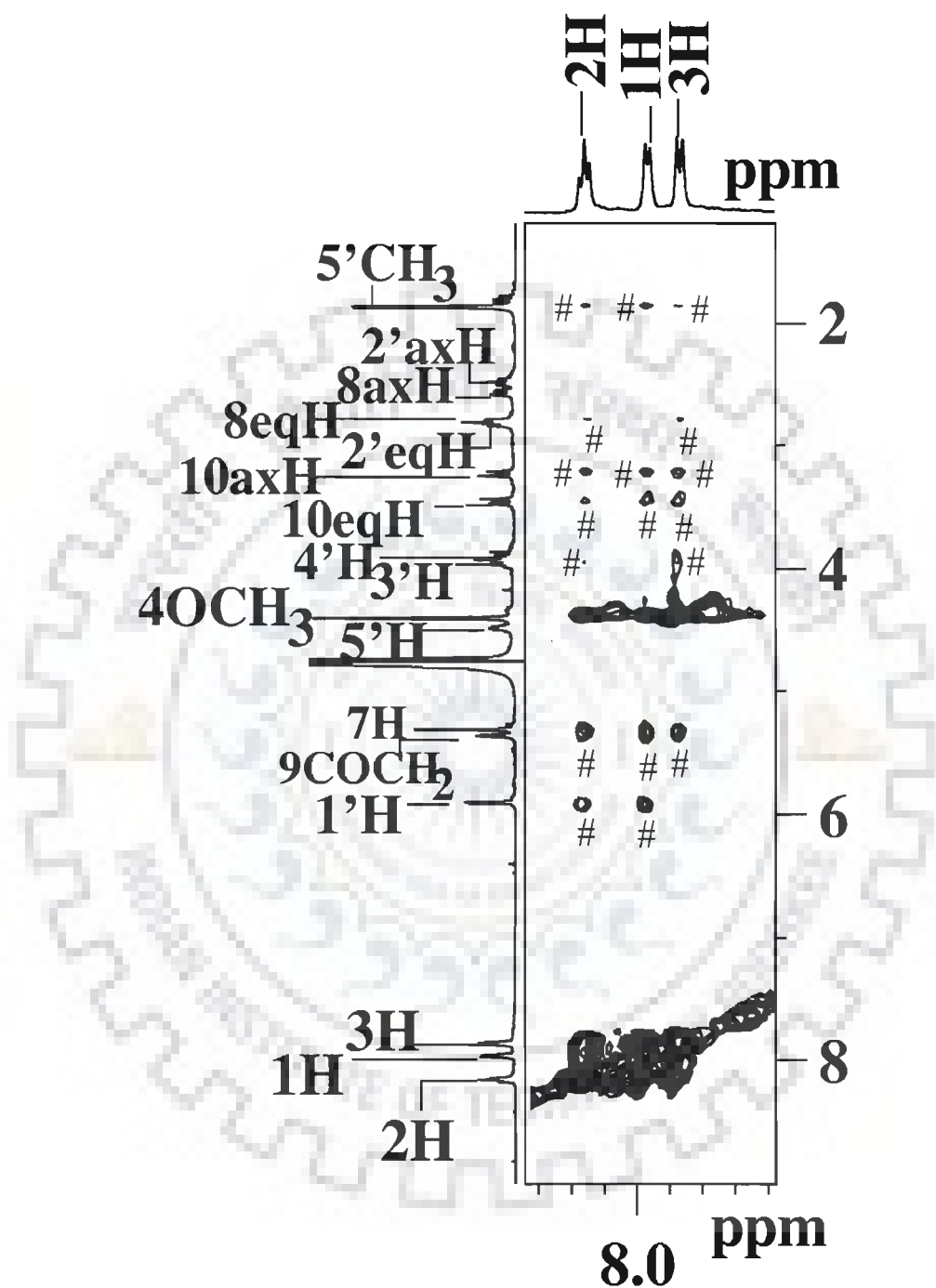


Fig. 13b: 2D NOESY spectra of 8 mM 4'-epiadriamycin in D₂O at 355 K at 500 MHz. The figure shows expansions of specific regions to highlight connectivity. (# indicates anti-parallel orientation).

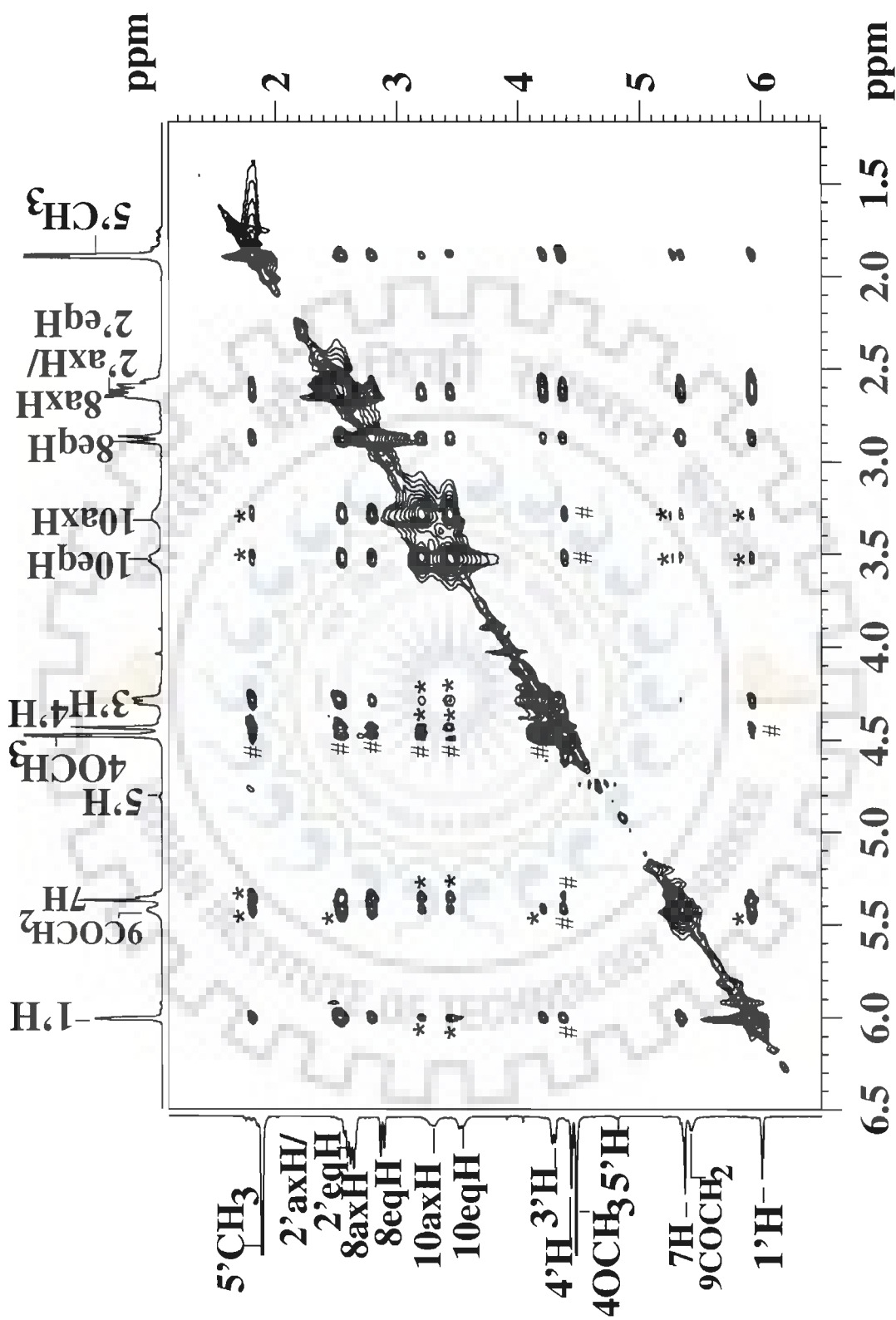


Fig. 14a: 2D NOESY spectra of 8 mM adriamycin in D_2O at 355 K at 500 MHz. The figure shows expansions of specific regions to highlight connectivities. (# indicates anti-parallel orientation and * indicating parallel mode of orientation).

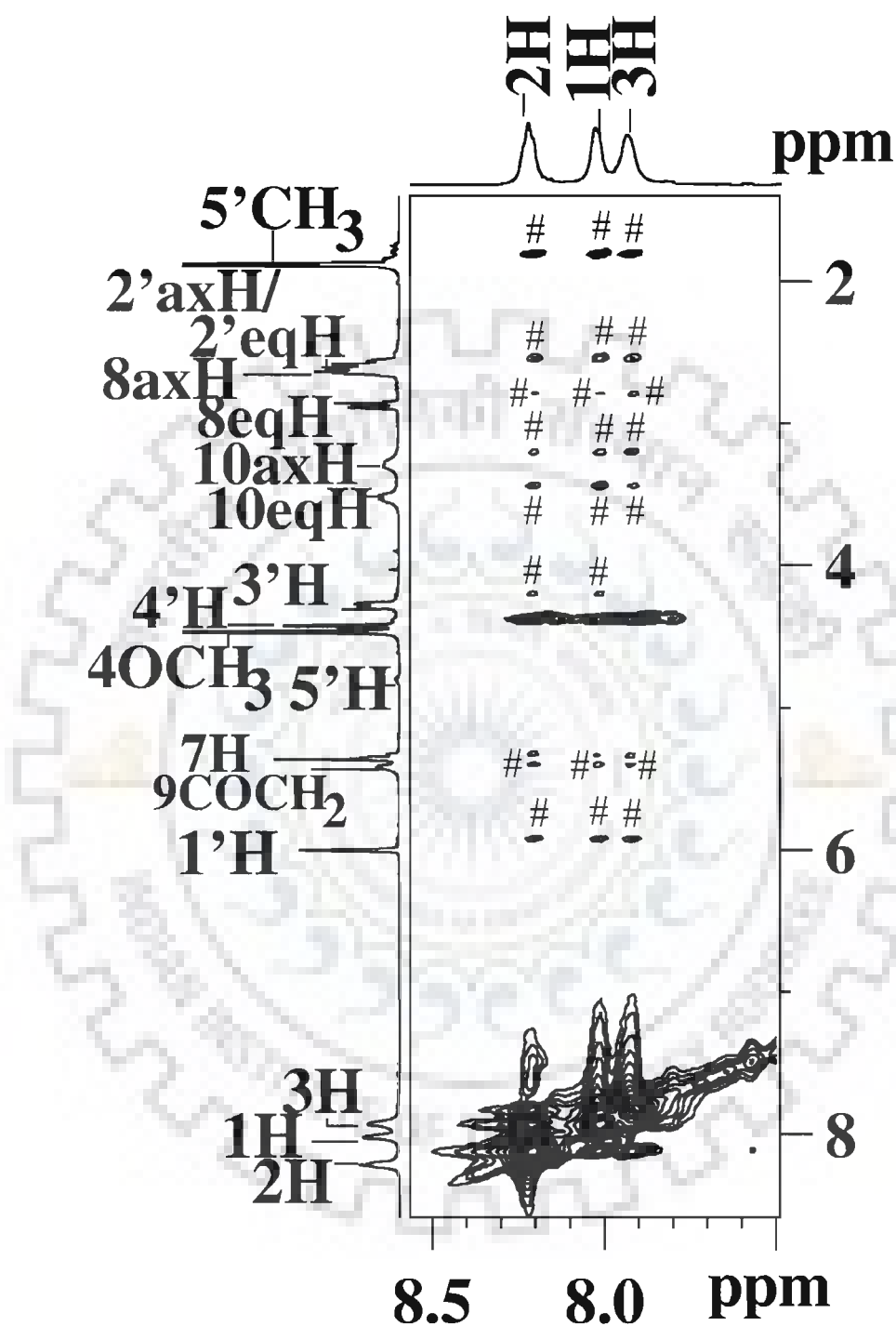


Fig. 14b: 2D NOESY spectra of 8 mM adriamycin in D₂O at 355 K at 500 MHz. The figure shows expansions of specific regions to highlight connectivities. (# indicates anti-parallel orientation).

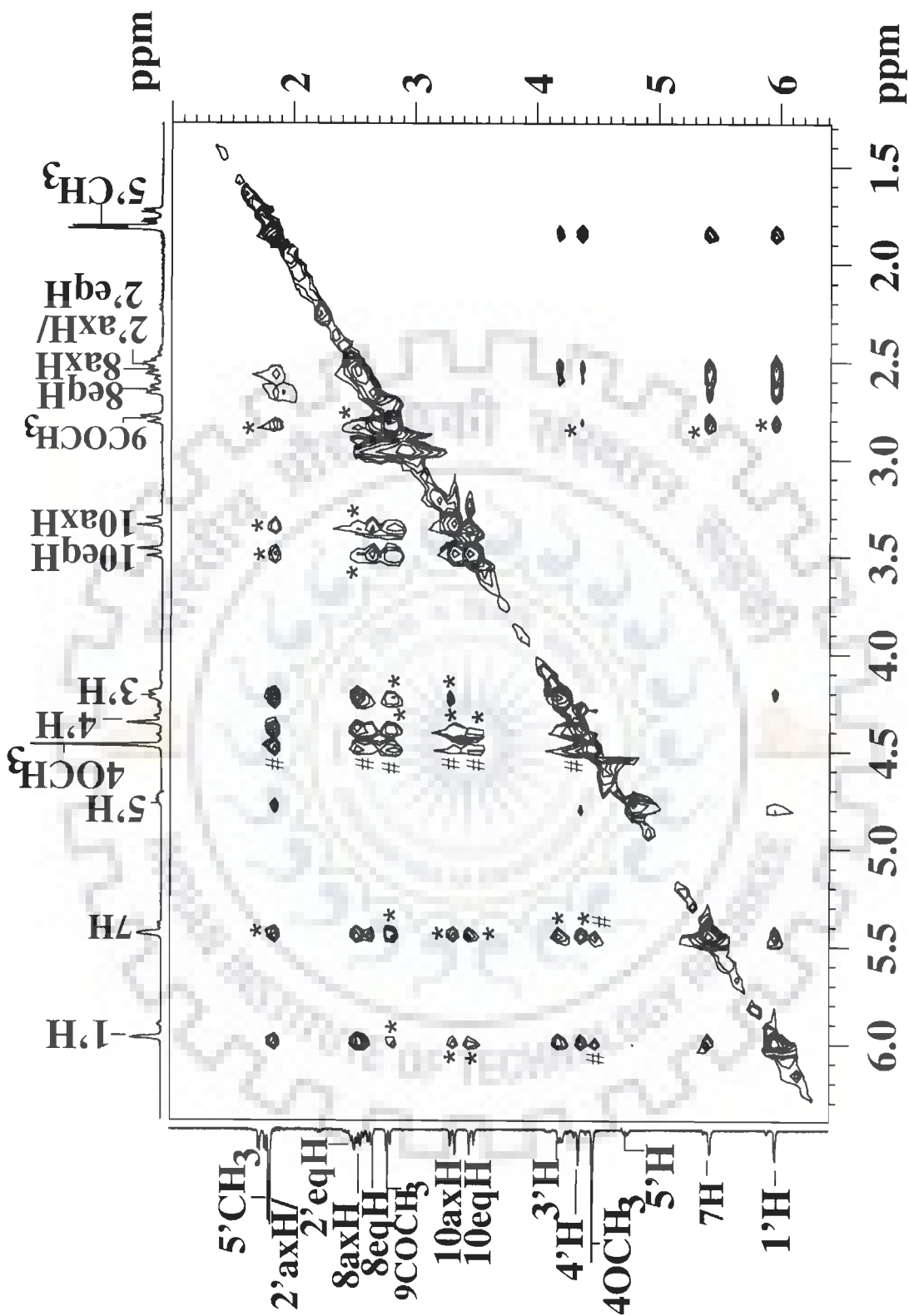


Fig. 15a: 2D NOESY spectra of 8 mM daunomycin in D_2O at 355 K at 500 MHz. The figure shows expansions of specific regions to highlight connectivities. (# indicates anti-parallel orientation and * indicating parallel mode of orientation).

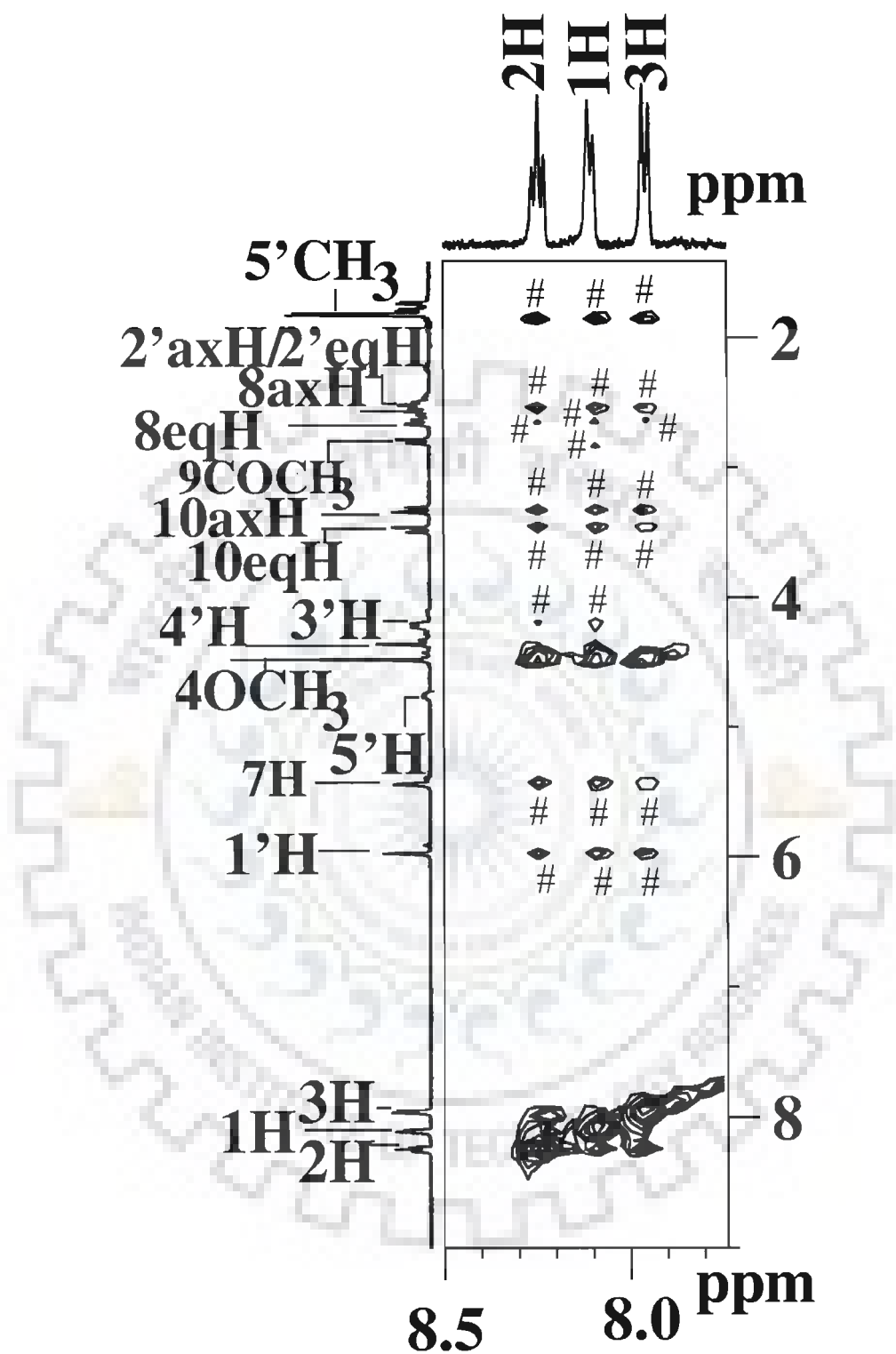


Fig. 15b: 2D NOESY spectra of 8 mM daunomycin in D_2O at 355 K at 500 MHz. The figure shows expansions of specific regions to highlight connectivities. (# indicates anti-parallel orientation).

Table: 3 Connectivities and inter-proton distances (Å) of 4'-epiadriamycin, adriamycin and daunomycin obtained from NOESY spectra ($\tau_m=400$ ms) at 355 K. The corresponding distances obtained from optimized rMD structure are also shown. Overlap of peak is shown by 'o' and '-' indicates absence of peak. 'E' denotes NOE observed for daunomycin at 303 K by Evstigneev et al., 2006.

Connectivities	4'-epiadriamycin		adriamycin		daunomycin	
	Distance (Å) obtained from NMR	Distance in rMD structure (Å)	Distance (Å) obtained from NMR	Distance in rMD structure (Å)	Distance (Å) obtained from NMR	Distance in rMD structure (Å)
INTRAMOLECULAR CONNECTIVITIES						
Spin-Spin coupled protons						
1H-2H	2.50	2.49	2.50	2.49	2.36	2.52
3H-2H	2.52	2.52	2.52	2.52	2.26	2.52
2'eqH-1'H	2.86	2.87	o	-	o	-
2'axH-1'H	2.78	2.36	o	-	o	-
4'H-3'H	o	-	o	-	o	-
4'H-5'H	o	-	o	-	o	-
4'H- 5'CH ₃	3.90	3.26	3.12	3.18	3.55	3.07
3'H-2'eqH	o	-	o	-	o	-
3'H-2'axH	o	-	o	-	o	-
2'axH-2'eqH	1.90	1.81	o	-	o	-
5'CH ₃ -5'H	2.93	2.29	2.32	2.44	2.44	2.73
8axH-7H	2.42	2.75	o	-	2.76	2.95
8eqH-7H	3.44	3.28	2.18	2.29	2.54	2.23
8axH-8eqH	o	-	o	-	o	-
10axH-10eqH	2.25	2.43	2.30	1.79	1.80	1.90
8eqH-10eqH	o	-	3.11	3.43	3.00	3.28
Within Sugar moiety						
1'H-3'H	-	-	3.30	3.95	2.26	2.24
1'H-4'H	4.87	3.30	o	-	o	-
1'H-5'H	3.55	3.56	-	-	3.26	3.73
1'H-5'CH ₃	3.55	3.49	3.91	3.51	3.93	3.88
3'H-5'H	-	-	-	-	-	-
4'H-5'H	3.71	3.04	-	-	ww	-
3'H-5'CH ₃	3.13	3.72	3.80	3.75	3.62	3.37
2'axH-4'H	3.27	3.69	o	-	o	-
2'eqH-4'H	3.96	2.36	o	-	o	-

(contd.)

Within Ring D						
4OCH ₃ -1H	4.01	4.15	2.93	3.00	4.63	4.76
4OCH ₃ -2H	3.62	3.95	2.50	2.58	2.54	2.68
4OCH ₃ -3H	2.44	2.58	2.21	2.58	2.28	2.62
Within Ring A						
8axH-10axH	o	-	o	-	o	-
8axH-10eqH	o	-	o	-	o	-
8eqH-10axH	o	-	3.02	3.26	2.81	2.68
10axH-9COCH ₂ / 9COCH ₃	3.70	3.10	2.47	2.47	o	-
10eqH-9COCH ₂ / 9COCH ₃	3.72	3.14	2.45	2.82	o	-
8axH-9COCH ₂ / 9COCH ₃	3.93	3.76	o	-	o	-
8eqH-9COCH ₂ / 9COCH ₃	3.16	3.06	2.54	2.30	o	-
Ring A with Sugar Protons						
7H-1'H	3.74	3.85	o	-	3.57	3.54
7H-2'eqH/2'axH	o	-	o	-	o	-
7H 5'CH ₃	3.88	3.81	3.49	4.07	4.04	4.13
7H-5'H	ww	-	-	-	-	-
8axH-1'H	o	-	o	-	o	-
8axH-3'H	o	-	o	-	o	-
8axH-5'CH ₃	o	-	o	-	o	-
8axH-5'H	o	-	o	-	o	-
8eqH-1'H	o	-	2.83	2.49	3.96	3.74
8eqH-3'H	o	-	3.56	4.00	3.05	3.38
8eqH-4'H	o	-	4.04	4.61	2.48	2.96
8eqH-5'CH ₃	4.45	4.84	3.18	3.73	2.98	2.65
8eqH-5'H	4.00	3.70	-	-	-	-
5'CH ₃ -9COCH ₂ / 9COCH ₃	3.30	3.15	3.28	3.07	3.25	3.10

(contd.)

PARALLEL ORIENTATION CONNECTIVITIES						
	4'- epiadriamycin		adriamycin		daunomycin	
Within Ring A						
7H-10axH	4.49	3.67	3.55	3.44	3.12	3.20
7H-10eqH	4.53	4.46	3.61	3.48	3.17	3.31
Ring A with Sugar protons						
10axH-1'H	ww	-	4.78	4.59	4.09	4.78
10axH-2'eqH	o	-	o	-	o	-
10axH-2'axH	o	-	o	-	o	-
10axH-3'H E	-	-	4.06	4.17	3.30	3.34
10axH-4'H	-	-	o	-	2.20	2.12
10axH-5'H E	4.74	4.33	-	-	-	-
10axH-5'CH ₃ E	4.99	4.79	4.94	4.76	4.13	4.41
10eqH-1'H	4.67	4.81	3.91	3.96	3.65	3.91
10eqH-2'eqH	o	-	o	-	o	-
10eqH-2'axH	o	-	o	-	o	-
10eqH-3'H E	-	-	3.93	4.15	-	-
10eqH-4'H	-	-	o	-	2.22	2.20
10eqH-5'H E	-	-	-	-	-	-
10eqH-5'CH ₃ E	4.41	4.68	3.75	3.73	3.08	3.90
9COCH ₂ -1'H	3.15	3.04	3.63	3.88	4.15	4.42
9COCH ₂ /9COCH ₃ - 2'eqH	o	-	o	-	o	-
9COCH ₂ /9COCH ₃ - 2'axH	o	-	o	-	o	-
9COCH ₂ /9COCH ₃ -3'H	-	-	4.81	4.59	4.62	4.37
9COCH ₂ /9COCH ₃ -4'H	4.02	4.39	o	-	o	-
9COCH ₂ /9COCH ₃ -5'H	4.12	4.63	-	-	-	-
9COCH ₂ /9COCH ₃ -7H	o	-	o	-	3.80	3.87
ANTI PARALLEL ORIENTATION CONNECTIVITIES						
Ring A with Ring D						
10axH-1H E	4.94	4.80	3.89	4.32	4.71	4.59
10axH-2H E	4.09	4.56	3.85	4.17	4.49	4.39
10axH-3H E	4.08	4.31	3.72	3.64	3.59	3.48
10axH-4OCH ₃ E	4.48	4.65	4.60	4.70	3.20	3.12
10eqH-1H E	4.28	4.39	4.84	4.72	4.47	4.42
10eqH-2H E	4.25	4.07	3.69	3.92	4.35	4.14
10eqH-3H E	3.68	3.78	2.79	2.54	4.29	4.33

(contd.)

		4'-epiadriamycin		adriamycin		daunomycin	
10eqH-4OCH ₃	E	4.52	4.45	4.58	4.72	3.22	3.18
9COCH ₂ /9COCH ₃ -1H		o	-	4.22	4.80	4.12	3.89
9COCH ₂ /9COCH ₃ -2H		o	-	3.88	4.45	-	-
9COCH ₂ /9COCH ₃ -3H		o	-	3.95	4.31	-	-
9COCH ₂ /9COCH ₃ -4OCH ₃		o	-	3.75	3.04	o	-
8eqH-1H	E	3.10	3.02	4.07	4.16	4.10	3.88
8eqH-2H	E	-	-	4.17	4.20	4.17	3.94
8eqH-3H	E	3.60	3.55	4.23	4.45	4.23	4.16
8eqH-4OCH ₃	E	o	-	4.61	4.67	o	-
8axH-1H	E	-	-	o	-	4.19	3.94
8axH-2H	E	-	-	o	-	3.52	3.06
8axH-3H	E	-	-	o	-	3.70	3.88
8axH-4OCH ₃	E	o	-	2.62	2.67	o	-
7H-1H	E	o	-	4.08	4.43	2.85	2.58
7H-2H	E	o	-	4.09	4.06	3.21	3.27
7H-3H	E	o	-	4.26	4.61	3.27	3.42
7H-4OCH ₃		o	-	4.60	4.92	o	-
Sugar with Ring D							
1'H-1H	E	3.05	3.46	2.76	2.96	3.38	3.07
1'H-2H	E	3.20	3.20	3.75	3.74	3.40	4.02
1'H-3H	E	-	-	2.75	2.49	3.06	3.27
1'H-4OCH ₃		4.50	5.05	4.50	4.57	4.50	5.31
2'eqH/2'axH-1H		-	-	o	-	o	-
2'eqH/2'axH-2H		o	-	o	-	o	-
2'eqH/2'axH-3H		o	-	o	-	o	-
2'eqH/2'axH-4OCH ₃		o	-	-	-	o	-
3'H-1H		-	-	4.04	4.81	4.48	4.02
3'H-2H		-	-	3.75	3.76	4.99	5.03
3'H-4OCH ₃		o	-	o	-	o	-
4'H-1H		-	-	o	-	o	-
4'H-2H		o	-	o	-	o	-
4'H-3H		o	-	o	-	o	-
4'H-4OCH ₃		o	-	o	-	o	-
5'CH ₃ -1H	E	4.84	4.80	4.74	4.72	3.41	3.91
5'CH ₃ -2H	E	4.89	4.87	4.57	4.17	4.39	4.38
5'CH ₃ -3H	E	4.93	4.99	4.73	4.19	4.45	4.02
5'CH ₃ -4OCH ₃		3.95	3.87	3.45	3.89	2.64	2.68
5'H-4OCH ₃		o	-	-	-	ww	-

The parallel mode of orientation is therefore different from that of Evstigneev et al. (Evstigneev et al., 2006). Our results show more cross peaks than that observed by Evstigneev et al. (Evstigneev et al., 2006). These are: (a) in parallel orientation, 7H-10axH / 10eqH; 10axH / 10eqH - 1'H / 2'eqH / 2'axH / 4'H; 9COCH₂ / 9COCH₃ - 1'H / 2'eqH / 2'axH / 3'H / 4'H / 5'H / 7H and (b) in anti-parallel orientation, 9COCH₂ / 9COCH₃ - 1H / 4OCH₃; 7H - 4OCH₃; 1'H - 4OCH₃; 2'eqH / 2'axH - 1H / 2H / 3H / 4OCH₃; 3'H - 1H / 2H / 4OCH₃; 4'H - 1H / 2H / 3H / 4OCH₃; 5'CH₃ - 4OCH₃. We also observe differences among the three drugs. For example, it is seen that in anti-parallel orientation, 9COCH₃ - 2H / 3H cross peak is absent in daunomycin but is present in adriamycin and 4'-epiadriamycin (9COCH₂ - 2H / 3H). This may be due to hydrophilicity of 9COCH₂ group which permits ordering of water molecule around it as compared to 9COCH₃ group. The cross peaks 4'H-1H, 10axH - 3'H / 4'H; 10eqH - 4'H present in adriamycin and daunomycin are absent in 4'-epiadriamycin, which may be attributed to inversion of the H and OH at 4' position of adriamycin / daunomycin sugar moiety. Thus, our results show that self-association observed by Evstigneev et al. (Evstigneev et al., 2006) in daunomycin exists in its analogues, adriamycin and 4'-epiadriamycin as well. The self associated structures are however specific in each case owing to difference in the chemical groups.

B. Restrained Molecular Dynamics (rMD) studies

The rMD studies are done using the inter-proton distances obtained from 2D NOESY spectra recorded at $\tau_m = 400$ ms by integrating the volume of each cross peak. The integration method is based on isolated spin pair approximation in which spin diffusion effect is insignificant. The distance between two protons 1H and 2H protons, $r(1H-2H) = 2.50 \text{ \AA}$, is used as an internal reference (Barthwal, et al., 1994). Pseudo atom corrections were used for methyl and other equivalent protons. The NOEs were categorized as strong, medium, and weak with the

corresponding distances set in the range 1.8-2.4 Å, 2.5-2.9 Å and 3.0-4.0 Å, respectively. The initial structure of dimer models have been built using builder module in INSIGHT II, version 2005 (Accelrys Inc., San Diego, California) software. The energy of the molecule was minimized using 1000 steps each of Steepest Descent and Conjugate Gradient to remove any internal strain due to short contacts in starting structure using CFF91 force field (Maple, et al., 1990; Maple, et al., 1988) in DISCOVER software version 2005 (Accelrys Inc., San Diego, California). Dielectric constant was fixed as 1.0 for calculation of electrostatic interactions. Conformational search was performed by using the following simulated annealing restrained molecular dynamics protocol. The molecule was heated to a temperature of 800 K in steps of 100 K so that the chances of molecule being trapped in local minima become least and it can reach global minima. Molecular dynamics was carried out for 100 ps (1000 iterations with time step of 1 fs) at 800 K during which 100 structures were saved at regular intervals of 1 ps. Each of them was then slowly cooled at 300 K in steps of 100 K. The force constants for NOEs of strong, medium and weak peaks were held constant as 25, 15 and 10 Kcal mole⁻¹ Å⁻², respectively. At the end of simulated annealing all the structures were minimized by 1000 steps of Conjugate Gradient until a predefined convergence limit of root mean square derivative of < 0.001 Kcal mole⁻¹ Å⁻¹ was reached. The complete protocol of rMD studies with the simulated annealing at 800 K was repeated by taking a different starting structure built using INSIGHT II version 2005 (Accelrys Inc., San Diego, California).

The dimer models of the drugs obtained from rMD simulations (Figs. 16-18) show that there is significant overlap of the aromatic rings and the daunosamine amino sugar. Upfield shift in 2H, 3H and 1H protons upto 0.56 ppm may be due to magnetic shielding arising from ring currents of π electrons. The daunosamine sugar moiety of one molecule of the drug interacts with the

chromophore of the other molecule of the same drug and vice-versa, thus there is possibility of H-bond formation between the O12 atoms of aromatic ring C of the chromophore of one molecule and the NH_3^+ group of the amino sugar ring of the other in daunomycin. This bond is absent in 4'-epiadriamycin and adriamycin. Adriamycin and 4'-epiadriamycin show 6O-H..O5' hydrogen bond, having a distance of 2.79 Å. Besides this, few van der Waal's interactions are also present: 5'CH₃-6O (2.19 Å) in parallel orientation of 4'-epiadriamycin and 12C-6O (2.50 Å) in anti-parallel orientation of adriamycin. The aggregation of aromatic molecules is known to be driven by stacking interactions, in which the main components are dispersive and hydrophobic attractions. The angle between planes of aromatic rings of two molecules of dimer in 4'-epiadriamycin is lower (13° for parallel and 38° for anti-parallel mode) in comparison to that of adriamycin (40° for parallel and 78° for anti-parallel mode) and daunomycin (62° for parallel and 83° for anti-parallel mode) indicating that 4'-epiadriamycin is better stacked. It is noteworthy that glycosidic torsional angle C7-O7-C1'-C2' in 4'-epiadriamycin, adriamycin and daunomycin is -149° (parallel), -143° (anti-parallel); -157° (parallel), -135° (anti-parallel) and -169° (parallel), -148° (anti-parallel), respectively. This angle is involved in anchoring of drug chromophore and positioning of daunosamine sugar between base pairs of DNA in the drug-DNA complex. It has been shown (Trieb et al., 2004) that this angle can adopt three conformations, that is, (1) 156-167° (2) 127-144° (3) 38-78°. Our rMD structure shows that 4'-epiadriamycin adopts only (2) conformer in both parallel and anti-parallel orientations while adriamycin and daunomycin adopt conformation (1) in parallel mode and conformation (2) in anti-parallel mode of orientation. This feature has important implications in biological action of these drugs, and is discussed later.

C. Absorption and Emission studies

4'-EPIADRIAMYCIN

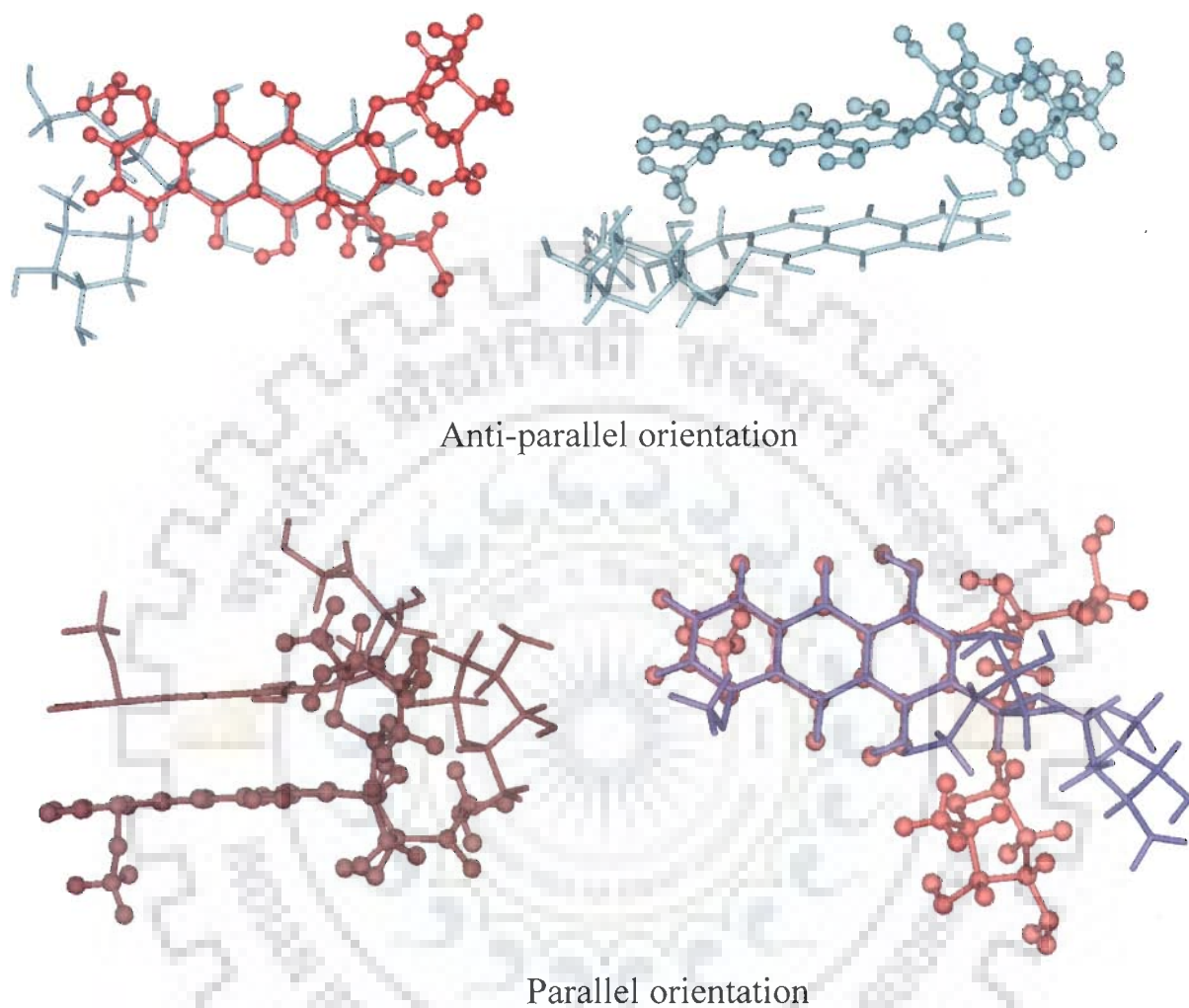


Fig. 16: Structure of self associated dimer of 4'-epiadriamycin based on restrained molecular dynamics simulations using experimental distance restraints from NOESY spectra

ADRIAMYCIN

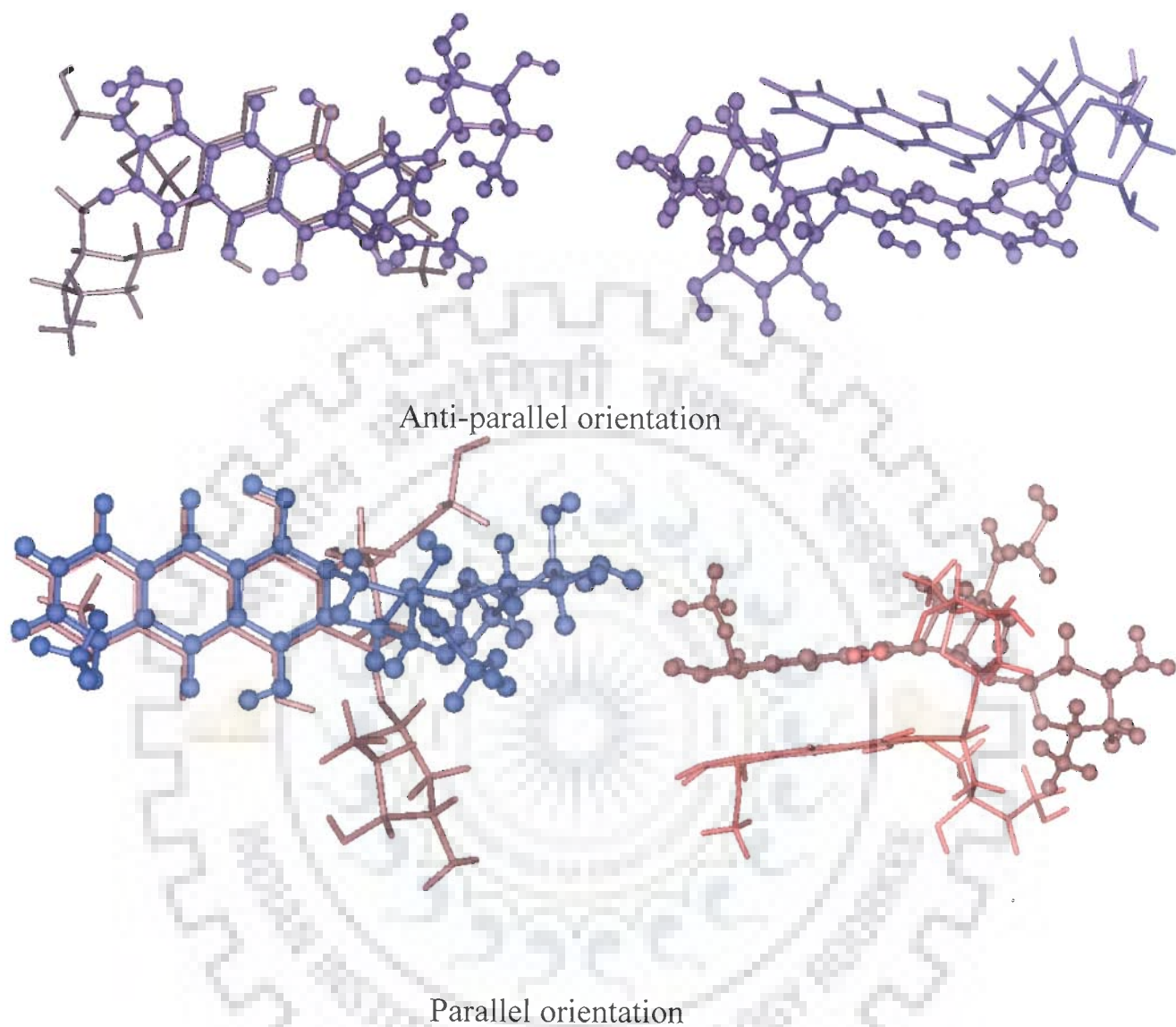


Fig. 17: Structure of self associated dimer of adriamycin based on restrained molecular dynamics simulations using experimental distance restraints from NOESY spectra

DAUNOMYCIN

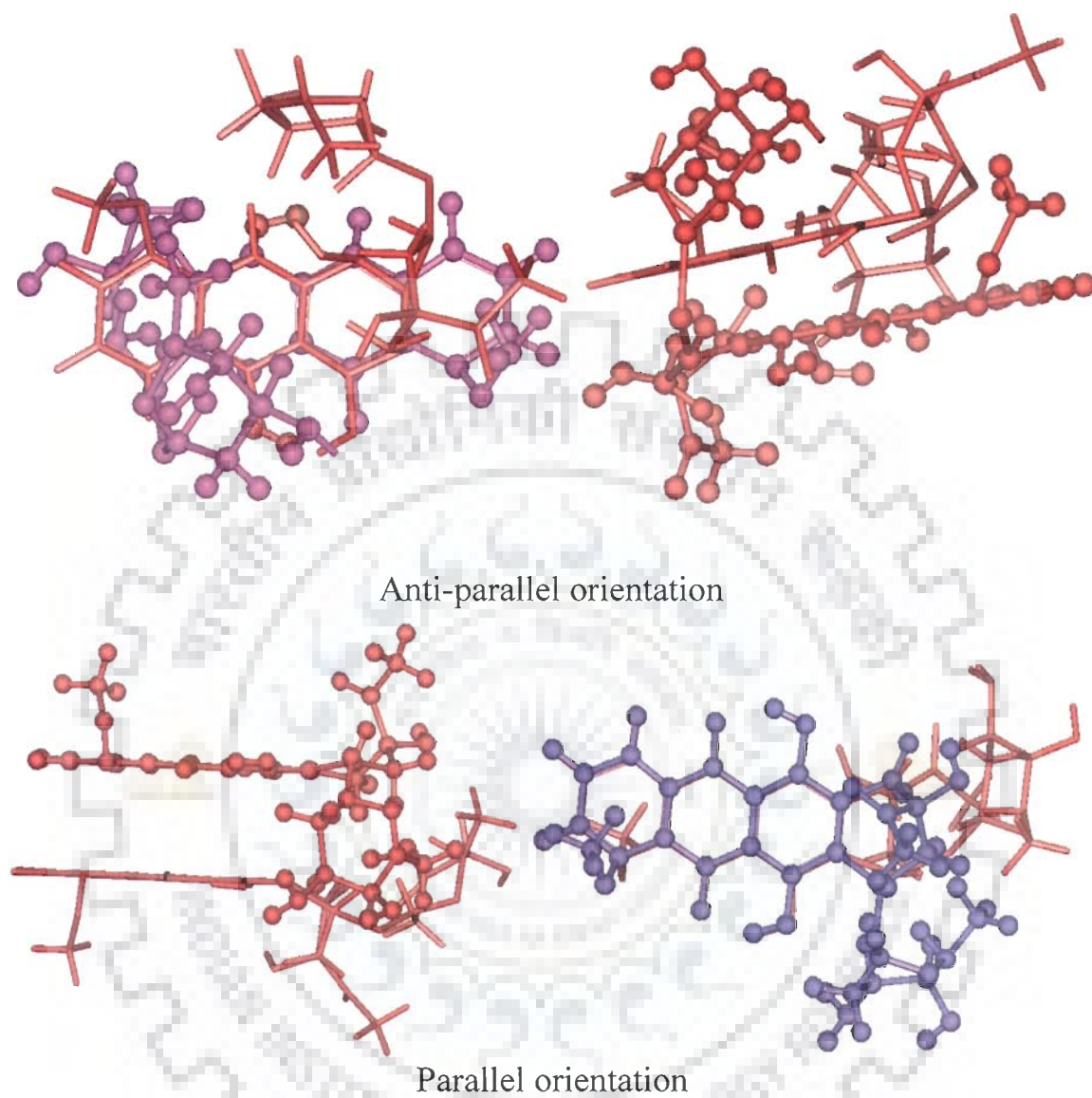


Fig. 18: Structure of self associated dimer of daunomycin based on restrained molecular dynamics simulations using experimental distance restraints from NOESY spectra

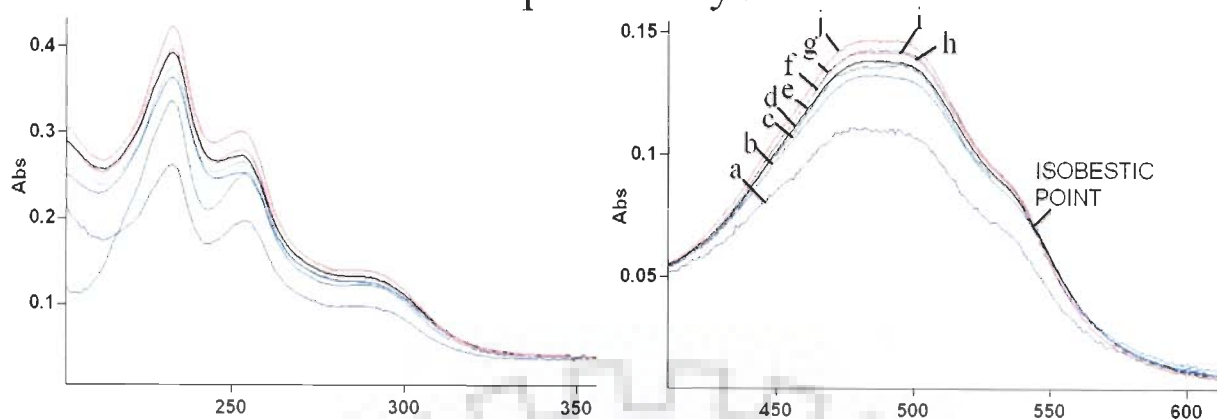
Visible absorbance spectra are recorded in CARY 100 Bio spectrophotometer. The concentration of drugs in buffer solution were determined spectrophotometrically at the λ_{\max} of 480 nm ($\epsilon = 11,500 \text{ M}^{-1}\text{cm}^{-1}$). All experiments were performed in the standard buffer containing 70 mM NaCl, 20 mM phosphate buffer, pH= 7.0 at 25°C. Absorbance and emission scans are done from 1, 3, 5, 6, 7, 8, 9, 10, 11, 12 μM concentration. The dimerization constant is calculated by using least square fitting curve (Kapuscinski, et al., 1985; Lee, et al., 1989) in MATLAB 7.0 version software. The ligand dimerization constants (K_D) were calculated according to the method described by von Tscherner and Schwarz, 1979: $K_D = C_T - C_M / 2C_M^2$ Where C_T is the total ligand concentration and C_M is the monomer concentration. The wavelength for maximum absorbance is 480 nm and the isobestic point is at 545 nm. The absorption spectra of drugs shows three bands in the visible region (529, 496, 479 nm) and three in the ultraviolet range (288, 252, 233 nm) (Marco et al., 1969). The three visible region bands are characteristic of the conjugated anthracycline rings; in the ultraviolet region, one at 288 nm is for aromatic ring and the other two, that is, 252, 233 nm are for daunosamine sugar moiety of the drugs. As the concentration of drug increases, there are weak but definite changes in the shape of their spectra. The maxima located at 288 and 496 nm vanish, while the absorption increases in the wavelength range 200 - 400 nm. For lower concentration ($\sim 6\text{-}7 \mu\text{M}$), the absorption follows the Beer-Lambert law. For higher concentrations deviations are observed. In dilute solution (1 μM) the 496 and 479 nm bands are of equal intensity, while in concentrated solution (12 μM), the spectrum is broader and the 496 nm band becomes less intense relative to the 479 nm band (Fig. 19). The chromophores of the anthracyclines are planar. There is uneven electronic charge distribution and such a charge distribution could favour the formation of stacked dimers. Using excitation wavelength (λ_{ex}) as 480 nm and emission wavelength (λ_{em}) as 592 nm, the emission

scan was done in spectrofluorimeter (make HORIBA Jobin, Horiba model Fluorolog -3). Fluorescence intensity gets quenched when the drugs start forming dimer. Since the dipole moment of the dimer is zero observed fluorescence is only due to the monomer species (Fig. 20) and there is no contribution from the dimer species. Also, there is no shift in the emission maxima with increase in concentration. The dimerization constant (K_D) is calculated by computer-aided extrapolation of the spectral changes to high dilution of the drugs, that is, least square fitting curve using software MATLAB 7.0 version. The concentration of monomer, dimer and the dimerization constant is calculated (Fig. 21) and the values are 21980 M^{-1} for 4'-epiadriamycin; 17420 M^{-1} for adriamycin and 19040 M^{-1} for daunomycin (Table 4) which are close to that obtained by Chaires et al. (Chaires et al., 1982). It is found that the magnitude of the self-association constant for 4'-epiadriamycin is higher than that of adriamycin and daunomycin, indicating that 4'-epiadriamycin has higher degree of self-aggregation than adriamycin and daunomycin. It may be noted that there is a possibility of the existence of higher aggregates at higher concentration.

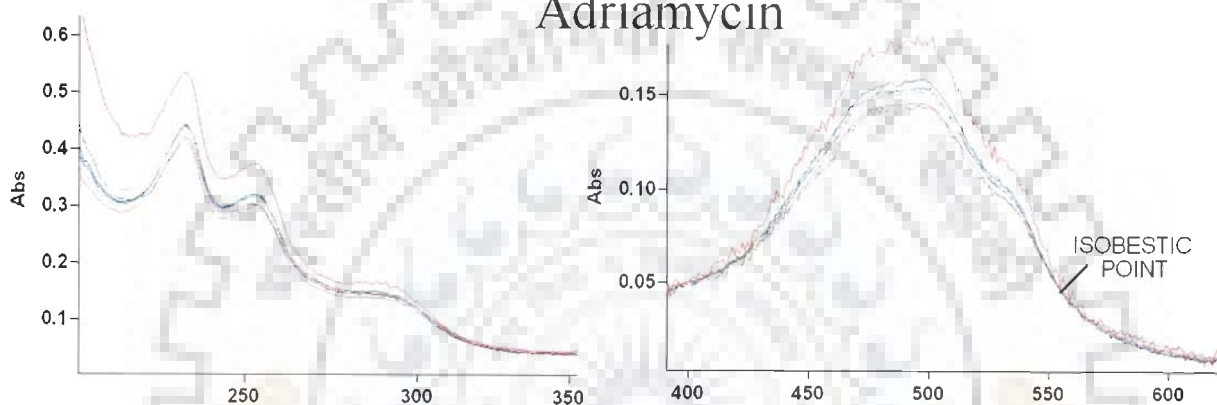
D. Diffusion Ordered Spectroscopy (DOSY) studies

DOSY experiment is done for the study of aggregation and the binding processes. It is a tool to distinguish between the complexed and noncomplexed forms in a mixture due to the differences in their relative diffusion coefficient values. It can also be utilized to obtain information about the relative strength of H-bonds, and about those components that show stronger binding affinities to a particular ligand in a pool of mixture of molecules. The DOSY technique has been developed to facilitate the complex mixture analysis without physical separation. DOSY enables identification and even structure elucidation of the individual components in a mixture resulting from the differences in their translational diffusion coefficients. To clarify the NMR assignment

4'-Epiadriamycin



Adriamycin



Daunomycin

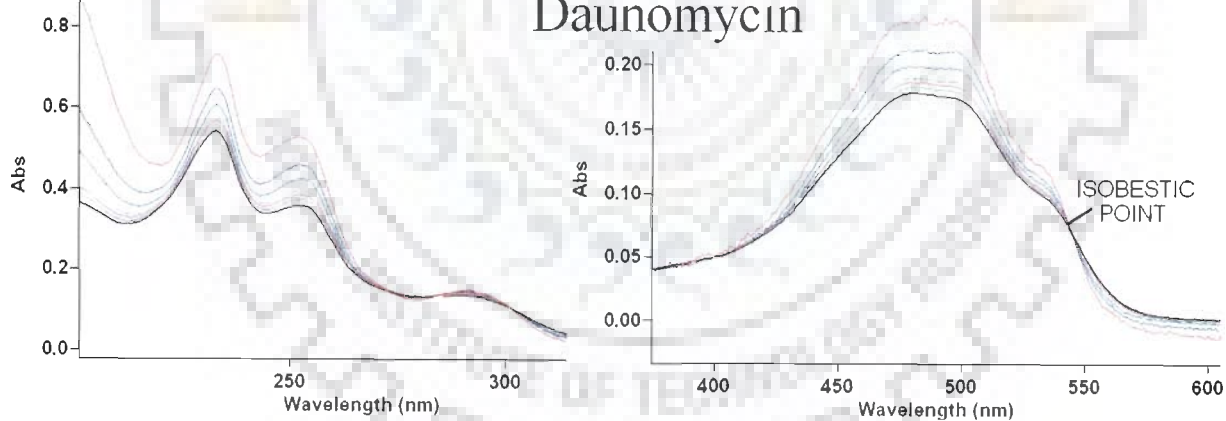


Fig. 19: Absorption Spectra of 4'-epiadriamycin, adriamycin and daunomycin as a function of concentration (a, b, c, d, e, f, g, h, i, j denotes 1, 3, 5, 6, 7, 8, 9, 10, 11 and 12 μM concentration)

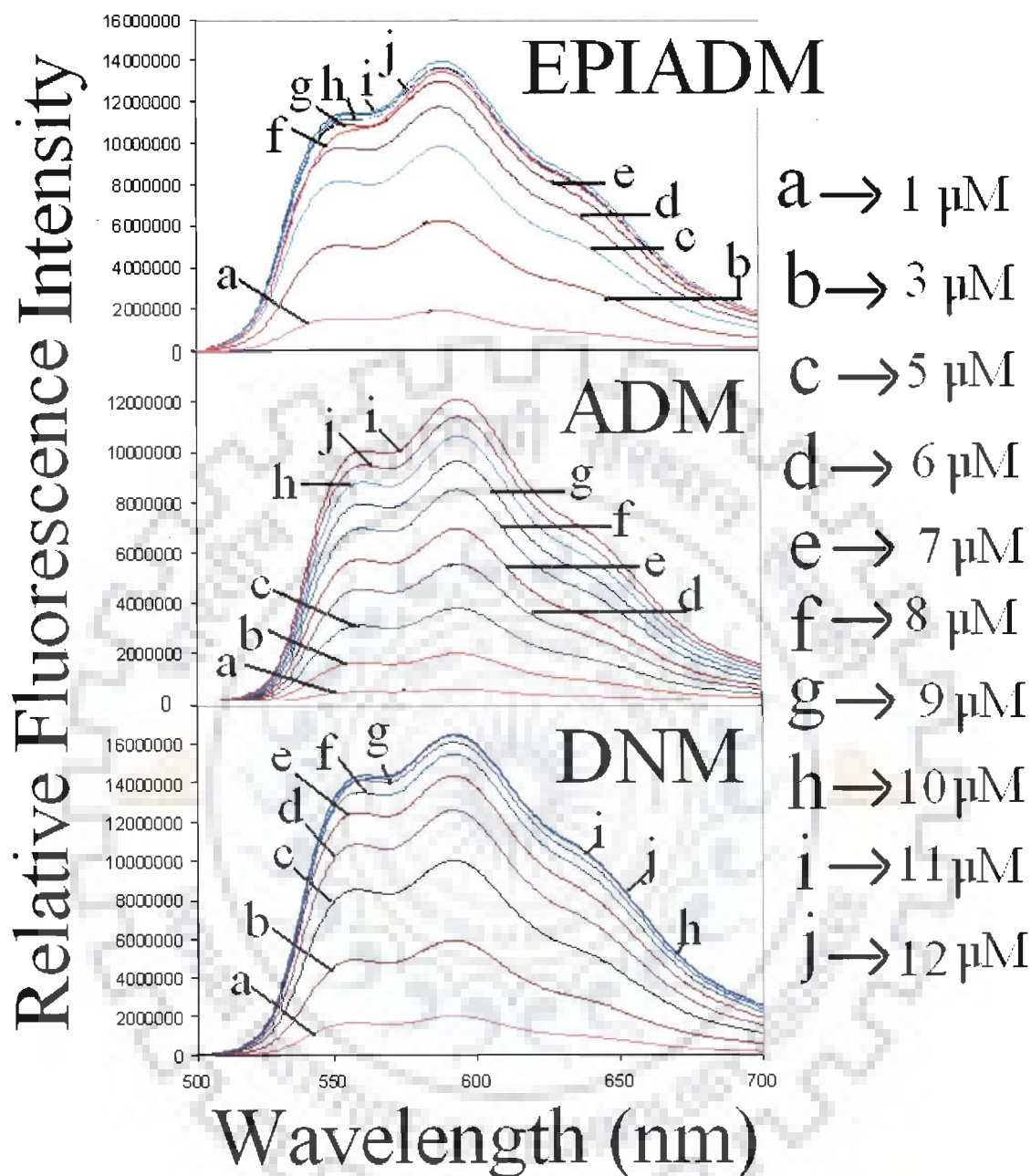


Fig. 20: Emission Spectra of 4'-epiadriamycin, adriamycin and daunomycin as a function of concentration

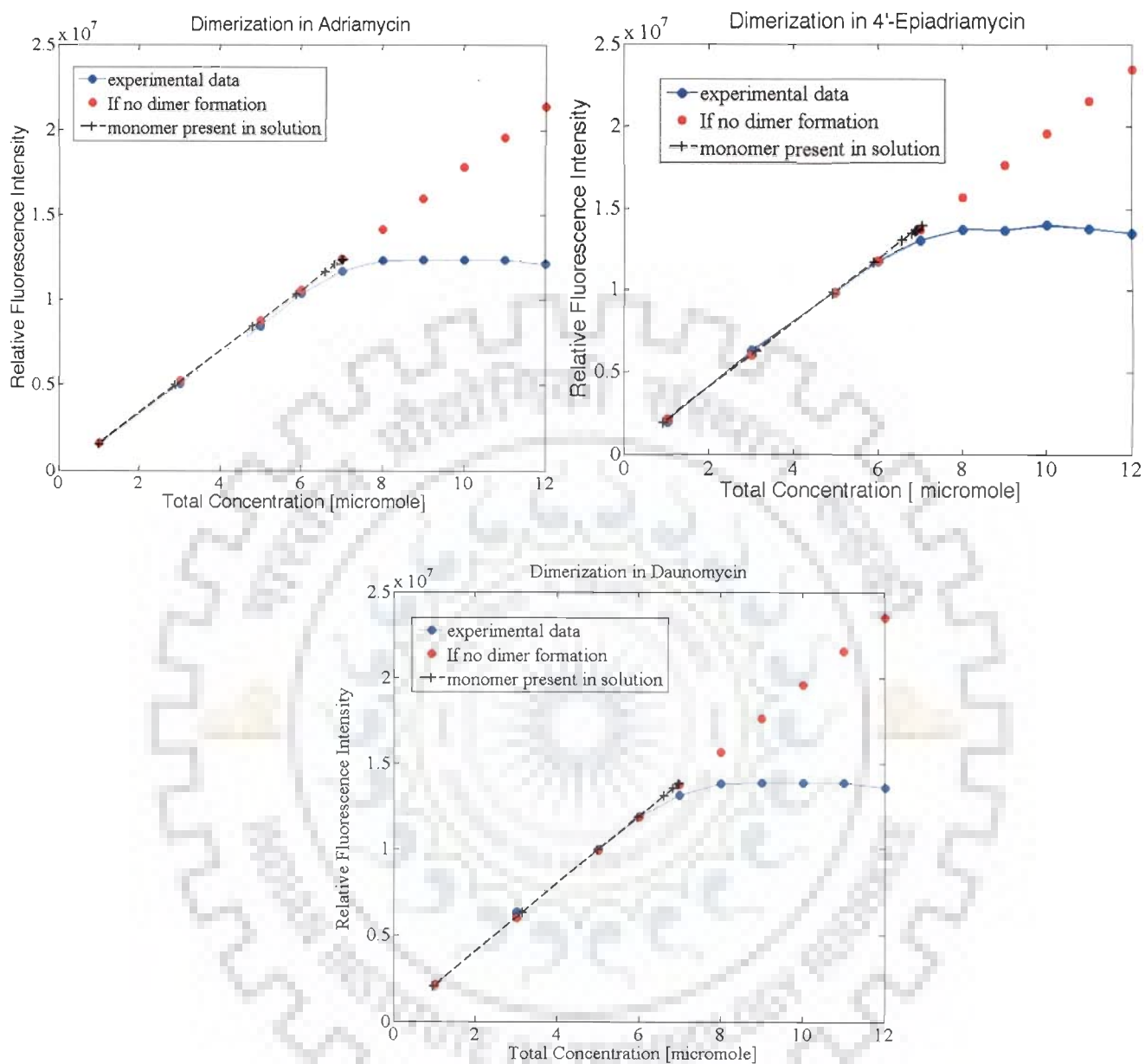


Fig. 21: Plot of Relative fluorescence Intensity versus concentration of the anthracycline drugs for the calculation of dimerization constant (K_d)

Table: 4 Dimerization Constant calculations for 4'-Epiadriamycin, adriamycin and daunomycin using fluorescence data.

4'-Epiadriamycin Conc (μM)	Monomer (μM)	Dimer (μM)	Dimerization constant 'K' ($\times 10^6 \text{ M}^{-1}$)
1.00	0.9232	0.0384	0.0450
3.00	2.8918	0.0541	0.0065
5.00	4.9464	0.0268	0.0011
6.00	5.9190	0.0405	0.0012
7.00	6.5788	0.2106	0.0049
8.00	6.9238	0.5381	0.0112
9.00	6.9004	1.0498	0.0220
10.00	7.0578	1.4711	0.0295
11.00	6.9439	2.0280	0.0421
12.00	6.7979	2.6011	0.0563
Mean			0.02198
Adriamycin Conc (μM)	Monomer (μM)	Dimer (μM)	Dimerization constant 'K' ($\times 10^6 \text{ M}^{-1}$)
1.00	0.9952	0.0024	0.0024
3.00	2.9018	0.0491	0.0058
5.00	4.8286	0.0857	0.0037
6.00	5.8870	0.0565	0.0016
7.00	6.6106	0.1947	0.0045
8.00	6.9868	0.5066	0.0104
9.00	7.0168	0.9916	0.0201
10.00	7.0207	1.4896	0.0302
11.00	7.0087	1.9956	0.0406
12.00	6.8494	2.5753	0.0549
Mean			0.01742
Daunomycin Conc (μM)	Monomer (μM)	Dimer (μM)	Dimerization constant 'K' ($\times 10^6 \text{ M}^{-1}$)
1.00	0.9664	0.0168	0.0180
3.00	2.8474	0.0763	0.0094
5.00	4.9887	0.0057	0.0002
6.00	5.9595	0.0203	0.0006
7.00	6.6232	0.1884	0.0043
8.00	6.9683	0.5159	0.0106
9.00	6.9958	1.0021	0.0205
10.00	6.9994	1.5003	0.0306
11.00	6.9884	2.0058	0.0411
12.00	6.8423	2.5789	0.0551
Mean			0.01904

of a complicated mixture, the DOSY technique is useful because the NMR signals belonging to one of the components appear aligned with the same diffusion coefficient value. The diffusion coefficient of the molecule is inversely proportional to the molecular radius. If the molecule is aggregating, their global size and molecular weight should be greater than the noncomplexed ones, and consequently they should exhibit different diffusion coefficient values. The observed diffusion is an average of the populations of the diffusion of the complexed and noncomplexed forms in equilibrium. A change in the chemical shift does not provide a sufficient indication about the strength of interaction between the components, which could be due to other effects influencing the chemical shift but the DOSY plots provide a better insight about the strength of such interactions which are clearly manifested in the diffusion dimension.

The drugs are known to exhibit self association at the concentration used. Our results show that the rate of exchange between monomer and dimer is apparently fast; therefore instead of two peaks only one peak is observed, which is averaged value of each weighted by its relative concentration. Adriamycin shows a diffusion rate which is intermediate between that of 4'-epiadriamycin and daunomycin, while daunomycin shows fastest diffusion (Fig. 22a-c). The diffusion coefficient is $1.84 \times 10^{-11} \text{ m}^2/\text{s}$ for 4'-epiadriamycin, $2.89 \times 10^{-11} \text{ m}^2/\text{s}$ for adriamycin and $1.52 \times 10^{-10} \text{ m}^2/\text{s}$ for daunomycin at 275 K. At 298 K, the corresponding values increase in the same order; being $1.53 \times 10^{-10} \text{ m}^2/\text{s}$, $1.63 \times 10^{-10} \text{ m}^2/\text{s}$ and $2.10 \times 10^{-10} \text{ m}^2/\text{s}$, respectively (Fig. 22a-c). The apparent diffusion rate is fastest for daunomycin and least for 4'-epiadriamycin. Since the rates are weighted by the relative concentrations of monomer and aggregated forms, it may be inferred that greater extent of self aggregation exists in 4'-epiadriamycin.

E. Electron Spray Ionization-Mass spectrometry Studies (ESI-MS)

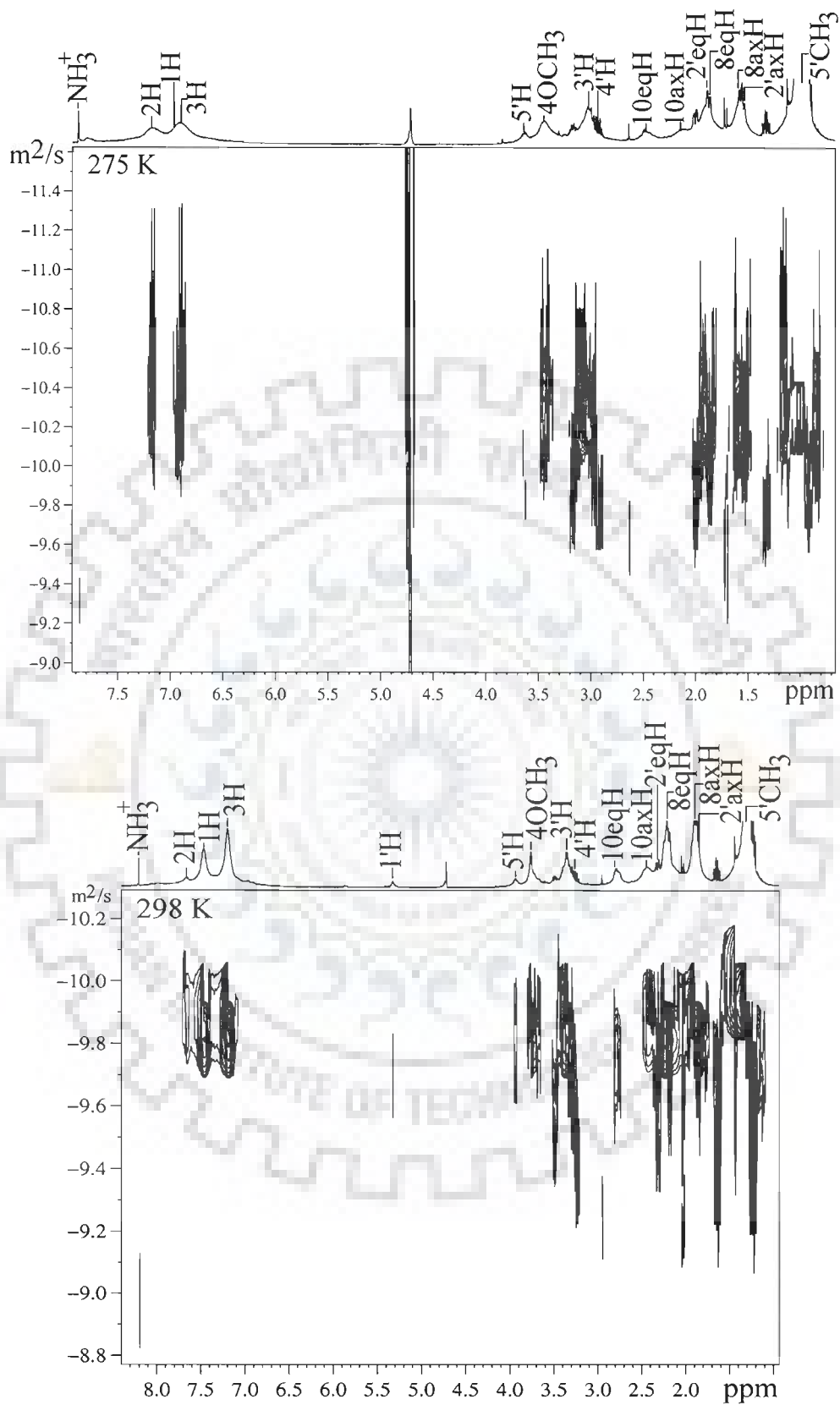


Fig. 22a: DOSY spectra of 8 mM 4'-epiadriamycin in D₂O

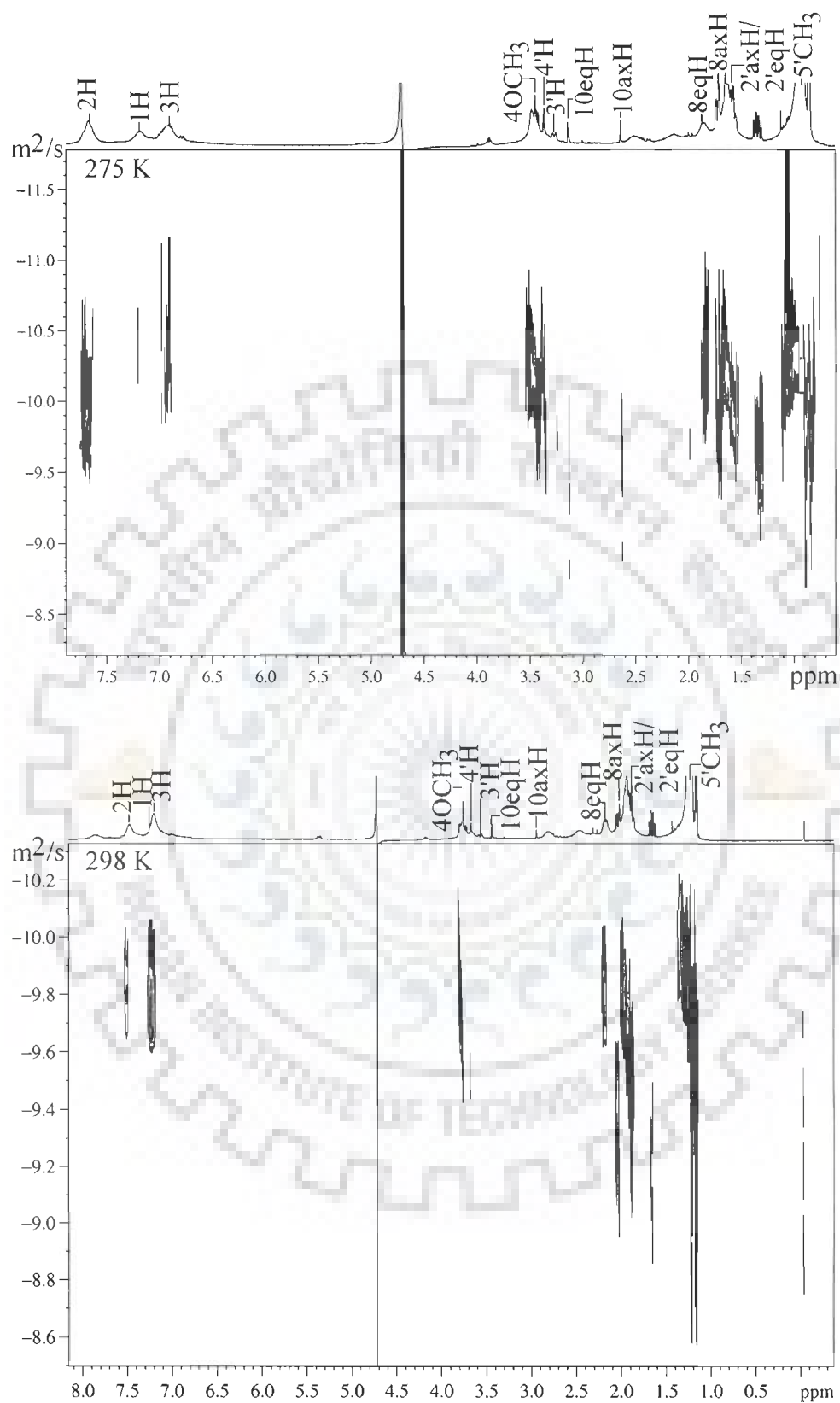


Fig. 22b: DOSY spectra of 8 mM adriamycin in D_2O

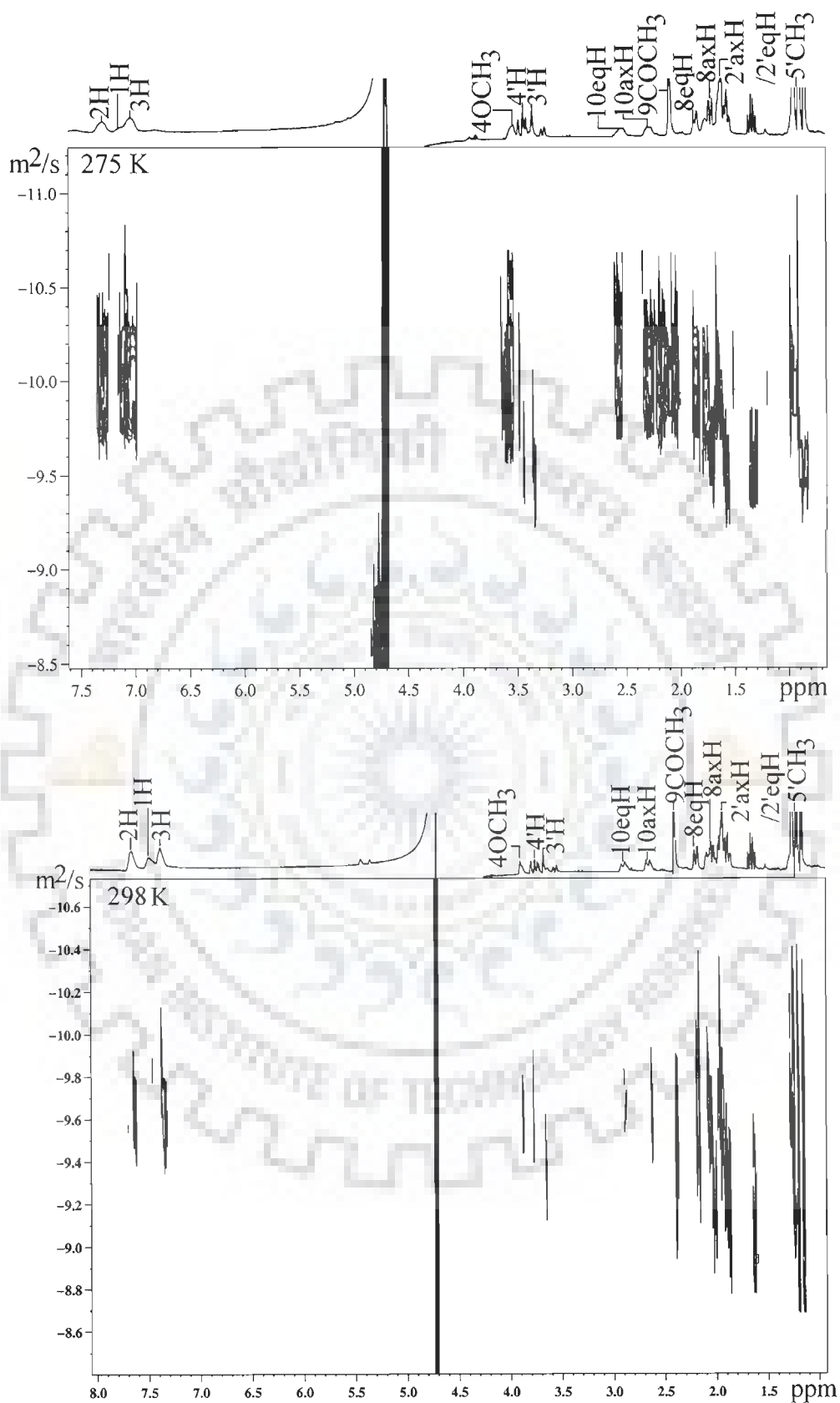


Fig. 22c: DOSY spectra of 8 mM daunomycin in D_2O

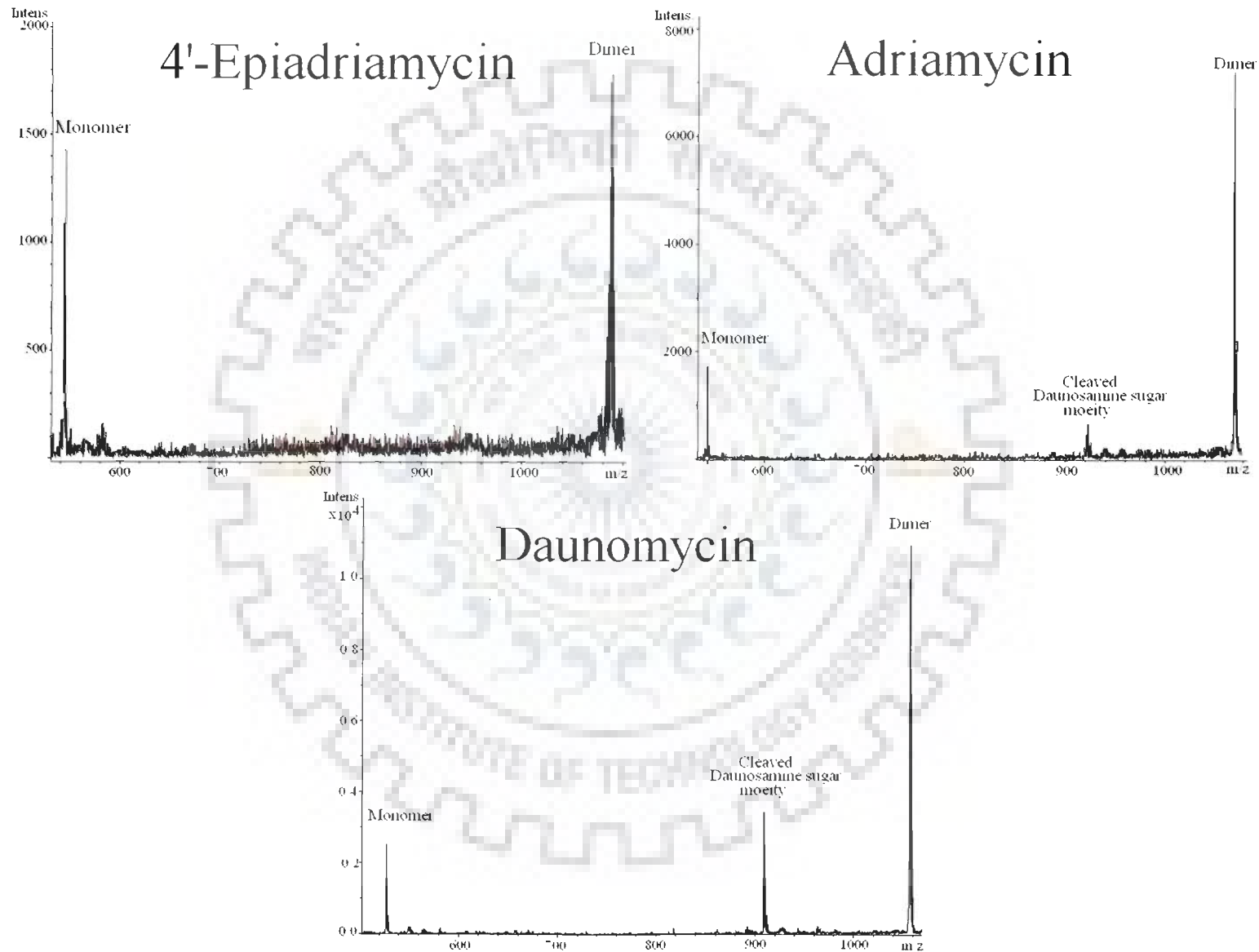


Fig. 23: Electron-Spray Ionization Mass Spectra (ESI-MS) of the anthracycline drugs showing the drugs exist in monomeric and dimeric state with single charge.

Positive-ion ESI-MS spectra are obtained on Esquire 4000 (Bruker Daltonics, Germany) with the normal ESI source. The 5 μM concentration solutions of drugs are prepared in the water:acetic acid mixture in the ratio of 90:10. The solutions are infused directly into the mass spectrometer at 240 $\mu\text{l/hr}$ rate. The parameters selected are: cone voltage 4.0 KV, nebulizer pressure 15 psi, dry gas flow rate 8 l/min and the capillary temperature 100 $^{\circ}\text{C}$. Data is collected for approximately 10 scans. The maximum accumulation time is 200 ms and scan range is 400-1700 m/z. The Electron Spray Ionization Mass Spectrometric studies of the three anthracycline drugs (Fig. 23) shows that the drugs exist in monomeric as well as dimeric state at 5 μM concentration in singly charged state. Adriamycin and 4'-epiadriamycin are epimers with same molecular weight, their intense peaks appear at 545 m/z ratio whereas for daunomycin it appears at 528 m/z ratio for the monomeric forms. Their dimeric species exist at 1089 and 1056 m/z, respectively corresponding to the molecular weight of the dimers with single charge. We did not observe any peak corresponding to trimer or higher aggregates with single / double charge. The mass spectrum gives a direct proof of the existence of dimer species due to self-aggregation and absence of trimer or higher aggregates. However it may be noted that Fig. 23 cannot be used to give a quantitative estimate of the relative amount of monomer and dimer since the process of electron spray ionization in gaseous phase may cleave the dimers or higher aggregates, if present. We observe a peak at $m/z = 908$ in mass spectra of daunomycin. This mass number corresponds to dimer ($m/z = 1056$) without daunosamine sugar moiety ($m/z = 148$). Similar peak is observed at $m/z = 941$ in adriamycin whereas no such corresponding signal is seen in 4'-epiadriamycin. This shows that cleavage is higher in daunomycin as compared to adriamycin while 4'-epiadriamycin does not show cleavage at all.

F. Biological Relevance

(a) Anticancer action: The anthracycline antibiotics are among the most effective antitumor medicines used in clinics for medicinal treatment of various types of malignant tumors. The dose of drugs is generally more than tens of micromoles. Self aggregation takes place at these high concentrations which will compete with binding to target DNA. The thermodynamical and structural analysis of intercalative binding of these drugs to DNA sequence therefore requires a precise pre-knowledge of self association. The self aggregation of these drugs also plays a biological role in influencing the selective transport of these substances through cell membrane as well as multiple drug resistance caused by proteins forming channels in bilayer lipid membrane (Evstigneev et al., 2006, Davies et al., 2001). Besides, several naturally occurring aromatic molecules consumed as a part of food (e.g. methyl xanthines, polyphenols) associate with these drugs. Alternately these drugs are used in combination with some aromatic molecules (Alberts et al., 1981; Adel et al., 1993). It has been shown that caffeine (present in tea, coffee, coca, chocolate) forms hetero association complexes with number of anticancer aromatic drugs, which effectively lowers the concentration of free ligands and thereby reduces the pharmacological activity of drugs. The major mechanism responsible for marked reduction in toxicity of adriamycin in cultured cell lines treated with caffeine (Piosik et al., 2002; Traganos et al., 1991) was found to be formation of adriamycin-caffeine complex. Caffeine is also able to block potential DNA binding site or remove the antibiotic already complexed with DNA, particularly in case of daunomycin. The relative importance of each process, hetero-association or competition for binding site on DNA, depends upon several factors. The specific conjugated aromatic ring system of anthracycline / anthraquinone and the side chains will influence van der Waal's dispersive forces responsible for overlap of aromatic rings, intermolecular interactions with side chains attached to aromatic ring, steric factors, hydrophobicity and intermolecular hydrogen bonding. It has been suggested

(Evstigneev et al., 2006) that the scavenging effect of cell detoxification can be used as a potential strategy of regulation of medico-biological activity of these drugs in clinical practice, say for example in reduction of the consequences of drug's overdosing during chemotherapy or in production of anti mutagenic effects in vivo.

Our results from physico-chemical techniques and restrained molecular dynamics indicate that there are specific differences in stacked structure of the three drugs. The stacked structure of 4'-epiadriamycin is better stabilized by dispersive forces due to reduced angles between planes of aromatic rings (13° for parallel orientation) resulting in immobilization of hydroxyl and NH_3^+ moieties, higher K_{eq} value and decreased diffusion constant in DOSY spectra. It has been shown that conformer (2) corresponding to glycosidic angle $\text{C7-O7-C1'-C2}' = 127\text{-}144^\circ$ is the biologically relevant conformer (Moore et al., 1989; Nunn et al, 1991; Wang et al., 1987). The readiness with which 4'-epiadriamycin adopts this conformation in both parallel and anti-parallel orientation, shows that its anti-proliferative activity is certainly not compromised as compared to daunomycin and adriamycin in spite of better self-association. A relatively more stable dimer of 4'-epiadriamycin may initially slow down uptake of drug through the cell membrane. However once absorbed, it may not let the drug get ejected out through channel across membrane, increasing thereby the efficacy of the drug.

(b) Toxicity: The ability to generate oxygen radicals during redox cycling and in vitro reductive glycosidic cleavage through the formation of tautomer 7-deoxydaunomycinone (Pan et al., 1980; Kleyer et al., 1983) is known to be responsible for cardiotoxicity. The kinetics of sugar moiety detachment has been related to conformation of cyclohexyl ring A (Malatesta et al., 1984). Our results from mass spectra have given a direct proof of cleavage and clearly show that it is negligible in 4'-epiadriamycin. These results may well explain why 4'-

epiadriamycin developed recently is better tolerated due to lesser cardiotoxicity than adriamycin and daunomycin (Arcamone et al., 1988).

4.2 Summary and Conclusions

1D Proton NMR of various drugs show upfield shifts upto 0.68 ppm in ring A and ring D on increasing concentration from 0.01 mM to 8.00 mM. This is attributed to the stacking of the chromophore rings. Temperature dependence studies show downfield shift upto 1.59 ppm with temperature for the aromatic protons indicating that these drugs exist in aggregated form. 2D NOESY spectra at 355 K show various inter-molecular and intra-molecular cross peaks which are evolved due to the stacking of aromatic chromophores of drug molecules. Restrained Molecular Dynamics studies show the existence of parallel and anti-parallel orientations between two aromatic rings in the dimer. To date no such structure of dimer has been reported for the 4'-epiadriamycin and adriamycin. The results in literature for daunomycin (Evstigneev et al., 2006) have structure similar to that observed by us although we get more inter-molecular contacts. Absorption and fluorescence studies show that aggregation starts at low concentration $\sim 10 \mu\text{M}$ and the observed isobestic point for absorption spectra is 545 nm. The DOSY studies indicate that the rate of diffusion increases in the following manner 4'-epiadriamycin < adriamycin < daunomycin. ESI-MS experiments clearly demonstrate the existence of dimers. Higher aggregates are not observed. The mass spectra of adriamycin and daunomycin also show presence of 7-deoxydaunomycinone resulting from cleavage of glycosidic bond. Absence of cleaved moiety in 4'-epiadriamycin gives direct proof of reduced cardiotoxicity due to generation of free radicals following the cleavage of glycosidic bond. The structural difference between stacked dimer of the three drugs may be related to competitive binding with DNA and hence different in their pharmacological action.

Studies on Complex of Adriamycin with d-(TGATCA)₂ by Phosphorus-31 Nuclear Magnetic Resonance Spectroscopy

The knowledge of detailed conformational changes at each phosphate site is important for characterization of the stereo dynamic properties of DNA chains. Phosphorus -31 NMR has been developed as a probe for studying conformational flexibility of nucleic acid backbone. This chapter contains the following studies of the complex of adriamycin-d-(TGATCA)₂ by one- and two-dimensional ³¹P NMR:

- The temperature dependence of ³¹P chemical shift of 3.42 mM d-(TGATCA)₂ duplex in the range of 275 - 328 K.
- The two dimensional ¹H - ³¹P Heteronuclear Multiple Bond Correlation (HMBC) of 3.42 mM d-(TGATCA)₂ at 278 K for assignment of ³¹P resonances.
- Titrations by recording ³¹P 1D NMR versus drug (D)/DNA duplex (N) ratio 0.1, 0.2, 0.3, 0.4, 0.5, 0.6, 0.7, 0.9, 1.0, 1.1, 1.2, 1.3, 1.4, 1.5, 1.6, 1.8, 2.0 at 275 and 318 K.
- 2D ³¹P - ³¹P exchange spectra of drug-DNA complex by a phase-sensitive NOESY using mixing time of 200 ms at 278 K for D/N = 1.0, 1.5 and 2.0.
- Temperature dependence of ³¹P NMR of the adriamycin-d-(TGATCA)₂ complex having D/N = 1.0, 1.5 and 2.0 in the range of 275 - 328 K.
- T₁ measurements of the 2:1 adriamycin-d-(TGATCA)₂ complex at 298 K.

5.1 Results and Discussion

A. d-(TGATCA)₂

One dimensional ³¹P NMR spectra of 3.42 mM d-(TGATCA)₂ is recorded in temperature range 275 - 328 K. (Fig. 1). The ³¹P resonances resolve into five distinct signals corresponding to the

five phosphate groups at the ambient temperature. The assignments of ^{31}P nuclei in d-(TGATCA)₂ were made by using the 2D ^1H - ^{31}P HMBC spectra (Fig. 2). The three-bond scalar couplings between (^{31}P)_n nuclei in the phosphate backbone and the ($\text{H}3'$)_n, ($\text{H}5'/\text{H}5''$)_{n+1} protons and four-bond coupling with ($\text{H}4'$)_n, ($\text{H}4'$)_{n+1} protons are observed (Fig. 2). The identification of the cross peaks were done on the basis of proton assignments, which have been done by using DQF COSY and 2D NOESY spectra (Barthwal et al., 2004). We are focusing mainly on H3' and H4' region as H5'/5'' region is overlapped highly. Two of the H4' signals (A3 and T4) are separated from the H5' overlapped regions and their connectivities through the four-bond couplings with G2pA3 and A3pT4 phosphates confirm the assignments (Table 1).

The increase or decrease in temperature from the ambient cause ^{31}P signals to shift towards each other and to overlap but there is no broadening (Fig. 1). This shows that the duplex is intact at lower and ambient temperature. There is a general downfield shift of several resonances with increasing temperature as well as a sharp decrease in line width with increase in temperature (Fig. 3a). The phosphorus double helical signals below T_m are substantially broader (8-7 Hz line width at half height) than the corresponding single-strand signals (the line width of free single helices at temperatures above T_m is 2-3 Hz) (Fig. 3b and Table 2). The T_m of the duplex is 292 K as the inflection point in the curves for all phosphates occurs at approximately this temperature (Fig. 3b). ^{31}P chemical shifts show the expected variation in the sugar-phosphate backbone conformation (Gorenstein et al., 1989; Gorenstein, 1992) as the duplex melts into a single strand, which is consistent with the change in the backbone conformation, generally g⁻ for P-O ester bonds in the duplex, to a single stranded random coil having random mix of g- and non-gauche conformations.

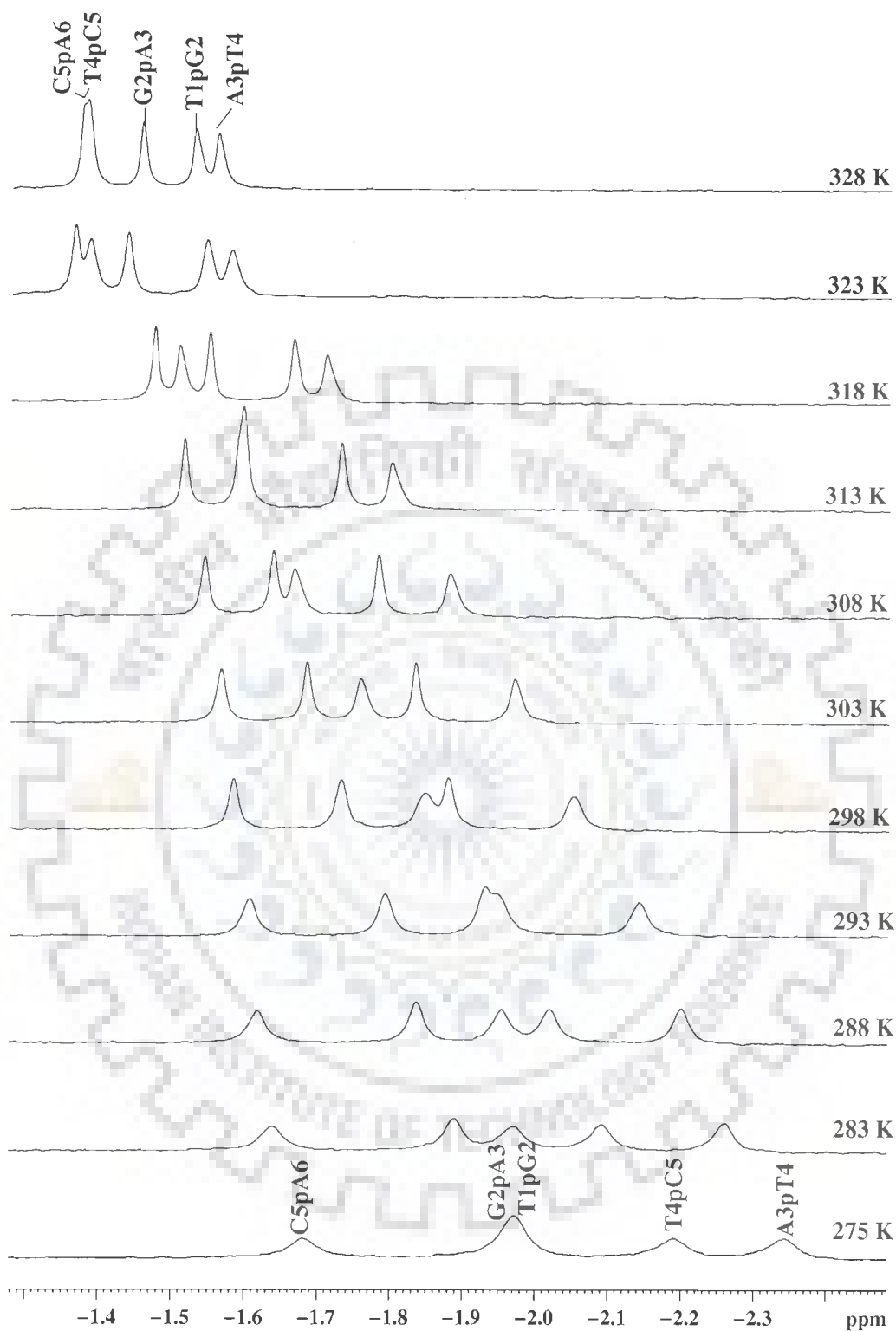


Fig. 1: ^{31}P NMR Spectra of 3.42 mM uncomplexed $d\text{-(TGATCA)}_2$ as a function of temperature

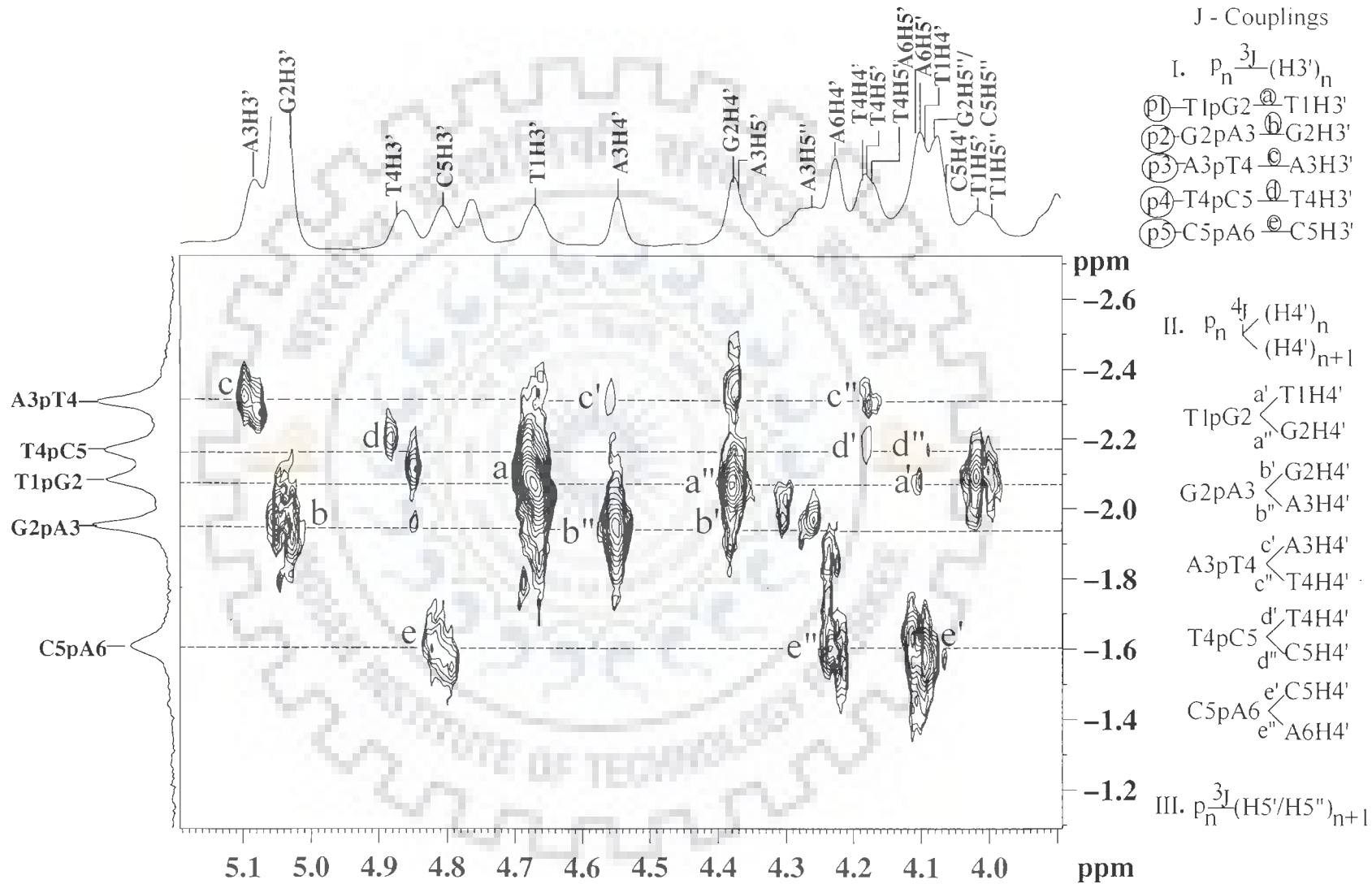


Fig. 2: Two Dimensional ^{31}P - ^1H Heteronuclear Multiple Bond Correlation (HMBC) spectra of 3.42 mM d-(TGATCA)₂ at 278 K

Table 1: ^{31}P chemical shift assignments (δ) of d-(TGATCA) $_2$ in the free duplex at different temperatures. The total change in chemical shift with temperature, $\Delta\delta = \delta_{328\text{K}} - \delta_{275\text{K}}$ is also shown.

Temperature(K)	T1pG2	G2pA3	A3pT4	T4pC5	C5pA6
275	-1.97	-1.97	-2.34	-2.19	-1.68
283	-1.97	-1.89	-2.26	-2.09	-1.64
288	-1.96	-1.84	-2.20	-2.02	-1.62
293	-1.93	-1.79	-2.14	-1.95	-1.61
298	-1.88	-1.73	-2.05	-1.85	-1.58
303	-1.83	-1.68	-1.97	-1.76	-1.57
308	-1.78	-1.64	-1.88	-1.67	-1.54
313	-1.73	-1.60	-1.80	-1.60	-1.52
318	-1.66	-1.55	-1.71	-1.51	-1.48
323	-1.55	-1.44	-1.58	-1.39	-1.37
328	-1.53	-1.46	-1.56	-1.38	-1.38
$\Delta\delta$	+0.44	+0.51	+0.78	+0.81	+0.30

Table 2: ^{31}P Line width of d-(TGATCA) $_2$ in the free duplex at different temperatures.

Temperature(K)	T1pG2	G2pA3	A3pT4	T4pC5	C5pA6
275	8.88	6.66	6.93	7.51	7.71
283	8.74	6.55	6.32	7.22	7.6
288	7.37	5.01	5.21	6.97	5.52
293	4.45	4.69	4.59	5.4	4.64
298	4.02	3.83	4.38	4.42	3.2
303	3.68	3.76	3.84	4.35	3.04
308	3.03	3.73	3.8	4.21	2.68
313	2.48	3.33	3.7	3.33	2.65
318	2.4	2.79	3.38	3.04	2.64
323	2.38	2.76	2.13	2.63	2.63
328	2.38	2.76	2.13	2.63	2.63

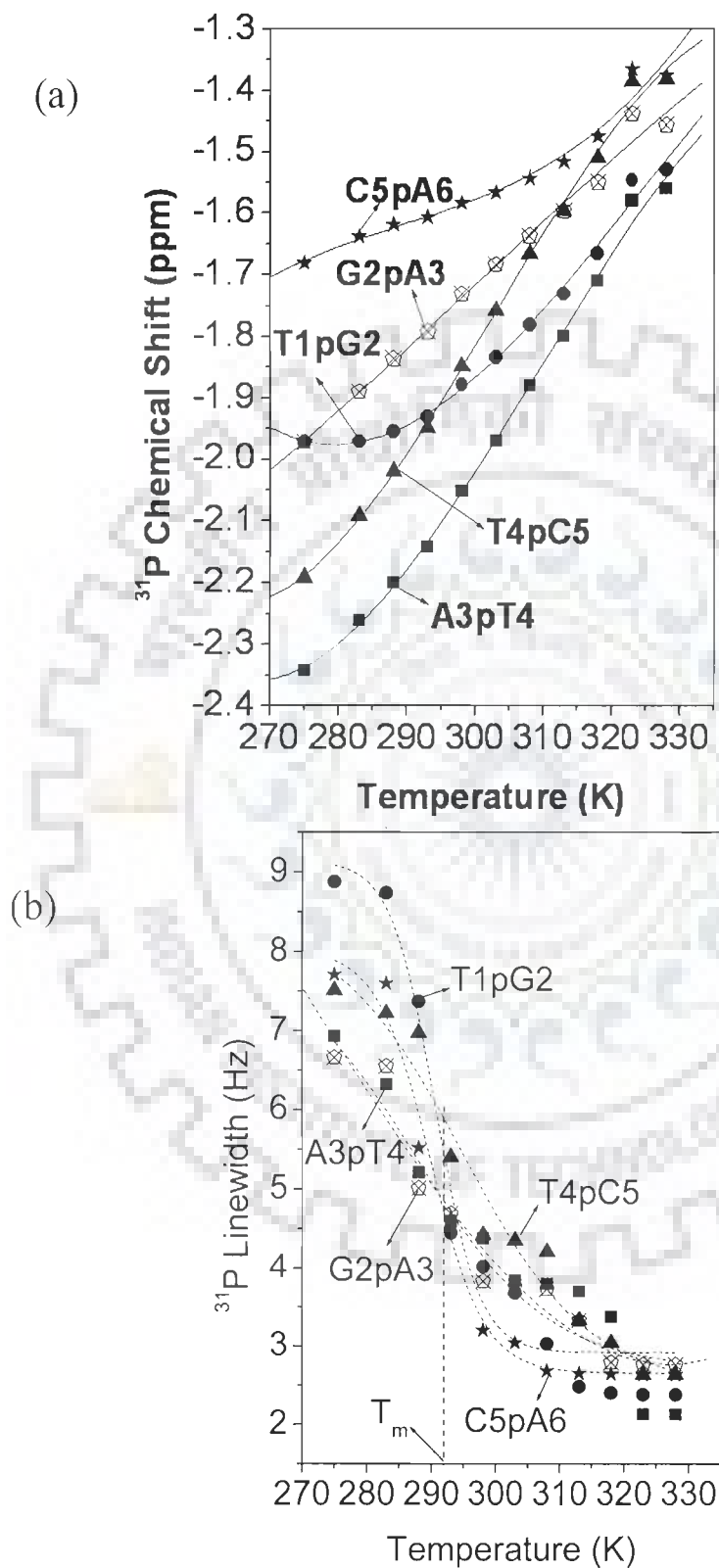


Fig. 3: ^{31}P (a) Chemical Shift (b) Line width of 3.42 mM uncomplexed d-(TGATCA)₂ as a function of temperature

B. Adriamycin-d-(TGATCA)₂ Complex

The complex of d-(TGATCA)₂ with adriamycin was made by addition of 10 μ l of adriamycin from the stock solution (20.49 mM) to the d-(TGATCA)₂ solution till it reaches a ratio of D/N = 2.0. The sample was prepared in 90% water and 10% D₂O. The addition of adriamycin to a solution of oligomer d-(TGATCA)₂ induces the appearance of five new peaks at low field in the ³¹P NMR spectrum as shown in Fig. 4a-b. The spectra were recorded at 275 K as well as 318 K (Fig. 5) to look at the slow and fast exchange. It is seen that even at 318 K there is no fast exchange as distinct bound ³¹P resonances are present (Fig. 5). In order to assign five new phosphorus resonances present in the ³¹P NMR spectra, ³¹P - ³¹P NOESY spectra at various D/N ratios 1.0, 1.5 and 2.0 are recorded at 278 K (Figs. 6 a-c). The five free phosphate resonances are already assigned (Table 1) through the ¹H-³¹P HMBC experiment. It is observed in Figs. 6a-c that each signal belonging to the phosphate group of free specie is correlated to another phosphate resonance shifted downfield, with respect to it, which is therefore the corresponding ³¹P signal of bound DNA. Accordingly, the bound and free phosphate resonances are assigned in the complex and designated with the superscript b and f, respectively (Table 3-5).

With increase in D/N ratio, there is no effect on the ³¹P chemical shift of the phosphate resonance signals. The line width of the free signals are found to increase from 9 upto 27 Hz with D/N ratio while that for bound signal e.g., T1pG2^b decreases (Fig. 7a and Table 6a). However corresponding area plot shows that intensity of ³¹P resonance signal of bound nucleotide phosphate increases in magnitude (Fig. 7b and Table 6b) and that of free nucleotide decreases. The binding appears to saturate at D/N ~ 2.0 (Fig. 7a and Fig. 7b) indicating that two drug molecules are apparently binding per DNA hexanucleotide. At both

275 K and 318 K, separate signals of bound and free nucleotides are observed indicating slow chemical exchange at NMR time scale. Irrespective of the D/N ratio, the T1pG2 and C5pA6 phosphorus signals shift most downfield by 1.3 and 1.07 ppm, respectively on binding. Sites adjacent to these are also affected while the central phosphate, A3pT4, is practically unaffected by binding.

(i) Chemical Shift

Local conformational heterogeneity in the sugar-phosphate backbone has been noted in the form of sequence specific variations or as a result of drug or protein binding to local regions of polynucleotides (Calladine, 1982; Dickerson, 1983; Saenger, 1984; Anderson et al., 1987). While ^1H NMR can provide detailed information on the overall conformation of the sugar rings and bases of oligonucleotides, it generally is unable to provide information on the conformation of the phosphate ester backbone since no direct inter-proton distance constraints are available though NOESY spectra. ^{31}P chemical shifts vary in response to local, sequence specific and induced environmental distortions in the duplex geometry (Calladine, 1982; Dickerson, 1983; Ott and Eckstein, 1985; Schroeder et al., 1989). Theoretical studies have shown that variation in conformation of two of the six torsional angles (α : O3'-P-O5'-C5' and ζ : C3'-O3'-P-O5') can cause perturbations in ^{31}P shifts. A switching from energetically more favorable B_I conformation ($\zeta = g^-, \alpha = g^-$) to the more flexible B_{II} conformation ($\zeta = t, \alpha = g^-$) having energy 1 Kcal/mol higher than B_I introduces a downfield shift of about 1.5 ppm (Gorenstein et al., 1977). The dispersion in ^{31}P chemical shifts of oligonucleotides has also been attributed to different populations of B_I and B_{II} states (Gorenstein, 1992). ^{31}P chemical shift has also been correlated with degree of unwinding of duplex DNA resulting from increase in the length of the sugar phosphate backbone to accommodate intercalation of drug

chromophore. Besides, the ester O-P-O bond angle distortions in drug-duplex DNA complexes also affect the chemical shift. Widening of ester O-P-O angle is expected to produce an upfield shift (Gorenstein, 1984; Gorenstein, 1975) while narrowing of this bond angle causes a downfield shift. Purely electrostatic associations between drug and nucleic acid on the other hand produce only small and generally upfield ^{31}P chemical shifts (Patel, 1979; Wilson et al., 1982).

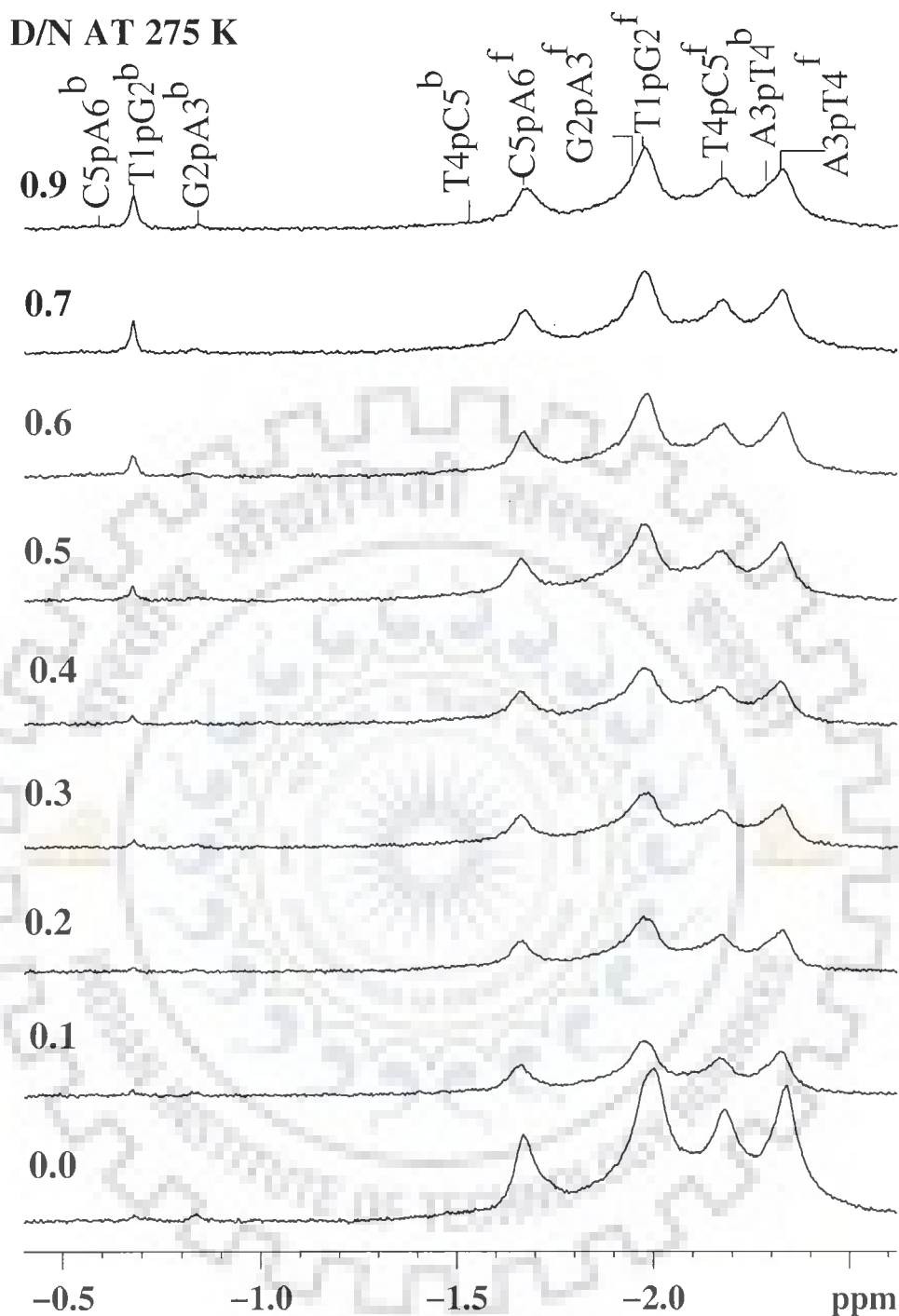
Our results on large observed downfield shift of 1.30 and 1.12 ppm (Table 3-4) in T1pG2 and C5pA6 respectively are supportive of intercalation of adriamycin chromophore between T1...A6 and G2...C5 base pairs. The shift may result due to increased population of trans conformation of ζ (hence B_{II} state), on unwinding of helix as well as distortions in ester O-P-O bonds. The intercalation at T1pG2 sites has apparently affected the neighboring sites as well, particularly the G2pA3 phosphate, perhaps through distortions in ester bond angles, while the central phosphate remains largely unaffected. A comparison with similar structures of complexes (Table 7a-b) of related drugs with d-(CGATCG) and d-(CGTACG), poly (dA.dT) obtained by ^{31}P NMR spectroscopic techniques (Ragg et al., 1988; Favier et al., 2001; Mazzini et al., 2004; Kotovych et al., 1986; Searle et al., 1988; Mazzini et al., 2003; Gorenstein et al., 1989) corroborate our findings. It may also be noted that such downfield shifts are absent in case of drugs which bind externally (Kotovych et al., 1986; Favier et al., 2001; Mazzini et al., 2004).

(ii) Line width

The observed broadening in line width in drug-DNA complexes have generally been attributed to (a) restricted dynamics (b) chemical shift dispersion due to local heterogeneity and (c) intermediate exchange rate (Jones et al., 1980; Levy et al., 1984). We observe slow

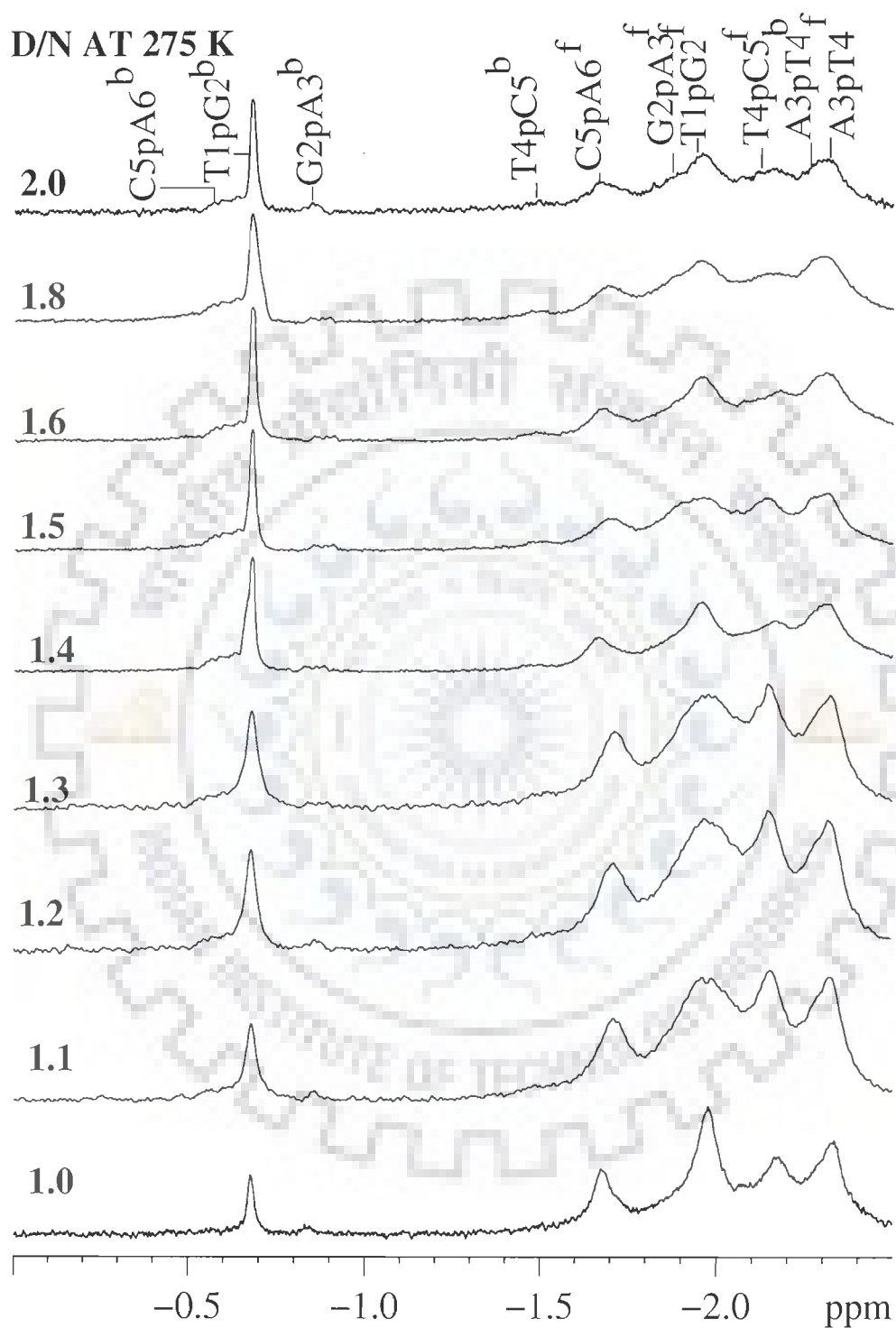
exchange between bound and free sites at all temperatures. The drug does not seem to affect the natural line width due to dynamics as line width of bound ^{31}P signal (eg. T1pG2) decreases while that of corresponding free ^{31}P shift increases with D/N ratio. We carried out spin-lattice relaxation time (T_1) measurement studies to see the effect of intercalation. Using the standard pulse sequence $180^\circ\text{-}\tau\text{-}90^\circ$ and delay (D1) of 10 sec, we got T_1 of phosphate signals of uncomplexed hexamer as 738.14 - 784.22 ms at 298 K. The corresponding signals of free phosphorus in 2:1 adriamycin-d-(TGATCA) $_2$ complex yielded T_1 value of 639.63 ms (broad signal). The relatively small observed difference ($\sim 15\%$) in T_1 of free phosphorus signals in uncomplexed DNA and drug-DNA complex, and hence T_2 or dynamics, cannot account for observed large broadening. The increase in line width of free phosphorus signals in drug-DNA complex is therefore not due to change in motional dynamics. The same has earlier been concluded by Levy et al (Levy et al., 1984) in ethidium bromide-DNA complex. Therefore the ^{31}P line widths are essentially determined by chemical shift dispersion alone. Presence of drug enhances chemical shift dispersion due to stronger differentiation of DNA phosphorus environment as a result of variations in phosphodiester bond angles O-P-O and ζ torsional angles. On the other hand, the bound phosphorus resonance in drug-DNA complex is sharp with ζ in a well defined trans conformation allowing on opening of intercalating T1...A6 and G2...C5 base pairs to $\sim 6.8 \text{ \AA}$ to accommodate adriamycin chromophore. The observed spin-lattice relaxation time (T_1) of T1pG2^b signal is 3.16 sec. However a better insight to the structural variations of the DNA hexamer due to binding of the drug can be obtained only by intermolecular NOE contacts in ^1H 2D NOESY spectra (following chapter).

(iii) Temperature Dependence Studies



(a)

Fig. 4(a-b): Proton decoupled ^{31}P NMR spectra of 3.42 mM d-(TGATCA) $_2$ in uncomplexed state (f) and complexed with adriamycin (b) with various increasing drug (D) to nucleic acid duplex (N) ratios, D/N, at 275 K



(b)

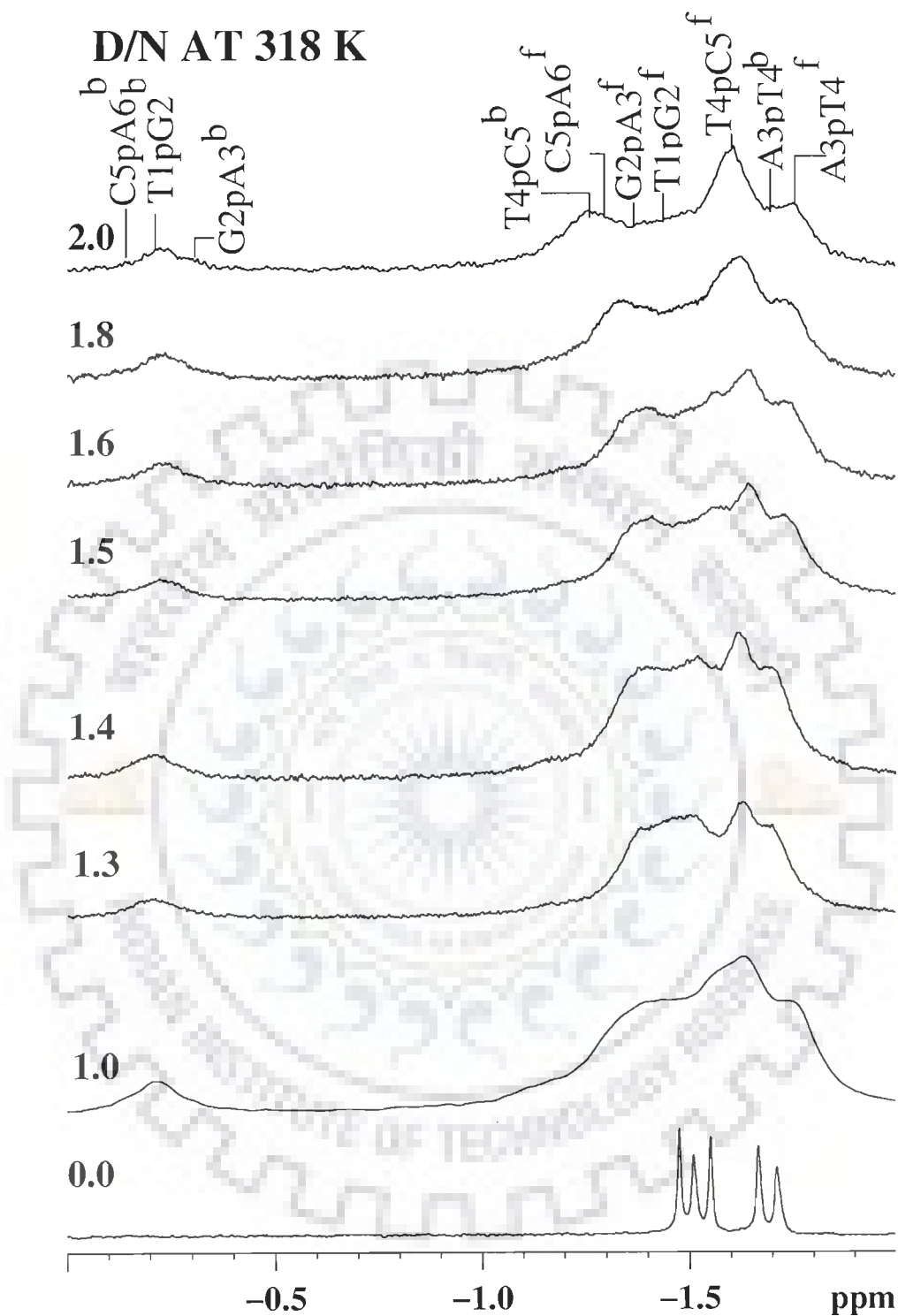


Fig. 5: Proton decoupled ^{31}P NMR spectra of 3.42 mM d-(TGATCA) $_2$ in uncomplexed state (f) and complexed with adriamycin (b) with increasing drug (D) to nucleic acid duplex (N) ratios, D/N, at 318 K

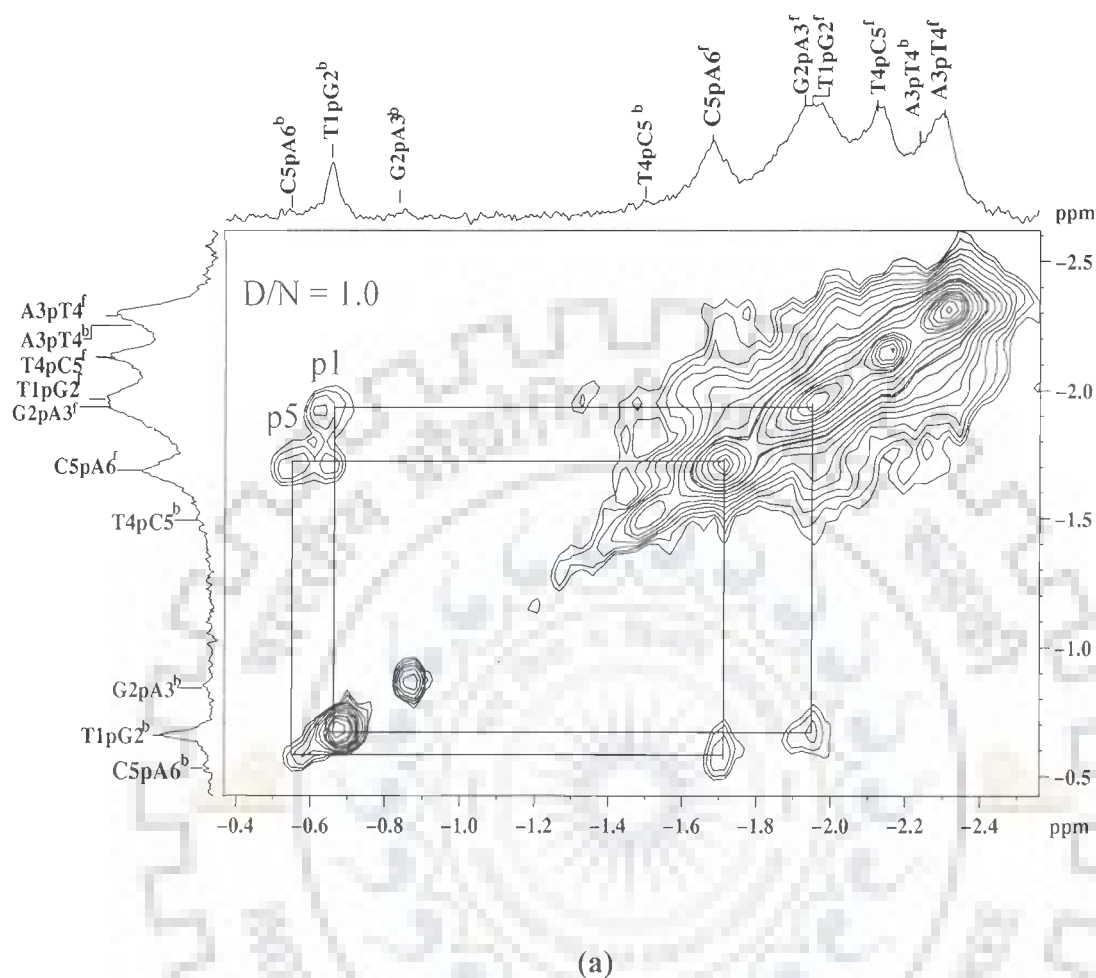


Fig. 6(a-c): ^{31}P - ^{31}P NOESY exchange spectrum at 200 ms of the complex of adriamycin with d-(TGATCA)₂ at drug (D) to nucleic acid duplex (N) ratios, D/N of (a) 1.0, (b) 1.5 and (c) 2.0 at 278K. Five cross peaks of bound and free DNA are labeled as p1 to p5 along 5' to 3' direction

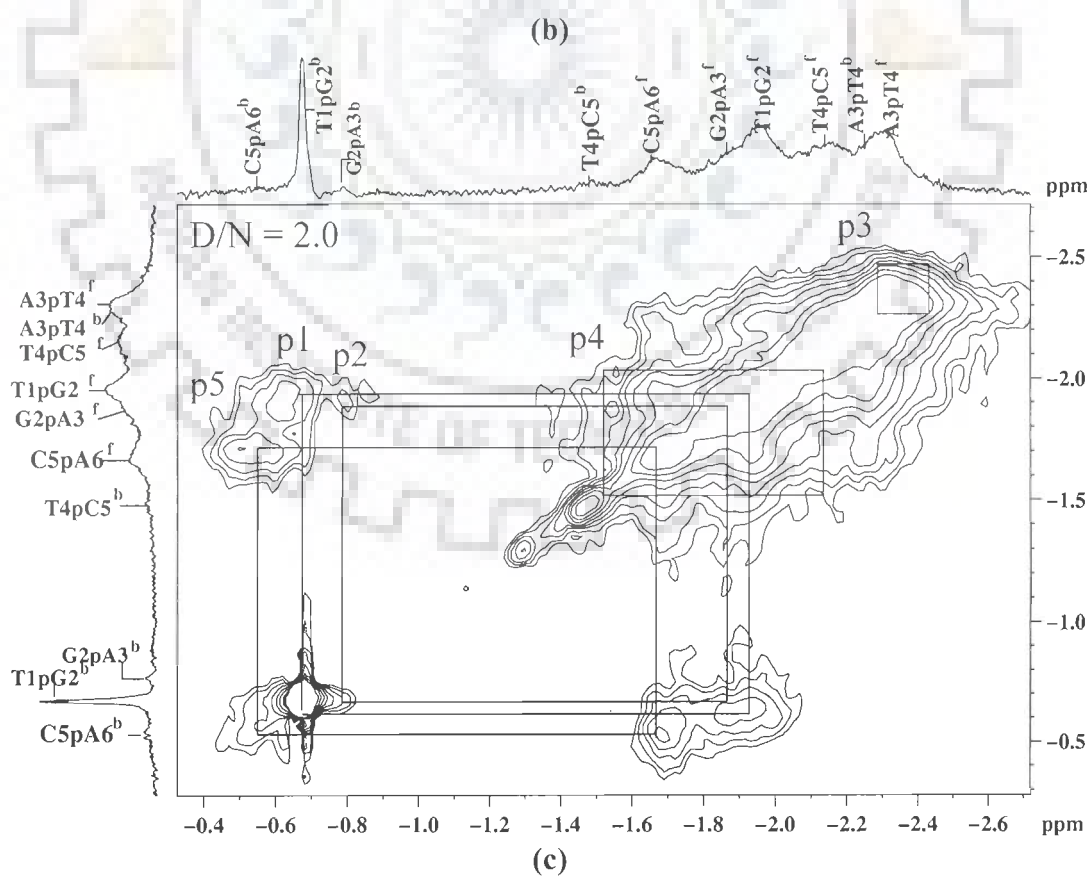
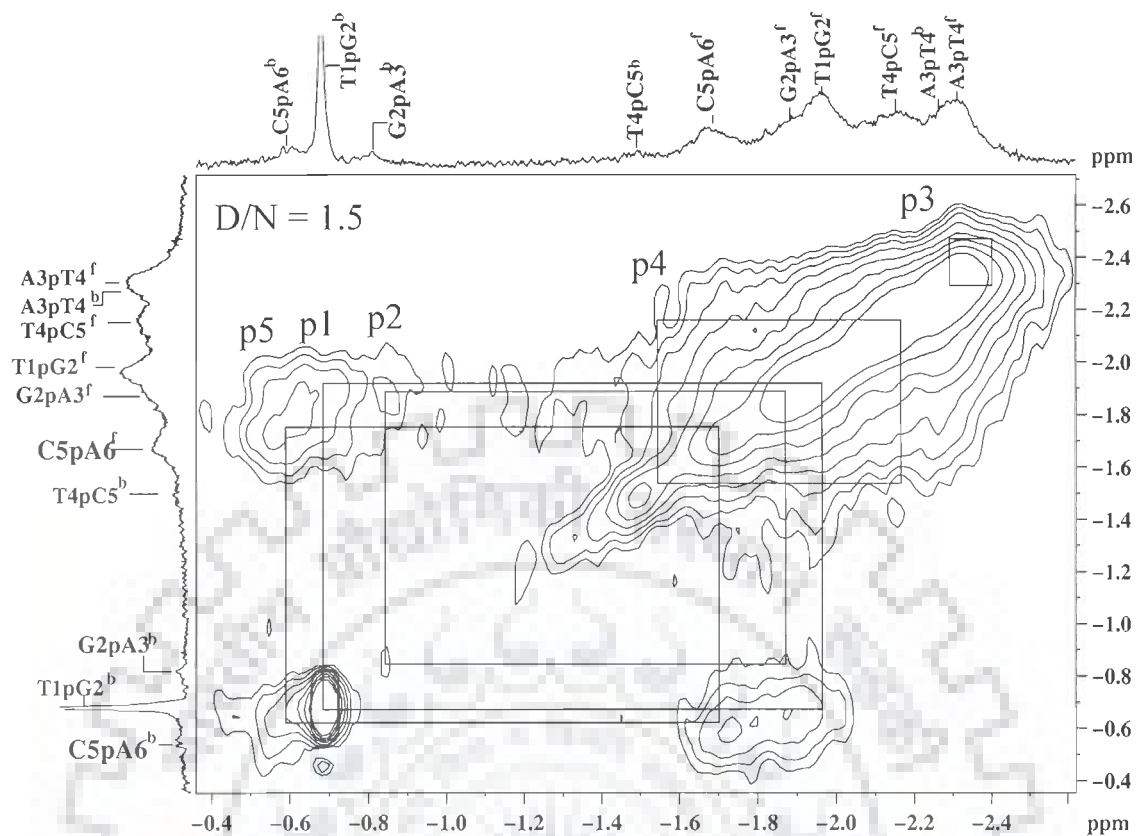


Table 3: Chemical shift of ^{31}P resonances of the phosphate groups of DNA oligomer, present in free and bound state, in the complex of adriamycin with d-(TGATCA) $_2$ at 275 K at different drug (D) to nucleic acid duplex (N) ratios (D / N). In the table, $\Delta \delta = \delta_b - \delta_f$ and +ve $\Delta \delta$ indicates downfield shift whereas -ve $\Delta \delta$ indicates upfield shift.

D/N at 275 K	T1pG2			G2pA3			A3pT4			T4pC5			C5pA6		
	δ^f	δ^b	$\Delta \delta$	δ^f	δ^b	$\Delta \delta$	δ^f	δ^b	$\Delta \delta$	δ^f	δ^b	$\Delta \delta$	δ^f	δ^b	$\Delta \delta$
0.0	-1.97	-	-	-1.97	-	-	-2.34	-	-	-2.19	-	-	-1.68	-	-
0.1	-1.97	-0.68	+1.29	-1.97	-0.82	+1.15	-2.32	-2.30	+0.02	-2.17	-1.46	+0.71	-1.66	-0.62	+1.04
0.2	-1.97	-0.68	+1.29	-1.97	-0.84	+1.13	-2.33	-2.31	+0.02	-2.17	-1.46	+0.71	-1.67	-0.63	+1.04
0.3	-1.98	-0.68	+1.30	-1.98	-0.84	+1.14	-2.32	-2.30	+0.02	-2.16	-1.45	+0.71	-1.66	-0.63	+1.03
0.4	-1.97	-0.68	+1.29	-1.97	-0.84	+1.13	-2.32	-2.30	+0.02	-2.16	-1.46	+0.70	-1.66	-0.63	+1.03
0.5	-1.98	-0.68	+1.30	-1.98	-0.84	+1.14	-2.32	-2.30	+0.02	-2.17	-1.49	+0.68	-1.66	-0.63	+1.03
0.6	-1.98	-0.68	+1.30	-1.98	-0.84	+1.14	-2.33	-2.31	+0.02	-2.18	-1.50	+0.68	-1.67	-0.63	+1.04
0.7	-1.98	-0.68	+1.30	-1.98	-0.84	+1.14	-2.33	-2.31	+0.02	-2.17	-1.50	+0.67	-1.67	-0.63	+1.04
0.9	-1.97	-0.68	+1.29	-1.97	-0.84	+1.13	-2.33	-2.31	+0.02	-2.17	-1.50	+0.67	-1.68	-0.64	+1.04
1.0	-1.97	-0.68	+1.29	-1.97	-0.86	+1.11	-2.33	-2.31	+0.02	-2.18	-1.51	+0.67	-1.69	-0.64	+1.05
1.1	-1.98	-0.68	+1.30	-1.96	-0.86	+1.10	-2.32	-2.30	+0.02	-2.15	-1.49	+0.66	-1.71	-0.62	+1.09
1.2	-1.97	-0.68	+1.29	-1.94	-0.85	+1.09	-2.31	-2.29	+0.02	-2.15	-1.48	+0.67	-1.71	-0.60	+1.11
1.3	-1.98	-0.68	+1.30	-1.94	-0.86	+1.08	-2.32	-2.30	+0.02	-2.14	-1.52	+0.62	-1.71	-0.59	+1.12
1.4	-1.95	-0.68	+1.27	-1.94	-0.88	+1.06	-2.30	-2.28	+0.02	-2.16	-1.47	+0.69	-1.67	-0.61	+1.06
1.5	-1.96	-0.68	+1.28	-1.91	-0.88	+1.03	-2.31	-2.29	+0.02	-2.15	-1.50	+0.65	-1.68	-0.61	+1.07
1.6	-1.96	-0.68	+1.28	-1.90	-0.88	+1.02	-2.31	-2.29	+0.02	-2.18	-1.48	+0.70	-1.68	-0.61	+1.07
1.8	-1.96	-0.68	+1.28	-1.88	-0.88	+1.00	-2.30	-2.28	+0.02	-2.17	-1.47	+0.70	-1.69	-0.61	+1.08
2.0	-1.94	-0.68	+1.26	-1.86	-0.88	+0.98	-2.27	-2.26	+0.01	-2.12	-1.47	+0.65	-1.68	-0.61	+1.07

Table 4: Chemical shift of ^{31}P resonances of the phosphate groups of DNA oligomer, present in free and bound state, in the complex of adriamycin with d-(TGATCA) $_2$ at 318 K at different drug (D) to nucleic acid duplex (N) ratios (D/N). In the table, $\Delta\delta = \delta_b - \delta_f$ and +ve $\Delta\delta$ indicates downfield shift whereas -ve $\Delta\delta$ indicates upfield shift.

D/N at 318 K	T1pG2			G2pA3			A3pT4			T4pC5			C5pA6		
	δ^f	δ^b	$\Delta\delta$	δ^f	δ^b	$\Delta\delta$	δ^f	δ^b	$\Delta\delta$	δ^f	δ^b	$\Delta\delta$	δ^f	δ^b	$\Delta\delta$
0.0	-1.66	-	-	-1.55	-	-	-1.71	-	-	-1.51	-	-	-1.48	-	-
1.0	-1.52	-0.22	+1.30	-1.50	-0.31	+1.19	-1.75	-1.71	+0.04	-1.63	-1.30	+0.33	-1.41	-0.13	+1.28
1.3	-1.50	-0.21	+1.29	-1.48	-0.25	+1.23	-1.68	-1.66	+0.02	-1.63	-1.24	+0.39	-1.38	-0.12	+1.26
1.4	-1.52	-0.22	+1.30	-1.46	-0.26	+1.20	-1.68	-1.67	+0.01	-1.61	-1.22	+0.39	-1.37	-0.11	+1.26
1.5	-1.56	-0.24	+1.32	-1.40	-0.27	+1.13	-1.73	-1.71	+0.02	-1.64	-1.18	+0.46	-1.33	-0.10	+1.23
1.6	-1.56	-0.24	+1.32	-1.48	-0.26	+1.22	-1.73	-1.70	+0.03	-1.63	-1.20	+0.43	-1.40	-0.11	+1.29
1.8	-1.49	-0.22	+1.27	-1.45	-0.28	+1.17	-1.74	-1.71	+0.03	-1.62	-1.22	+0.40	-1.37	-0.14	+1.23
2.0	-1.45	-0.22	+1.23	-1.44	-0.28	+1.16	-1.75	-1.74	+0.01	-1.60	-1.26	+0.34	-1.40	-0.14	+1.26

Table 5: ^{31}P chemical shift assignments of free (δ^f) and bound (δ^b) phosphate groups in the adriamycin-d-(TGATCA) $_2$ complex at 278 K at drug (D) to nucleic acid duplex (N) ratios, D/N = 1, 1.5 and 2.0. The change in chemical shift, $\Delta\delta = \delta^b - \delta^f$, due to binding is also indicated for the three complexes. +ve $\Delta\delta$ indicates downfield shift.

	D/N = 1			D/N = 1.5			D/N = 2.0		
	δ^f	δ^b	$\Delta\delta$	δ^f	δ^b	$\Delta\delta$	δ^f	δ^b	$\Delta\delta$
T1pG2	-1.97	-0.68	+1.29	-1.96	-0.68	+1.28	-1.94	-0.68	+1.26
G2pA3	-1.95	-0.86	+1.09	-1.91	-0.78	+1.13	-1.86	-0.80	+1.06
A3pT4	-2.33	-2.31	+0.02	-2.31	-2.29	+0.02	-2.27	-2.26	+0.01
T4pC5	-2.18	-1.51	+0.67	-2.15	-1.5	+0.65	-2.12	-1.47	+0.65
C5pA6	-1.69	-0.58	+1.11	-1.68	-0.57	+1.11	-1.68	-0.54	+1.14

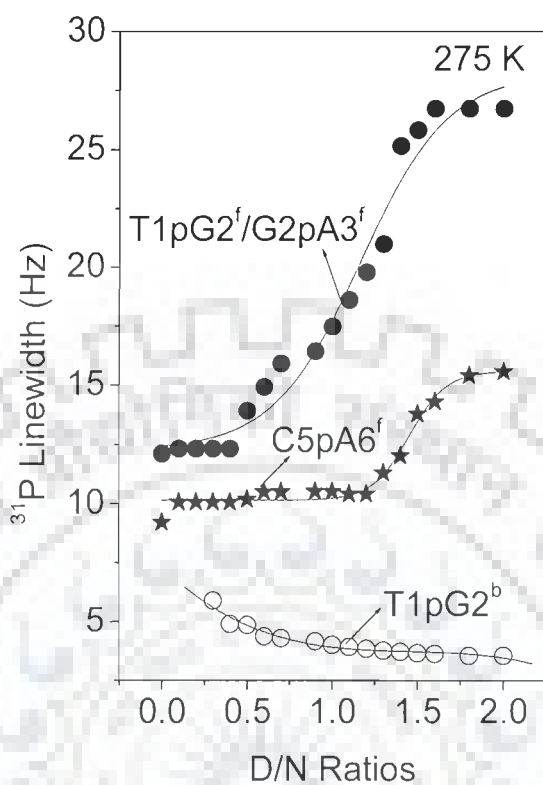


Fig. 7(a): ^{31}P Line width plot of ADM-d-(TGATCA)₂ complex as a function of D/N ratios at 275 K

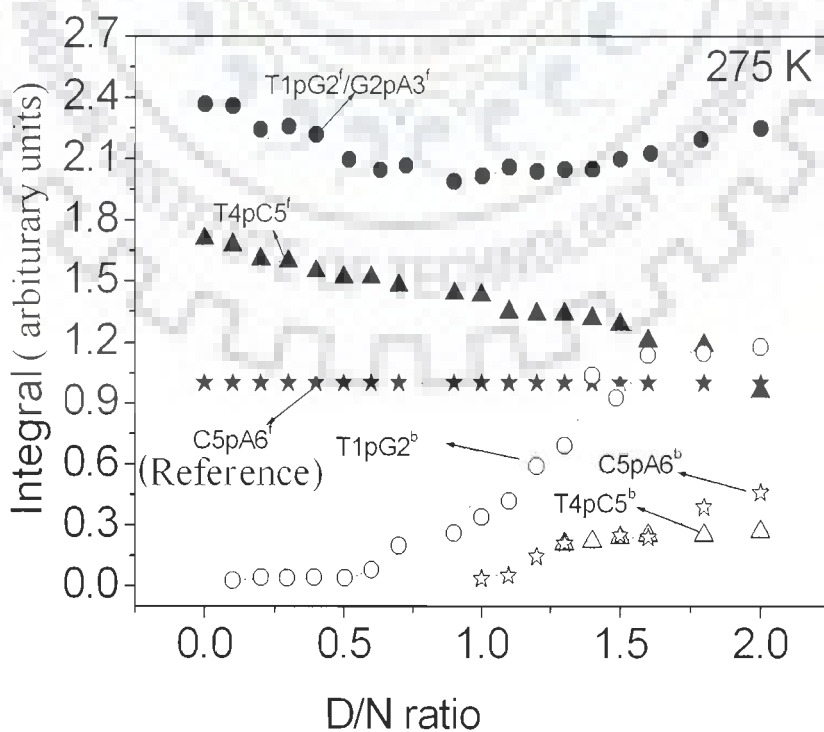


Fig. 7(b): The Integral plot as a function of D/N ratios at 275 K

Table 6a: ^{31}P The Line width plot as a function of D/N ratios at 275 K

D/N at 275 K	T1pG2 ^f /G2pA3 ^f	C5pA6 ^f	T1pG2 ^b
0.0	12.11	9.21	-
0.1	12.32	10.07	-
0.2	12.32	10.07	-
0.3	12.32	10.07	5.89
0.4	12.32	10.07	4.90
0.5	13.92	10.19	4.85
0.6	14.92	10.50	4.37
0.7	15.92	10.50	4.29
0.9	16.44	10.52	4.16
1.0	17.49	10.52	4.01
1.1	18.61	10.42	3.92
1.2	19.79	10.42	3.85
1.3	20.99	11.30	3.77
1.4	25.15	12.02	3.71
1.5	25.83	13.79	3.66
1.6	26.74	14.3	3.63
1.8	26.34	15.42	3.55
2.0	26.34	15.58	3.55

Table 6b: The Integral plot as a function of D/N ratios at 275 K

D/N at 275 K	T4pC5 ^f	T1pG2 ^f / G2pA3 ^f	C5pA6 ^f	T4pC5 ^b	T1pG2 ^b	C5pA6 ^b
0.0	1.71	2.37	1	-	-	-
0.1	1.68	2.36	1	-	0.03	-
0.2	1.61	2.17	1	-	0.04	-
0.3	1.60	2.26	1	-	0.06	-
0.4	1.55	2.22	1	-	0.08	-
0.5	1.52	1.93	1	-	0.10	-
0.6	1.52	1.87	1	-	0.14	-
0.7	1.48	2.39	1	-	0.20	-
0.9	1.44	1.99	1	-	0.26	-
1.0	1.43	1.96	1	-	0.34	0.03
1.1	1.35	2.06	1	-	0.42	0.05
1.2	1.34	2.04	1	-	0.59	0.15
1.3	1.34	2.05	1	0.21	0.69	0.21
1.4	1.32	2.05	1	0.22	1.08	0.08
1.5	1.29	2.10	1	0.24	1.04	0.25
1.6	1.21	2.19	1	0.25	1.14	0.24
1.8	1.19	2.24	1	0.25	1.15	0.39
2.0	0.96	2.25	1	0.27	1.18	0.46

Table 7a: Chemical shift of free (δ^f), bound (δ^b), and change in chemical shift due to binding, $\Delta\delta = \delta^b - \delta^f$ in phosphate groups of some of the drug–DNA complexes taken from literature. +ve $\Delta\delta$ indicates downfield shift.

Phosphate Group	Mazzini et al., 1988 d-(CGATCG) ₂ + Adriamycin			Mazzini et al., 1988 d-(CGTACG) ₂ + Adriamycin			Searle et al., 1988 d-(GCATGC) ₂ + Nogalamycin		
	δ^f	δ^b	$\Delta\delta$	δ^f	δ^b	$\Delta\delta$	δ^f	δ^{b*}	$\Delta\delta$
C1pG2/ G1pC2	-0.91	-0.48	+0.43	-1.03	-0.58	+0.45	-3.30	-2.90	+0.20
G2pA3/ C2pA3	-0.86	0.67	+1.53	-1.40	-0.56	+0.84	-3.00	-2.50	+0.50
A3pT4/ T3pA4	-1.26	-1.28	-0.2	-1.12	-1.26	-0.14	-3.40	-3.20	+0.20
T4pC5/ T4pG6	-1.06	-1.12	-0.06	-1.20	-1.34	-0.14	-3.10	-1.60	+1.50
C5pG6/ G5pC6	-0.73	0.84	+1.57	-0.90	+0.63	+1.53	-3.00	-3.00	+0.00
Phosphate Group	Mazzini et al., 1988 d-(CGATCG) ₂ + Morpholinodoxorubicin			Mazzini et al., 1988 d-(CGTACG) ₂ + Morpholinodoxorubicin			Ragg et al., 1988 d-(CGTACG) ₂ + Daunorubicin		
	δ^f	δ^b	$\Delta\delta$	δ^f	δ^b	$\Delta\delta$	δ^f	δ^b	$\Delta\delta$
C1pG2	-0.91	-0.32	+0.59	-1.03	-0.56	+0.47	-1.02	-1.45	+0.43
G2pA3 / G2pT3	-0.86	0.19	+1.05	-1.40	-0.50	+0.90	-1.42	-1.95	+0.53
A3pT4/ T3pA4	-1.26	-1.36	-0.10	-1.12	-1.45	-0.33	-1.08	-1.28	-0.20
T4pC5/ A4pC5	-1.06	-1.11	-0.05	-1.20	-1.46	-0.26	-1.28	-1.48	-0.20
C5pG6	-0.73	0.52	+1.25	-0.90	+0.22	+1.12	-0.88	+0.44	+1.32

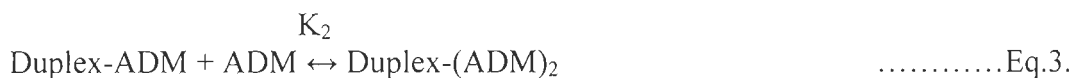
* Tentative assignment

Table 7b: Chemical shift of free (δ^f), bound (δ^b), and the change in chemical shift due to binding, $\Delta\delta = \delta^b - \delta^f$ in phosphate resonances of some of the drug–DNA complexes taken from literature. +ve $\Delta\delta$ indicates downfield shift.

Phosphate Group	Lown et al., 1985 d-(CGCG) ₂ + mitoxantrone			Kotovych et al., 1986 d-(CGATCG) ₂ + mitoxantrone			Favier et al., 2001 d-(CGATCG) ₂ + pyridopurine			Mazinni et al., 2003 d-(AAGAATTCTT) ₂ + berberine					
	δ^f	δ^b	$\Delta\delta$		δ^f	δ^b	$\Delta\delta$		δ^f	δ^b	$\Delta\delta$		δ^f	δ^b	$\Delta\delta$
C1pG2	-3.46	-3.31	+0.15	C1pG2	-1.71	-1.70	+0.01	C1pG2	1.2	1.1	-0.1	A1pA2	-1.31	-1.19	+0.12
G2pA3	-3.30	-3.40	-0.10	G2pA3	-1.71	-1.70	+0.01	G2pA3	1.1	1.1	0.0	A2pG3	-1.00	-0.98	+0.02
C3pG4	-3.46	-3.31	+0.15	A3pT4	-2.19	-2.21	-0.02	A3pT4	0.7	0.8	-0.1	G3pA4	-1.14	-1.12	+0.02
				T4pC5	-1.95	-1.97	-0.02	T4pC5	0.4	0.5	-0.1	A4pA5	-1.40	-1.23	+0.17
				C5pG6	-1.59	-1.25	+0.34	C5pG6	1.2	1.2	0.0	A5pT6	-1.37	-1.40	+0.03
Mazzini et al., 2004 Topotecan+d(CGTAACG) ₂				Mazzini et al., 2004 Camptothecin+d(CGTAACG) ₂				Mazzini et al., 2004 Camptothecin+d(CGTAACG) ₂				T6pT7	-1.18	-1.10	+0.08
C1pG2	-1.00	-1.00	0.00	C1pG2	-0.88	-0.95	+0.07	C1pG2	-0.94	-0.96	+0.02	T7pC8	-1.11	-1.07	+0.04
G2pT3	-1.29	-1.35	-0.06	G2pT3	-1.32	-1.33	+0.01	G2pT3	-1.33	-1.33	+0.00	C8pT9	-1.14	-1.10	+0.04
T3pA4	-1.08	-1.10	-0.02	T3pA4	-1.14	-1.17	-0.03	T3pA4	-1.03	-1.03	+0.00	T9pT10	-1.04	-1.07	+0.03
A4pC5	-1.12	-1.20	-0.08	A4pC5	-1.14	-1.17	-0.03	A4pC5	-1.33	-1.33	+0.00				
C5pG6	-0.90	-1.00	-0.10	C5pG6	-0.78	-0.85	+0.07	T5pA6	-1.10	-1.13	-0.03				
								A6pC7	-1.09	-1.11	+0.02				
								C7pG8	-0.82	-0.84	-0.02				

We have recorded the ^{31}P 1D spectra versus temperature for D/N ratios 1.0, 1.5 and 2.0 (Fig. 8a-c). The variations in chemical shift of free and bound species are shown in Fig. 9a-e. With increase in temperature, there is downfield shift of the ^{31}P resonances (Table 8, 9a-b). The ^{31}P free nucleotide resonances coalesce to form a single very broad peak. The bound ^{31}P resonance signal, especially the signal at the intercalation site (T1pG2), gets broadened. On formation of the complex, the T_m of the complex is 315 K and is thus enhanced by 23 K ($\Delta T_m = 315 \text{ K} - 292 \text{ K}$) (Fig.10 and Table 10). At temperatures much below T_m , the ^{31}P signals in adriamycin-d-(TGATCA)₂ complex are sharp because the rate of exchange of the phosphates in the two sites is slow. A comparison of melting curve of uncomplexed d-(TGATCA)₂ with corresponding free ^{31}P resonances in 2:1 adriamycin-d-(TGATCA)₂ complex (Fig. 9d and Table 9a) shows that there are no major differences between the two curves, as expected. The bound ^{31}P resonances (Fig. 9e and Table 9b) on the other hand show that $\delta_{328} - \delta_{275}$ is significantly larger ($\Delta\delta \sim 0.6, 0.7$ and 0.6 ppm for T1pG2^b, G2pA3^b and C5pA6^b, respectively) than that for corresponding free ^{31}P resonances in drug-DNA complex ($\Delta\delta \sim 0.3$ ppm for C5pA6^f). These results are indicative of the fact that the intercalation of drug at T1pG2 and C5pA6 site acts as a stabilizing factor, the effect of which is also seen in adjacent base pair, that is, G2pA3 site. Apparently the drug is bound to DNA at higher temperature as well. At T4pC5 site, the bound signal has $\Delta\delta \sim 0.2$ ppm which is less than the free resonance signal ($\Delta\delta \sim 0.7$ ppm), showing that the T4pC5 site is destabilized in comparison to G2pA3 on the complex formation. Although the variations in phosphodiester bond angles O-P-O are present at both G2pA3 and T4pC5 sites. The phenomenon of duplex to single strand transition takes place along with the following reactions that exist.





Eq. 1 shows melting of the duplex with $K_M = 1.82 \times 10^{-3} \text{ M}^{-1}$ (Fig. 3a). Eq. 4 shows aggregation of adriamycin which may compete with intercalation process ($K_D = 1.5 \times 10^4 \text{ M}^{-1}$ from chapter 3). In Eq. 2 and 3, K_1 and K_2 are the binding constants at D/N 1:1 and 2:1, respectively, whose values are $1.49 \times 10^4 \text{ M}^{-1}$ and $1.03 \times 10^4 \text{ M}^{-1}$. Table 6b shows the area plot of various D/N ratios and equilibrium constant (K_1 at D/N 1:1) and (K_2 at D/N 2:1) is calculated from the D/N ratios.

Fig.11 and Table 11 shows the area plot of the phosphorus at D/N ratio = 1:1, 1.5:1, 2:1 complex. From this plot, thermodynamic parameters are calculated which include equilibrium constant calculation. Then plot was made of K_{eq} versus $1/T$ using Vant Hoff's Equation for C5pA6. From this plot, entropy (ΔS), enthalpy (ΔH) and the free energy (ΔG) is calculated.

$$\Delta G = \Delta H - T\Delta S$$

Thermodynamic Parameters	C5pA6
ΔS	16.51 J/Mole/K
ΔH	-15.59 KJ/Mole
$\Delta G_{275 \text{ K}}$	-4555.84 KJ
$\Delta G_{328 \text{ K}}$	-5430.87 KJ

These values are consistent with those reported in literature (Breslauer, 1987). It may be noted that the temperature dependence of the bound phosphorus signal in drug-DNA complex has been reported for ethidium bromide-PolyA.PolyU (Gorenstein et al., 1989) and daunorubicin-d-(CGATCG)₂ complex (Ragg et al., 1988) in literature. It has been found that as the temperature is increased, the bound ³¹P signal shifts gradually upfield. As the temperature is further increased (50 °C and 80 °C, respectively in these two complexes) the downfield, intercalating drug / helix signal (that is, bound signal) disappears and coalesces with the upfield signal to form a single very broad peak. This is in sharp contrast to our results which show that the bound ³¹P signals

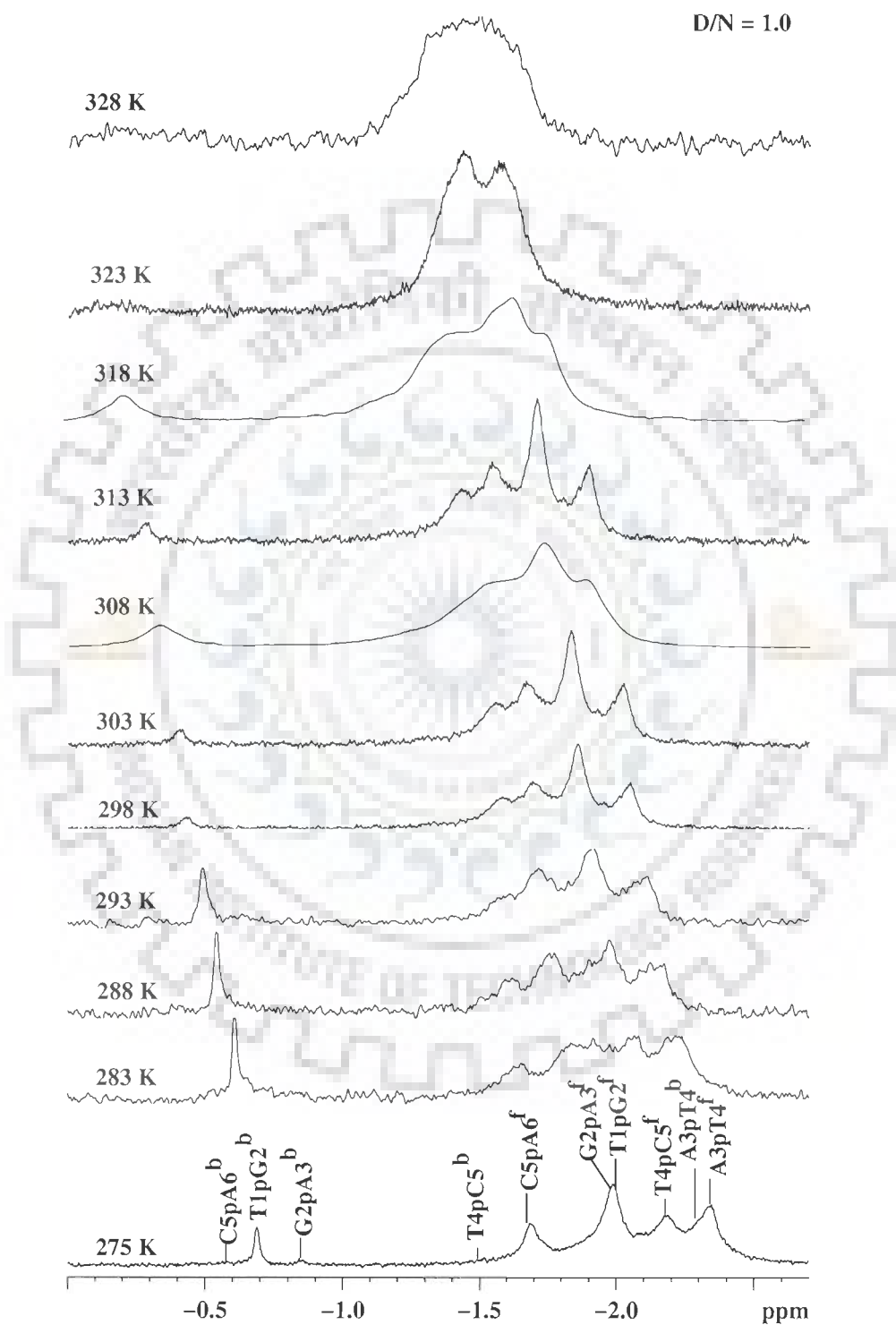


Fig. 8(a): Proton decoupled ^{31}P NMR spectra of d-(TGATCA)₂ complexed with adriamycin as a function of temperature at D/N ratio 1.0

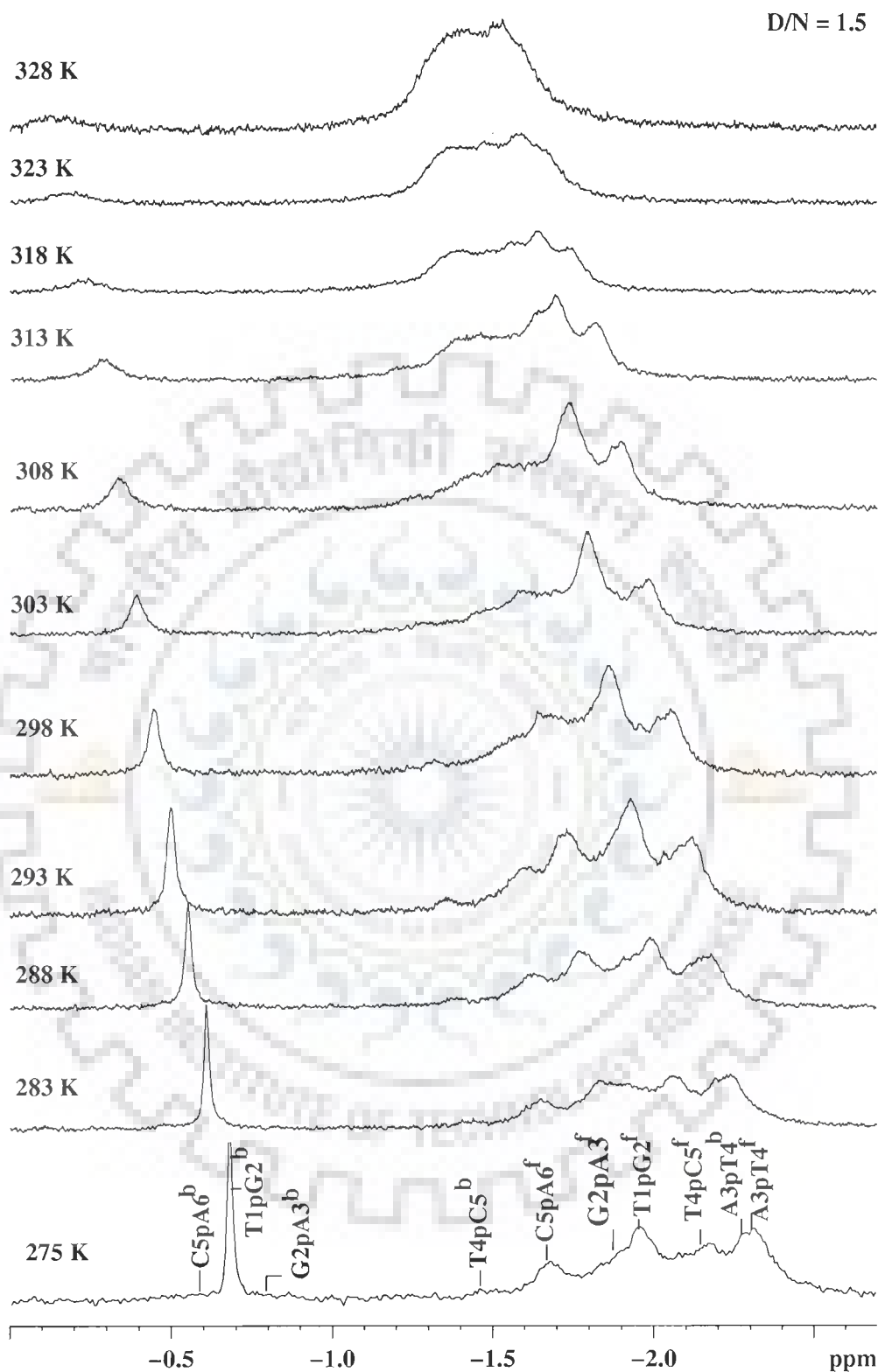


Fig. 8b: Proton decoupled ^{31}P NMR spectra of d-(TGATCA)₂ complexed with adriamycin as a function of temperature at D/N ratio 1.5

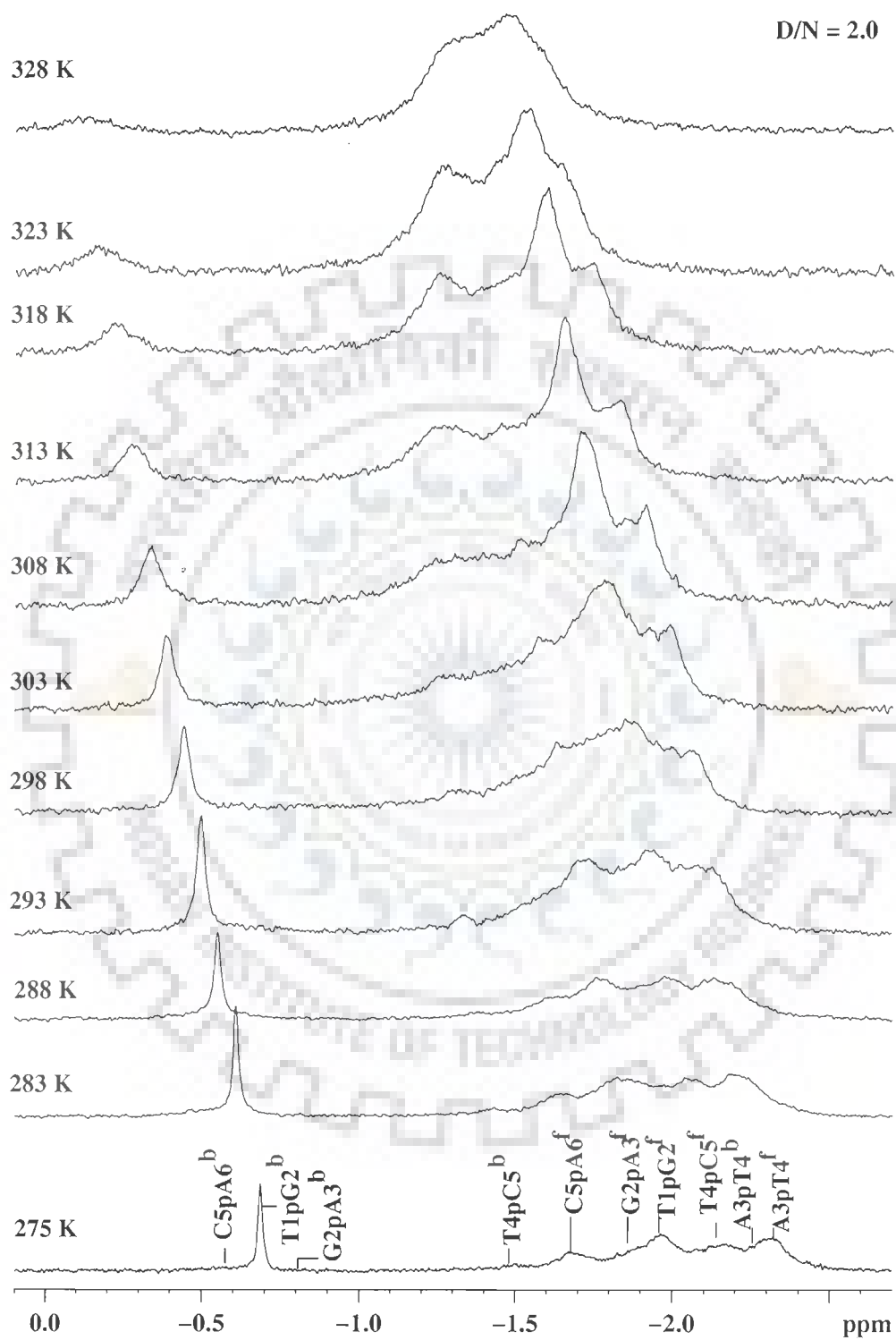


Fig. 8c: Proton decoupled ^{31}P NMR spectra of d-(TGATCA)₂ complexed with adriamycin as a function of temperature at D/N ratio 2.0

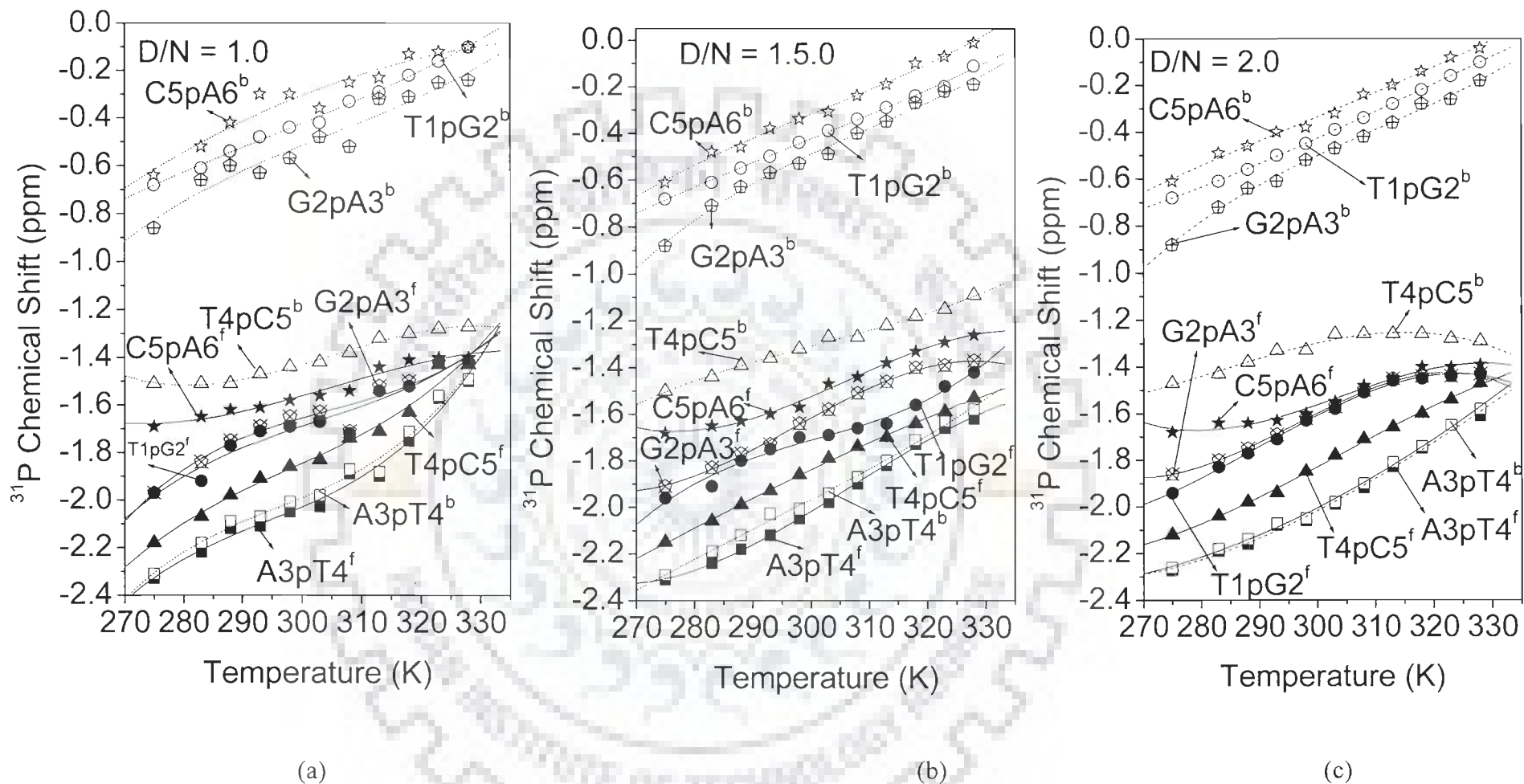


Fig. 9: Free (f) and bound (b) ^{31}P chemical shift of adriamycin-d-(TGATCA) $_2$ complex as a function of temperature in the range of 275-328 K at D/N ratios of (a) 1.0 (b) 1.5 (c) 2.0

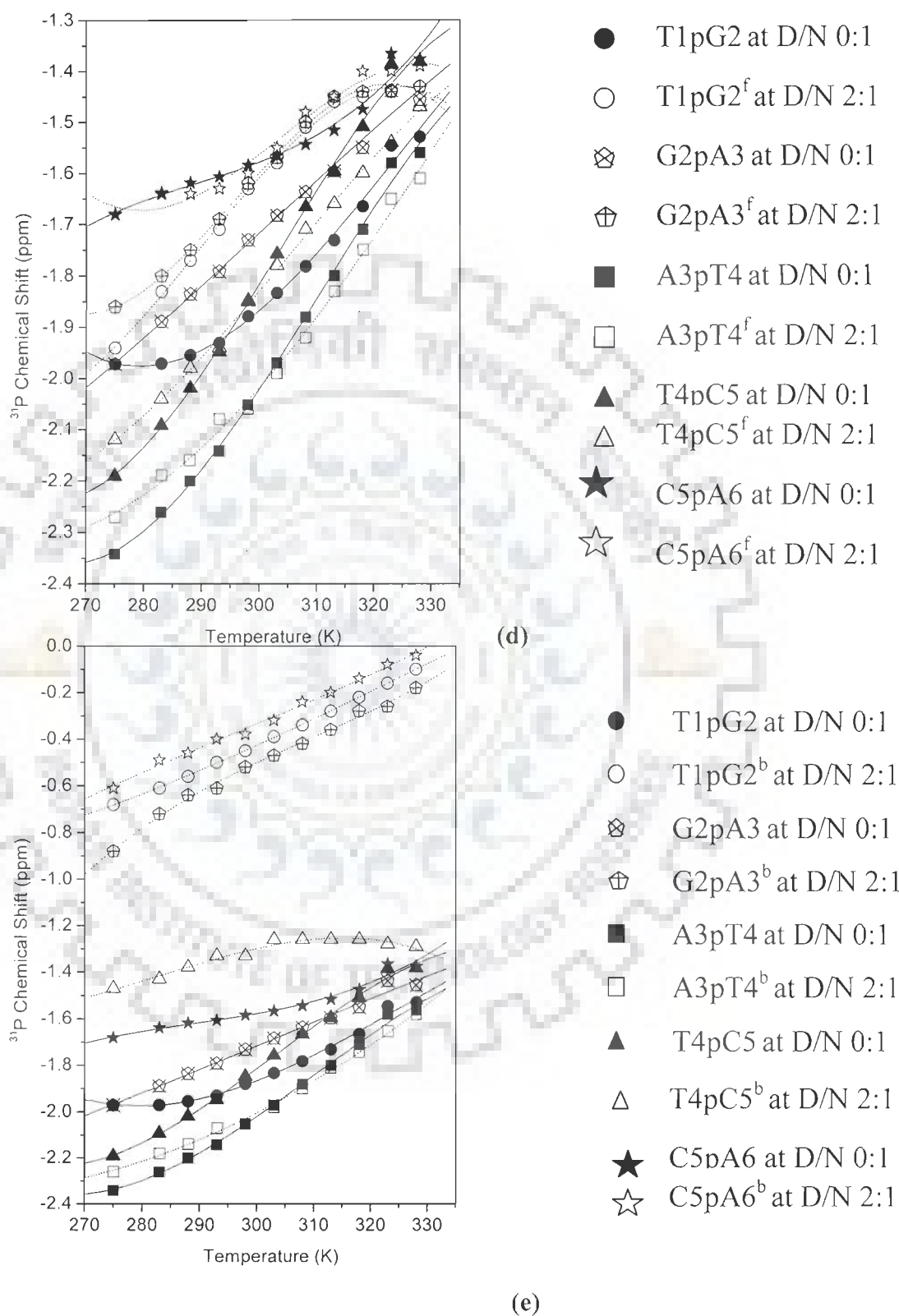


Fig. 9: (d) Free and (e) Bound resonances of the adriamycin-d-(TGATCA)₂ complex (2:1) along with the uncomplexed d-(TGATCA)₂

Table 8: ^{31}P chemical shift adriamycin-d-(TGATCA) $_2$ complex (D/N = 1.0, 1.5, 2.0) as a function of temperature in the range 275-328 K where $\Delta\delta = \delta_{328\text{K}} - \delta_{275\text{K}}$ and $\Delta\delta' = \delta^b - \delta^f$

Temp. (K) at (1:1)	T1pG2			G2pA3			A3pT4			T4pC5			C5pA6		
	δ^f	δ^b	$\Delta\delta'$	δ^f	δ^b	$\Delta\delta'$	δ^f	δ^b	$\Delta\delta'$	δ^f	δ^b	$\Delta\delta'$	δ^f	δ^b	$\Delta\delta'$
275	-1.97	-0.68	+1.29	-1.97	-0.86	+1.11	-2.33	-2.31	+0.02	-2.18	-1.51	+0.67	-1.69	-0.64	+1.05
283	-1.92	-0.61	+1.31	-1.84	-0.66	+1.18	-2.22	-2.18	+0.04	-2.07	-1.51	+0.56	-1.65	-0.52	+1.13
288	-1.77	-0.54	+1.23	-1.75	-0.6	+1.15	-2.12	-2.09	+0.03	-1.98	-1.51	+0.47	-1.62	-0.42	+1.20
293	-1.71	-0.48	+1.23	-1.69	-0.63	+1.06	-2.11	-2.07	+0.04	-1.91	-1.47	+0.44	-1.61	-0.3	+1.31
298	-1.69	-0.44	+1.25	-1.65	-0.57	+1.08	-2.05	-2.01	+0.04	-1.86	-1.44	+0.42	-1.58	-0.3	+1.28
303	-1.67	-0.42	+1.25	-1.63	-0.48	+1.15	-2.03	-1.98	+0.05	-1.83	-1.42	+0.41	-1.56	-0.36	+1.20
308	-1.72	-0.33	+1.39	-1.71	-0.52	+1.19	-1.89	-1.87	+0.02	-1.74	-1.38	+0.36	-1.54	-0.25	+1.29
313	-1.54	-0.29	+1.25	-1.52	-0.32	+1.20	-1.9	-1.88	+0.02	-1.71	-1.32	+0.39	-1.44	-0.23	+1.21
318	-1.52	-0.22	+1.30	-1.5	-0.31	+1.19	-1.75	-1.71	+0.04	-1.63	-1.3	+0.33	-1.41	-0.13	+1.28
323	-1.42	-0.16	+1.26	-1.42	-0.25	+1.17	-1.57	-1.56	+0.01	-1.43	-1.28	+0.15	-1.4	-0.12	+1.28
328	-1.42	-0.1	+1.32	-1.42	-0.24	+1.18	-1.5	-1.49	+0.01	-1.43	-1.27	+0.16	-1.4	-0.1	+1.30
$\Delta\delta$	+0.55	+0.58		+0.55	+0.62		+0.83	+0.82		+0.75	+0.24		+0.29	+0.54	
Temp. (K) at (1.5:1)	δ^f	δ^b	$\Delta\delta'$	δ^f	δ^b	$\Delta\delta'$	δ^f	δ^b	$\Delta\delta'$	δ^f	δ^b	$\Delta\delta'$	δ^f	δ^b	$\Delta\delta'$
275	-1.96	-0.68	+1.28	-1.91	-0.88	+1.03	-2.31	-2.29	+0.02	-2.15	-1.5	+0.65	-1.68	-0.61	+1.07
283	-1.91	-0.61	+1.3	-1.83	-0.71	+1.12	-2.24	-2.19	+0.05	-2.06	-1.44	+0.62	-1.65	-0.48	+1.17
288	-1.8	-0.55	+1.25	-1.77	-0.63	+1.14	-2.18	-2.12	+0.06	-1.99	-1.39	+0.6	-1.63	-0.46	+1.17
293	-1.75	-0.5	+1.25	-1.73	-0.57	+1.16	-2.12	-2.03	+0.09	-1.93	-1.36	+0.57	-1.6	-0.38	+1.22
298	-1.7	-0.44	+1.26	-1.64	-0.53	+1.11	-2.05	-2.01	+0.04	-1.86	-1.32	+0.54	-1.57	-0.34	+1.23
303	-1.69	-0.39	+1.3	-1.58	-0.49	+1.09	-1.98	-1.94	+0.04	-1.79	-1.27	+0.52	-1.47	-0.31	+1.16
308	-1.66	-0.34	+1.32	-1.51	-0.4	+1.11	-1.9	-1.87	+0.03	-1.74	-1.27	+0.47	-1.44	-0.24	+1.20
313	-1.64	-0.29	+1.35	-1.46	-0.35	+1.11	-1.82	-1.8	+0.02	-1.7	-1.22	+0.48	-1.38	-0.19	+1.19
318	-1.56	-0.24	+1.32	-1.4	-0.27	+1.13	-1.73	-1.71	+0.02	-1.64	-1.18	+0.46	-1.33	-0.1	+1.23
323	-1.48	-0.2	+1.28	-1.39	-0.22	+1.17	-1.66	-1.63	+0.03	-1.59	-1.15	+0.44	-1.29	-0.07	+1.22
328	-1.42	-0.11	+1.31	-1.37	-0.19	+1.18	-1.62	-1.58	+0.04	-1.53	-1.09	+0.44	-1.26	-0.01	+1.25
$\Delta\delta$	+0.54	+0.57		+0.54	+0.69		+0.69	+0.71		+0.62	+0.41		+0.42	+0.6	

Contd.

Table 8 (Contd.)

D/N =2:1	T1pG2			G2pA3			A3pT4			T4pC5			C5pA6		
Temp. (K)	δ^f	δ^b	$\Delta \delta'$	δ^f	δ^b	$\Delta \delta'$	δ^f	δ^b	$\Delta \delta'$	δ^f	δ^b	$\Delta \delta'$	δ^f	δ^b	$\Delta \delta'$
275	-1.94	-0.68	+1.26	-1.86	-0.88	+0.98	-2.27	-2.26	+0.01	-2.12	-1.47	+0.65	-1.68	-0.61	+1.07
283	-1.83	-0.61	+1.22	-1.8	-0.72	+1.08	-2.19	-2.18	+0.01	-2.04	-1.43	+0.61	-1.64	-0.49	+1.15
288	-1.77	-0.56	+1.21	-1.75	-0.64	+1.11	-2.16	-2.14	+0.02	-1.98	-1.38	+0.6	-1.64	-0.46	+1.18
293	-1.71	-0.5	+1.21	-1.69	-0.61	+1.08	-2.08	-2.07	+0.01	-1.94	-1.33	+0.61	-1.63	-0.4	+1.23
298	-1.63	-0.45	+1.18	-1.62	-0.52	+1.1	-2.06	-2.05	+0.01	-1.85	-1.33	+0.52	-1.6	-0.38	+1.22
303	-1.58	-0.39	+1.19	-1.57	-0.47	+1.1	-1.99	-1.98	+0.01	-1.78	-1.26	+0.52	-1.55	-0.32	+1.23
308	-1.51	-0.34	+1.17	-1.5	-0.42	+1.08	-1.92	-1.9	+0.02	-1.71	-1.26	+0.45	-1.48	-0.24	+1.24
313	-1.46	-0.28	+1.18	-1.45	-0.36	+1.09	-1.83	-1.81	+0.02	-1.66	-1.26	+0.4	-1.45	-0.2	+1.25
318	-1.45	-0.22	+1.23	-1.44	-0.28	+1.16	-1.75	-1.74	+0.01	-1.6	-1.26	+0.34	-1.4	-0.14	+1.26
323	-1.44	-0.16	+1.28	-1.44	-0.26	+1.18	-1.65	-1.65	+0	-1.54	-1.28	+0.26	-1.4	-0.08	+1.32
328	-1.43	-0.1	+1.33	-1.43	-0.18	+1.25	-1.61	-1.58	+0.03	-1.47	-1.29	+0.18	-1.39	-0.04	+1.35
$\Delta \delta$	+0.51	+0.58		+0.43	+0.7		+0.66	+0.68		+0.65	+0.18		+0.29	+0.57	

+ve $\Delta \delta$ indicates downfield shift

-ve $\Delta \delta$ indicates up field shift

Table 9a-b: Free and bound resonances of the adriamycin-d-(TGATCA)₂ complex (2:1) along with the alone d-(TGATCA)₂ signals as a function of temperature in the range 275-328 K where $\Delta\delta = \delta_{328\text{K}} - \delta_{275\text{K}}$.

(a) Temp. (K)	T1pG2 ^f (2:1)	G2pA3 ^f (2:1)	A3pT4 ^f (2:1)	T4pC5 ^f (2:1)	C5pA6 ^f (2:1)	T1pG2 (0:1)	G2pA3 (0:1)	A3pT4 (0:1)	T4pC5 (0:1)	C5pA6 (0:1)
275	-1.94	-1.86	-2.27	-2.12	-1.68	-1.97	-1.97	-2.34	-2.19	-1.68
283	-1.83	-1.8	-2.19	-2.04	-1.64	-1.97	-1.89	-2.26	-2.09	-1.64
288	-1.77	-1.75	-2.16	-1.98	-1.64	-1.95	-1.84	-2.20	-2.02	-1.62
293	-1.71	-1.69	-2.08	-1.94	-1.63	-1.93	-1.79	-2.14	-1.95	-1.61
298	-1.63	-1.62	-2.06	-1.85	-1.6	-1.88	-1.73	-2.05	-1.85	-1.58
303	-1.58	-1.57	-1.99	-1.78	-1.55	-1.83	-1.68	-1.97	-1.76	-1.57
308	-1.51	-1.5	-1.92	-1.71	-1.48	-1.78	-1.64	-1.88	-1.67	-1.54
313	-1.46	-1.45	-1.83	-1.66	-1.45	-1.73	-1.60	-1.80	-1.60	-1.52
318	-1.45	-1.44	-1.75	-1.6	-1.4	-1.66	-1.55	-1.71	-1.51	-1.48
323	-1.44	-1.44	-1.65	-1.54	-1.4	-1.55	-1.44	-1.58	-1.39	-1.37
328	-1.43	-1.43	-1.61	-1.47	-1.39	-1.53	-1.46	-1.56	-1.38	-1.38
$\Delta\delta$	+0.51	+0.43	+0.66	+0.65	+0.29	+0.44	+0.51	+0.78	+0.81	+0.30
(b) Temp. (K)	T1pG2 ^b (2:1)	G2pA3 ^b (2:1)	A3pT4 ^b (2:1)	T4pC5 ^b (2:1)	C5pA6 ^b (2:1)	T1pG2 (0:1)	G2pA3 (0:1)	A3pT4 (0:1)	T4pC5 (0:1)	C5pA6 (0:1)
275	-0.68	-0.88	-2.26	-1.47	-0.61	-1.97	-1.97	-2.34	-2.19	-1.68
283	-0.61	-0.72	-2.18	-1.43	-0.49	-1.97	-1.89	-2.26	-2.09	-1.64
288	-0.56	-0.64	-2.14	-1.38	-0.46	-1.95	-1.84	-2.20	-2.02	-1.62
293	-0.5	-0.61	-2.07	-1.33	-0.4	-1.93	-1.79	-2.14	-1.95	-1.61
298	-0.45	-0.52	-2.05	-1.33	-0.38	-1.88	-1.73	-2.05	-1.85	-1.58
303	-0.39	-0.47	-1.98	-1.26	-0.32	-1.83	-1.68	-1.97	-1.76	-1.57
308	-0.34	-0.42	-1.9	-1.26	-0.24	-1.78	-1.64	-1.88	-1.67	-1.54
313	-0.28	-0.36	-1.81	-1.26	-0.2	-1.73	-1.60	-1.80	-1.60	-1.52
318	-0.22	-0.28	-1.74	-1.26	-0.14	-1.66	-1.55	-1.71	-1.51	-1.48
323	-0.16	-0.26	-1.65	-1.28	-0.08	-1.55	-1.44	-1.58	-1.39	-1.37
328	-0.1	-0.18	-1.58	-1.29	-0.04	-1.53	-1.46	-1.56	-1.38	-1.38
$\Delta\delta$	+0.58	+0.7	+0.68	+0.18	+0.57	+0.44	+0.51	+0.78	+0.81	+0.30

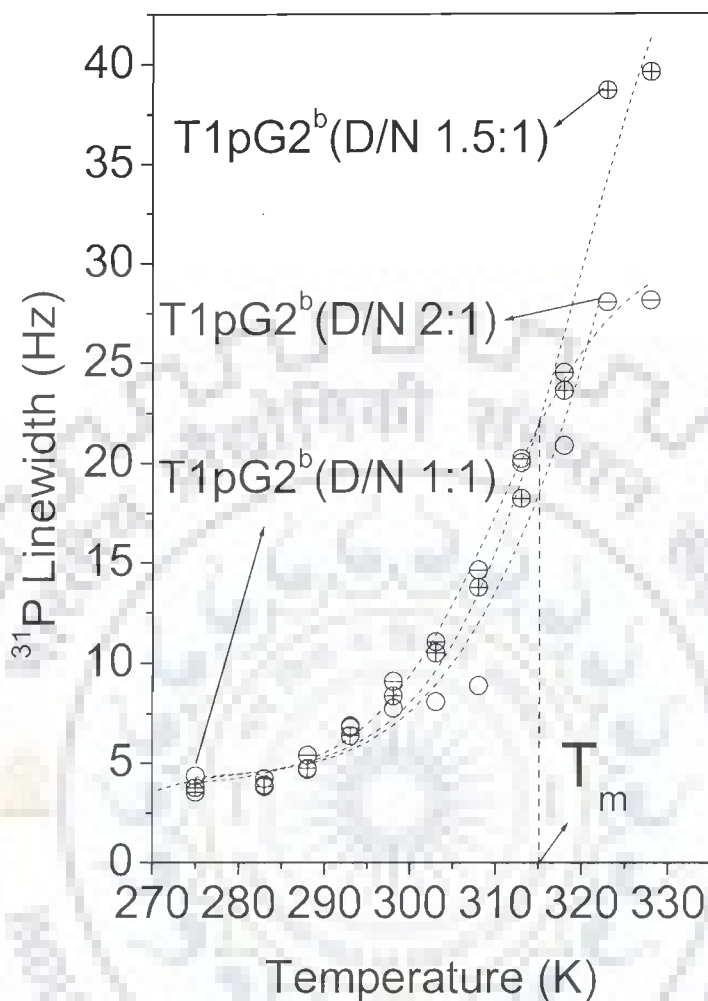


Fig. 10: ^{31}P Line width (Hz) plot of adriamycin-d-(TGATCA) $_2$ complex as a function of Temperature at D/N ratios of 1.0, 1.5 and 2.0.

Table 10: ^{31}P Line width (Hz) of adriamycin-d-(TGATCA) $_2$ complex as a function of Temperature at D/N ratios = 1.0, 1.5, 2.0.

Temp. (K)	T1pG2 ^b (1:1)	T1pG2 ^b (1.5:1)	T1pG2 ^b (2:1)
275	4.36	3.78	3.55
283	3.93	3.83	4.23
288	4.68	4.76	5.39
293	6.87	6.38	6.77
298	7.75	8.36	9.08
303	8.07	10.49	11.04
308	8.87	13.75	14.64
313	20.02	18.22	20.21
318	20.87	23.62	24.51
323	-	38.67	28.04
328	-	39.59	28.12

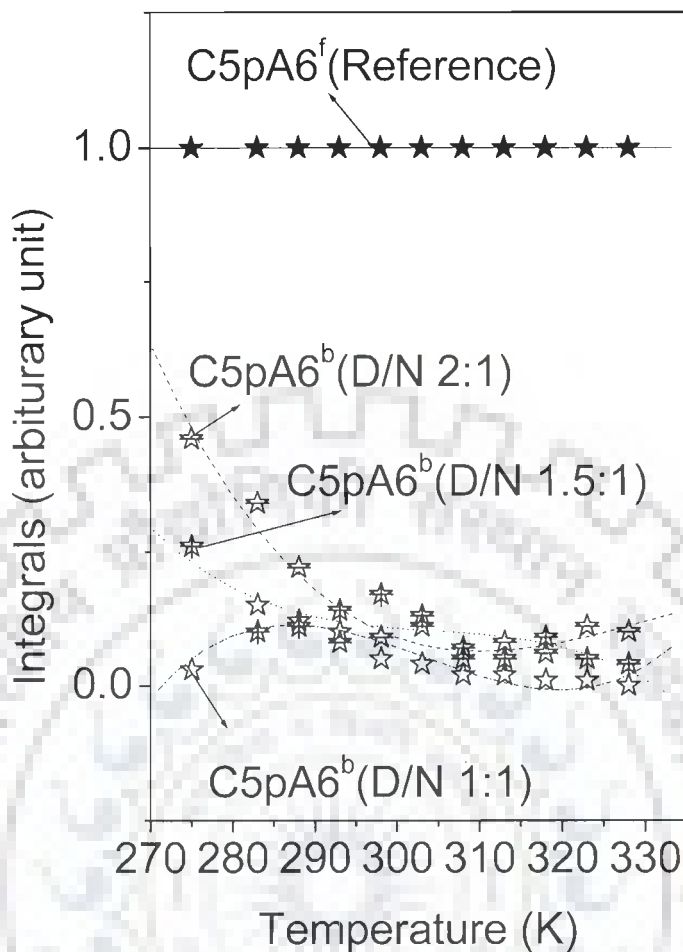


Fig. 11: The area plot of ^{31}P resonances as a function of Temperature at D/N ratios of 1.0, 1.5 and 2.0

Table 11: The area plot of ^{31}P resonances as a function of Temperature at D/N ratios = 1.0, 1.5, 2.0.

Temp. (K)	C5pA6 ^f (Reference)	C5pA6 ^b (1:1)	C5pA6 ^b (1.5:1)	C5pA6 ^b (2:1)
275.00	1.00	0.03	0.26	0.46
283.00	1.00	0.15	0.10	0.34
288.00	1.00	0.12	0.11	0.22
293.00	1.00	0.10	0.14	0.08
298.00	1.00	0.05	0.17	0.09
303.00	1.00	0.04	0.13	0.11
308.00	1.00	0.02	0.07	0.05
313.00	1.00	0.02	0.05	0.08
318.00	1.00	0.01	0.09	0.06
323.00	1.00	0.01	0.05	0.11
328.00	1.00	0.00	0.04	0.10

shift gradually downfield with temperature up to 55 °C. The drug is therefore still bound to DNA. We therefore conclude that binding in our complex is comparatively stronger. In general, the present studies indicate that even for intercalating drugs, there is no generalized trend that occurs. The binding of drug to DNA is in fact drug-specific as well as DNA-sequence specific.

5.2 Summary and Conclusions

Temperature dependence studies of the uncomplexed DNA hexamer showed that there is duplex to single strand transition. The ^{31}P resonance assignment was performed using $^1\text{H} - ^{31}\text{P}$ HMBC. On adding drug, new set of 5 peaks (bound phosphorus signals) appear which are in slow exchange with the corresponding free species. Titrations at various D/N ratio showed that there was systematic regular variation in signal strengths and line widths. ^{31}P - ^{31}P NOESY exchange clearly proves the fact that there are bound and free species in slow exchange on NMR time scale and yielded $\Delta\delta$ of the drug-DNA complex. The downfield shifts up to ~ 1.3 ppm in T1pG2 and C5pA6 phosphorus signals is attributed to change in the conformation of ζ torsional angle from g- to trans state so as to open the base pairs at these steps. The distortions in O-P-O phosphodiester bond angle also contribute to downfield shifts in intercalative and adjacent sites. The line width of free signals increases while that of bound phosphorus signals decreases with D/N ratio. This could be due to chemical shift dispersion in free phosphorus signals and well defined trans conformation of T1pG2^b signal and is not related to motional dynamics. Temperature dependence studies show that intercalating drug stabilizes the complex even at higher temperature. Comparing our results with literature shows that the binding of drug to DNA is drug-specific as well as DNA-sequence specific.

Studies on Adriamycin complexed with d-(TGATCA)₂ by Proton Nuclear Magnetic Resonance Spectroscopy and Restrained Molecular Dynamics Simulations

To understand the drug-DNA interactions, specific intermolecular contacts between drug and DNA molecules are to be extracted. For this, the solution structure of 2:1 adriamycin-d-(TGATCA)₂ complex has been determined using restrained molecular dynamics simulations. We report here the following studies on adriamycin-d-(TGATCA)₂ complex (Fig. 1a-b) by proton NMR followed by restrained molecular dynamics simulations.

- 1D ¹H NMR titration studies of adriamycin-d-(TGATCA)₂ complex at various drug (D)/DNA duplex (N) ratios of 0.1, 0.2, 0.3, 0.4, 0.5, 0.6, 0.7, 0.9, 1.0, 1.1, 1.2, 1.3, 1.4, 1.5, 1.6, 1.8 and 2.0 at 275 K in 90% water and 10% D₂O.
- 1D NMR study as a function of temperature in the range 275-328 K at D/N = 1.0, 1.5, 2.0.
- 2D NOESY at D/N = 1.0, 1.5, 2.0 using mixing time $\tau_m = 200, 300$ ms at 275 K in 90% H₂O and 10% D₂O.
- Life-time fluorescence measurement studies for 2:1 complex of adriamycin-d-(TGATCA)₂.
- Diffusion Ordered Spectroscopy (DOSY) experiments of 2:1 complex of adriamycin-d-(TGATCA)₂, uncomplexed d-(TGATCA)₂ and free adriamycin at 275 and 298 K.
- Restrained molecular dynamics studies on the solution structure for the complex of adriamycin with d-(TGATCA)₂ in drug to DNA duplex ratio of 2:1 using inter-proton distances obtained from 2D NOESY as restraints.
- Analysis of the converged structure in terms of time average of the various conformational and helical parameters as well as fluctuations and correlations among different structural parameters.

6.1 Results and Discussion

(A) NMR studies on complex of adriamycin-d-(TGATCA)₂

The proton NMR spectra of the complex of adriamycin-d-(TGATCA)₂ at various drug (D)/DNA duplex (N) ratios, D/N = 0.1, 0.2, 0.3, 0.4, 0.5, 0.6, 0.7, 0.9, 1.0, 1.1, 1.2, 1.3, 1.4, 1.5, 1.6, 1.8, 2.0 at 275 K are shown in Fig. 2(a-d). This temperature is chosen as imino protons signals are sharpened and intensified at this temperature. Besides, DNA is expected to be present completely in duplex state at 275 K. There is one set of major conformer of the drug bound to DNA. Spectral assignments (Table 1 and 2) are done on the basis of 2D NMR based conformational analysis of uncomplexed d-(TGATCA)₂ (Barthwal et al., 2004) using standard strategies adopted for B-DNA structure and uncomplexed drug (Barthwal et al., 1994; Barthwal et al., 1996). The observation of the shifts on cumulative addition of drug to DNA and the plot of area helped to resolve the overlapping resonance peaks. On addition of adriamycin to d-(TGATCA)₂, new drug proton signals are seen which increase in intensity with D/N ratio. This is evident from the resonance signals of 1H, 7H, 5'CH₃, 2H and 3H protons in Fig. 2a-d. The initially sharp NMR spectral lines of free DNA duplex broaden significantly without the appearance of a new set of NMR resonances for the bound complex. The line widths of all drug and nucleotide protons are relatively large and similar. Both the nucleotide and drug protons, each having one set of resonances, shift gradually from their position in uncomplexed state with D/N ratio (Table 3 and 4, Fig. 3a-d and 4). The spectra of the complex of adriamycin-d-(TGATCA)₂ as a function of temperatures are obtained at D/N = 1.0, 1.5, 2.0 at the range 275 - 328 K Fig. 5(a-i). The variation in chemical shift with temperature is shown in Fig. 6a-c and 7 (Table 5a-c and 6).

In uncomplexed or free d-(TGATCA)₂, T4NH and G2NH peaks appear at 13.69 and 12.86 ppm, respectively while the T1NH resonance is not seen presumably due to exchange with water

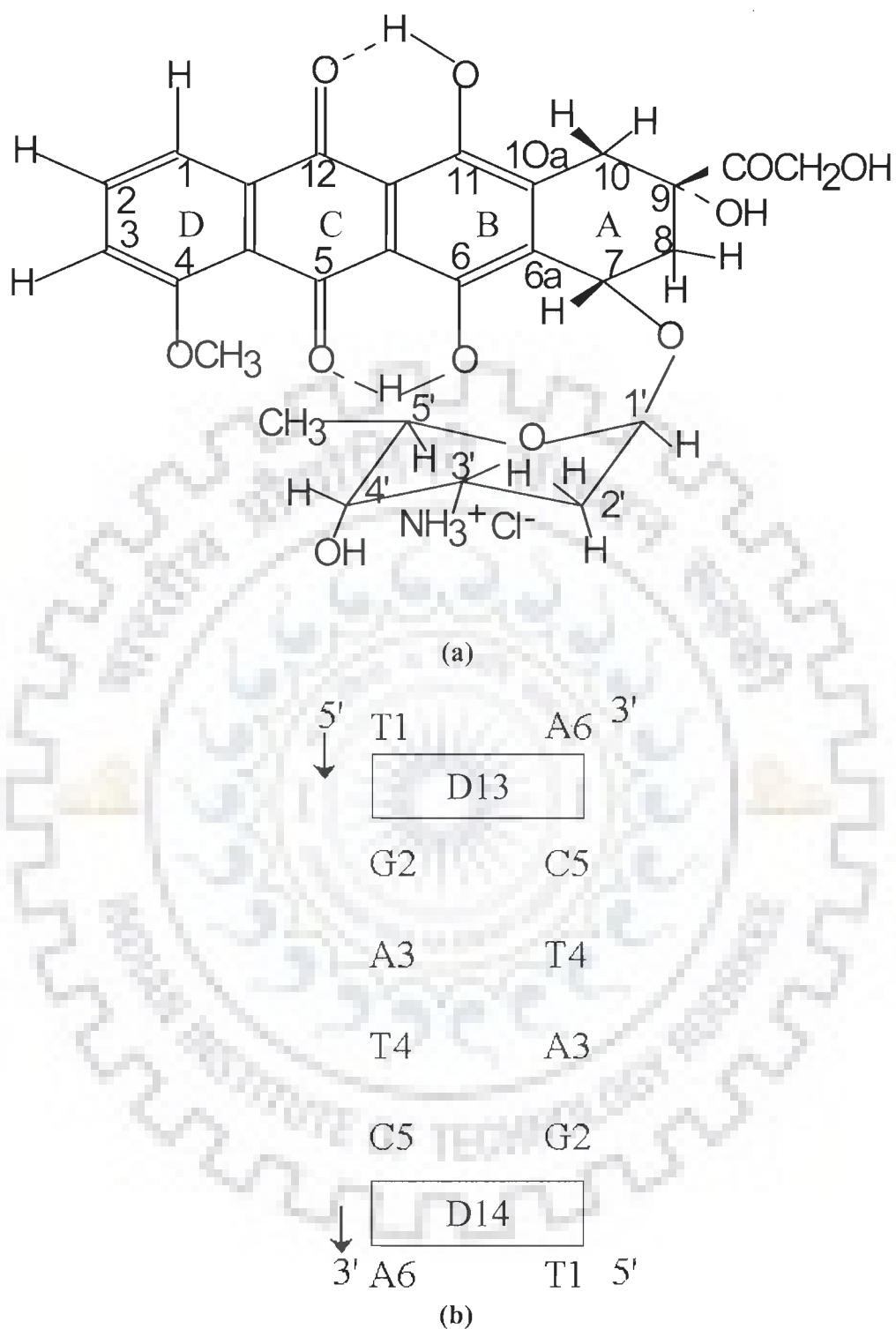


Fig. 1: (a) Molecular structure of adriamycin (b) Schematic representation of the 2:1 adriamycin-d-(TGATCA)₂ complex.

Table 1: Chemical shift (ppm) of nucleic acid protons in uncomplexed state (δ^f) and that bound to drug (δ^b) at drug (D) to nucleic acid duplex (N) ratio D/N = 2.0 at 275 K. Also shown here is the change in chemical shift on binding, that is. $\Delta\delta = \delta^b_{(D/N=2.0)} - \delta^f$ and $^{\#}\Delta\delta = ^{\#}\delta^b - ^{\#}\delta^f$

Proton	T1			G2			A3			T4			C5			A6		
	δ^b	δ^f	$\Delta\delta$	δ^b	δ^f	$\Delta\delta$	δ^b	δ^f	$\Delta\delta$	δ^b	δ^f	$\Delta\delta$	δ^b	δ^f	$\Delta\delta$	δ^b	δ^f	$\Delta\delta$
H8/H6	7.36	7.39	-0.03	8.03	8.04	-0.01	8.32	8.34	-0.02	7.22	7.23	-0.01	7.49	7.50	-0.01	8.23	8.26	-0.03
H1'	5.74	5.80	-0.06	5.54	5.56	-0.02	6.32	6.34	-0.02	5.98	5.99	-0.01	5.70	5.77	-0.07	6.29	6.30	-0.01
H2'	1.83	1.84	-0.01	2.74	2.80	-0.06	2.73	2.79	-0.06	2.06	2.04	+0.02	2.02	2.08	-0.06	2.79	2.78	+0.01
H2''	2.24	2.28	-0.04	2.92	2.88	+0.04	2.99	3.00	-0.01	2.34	2.42	-0.08	2.32	2.33	-0.01	2.45	2.50	-0.05
H3'	4.65	4.67	-0.02	5.02	5.09	-0.07	5.07	5.11	-0.04	4.84	4.87	-0.03	4.81	4.82	-0.01	4.72	4.76	-0.04
H4'	4.08	4.06	+0.02	4.28	4.36	-0.08	4.52	4.55	-0.03	4.20	4.14	+0.06	4.02	4.04	-0.02	4.22	4.16	+0.06
H5'	3.68	3.69	-0.01	4.13	4.04	+0.09	4.32	4.35	-0.03	4.13	4.04	+0.09	4.06	4.09	-0.03	4.17	4.19	-0.02
H5''	3.65	3.63	+0.02	4.02	3.94	+0.08	4.10	4.21	-0.11	4.02	4.07	-0.05	3.85	3.95	-0.10	3.94	4.06	-0.12
H5/H2	*	*	*	*	*	*	7.96	7.92	+0.04	*	*	*	5.65	5.74	-0.09	7.99	7.95	+0.04
NH ₂ ^b	*	*	*	7.71	7.70	+0.01	7.63	7.65	-0.02	*	*	*	8.38	8.49	-0.11	7.78	7.75	+0.03
NH ₂ ^{nb}	*	*	*	5.86	5.87	-0.01	6.09	6.23	-0.14	*	*	*	7.15	7.13	+0.02	6.25	6.34	-0.09
	[#] δ^b	[#] δ^f	[#] $\Delta\delta$	[#] δ^b	[#] δ^f	[#] $\Delta\delta$				[#] δ^b	[#] δ^f	[#] $\Delta\delta$						
NH	11.96	12.12	-0.16	12.66	12.86	-0.20	*	*	*	13.75	13.69	0.06	*	*	*	*	*	*
CH ₃	1.58	1.65	-0.07	*	*	*	*	*	*	1.33	1.44	-0.11	*	*	*	*	*	*

-ve $\Delta\delta$ indicates upfield shift
+ve $\Delta\delta$ indicates downfield shift.

Table 2: Chemical shift (ppm) of drug protons in uncomplexed monomer a state (δ^{monomer} concentration 0.01 mM, 298 K), free (δ^f) and that bound (δ^b) to nucleic acid duplex at drug (D) to DNA (N) ratio, D/N =2.0 at 275 K. Also shown here is the change in chemical shift, due to binding, that is, $\Delta\delta = \delta^b_{(D/N=2)} - \delta^f$ and $\Delta\delta' = \delta^b_{(D/N=2)} - \delta^{\text{monomer}}$

Protons	$\delta^b_{(D/N=2)}$	δ^f	$\Delta\delta = \delta^b_{(D/N=2)} - \delta^f$	δ^{monomer}	$\Delta\delta' = \delta^b_{(D/N=2)} - \delta^{\text{monomer}}$
1H	7.61	7.46	+0.15	7.86	-0.25
2H	7.78	7.69	+0.09	7.87	-0.09
3H	7.42	7.44	-0.02	7.58	-0.16
7H	4.63	4.79	-0.16	4.69	-0.06
1'H	5.61	5.52	+0.09	5.54	+0.07
3'H	3.94	3.75	+0.19	3.58	+0.36
4'H	4.15	3.86	+0.29	3.76	+0.39
5'H	4.23	4.29	-0.06	4.26	-0.03
5'CH ₃	1.23	1.32	-0.09	1.25	-0.02
4OCH ₃	3.98	3.93	+0.05	4.02	-0.04
9COCH ₂	4.49	4.85	-0.36	4.77	-0.28
14OH	-	5.91	-	-	-
6 OH	13.25	13.31	-0.06	-	-
11OH	12.34	12.70	-0.36	-	-
9OH	5.30	6.48	-1.18	-	-
4'OH	4.79	4.61	+0.18	-	-
8 _{eq} H	2.22	2.25	-0.03	2.28	-0.06
8 _{ax} H	1.83	2.08	-0.25	2.16	-0.33
2' _{ax} H	1.68	2.00	-0.32	1.88	-0.20
2' _{eq} H	1.83	2.00	-0.17	1.88	-0.05
10 _{eq} H	3.00	2.98	+0.02	3.16	-0.16
10 _{ax} H	2.79	2.62	+0.17	2.90	-0.11
3NH ₃ ⁺	8.97	8.45	+0.52	-	-

-ve $\Delta\delta$ indicates upfield shift
+ve $\Delta\delta$ indicates downfield shift.

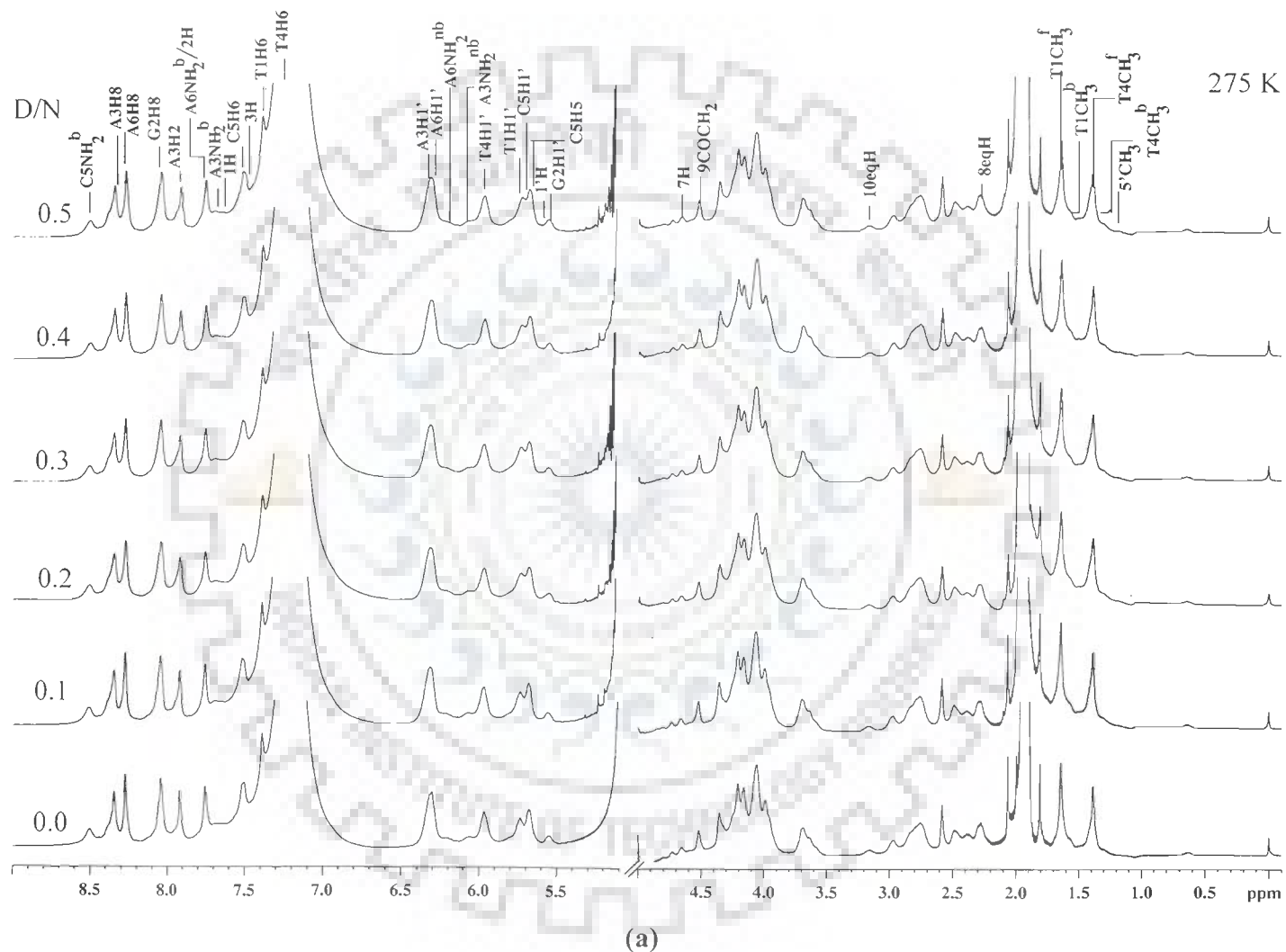
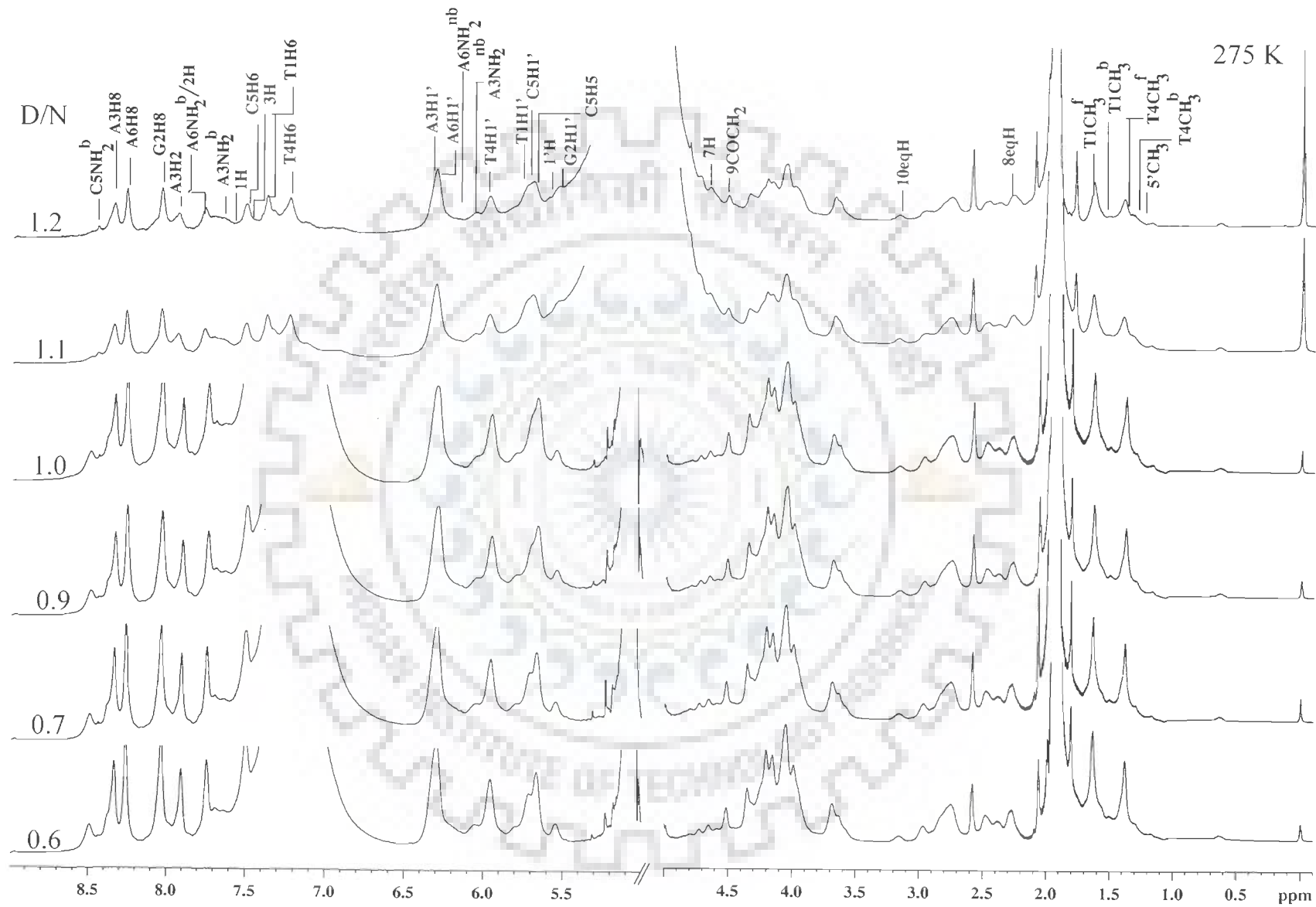
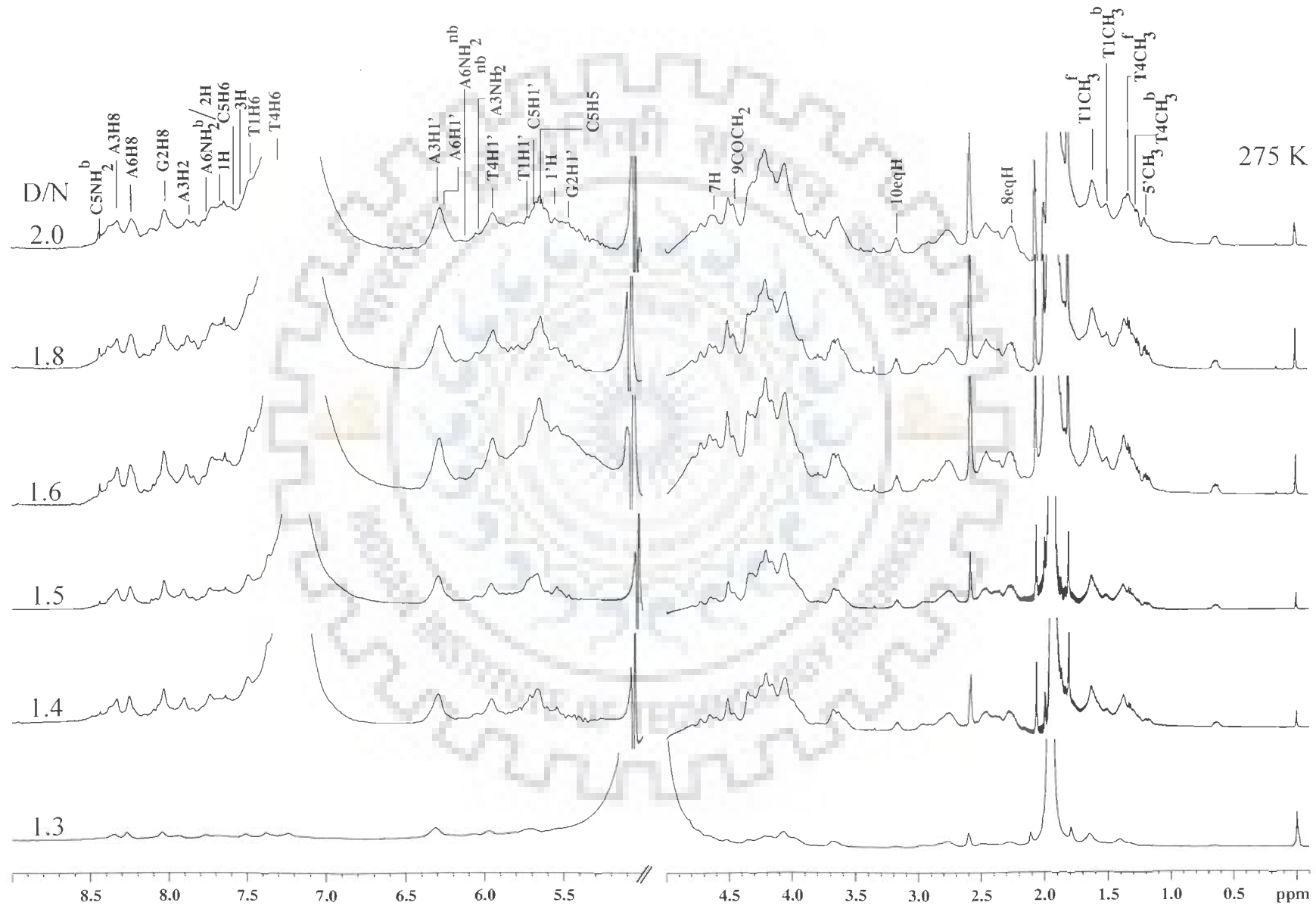


Fig. 2a-d: Proton NMR spectrum of adriamycin-d(TGATCA)₂ complex as a function of added drug (D) to DNA (N) duplex stoichiometric ratios (D/N) of 0.0, 0.1, 0.2, 0.3, 0.4, 0.5, 0.6, 0.7, 0.9, 1.0, 1.1, 1.2, 1.3, 1.4, 1.5, 1.6, 1.8, 2.0 at 275 K in H₂O/D₂O.



(b)



(c)

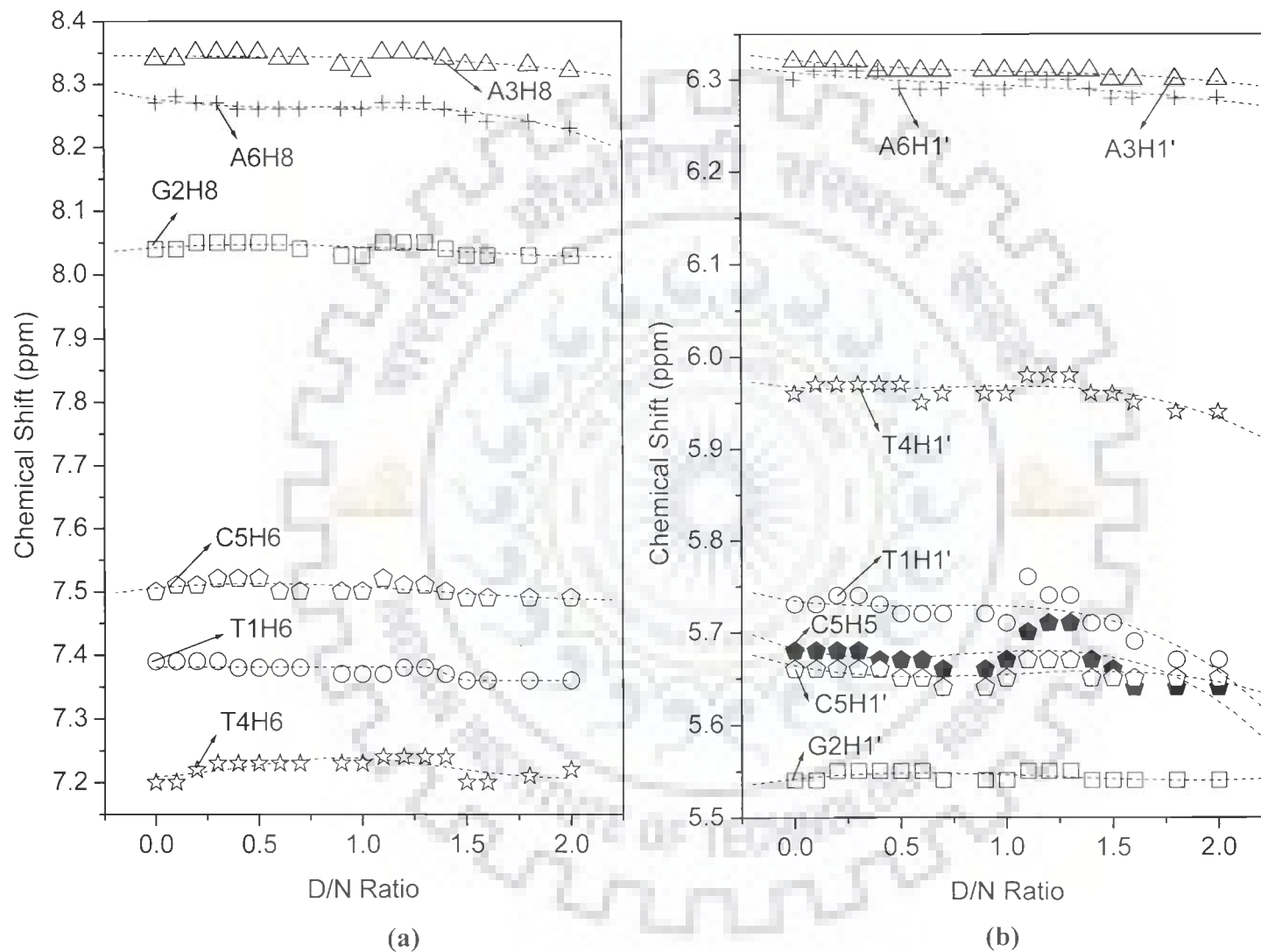
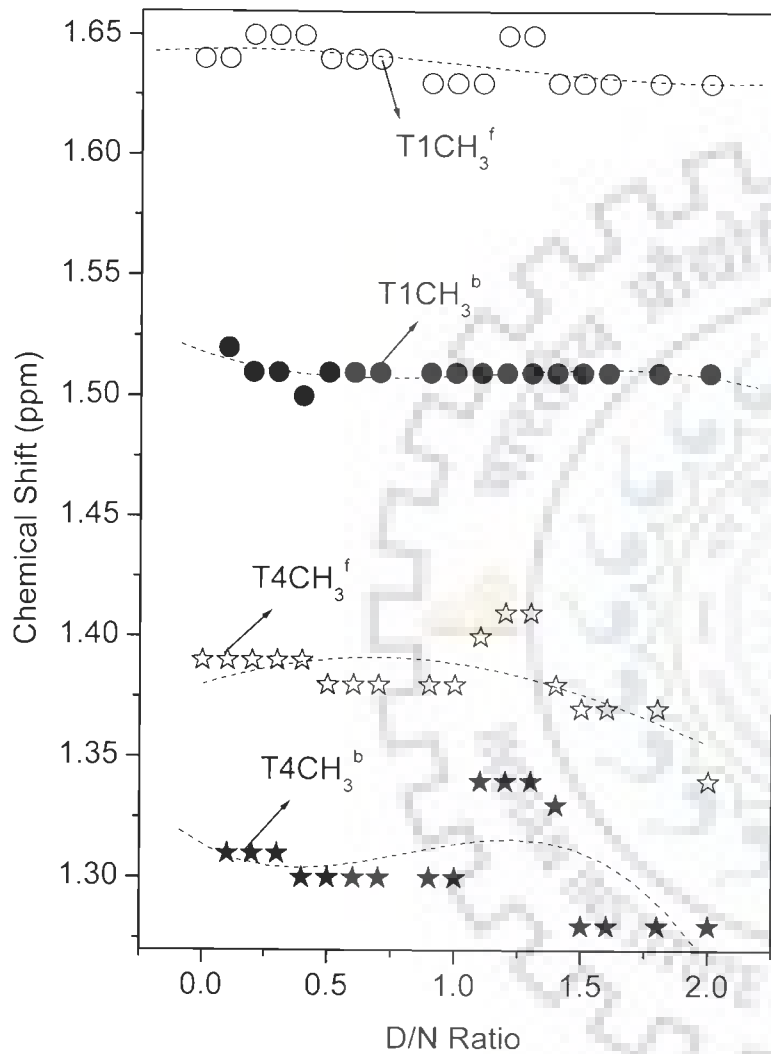
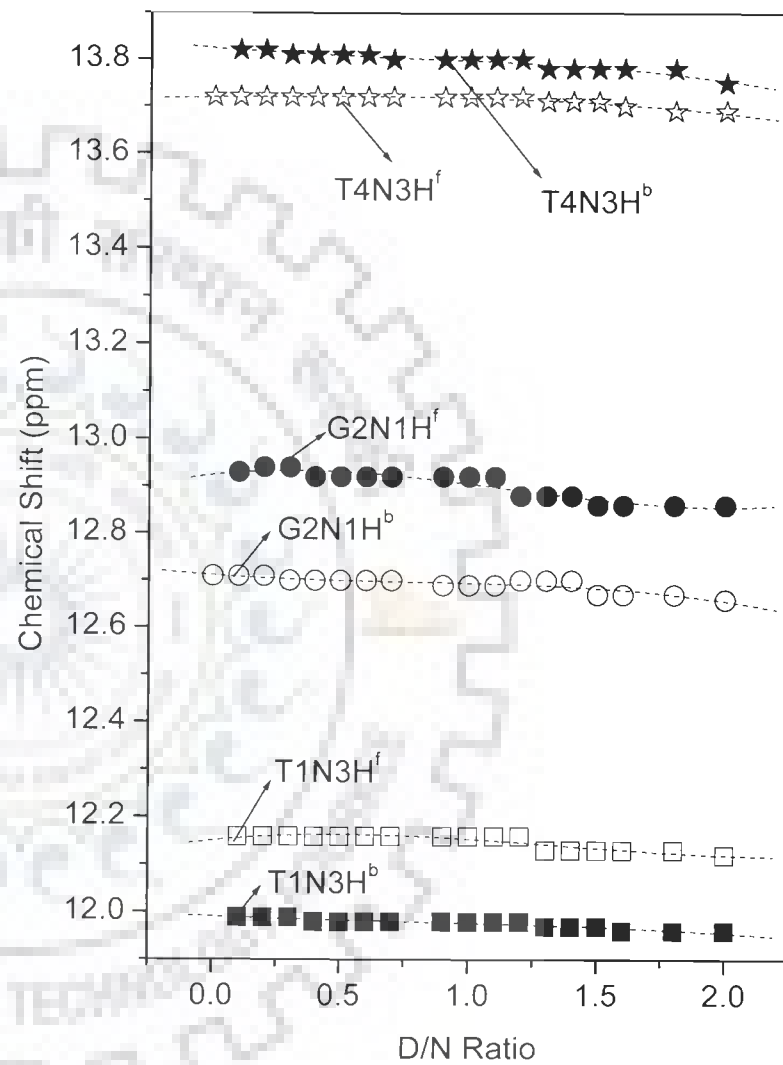


Fig. 3a-d: Chemical Shift of various protons of $d(TGATCA)_2$ in adriamycin- $d(TGATCA)_2$ complex as a function of various drug to DNA ratios (D/N).



(c)



(d)

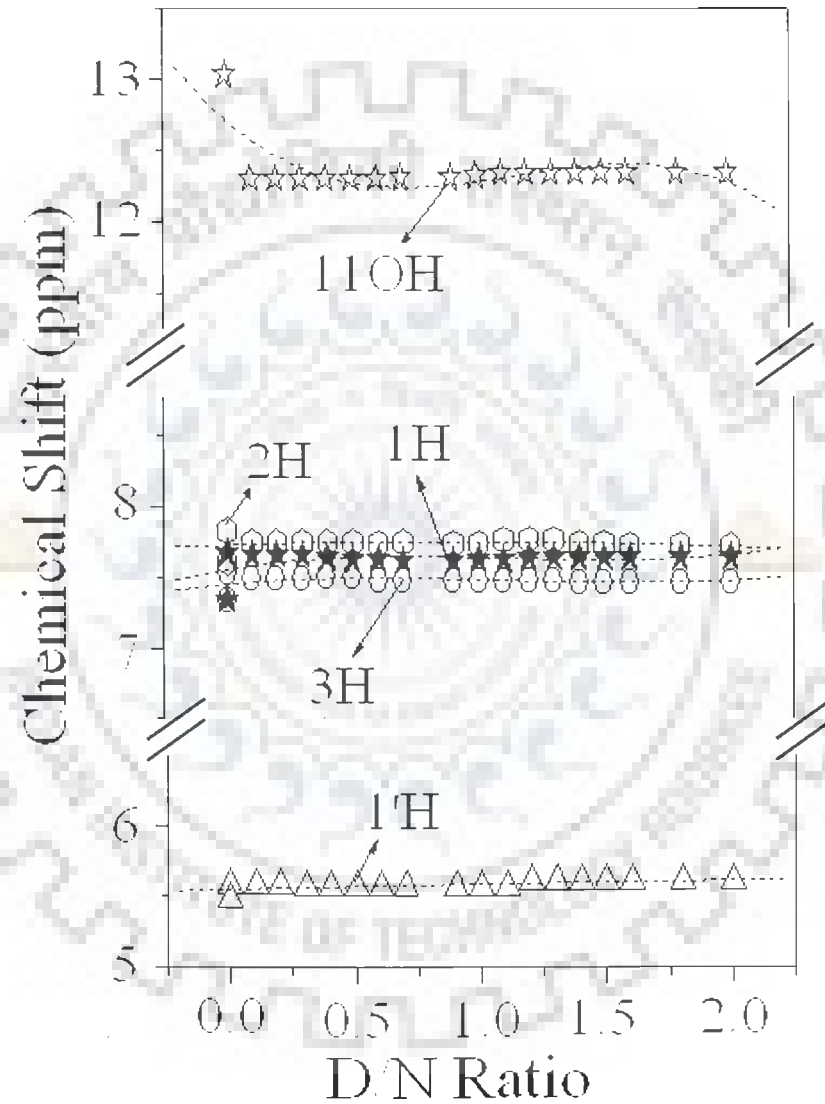


Fig. 4: Chemical Shift of various protons of adriamycin in adriamycin-d-(TGATCA)₂ complex as a function of various drug to DNA ratios (D/N).

Table 3: Chemical shift (ppm) of nucleotide protons as a function of drug (D) to nucleic acid duplex (N) ratio, D/N, at 275 K. Also shown here is the change in chemical shift on binding, that is, $\Delta\delta = \delta_{(D/N=2.0)} - \delta_{(D/N=0.0)}$ equivalent to $\delta_{\text{Total}} = \delta_{(D/N=2.0)}^b - \delta^f$.

D/N Ratios	T1H1'	G2H1'	A3H1'	T4H1'	C5H1'	A6H1'	T1CH ₃ ^f	T1CH ₃ ^b	T4CH ₃ ^f	T4CH ₃ ^b
0.0	5.73	5.54	6.32	5.96	5.68	6.30	1.64	-	1.39	-
0.1	5.73	5.54	6.32	5.97	5.68	6.31	1.64	1.52	1.39	1.31
0.2	5.74	5.55	6.32	5.97	5.68	6.31	1.65	1.51	1.39	1.31
0.3	5.74	5.55	6.32	5.97	5.68	6.31	1.65	1.51	1.39	1.31
0.4	5.73	5.55	6.31	5.97	5.67	6.31	1.65	1.50	1.39	1.30
0.5	5.72	5.55	6.31	5.97	5.67	6.29	1.64	1.51	1.38	1.30
0.6	5.72	5.55	6.31	5.95	5.67	6.29	1.64	1.51	1.38	1.30
0.7	5.72	5.54	6.31	5.96	5.66	6.29	1.64	1.51	1.38	1.30
0.9	5.72	5.54	6.31	5.96	5.66	6.29	1.63	1.51	1.38	1.30
1.0	5.71	5.54	6.31	5.96	5.67	6.29	1.63	1.51	1.38	1.30
1.1	5.76	5.55	6.31	5.98	5.70	6.30	1.63	1.51	1.40	1.34
1.2	5.74	5.55	6.31	5.98	5.71	6.30	1.65	1.51	1.41	1.34
1.3	5.74	5.55	6.31	5.98	5.71	6.30	1.65	1.51	1.41	1.34
1.4	5.71	5.54	6.31	5.96	5.67	6.29	1.63	1.51	1.38	1.33
1.5	5.71	5.54	6.30	5.96	5.66	6.28	1.63	1.51	1.37	1.28
1.6	5.69	5.54	6.30	5.95	5.64	6.28	1.63	1.51	1.37	1.28
1.8	5.67	5.54	6.30	5.94	5.64	6.28	1.63	1.51	1.37	1.28
2.0	5.67	5.54	6.30	5.94	5.64	6.28	1.63	1.51	1.34	1.28
$\Delta\delta$	-0.06	0.0	-0.02	-0.02	-0.04	-0.02	-	-	-	-

-ve $\Delta\delta$ indicates upfield shift
+ve $\Delta\delta$ indicates downfield shift.

(contd.)

Table 3 (contd.)

D/N Ratios	T1H6	G2H8	A3H8	T4H6	C5H6	A6H8	C5H5	T1NH ^b	T1NH ^f	G2NH ^b	G2NH ^f	T4NH ^b	T4NH ^f
0.0	7.39	8.04	8.34	7.20	7.50	8.27	5.66	-	-		12.71	-	13.72
0.1	7.39	8.04	8.34	7.20	7.51	8.28	5.66	11.99	12.16	12.71	12.93	13.82	13.72
0.2	7.39	8.05	8.35	7.22	7.51	8.27	5.66	11.99	12.16	12.71	12.94	13.82	13.72
0.3	7.39	8.05	8.35	7.23	7.52	8.27	5.66	11.99	12.16	12.70	12.94	13.81	13.72
0.4	7.38	8.05	8.35	7.23	7.52	8.26	5.66	11.98	12.16	12.70	12.92	13.81	13.72
0.5	7.38	8.05	8.35	7.23	7.52	8.26	5.65	11.98	12.16	12.70	12.92	13.81	13.72
0.6	7.38	8.05	8.34	7.23	7.50	8.26	5.65	11.98	12.16	12.70	12.92	13.81	13.72
0.7	7.38	8.04	8.34	7.23	7.50	8.26	5.64	11.98	12.16	12.70	12.92	13.80	13.72
0.9	7.37	8.03	8.33	7.23	7.50	8.26	5.64	11.98	12.16	12.69	12.92	13.80	13.72
1.0	7.37	8.03	8.32	7.23	7.50	8.26	5.65	11.98	12.16	12.69	12.92	13.80	13.72
1.1	7.37	8.05	8.35	7.24	7.52	8.27	5.67	11.98	12.16	12.69	12.92	13.80	13.72
1.2	7.38	8.05	8.35	7.24	7.51	8.27	5.67	11.98	12.16	12.70	12.88	13.80	13.72
1.3	7.38	8.05	8.35	7.24	7.51	8.27	5.67	11.97	12.13	12.70	12.88	13.78	13.71
1.4	7.37	8.04	8.34	7.24	7.50	8.26	5.65	11.97	12.13	12.70	12.88	13.78	13.71
1.5	7.36	8.03	8.33	7.20	7.49	8.25	5.65	11.97	12.13	12.67	12.86	13.78	13.71
1.6	7.36	8.03	8.33	7.20	7.49	8.24	5.65	11.96	12.13	12.67	12.86	13.78	13.70
1.8	7.36	8.03	8.33	7.21	7.49	8.24	5.65	11.96	12.13	12.67	12.86	13.78	13.69
2.0	7.36	8.03	8.32	7.22	7.49	8.23	5.65	11.96	12.12	12.66	12.86	13.75	13.69
$\Delta\delta$	-0.03	-0.01	-0.02	+0.02	-0.01	-0.04	-0.01	-	-	-	-	-	-

-ve $\Delta\delta$ indicates upfield shift
+ve $\Delta\delta$ indicates downfield shift.

Table 4: Chemical shift (ppm) of drug protons as a function of drug (D) to nucleic acid duplex (N) ratio, D/N, at 275 K. Also shown here is the maximum change in chemical shift due to binding, with respect to drug in free self associated form, δ^f , (20.49 mM, 275 K) as well as the drug in monomeric form, δ^{monomer} (0.01 mM, 298 K) δ^b of the bound form for D/N = 2.0.

D/N Ratios	3H	2H	1H	1'H	11OH
δ^{monomer}	7.58	7.87	7.86	5.54	-
δ^f	7.44	7.69	7.46	5.52	12.70
0.1	7.49	7.75	7.66	5.58	12.30
0.2	7.49	7.75	7.66	5.58	12.30
0.3	7.49	7.75	7.66	5.57	12.30
0.4	7.50	7.75	7.64	5.57	12.30
0.5	7.50	7.75	7.63	5.57	12.30
0.6	7.48	7.74	7.63	5.57	12.30
0.7	7.48	7.75	7.62	5.57	12.31
0.9	7.48	7.74	7.62	5.57	12.31
1.0	7.48	7.74	7.63	5.57	12.32
1.1	7.48	7.77	7.63	5.57	12.34
1.2	7.48	7.77	7.63	5.61	12.34
1.3	7.48	7.77	7.63	5.61	12.34
1.4	7.47	7.77	7.63	5.61	12.34
1.5	7.47	7.78	7.63	5.61	12.34
1.6	7.47	7.78	7.61	5.61	12.34
1.8	7.47	7.78	7.61	5.61	12.34
2.0	7.42	7.78	7.61	5.61	12.34
$\Delta\delta = \delta^b - \delta^{\text{monomer}}$	-0.16	-0.09	-0.25	+0.07	-
$\Delta\delta' = \delta^b - \delta^f$	-0.02	+0.09	+0.15	+0.09	-0.36

-ve $\Delta\delta$ indicates upfield shift
+ve $\Delta\delta$ indicates downfield shift.

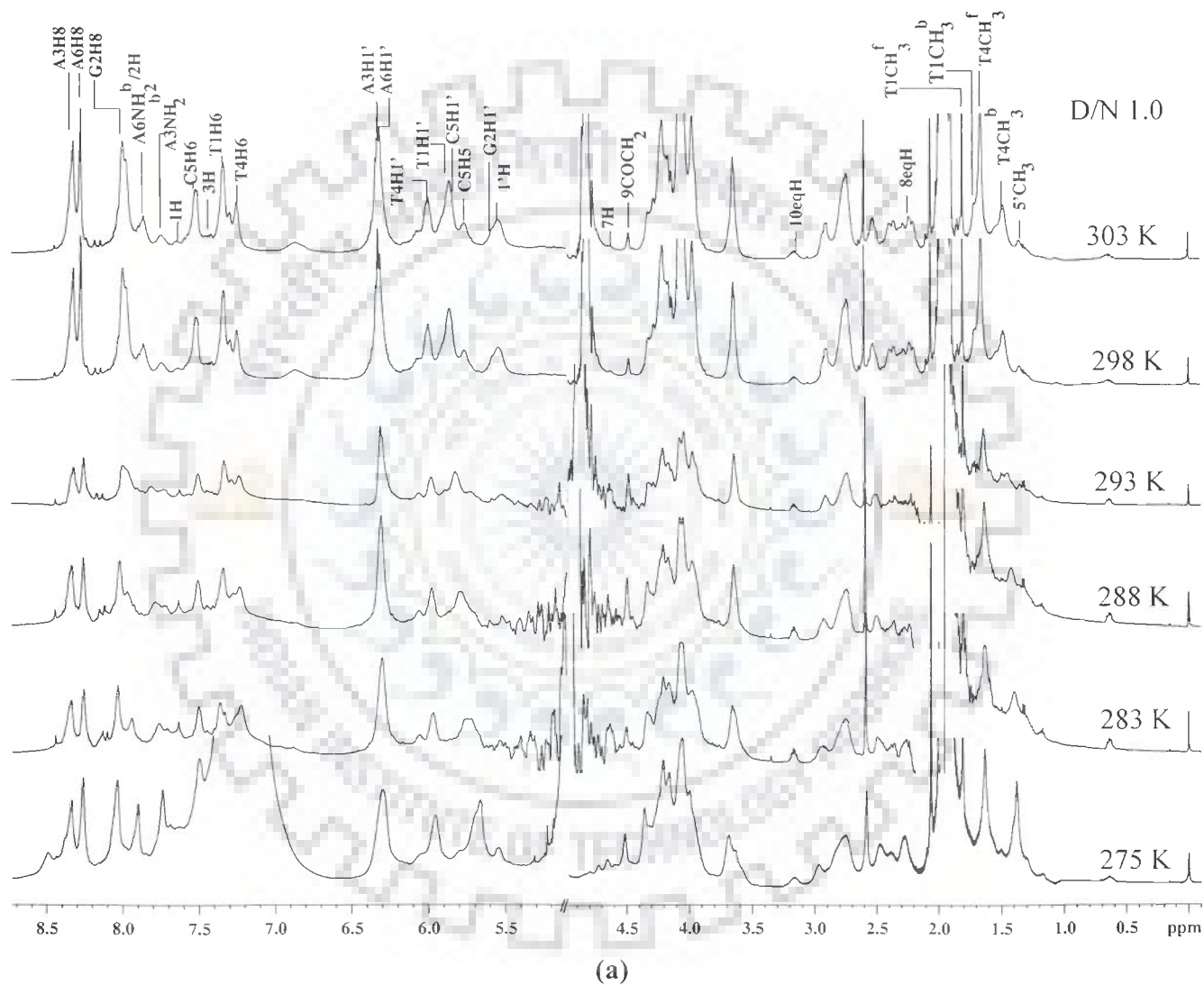
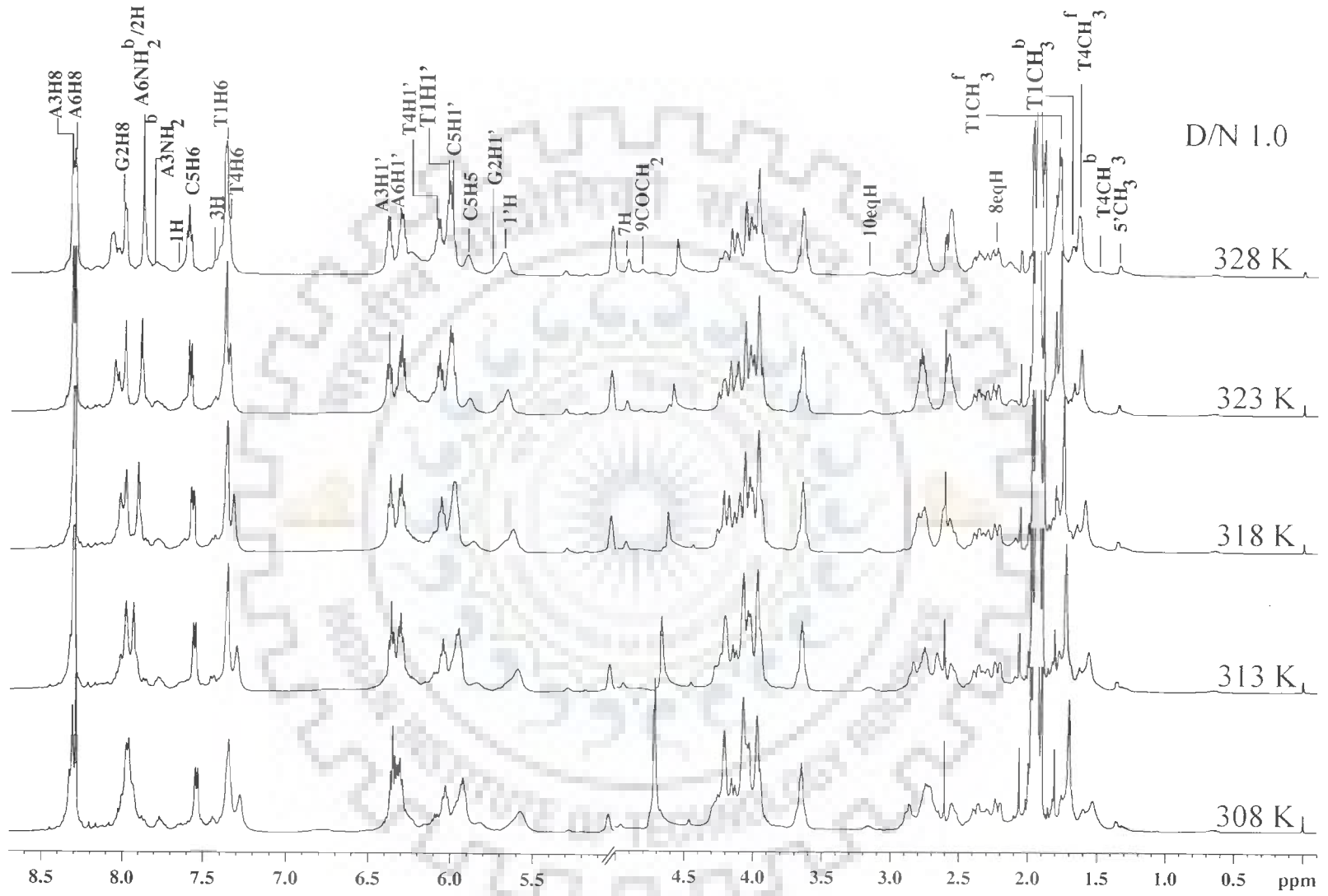


Fig. 5a-i: Proton NMR spectrum of adriamycin-d (TGATCA)₂ complex as a function of temperature (275 - 328 K) at drug (D) to DNA (N) duplex ratios (D/N) of 1.0, 1.5, 2.0 in H₂O/D₂O.



(b)

D/N 1.0

328 K

323 K

318 K

313 K

308 K

303 K

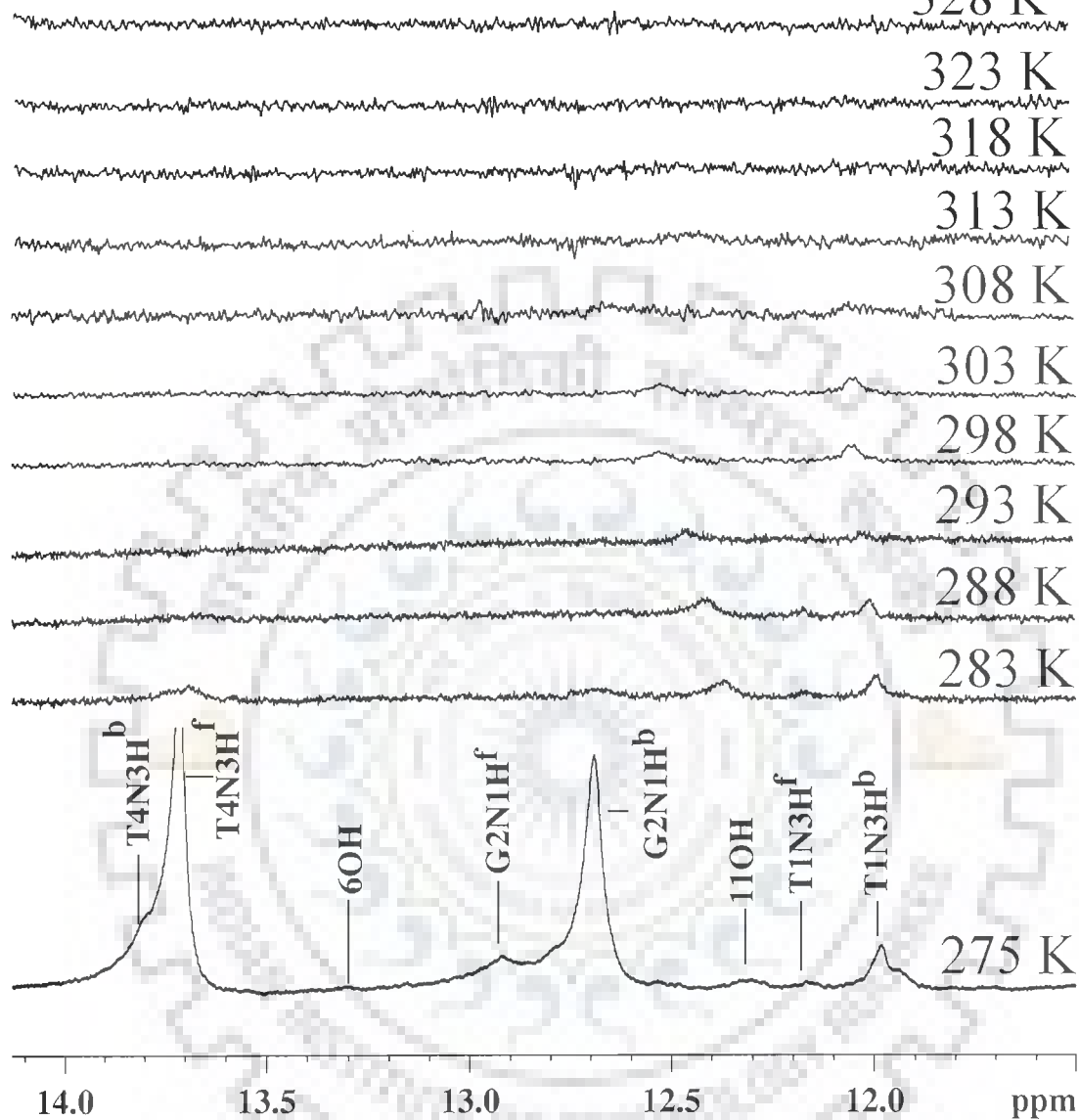
298 K

293 K

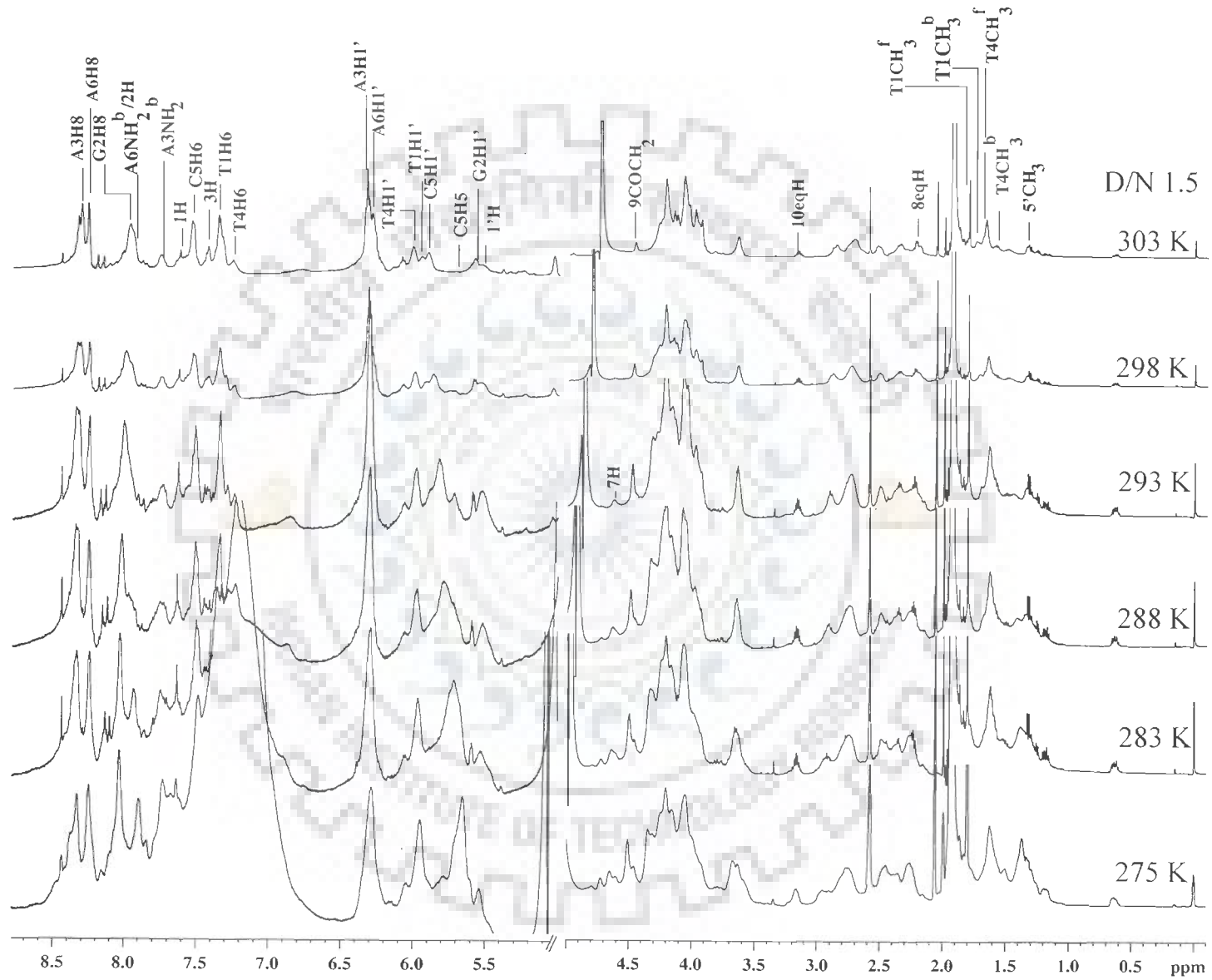
288 K

283 K

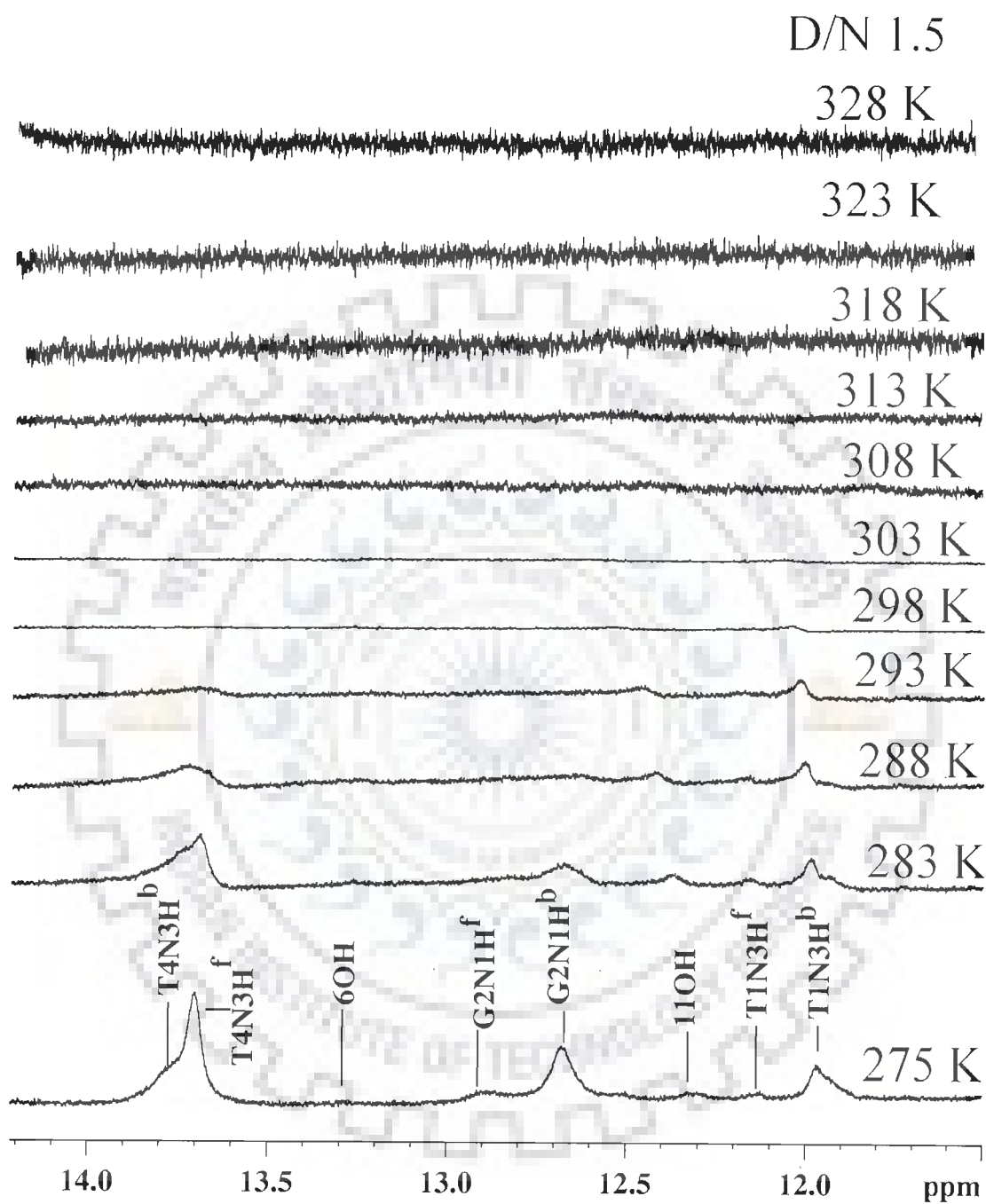
275 K



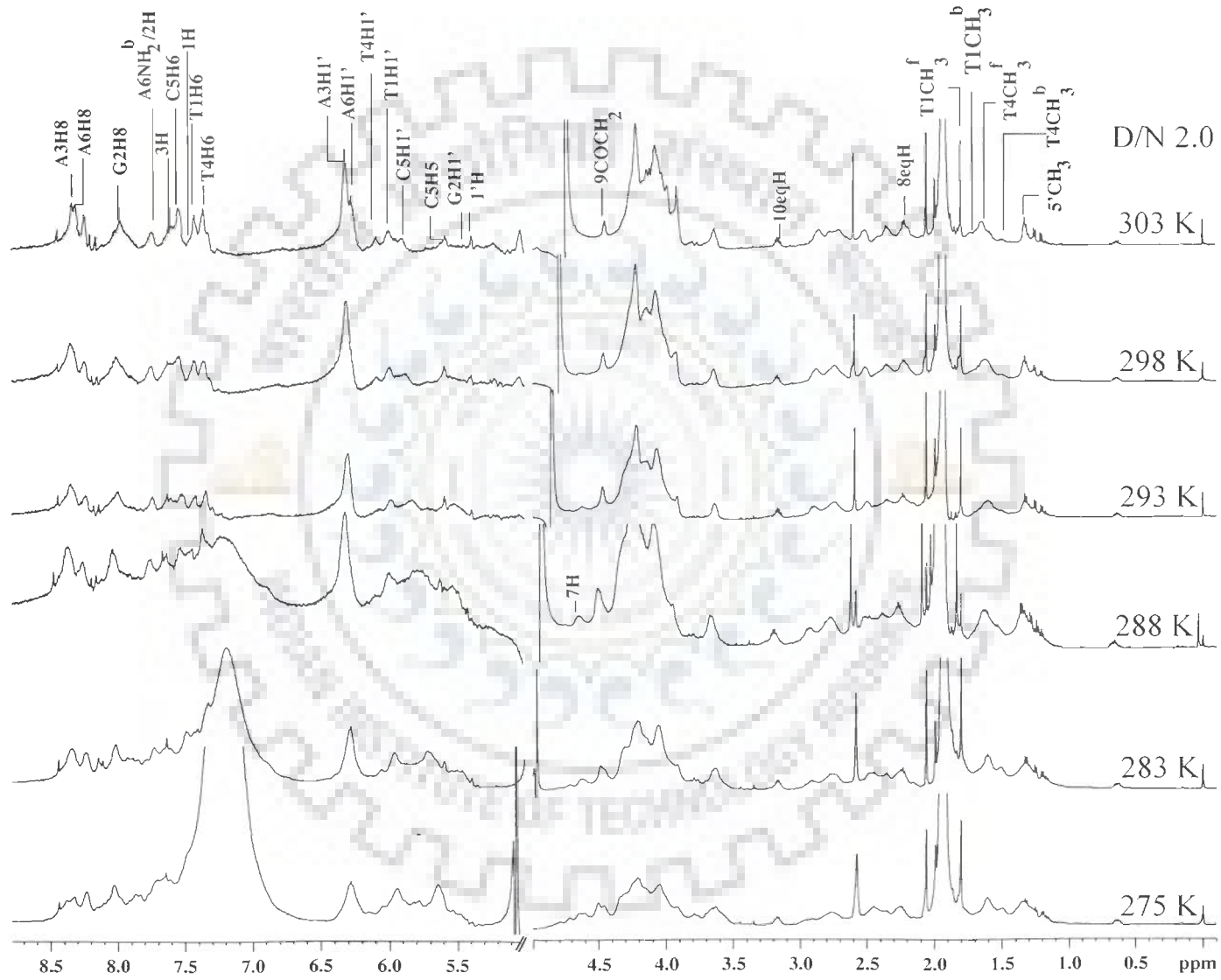
(c)



(d)



(f)



(g)

D/N 2.0

328 K

323 K

318 K

313 K

308 K

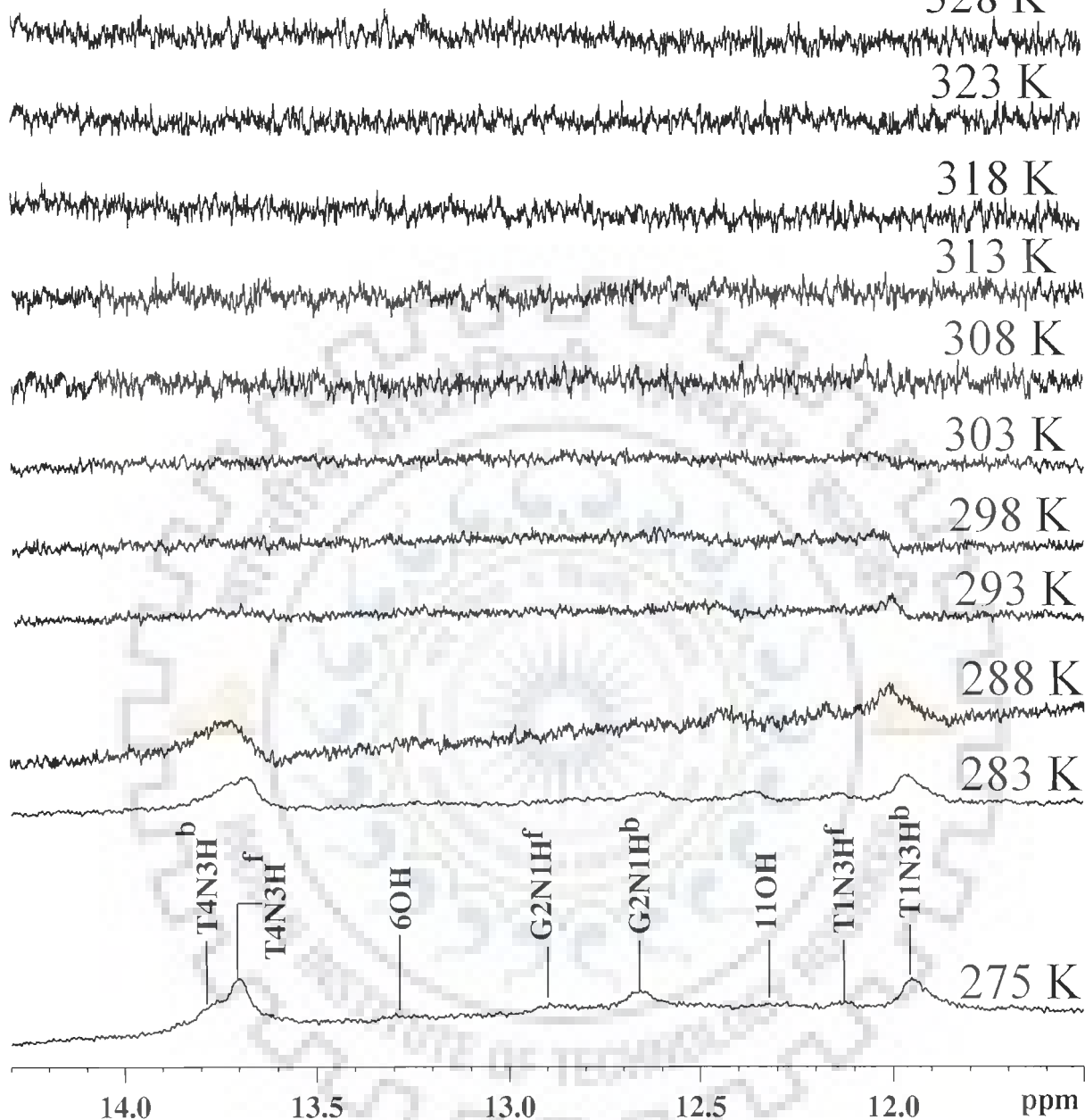
303 K

298 K

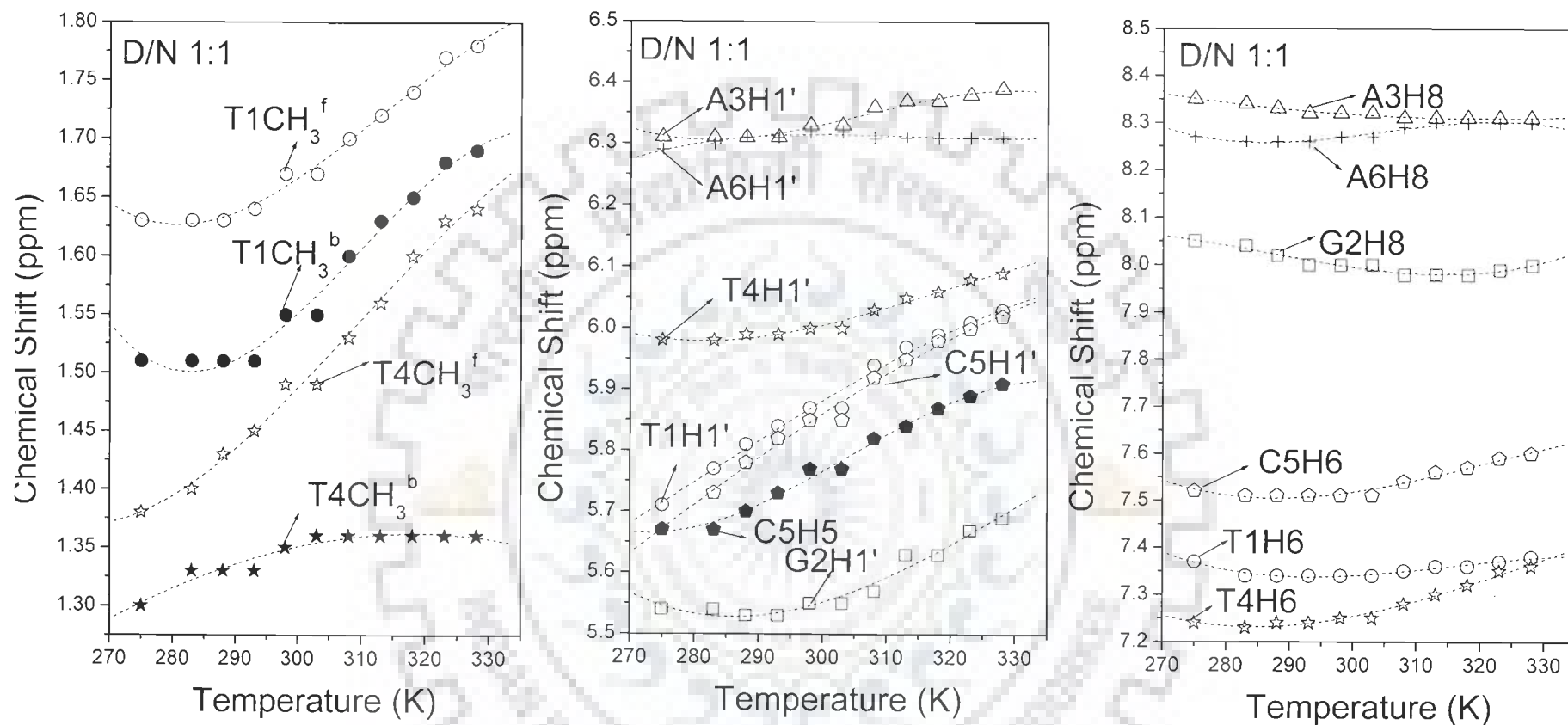
293 K

288 K

283 K

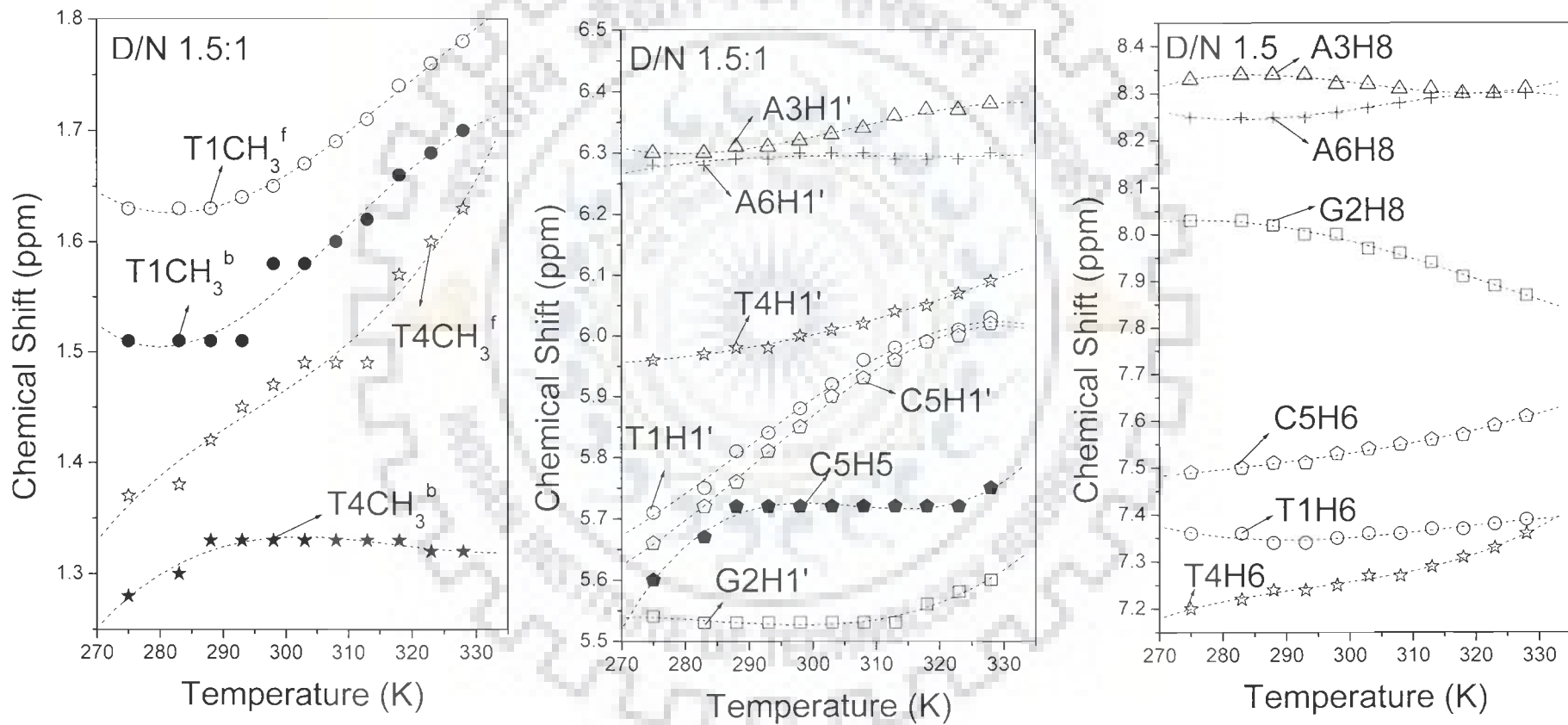


(i)

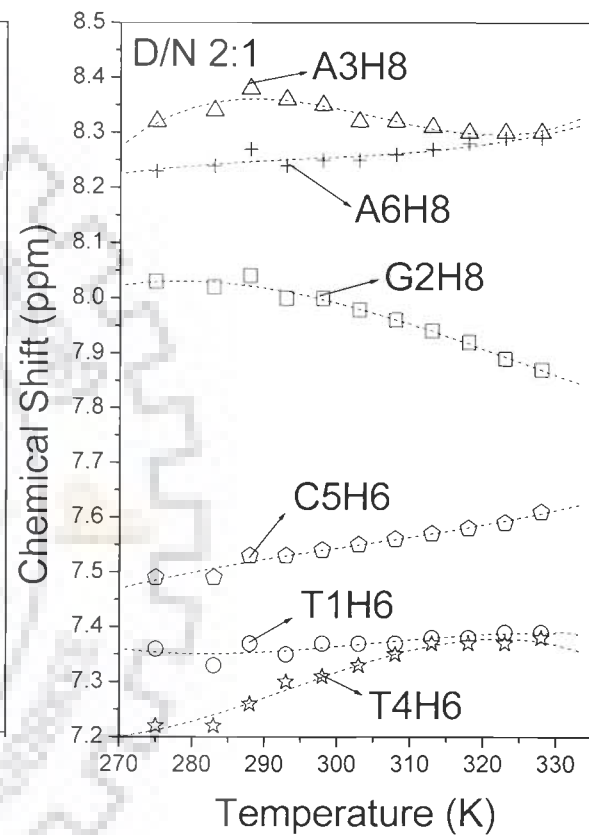
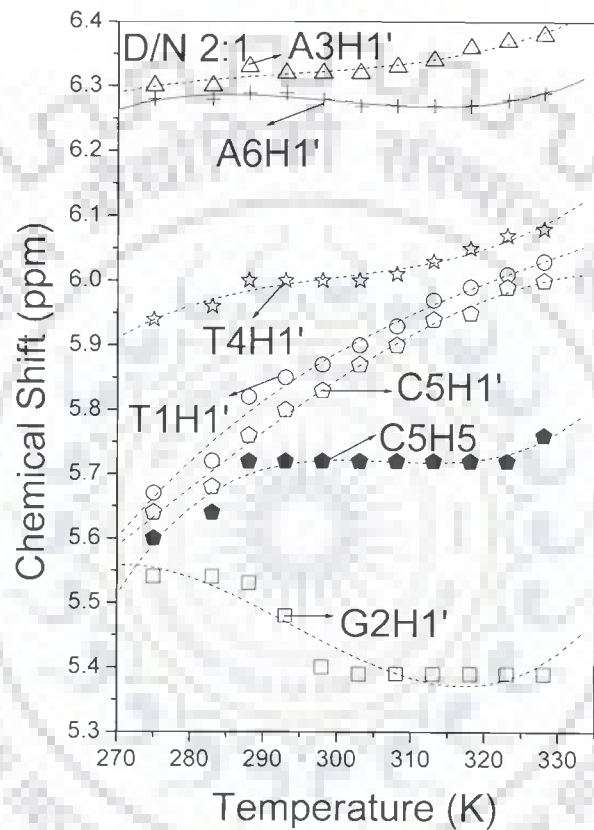
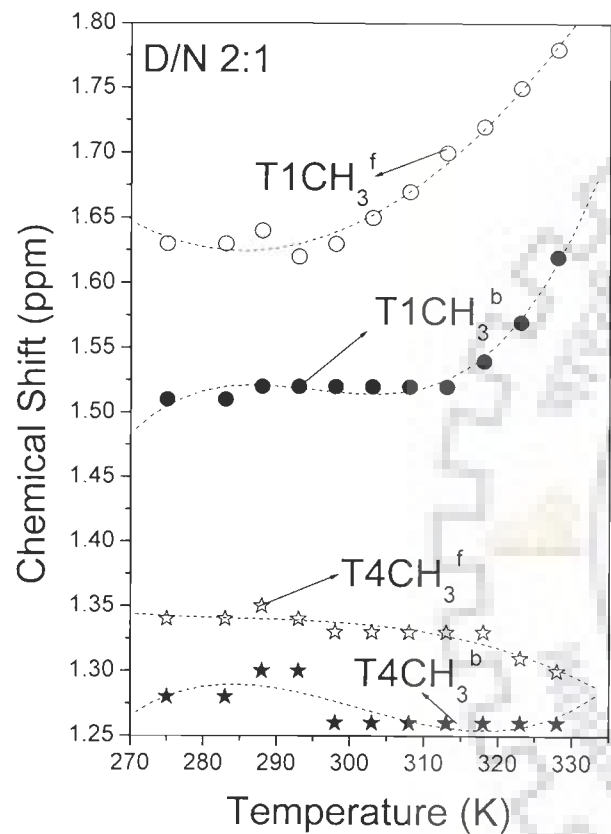


(a)

Fig. 6a-c: Chemical Shift of various protons of d-(TGATCA)₂ in adriamycin-d(TGATCA)₂ complex as a function of temperature (275 - 328 K) at drug (D) to DNA (N) duplex ratios (D/N) of 1.0, 1.5, 2.0 in H₂O/D₂O.



(b)



(c)

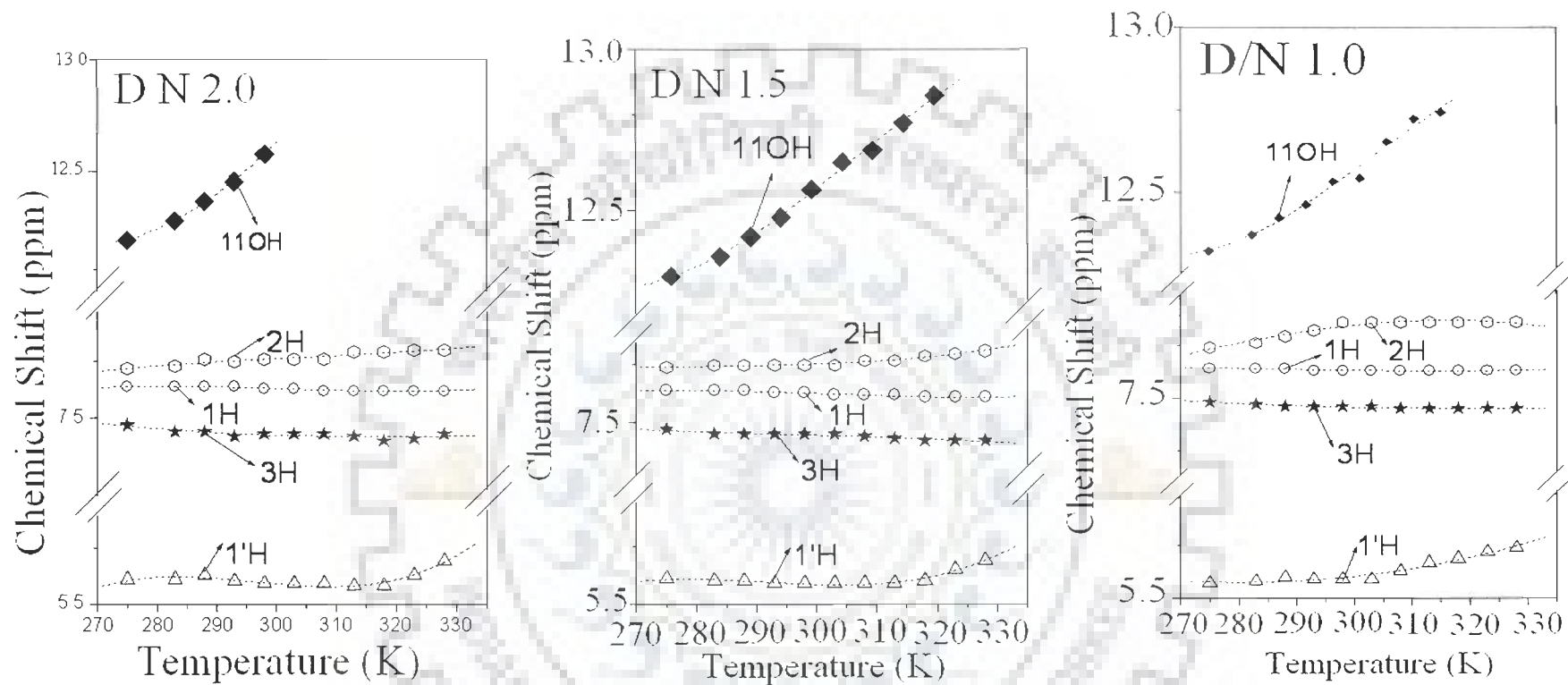


Fig. 7: Chemical Shift of various drug protons in adriamycin-d-(TGATCA)₂ complex as a function of temperature (275 - 328 K) at drug (D) to DNA (N) duplex ratios (D/N) of 1.0, 1.5, 2.0 in H₂O/D₂O.

Table 5a: Chemical shift (ppm) of nucleic acid protons in drug – DNA complex having D/N = 1.0 as a function of temperature. Also shown here is the net change in chemical shift with temperature, that is, $\Delta\delta = \delta_{(328\text{ K})} - \delta_{(275\text{ K})}$ -ve $\Delta\delta$ indicates upfield shift and +ve $\Delta\delta$ indicates downfield shift.

Temp. (K)	T1H1'	G2H1'	A3H1'	T4H1'	C5H1'	A6H1'	T1CH ₃ ^f	T1CH ₃ ^b	T4CH ₃ ^f	T4CH ₃ ^b	T1H6	
275	5.71	5.54	6.31	5.98	5.67	6.29	1.63	1.51	1.38	1.30	7.37	
283	5.77	5.54	6.31	5.98	5.73	6.30	1.63	1.51	1.40	1.33	7.34	
288	5.81	5.53	6.31	5.99	5.78	6.31	1.63	1.51	1.43	1.33	7.34	
293	5.84	5.53	6.31	5.99	5.82	6.31	1.64	1.51	1.45	1.33	7.34	
298	5.87	5.55	6.33	6.00	5.85	6.32	1.67	1.55	1.49	1.35	7.34	
303	5.87	5.55	6.33	6.00	5.85	6.32	1.67	1.55	1.49	1.36	7.34	
308	5.94	5.57	6.36	6.03	5.92	6.31	1.70	1.60	1.53	1.36	7.35	
313	5.97	5.63	6.37	6.05	5.95	6.31	1.72	1.63	1.56	1.36	7.36	
318	5.99	5.63	6.37	6.06	5.98	6.31	1.74	1.65	1.60	1.36	7.36	
323	6.01	5.67	6.38	6.08	6.00	6.31	1.77	1.68	1.63	1.36	7.37	
328	6.03	5.69	6.39	6.09	6.02	6.31	1.78	1.69	1.64	1.36	7.38	
$\Delta\delta$	+0.32	+0.15	+0.08	+0.11	+0.35	+0.02	+0.15	+0.18	+0.26	+0.06	+0.01	
Temp. (K)	G2H8	A3H8	T4H6	C5H6	A6H8	C5H5	T1NH ^b	T1NH ^f	G2NH ^b	G2NH ^f	T4NH ^f	T4NH ^b
275	8.05	8.35	7.24	7.52	8.27	5.67	11.98	12.16	12.69	12.92	13.72	13.81
283	8.04	8.34	7.23	7.51	8.26	5.67	11.99	12.16	12.70	-	13.69	-
288	8.02	8.33	7.24	7.51	8.26	5.70	12.01	12.16	-	-	13.69	-
293	8.00	8.32	7.24	7.51	8.26	5.73	12.01	-	-	-	-	-
298	8.00	8.32	7.25	7.51	8.27	5.77	12.05	-	-	-	-	-
303	8.00	8.32	7.25	7.51	8.27	5.77	12.05	-	-	-	-	-
308	7.98	8.31	7.28	7.54	8.29	5.82	12.10	-	-	-	-	-
313	7.98	8.31	7.30	7.56	8.30	5.84	12.10	-	-	-	-	-
318	7.98	8.31	7.32	7.57	8.30	5.87	-	-	-	-	-	-
323	7.99	8.31	7.35	7.59	8.30	5.89	-	-	-	-	-	-
328	8.00	8.31	7.36	7.60	8.30	5.91	-	-	-	-	-	-
$\Delta\delta$	-0.05	-0.04	+0.12	+0.08	+0.03	+0.24	-	-	-	-	-	-

Table 5b: Chemical shift (ppm) of nucleic acid protons in drug – DNA complex having D/N = 1.5 as a function of temperature. Also shown here is the net change in chemical shift with temperature, that is, $\Delta\delta = \delta_{(328\text{ K})} - \delta_{(275\text{ K})}$ -ve $\Delta\delta$ indicates upfield shift and +ve $\Delta\delta$ indicates downfield shift.

Temp. (K)	T1H1'	G2H1'	A3H1'	T4H1'	C5H1'	A6H1'	T1CH ₃ ^f	T1CH ₃ ^b	T4CH ₃ ^f	T4CH ₃ ^b	T1H6	
275	5.71	5.54	6.30	5.96	5.66	6.28	1.63	1.51	1.37	1.28	7.36	
283	5.75	5.53	6.30	5.97	5.72	6.28	1.63	1.51	1.38	1.30	7.36	
288	5.81	5.53	6.31	5.98	5.76	6.29	1.63	1.51	1.42	1.33	7.34	
293	5.84	5.53	6.31	5.98	5.81	6.29	1.64	1.51	1.45	1.33	7.34	
298	5.88	5.53	6.32	6.00	5.85	6.30	1.65	1.58	1.47	1.33	7.35	
303	5.92	5.53	6.33	6.01	5.90	6.30	1.67	1.58	1.49	1.33	7.36	
308	5.96	5.53	6.34	6.02	5.93	6.30	1.69	1.60	1.49	1.33	7.36	
313	5.98	5.53	6.36	6.04	5.96	6.29	1.71	1.62	1.49	1.33	7.37	
318	5.99	5.56	6.37	6.05	5.99	6.29	1.74	1.66	1.57	1.33	7.37	
323	6.01	5.58	6.37	6.07	6.00	6.29	1.76	1.68	1.60	1.32	7.38	
328	6.03	5.60	6.38	6.09	6.02	6.30	1.78	1.70	1.63	1.32	7.39	
$\Delta\delta$	+0.32	+0.06	+0.08	+0.13	+0.36	+0.02	+0.15	+0.19	+0.26	+0.04	+0.03	
Temp. (K)	G2H8	A3H8	T4H6	C5H6	A6H8	C5H5	T1NH ^b	T1NH ^f	G2NH ^b	G2NH ^f	T4NH ^f	T4NH ^b
275	8.03	8.33	7.20	7.49	8.25	5.60	11.97	12.13	12.67	12.86	13.69	13.76
283	8.03	8.34	7.22	7.50	8.25	5.67	11.98	12.17	12.67	12.82	13.69	13.76
288	8.02	8.34	7.24	7.51	8.25	5.72	12.00	12.17	12.67	12.80	13.69	13.76
293	8.00	8.34	7.24	7.51	8.25	5.72	12.02	12.17	12.67	12.80	13.69	13.76
298	8.00	8.32	7.25	7.53	8.26	5.72	12.04	-	-	-	-	-
303	7.97	8.32	7.27	7.54	8.27	5.72	12.06	-	-	-	-	-
308	7.96	8.31	7.27	7.55	8.28	5.72	12.06	-	-	-	-	-
313	7.94	8.31	7.29	7.56	8.29	5.72	12.06	-	-	-	-	-
318	7.91	8.30	7.31	7.57	8.30	5.72	-	-	-	-	-	-
323	7.89	8.30	7.33	7.59	8.30	5.72	-	-	-	-	-	-
328	7.87	8.31	7.36	7.61	8.30	5.75	-	-	-	-	-	-
$\Delta\delta$	-0.16	-0.02	+0.16	+0.12	+0.05	+0.15	-	-	-	-	-	-

Table 5c: Chemical shift (ppm) of nucleic acid protons in drug – DNA complex having D/N = 2.0 as a function of temperature. Also shown here is the net change in chemical shift with temperature, that is, $\Delta\delta = \delta_{(328\text{ K})} - \delta_{(275\text{ K})}$ -ve $\Delta\delta$ indicates upfield shift and +ve $\Delta\delta$ indicates downfield shift.

Temp. (K)	T1H1'	G2H1'	A3H1'	T4H1'	C5H1'	A6H1'	T1CH ₃ ^f	T1CH ₃ ^b	T4CH ₃ ^f	T4CH ₃ ^b	T1H6
275	5.67	5.54	6.30	5.94	5.64	6.28	1.63	1.51	1.34	1.28	7.36
283	5.72	5.54	6.30	5.96	5.68	6.28	1.63	1.51	1.34	1.28	7.33
288	5.82	5.53	6.33	6.00	5.76	6.29	1.64	1.52	1.35	1.30	7.37
293	5.85	5.48	6.32	6.00	5.80	6.29	1.62	1.52	1.34	1.30	7.35
298	5.87	5.40	6.32	6.00	5.83	6.28	1.63	1.52	1.33	1.26	7.37
303	5.90	5.39	6.32	6.00	5.87	6.27	1.65	1.52	1.33	1.26	7.37
308	5.93	5.39	6.33	6.01	5.90	6.27	1.67	1.52	1.33	1.26	7.37
313	5.97	5.39	6.34	6.03	5.94	6.27	1.70	1.52	1.33	1.26	7.38
318	5.99	5.39	6.36	6.05	5.95	6.27	1.72	1.54	1.33	1.26	7.38
323	6.01	5.39	6.37	6.07	5.99	6.28	1.75	1.57	1.31	1.26	7.39
328	6.03	5.39	6.38	6.08	6.00	6.29	1.78	1.62	1.30	1.26	7.39
$\Delta\delta$	+0.36	-0.15	+0.08	+0.14	+0.36	+0.01	+0.15	+0.11	-0.04	-0.02	+0.03

Temp. (K)	G2H8	A3H8	T4H6	C5H6	A6H8	C5H5	T1NH ^b	T1NH ^f	G2NH ^b	G2NH ^f	T4NH ^f	T4NH ^b
275	8.03	8.32	7.22	7.49	8.23	5.60	11.96	12.13	12.66	12.86	13.70	13.76
283	8.02	8.34	7.22	7.49	8.24	5.64	11.96	12.13	12.66	12.88	13.70	-
288	8.04	8.38	7.26	7.53	8.27	5.72	12.01	12.18	12.65	12.88	13.70	-
293	8.00	8.36	7.30	7.53	8.24	5.72	12.01	-	12.65	-	-	-
298	8.00	8.35	7.31	7.54	8.25	5.72	12.04	-	-	-	-	-
303	7.98	8.32	7.33	7.55	8.25	5.72	12.04	-	-	-	-	-
308	7.96	8.32	7.35	7.56	8.26	5.72	-	-	-	-	-	-
313	7.94	8.31	7.37	7.57	8.27	5.72	-	-	-	-	-	-
318	7.92	8.30	7.37	7.58	8.28	5.72	-	-	-	-	-	-
323	7.89	8.30	7.37	7.59	8.29	5.72	-	-	-	-	-	-
328	7.87	8.30	7.38	7.61	8.29	5.76	-	-	-	-	-	-
$\Delta\delta$	-0.16	-0.02	+0.16	+0.12	+0.06	+0.16	-	-	-	-	-	-

Table 6: Chemical shift (ppm) of some of the drug protons in drug-DNA complex having D/N = 1.0, 1.5 and 2.0 as a function of temperature. Also shown here is the total change in chemical shift, $\Delta\delta = \delta_{328\text{ K}} - \delta_{275\text{ K}}$. -ve $\Delta\delta$ indicates upfield shift and +ve $\Delta\delta$ indicates downfield shift.

Temp.(K)	D/N = 1:1					D/N = 1.5:1					D/N = 2:1				
	3H	2H	1H	1'H	11OH	3H	2H	1H	1'H	11OH	3H	2H	1H	1'H	11OH
275	7.48	7.74	7.64	5.57	12.32	7.47	7.74	7.64	5.61	12.32	7.47	7.72	7.64	5.61	12.32
283	7.47	7.76	7.64	5.58	12.37	7.45	7.75	7.64	5.60	12.37	7.44	7.73	7.64	5.61	12.37
288	7.46	7.79	7.64	5.6	12.42	7.45	7.75	7.64	5.60	12.42	7.44	7.76	7.64	5.63	12.42
293	7.46	7.82	7.63	5.59	12.46	7.45	7.75	7.63	5.59	12.47	7.42	7.75	7.64	5.60	12.47
298	7.46	7.86	7.63	5.59	12.53	7.45	7.75	7.63	5.59	12.54	7.43	7.76	7.63	5.59	12.54
303	7.46	7.86	7.63	5.59	12.54	7.45	7.75	7.62	5.59	12.61	7.43	7.76	7.63	5.59	-
308	7.45	7.86	7.63	5.63	12.65	7.44	7.77	7.62	5.59	12.64	7.43	7.76	7.62	5.59	-
313	7.45	7.86	7.63	5.67	12.72	7.43	7.77	7.62	5.59	12.71	7.42	7.79	7.62	5.58	-
318	7.45	7.86	7.63	5.69	12.74	7.42	7.79	7.61	5.60	12.78	7.40	7.79	7.62	5.58	-
323	7.45	7.86	7.63	5.72	-	7.42	7.80	7.61	5.65	-	7.41	7.80	7.62	5.63	-
328	7.45	7.86	7.63	5.74	-	7.42	7.81	7.61	5.69	-	7.43	7.80	7.62	5.69	-
$\Delta\delta$	-0.03	+0.12	-0.01	+0.17	+0.42	-0.05	+0.07	-0.03	+0.08	+0.46	-0.04	+0.08	-0.02	+0.08	+0.22

solvent. On successive addition of adriamycin to DNA, four additional resonance peaks are observed at 12.12, 11.96, 12.66, 13.75 ppm. In 2D NOESY spectra (Fig. 8a-b) pairs of protons resonating at 12.12, 11.96; 12.66, 12.86 and 13.69, 13.75 give cross peaks with each other. Since T4NH and G2NH appear at 13.69 and 12.86 ppm in uncomplexed / d-(TGATCA)₂, the peaks at 13.75 and 12.66 ppm get assigned to T4NH and G2NH in the complex of d-(TGATCA)₂ with drug at D/N= 2.0 (designated as T4NH^b and G2NH^b). The remaining pair (12.12, 11.96 ppm), gets assigned to T1NH present in free (T1NH^f 12.12 ppm) and bound state (T1NH^b 11.96 ppm). The area under the NH peaks, confirmed that the T1NH / G2NH / T4NH indeed split in to two sets of peaks. The ratio of area of T4NH^f to T4NH^b decreased from 4:1 (approximately) at D/N ratio of 1.0 to 2:1 at D/N ratio of 2.0 that is, on addition of an increasing amount of drug to DNA. It is noted that the intensity of T1NH^f peaks is significantly lesser than that of G2NH^f and T4NH^f. Also the NOE cross peak of T1NH^f and G2NH^f resonance corresponding to a distance of 3.70 Å in standard B-DNA structures is considerably weaker in intensity than the NOE cross peak of T4NH^f and G2NH^f which corresponds to a distance of 3.72 Å. This suggests that T1NH proton which completely exchanges with water in free d-(TGATCA)₂, is immobilized in the drug-DNA complex although it is still fraying to some extent being the terminal base pair of DNA. Accordingly the line width of T1NH^b is found to be greater than that of G2NH^b and T4NH^b.

It is observed that the sharp T1CH₃ and T4CH₃ peaks appearing at 1.65 and 1.44 ppm, respectively in d-(TGATCA)₂ decrease in intensity as D/N ratio increases and two new relatively broad peaks appearing at 1.58 and 1.33 ppm, respectively start growing in intensity with D/N (Fig. 2a-c); the same is also manifested in the area plots. These peaks exchange with each other and hence the peak at 1.58 and 1.33 ppm get assigned to T1CH₃ and T4CH₃ of DNA

bound to the drug molecule ($T1CH_3^b$ and $T4CH_3^b$), respectively. $T4CH_3^b$ shows all expected interproton NOE connectivities, that is, to $A3H2'$, $A3H2''$, $A3H8$, $T4H6$, $A3H1'$ (Fig. 8e-g). These NOE cross peaks are weaker in intensity than the corresponding NOEs of $T1CH_3^f$ and $T4CH_3^f$ protons resonating at 1.65 and 1.44 ppm, respectively. The existence of two sets of $T4NH$, $T1NH$, $G2NH$, $T1CH_3$ and $T4CH_3$ clearly demonstrates that the drug indeed binds to the DNA hexamer and there is a slow exchange of free and bound DNA on NMR time scale at 275 K. This is consistent with our observations of ^{31}P NMR spectra (Chapter 5) in which bound and free ^{31}P resonances showed slow exchange.

Change in Chemical Shift due to complexation: The palindromic symmetry of the system implies that two intercalative sites are available for the drug. The change in chemical shift ($\Delta\delta$) of base and $H1'$ protons with ratios are gradual and small in magnitude. The $\Delta\delta$ increases with D/N ratio as more and more DNA oligomer binds to the drug and a maximum of 0.06 ppm upfield shift is observed for $T1H1'$ and $C5H1'$ protons. Two of the bound imino protons on the DNA oligomer are upfield shifted with respect to the corresponding imino protons in free state (Table 1, Fig. 8a-b); the shift being 0.16 and 0.20 ppm for $T1NH$ and $G2NH$, respectively. Such changes may be attributed to stacking or structural changes in complexation which may however be compensatory in nature. We have followed the 1H resonance signals on addition of increasing amount of drug in the temperature range 275-328 K at steps of 5 K (Table 5a-c, Fig. 5a-i). It is observed that there is variation of chemical shift with temperature showing downfield shift of 0.32 ppm for $T1H1'$ and 0.35 ppm for $C5H1'$. This indicates that structurally only one complex is being formed and the chemical shift at any one temperature is an average of bound and unbound DNA/drug, the equilibrium of which is likely to shift with temperature. $T4NH$, $G2NH$ and $T1NH$ also show slight downfield shift (Fig. 5a-i). These changes may be due to several

reasons such as destacking/decreased intercalation, duplex to single strand transition, etc. The integral values of T4NH, G2NH, T1NH, T1CH₃ and T4CH₃ in bound and free state also confirm that only one bound species exists in this temperature range. The T1NH^b and 11OH peaks are seen in the spectra of 1.5:1 drug-DNA complex at 308 K indicates that the drug is bound to DNA and the complex exists. In fact T1NH is immobilized in the complex whereas in uncomplexed DNA, it exchanges with water.

There is a gradual shift in drug protons on binding to DNA. The ring protons, 1H, 2H and 3H, shift upfield substantially up to 0.25 ppm with respect to the chemical shift position of drug monomer, δ^{monomer} in 2:1 drug to DNA complex at 275 K (Table 4) due to stacking. There is downfield shift ($\Delta\delta = \delta^{\text{b}} - \delta^{\text{f}}$) of 0.09 ppm for 2H, 0.15 ppm for 1H and 0.09 ppm for 1'H proton (Table 4). 6OH and 11OH peaks appear at about 13.25 and 12.34 ppm. The cross peak between 11OH and 8eqH, 8axH; 6OH and 4OCH₃ are the basis of assignment of 11OH and 6OH. The upfield shift of 11OH proton by 0.36 ppm shows stacking is taking place through drug chromophore. There is an upfield shift of 1.18 ppm in 9OH and 0.36 ppm in 9COCH₂ protons on the complex formation which indicates direct interaction of 9OH and 9COCH₂ of drug chromophore with base pair of DNA. The change in chemical shift with temperature is observed for 1H, 2H, 3H, 1'H and 11OH protons (Table 6, Fig. 7), which are presumably close to oligomer due to stacking of adriamycin chromophore with base pair of DNA.

The observed change in chemical shift of drug and DNA protons in 2:1 drug to DNA complex with respect to the corresponding chemical shifts in free drug in monomer form and free DNA (Barthwal et al., 1996) are shown in Table 2 and 1, respectively. This may be attributed to 2:1 stoichiometric drug-DNA complex to a first approximation since minor conformer and free drug/free DNA are also present. The upfield shifts of several drug protons in ring A and D is

consistent with the results reported on binding of adriamycin to oligonucleotide sequences in literature (Chaires et al., 1985; Nuss et al., 1981; Philips et al., 1980; Barthwal et al., 1994; Barthwal et al., 1996). These have been attributed to intercalation of drug chromophore between base pairs of DNA, which move apart to a distance of $\sim 6.8 \text{ \AA}$ on binding to drug (Nunn et al., 1991; Leonard et al., 1992; d'Estaintot et al., 1992) and are characteristic of stacking interaction between aromatic/conjugated rings (Chaires et al., 1985; Nuss et al., 1981; Philips et al., 1980; Barthwal et al., 1994; Barthwal et al., 1996). The relatively smaller change in 1H and 2H protons of drug, also reported earlier (Chaires et al., 1985; Nuss et al., 1981; Philips et al., 1980; Barthwal et al., 1994; Barthwal et al., 1996), is due to specific positioning of drug chromophore between base pairs such that the ring A partially protrudes out of base pairs resulting in much lesser overlap with adjacent base pairs and hence experiencing less ring current shifts. The base pair protons (H8, H6, H2, H5, CH₃) and deoxyribose H1' protons (being close to aromatic ring) of the intercalating base pair of DNA show ring current effect to a much lesser extent since they are destacked from the neighboring base pair in free DNA and then stacked with the conjugated aromatic rings ABCD (Fig. 1a) of adriamycin. The observed chemical shift at different temperatures (Fig. 7) is distinctly different from that of free drug in monomer / self associated form or free DNA. These changes in chemical shift may be due to structural alterations on binding and cannot be correlated directly to a specific structural parameter; hence not a sufficient marker of interaction. Therefore one needs to look at the structure of the specific complex by alternate ways, such as inter-proton contacts. 2D NOESY data infer that most of the drug exists in complexed form and 2:1 molecular complex is the major conformer.

Conformational features of DNA and drug in the complex

The NOESY spectra of drug-DNA complex at stoichiometric D/N ratio of 1.0 have been investigated extensively at mixing time (τ_m) of 300 and 200 ms. The intensities of cross peak have been estimated qualitatively as strong intense (ss), strong (s) medium (ws) and weakly intense (w) and very weak (ww) for distances of about 1.8 - 2.5, 2.5 - 3.0, 3.0 - 3.5, 3.5 - 4.0, and 4.0 - 5.0 Å, respectively from the spectra recorded at $\tau_m = 200$ ms. The inter-proton distances have also been evaluated by taking distance C5H5-C5H6 = 2.45 Å for $\tau_m = 200$ ms as an internal standard. The observed NOEs for (a) connectivities involving amino and imino protons of base pairs (b) sequential connectivities (c) intranucleotide connectivities within sugar and intranucleotide base to sugar connectivities are given in Table 7-10. Several short interproton distances (< 5 Å) from 5' to 3' direction along the oligonucleotide sequence are generally observed in NOESY spectra. Table 7-10 gives the NOE intensities observed within the DNA hexamer.

(a) Base pairing: The observation of NOEs C5N4H₂^b - G2N1H^f, T4NH^b - A3H2, T4NH^b - A3N6H₂^b establish Watson-Crick base pairing between G2...C5 and A3...T4 base pairs in the duplex. The sequential connectivity between T4N3H^b - G2N1H^b the imino protons is also observed (Table 10 and Fig. 8c-d). The T1NH^b-A6H2 cross peak shows the presence of T1.....A6 base pair. However the sequential connectivity between T1 and G2 is absent. This clearly demonstrates that DNA duplex is intact and apparently the distance between base pairs is increased (~ 7 Å) at T1pG2 base pair step to accommodate the drug chromophore as expected on binding of typical intercalator to DNA molecule. Other pair peaks are listed in Table 10.

(b) Sequential connectivities of d-(TGATCA)₂: The sequential base (H6/H8)_n to (H1')_{n-1}, (H2')_{n-1}, (H2'')_{n-1}, (H3')_{n-1}, base (H6/H8)_{n-1} connectivities are not observed between first - second base pair step (T1pG2) and fifth-sixth base pair steps (C5pA6) (Table 9 and Fig. 8e-j). Intense NOE cross peaks are observed for several sequential connectivities between the steps, G2pA3,

A3pT4 and T4pC5, as expected for right handed B-DNA type conformations. The intensities corresponding to these sequential NOE connectivities, $(H1', H2', H2'')_{n-1} - (\text{base } H8/H6)_n$ are found to be in the range 2.5-4.0 Å (Table 9). Thus the drug chromophore intercalates at T1pG2 and C5pA6 steps, as reported in X-ray crystallographic studies (Nunn et al., 1991; Leonard et al., 1992; d'Estaintot et al., 1992). This is also evident from several observed intermolecular NOE connectivities between drug and DNA protons in the complex discussed later. The cross peaks A3H8-G2H8 (5.0 Å), T4CH₃-A3H8 (3.8 Å), T4H6-A3H8 (4.8 Å) and C5H5-T4H6 (3.9 Å) have earlier been observed in the spectra of d-(CGATCG)₂ (Barthwal et al., 2003) and d-(TGATCA)₂ (Barthwal et al., 2004). These observations are indicative of good base to base stacking at these base pair steps. In the complex of adriamycin with d-(TGATCA)₂, we observe two of these NOE connectivities, that is, A3H8-T4CH₃ and T4H6-C5H5 (Table 9 and Fig. 8m-n). The stacking pattern in the base pairs adjacent to the intercalation site appears to have changed on complexation.

(c) Conformational feature of hexamer: Sugar conformation may be determined from the integrals of cross peaks in NOESY spectra (Table 7) at 275 K. The deoxyribose conformation may be estimated from intra-sugar distances of a nucleotide residue. Intra residue inter-proton distances H1'-H2', H1'-H2'', H2'-H3', H2''-H3', H2'-H4' and H3'-H4' vary with P_S and χ_S in a narrow range, on the other hand, H1'-H4' and H2''-H4' distances vary significantly with P_S and χ_S, respectively (Wüthrich, 1986) and may be used for conformational analysis. The NOE connectivity corresponding to H1'-H4' for G2 residue is weakly intense as compared to that of A3 residue (Table 7 and Table 8k, l, o) indicating that pseudo rotation phase angle for G2 residue is ~162-180° while that for A3 may be ≤ 162°. The H2''-H4' distance serves as a marker for mole fraction of S-conformer, χ_S, since its value of 3.8 Å for P = 162° decreases to 2.2 Å as P decreases to 18°. The observed values of H2''-H4' distance (Table 7) show that fraction of N

conformer decreases in the order C5 > T1, T4, A6, G2 > A3. The observed intense cross peaks H2''-H3' and H3'-H4' show that S-conformation is predominant.

Among purines, the intensity of H8-H1' cross peak in Fig. 8m decreases in order A6 > A3 > G2 so that χ value for G2 is close to that of B DNA $\sim -105^\circ$ while that for A6 and A3 residues deviates from -105° (Table 8 and Fig. 8h-j). Among pyrimidines, H6-H1' cross peak intensity decreases C5 > T4 > T1 (Fig. 8h) so that corresponding χ of T1 is close to $\sim -105^\circ$ whereas, C5, T4 deviates from this value. However H6-H2' for T1 residue gives unusual high value of distance (Fig. 8f, Table 8) which correspond to $\chi \sim -150^\circ$ (wuthrich, 1986) and H8/H6-H2'' NOE cross peaks show that the distance is least in A6 residue among the purines and C5 in pyrimidines, thus these two residues may be adopt $\chi = -90^\circ$ (Barthwal et al., 2006).

Conformation of Drug

The intramolecular NOE connectivities within the drug molecule in the drug-DNA complex give information about the conformation of drug (Table 11). The intensity of few of the drug protons are decreasing with D/N ratio. This is due to broadening of peaks at higher ratios. The conformation of ring A as well as daunosamine sugar has changed due to binding. As a result the relative orientation of ring A protons with sugar protons is affected. The distance of 7H and 8eqH to 1'H, 3'H and 5'H have increased and corresponding NOE connectivity is not observed. The distance of a 9COCH₂ proton from 3'H proton has decreased while its distance from 10eqH has increased (no cross peak observed at 2:1 ratio). Apparently, 9COCH₂ has moved closer to daunosamine sugar moiety. Such changes have been observed in X-ray crystal structure of complexes of daunomycin with d-(TGATCA)₂ (Nunn et al., 1991). No such studies have been carried out in solution state by NMR techniques. The NMR structure of bisdaunorubicin with d-

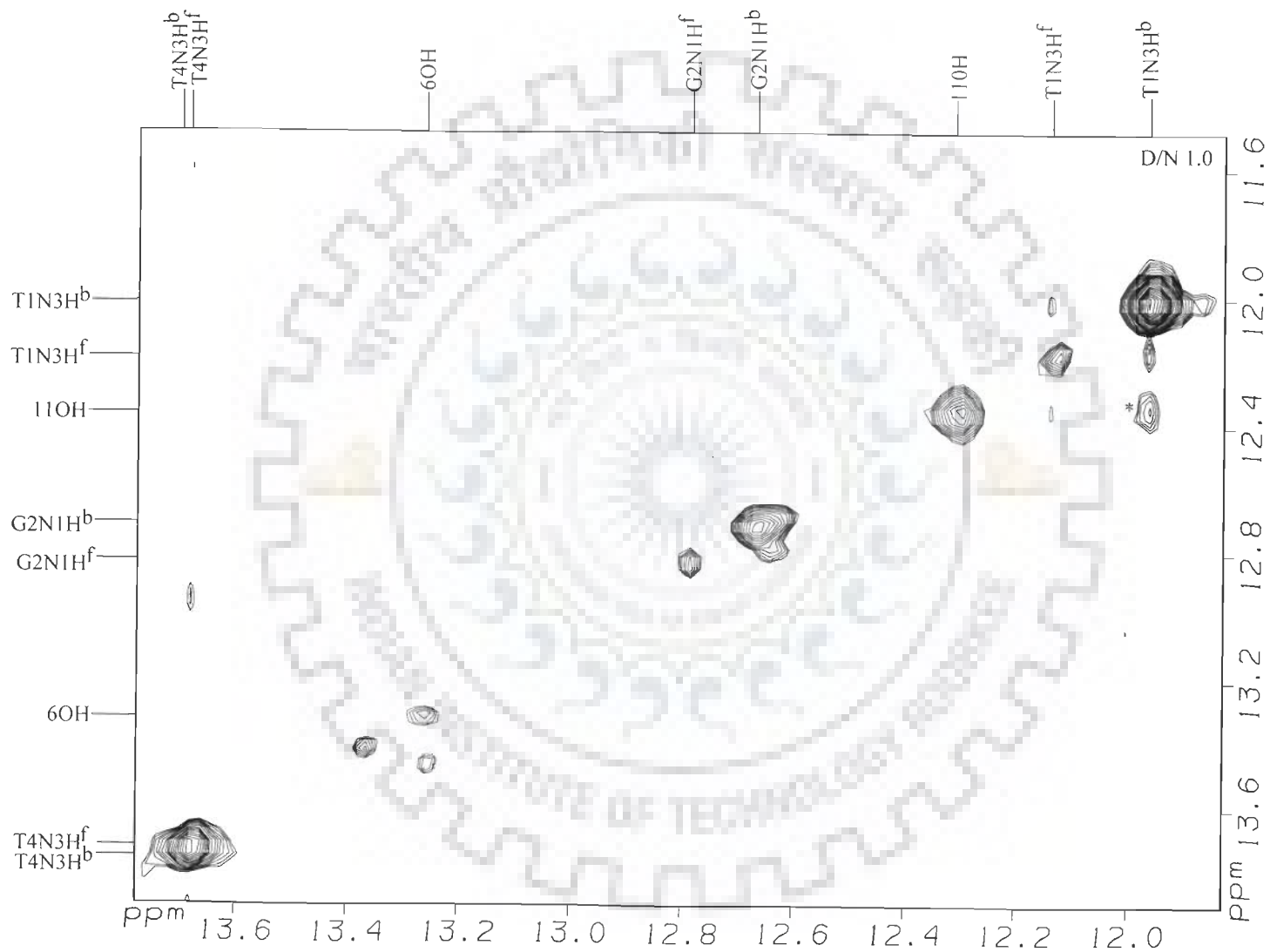
TGTACA (Robinson et al., 1997) does indicate bending of 9OH group towards daunosamine sugar.

Intermolecular Interactions

Several intermolecular contacts have been observed in the NOESY spectra (Fig. 8a-o) of major conformer and are listed in Table 12. The existence of NOESY cross peaks T1CH₃-7H, T1CH₃-10axH, T1CH₃-10eqH, C5H6-1H, C5H6-2H, C5H6-3H, C5H6-4OCH₃ (intense NOE cross peak) and C5H5-4OCH₃ (weakly intense cross peak) indicates that the drug chromophore stacks with T1 and C5 residues. Since the 4OCH₃ proton is closer to C5H6 and C5H5 protons while 7H, 10axH, 10eqH protons are close to T1CH₃ protons, the drug chromophore is oriented in a direction perpendicular to the long axis of T1.A6 and G2.C5 base pairs. As a result of stacking interactions, the 1'H atom of drug comes in close proximity of A3H1' and A3H2' atoms. The daunosamine sugar is in close proximity of third base pair as 5'CH₃ shows NOE cross peaks with protons of A3 residue. Table 12 shows several other NOEs between drug and DNA proton in which ambiguity arises due to the fact that more than one proton resonates at the same chemical shift position. For example, pairs of protons T1H3', 7H; G2H1', 1'H; T1H2', 8axH/2'eqH; resonate at same frequency. We have therefore selected some intermolecular NOE connectivities discussed above to build a model of drug-DNA complex. Several intramolecular NOE connectivities within the drug and DNA molecules have also been incorporated as NMR restraints. The structure obtained after restrained energy minimization followed by restrained molecular dynamics for 100 ps is shown in Fig. 9. It is observed that some of the NOEs observed between overlapping resonant peaks are possible as their corresponding distance in rMD structure is within 4.5 Å. The structure derived by rMD simulations is indeed defined by experimental NOE restraints. The comparison of the distance obtained by NMR and rMD is

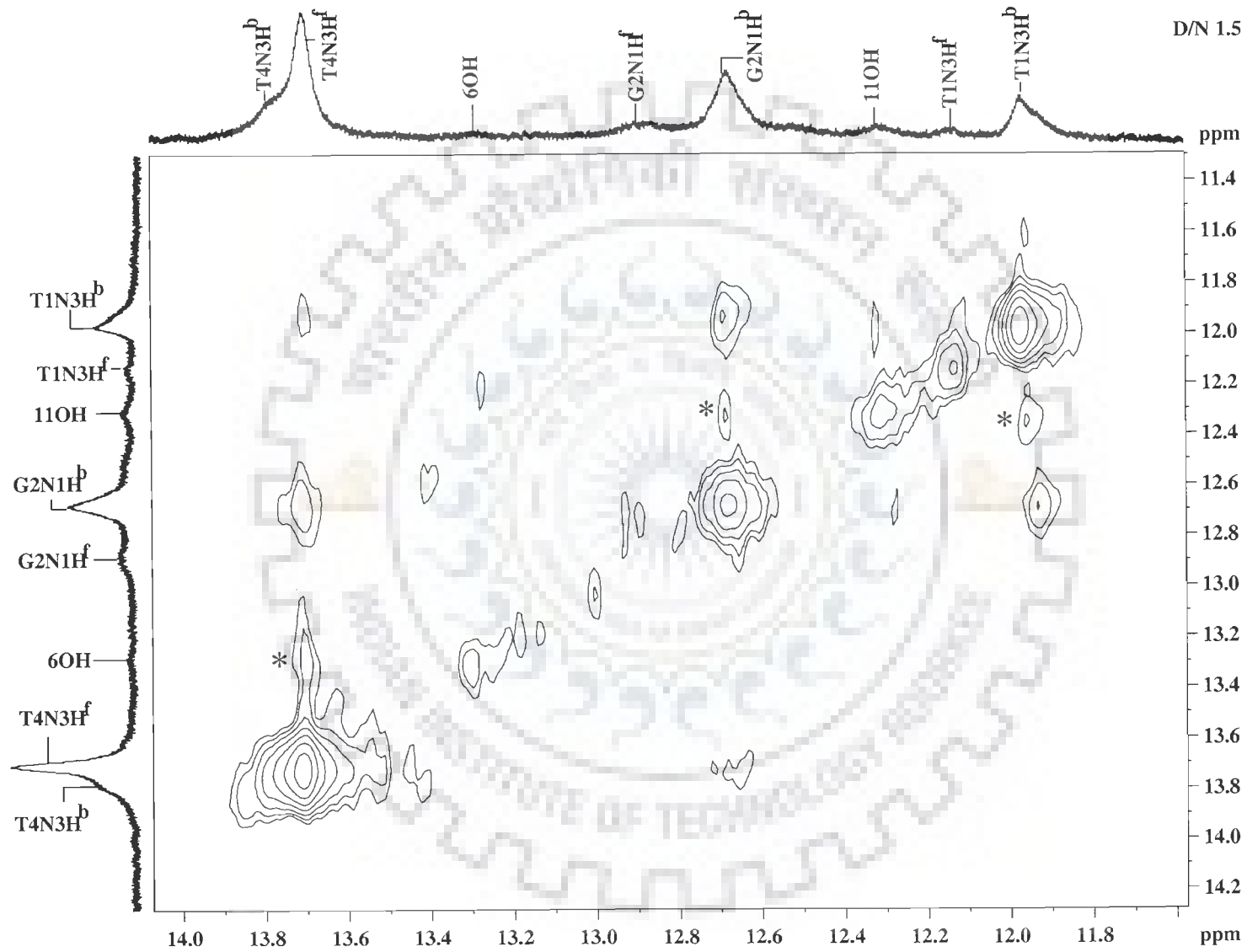
given in Table 13. This geometry would lead to upfield shifts in ring D and ring A protons due to anisotropic ring current effects from the adjacent base pairs. This is consistent with the observed upfield shifts of 0.16-0.36 ppm in -9COCH_2 , 7H , 8eqH and 8axH protons. Ring A is seen to protrude out, somewhat towards the solvent and is consistent with the observed small upfield shifts in 1H , 2H and 3H protons, being ~ 0.2 ppm. On accommodating the aromatic chromophore of drug between adjacent base pairs, the overlap geometry is considerably altered leading to shifts in their resonance positions although the base pairs are well stacked.

We have derived the values of pseudorotation phase and glycosidic bond rotation in the rMD structure (Table 14a-b) and compared them with that obtained earlier in similar X-ray crystallographic structures (Nunn et al., 1991; Leonard et al., 1992; d'Estaintot et al., 1992) with $\text{d}-(\text{TGATCA})_2$ and daunomycin, 4'-epiadriamycin. NMR studies are done on bisdaunomycin to $\text{d}-(\text{TGTACA})_2$ (Robinson, et al., 1997), daunorubicin- $\text{d}-(\text{TGATCA})_2$ (Barthwal et al., 2006). There are no such studies on binding of adriamycin/4'-epiadriamycin to $\text{d}-(\text{TGATCA})_2$ hexamer sequence by NMR techniques. The corresponding studies on NMR based structure of bisdaunomycin to $\text{d}-(\text{TGTACA})_2$ (Robinson, et al., 1997) result in a severely distorted B-DNA duplex and the detailed interactions are quite different. Table 14a shows that G2 and A3 residues have pseudorotation phase angle of 165° and 150° , respectively. The 2D NOESY spectra show glycosidic angle, χ , for T1 -150° , G2 -105° and A6 -90° . Similar structure has been obtained by rMD simulations based on NOE restraints exhibits anti conformation for T1 (-146°); G2 (-75°); high anti for A6 residue (-88°) Table 14b. Same values have been observed in literature (Frederick et al., 1990; Mazzini et al., 1998; Barthwal et al., 1994). Thus these results show the feasibility and relevance of NMR studies of adriamycin bound to $\text{d}-(\text{TGATCA})_2$. Some of the features such as NOE connectivities $\text{A3H1}'-5'\text{CH}_3$ and $\text{G6H1}'/\text{A6H1}'-1'\text{H}$ are common to

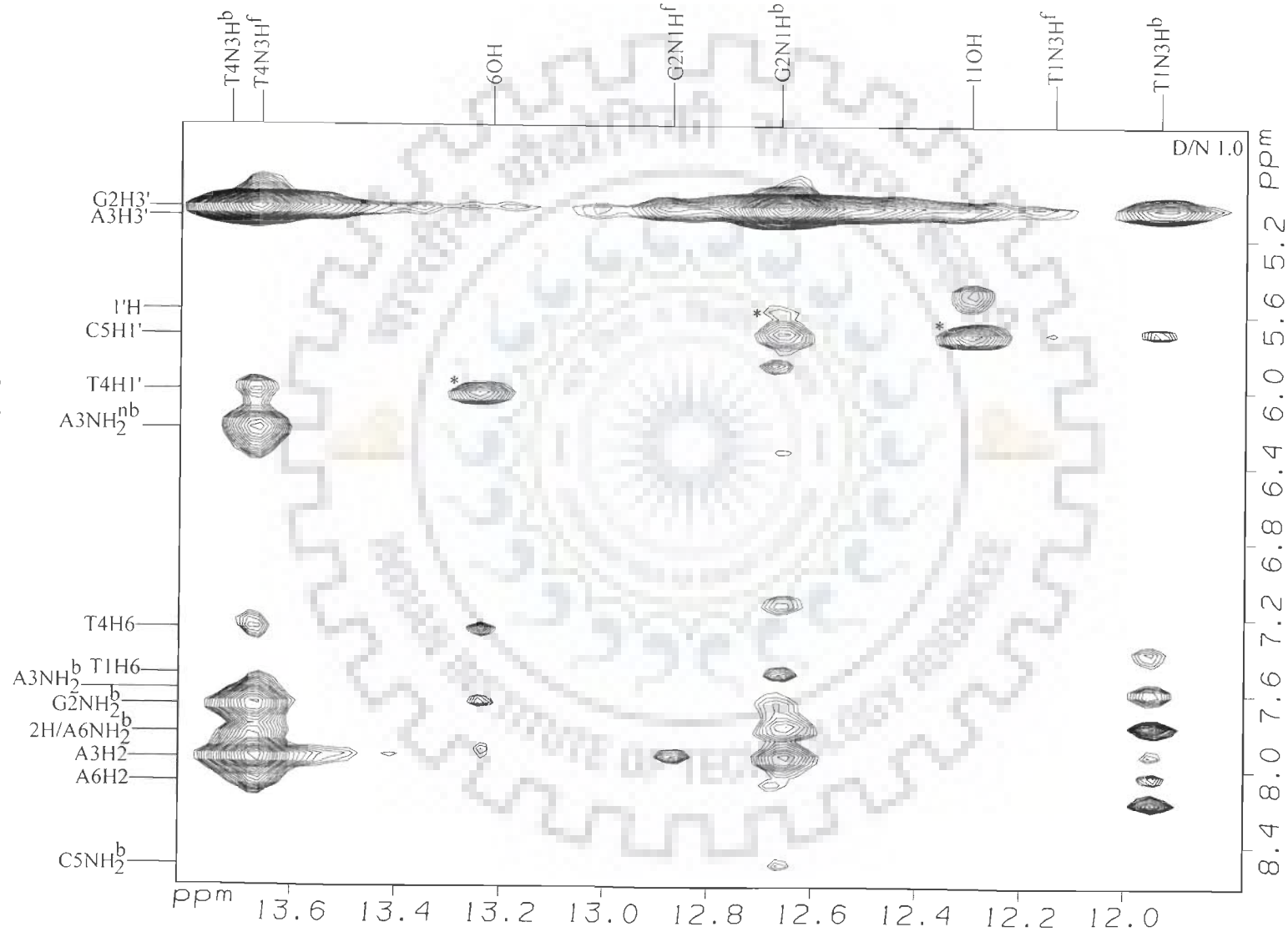


(a)

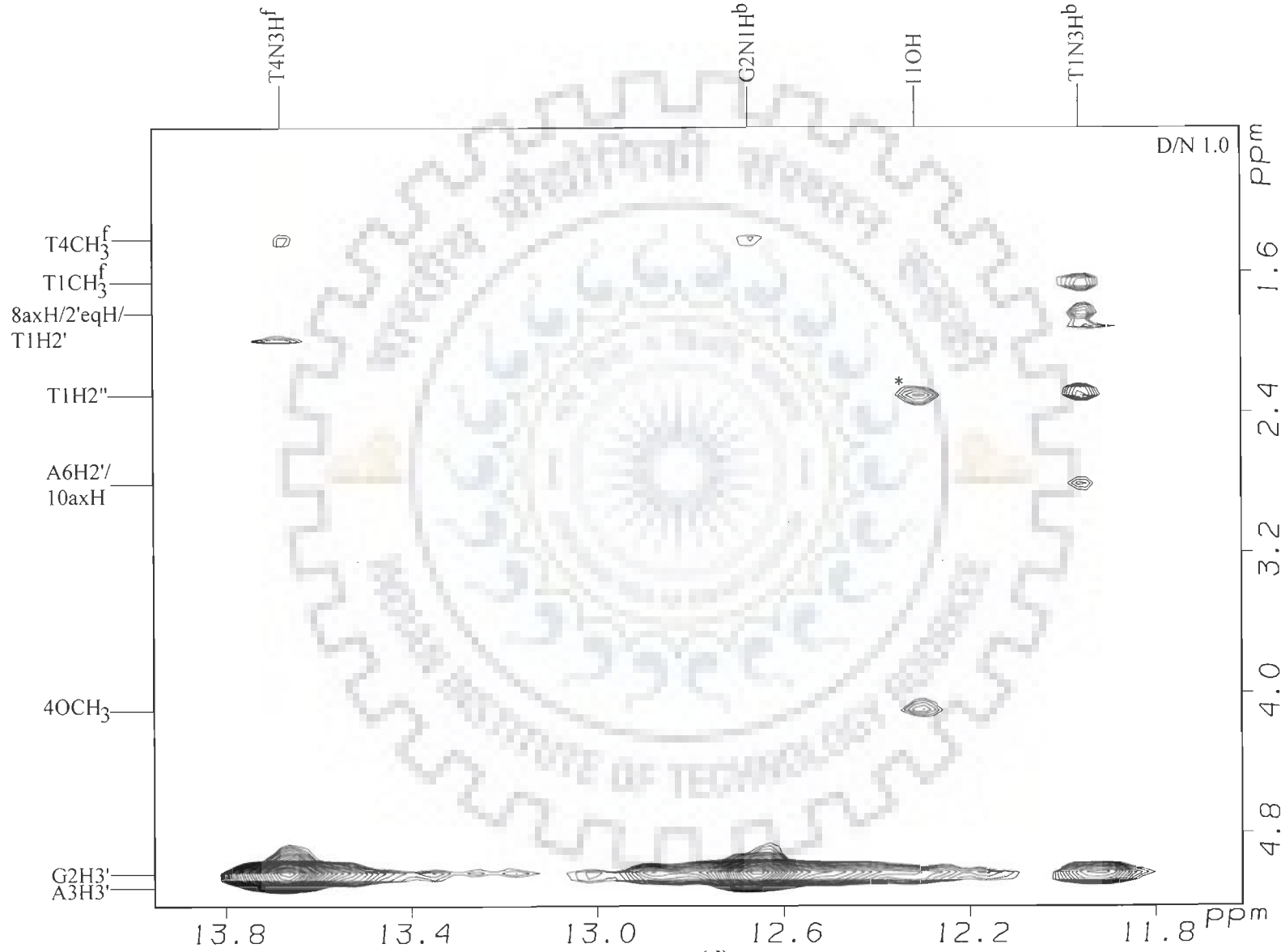
Fig. 8a-o: Expansions of various regions of 2D NOESY spectrum of adriamycin-d (TGATCA)₂ complex in H₂O/D₂O and intermolecular cross peaks are shown by asterisk (*) between drug and DNA at $\tau_m = 200$ ms and at 275 K.



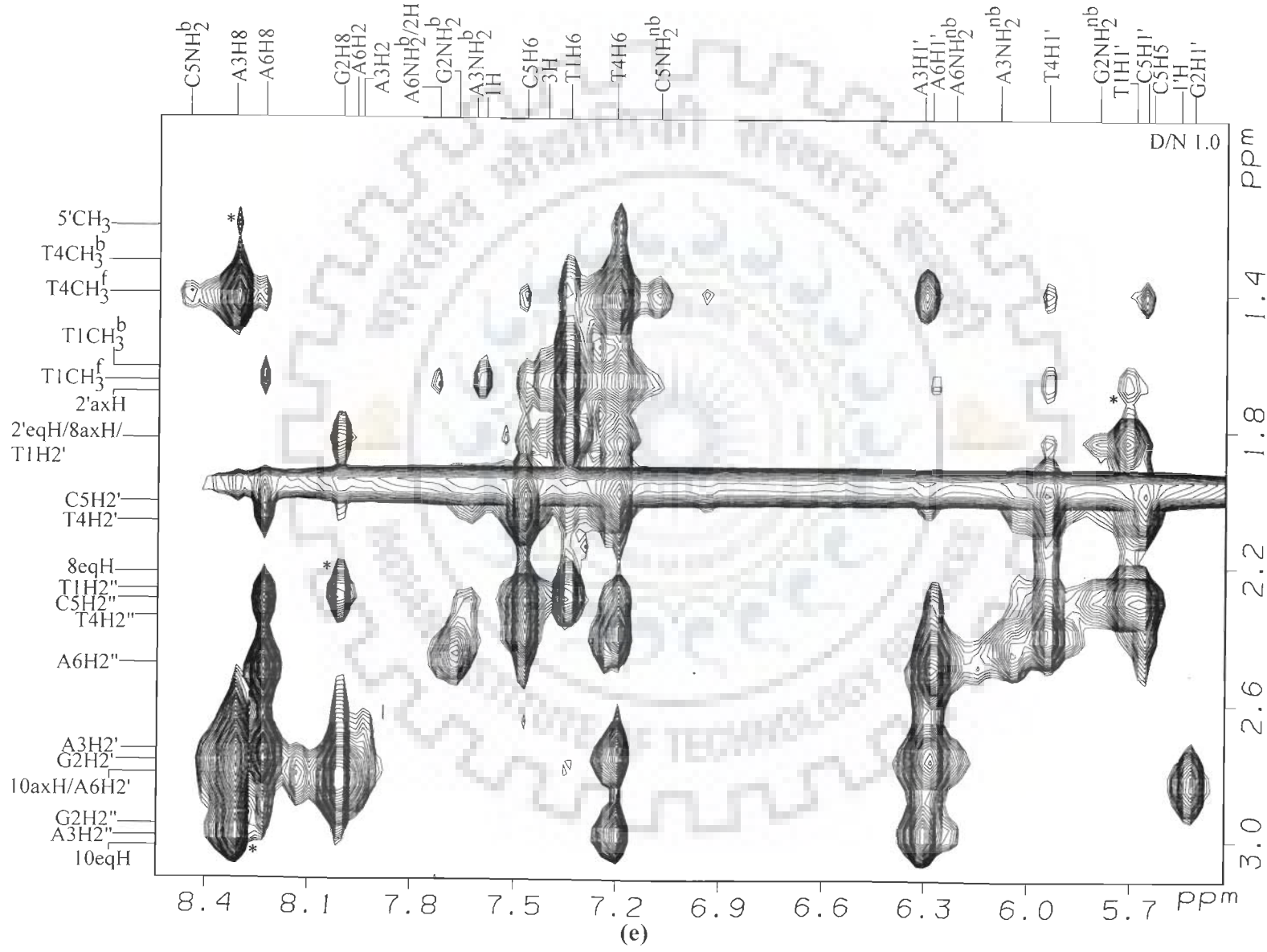
(b)

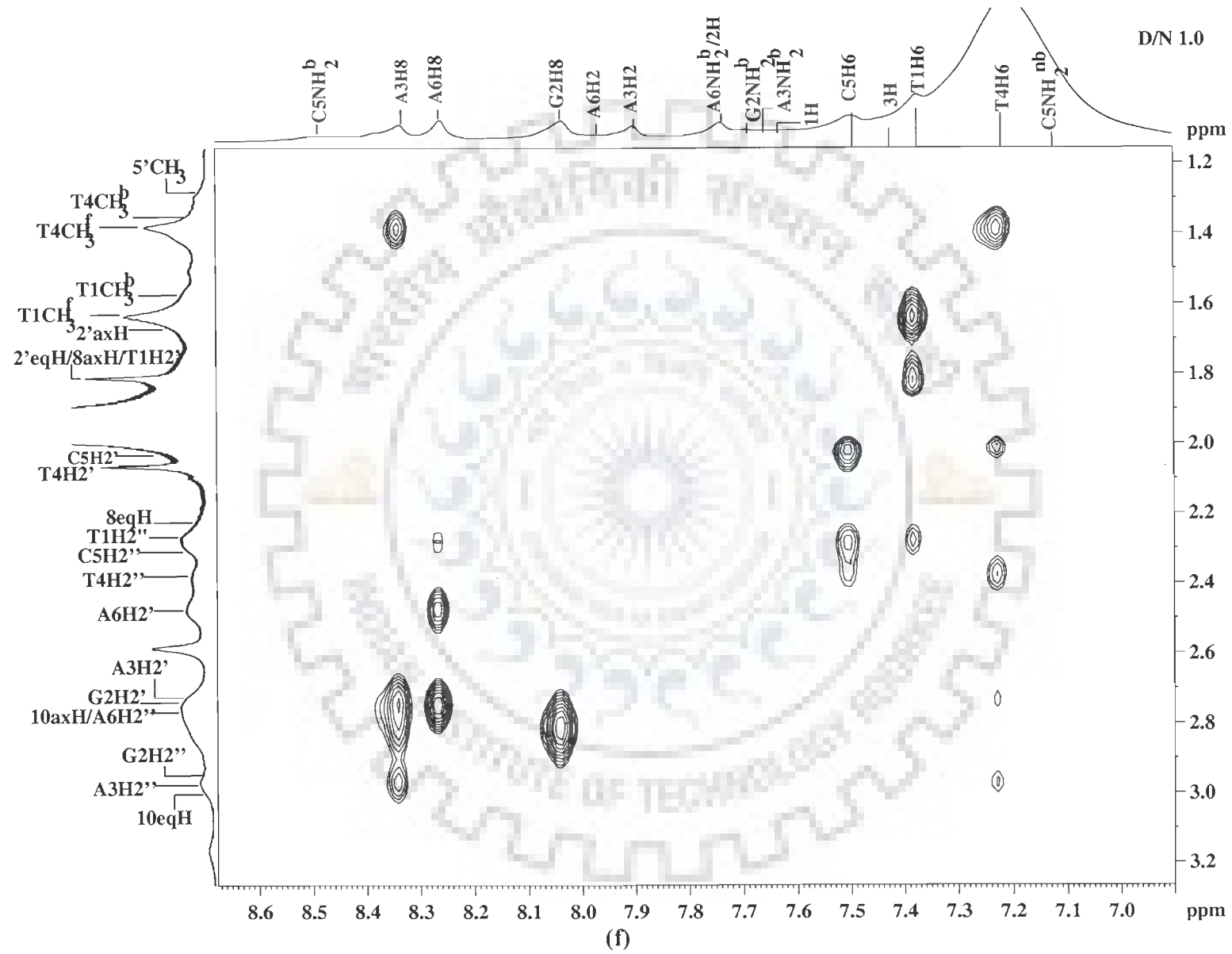


(c)

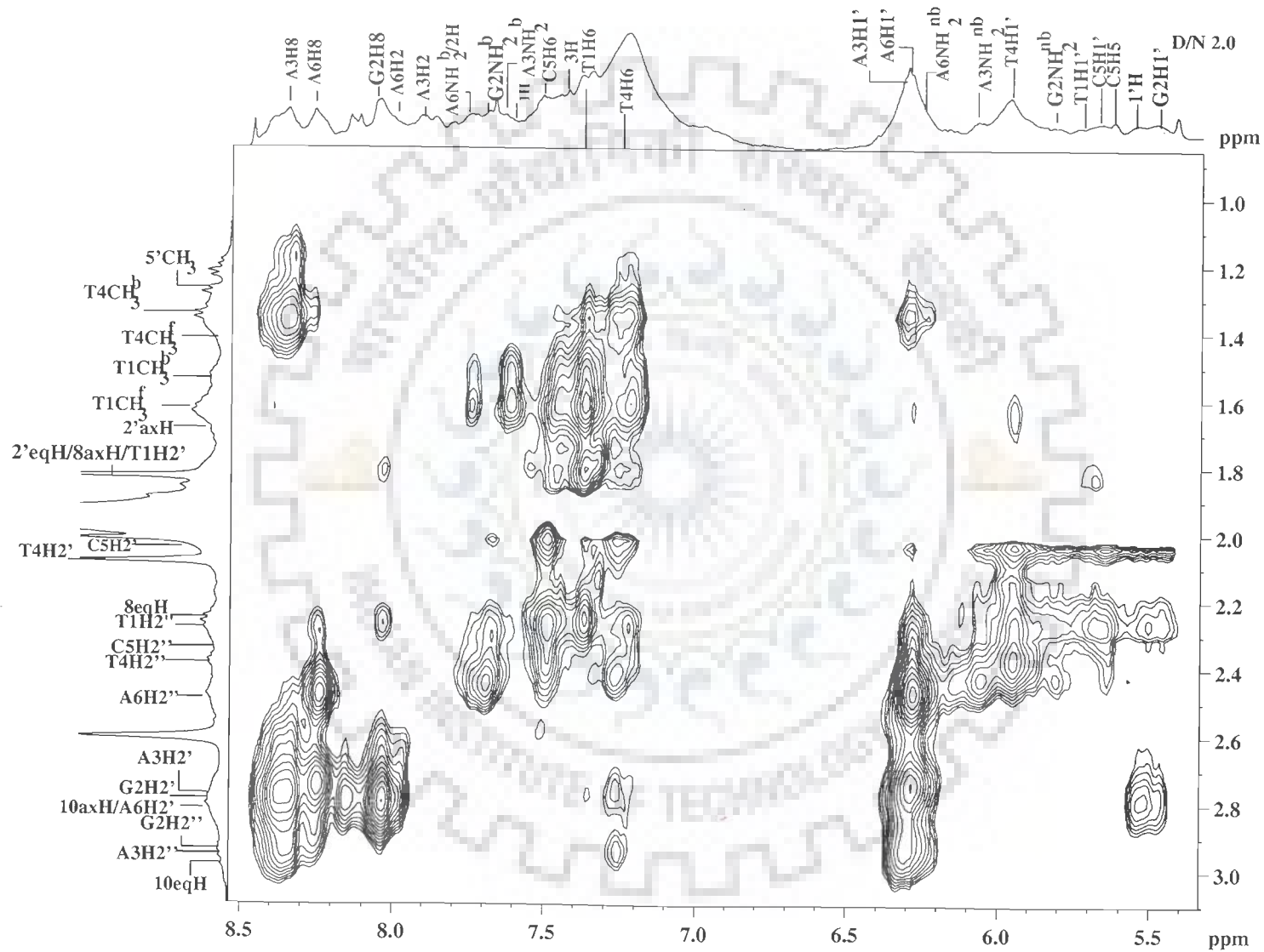


(d)

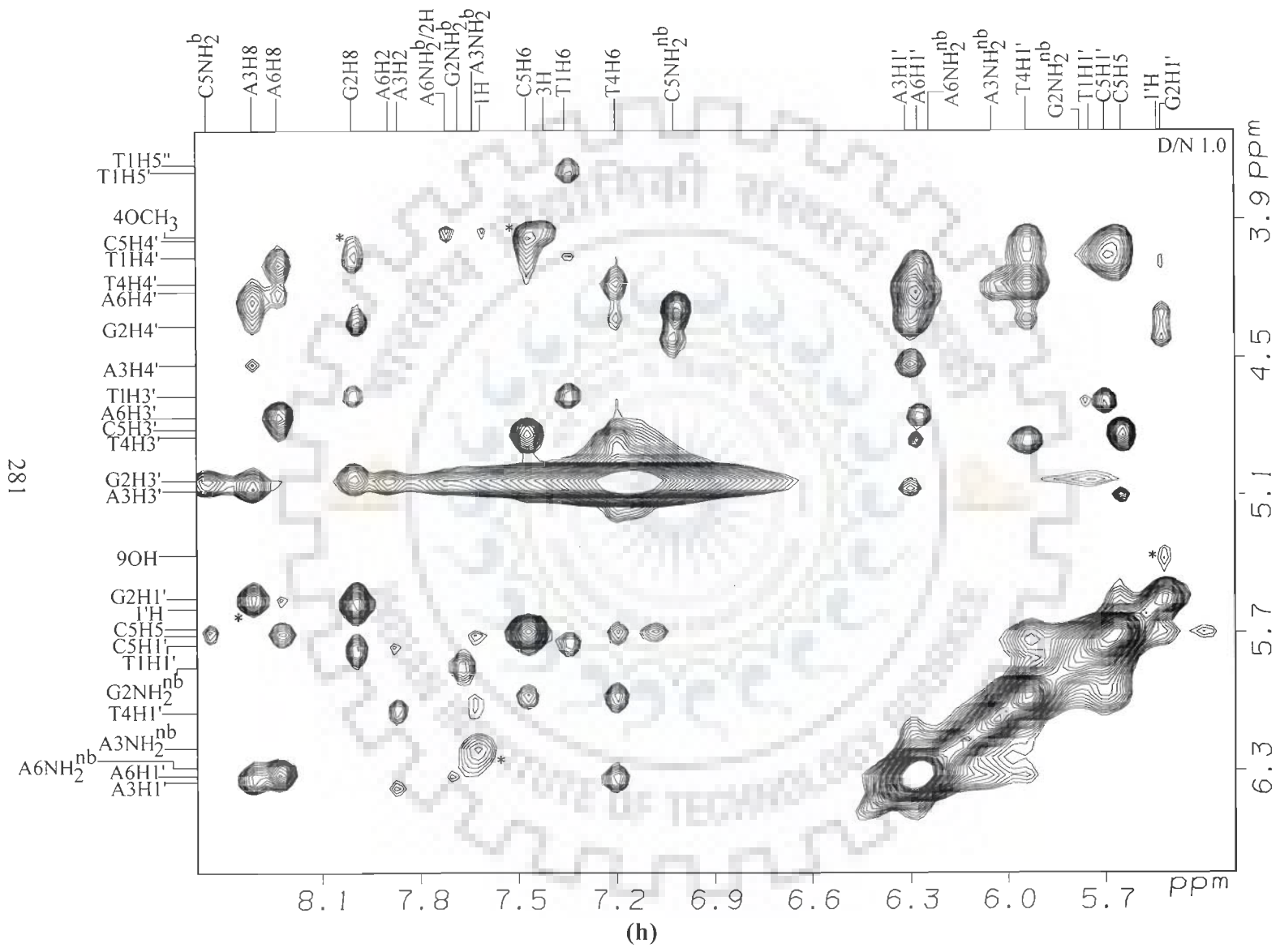




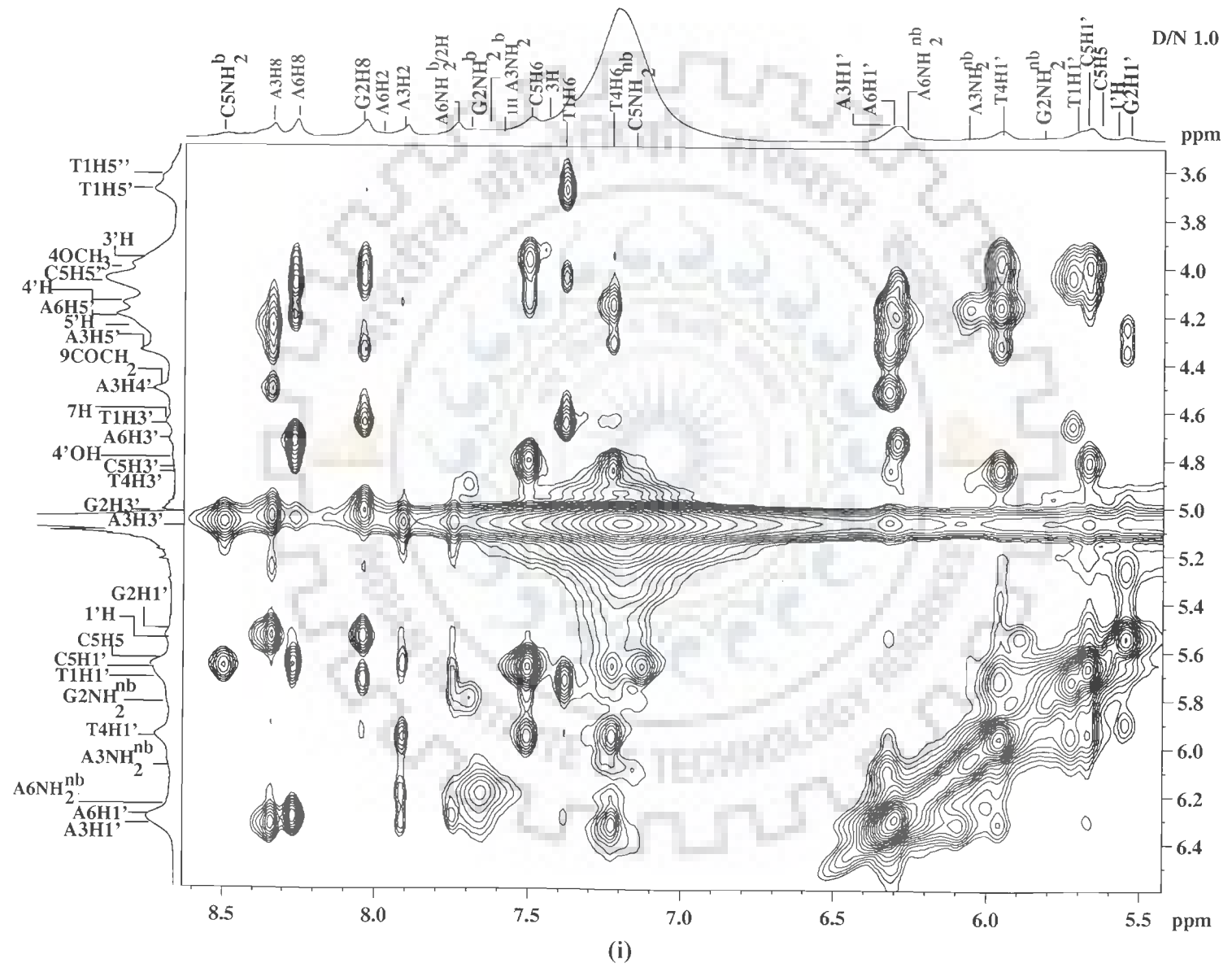
280

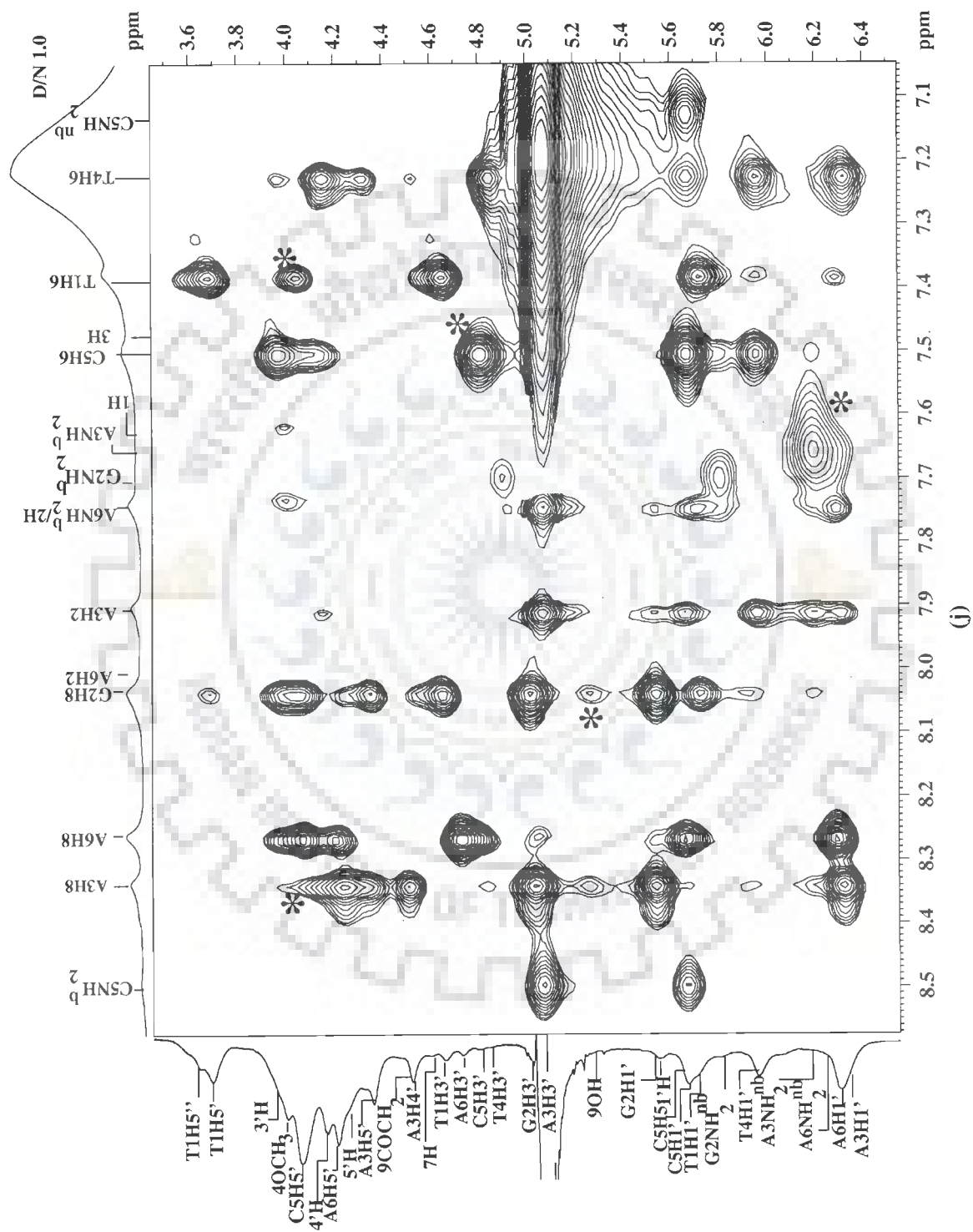


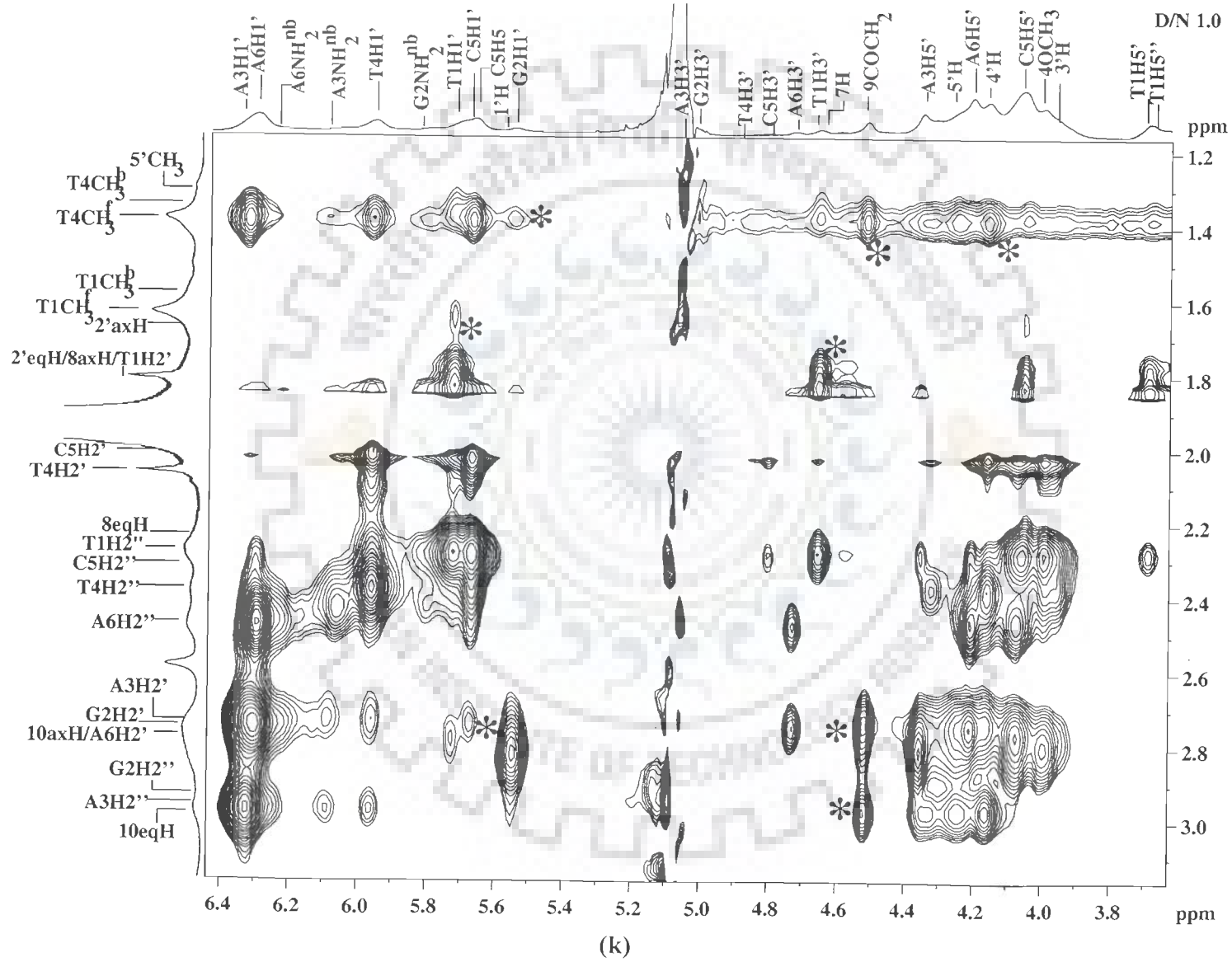
(g)

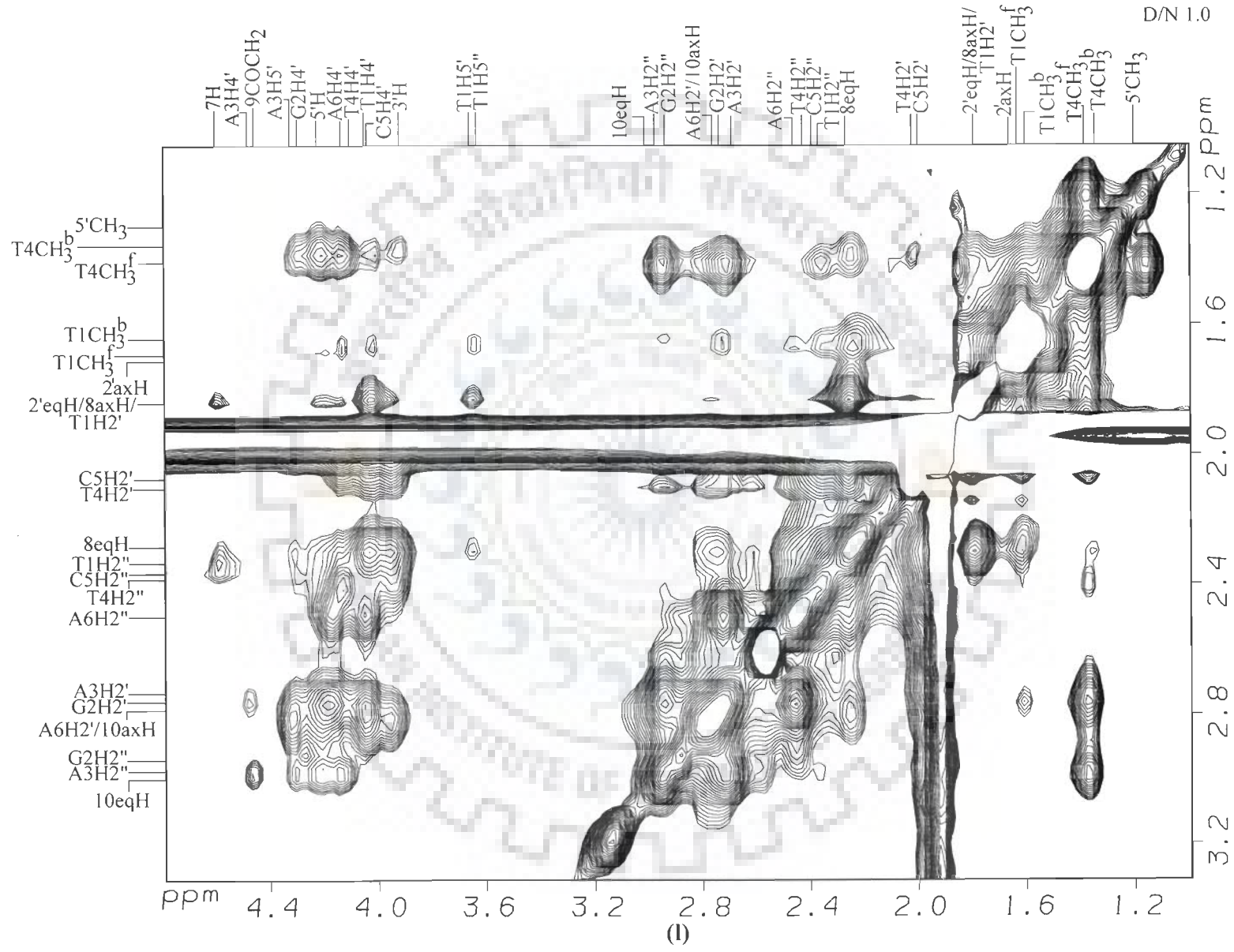


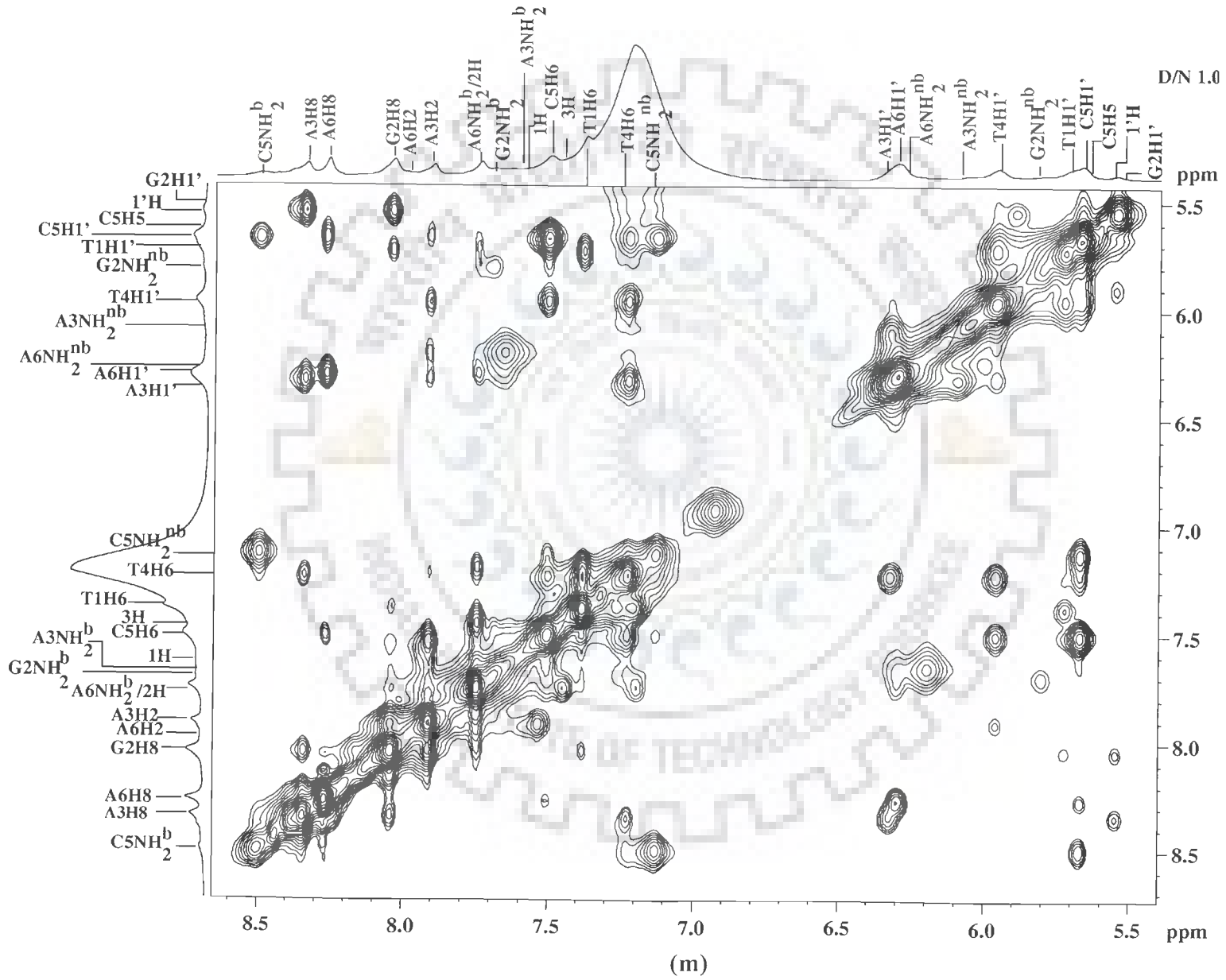
(h)











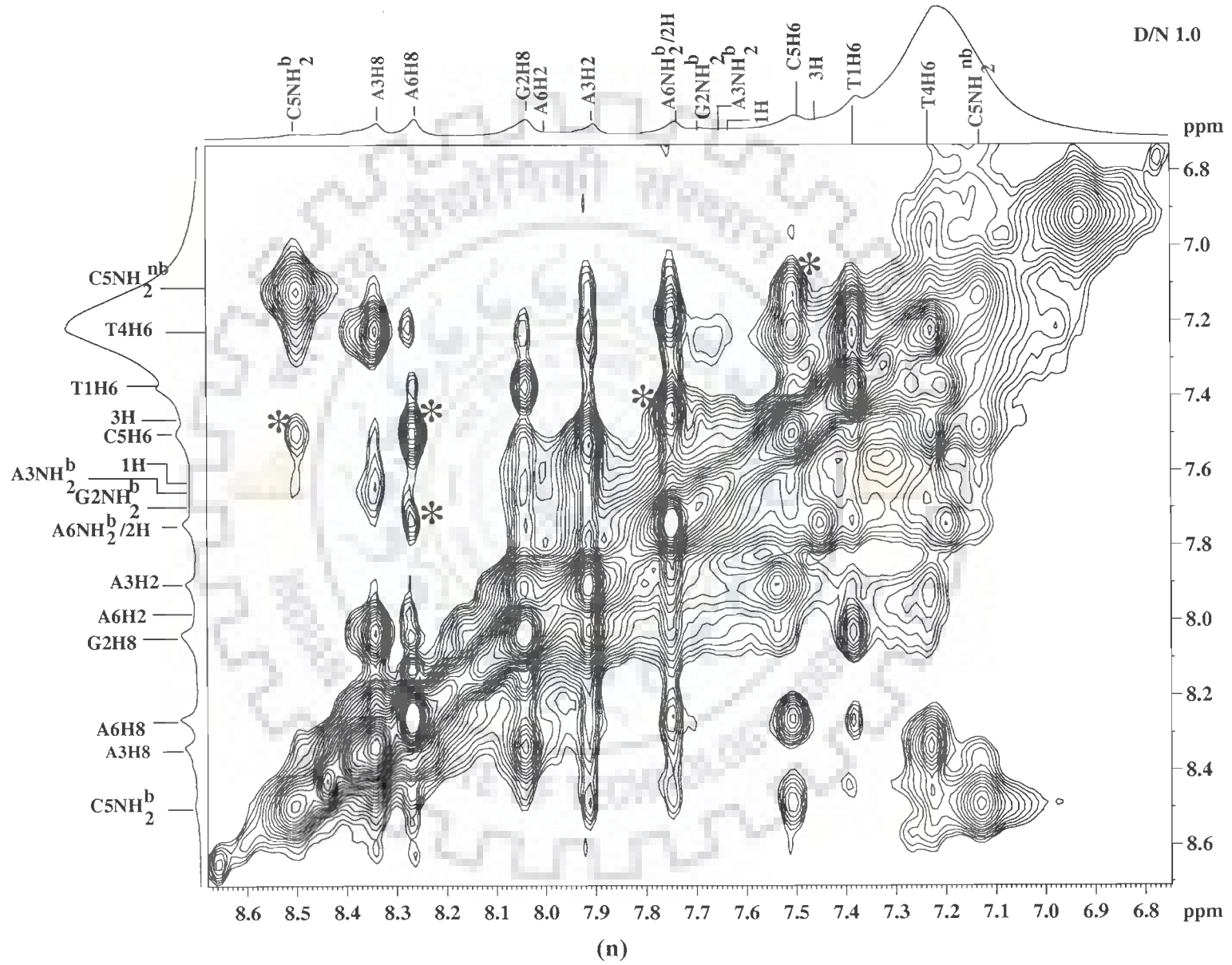


Table 7: Interproton distances (Å) obtained from intranucleotide NOE connectivities (d_i) within sugar protons of hexanucleotide of the drug-DNA complex at D/N = 1.0 at 275 K estimated from NOESY spectra (Fig. 8k, l, o) using C5H6-C5H5 = 2.45 Å as a standard reference. Overlap of peaks is indicated as o. – indicates absence of cross peak.

Protons	T1	G2	A3	T4	C5	A6
H1'-H2'	2.84	2.82	2.81	2.82	2.80	2.85
H1'-H2''	2.18	2.19	2.20	2.20	2.21	2.18
H1'-H3'	3.84	-	3.74	3.54	3.65	3.69
H1'-H4'	o	3.30	3.03	o	o	o
H2'-H3'	2.32	2.30	o	o	2.32	2.30
H2''-H3'	2.58	2.50	2.51	2.52	2.55	2.50
H2'-H4'	3.59	3.58	3.65	o	3.60	3.57
H2''-H4'	3.08	3.15	3.62	3.10	3.01	3.12
H2'-H2''	1.81	1.82	1.80	o	o	1.83
H3'-H4'	2.52	o	2.58	2.55	2.54	2.60
H5'-H5''	1.82	o	o	o	o	o

Table 8: Interproton distances (Å) obtained from intra nucleotide NOE connectivities (d_i) of base to sugar protons of nucleic acid in drug-DNA complex at D/N = 1.0 at 275 K estimated from NOESY spectra (Fig. 8e-j) using C5H6-C5H5 = 2.45 Å as a standard reference. – indicates absence of cross peak.

Protons	T1	G2	A3	T4	C5	A6
H8/H6-H1'	3.81	3.80	3.78	3.79	o	3.74
H8/H6-H2'	3.41	o	2.22	2.50	2.08	2.28
H8/H6-H2''	4.04	o	3.62	3.65	3.68	3.34
H8/H6-H3'	3.80	3.78	3.76	3.72	3.75	3.75
H8/H6-H4'	3.80	3.75	3.09	3.67	3.11	3.15
H8/H6-H5'	2.54	3.92	3.37	2.80	2.33	2.23
H8/H6-H5''	3.42	2.85	2.84	3.03	2.03	3.18
H8/H6-CH ₃ ^f	1.89	-	-	2.04	-	-
H8/H6-CH ₃ ^b	2.29	-	-	2.87	-	-

Table 9: Some of the inter residue sequential NOE cross peaks (ds) of nucleotide protons in the drug-DNA complex observed in NOESY spectra in the drug - DNA complex at Drug/DNA ratio (D/N) = 1.0, 1.5 and 2.0 at 275 K. The very strong (ss), strong (s), medium (ws), weak (w), very weakly (ww) intense cross peaks correspond to distances in the range ss 1.8 - 2.5 Å, s 2.5 - 3.0 Å, ws 3.0 - 3.5 Å, w 3.5 - 4.0 Å, ww 4.0 - 5.0 Å, respectively in the NOESY spectra, Fig. 8e-o. Overlap of cross peaks is indicated as o.

Inter-residues Sequential peaks	D/N 1.0	D/N 1.5	D/N 2.0	Inter-residues Sequential peaks	D/N 1.0	D/N 1.5	D/N 2.0
G2H8-T1H1'	ww	ww	-	T4H6-A3H2''	s	s	s
G2H8-T1H2'	-	-	-	T4H6-A3H3'	s	ws	s
G2H8-T1H2''	-	-	-	T4H6-A3H8	s	s	s
G2H8-T1CH ₃	-	-	-	T4CH ₃ -A3H8	ws	w	w
G2H8-T1H6	w	ww	-	C5H6-T4H1'	s	s	ws
G2H1'-T1H6	-	-	-	C5H6-T4H2''	s	s	s
G2H8-T1H3'	ww	-	-	C5H6-T4H2'	s	s	s
G2H5''-T1H1'	-	-	-	C5H6-T4H3'	s	s	s
G2H2'-T1H2''	-	-	-	C5H5-T4H6	ws	w	w
G2H5''-T1H2''	-	-	-	C5H5-T4H4'	w	w	s
G2H5''-T1H4'	-	-	-	C5H5-T4H5'	ws	ws	ws
A3H8-G2H1'	s	s	ws	C5H5-T4CH ₃	w	w	w
A3H8-G2H2'	ws	ws	s	A6H8-C5H6	ww	ww	-
A3H8-G2H2''	ws	ws	s	A6H8-C5H1'	w	w	-
A3H8-G2H8	s	s	s	A6H8-C5H2''	ww	ws	-
T4H6-A3H1'	s	s	s	A6H8-C5H2'	w	ws	-
T4H6-A3H2'	s	s	s	A6H8-C5H3'	ww	w	-

Table 10: Some of the inter-proton distances within the nucleic acid in drug-DNA complex at various D/N ratios estimated from NOESY spectra (Fig. 8a-o) at 275 K using C5H6-C5H5 = 2.45 Å as a standard reference. The corresponding distances in standard B- DNA are also shown here for reference.

	Standard B- DNA	1.0 Complex	1.5 Complex	2.0 Complex
ds peaks Distance (Å)				
G2N1H ^b -T1N3H ^b	4.0	-	-	-
G2N1H ^b -T1H6	5.6	ww	-	-
G2N1H ^b -T1H1'	5.2	-	-	-
G2N2H ₂ ^b -T1H1'	4.9	-	-	-
G2N1H ^b -T1H2'	-	-	-	-
G2N1H ^b -T1H2''	-	-	-	-
A3N6H ₂ ^b -G2N1H ^b	4.5	ww	ww	-
A3H2-G2N1H ^b	3.7	w	ww	-
A3H2-G2N2H ₂ ^b	3.5	ws	ws	w
T4N3H-A3H2	4.0	ws	w	w
T4CH ₃ ^b -A3H2'	-	ws	ww	-
T4CH ₃ ^f -A3H8	5.6	s	ws	ws
T4CH ₃ ^b -A3H8	-	w	w	w
T4CH ₃ ^f -A3H2'	-	s	ww	-
T4CH ₃ ^f -A3H2''	-	s	ww	-
T4CH ₃ ^f -A3H1'	-	ws	w	-
T4CH ₃ ^b -A3H1'	-	w	w	ww
T4CH ₃ ^f -A3N6H ₂ ^{nb}	3.9	-	w	-
C5H6-T4CH ₃ ^f	2.7	w	w	ww
C5H6-T4CH ₃ ^b	-	-	w	ww
C5N4H ₂ ^{nb} -T4N3H	5.5	-	ww	ww
C5N4H ₂ ^b -T4N3H	3.9	-	-	-
C5N4H ₂ ^{nb} -T4CH ₃ ^f	4.8	ws	w	ww
C5N4H ₂ ^{nb} -T4CH ₃ ^b	-	-	w	ww
C5N4H ₂ ^b -T4CH ₃ ^f	5.1	s	w	-
C5N4H ₂ ^b -T4CH ₃ ^b	-	-	ww	-
dps				
T1N3H-C5N4H ₂ ^b	2.9	-	-	-

(contd.)

(contd.)

T1N3H-C5N4H ₂ ^{nb}	-	-	-	-
G2N1H ^b -A6H2''	-	-	-	-
G2N1H ^f -A6H2''	-	-	-	-
G2N1H ^f -A6N2H ₂ ^b	4.1	w	ww	-
G2N1H ^f -A6N2H ₂ ^{nb}	5.0	ww	-	-
G2N2H ₂ ^{nb} -A6N2H ₂ ^b	4.1	w	w	ww
G2N1H ^f -T4CH ₃ ^f	-	ww	-	-
A3N6H ₂ ^b -C5N4H ₂ ^b	3.6	-	-	-
T4N3H-T4N3H	2.9	s	s	s
T4N3H-G2N1H	3.6	-	ws	-
T4CH ₃ ^f -T4H6	-	s	w	w
T4CH ₃ ^b -T4H6	-	ws	w	w
T4CH ₃ ^f -T4H2'	-	ws	-	-
T4CH ₃ ^f -T4H2''	-	ws	-	-
dpi peaks				
T1N3H-A6H2	2.8	-	-	-
T1N3H-A6N6H ₂ ^b	2.3	ww	ww	-
T1N3H-A6N6H ₂ ^{nb}	3.9	-	-	-
G2N1H ^f -C5N4H ₂ ^{nb}	4.0	w	w	-
A3H2-T4N3H ^f	2.8	ss	s	s
A3N6H ₂ ^{nb} -T4N3H ^f	3.8	s	ws	ws
A3N6H ₂ ^b -T4N3H ^f	2.5	s	ws	ws
C5N4H ₂ ^b -G2N1H	2.5	-	ww	-
di peaks				
G2N1H-G2N2H ₂ ^{b/nb}	2.3 ^b / 3.4 ^{nb}	w	w	-
A3H2-A3N6H ₂ ^{nb}	5.2	w	-	-
A3H2-A3N6H ₂ ^b	4.4	w	ww	-
A3N6H ₂ ^b -A3N6H ₂ ^{nb}	1.7	ss	s	ws
A3N6H ₂ ^{b/nb} -A3H8	5.1 ^b / 4.8 ^{nb}	ww	-	-
T4N3H-T4CH ₃	4.9	ww	ww	ww
C5N4H ₂ ^{b/nb} -C5H5	3.5 ^b / 2.4 ^{nb}	s/s	ww/w	ww/w
C5N4H ₂ ^{b/nb} -C5H6	5.3 ^b / 4.6 ^{nb}	ws	ww	ww

Table 11: Intensities of NOE cross peaks (di) within the drug molecule in the drug-DNA complex at D/N = 1.0 and 2.0 at 275 K. The very strong (ss), strong (s), medium (ws), weak (w) and very weakly (ww) intense cross peaks refer to distances in the range ss 1.8 – 2.5 Å, s 2.5 – 3.0 Å, ws 3.0 – 3.5 Å, w 3.5 – 4.0 Å, ww 4 – 5 Å, respectively from the NOESY spectra, Fig. 8a-o. Overlap of peaks is indicated as o.

J coupled Protons	Uncomplexed drug	D/N = 1.0	D/N = 1.5	D/N = 2.0	Ring A with sugar Protons	Uncomplexed drug	D/N = 1.0	D/N = 1.5	D/N = 2.0
1H-2H	ss	s	ws	ws	7H-1'H	ws	-	-	-
2H-3H	ss	s	ws	ws	7H-3'H	ws	-	-	-
1'H-2' _{ax} H	o	-	-	-	7H-5'H	s	w	w	w
1'H-2' _{eq} H	o	-	w	w	7H-4'H	s	-	o	o
3'H-4'H	ss	s	ws	ws	7H-5CH ₃	ww	-	w	-
4'H-5'H	ss	s	ws	ws	8 _{ax} H-1'H	o	o	o	o
3'H-2' _{ax} H	o	ws	w	-	8 _{ax} H-3'H	o	w	o	o
3'H-2' _{eq} H	o	ws	w	w	8 _{ax} H-4'H	o	ww	o	w
2' _{ax} H-2' _{eq} H	o	s	s	s	8 _{ax} H-5'H	o	w	o	w
5'H-5'CH ₃	s	-	s	s	8 _{ax} H-5'CH ₃	w	-	ws	ws
7H-8 _{ax} H	s	s	-	-	8 _{eq} H-1'H	ws	w	w	-
7H-8 _{eq} H	w	s	ws	ws	8 _{eq} H-3'H	ws	ws	-	-
8 _{ax} H-8 _{eq} H	ss	ss	s	s	8 _{eq} H-4'H	ws	ws	-	-
10 _{ax} H-10 _{eq} H	ss	ss	s	s	8 _{eq} H-5'H	ws	w	-	-
Within Ring D Protons					8 _{eq} H-5'CH ₃	w	w	-	w
2H-4OCH ₃	ws	ws	ws	ws	9COCH ₂ -3'H	w	ws	w	w
1H-4OCH ₃	w	w	w	ws	9COCH ₂ -1'H	w	-	-	w
3H-4OCH ₃	s	s	s	s	9COCH ₂ -5'H	s	s	w	ws
Within Sugar Protons					Within Ring A Protons				
1'H-3'H	ws	ws	w	-	10 _{ax} H-8 _{ax} H	ws	s	-	-
1'H-4'H	w	-	ws	-	10 _{ax} H-8 _{eq} H	s	ss	-	-
1'H-5'H	w	s	ws	ws	10 _{eq} H-8 _{ax} H	-	w	-	-
1'H-5CH ₃	ww	-	-	-	10 _{eq} H-8 _{eq} H	-	-	w	w
3'H-5'H	o	o	o	o	10 _{eq} H-9COCH ₂	ws	ws	w	-
3'H-5'CH ₃	ww	-	w	-	10 _{ax} H-9COCH ₂	s	s	w	w
4'H-2' _{ax} H	o	-	o	ws	8 _{ax} H-9COCH ₂	-	w	ws	-
4'H-2' _{eq} H	o	-	o	ws	8 _{eq} H-9COCH ₂	-	-	ws	-
4'H-5'CH ₃	ws	-	ws	ws					

Table 12: Relative intensities of intermolecular NOE connectivities between hexanucleotide and the drug molecule in the drug–DNA complex at drug to DNA ratio D/N = 1.0, 1.5 and 2.0 from NOESY spectra (Fig. 8a-o) at 275 K. The very strong (ss), strong (s), medium (ws) and weakly (w) intense cross peaks correspond to distance of ss 1.8 – 2.5 Å, s 2.5 – 3.0 Å, ws 3.0 – 3.5 Å, w 3.5- 4.0 Å, ww 4 - 5 Å. '-' indicates absence of peaks due to broadening.

S.No	Intermolecular Cross peak	D/N =1.0	D/N =1.5	D/N =2.0	S.No	Intermolecular Cross peak	D/N = 1.0	D/N = 1.5	D/N = 2.0
1.	T1CH ₃ ^b -7H	w	-	-	30.	C5H6-4OCH ₃	ws	ws	ws
2.	T1H2''/C5H2''-7H	ws	ws	-	31.	A6H1'/A6NH ₂ ^{nb} -1H	ws	ws	ws
3.	G2H2''/A3H2''-9COCH ₂	w	w	w	32.	C5H1'/C5H5-3'H/4OCH ₃	ws	ws	ws
4.	T4CH ₃ ^f -5'H	ws	-	-	33.	A3H8-5'CH ₃	w	w	ws
5.	T4CH ₃ ^b -5'H	ws	ws	ws	34.	A3H8-10eqH	ww	w	w
6.	T4CH ₃ ^f -3'H	w	-	-	35.	G2H8-8eqH	ww	ww	ww
7.	T4CH ₃ ^b -3'H	ww	ww	-	36.	T1CH ₃ ^b -1H	ws	ws	ws
8.	A3H2''-5'H	ww	ww	ww	37.	T1CH ₃ ^b -3H	ws	ws	ws
9.	A3H2''-5'CH ₃	ww	ww	-	38.	T4H6-5'CH ₃	ww	ww	ww
10.	T1CH ₃ ^f -10eqH	ws	ww	ww	39.	A6H8-3H	w	ww	ww
11.	T1CH ₃ ^b -10eqH	w	ww	ww	40.	G2H8-1H	w	w	w
12.	A3H2''-5'CH ₃	ws	ww	ww	41.	C5NH ₂ ^{nb} -3H	w	ww	ww
13.	T4CH ₃ ^f -5'CH ₃	ww	ww	-	42.	T1H6-1H	ww	ww	ww
14.	T4CH ₃ ^b -5'CH ₃	ww	ww	-	43.	A3H5'-1'H	ww	ww	ww
15.	T1N3H ^b -11OH	ww	ww	-	44.	C5H5''-5'H	ww	ww	ww
16.	A6H2-6OH	ww	-	-	45.	T1H5'/T1H5''-8eqH	ws	ww	-
17.	T1H2''-11OH	ws	-	-	46.	G2H4'-8eqH	w	-	-
18.	G2H3'-11OH	w	-	-	47.	C5H3'-8eqH	s	w	ww
19.	C5H5/C5H1'-11OH	ws	ws	-	48.	A3H3'-2'axH	w	ww	-
20.	A6H5''-11OH	-	-	w	49.	G2H2''-9COCH ₂	w	ww	ww
21.	T1N3H ^b -7H	-	-	w	50.	A3H1'-4'OH	w	ww	ww
22.	T1N3H ^b -4OCH ₃	ww	-	-	51.	C5NH ₂ ^b -9COCH ₂	ww	-	-
23.	A6H8-4OCH ₃	ws	ws	ws	52.	T4H6-5'H	ww	ww	ww
24.	G2H8-9OH	ww	-	-	53.	C5NH ₂ ^b -5'H	ww	ww	ww
25.	C5H1'/C5H5-9OH	-	ww	ww	54.	T1H6-8eqH	s	-	-
26.	C5NH ₂ ^{nb} -9OH	-	w	w	55.	C5H6-8eqH	s	-	-
27.	G2H1'-9OH	ws	ws	ws	56.	A6H1'-3H	w	w	w
28.	G2H1'-1'H	w	ww	ww	57.	A6H8-1H	w	w	w
29.	A3H8-1'H	ww	ww	ww	58.	G2NH ^b -11OH	ws	ws	ws

Table 13: Inter-proton distances (Å) obtained from intermolecular NOE connectivities between hexanucleotide and the drug molecule in the drug–DNA complex from NOESY spectra (Fig. 8a-o) at 275 K. (Distances are taken for rMD model from intramolecular and intermolecular peaks of drug and DNA).

S.No.	Intermolecular Cross peak	NMR (Å)	rMD (Å)
1.	T1CH ₃ ^b -7H	3.50	3.53
2.	T4CH ₃ ^b -5'H	3.20	3.31
3.	T4CH ₃ ^b -3'H	3.80	3.95
4.	T4CH ₃ ^f - 5'CH ₃	4.10	4.11
5.	T4CH ₃ ^b - 5'CH ₃	4.15	4.11
6.	T1N3H ^b -11OH	4.30	4.15
7.	A6H2-6OH	4.50	4.54
8.	T1H2 ^m -11OH	3.30	3.12
9.	G2H1'-9OH	2.70	2.58
10.	A6H8-3H	4.10	4.17
11.	T1N3H ^b -7H	4.35	4.16
12.	A6H8-4OCH ₃	3.45	3.35
13.	C5NH ₂ ^b -3H	3.70	3.80
14.	T1H6-1H	4.85	4.75
15.	A3H5'-1'H	4.60	4.59
16.	A3H1'- 4'OH	2.50	2.30
17.	C5NH ₂ ^b -9COCH ₂	4.60	4.67
18.	T4H6-5'H	4.75	4.79
19.	C5NH ₂ ^b -3H	3.50	3.43
20.	C5H6-4OCH ₃	3.25	3.17
21.	A6H1'-1H	4.50	4.61

Table 14 a: Comparison of deoxyribose conformation (pseudorotation °)

	Present Work		CGA+ mor ^a	CGA+ adm ^b	CGA+ dnm ^c	CpG+ dnm ^d
	NMR	rMD				
T1	153-162	138	143	158	160	153
G2	180	165	136	141	142	135
A3	153-162	150	73	129	131	
T4	144	125	130	124	122	
C5	153-162	179	119	151	141	
A6	162	176	142	161	165	

^a CGATCG + morpholinodoxorubicin (Mazzini et al., 1998)

^b CGATCG + adriamycin (Frederick et al., 1990)

^c CGATCG + daunomycin (Frederick et al., 1990)

^d CpG + daunomycin (Barthwal et al., 1994)

Table 14b: Comparison of glycosidic bond rotation ($^{\circ}$)

	Present Work			CGA+mor ^a	CGA+adm ^b
		NMR	rMD		
T1	anti	-150	-146	-125, -159	148
G2	High anti	-105	-75	-131, -92	-90
A3	Anti	-105 to -140	-128	-148, -146	-130
T4	Anti	-105 to -140	-112	-141, -123	-113
C5	High anti	-90	-75	-105, -112	-90
A6	High anti	-90	-88	-104, -110	-90

^a CGATCG + morpholinodoxorubicin (Mazzini et al., 1998)

^b CGATCG + adriamycin (Frederick et al., 1990)

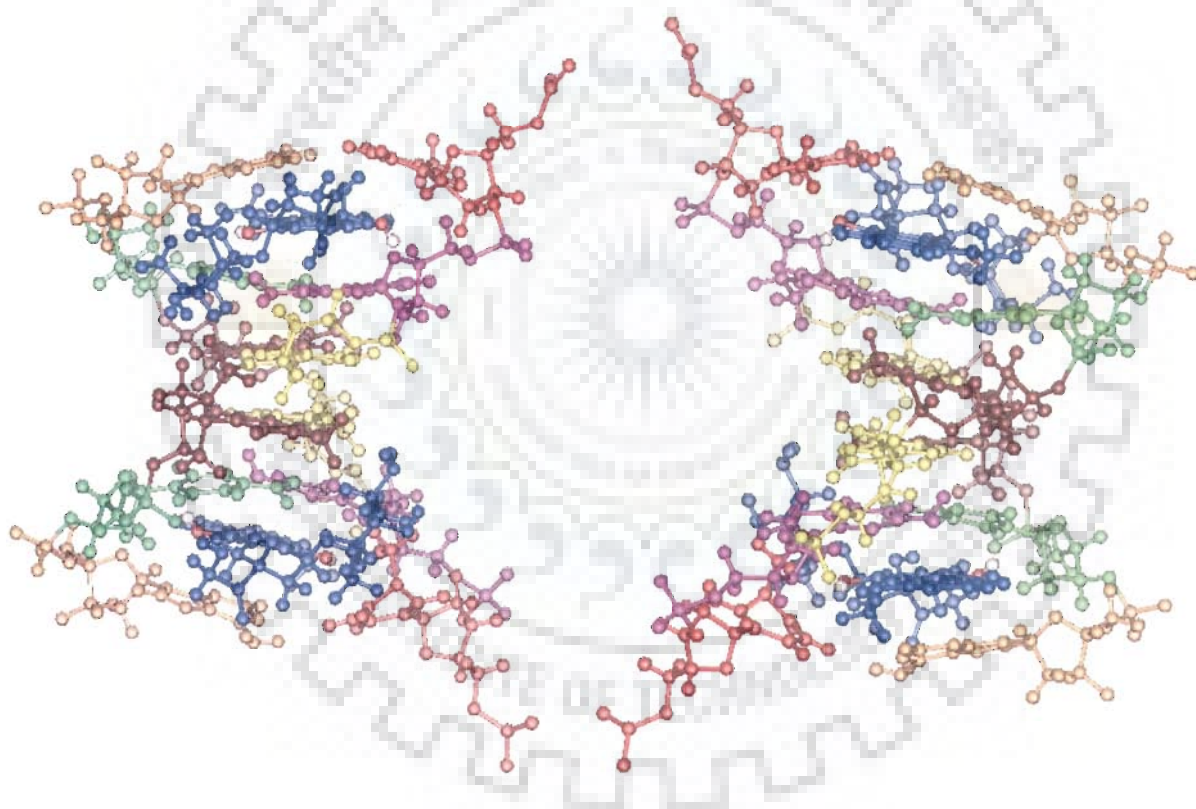


Fig. 9: The stereoview of final rMD structure of d-(TGATCA)₂-adriamycin derived from the NOE data.

complexes with d-(CGATCG)₂ (Wang et al., 1987; Jain et al., 2005) and d-(TGATCA)₂. But various other detailed structural features appear to be unique to the drug-DNA complex studied. This reflects on drug-specific or DNA sequence specific interactions at molecular level and is relevant to differences in molecular basis of their action.

(B) TCSPC Analysis: Time-resolved fluorescence measurements

Time resolved fluorescence decays were obtained by the Time-Correlated Single-Photon Counting method on the Spectrofluorimeter (model FluoroLog-TCSPC, make HORIBA Jobin Yvon Spex), used for the life time measurement study. The excitation source, $\lambda_{\text{ex}} = 470$ nm was a fixed-wavelength NanoLED. The emission was detected at the emission wavelength, $\lambda_{\text{em}} = 593$ nm. The fluorescence emission of the drug and its complex with d-(TGATCA)₂ was counted by a micro channel plate photo multiplier tube, after passing through the monochromator and processed through constant fraction discriminator (CFD), time-to-amplitude converter (TAC) and multi channel analyzer (MCA). All measurements were performed at 298 K in water. The fluorescence decay was obtained and all the parameters were systematically analysed and processed by the software program DAS provided by FluoroLog-TCSPC instrument.

From TCSPC analysis, it is seen that the fluorescence decay curve profile of free drug was monoexponential according to the equation $I(t) = B \exp(-t/\tau)$ where B is the pre-exponential factor and τ is the fluorescence lifetime of the free drug. However, in the presence of DNA (intercalated form), the drug exhibited biexponential function corresponding to the equation $I(t) = B_1 \exp(-t/\tau_1) + B_2 \exp(-t/\tau_2)$, where B_1 and B_2 are the pre-exponential factors and τ_1 and τ_2 are the fluorescence lifetimes of the fluorophores. The biexponential function with two lifetimes (τ_1 and τ_2) and two amplitudes (B_1 and B_2), indicate the presence of both free and intercalated drug correspondingly (Qu et al, 2001; Johnson et al, 2003).

The lifetime of free adriamycin is found to be $\tau = 1.03$ ns and amplitude is $B = 0.09$. On the formation of adriamycin-d-(TGATCA)₂ 2:1 complex, $\tau_1 = 0.79$ ns, $\tau_2 = 1.43$ ns; $B_1 = 0.07$ and $B_2 = 0.03$. In the present study the smaller B_1 and higher B lifetime components representing the intercalated and free form of the drug. The τ_1 value ($\tau_1 = 0.79$ ns) of the complex is less than that of τ value ($\tau = 1.03$ ns) of free adriamycin, showing that there is shortening of the decay time of adriamycin due to intercalation (Table 15, Fig. 10). This clearly indicates the result of complexation of the DNA base with the drug and is due to electron transfer from the d-(TGATCA)₂ to adriamycin. The $\tau_2 = 1.43$ ns component may reflect the other conformations of unprivileged structures. Thus there is clear indication that adriamycin is intercalating in the d-(TGATCA)₂ hexamer sequence and forming the complex.

(C) Diffusion Ordered Spectroscopy (DOSY) studies on adriamycin-d-(TGATCA)₂ complex

DOSY is a tool to distinguish between the complexed and noncomplexed forms in a mixture due to the differences in their relative diffusion coefficient values. It can also be utilized to obtain information about the relative strength of H-bonds, and about those components that show stronger binding affinities to a particular ligand in a pool of mixture of molecules. The observed diffusion is an average of the populations of the diffusion of the complexed and noncomplexed forms in equilibrium. A change in the chemical shift does not provide a sufficient indication about the strength of interaction between the components, which could be due to other effects influencing the chemical shift but the DOSY plots provide a better insight about the strength of such interactions which are clearly manifested in the diffusion dimension.

DOSY spectra of adriamycin-d-(TGATCA)₂ complex of 2:1 D/N ratio is compared with that of adriamycin (Fig. 22b in chapter 4) and d-(TGATCA)₂ alone at 275 (Fig. 11a) and 298 K (Fig.

Table 15: Lifetimes parameters of Adriamycin fluorescence and its 2:1 complex with d-(TGATCA)₂ in water at 298 K.

samples	Lifetime decay (ns)	Amplitude	Lifetime decay (ns)	Amplitude
	τ_1	B_1	τ_2	B_2
Adriamycin	1.03	0.09	-	-
d-(TGATCA) ₂ -Adriamycin 2:1 complex	0.79	0.07	1.43	0.03

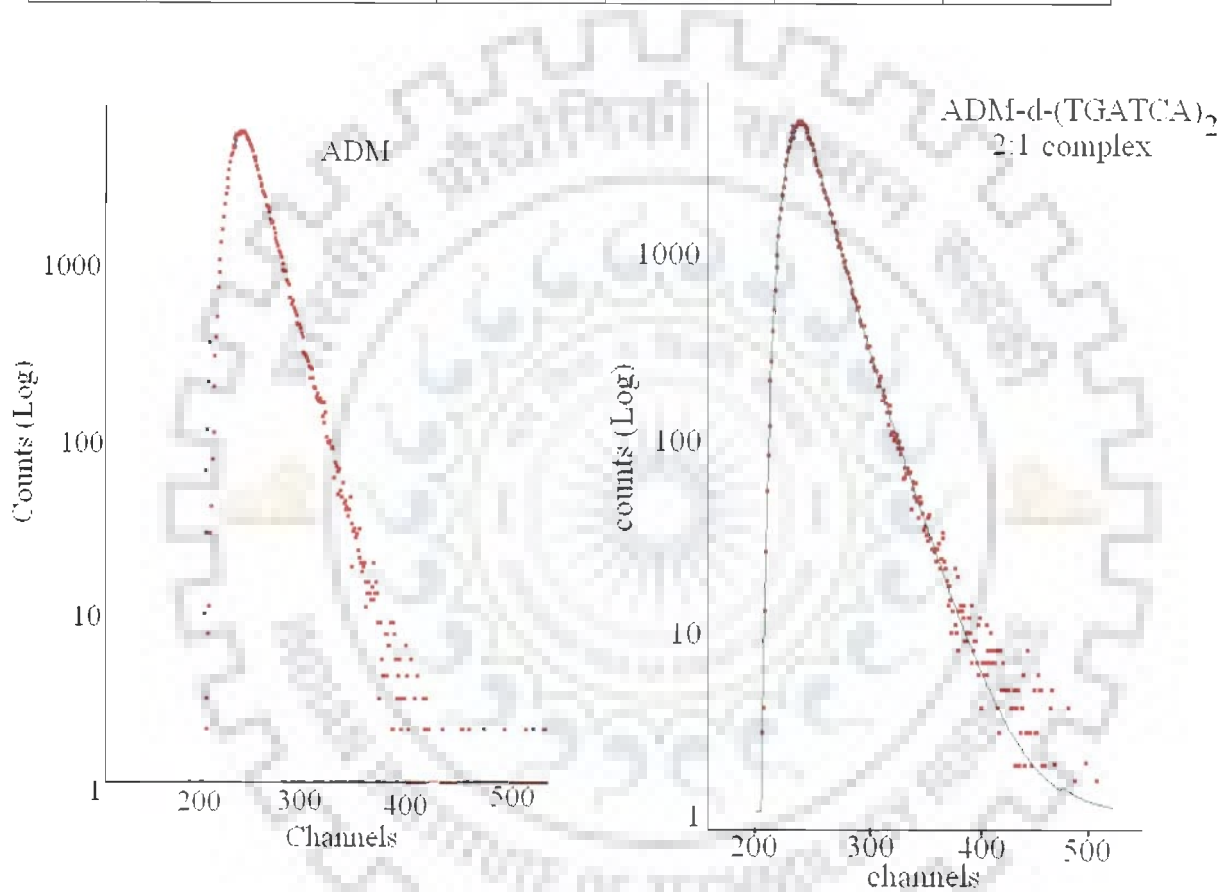
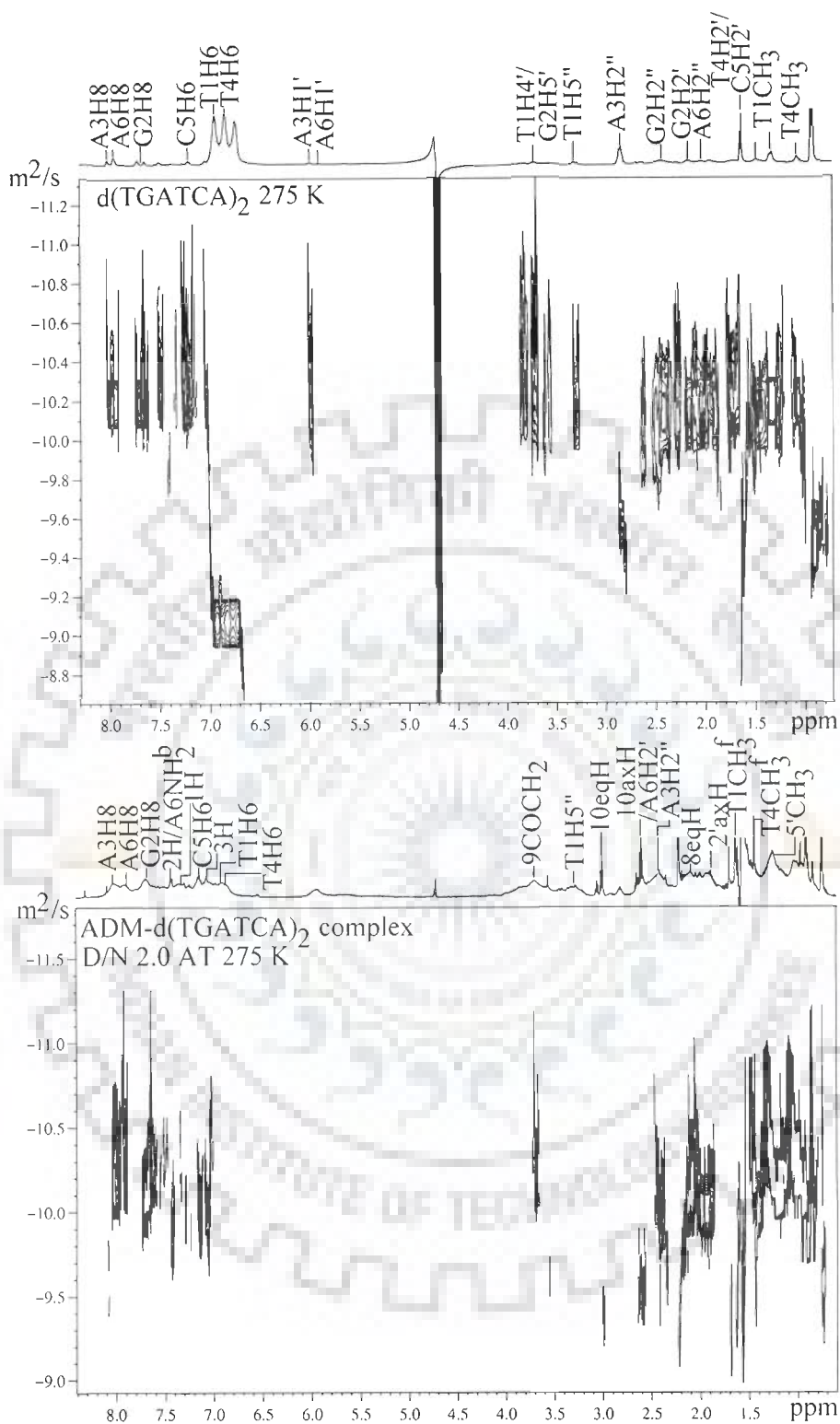
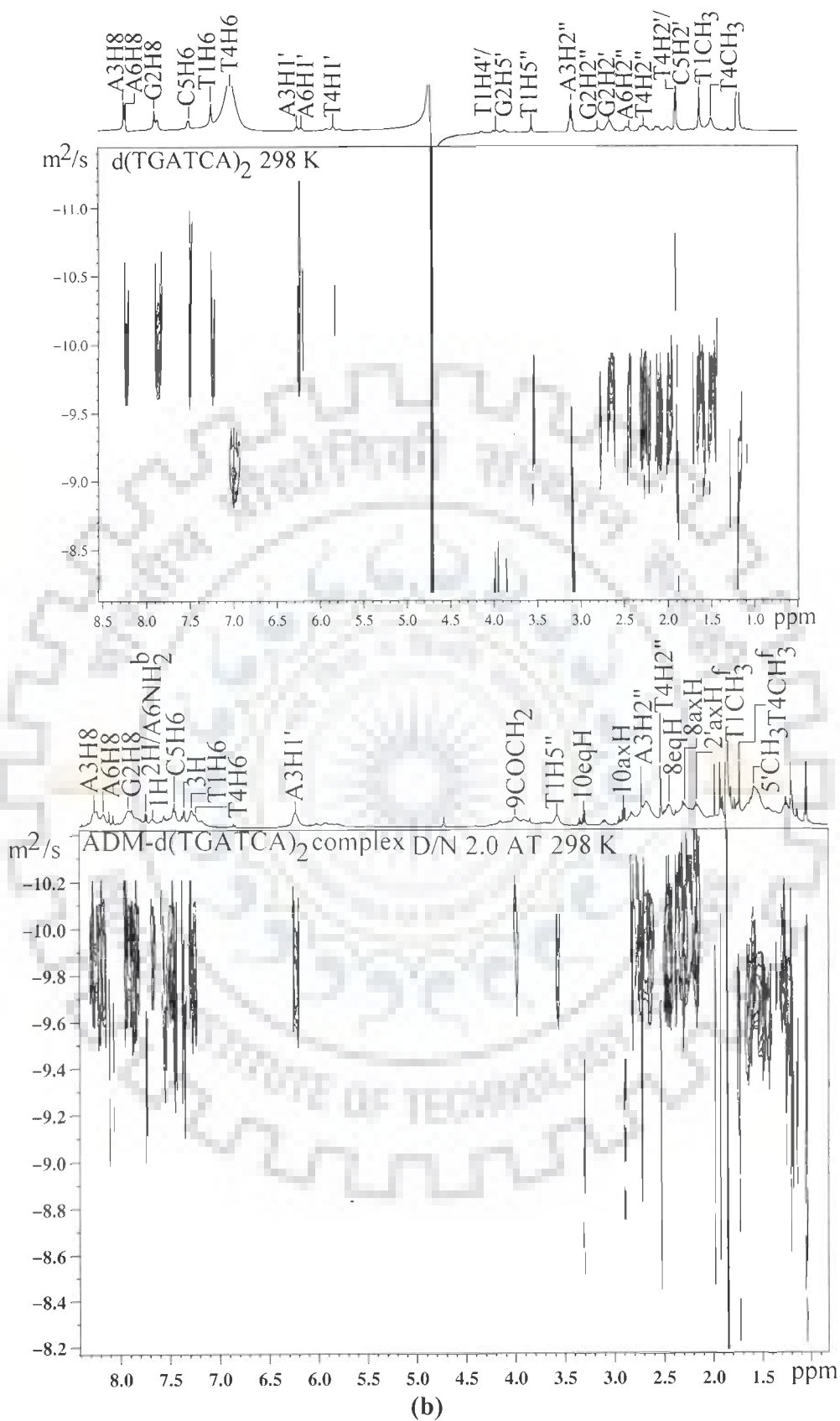


Fig. 10: Fluorescence lifetime decay measurement profile of adriamycin and 2:1 adriamycin-d (TGATCA)₂ complex.



(a)

Fig. 11: DOSY of $d\text{-(TGATCA)}_2$ and adriamycin- $(\text{TGATCA})_2$ complex in D_2O at (a) 275 (b) 298 K.



11b). On complex formation, the diffusion coefficient value decreases of the drug resonances in the complex in comparison to that in the drug alone. The corresponding values of the drug resonances in complex and the drug alone are 1.33×10^{-11} and 1.63×10^{-10} m²/s, respectively and that of d-(TGATCA)₂ in the complex and alone hexamer are 1.57×10^{-10} and 2.32×10^{-10} m²/s, respectively at 298 K. At 275 K, the diffusion coefficient value for the same hexamer signal for complexed and uncomplexed DNA are 3.17×10^{-11} and 7.46×10^{-11} m²/s, respectively, while that for bound and free drug resonance, the values are 7.11×10^{-11} and 1.04×10^{-10} m²/s, respectively. This is because of the interaction of the drug with DNA which slower the rate of diffusion, same is found with d-(TGATCA)₂ alone. However, only one set of peaks is present. This is due to averaging of the diffusion coefficients. The exchange is slower at 275 K in comparison to that obtained at 298 K on the diffusion time scale.

(D) Restrained Molecular Dynamics Studies

The nucleotides are labeled from T1 to A6 in the 5' to 3' direction on strand 1 and from T7 to A12 on strand 2 with T1 base paired to A12. The adriamycin molecules are numbered D13 and D14 and the atomic numbering scheme for the molecule is shown in Fig. 1b. The initial structure of d-(TGATCA)₂ was built using the biopolymer module in INSIGHT II, version 2005 (Accelrys Inc., San Diego, California) on Silicon Graphics Fuel workstation. The energy of the molecule was minimized using 1000 steps each of Steepest Descent and Conjugate Gradient to remove any internal strain due to short contacts in starting structure using CFF91 force field in DISCOVER software version 2005 (Accelrys Inc., San Diego, California). Dielectric constant was fixed as 1.0 for calculation of electrostatic interactions. Conformational search was performed using the following simulated annealing restrained molecular dynamics protocol. The molecule was heated to a temperature of 800 K in steps of 100 K so that the chances of molecule being trapped in

local minima become least and it can reach global minima. Molecular dynamics was carried out for 100 ps (1000 iterations with time step of 1 fs) at 800 K during which 100 structures were saved at regular intervals of 1 ps. Each of them was then slowly cooled at 300 K in steps of 100 K. The force constants for NOEs for strong (1.8 – 3.0 Å), medium (3.0 – 4.0 Å) and weak (4.0 – 5.0 Å) peaks were held constant as 25, 15 and 10 Kcal mole⁻¹ Å⁻², respectively. At the end of simulated annealing all the structures were minimized by 1000 steps of Steepest Descent until a predefined convergence limit of root mean square derivative of < 0.001 Kcal mole⁻¹ Å⁻¹ was reached.

The best-fit refined structure showing all atoms are given in Fig. 12 showing the front and side view of the complex. The drug-DNA complex is stabilized via close contacts which involve specific hydrogen bonding and van der Waal's interactions (Table 16). The 100 structures are saved at a regular interval of one ps during 100 ps molecular dynamics simulations. The various superimposed structures obtained by restrained molecular dynamics simulations are shown in Fig. 13. The root mean square deviation between the rMD structure and the starting structure is quite large but among various final structures is very low. This is generally acknowledged as an indication that convergence has been achieved. Table 17 indicates an assessment of refined structure in terms of energetics. The total energy of the final structure is 463 Kcal mole⁻¹, which is much lower than the initial B-DNA structure. The restraint energy has also been reduced from 477 Kcal mole⁻¹ to 377 Kcal mole⁻¹. Table 18 shows the pairwise as well as residue wise root mean square deviations (RMSD) of the complex. The starting structure was chosen as reference and the value of target RMSD is chosen to be zero.

Conformation of DNA

All helical parameters, backbone torsional angles and sugar conformations of the resulting rMD structures were thoroughly analysed with the program CURVES, version 5.1 (Lavery et al., 1996; Lavery et al., 1989). Plot of some helicoidal parameters (global, unless specified otherwise) as a function of residue position in the duplex is shown in Fig. 14(a-b) along with that for two classical structures of A-DNA and B-DNA. Among the base pair axis parameters, the x-displacement (dx) and y-displacement (dy) are found to vary to a large extent for all base pairs. Large displacements are generally observed in intercalated complexes (Nunn et al., 1991; d'Estaintot et al., 1992; Leonard et al., 1992). The base pairs are inclined at an angle (η) up to 8° , the inclination being larger at 5' end. The tip angle fluctuates along the base sequence. The variation in shear, stretch, stagger, and buckle is fairly large for the TG and CA base pairs at both the ends. It is noteworthy that in the X-ray crystal structure of the daunomycin and 4'-epiadriamycin with d-TGATCA (Nunn et al., 1991; d'Estaintot et al., 1992; Leonard et al., 1992) also, stagger is found to be more for TG and CA base pairs and large values of buckle due to intercalation have been reported. The values of buckle varies from $+10^\circ$ to -20° at the intercalation site which is in consistency with that reported by Trieb et al., that is $+15^\circ$ to -15° (Trieb et al., 2004). The propeller twist at either ends are negative and large, indicating that the ends are not having fraying effects. The inter-base parameters shift (Dx) and slide (Dy), vary in the range -0.62 to $+1.52$ Å. The rise per residue (Dz) is ~ 3.0 Å at A3pT4 base pair step while that at T1pG2 and C5pA6 base pair step increases up to 7.2 Å to accommodate drug chromophore. The intercalation results in large amount of tilt ($\tau = 9.46^\circ$ to -9.46°) in base pairs. The roll angle (ρ) varies within $\pm 11^\circ$. Positive roll opens the angle between the base pairs towards the minor groove; as a result a wider minor groove and bending towards major groove causing a curvature in the helix occurs. The large positive roll at G2pA3 ($+11^\circ$) and T4pC5

(+11°) steps also indicates reduced base stacking. This is due to the fact that intercalating anthracycline ring chromophore is oriented approximately perpendicular to the base pair axis in the helix, as found in the crystal structures of the complexes. The large negative values of the roll (-9°) for T1pG2 and C5pA6 base pair step is compensated by a decrease in propeller twist to -4° at T1pG2 and C5pA6 base pair step so as to prevent de-stacking of the bases. The local inter base parameters also show positive roll angle at both the ends of the helix and negative roll in the centre. The twist (Ω) varies in the range 27.0 - 39.0°. The twist angle values at the intercalation steps indicate that there is unwinding of DNA at these steps. Also there is unwinding of DNA at the steps adjacent to the intercalation steps. The unwinding of DNA at the site of intercalation is upto 12° and is consistent with that reported by viscosity techniques (Patcher et al., 1982). The width and depth of major groove is found to be 13.20 and 1.70 Å while the corresponding values for minor groove are 8.19 and 3.81 Å, respectively and their depth is lower than that in standard B-DNA structures. The wider minor groove presumably allows proximity of daunosamine sugar moiety.

The backbone torsional angles along with corresponding values for canonical B-DNA and A-DNA are plotted in Fig. 15. The torsional angles α , β and γ adopt gauche⁻, trans and gauche⁺ conformations, respectively. The torsional angle ζ , however, deviates from the normal gauche⁻ conformation and adopts a trans conformation for the G2 and C5 bases. This is due to the opening of base pairs at these sites. This is accompanied by a corresponding deviation in torsional angle ϵ for G2 and C5 bases to a lower negative value of -131° and -98°, respectively, as compared to a value to 155° found in B-DNA structures. The torsional angle, δ as well as pseudorotation phase angle P, is deviated from the normal range around C2' endo conformation. The glycosidic bond rotation, χ , of the DNA molecule measuring rotation of base around sugar

varies along base sequence. The χ angles are as follows: T1, -146° ; G2, -75° ; A3, -128° ; T4, -112° ; C5, -75° ; A6, -88° . On T1pG2 side of the backbone, the 2'-deoxythymidine residue on the 5'-end site changes the glycosyl angle from an anti (-98° in B-DNA) to a low anti value (-146°). At the same time by adjusting ε angle from a near trans (155° in B-DNA) to a somewhat lower value (121°), it allows the adjacent bases to separate from 3.4 to 6.4 Å.

On the T1pG2 side, both nucleotide units maintain the glycosyl angle at anti value (-146° , -75°). But the ε value is changed from 155° to 131° in the G2 residue; it is possible to separate the neighboring G2 and T1 bases to a distance of ~ 6.4 Å. This can be achieved by coupling it with the rotation of the phosphodiester linkage from a normal gauche-, gauche- conformation to a trans, gauche-, as observed in X-ray crystallography (Wang et al., 1987; Frederick et al., 1990; Moore et al., 1989; Williams et al., 1990) and NMR (Mazzini et al., 1998) structures of similar complexes. The change in phosphodiester linkage gets reflected as downfield shift in phosphorus-31 NMR spectra or alternately in the backbone torsional angles ε , ζ , α and β . A correlation between these torsional angles has been found on the basis of a number of B-DNA crystal structures, which have shown that two conformational states are usually observed in B-DNA, namely B_I and B_{II} . The B_I state is characterized by torsional angles α , -62° ; β , 176° ; γ , 48° ; δ , 128° ; ε , -176° ; ζ , -95° ; and χ , -102° to -119° ; while the B_{II} state is characterized by α , -62° ; β , 176° ; γ , 48° ; δ , 144° ; ε , -114° ; ζ , -174° ; and χ , -89° . Our results (Table 19) show that both T1 and A6 residues tend to adopt B_{II} conformation. The G2 and C5 residue also adopt B_{II} conformation due to intercalation. The A3 and T4 residues remain in stable state. It has been shown that in the crystal structure of daunomycin with d-TGATCA (Nunn et al., 1991), γ of A3 residue is 24° ; G2 and C5 residues are close to B_{II} conformations adopting ε and ξ angles of -131° , 155° and -98° , 167° , respectively. G2 and C5 residues adopt B_{II} conformation in X-ray

crystal structure of 4'-epiadriamycin with d-TGATCA (d'Estaintot et al., 1992) also. Our results show that two strands of DNA are symmetrical. The β angle of both A3 and T4 residues showed lower values, 169 and 170° respectively (Table 19). A lower value of β has been reported in X-ray crystal structure of 4'-epiadriamycin with d-TGATCA (d'Estaintot et al., 1992) but not in the complex of daunomycin with d-TGATCA (Nunn et al., 1991). A lower value of β angle has been associated with change in phosphodiester bond from idealized *g-g-* conformation to *tg-* observed in some crystal structures (Frederick et al., 1990).

A correlation between ζ and ϵ shows (Fig. 16) that the variations in these two angles are coupled. The torsional angle ϵ deviates from the normal value of -176° to values in the range $\sim 98^\circ$ whenever ζ angle adopts trans conformation, say for example in C5 residue. These values of torsional angles are close to the characteristic value of ϵ , -114° ; ζ , 174° ; χ , -89° ; for B_{II} conformation of DNA and are indeed the most populated conformations (Fig. 16). G2 adopts B_{II} conformational state in 99 structures while it adopts B_I conformational state in 1 structure. The A3 residue show a large amount of scatter of data in ϵ - ζ correlation (Fig. 16) but a distinct preference for B_I conformation is observed. An interesting behavior of phosphodiester linkage emerges from this data; if the phosphodiester bonds show B_I conformation in one strand, then the corresponding bonds on opposite strand are in B_{II} conformation. Such correlation has recently been observed by Trieb et al. (Trieb et al., 2004) on intercalation of daunomycin in $d(\text{CGCGGATCGCGCG})_2$ by molecular dynamics simulations. It has been suggested that there appears to be a possibility to directly influence the DNA backbone through complexation and hence lead to a redirection of intercalation caused structural changes to the backbone. Also there has been evidence in literature that on stretching of DNA, B_{II} conformation becomes

energetically more favorable and more pronounced (Winger et al., 1998; Kosikov et al., 1999; Bertucat et al., 1998; Grzeskowiak et al., 1991).

Conformation of Adriamycin

Adriamycin consists of three fused aromatic rings B, C and D bound to a cyclohexane ring, ring A, with an amino sugar attached at C7 position. The bond distances and bond angles are generally within the limit of accepted values. The average C-C distance in BCD ring is 1.41 Å. The aromatic part of a glycon is quite planar with rms distance of 1.3 Å for the least squares plane calculated from all the atoms of rings B, C and D without the exocyclic atoms. If all the exocyclic oxygen atoms (O4, O5, O6, O11, O12) as well as C7 and C10 are included in the calculations the rms distance is 1.1 Å. Few deviations greater than 0.1 Å are observed; e.g. C21 lying 0.61 Å on one side of BCD plane.

The orientation of 4OCH₃ group is such that methyl group is pointed away from O5 atom and protrudes into the solvent region. The distance between keto O5 and phenolic O6 and between keto O11 and phenolic O12 are 1.80 Å and 2.27 Å, respectively. Thus they presumably form intramolecular hydrogen bonds. During the course of restrained molecular dynamics simulations, it was observed that O11-H11...O12 had greater tendency to form intramolecular hydrogen bond than O6-H6...O5. Infact, out of the 100 structures saved at equal intervals during 100 ps run of dynamics, O11-H11...O12 hydrogen bond existed in all the 100 structures. The corresponding O6-H6...O5 intramolecular hydrogen bond was observed only in 98 structures and the H6 atom faced C7 atom in other 9 structures with no possibility of existence of hydrogen bond.

The torsional angles of the adriamycin molecule in the complex are listed along with those obtained in similar X-ray crystal structures (Nunn et al., 1991; d'Estaintot et al., 1992; Leonard et al., 1992) and free daunomycin (Neidle et al., 1977) molecule in Table 20. The torsional

angles around C19-C20 and C20-C7 bonds are -20° and 33° , respectively. All the atoms except C9 and C8 atom are almost in a plane with a maximum deviation of 2.0 Å. The atom C9 is displaced by 0.98 Å in the same direction as the amino sugar relative to the plane of aglycon and C9-O9 bond is almost orthogonal to the plane of ring A. O7 and O9 atom can no longer form intramolecular hydrogen bond in contrast to that observed in crystal structure of free daunomycin and related anthracycline antibiotics (Neidle et al., 1977; von Dreele et al., 1977; Anguilli et al., 1971; Courseille et al., 1979). The torsional angle in the glycosyl linkage is lower than that in the free daunomycin molecule as well as that in corresponding crystal structure of complex of daunomycin with d-TGATCA (Nunn et al., 1991). During simulations, the torsional angle C7-O7-C1'-C2' lies in the range 106° to 157° in 98 structures while it has the value 170° , as in uncomplexed daunomycin, in two of the 100 structures saved. The amino sugar is in chair conformation with all the side chains pointed away from the aglycon. The torsional angle about C3'-C4' bond is particularly lower (52°) than the expected ideal gauche value (near $\pm 60^\circ$). The C2', C3', C5', O5' atoms are coplanar while the atom C4' is displaced by 0.86 Å away from chromophore while C1' are displaced towards aglycon by the same magnitude.

Adriamycin-d-(TGATCA)₂ Interactions

A view showing the stacking interaction of the anthracycline chromophore between the bases is presented in Fig. 17a-b. This clearly shows the manner in which the aglycon chromophore is placed between adjoining base pairs, lying almost orthogonal to the long axis of T1.A12 and G2.C11 base pairs. Fig. 18 shows the stacking of G2.C11 base pair over A3.T10 base pair and A3.T10 base pair over T4.A9 base pair, respectively. These are somewhat similar to that existing in canonical B-DNA structures but there are significant deviations from the pseudo 2-fold symmetry relating the backbones of the B-DNA molecules. The helix axis also is not in the same

position in any two base pairs as would be expected for a perfect B-DNA conformation. The G2.C11 base pair is translated towards the minor groove relative to A3.T10 by about 1.2 Å. This represents an alteration in the base stacking at a site one removed from the intercalative site. An opposite translation of the axis of G2.C11 base pair by about 0.5 Å relative to T1.A12 is also seen around the intercalator in Fig. 18. The stacking of A3.T10 base pair over the T4.A9 base pair at the center of the molecule shows stacking that is typical of purine-pyrimidine sequences in B-DNA except that the two base pairs are translated along the long axis of base pair by about 1 Å. These changes in stacking patterns among adjacent base pairs (including third base pair) get reflected in the changes in chemical shift of base protons in the NMR spectra on binding.

One of the significant features of anthracycline antibiotics is that changing substituent groups at ring A, ring D or daunosamine sugar have moderate or no influence on its biological activity. Some constituent groups are however important for biological function. Fig. 19 shows the position of drug with respect to DNA molecule to illustrate some of the hydrogen bonding interactions and close van der waals contacts. It is found that the hydroxyl oxygen atom of 9OH in ring A is within the hydrogen bonding distance of N3 and N2 atoms of guanine base G2. The distance between O9 and G2N3 atom is 2.90 Å and varies in the range 2.85-3.60 Å in the 100 structures saved at equal intervals during 100 ps rMD simulations indicating thereby that a strong hydrogen bond exists. The distance of O9 from G2N2 atom is 3.0 Å and varies in the range 2.99-4.01 Å suggesting the existence of another weak hydrogen bond. The O9 atom forms a close van der waal contact of 3.18 Å with O4' atom of G2 residue. O7 atom of drug, which links the chromophore and amino sugar, is close to N2 of G2 residue with a separation of 2.7 Å. The distance of O7 atom from O9 atom of 9OH hydroxyl group in ring A is 3.75 Å so that there is no

possibility of intramolecular hydrogen bond between O7 and 9OH in contrast to that found in X-ray crystal structures of daunomycin in its uncomplexed form (Neidle et al., 1977; von Dreele et al., 1977; Anguilli et al., 1971; Courseille et al., 1979). During the entire course of simulations, the O7-9OH hydrogen bond does not exist. Thus the hydroxyl group on O9 atom, which appears to be important for biological activity, is involved with two hydrogen bonds to a guanine residue adjacent to the chromophore, donating one to N3 and receiving one from N2 atom. Also the 9OH-G2N3 hydrogen bond is shorter than 9O-G2N2H hydrogen bond. In order to have these two hydrogen bonding interactions, O9 and O7 atoms are close to G2 residue in such a way that 9OH is away from O7 atom. This hydrogen bonding interaction is sensitive to conformation of ring A, which is observed to be different from that in uncomplexed daunomycin (Table 20).

The X-ray crystallographic structure of daunomycin with d-TGTACA (Nunn et al., 1991) shows that carbonyl oxygen at C13 position of ring A is bonded to O2 of the ring T1 residue through a bridging water molecule while that in daunomycin-d-TGATCA complex shows water molecule hydrogen bonding to O13 without any further interaction. The distance between O13 and O2 of T1 in our rMD structure is 3.94 Å so that possibility of hydrogen bond through bridging water molecule exists. Further the distance between O5 and C5N1 atoms is 3.35 Å that between O4 and O1P of residue A6 is 9.12 Å and between 4OCH₃ and O1P of residue A6 is 9.06 Å. This suggests that a hydrogen bond involving O4 and O5 atom with phosphate groups of A6 residue are possible through two water molecules acting as bridges in between them. The amino group in the daunosamine sugar has been implicated in the electrostatic interactions between the daunomycin and the phosphate group of the nucleic acid (Gabbay et al., 1976). However, in X-ray crystal structure of daunomycin-d-TGATCA (Nunn et al., 1991) the amino group forms hydrogen bonds via its three hydrogen atoms to oxygen atoms in the neighbouring T4 and C5 residues, that is,

C5O2, C5O4' and T4O2 having separation of 2.6, 2.8 and 3.1 Å, respectively. In our rMD structures, these distances N-H...O with C5O2, C5O4' and T4O2 atoms are 3.04, 2.96 and 2.67 Å, respectively so that hydrogen bond between amino group and O2 of T4 residue may only be a strong hydrogen bond. It has been shown that ammonium group of daunosamine sugar contributes significantly to the binding (Wang et al., 1987; Frederick et al., 1990; Moore et al., 1989; Williams et al., 1990; Nunn et al., 1991; d'Estaintot et al., 1992; Leonard et al., 1992). It shows considerable positional variability and thermal mobility (Lipscomb et al., 1994; Williams et al., 1990). We have therefore looked into these hydrogen bonding contacts during the course of 100 ps simulations. We find that the distance of nitrogen of NH_3^+ from C5O2, C5O4' and T4O2 atoms are in the range 3.0-4.9, 2.8-4.7 and 2.5-3.9 Å, respectively. At the other site of intercalation, the distance of NH_3^+ from C11O2, C11O4' and T10O2 atoms are in the range of 3.1-4.9, 3.3-4.8 and 3.0-3.9 Å, respectively. If we consider 3.3 Å as the cutoff distance for the hydrogen bond, then at least two of the bonds of reasonable good strength exist in the complex. The distance of NH_3^+ from O4' of T4/T10 is in the range 4.2-7.0 Å so that there are no contacts through hydrogen bonds as seen in X-ray crystal structures of daunomycin with d-CGTACG (Wang et al., 1987) and d-TGTACA (Nunn et al., 1991).

An interesting feature of anthracycline complexes is the flexibility of glycosidic bond rotation, which has a role in anchoring the intercalator in the minor groove of DNA. We find that the glycosidic dihedral angle C7-O7-C1'-C2' varies within a range of angles, 106°-157°. This dihedral angle adopts an angle of 162°-168° in uncomplexed daunomycin and its analogues (Neidle et al., 1977; von Dreele et al., 1977; Anguilli et al., 1971; Courseille et al., 1979). In the X-ray crystal structure of daunomycin complexed to d-TGATCA (Nunn et al., 1991) it is 127° while in several other structures of similar complexes it lies in the range 132°-163° (Wang et al., 1987; Frederick et

al., 1990; Moore et al., 1989; Nunn et al., 1991; d'Estaintot et al., 1992; Leonard et al., 1992). The molecular dynamics simulations of daunomycin with d-(CGCGCGATCGCGCG)₂ have shown (Trieb et al., 2004) that three distinct conformational states can exist; the first one is 152°-162°, second at 135°-138° and a third is 57-61°. The energy barrier between 137° and 159° conformations is 0.3 - 0.7 Kcal mole⁻¹ and between 137° and 59° is 1.4 Kcal mole⁻¹. We did not observe the presence of 59° conformation during the course of simulations. Apparently only 137° and 159° conformations were readily accessible kinetically. The flexibility of glycosidic bond permits the daunosamine sugar moiety to point towards the minor groove and builds stabilizing contacts with DNA through NH₃⁺ moiety. Trieb et al (Trieb et al., 2004) have shown that in the first conformation centered at 157°, the nitrogen of NH₃⁺ moiety is at a distance of 5.5, 5.1 and 3.2 Å from C5O4', T4O2 and T4O4', respectively. In the second conformation centered at 137°, the corresponding distances are 3.2, 3.0 and > 6.0 Å, respectively while in the third conformation centered at 59°, the distances of nitrogen from G6O4' and G6O5' are 3.4 and 3.0 Å, respectively. In our complex, the distance of nitrogen from C5O4' / C11O4', T4O2 / T10O2 and T4O4' / T10O4' is in the range 3.0-4.8 Å and that from G2O4' and G2O5' is in the range 8.0 – 11.0 Å. Thus our results are in agreement with the correlation of glycosidic bond with stabilizing hydrogen bonding contacts through NH₃⁺ group suggested by Trieb et al (Trieb et al., 2004). It is important to note that the conformation of glycosidic bond is also related to cleavage of C7-O7 bond and production of free radicals, which are responsible for cardiotoxicity.

During the course of simulations, it was observed that the hydrogen atom of 6OH group of ring B of adriamycin pointed towards O5 atoms in 98 structures and was away from O5 atoms but pointed towards O7 atom in 2 structures. The hydrogen of 11OH on the other hand pointed towards O12 in all the structures. Thus both hydrogen bonds, 6OH...5O and 11OH...12, are not stabilized in all

the structures. This is in sharp contrast to the existence of both hydrogen bonds in the uncomplexed daunomycin, adriamycin and 4'-epiadriamycin (chapter 3) investigated by us using molecular dynamics simulations using NMR restraints. In order to see if the stability of these hydrogen bonds is related to glycosidic bond rotation, we looked into their correlation in various structures. We find out that the presence and absence of hydrogen bonds is not dependent on the glycosidic bond which varies independently in the range 106° - 157° . However on positioning of hydrogen atom of 11OH towards ring A, its distance from 10eqH, 10axH and O13 atoms is considerably decreased, as expected. Several other non-bonded van der waals interactions have been observed (Table 16) which may be important in stabilizing the complex. The 10eqH is close to G2N3 atom (3.46 Å); 10eqH has close contact with G2O4' atom (2.32 Å); 8axH is close to A6H2 atom 2.02 Å; A3H4' is closed to 5'CH₃ group (4.5 Å). Several of these contacts have been observed in X-ray crystal structures of daunomycin with d-CGTACG (Wang et al., 1987); for example contact between 8axH and G6H1N2 having a distance of 2.43 Å corresponds to A6H2-8axH contact in our rMD structure. In addition there are contacts involving O5, O6, 6OH atoms which are at a distance of 4.84, 5.05 and 4.43 Å from C5H1' atom, respectively. Further, 4OCH₃ is close to C5H2' atom which is 3.89 Å away. These observations are significant and establish the involvement of 4OCH₃, O5, O6, 6OH and ring A protons 2'eqH, 10eqH, 8axH etc. in stabilizing the drug-DNA complex, Summarizing the interactions, we find that atoms on one side of planer anthracycline ring, that is, 4OCH₃, O5, O6, 6OH, O7 as well as ring A protons and daunosamine sugar protons are involved in highly specific interactions with DNA and apparently the atoms/groups of atom in position 1, 2, 3, 11, 12 are not critical for binding (Fig. 19).

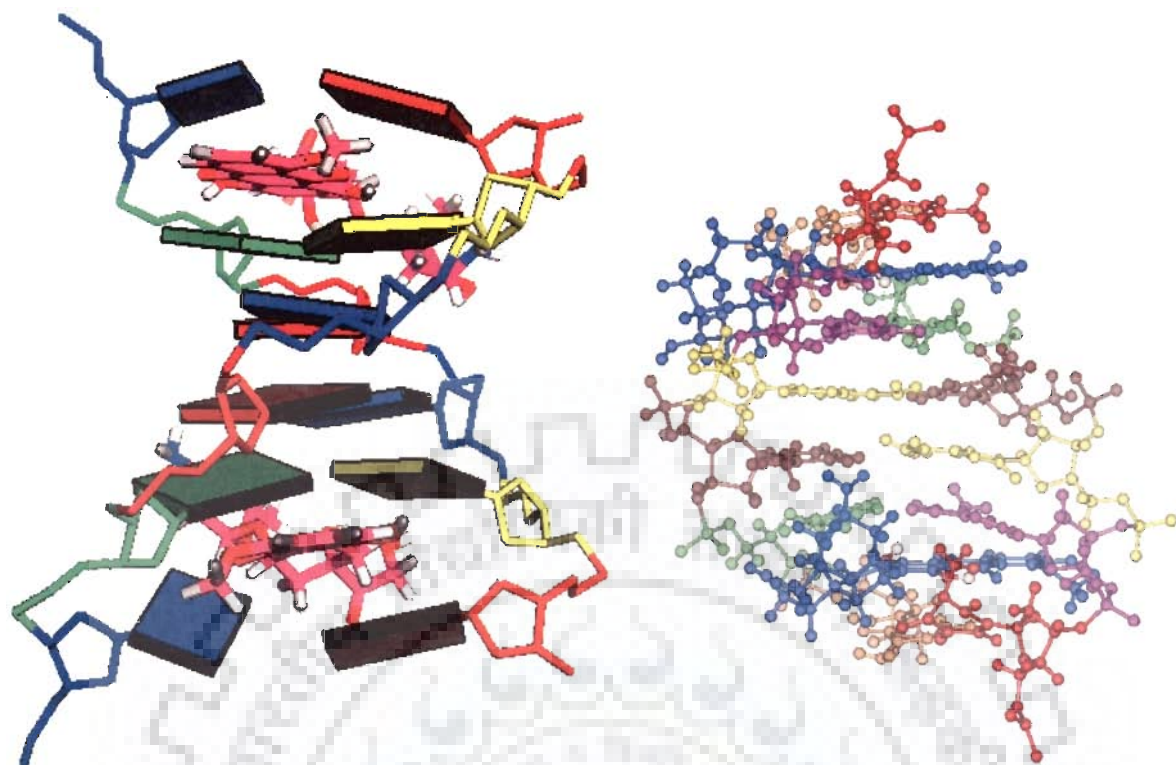


Fig. 12: Front view and Side view of the final structure obtained by restrained molecular dynamics simulations.

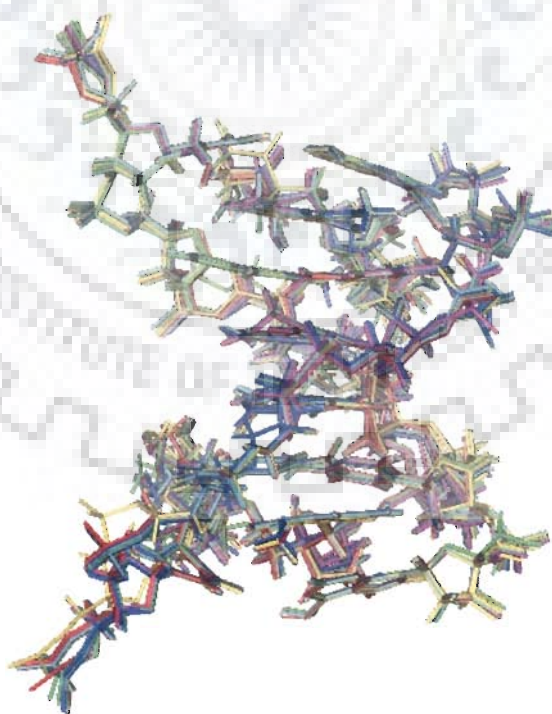
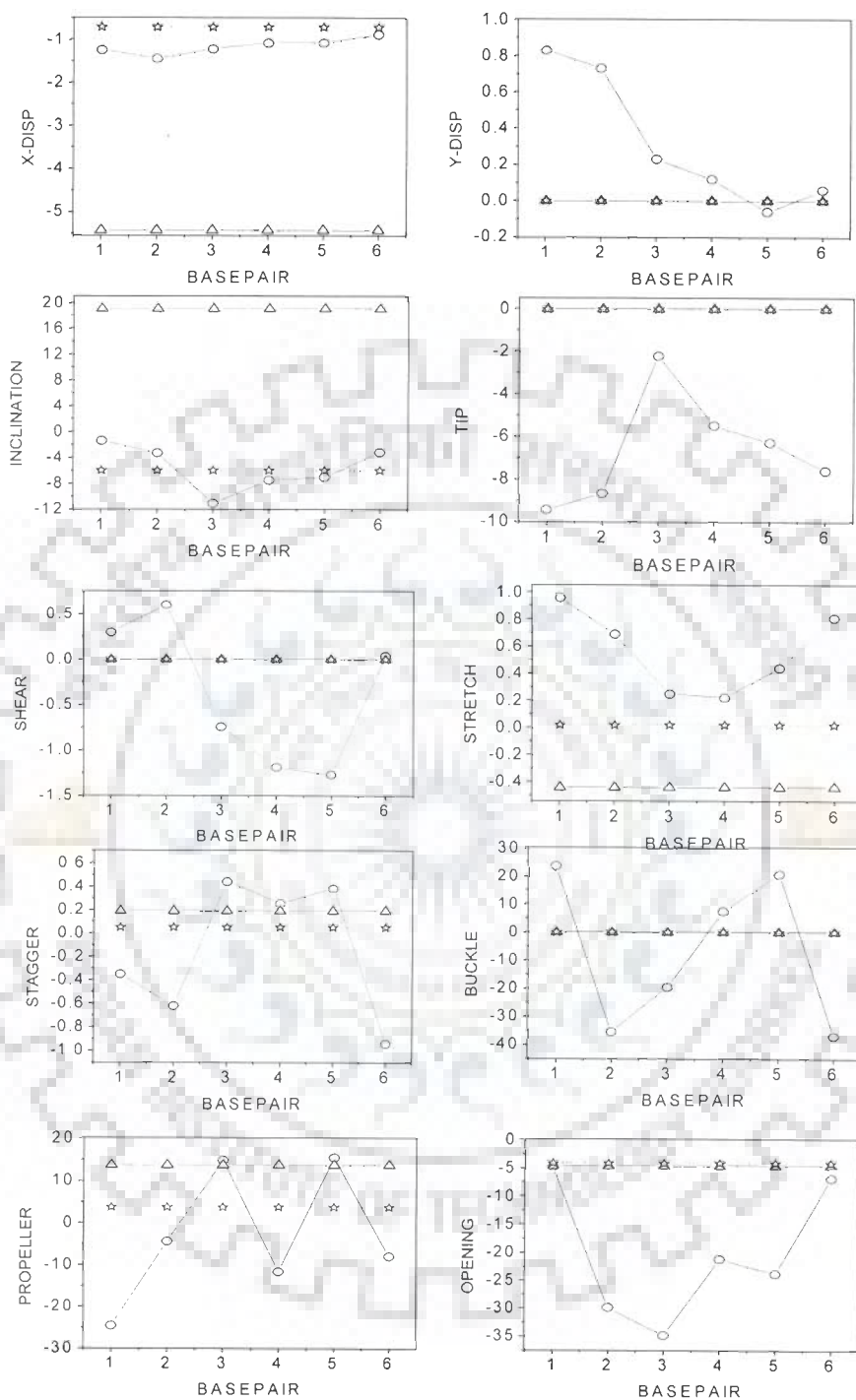
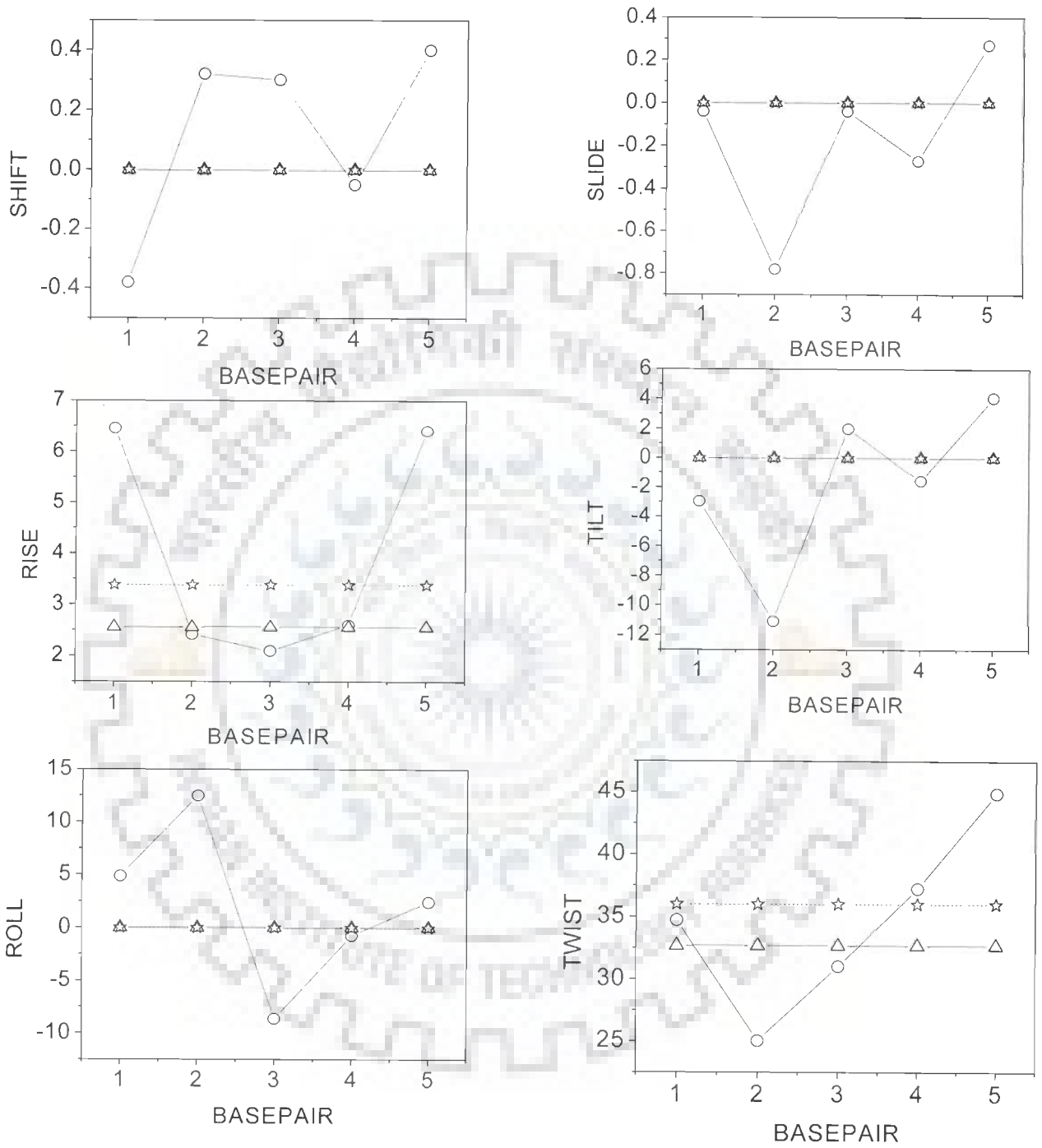


Fig.13: Superimposed structures obtained by restrained molecular dynamics simulations.



(a)

Fig. 14(a) and (b) Helical parameters for d-(TGATCA)₂ complexed with adriamycin calculated for structure obtained by restrained molecular dynamics simulations (○) and that for standard A-DNA (△), B-DNA (☆)



(b)

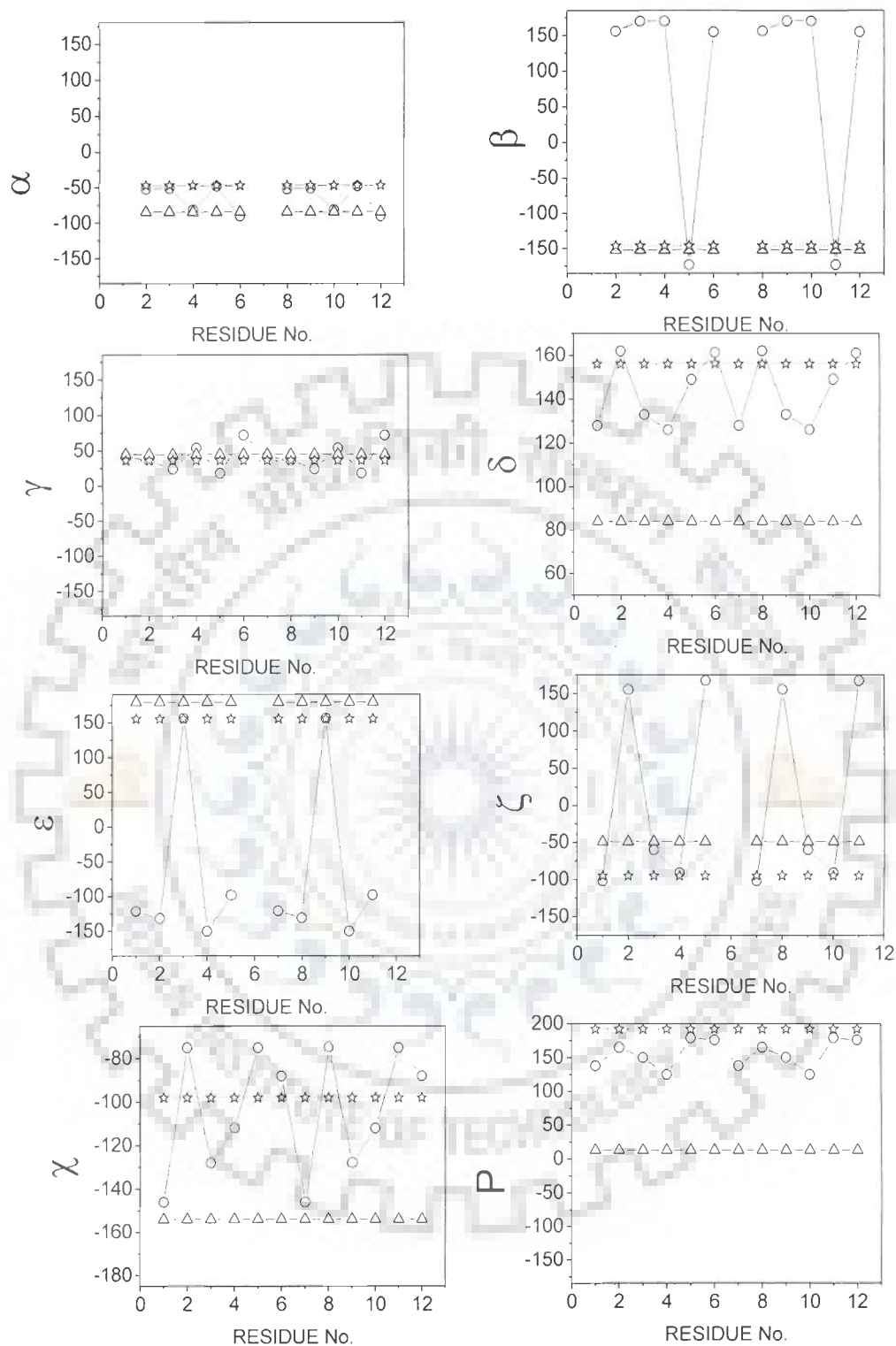


Fig. 15 Backbone torsional angles for d-(TGATCA)₂ complexed with adriamycin calculated for structure obtained by restrained molecular dynamics simulations (○) and that for standard A-DNA (△), B-DNA (☆)

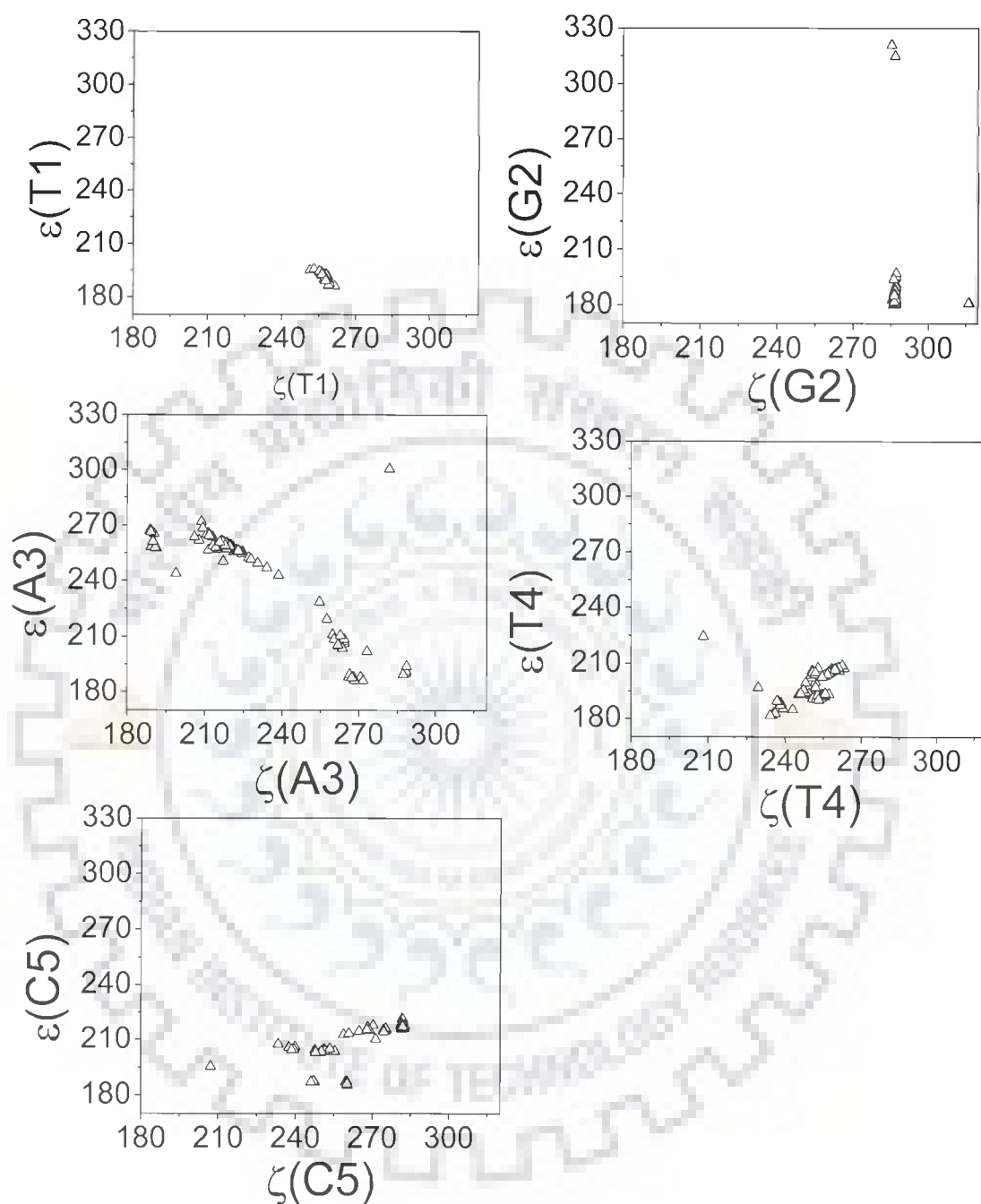


Fig. 16: Correlation between ϵ and ζ torsional angle in the structures obtained after 100 ps rMD simulation.

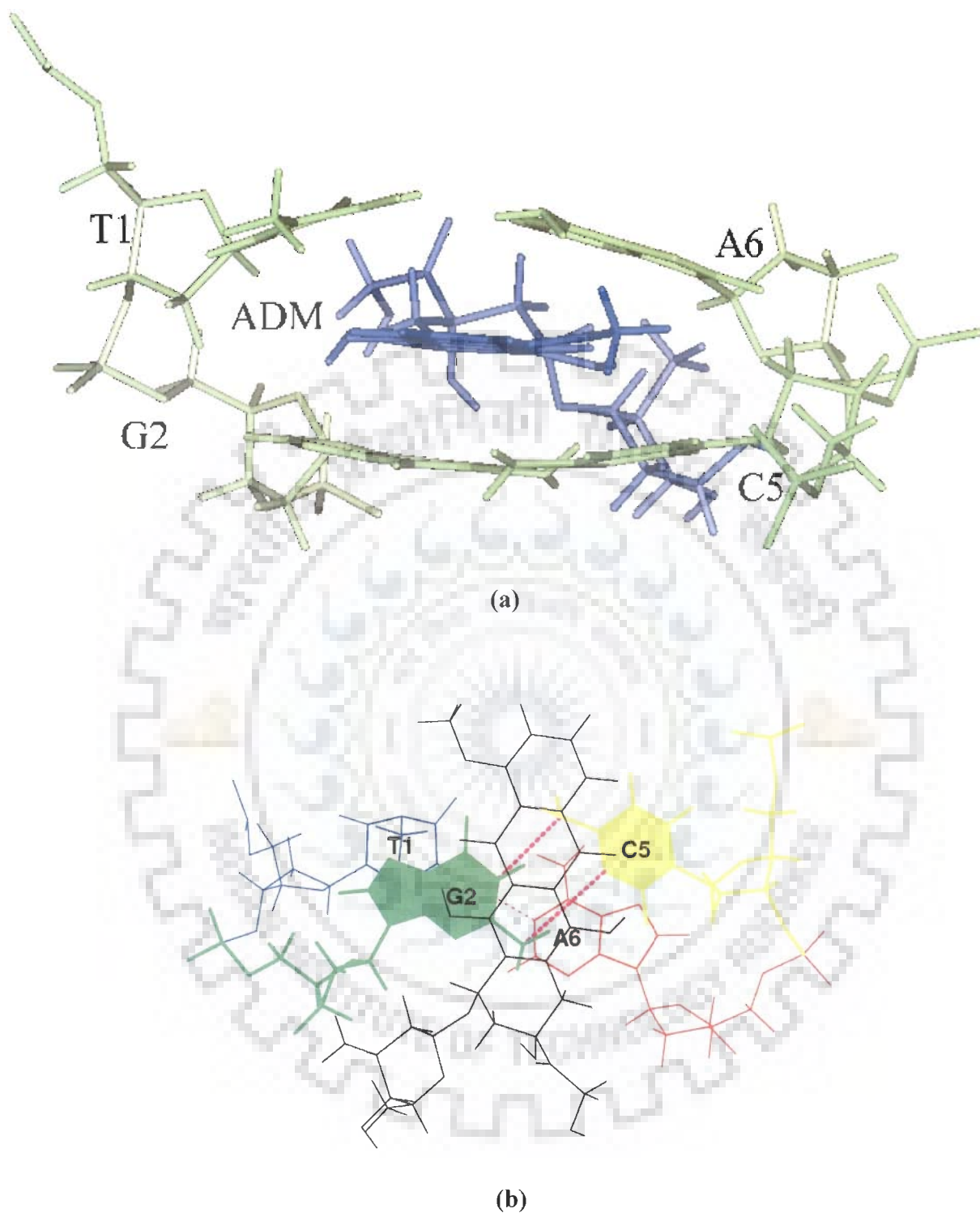


Fig. 17: Drug-DNA stacking interaction in the intercalation site showing the orientation of the adriamycin with respect to base pairs (a) front view (b) top view.

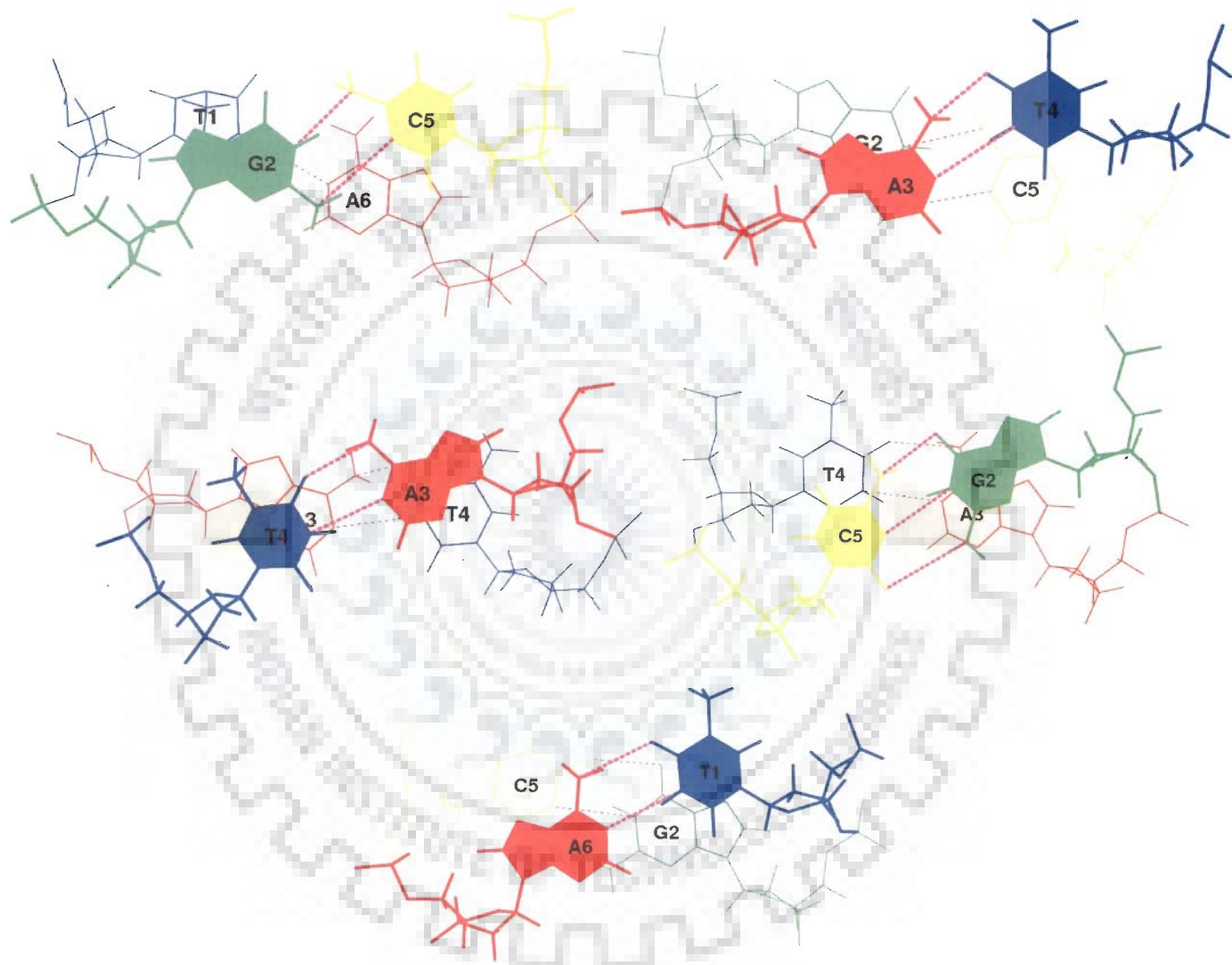


Fig. 18: Overlap of base pairs at different base pair steps in $d\text{-(TGATCA)}_2$ + adriamycin complex showing stacking interactions.

Table 16: Close contacts (Å) between drug and DNA molecule

Van der Waal's contacts			H-Bond contacts		
S.No.	Protons	Distance (Å)	S.No.	Protons	Distance (Å)
1	T1C4-7H	2.33	1	G2N2-O9	2.93
2	G2O4'-O9	2.52	2	G2N3-O9	2.54
3	G2N2-C11a	2.63	3	C5N3-O5	2.58
4	G2N3-5C	2.31	4	A6N7-O5	2.76
5	G2C2-C5a	2.49	5	A6N3-11O	2.87
6	G2NH ₂ ^{nb} -O11	1.90	6	A6NH ₂ ^{nb} -O4	2.31
7	G2C5-11OH	2.30	7	T1N1-11O	2.82
8	G2N7-11OH	1.95	8	G2N7-11O	2.67
9	G2C6-C11a	2.74	9	G2N7-11OH	1.95
10	G2C5-11C	2.72	10	G2NH ₂ ^{nb} -11O	1.90
11	G2C4-C10a	2.78	11	A3P-14OH	1.69
12	G2N3-C10a	2.59	12	T4P-4'OH	1.70
13	G2C2-C7	2.72	13	C5P-14OH	1.69
14	G2NH ₂ ^b -O7	2.15	14	C5N3-11O	2.91
15	G2NH ₂ ^{nb} -6C	2.34	15	C5NH ₂ ^b -O7	2.13
16	G2P-14OH	1.69	16	C5NH ₂ ^b -O9	2.01
17	G2P-4'OH	1.70	17	A6N9-11O	2.91
18	G2P-14OH	1.69	18	A6NH ₂ ^{nb} -O13	2.42
19	C5C5-10axH	2.38			
20	C5NH ₂ ^b -O7	2.13			
21	C5NH ₂ ^b -O9	2.01			
22	C5H5-9OH	1.96			
23	A6NH ₂ ^b -8eqH	1.93			
24	A6N3-7H	2.19			
25	A6C2-6C	2.78			
26	A6H2-8eqH	1.98			

Table 17: Energy terms (Kcal mole⁻¹) for starting model and final rMD structure

Energies (Kcal mole ⁻¹)	Adriamycin -d-(TGATCA) ₂ complex	
	Initial	Final
Total	1618	463
Bond	94	89
Angle	686	613
Dihedral	34	47
Van der Waal	257	280
Repulsion	2301	2329
Dispersive	-2044	-2049
Electrostatic	598	497
Restraint	477	377

Table 18: Summary of experimental restraints and statistical analysis of final structure generated by restrained molecular dynamics (rMD)

Parameters	No. of distance restraints
Intra residue	180
Inter residue	68
Total NOE violations	34
Average pairwise RMSD	Initial = 0.0 Final = 0.85
Average residue wise RMSD	T1 = 0.225, G2 = 0.121, A3 = 0.103, T4 = 0.063, C5 = 0.052, A6 = 0.057
Minor groove	Width = 13.20 Å; Depth = 1.70 Å
Major groove	Width = 8.19 Å; Depth = 3.81 Å

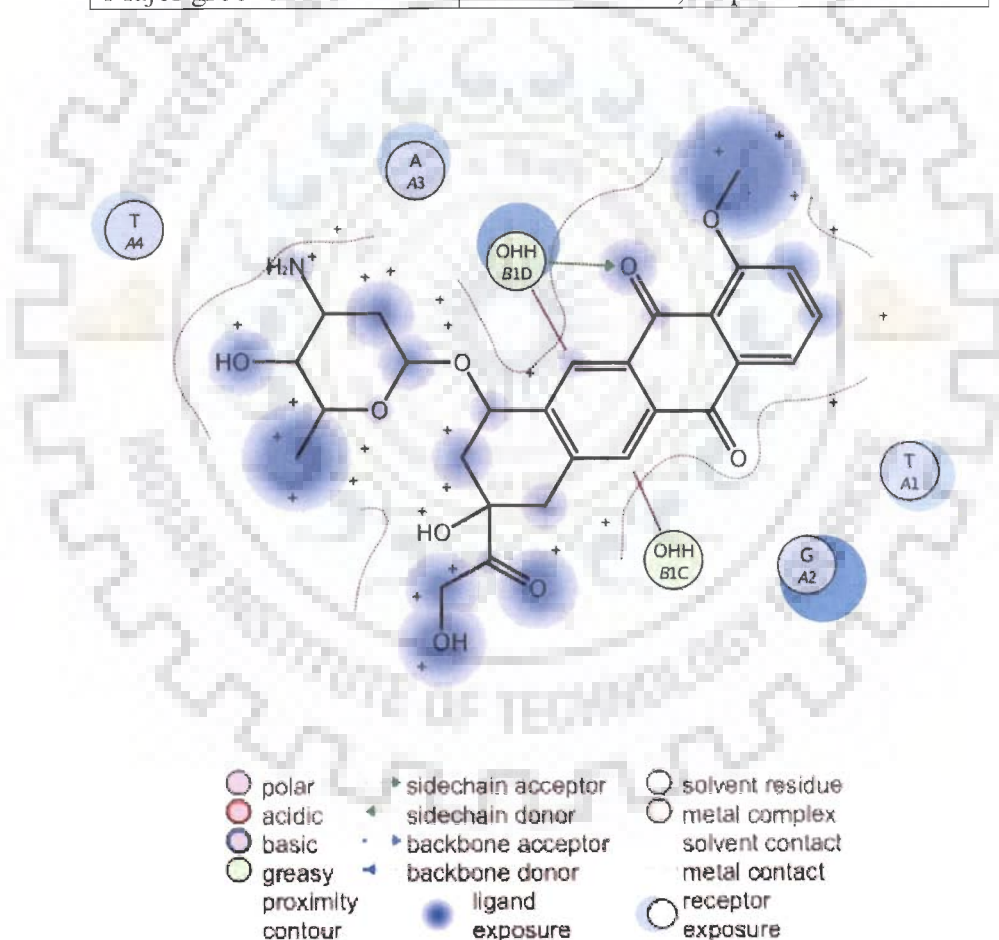


Fig. 19: Various Interactions present in 2:1 adriamycin-d-(TGATCA)₂ complex.

Table 19: Backbone torsional angles ($^{\circ}$), pseudorotation phase angle ($^{\circ}$) and glycosidic bond rotation ($^{\circ}$) of the final structure

Residues	α	β	γ	δ	ϵ	ζ	χ	P
T1	-	-	42	128	-121	-102	-146	138
G2	-52	156	36	162	-131	155	-75	165
A3	-51	170	24	133	156	-60	-128	150
T4	-81	170	54	126	-150	-91	-112	125
C5	-48	-173	18	149	-98	167	-75	179
A6	-90	155	72	161	-	-	-88	176
T7	-	-	42	128	-121	-102	-146	138
G8	-52	156	36	162	-131	155	-75	165
A9	-51	170	24	133	156	-60	-128	150
T10	-81	170	54	126	-150	-91	-112	125
C11	-48	-173	18	149	-98	167	-75	179
A12	-90	155	72	161	-	-	-88	176
B-DNA	-47	-146	36	156	155	-95	-98	192
A-DNA	-84	-152	45	84	179	-49	-154	13

Table 20: Selected torsional angles ($^{\circ}$) of the adriamycin in the complex and their comparison with similar structures available in literature. ^aTGATCA + daunomycin (Nunn et al., 1991); ^bTGTACA + daunomycin (Nunn et al., 1991); ^cTGATCA + 4'-epiadriamycin (Estaintot et al., 1992); ^dTGTACA + 4'-epiadriamycin (Leonard et al., 1992); ^edaunomycin (Neidle et al., 1977)

TORSIONAL ANGLES	Present Work TGA + adm	TGA + dnm ^a	TGT + dnm ^b	TGA + 4'-epi ^c	TGT + 4'-epi ^d	dnm ^e
RING A						
C20-C7-C8-C9	-55	-56	-40	-45	-50	-48
C7-C8-C9-C10	61	66	55	68	63	58
C8-C9-C10-C19	-48	-35	-44	-60	-42	-38
C9-C10-C19-C20	29	-2	27	33	14	14
C10-C19-C20-C7	-20	10	-11	-8	-1	-5
C19-C20-C7-C8	33	18	14	13	18	20
GLYCOSYL						
C8-C7-O7-C1'	73	129	120	96	95	125
C20-C7-O7-C1'	-161	-115	-125	-139	-142	-114
C7-O7-C1'-O5'	-106	-115	-105	-102	-81	-68
C7-O7-C1'-C2'	133	127	137	132	159	167
AMINO SUGAR						
O5'-C1'-C2'-C3'	55	-49	-60	-31	-53	-54
C1'-C2'-C3'-C4'	-52	50	49	41	52	56
C2'-C3'-C4'-C5'	52	-20	-17	-53	54	-61
C3'-C4'-C5'-O5'	-53	-16	-5	61	57	61
C4'-C5'-O5'-C1'	-54	19	-9	-55	-59	-59
C5'-O5'-C1'-C2'	-56	17	42	36	57	57

6.2 Summary and Conclusions

Large upfield shifts are observed in T1CH₃, G2H1', T1NH and A6H2' protons on binding of drug to DNA hexamer sequence. The 3H, 7H, 8axH, 2'axH protons of the drug are shifted upfield up to 0.3 ppm in the complex. Sequential nOe (nuclear Overhauser effect) connectivities between T1pG2 and C5pA6 steps are not observed and the drug chromophore intercalates at these base pair steps. Presence of several other intermolecular nOes, that is, T1CH₃-7H, T1CH₃-8axH and C5H6-4OCH₃ corroborate the same. The daunosamine sugar protons are in close proximity of third base pair. Presence of both B_I and B_{II} conformations have been detected at some of the base pair steps. The observed sequence dependant variations in DNA occur presumably to allow intercalation of the drug chromophore and proximity of daunosamine sugar to the third base pair, A3T10. The conformation of the drug also changes in order to have interaction with G2 base. The results have been compared with similar structures of complexes of daunomycin and 4'-epiadriamycin with d-(TGATCA)₂, obtained by X-ray crystallography techniques. Our studies establish the role of 9OH, C13O13, NH₃⁺, 7O, 4OCH₃ groups in binding to DNA. Besides this, life time measurement study has been done to show that there is shortening of decay time on complex formation in comparison to the uncomplexed drug due to electron transfer from the DNA base to the drug molecule. The nonspecific interactions as well as those essential for biological activity are discussed. The DOSY spectral analysis also show that the rate of diffusion decreases due to the binding of drug to DNA hexamer. The present study is the first restrained molecular dynamics studies on the solution structure of adriamycin with d-(TGATCA)₂ hexamer sequence of DNA. The rMD simulations of adriamycin- d-(TGATCA)₂ complex based on intermolecular and intramolecular NOEs have led to a detailed conformational analysis. The drug is found to intercalate between TG and CA base pairs at two

d-TpG and d-CpA sites which result in π - π stacking, dipole-dipole interactions, hydrogen bonding and van der waal's interactions. The drug-DNA complex is stabilized by intercalation of drug chromophore at T1pG2 and C5pA6 sites, several hydrogen bonding and van der waal's interactions involving 4OCH₃, O5, 6OH, and NH₃⁺ moiety of daunosamine sugar, and rings A protons. The adriamycin molecule also adjusted its conformation in order to fit tightly into the double helix; the ring A conformation has changed to permit 9OH and 9CO to come in close contact with G2 base. The role of various functional groups leading to molecular basis of drug action is discussed and correlated to the available biochemical evidence.



Studies on Complex of 4'-Epiadriamycin with d-(CGATCG)₂ by Phosphorus-31 Nuclear Magnetic Resonance Spectroscopy

³¹P NMR is a useful probe for the geometric arrangement about the phosphate group since it provides direct information about phosphate residues, due to its high sensitivity to chemical (solvent, pH, metal ions) and structural (valence bond and torsion angles) environment. Especially the latter dependency is regarded as a promising tool in the study of nucleic acid constituents and its stereo dynamic properties. This chapter contains the following studies of the complex of 4'-epiadriamycin-d-(CGATCG)₂ by one- and two-dimensional ³¹P NMR.

- The temperature dependence of ³¹P chemical shift of 4.62 mM d-(CGATCG)₂ duplex in the range of 275 - 328 K.
- The two dimensional ¹H - ³¹P Heteronuclear Multiple Bond Correlation (HMBC) of 4.62 mM d-(CGATCG)₂ at 298 K for the assignment of ³¹P resonances.
- Titrations by recording ³¹P 1D NMR versus drug (D)/DNA duplex (N) ratio, 0.16, 0.32, 0.48, 0.64, 0.80, 0.96, 1.11, 1.27, 1.43, 1.53, 1.60, 1.75, 1.91 and 2.03 at 275, 298 and 318 K.
- 2D ³¹P - ³¹P exchange spectra of 4'-epiadriamycin-d-(CGATCG)₂ complex by a phase-sensitive NOESY with mixing time of 200 ms at 298 K for D/N = 1.0, 1.5 and 2.0.
- Temperature dependent ³¹P NMR of the 4'-epiadriamycin-d-(CGATCG)₂ complex having D/N = 1.0, 1.5 and 2.0 in the range of 275 - 328 K.
- T₁ measurements of the 2:1 4'-epiadriamycin-d-(CGATCG)₂ complex at 298 K.

7.1 Results and Discussion

A. d-(CGATCG)₂

^{31}P 1D variable temperature experiments are recorded for 4.62 mM d-(CGATCG)₂ in 275 - 328 K range (Fig. 1). The ^{31}P resonances resolve into five distinct signals corresponding to the five phosphate groups at the ambient temperature. The assignments of ^{31}P nuclei in d-(CGATCG)₂ were performed by using the 2D ^1H - ^{31}P HMBC (Fig. 2). The three-bond scalar couplings between (^{31}P)_n nuclei in the phosphate backbone and the (H3')_n, (H5'/H5'')_{n+1} protons and four-bond coupling with (H4')_n, (H4')_{n+1} protons are observed (Fig. 2). The identification of the cross peaks were done on the basis of proton assignments, which have been done by using DQF COSY and 2D NOESY spectra (Barthwal et al., 2003). We are focusing mainly on H3' and H4' region for the assignment purpose as H5'/5'' are overlapped highly. Two of the H4' signals (A3 and T4) are separated from the H5' overlapped regions and their connectivities through the four-bond couplings with G2pA3 and A3pT4 phosphates, confirm the assignments (Table 1).

The increase or decrease in temperature from the ambient cause ^{31}P signals to shift towards each other and to overlap but there is no broadening (Fig. 1 and Table 1). This shows that the duplex is intact at lower and ambient temperature. There is a general downfield shift (Fig. 3a) of ^{31}P resonances with increasing temperature which is consistent with the change in the backbone conformation, generally g⁻ for P-O ester bonds in the duplex, to a single stranded having random mix of g- and non-gauche conformations. Thus the temperature dependence of ^{31}P chemical shifts provides an important monitor of both melting and premelting structural transitions in the phosphate ester backbone. There is a sharp decrease in line width with temperature. The ^{31}P double helical signals below T_m are substantially broader (25-15 Hz line width at half height) than the corresponding single-strand signals (line width of free single helices at temperatures above T_m is 3-5 Hz) (Fig. 3b and Table 2). The T_m of the duplex is 288 K as the inflection point in the curves for all phosphates occurs at approximately this temperature (Fig. 3b).

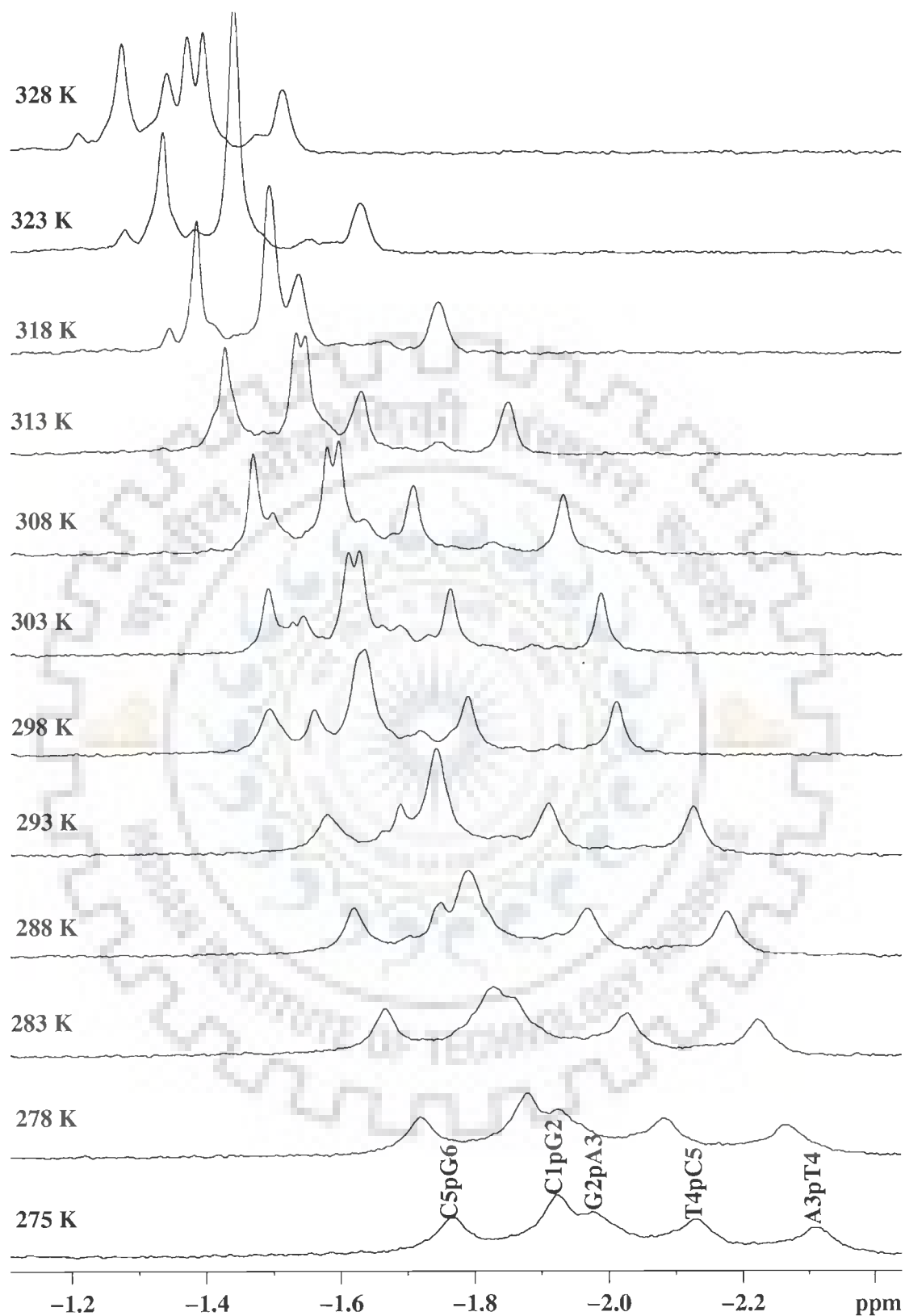


Fig. 1: ^{31}P NMR Spectra of 4.62 mM d-(CGATCG)₂ as a function of temperature

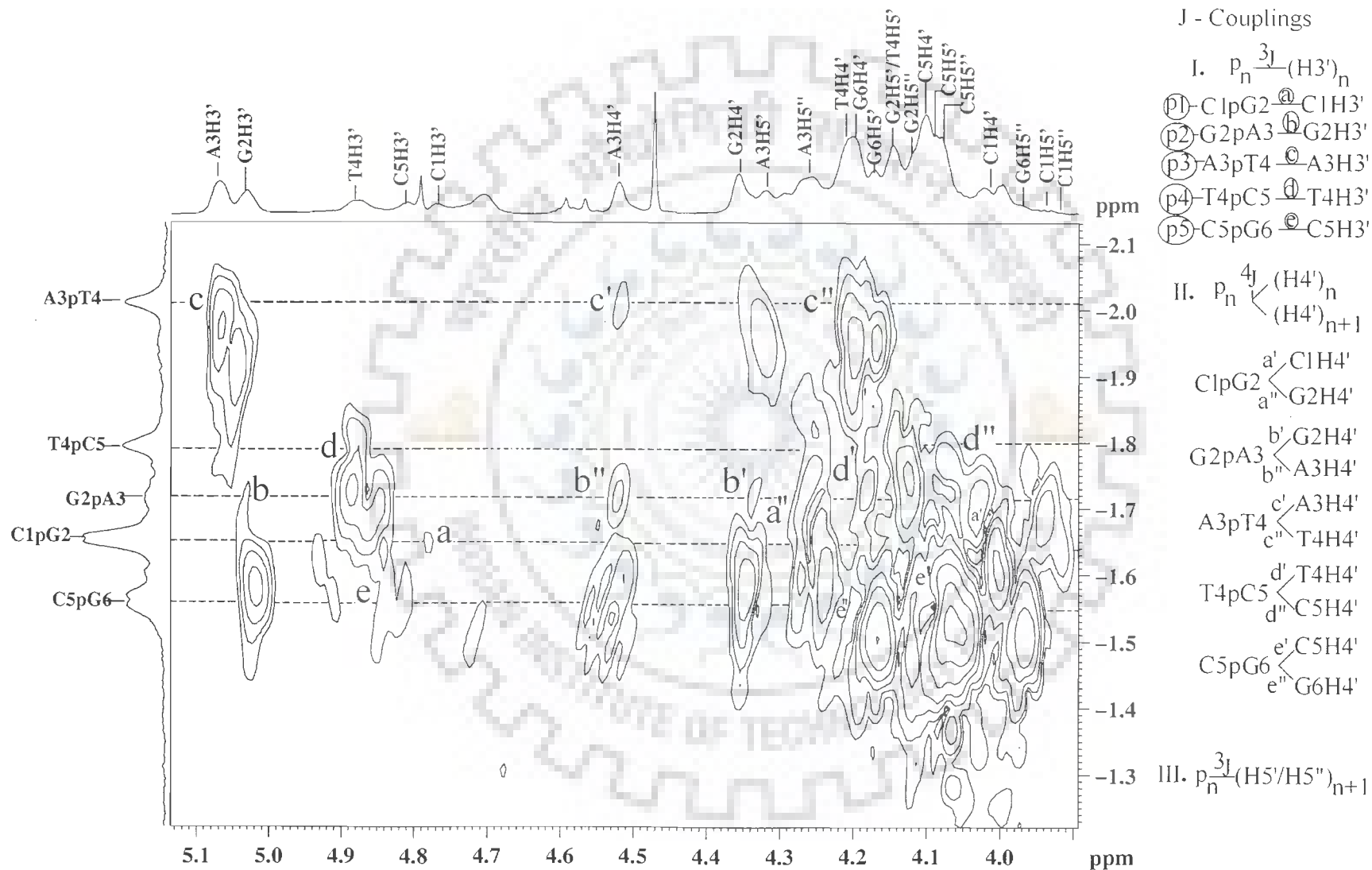


Fig. 2: Two dimensional ^{31}P - ^1H Heteronuclear Multiple Bond Correlation (HMBC) Spectra 4.62 mM d-(CGATCG)₂ at 298K

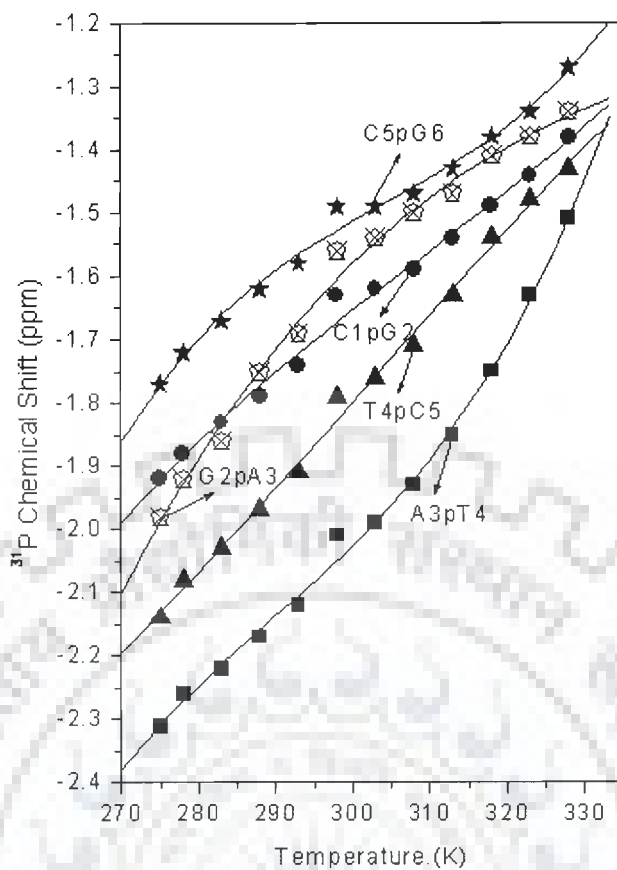


Fig. 3(a): ^{31}P Chemical Shift of 4.62 mM d-(CGATCG) $_2$ as a function of temperature

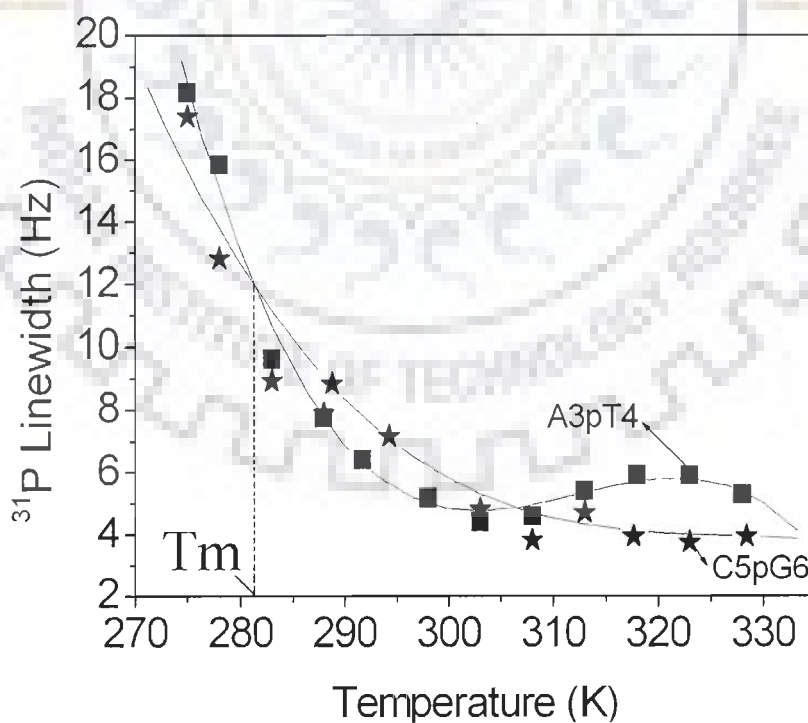


Fig. 3(b): ^{31}P Line width (Hz) of 4.62 mM d-(CGATCG) $_2$ as a function of temperature

Table 1: ^{31}P chemical shift assignments (δ) of d-(CGATCG) $_2$ in the free duplex at different temperatures. The total change in chemical shift with temperature, $\Delta\delta = \delta_{328\text{K}} - \delta_{275\text{K}}$ is also shown.

Temperature(K)	C1pG2	G2pA3	A3pT4	T4pC5	C5pG6
275	-1.92	-1.98	-2.31	-2.14	-1.77
278	-1.88	-1.92	-2.26	-2.08	-1.72
283	-1.83	-1.86	-2.22	-2.03	-1.67
288	-1.79	-1.75	-2.17	-1.97	-1.62
293	-1.74	-1.69	-2.12	-1.91	-1.58
298	-1.63	-1.56	-2.01	-1.79	-1.49
303	-1.62	-1.54	-1.99	-1.76	-1.49
308	-1.59	-1.50	-1.93	-1.71	-1.47
313	-1.54	-1.47	-1.85	-1.63	-1.43
318	-1.49	-1.41	-1.75	-1.54	-1.38
323	-1.44	-1.38	-1.63	-1.48	-1.34
328	-1.38	-1.34	-1.51	-1.43	-1.27
$\Delta\delta$	+0.54	+0.64	+0.80	+0.71	+0.50

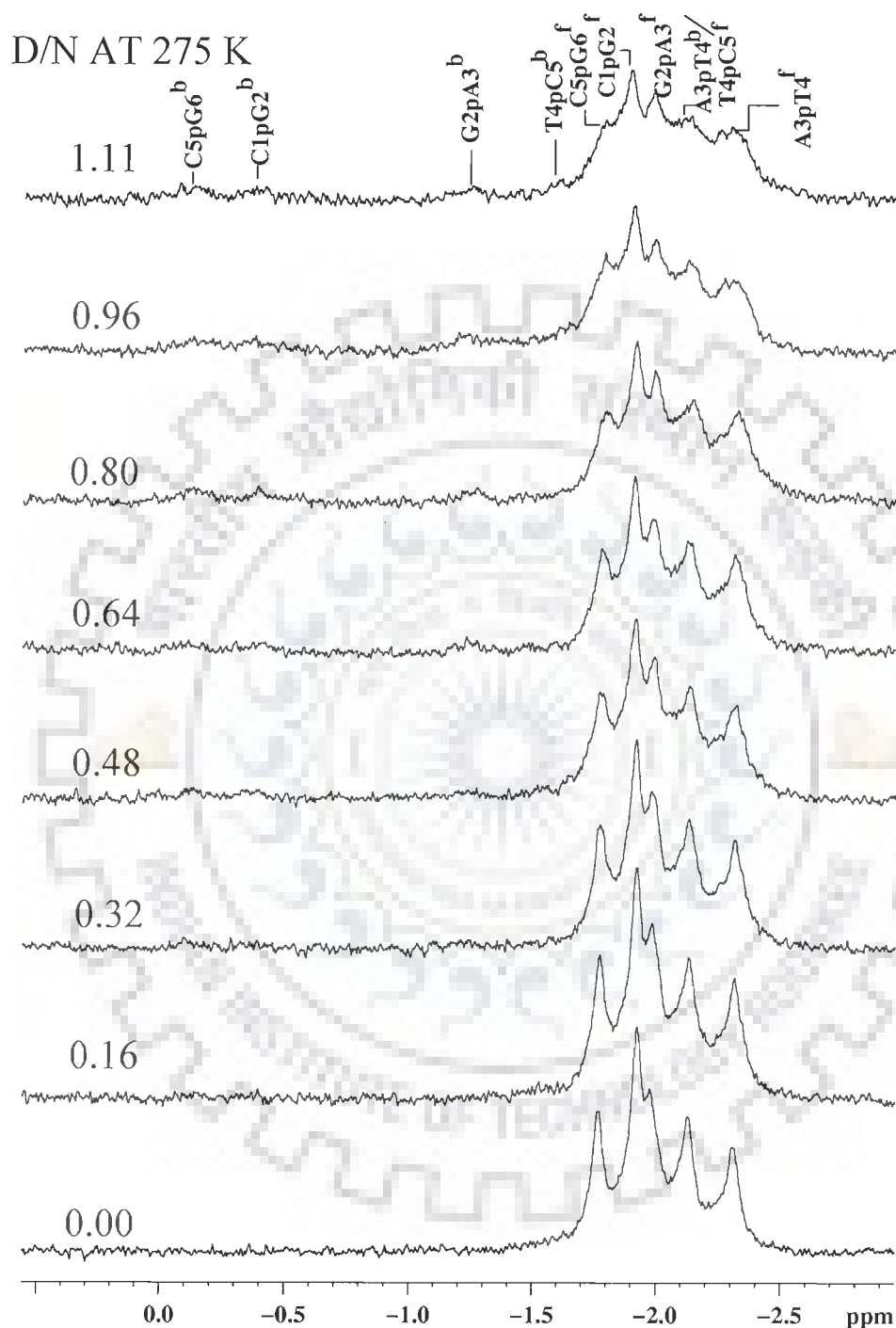
Table 2: ^{31}P Line width (Hz) of d-(CGATCG) $_2$ in the free duplex at different temperatures

Temperature(K)	C1pG2	G2pA3	A3pT4	T4pC5	C5pG6
275	24.26	24.26	18.16	10.92	17.40
278	21.55	21.55	15.84	9.75	12.82
283	19.31	19.31	9.60	14.09	8.92
288	13.92	13.92	7.75	6.96	7.88
293	7.94	7.94	6.66	7.66	9.84
298	8.13	8.13	5.18	6.19	7.93
303	8.21	17.14	4.41	4.74	4.81
308	7.85	3.82	4.59	4.90	3.82
313	6.81	4.71	5.41	6.02	4.71
318	4.55	3.21	5.91	4.55	3.21
323	3.95	3.75	5.89	3.95	3.75
328	2.98	2.98	5.28	2.98	4.55

Thus ^{31}P chemical shifts show the expected variation in the sugar-phosphate backbone conformation as the duplex melts into a single strand (Gorenstein, 1992).

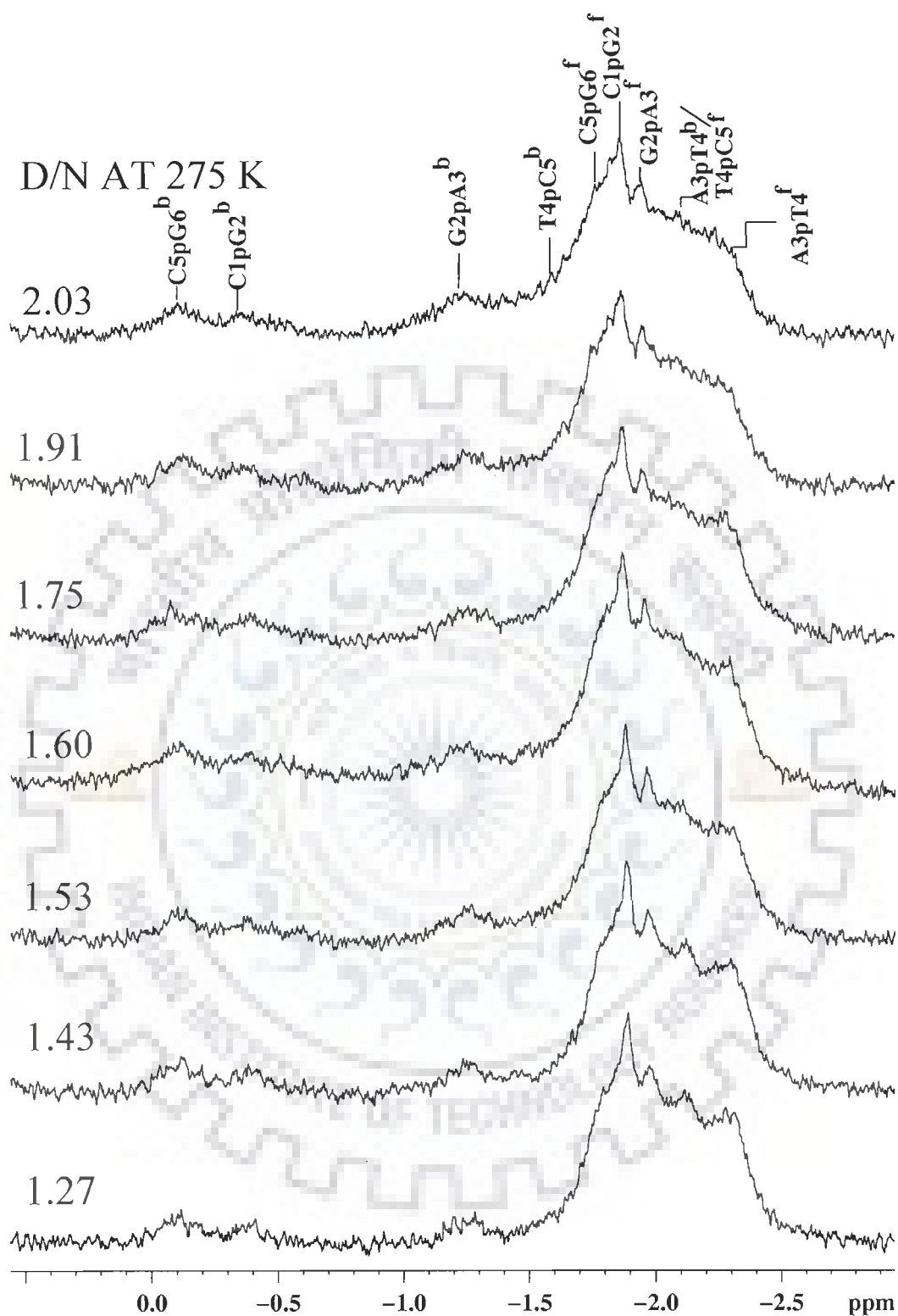
B. 4'-Epiadriamycin-d-(CGATCG)₂ Complex

The complex of d-(CGATCG)₂ with 4'-epiadriamycin was made by addition of 6 μl of 4'-epiadriamycin from the stock solution (88.33 mM) to the d-(CGATCG)₂ solution till it reaches 2:1 ratio. The sample was prepared in 90% water and 10% D₂O. The addition of 4'-epiadriamycin to a solution of the oligomer d-(CGATCG)₂ induces the appearance of five new peaks at low field in the ^{31}P NMR spectrum, as shown in Fig. 4a-d. The spectra were recorded at 275 (Fig. 4a-b), 298 (Fig. 4c-d) and 318 K (Fig. 4e-f) to look at the slow and fast exchange. At 275 and 298 K, there is slow exchange hence bound and free peaks are coming separately, but at 318 K there is fast exchange, as the bound and free ^{31}P resonances are present at the same position at this temperature, along with the phenomenon of duplex to single strand transition taking place (Fig. 4e-f). Increasing the concentration of drug produces downfield shifts and line broadening. The intensity of bound resonances increases with D/N ratios and that of free nucleotide decreases at 275 and 298 K (Fig. 4a-d). This shows that at 318 K, the bound DNA species decreases and the free increases, thus causing unbinding of the drug at higher temperature. However, the line width of the bound phosphorus signals increases from 9 to 30-40 Hz with increasing D/N ratios. At higher ratios the peaks are too broad to resolve. The assignment of five new phosphorus resonance signals are done by ^{31}P - ^{31}P 2D NOESY spectra (Figs. 5 a-c) at various D/N ratios 1.0, 1.5, 2.0 at 298 K. The five free phosphate resonances are already assigned (Table 1) through the ^1H - ^{31}P HMBC experiment. It is observed in Figs. 5a-c that each signal belonging to the phosphate group of free specie is correlated to another phosphate resonance shifted downfield, with respect to it, which is therefore the corresponding

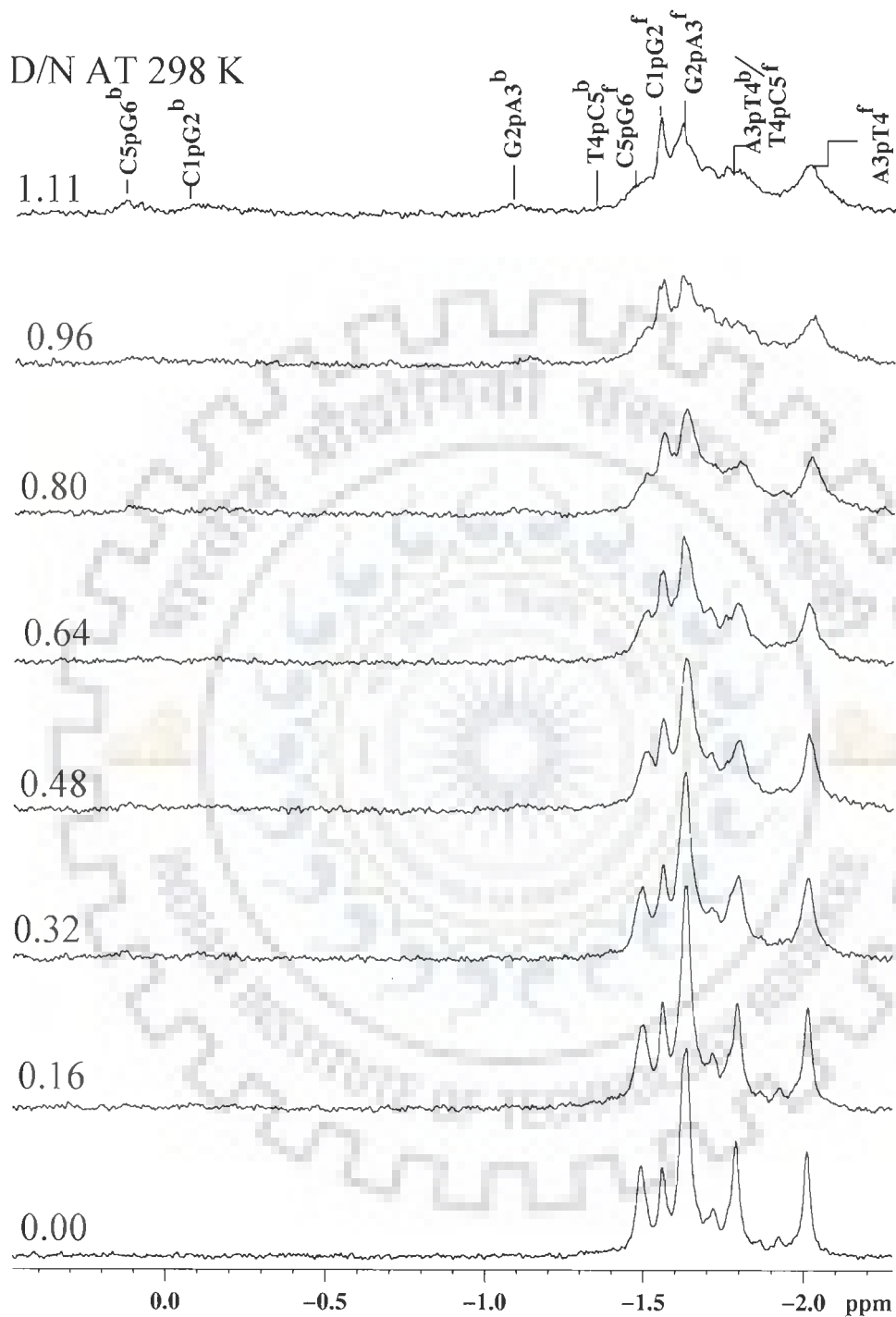


(a)

Fig. 4(a-b): Proton decoupled ^{31}P NMR spectra of 4.62 mM d-(CGATCG)₂ in uncomplexed state and complexed with 4'-epiadriamycin with increasing drug (D) to nucleic acid duplex (N) ratios, D/N, at 275 K

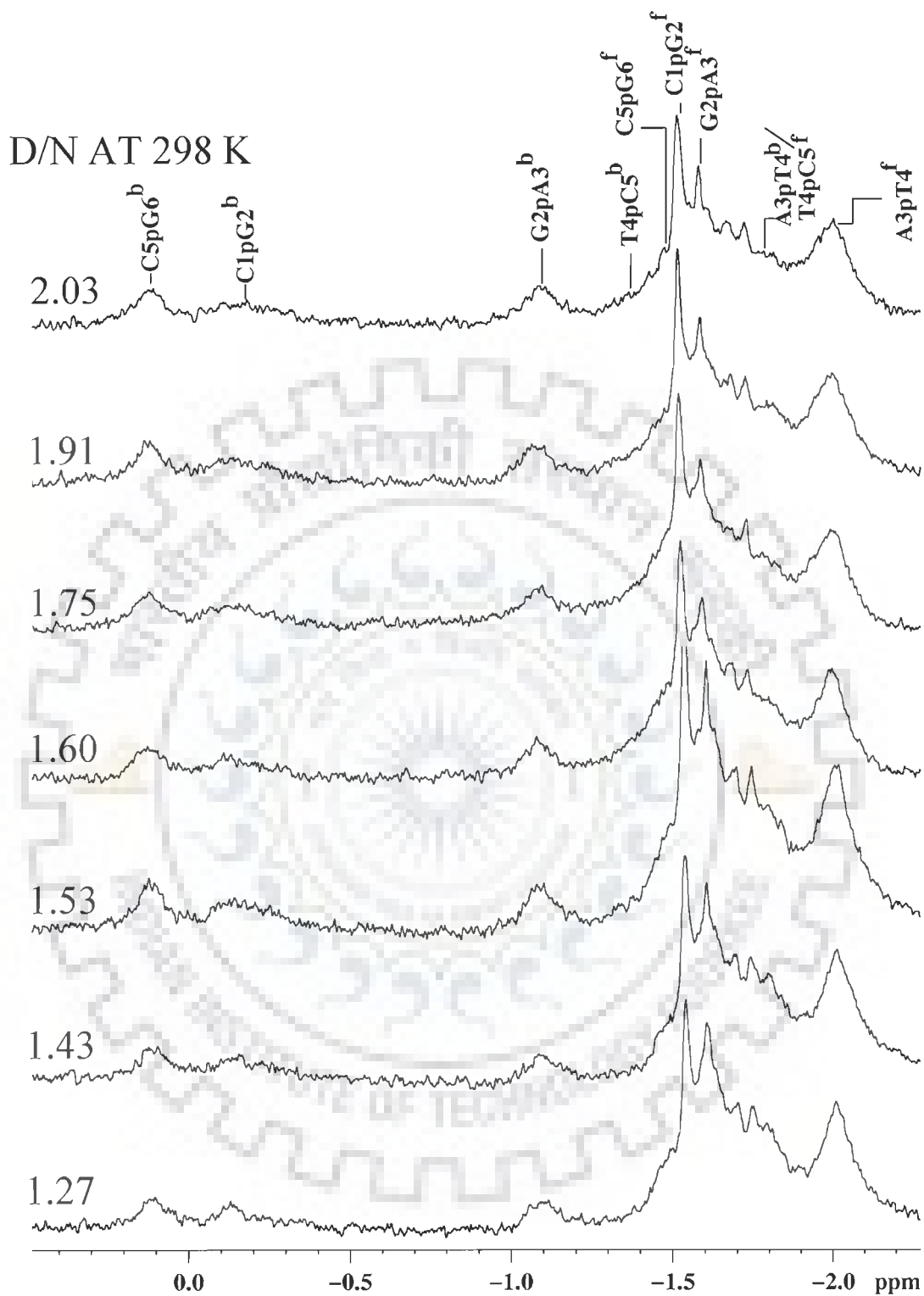


(b)

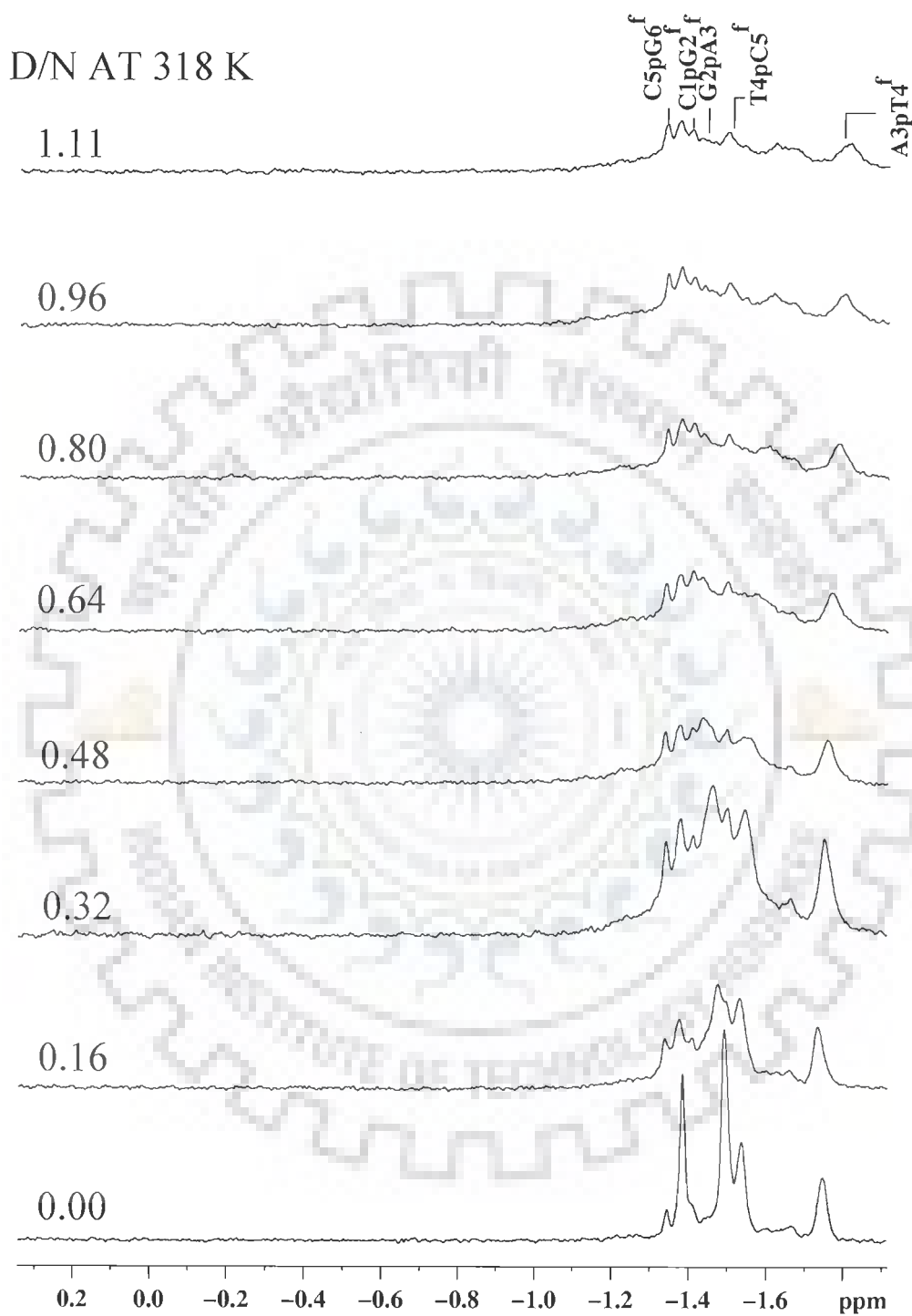


(c)

Fig. 4(c-d): Proton decoupled ^{31}P NMR spectra of 4.62 mM d-(CGATCG) $_2$ in uncomplexed state and complexed with 4'-epidriamycin with increasing drug (D) to nucleic acid duplex (N) ratios, D/N, at 298 K

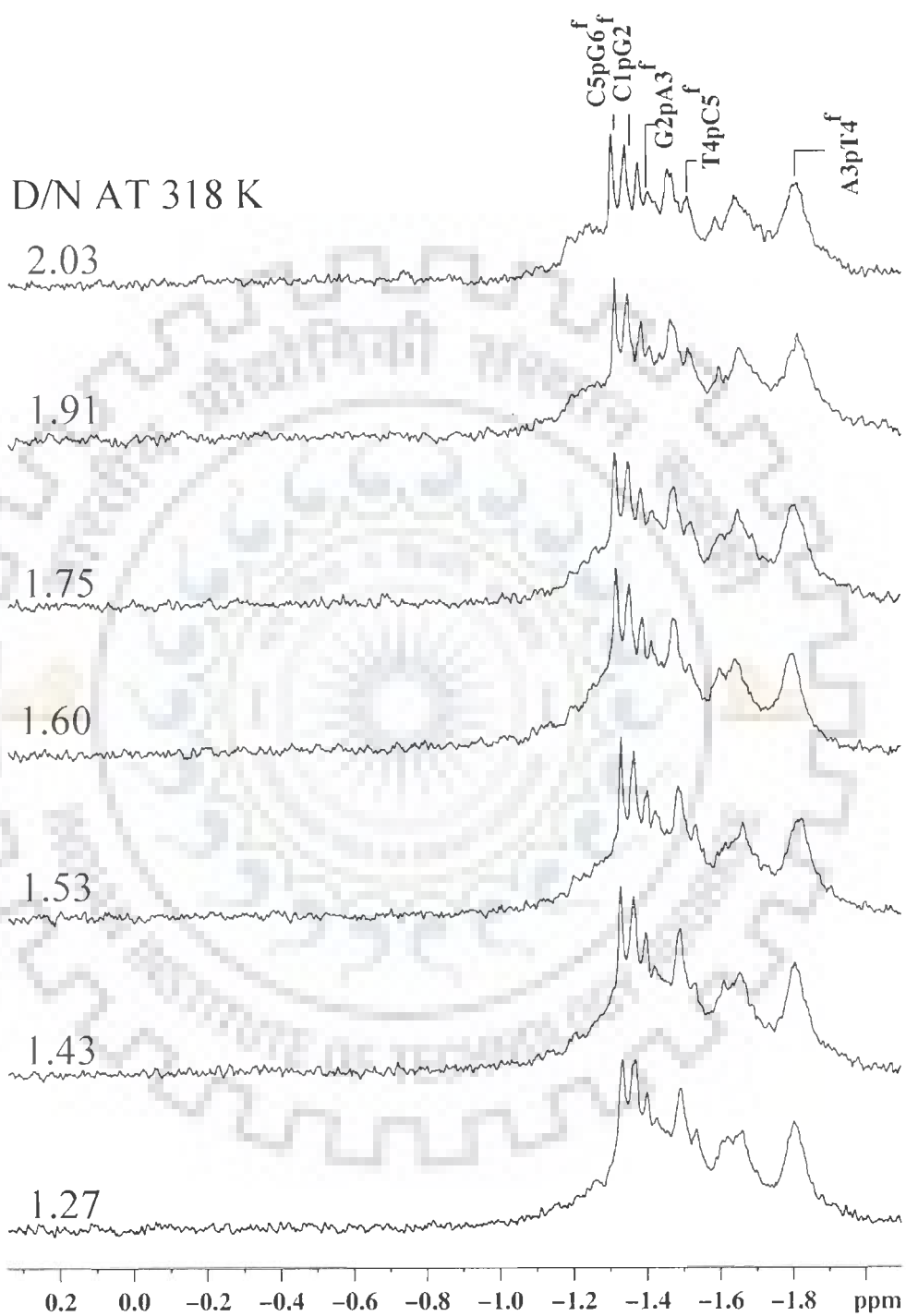


(d)



(e)

Fig. 4 (e-f): Proton decoupled ^{31}P NMR spectra of 4.62 mM d-(CGATCG)₂ in uncomplexed state and complexed with 4'-epiadriamycin with increasing drug (D) to nucleic acid duplex (N) ratios, D/N, at 318 K



(f)

^{31}P signal of bound DNA. Accordingly, the bound and free phosphate resonances are assigned in the complex (Table 3-5). The chemical shift of free and bound signals does not change with D/N ratios at all the three temperatures, that is, 275, 298 and 318 K (Figs. 6a-c).

(i) Chemical Shift

The significantly large downfield shift in C5pG6 (1.72 ppm) and C1pG2 (1.52 ppm) resonances indicate that intercalation occurs at these steps. The sites adjacent to the intercalation sites are affected and show downfield shifts of G2pA3 (0.67 ppm) and T4pC5 (0.47 ppm). The A3pT4 resonance (0.22 ppm) is least affected (Table 6). The observed shifts are markedly different from that observed in adriamycin-d-(TGATCA)₂ complex (Table 3, Chapter 5). As discussed in chapter 5, downfield shifts induced by drug are associated with the change in ζ torsional angle from g- to trans conformation and the ester O-P-O bond angle distortion. Thus we may infer that 4'-epiadriamycin induces an increase in the g, t conformation for C1pG2 and C5pG6 to accommodate insertion of drug aromatic chromophore. The downfield shift of adjacent site, G2pA3 seems to indicate distortions in O-P-O bond angle at the level of these phosphate bonds. The results are comparable with similar structures of complexes of related intercalating drugs in literature (Table 7a, Chapter 5).

(ii) Line width

The observed broadening in line width in drug-DNA complex has been attributed to chemical shift dispersion due to local heterogeneity (Jones et al., 1980; Levy et al., 1984). We observe slow exchange between bound and free ^{31}P resonance signals only at low temperatures. The drug does not seem to affect the natural line width due to dynamics as line width of bound ^{31}P signal (eg. C1pG2) decreases while that of corresponding free ^{31}P shift increases with D/N ratio. We carried out spin-lattice relaxation time (T_1) measurement studies to see the effect of intercalation.

The sharp ^{31}P NMR signals in $d\text{-(CGATCG)}_2$ get broadened on adding 4'-epiadriamycin. Using the standard pulse sequence $180^\circ\text{-}\tau\text{-}90^\circ\text{-}\tau$ and delay (D1) of 10 sec, we got T_1 of phosphate signals of uncomplexed hexamer as 984.11 ms at 298 K. The corresponding signals of free phosphorus in 2:1 4'-epiadriamycin- $d\text{-(CGATCG)}_2$ complex yielded T_1 value of 771.87 ms (broad signal). The relatively less difference ($\sim 25\%$) in T_1 of free phosphorus signals in uncomplexed DNA and drug-DNA complex, and hence T_2 or dynamics, cannot account for observed large broadening. The increase in line width of free phosphorus signals in drug-DNA complex is therefore not due to change in motional dynamics. The same has earlier been concluded by Levy et al (Levy et al., 1984) in ethidium bromide-DNA complex. Therefore the ^{31}P line widths are essentially determined by chemical shift dispersion alone. Presence of drug enhances chemical shift dispersion due to stronger differentiation of DNA phosphorus environment as a result of variations in phosphodiester bond angles O-P-O and ζ torsional angles. On the other hand, the bound phosphorus resonance in drug-DNA complex is sharp with ζ in a well defined trans conformation allowing on opening of intercalating C1...G6 and G2...C5 base pairs to $\sim 6.8 \text{ \AA}$ to accommodate 4'-epiadriamycin chromophore. The observed spin-lattice relaxation time (T_1) of C1pG2^b signal is 835.23 ms which shows that the relaxation is faster in complex and the corresponding correlation time is short. However a better insight to the structural variations of the DNA hexamer due to binding of the drug can be obtained only by intermolecular NOE contacts in ^1H 2D NOESY spectra (following chapter).

Temperature Dependence Studies

The ^{31}P 1D spectra versus temperature was also recorded at the D/N 1.0, 1.5 and 2.0 (Fig. 7a-f). The variations in chemical shift of free and bound species are shown in Figs. 8a-e. With increase in temperature, there is downfield shift of both bound as well as free ^{31}P resonances (Table 7a-c

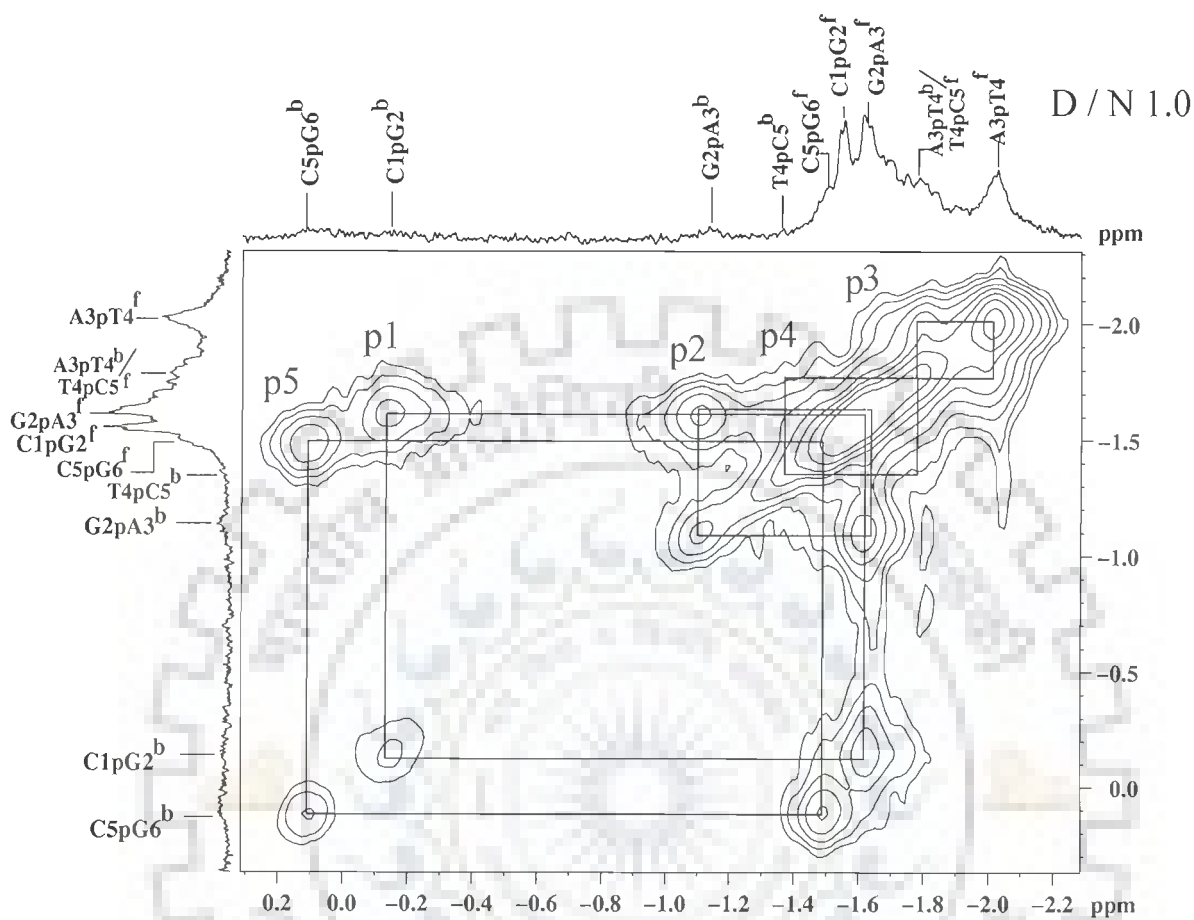


Fig. 5: ^{31}P - ^{31}P NOESY exchange spectrum at 100 ms of the complex of 4'-epiadriamycin with d-(CGATCG)₂ at drug (D) to nucleic acid duplex (N) ratios, D/N of (a) 1, (b) 1.5, and (c) 2.0 at 298K. Five cross peaks of bound and free DNA are labeled as p1 to p5 along 5' to 3' direction.

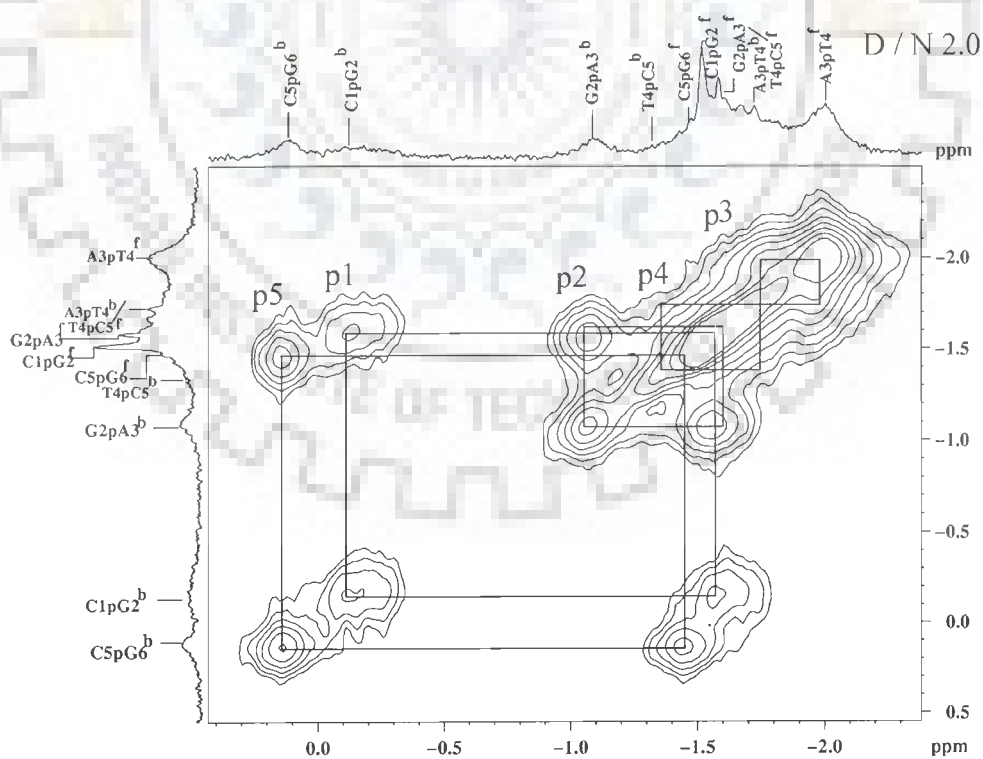
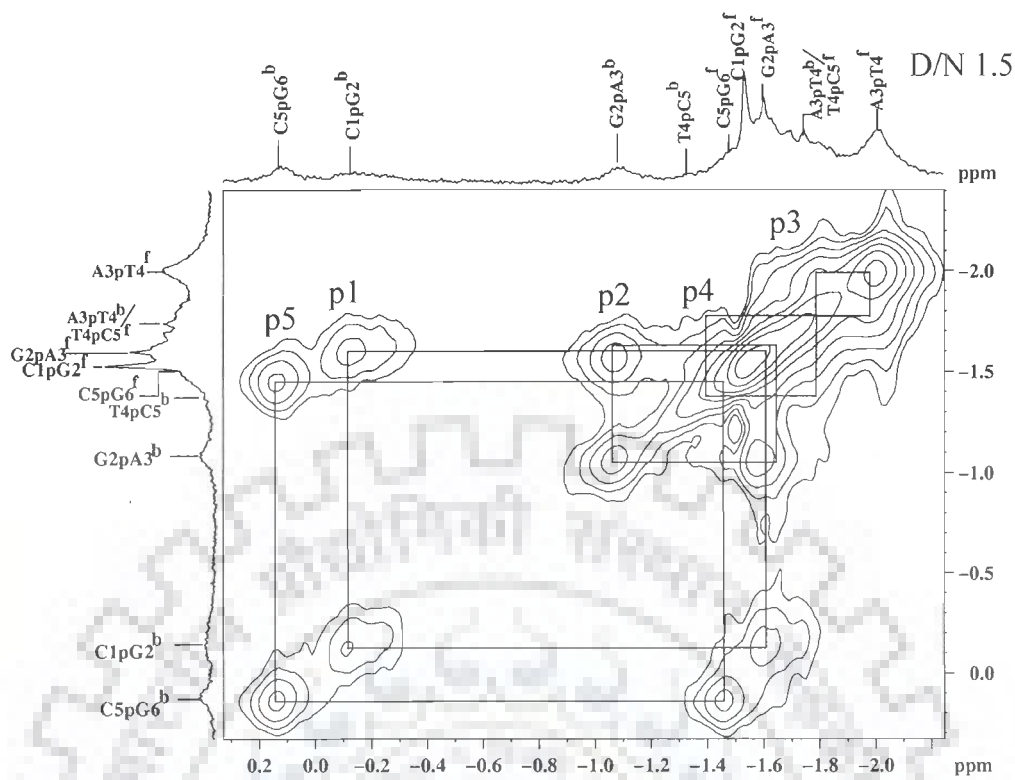


Table 3: Chemical shift of ^{31}P resonances of the phosphate groups of DNA oligomer, present in free and bound state, in the complex of 4'-Epiadriamycin with d-(CGATCG) $_2$ at 275 K at different drug (D) to nucleic acid duplex (N) ratios (D / N). In the table, $\Delta\delta = \delta_b - \delta_f$ and $\Delta\delta' = \delta_{(D/N\ 2.03)} - \delta_{(D/N\ 0.0)}$, +ve $\Delta\delta$ indicates downfield shift whereas -ve $\Delta\delta$ indicates upfield shift.

D/N Ratios	C1pG2			G2pA3			A3pT4			T4pC5			C5pG6		
	δ_f	δ_b	$\Delta\delta$	δ_f	δ_b	$\Delta\delta$	δ_f	δ_b	$\Delta\delta$	δ_f	δ_b	$\Delta\delta$	δ_f	δ_b	$\Delta\delta$
0.00	-1.92	-	-	-1.98	-	-	-2.31	-	-	-2.14	-	-	-1.77	-	-
0.16	-1.92	-0.38	+1.54	-1.98	-	-	-2.32	-2.14	+0.18	-2.14	-1.32	+0.82	-1.77	-0.14	+1.63
0.32	-1.92	-0.38	+1.54	-1.98	-1.21	+0.77	-2.32	-2.14	+0.18	-2.14	-1.33	+0.81	-1.77	-0.12	+1.65
0.48	-1.92	-0.38	+1.54	-1.99	-1.24	+0.75	-2.32	-2.14	+0.18	-2.14	-1.38	+0.76	-1.78	-0.12	+1.66
0.64	-1.91	-0.38	+1.53	-1.99	-1.24	+0.75	-2.32	-2.14	+0.18	-2.14	-1.45	+0.69	-1.78	-0.12	+1.66
0.80	-1.91	-0.38	+1.53	-1.99	-1.24	+0.75	-2.32	-2.14	+0.18	-2.14	-1.45	+0.69	-1.79	-0.12	+1.67
0.96	-1.90	-0.37	+1.53	-1.99	-1.24	+0.75	-2.32	-2.14	+0.18	-2.14	-1.48	+0.66	-1.79	-0.12	+1.67
1.11	-1.89	-0.37	+1.52	-1.99	-1.25	+0.74	-2.32	-2.14	+0.18	-2.14	-1.59	+0.55	-1.79	-0.13	+1.66
1.27	-1.89	-0.37	+1.52	-1.99	-1.27	+0.72	-2.32	-2.13	+0.19	-2.13	-1.59	+0.54	-1.79	-0.11	+1.68
1.43	-1.88	-0.37	+1.51	-1.97	-1.27	+0.70	-2.32	-2.12	+0.20	-2.12	-1.60	+0.52	-1.79	-0.11	+1.68
1.53	-1.88	-0.37	+1.51	-1.96	-1.27	+0.69	-2.32	-2.10	+0.22	-2.10	-1.60	+0.50	-1.79	-0.10	+1.69
1.60	-1.87	-0.37	+1.50	-1.96	-1.27	+0.69	-2.30	-2.10	+0.20	-2.10	-1.61	+0.49	-1.79	-0.10	+1.69
1.75	-1.87	-0.37	+1.50	-1.94	-1.27	+0.67	-2.30	-2.09	+0.21	-2.09	-1.61	+0.48	-1.80	-0.09	+1.71
1.91	-1.86	-0.37	+1.49	-1.94	-1.27	+0.67	-2.30	-2.08	+0.22	-2.08	-1.61	+0.47	-1.80	-0.09	+1.71
2.03	-1.86	-0.34	+1.52	-1.94	-1.27	+0.67	-2.30	-2.08	+0.22	-2.08	-1.61	+0.47	-1.81	-0.09	+1.72
$\Delta\delta'$	+0.06	+0.04		+0.04	-0.06		+0.01	+0.06		+0.06	-0.29		-0.04	+0.05	

Table 4: Chemical shift of ^{31}P resonances of the phosphate groups of DNA oligomer, present in free and bound state, in the complex of 4'-Epiadriamycin with d-(CGATCG) $_2$ at 298 K at different drug (D) to nucleic acid duplex (N) ratios (D/N). In the table, $\Delta\delta = \delta_b - \delta_f$ and $\Delta\delta' = \delta_{(D/N\ 2.03)} - \delta_{(D/N\ 0.0)}$; +ve $\Delta\delta$ indicates downfield shift whereas -ve $\Delta\delta$ indicates upfield shift.

D/N Ratios	C1pG2			G2pA3			A3pT4			T4pC5			C5pG6		
	δ_f	δ_b	$\Delta\delta$	δ_f	δ_b	$\Delta\delta$	δ_f	δ_b	$\Delta\delta$	δ_f	δ_b	$\Delta\delta$	δ_f	δ_b	$\Delta\delta$
0.00	-1.56	-	-	-1.63	-	-	-2.01	-	-	-1.79	-	-	-1.49	-	-
0.16	-1.56	-	-	-1.63	-	-	-2.01	-1.79	+0.22	-1.79	-1.35	+0.44	-1.49	-	-
0.32	-1.56	-	-	-1.62	-	-	-2.01	-1.79	+0.22	-1.79	-1.35	+0.44	-1.49	-	-
0.48	-1.56	-0.13	+1.43	-1.62	-1.11	+0.51	-2.01	-1.79	+0.22	-1.79	-1.35	+0.44	-1.50	+0.13	+1.63
0.64	-1.55	-0.14	+1.41	-1.62	-1.11	+0.51	-2.01	-1.78	+0.23	-1.78	-1.35	+0.43	-1.50	+0.12	+1.62
0.80	-1.55	-0.14	+1.41	-1.62	-1.11	+0.51	-2.01	-1.79	+0.22	-1.79	-1.35	+0.44	-1.50	+0.11	+1.61
0.96	-1.55	-0.15	+1.40	-1.61	-1.15	+0.46	-2.02	-1.79	+0.23	-1.79	-1.35	+0.44	-1.50	+0.11	+1.61
1.11	-1.54	-0.10	+1.44	-1.61	-1.08	+0.53	-2.00	-1.79	+0.21	-1.79	-1.35	+0.44	-1.50	+0.12	+1.62
1.27	-1.54	-0.12	+1.42	-1.60	-1.10	+0.50	-2.00	-1.79	+0.21	-1.79	-1.37	+0.42	-1.50	+0.11	+1.61
1.43	-1.53	-0.12	+1.41	-1.60	-1.09	+0.51	-2.00	-1.79	+0.21	-1.79	-1.37	+0.42	-1.50	+0.11	+1.61
1.53	-1.53	-0.12	+1.41	-1.60	-1.08	+0.52	-2.00	-1.78	+0.22	-1.78	-1.38	+0.40	-1.50	+0.11	+1.61
1.60	-1.52	-0.12	+1.40	-1.58	-1.08	+0.50	-1.99	-1.78	+0.21	-1.78	-1.38	+0.40	-1.48	+0.12	+1.60
1.75	-1.51	-0.12	+1.39	-1.58	-1.08	+0.50	-1.99	-1.78	+0.21	-1.78	-1.38	+0.40	-1.48	+0.12	+1.60
1.91	-1.51	-0.11	+1.40	-1.58	-1.07	+0.51	-1.99	-1.78	+0.21	-1.78	-1.38	+0.40	-1.47	+0.12	+1.59
2.03	-1.51	-0.10	+1.41	-1.58	-1.07	+0.51	-1.99	-1.78	+0.21	-1.78	-1.38	+0.40	-1.47	+0.12	+1.59
$\Delta\delta'$	+0.05	+0.03		+0.05	+0.04		+0.02	+0.01		+0.01	-0.03		+0.02	-0.01	

Table 5: Chemical shift of ^{31}P resonances of the phosphate groups of DNA oligomer, present in free and bound state, in the complex of 4'-Epiadriamycin with d-(CGATCG) $_2$ at 318 K at different drug (D) to nucleic acid duplex (N) ratios (D/N). In the table, $\Delta\delta = \delta_{(D/N = 2.03)} - \delta_{(D/N = 0.0)}$ and +ve $\Delta\delta$ indicates downfield shift whereas -ve $\Delta\delta$ indicates upfield shift.

D/N Ratios	C1pG2	G2pA3	A3pT4	T4pC5	C5pG6
0.00	-1.41	-1.49	-1.75	-1.54	-1.38
0.16	-1.41	-1.47	-1.73	-1.53	-1.36
0.32	-1.41	-1.46	-1.75	-1.54	-1.36
0.48	-1.41	-1.43	-1.76	-1.54	-1.35
0.64	-1.41	-1.43	-1.77	-1.54	-1.35
0.80	-1.41	-1.43	-1.78	-1.54	-1.35
0.96	-1.38	-1.41	-1.80	-1.54	-1.35
1.11	-1.40	-1.42	-1.81	-1.54	-1.35
1.27	-1.40	-1.42	-1.80	-1.53	-1.34
1.43	-1.39	-1.41	-1.80	-1.53	-1.34
1.53	-1.39	-1.36	-1.81	-1.53	-1.33
1.60	-1.38	-1.40	-1.80	-1.51	-1.33
1.75	-1.38	-1.40	-1.80	-1.51	-1.33
1.91	-1.38	-1.40	-1.81	-1.51	-1.33
2.03	-1.37	-1.40	-1.81	-1.51	-1.32
$\Delta\delta$	+0.04	+0.09	-0.06	+0.03	+0.06

Table 6: ^{31}P chemical shift assignments of free (δ^f) and bound (δ^b) phosphate groups in the 4'-Epiadriamycin–d-(CGATCG) $_2$ complex at drug (D) to nucleic acid duplex (N) ratios, D / N = 1, 1.5 and 2.0. The change in chemical shift, $\Delta\delta = \delta^b - \delta^f$, due to binding is also indicated for the three complexes. +ve $\Delta\delta$ indicates downfield shift.

At 298 K Phosphate group	D/N 1:1			D/N 1.5:1			D/N 2:1		
	δ_b	δ_f	$\Delta\delta$	δ_b	δ_f	$\Delta\delta$	δ_b	δ_f	$\Delta\delta$
C1pG2	-0.15	-1.55	+1.40	-0.12	-1.53	+1.41	-0.10	-1.51	+1.41
G2pA3	-1.15	-1.61	+0.46	-1.08	-1.60	+0.52	-1.07	-1.58	+0.51
A3pT4	-1.79	-2.02	+0.23	-1.78	-2.00	+0.22	-1.78	-1.99	+0.21
T4pC5	-1.35	-1.79	+0.44	-1.38	-1.78	+0.40	-1.38	-1.78	+0.40
C5pG6	+0.11	-1.50	+1.61	+0.11	-1.50	+1.61	+0.12	-1.47	+1.59

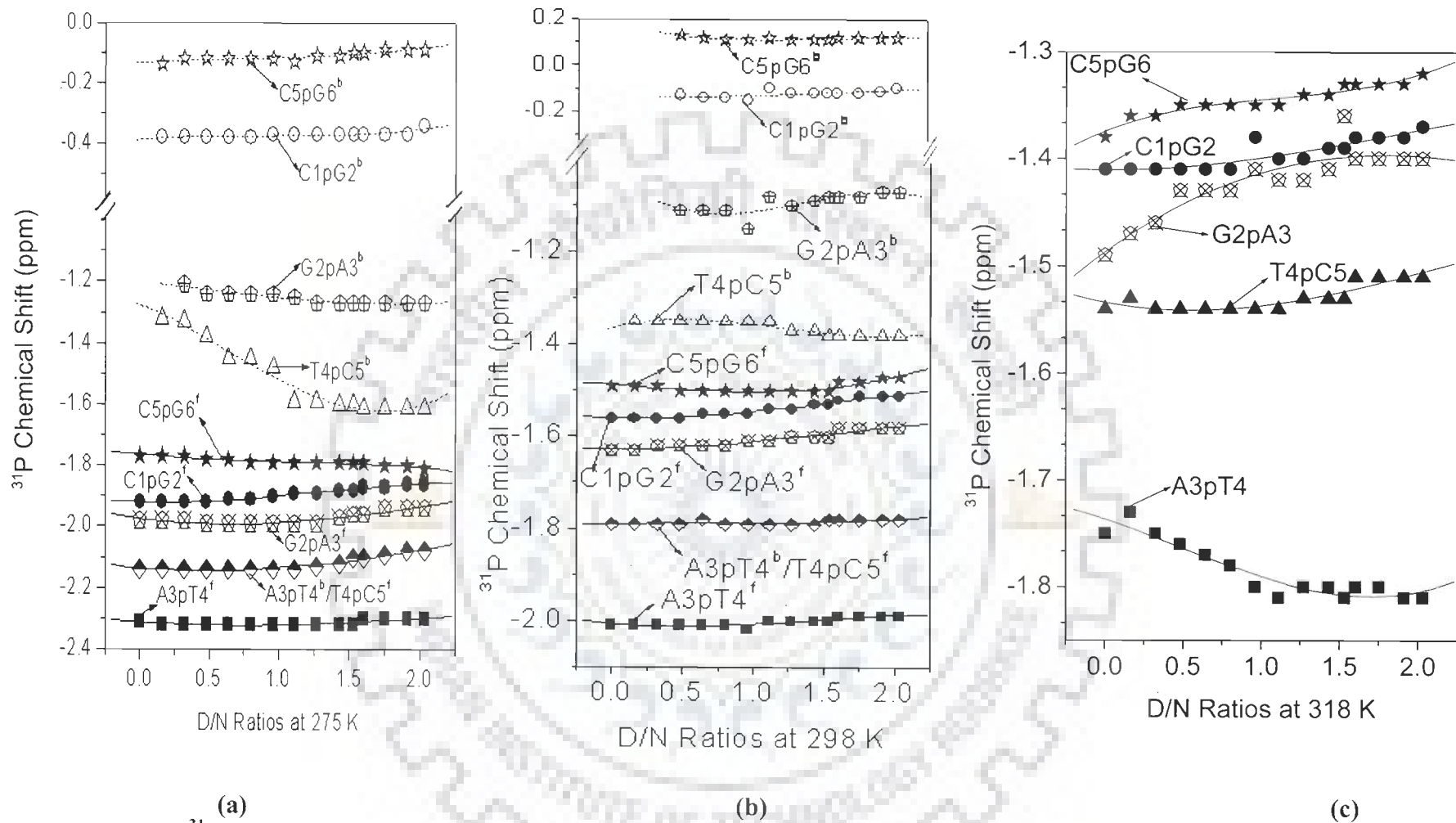


Fig. 6(a-c): ^{31}P Chemical Shift of d-(CGATCG)₂ in free and bound state complexed with 4'-epiadriamycin with increasing drug (D) to nucleic acid duplex (N) ratios, D/N, at (a) 275 K (b) 298 K (c) 318 K

and 8a-b). On formation of the complex of d-(CGATCG)₂ with 4'-epiadriamycin, the T_m of the complex is 301 K and is thus enhanced by 13 K ($\Delta T_m = 301 - 288$ K) (Figs. 8a-c and Table 7a-c). At temperatures much below T_m, the ³¹P signals in 4'-epiadriamycin-d-(CGATCG)₂ complex are sharp because the rate of exchange of the phosphates in the two sites is slow. A comparison of melting curve of uncomplexed d-(CGATCG)₂ with corresponding free ³¹P resonances in 2:1 4'-epiadriamycin-d-(CGATCG)₂ complex (Fig. 8d and Table 8a) shows that there are no major differences between the two curves, as expected. The bound ³¹P resonances (Fig. 8e and Table 8b) show $\delta_{328} - \delta_{275}$ is slightly smaller ($\Delta\delta \sim 0.2, 0.2$ and 0.3 ppm for C1pG2, G2pA3 and C5pG6, respectively) than the corresponding ³¹P signals of free resonances in drug-DNA complex ($\Delta\delta \sim 0.6$ ppm). This is in sharp contrast to results obtained in chapter 5 for adriamycin-d-(TGATCA)₂ complex (Table 9a-b, Chapter 5). The phenomenon of duplex to single strand transition is taking place along with the transition from binding to unbinding of the drug. At 298 K, the d-(CGATCG)₂ complexed with 4'-epiadriamycin exist entirely as double helix but with slight broadening of peaks, may be because of the intercalation of the drug acting as the stabilizing factor. At 318 K, the signals are in the fast exchange regime, and are not sufficiently narrow to be followed individually through the titration. The phenomenon of duplex to single strand transition along with self association of drug and binding to DNA in D/N ratio of 1.0 or 2.0 show the same as mentioned above. The values are not calculated as the signals are not that sharp so as to measure the integral or the line width of it.

Comparative study of adriamycin-d-(TGATCA)₂ and 4'-epiadriamycin-d-(CGATCG)₂ complexes

The present studies on adriamycin-d-(TGATCA)₂ and 4'-epiadriamycin-d-(CGATCG)₂ complexes clearly demonstrate that drugs which intercalate between base pairs of DNA by

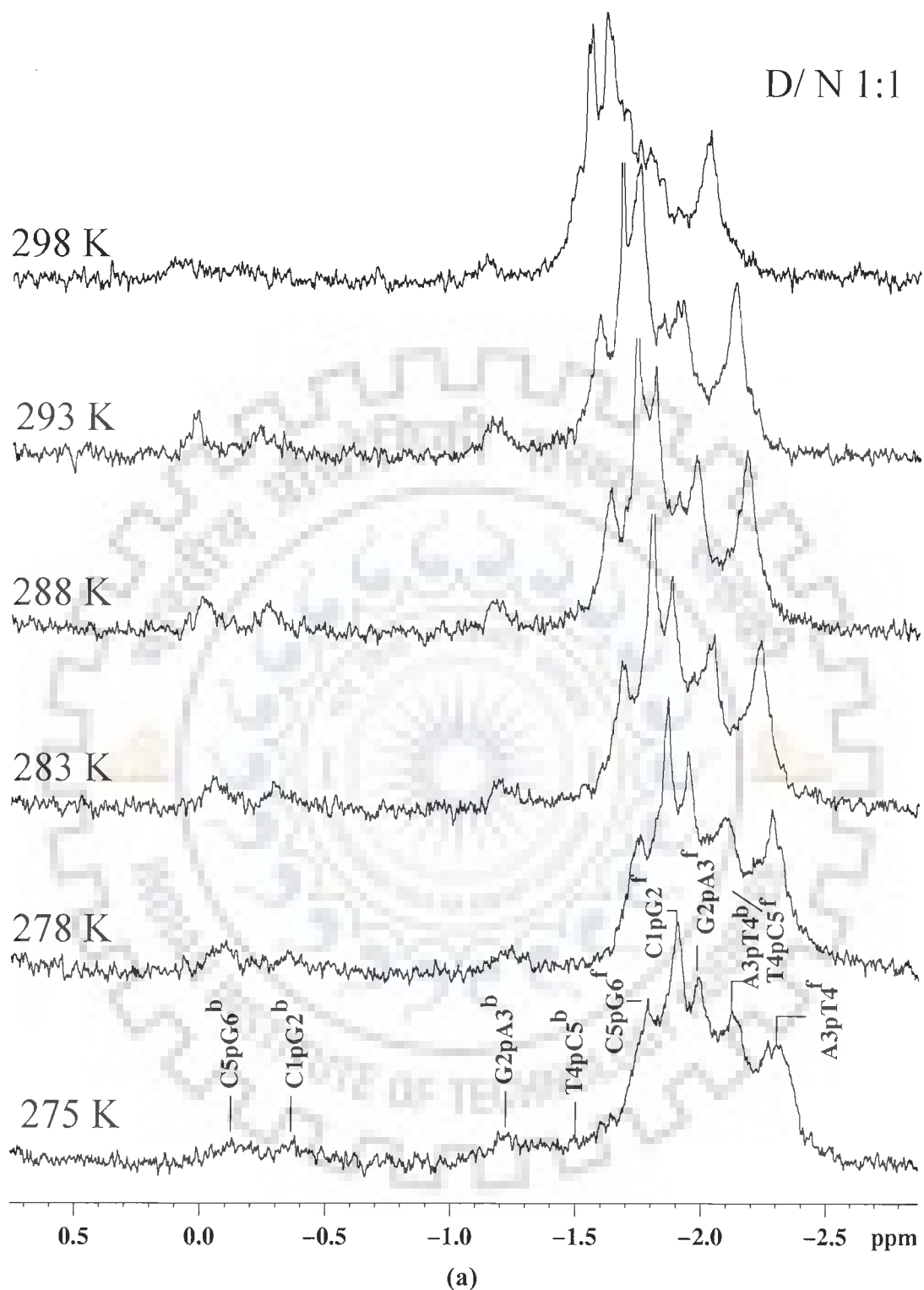
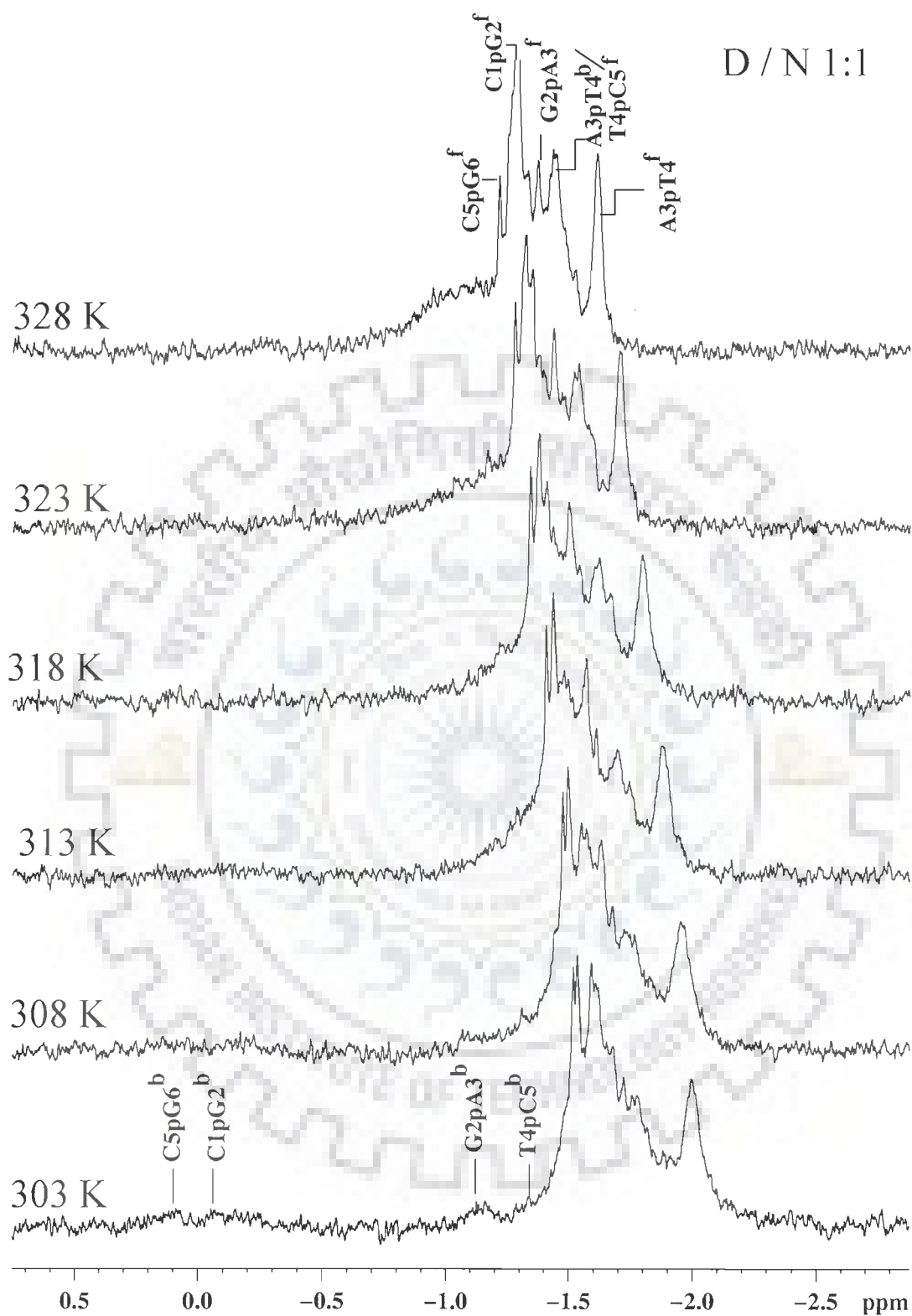


Fig. 7(a-b): Proton decoupled ^{31}P NMR spectra of d-(CGATCG)₂ complexed with 4'-Epiadriamycin (D/N = 1.0) as a function of temperature in the range 275–328 K



(b)

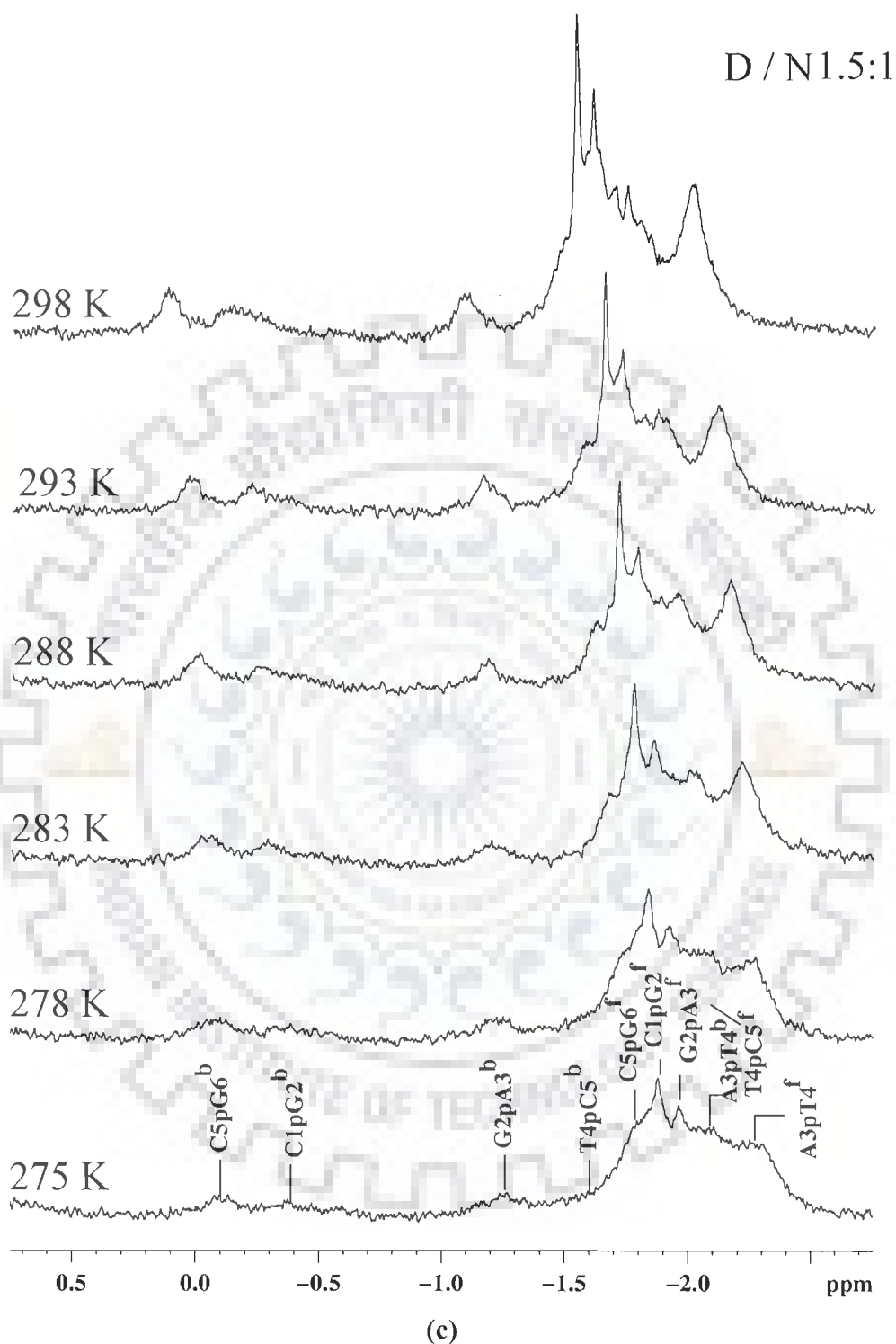
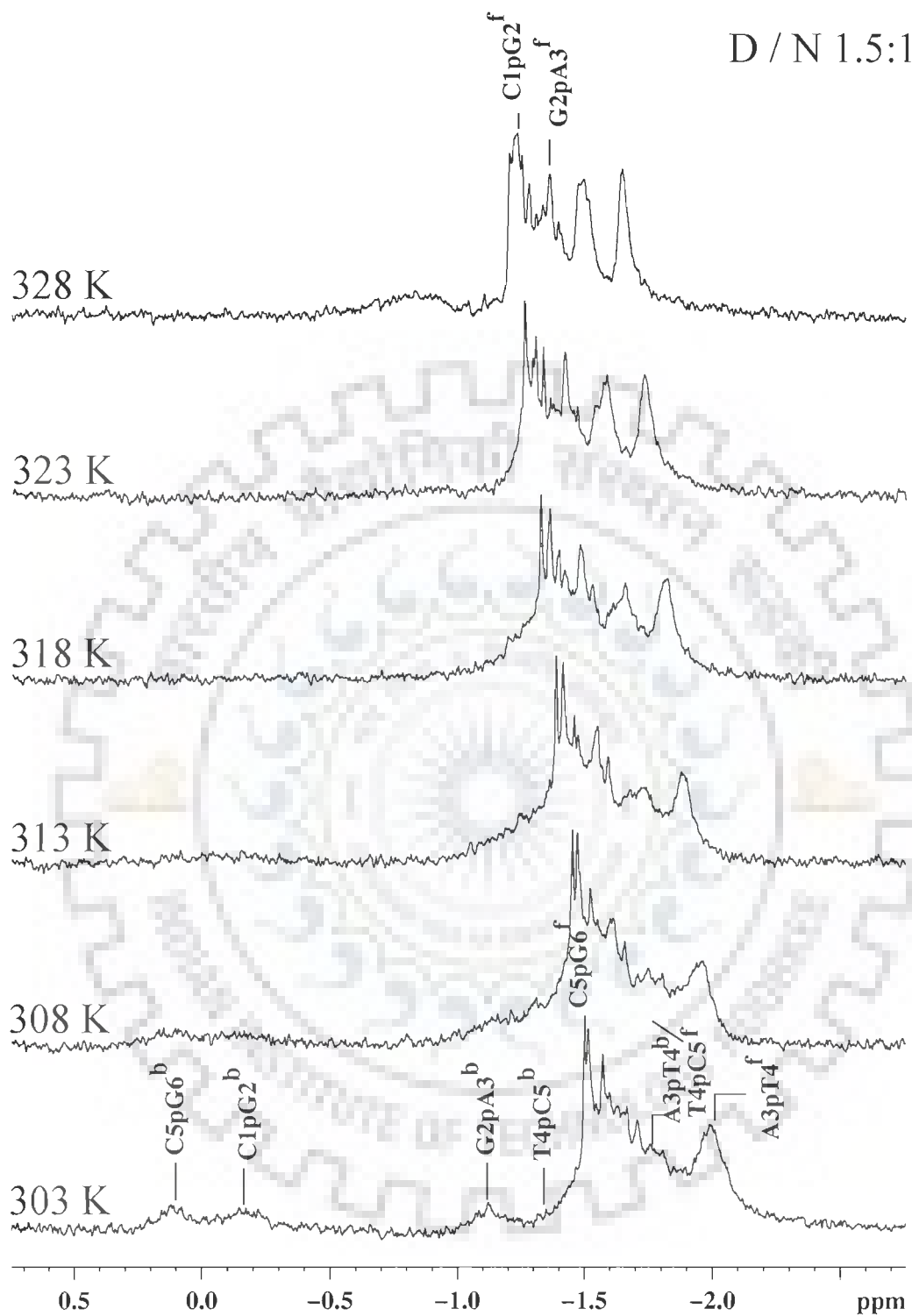
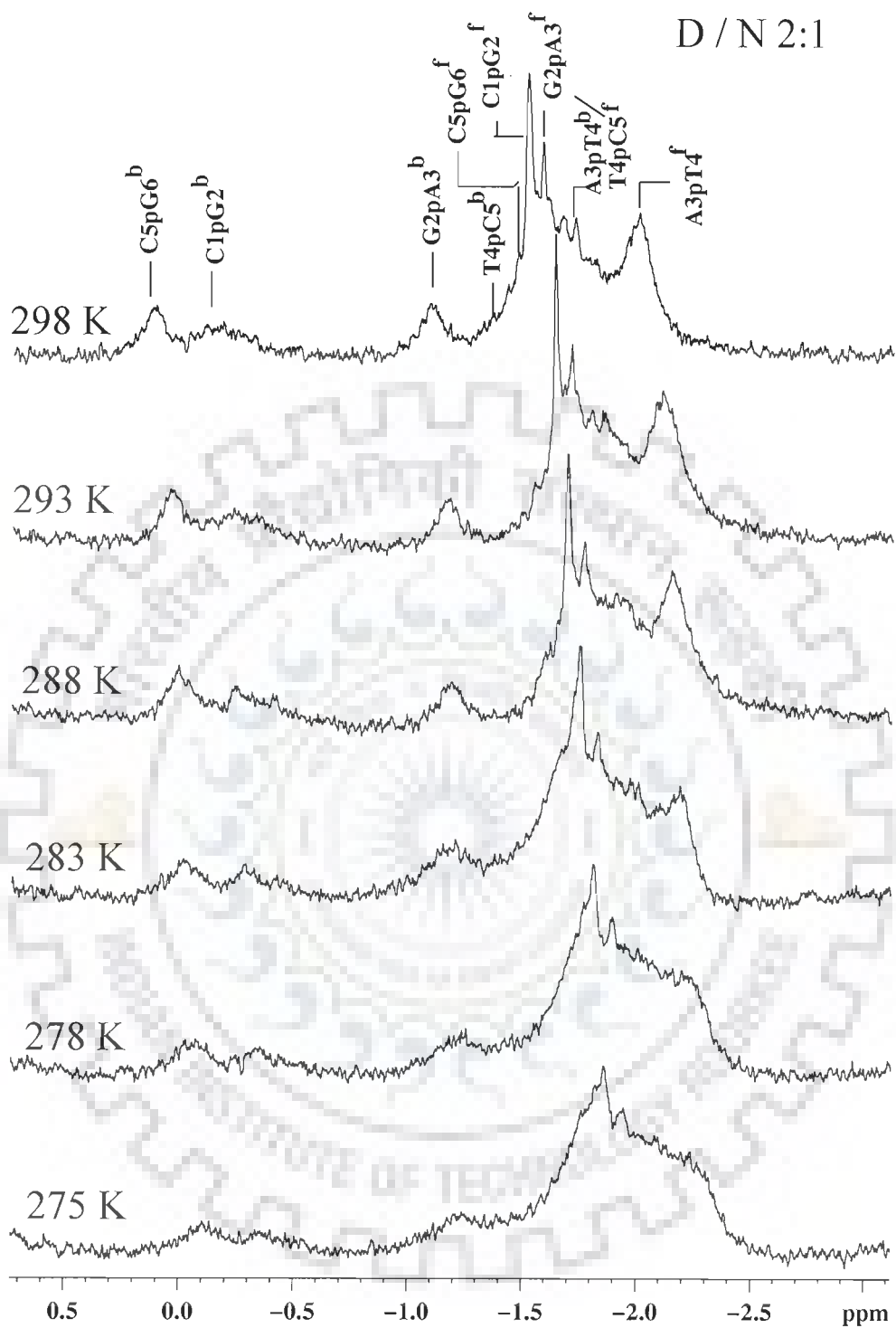


Fig. 7(c-d): Proton decoupled ^{31}P NMR spectra of d-(CGATCG) $_2$ complexed with 4'-Epiadriamycin (D/N = 1.5) as a function of temperature in the range 275-328 K

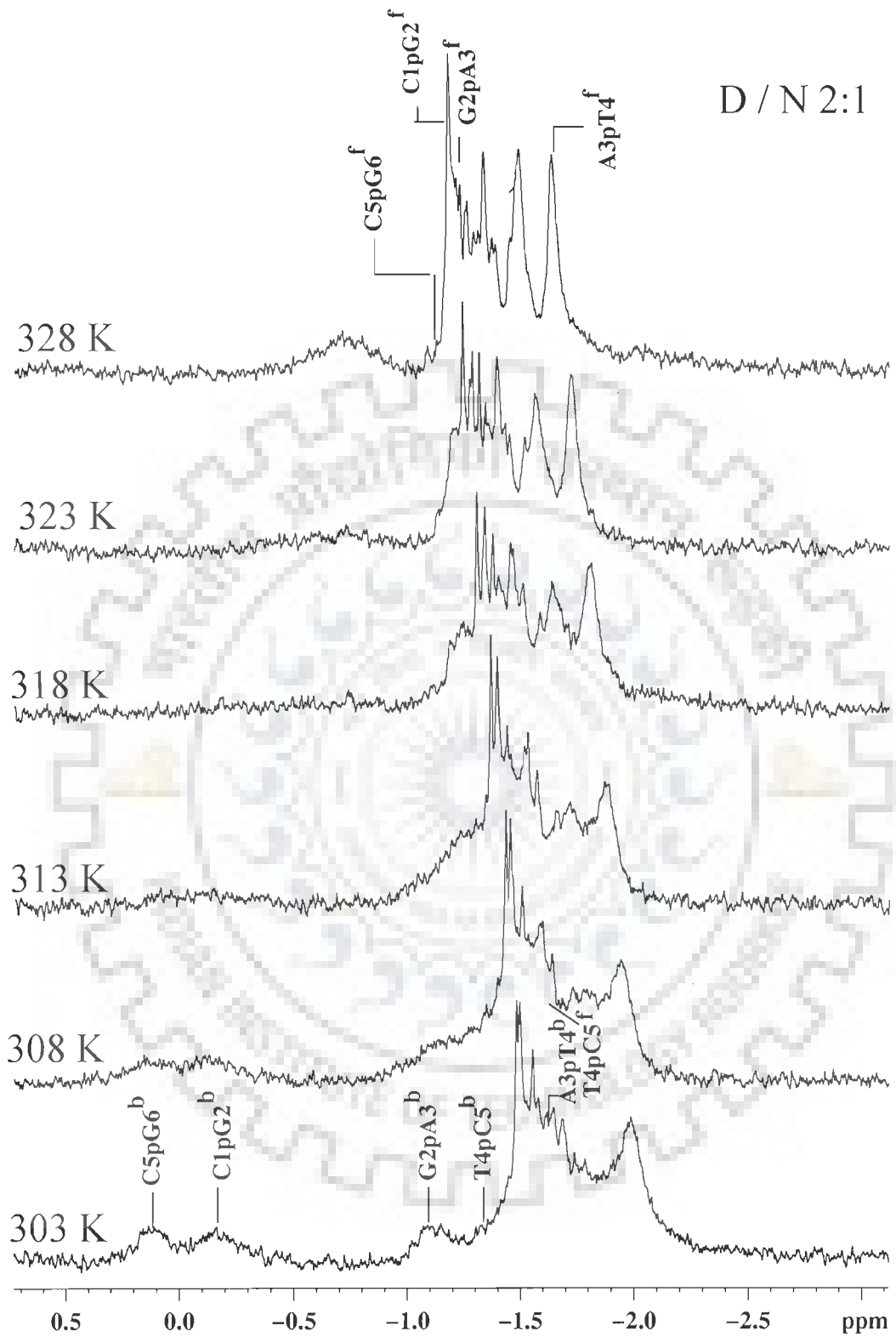


(d)



(e)

Fig. 7(e-f): Proton decoupled ^{31}P NMR spectra of $d\text{-(CGATCG)}_2$ complexed with 4'-Epiadriamycin (D/N = 2.0) as a function of temperature in the range 275-328 K



(f)

Table 7a: ^{31}P chemical shift $d\text{-(CGATCG)}_2 - 4'\text{-Epiadriamycin}$ complex ($D/N = 1.0$) as a function of temperature in the range 275 – 328 K. In the table, $\Delta\delta = \delta_b - \delta_f$ and $\Delta\delta' = \delta_{(328\text{ K})} - \delta_{(275\text{ K})}$; +ve $\Delta\delta$ indicates downfield shift whereas -ve $\Delta\delta$ indicates upfield shift.

Temp. (K)	C1pG2			G2pA3			A3pT4			T4pC5			C5pG6		
	δ_f	δ_b	$\Delta\delta$	δ_f	δ_b	$\Delta\delta$	δ_f	δ_b	$\Delta\delta$	δ_f	δ_b	$\Delta\delta$	δ_f	δ_b	$\Delta\delta$
275	-1.90	-0.37	+1.53	-1.99	-1.24	+0.75	-2.32	-2.14	+0.18	-2.14	-1.48	+0.66	-1.79	-0.12	+1.67
278	-1.87	-0.35	+1.52	-1.95	-1.24	+0.71	-2.28	-2.10	+0.18	-2.10	-1.46	+0.64	-1.75	-0.10	+1.65
283	-1.80	-0.29	+1.51	-1.88	-1.19	+0.69	-2.23	-2.04	+0.19	-2.04	-1.43	+0.61	-1.69	-0.05	+1.64
288	-1.74	-0.26	+1.48	-1.81	-1.19	+0.62	-2.17	-1.98	+0.19	-1.98	-1.39	+0.59	-1.64	0.00	+1.64
293	-1.68	-0.23	+1.45	-1.75	-1.15	+0.60	-2.12	-1.90	+0.22	-1.90	-1.38	+0.52	-1.59	+0.03	+1.62
298	-1.55	-0.15	+1.40	-1.61	-1.11	+0.50	-2.02	-1.79	+0.23	-1.79	-1.35	+0.44	-1.50	+0.11	+1.61
303	-1.52	-		-1.59	-		-2.00	-1.72	+0.28	-1.72	-		-1.48	-	
308	-1.48	-		-1.55	-		-1.95	-1.67	+0.28	-1.67	-		-1.45	-	
313	-1.43	-		-1.47	-		-1.88	-1.61	+0.27	-1.61	-		-1.40	-	
318	-1.38	-		-1.41	-		-1.80	-1.54	+0.26	-1.54	-		-1.35	-	
323	-1.32	-		-1.35	-		-1.70	-1.52	+0.18	-1.52	-		-1.28	-	
328	-1.29	-		-1.32	-		-1.61	-1.44	+0.17	-1.44	-		-1.21	-	
$\Delta\delta'$	+0.61	+0.22		+0.67	+0.13		+0.71	+0.70		+0.70	+0.13		+0.58	+0.23	

Table 7b: ³¹P chemical shift d-(CGATCG)₂ – 4'-Epiadriamycin complex (D/N = 1.5) as a function of temperature in the range 275 – 328 K. In the table, $\Delta\delta = \delta_b - \delta_f$ and $\Delta\delta' = \delta_{(328\text{ K})} - \delta_{(275\text{ K})}$; +ve $\Delta\delta$ indicates downfield shift whereas -ve $\Delta\delta$ indicates upfield shift.

Temp. (K)	C1pG2			G2pA3			A3pT4			T4pC5			C5pG6		
	δ_f	δ_b	$\Delta\delta$	δ_f	δ_b	$\Delta\delta$	δ_f	δ_b	$\Delta\delta$	δ_f	δ_b	$\Delta\delta$	δ_f	δ_b	$\Delta\delta$
275	-1.88	-0.37	+1.51	-1.96	-1.27	+0.69	-2.32	-2.10	+0.22	-2.10	-1.60	+0.50	-1.79	-0.10	+1.69
278	-1.84	-0.37	+1.47	-1.92	-1.27	+0.65	-2.27	-2.10	+0.17	-2.10	-1.58	+0.52	-1.74	-0.10	+1.64
283	-1.77	-0.28	+1.49	-1.86	-1.21	+0.65	-2.21	-2.00	+0.21	-2.00	-1.56	+0.44	-1.67	-0.06	+1.61
288	-1.71	-0.26	+1.45	-1.79	-1.18	+0.61	-2.17	-1.96	+0.21	-1.96	-1.49	+0.47	-1.62	-0.01	+1.61
293	-1.65	-0.22	+1.43	-1.73	-1.16	+0.57	-2.11	-1.86	+0.25	-1.86	-1.44	+0.42	-1.58	+0.04	+1.62
298	-1.53	-0.12	+1.41	-1.60	-1.08	+0.52	-2.00	-1.78	+0.22	-1.78	-1.38	+0.40	-1.50	+0.13	+1.63
303	-1.51	-0.12	+1.39	-1.57	-1.08	+0.49	-1.99	-1.71	+0.28	-1.71	-1.35	+0.36	-1.49	+0.12	+1.61
308	-1.46	-0.12	+1.34	-1.52	-1.08	+0.44	-1.96	-1.66	+0.30	-1.66	-1.31	+0.35	-1.45	+0.13	+1.58
313	-1.41	-		-1.46	-		-1.88	-1.59	+0.29	-1.59	-1.25	+0.34	-1.38	-	
318	-1.36	-		-1.39	-		-1.81	-1.53	+0.28	-1.53	-1.22	+0.31	-1.33	-	
323	-1.30	-		-1.36	-		-1.73	-1.46	+0.27	-1.46	-		-1.26	-	
328	-1.23	-		-1.33	-		-1.65	-1.40	+0.25	-1.40	-		-1.20	-	
$\Delta\delta'$	+0.65	+0.25		+0.63	+0.19		+0.67	+0.70		+0.70	+0.38		+0.59	+0.23	

Table 7c: ^{31}P chemical shift d-(CGATCG) $_2$ – 4'-Epiadriamycin complex (D/N = 2.0) as a function of temperature in the range 275 – 328 K. In the table, $\Delta\delta = \delta_b - \delta_f$ and $\Delta\delta' = \delta_{(328\text{ K})} - \delta_{(275\text{ K})}$; +ve $\Delta\delta$ indicates downfield shift whereas -ve $\Delta\delta$ indicates upfield shift.

Temp. (K)	C1pG2			G2pA3			A3pT4			T4pC5			C5pG6		
	δ_f	δ_b	$\Delta\delta$	δ_f	δ_b	$\Delta\delta$	δ_f	δ_b	$\Delta\delta$	δ_f	δ_b	$\Delta\delta$	δ_f	δ_b	$\Delta\delta$
275	-1.86	-0.34	+1.52	-1.94	-1.27	+0.67	-2.30	-2.08	+0.22	-2.08	-1.61	+0.47	-1.81	-0.09	+1.72
278	-1.81	-0.34	+1.47	-1.89	-1.25	+0.64	-2.22	-2.03	+0.19	-2.03	-1.58	+0.45	-1.76	-0.07	+1.69
283	-1.75	-0.28	+1.47	-1.82	-1.21	+0.61	-2.19	-1.97	+0.22	-1.97	-1.53	+0.44	-1.67	-0.02	+1.65
288	-1.69	-0.24	+1.45	-1.76	-1.18	+0.58	-2.15	-1.93	+0.22	-1.93	-1.51	+0.42	-1.64	+0.02	+1.66
293	-1.63	-0.21	+1.42	-1.70	-1.16	+0.54	-2.10	-1.84	+0.26	-1.84	-1.47	+0.37	-1.58	+0.05	+1.63
298	-1.51	-0.10	+1.41	-1.58	-1.07	+0.51	-1.99	-1.78	+0.21	-1.78	-1.38	+0.40	-1.47	+0.13	+1.60
303	-1.49	-0.10	+1.39	-1.55	-1.07	+0.48	-1.98	-1.76	+0.22	-1.76	-1.34	+0.42	-1.47	+0.14	+1.61
308	-1.44	-0.10	+1.34	-1.50	-1.07	+0.43	-1.94	-1.72	+0.22	-1.72	-1.27	+0.45	-1.43	+0.16	+1.59
313	-1.39	-		-1.44	-		-1.88	-1.65	+0.23	-1.65	-1.23	+0.42	-1.36	-	
318	-1.37	-		-1.40	-		-1.81	-1.51	+0.30	-1.51	-1.23	+0.28	-1.32	-	
323	-1.27	-		-1.34	-		-1.72	-1.43	+0.29	-1.43	-1.20	+0.23	-1.23	-	
328	-1.20	-		-1.33	-		-1.63	-1.37	+0.26	-1.37	-		-1.17	-	
$\Delta\delta'$	+0.66	+0.24		+0.61	+0.20		+0.67	+0.71		+0.71	+0.41		+0.64	+0.25	

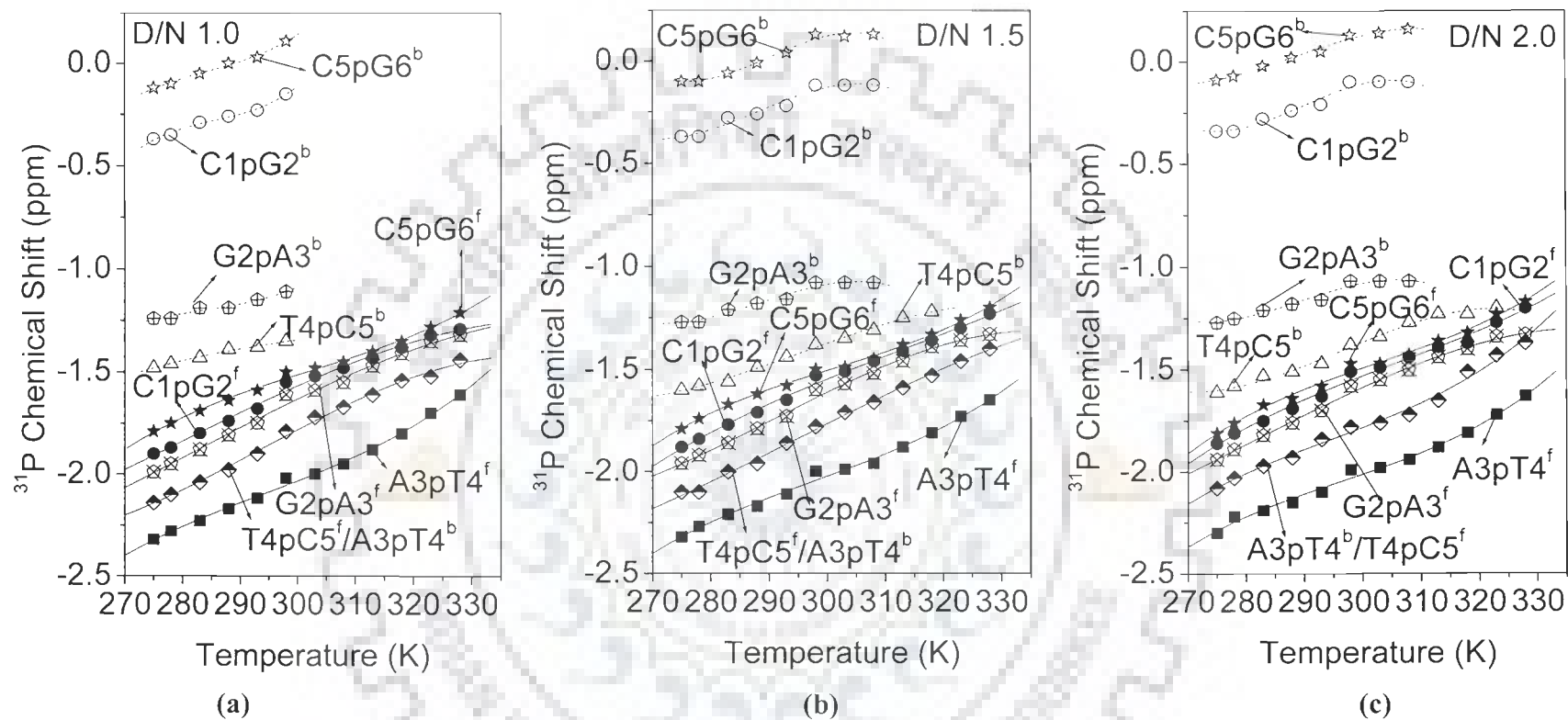


Fig. 8 Free (f) and bound (b) ^{31}P Chemical Shift of $d\text{-(CGATCG)}_2$ complexed with 4'-Epiadriamycin as a function of temperature in the range 275–328 K at D/N ratio (a) 1.0 (b) 1.5 (c) 2.0

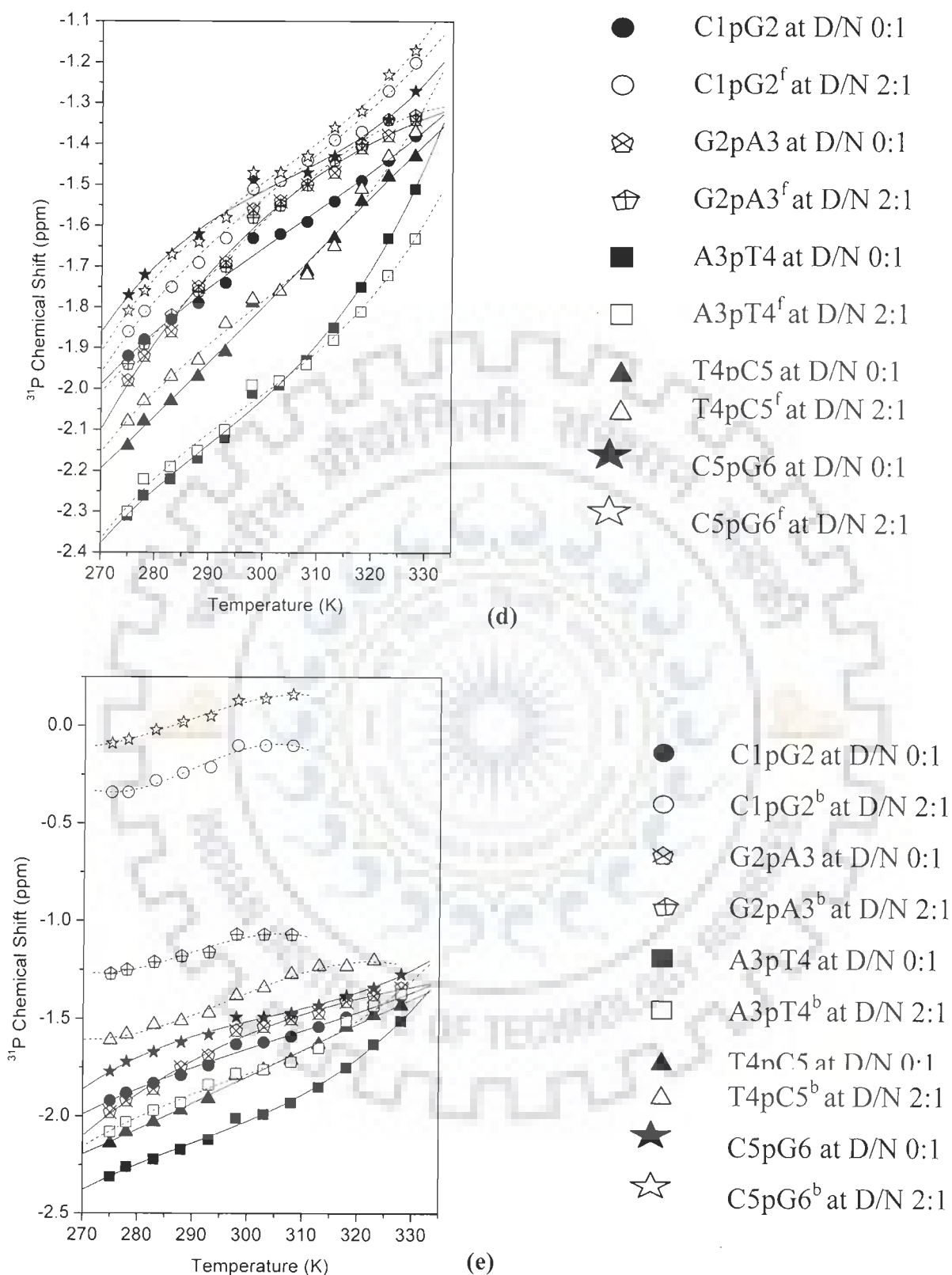


Fig. 8: (d) Free and (e) Bound resonances of the d-(CGATCA)₂-4'-epiadriamycin complex (2:1) along with the uncomplexed d-(CGATCG)₂

Table 8a-b: Free and bound resonances of the 4'-Epiadriamycin-d(CGATCG)₂ complex (2:1) along with the alone d-(CGATCG)₂ signals.

(a)										
Temp. (K)	C1pG2 ^f (2:1)	G2pA3 ^f (2:1)	A3pT4 ^f (2:1)	T4pC5 ^f (2:1)	C5pG6 ^f (2:1)	C1pG2 (0:1)	G2pA3 (0:1)	A3pT4 (0:1)	T4pC5 (0:1)	C5pG6 (0:1)
275	-1.86	-1.94	-2.30	-2.08	-1.81	-1.92	-1.98	-2.31	-2.14	-1.77
278	-1.81	-1.89	-2.22	-2.03	-1.76	-1.88	-1.92	-2.26	-2.08	-1.72
283	-1.75	-1.82	-2.19	-1.97	-1.67	-1.83	-1.86	-2.22	-2.03	-1.67
288	-1.69	-1.76	-2.15	-1.93	-1.64	-1.79	-1.75	-2.17	-1.97	-1.62
293	-1.63	-1.70	-2.10	-1.84	-1.58	-1.74	-1.69	-2.12	-1.91	-1.58
298	-1.51	-1.58	-1.99	-1.78	-1.47	-1.63	-1.56	-2.01	-1.79	-1.49
303	-1.49	-1.55	-1.98	-1.76	-1.47	-1.62	-1.54	-1.99	-1.76	-1.49
308	-1.44	-1.50	-1.94	-1.72	-1.43	-1.59	-1.50	-1.93	-1.71	-1.47
313	-1.39	-1.44	-1.88	-1.65	-1.36	-1.54	-1.47	-1.85	-1.63	-1.43
318	-1.37	-1.40	-1.81	-1.51	-1.32	-1.49	-1.41	-1.75	-1.54	-1.38
323	-1.27	-1.34	-1.72	-1.43	-1.23	-1.44	-1.38	-1.63	-1.48	-1.34
328	-1.20	-1.33	-1.63	-1.37	-1.17	-1.38	-1.34	-1.51	-1.43	-1.27
$\Delta \delta$	+0.66	+0.61	+0.67	+0.71	+0.64	+0.54	+0.64	+0.80	+0.71	+0.50
(b)										
Temp. (K)	C1pG2 ^b (2:1)	G2pA3 ^b (2:1)	A3pT4 ^b (2:1)	T4pC5 ^b (2:1)	C5pG6 ^b (2:1)	C1pG2 (0:1)	G2pA3 (0:1)	A3pT4 (0:1)	T4pC5 (0:1)	C5pG6 (0:1)
275	-0.34	-1.27	-2.08	-1.61	-0.09	-1.92	-1.98	-2.31	-2.14	-1.77
278	-0.34	-1.25	-2.03	-1.58	-0.07	-1.88	-1.92	-2.26	-2.08	-1.72
283	-0.28	-1.21	-1.97	-1.53	-0.02	-1.83	-1.86	-2.22	-2.03	-1.67
288	-0.24	-1.18	-1.93	-1.51	+0.02	-1.79	-1.75	-2.17	-1.97	-1.62
293	-0.21	-1.16	-1.84	-1.47	+0.05	-1.74	-1.69	-2.12	-1.91	-1.58
298	-0.10	-1.07	-1.78	-1.38	+0.13	-1.63	-1.56	-2.01	-1.79	-1.49
303	-0.10	-1.07	-1.76	-1.34	+0.14	-1.62	-1.54	-1.99	-1.76	-1.49
308	-0.10	-1.07	-1.72	-1.27	+0.16	-1.59	-1.50	-1.93	-1.71	-1.47
313	-	-	-1.65	-1.23	-	-1.54	-1.47	-1.85	-1.63	-1.43
318	-	-	-1.51	-1.23	-	-1.49	-1.41	-1.75	-1.54	-1.38
323	-	-	-1.43	-1.20	-	-1.44	-1.38	-1.63	-1.48	-1.34
328	-	-	-1.37	-	-	-1.38	-1.34	-1.51	-1.43	-1.27
$\Delta \delta$	+0.24	+0.20	+0.71	+0.41	+0.25	+0.54	+0.64	+0.80	+0.71	+0.50

stretching of DNA backbone cause large downfield shift (1.0 – 1.7 ppm) of the phosphates at intercalation or adjacent site. On the other hand, berberine and pyridopurine, which are known to bind externally to DNA do not affect chemical shift of any of the ^{31}P resonances significantly ($\Delta\delta < 0.2$ ppm). Secondly, we observe maximum shift due to binding directly at each intercalation step, C1pG2 / T1pG2 and C5pG6 / C5pA6; although the $\Delta\delta$ ($\delta^b - \delta^f$) due to binding, variation with temperature ($\delta_{328} - \delta_{275}$) and line width of resonances in each drug – DNA complex is different in each of the two complexes studied. Comparison with similar complexes (Table 7a-b of chapter 5) of daunomycin, adriamycin and morpholinodoxorubicin with d-(CGATCG)₂ and d-(CGTACG)₂ sequences reported in literature (Mazzini et al., 1988; Ragg et al., 1988), show a different behavior. The maximum shift, $\Delta\delta = 1.0 - 1.6$ ppm is observed at one site of intercalation C5pG6 only. The other intercalation site, C1pG2, is less (~ 0.5 ppm) affected but the site adjacent to it, G2pA3 / G2pT3, is affected more (up to 1.5 ppm). Thus the changes are specific and bear the signature of drug and sequence of bases to which it binds. Since they are related to relative population of B_I / B_{II} states, backbone stretching (change in torsional angle ζ) and O-P-O bond angles, it may be inferred that each drug distorts the DNA on binding to it in a unique way. Alternately the DNA backbone adopts a conformation that is specific for each drug on intercalation of the drug chromophore. The exact structural variations, that is, change in unwinding angle, stretching of backbone causing change in six torsional angles along the entire backbone, distortions in O-P-O bond, change in sugar pucker, etc., can be ascertained by detailed conformational analysis of complex using say inter-proton NOE constraints. The difference in distortions induced in DNA due to binding will affect the manner in which they bind to topoisomerase-I-enzyme and form ternary complex of drug-enzyme-DNA. This eventually shifts DNA cleavage-religation equilibrium action of topoisomerase II towards cleavage and causes multiple DNA strand breaks which are responsible for their anticancer action. Thus ^{31}P NMR

spectra alone can be used as a rapid tool to characterize different drug-DNA complexes. Various drugs on binding to DNA induce alterations in backbone conformation which are drug specific and base sequence specific. The exact way of binding to DNA is expected to influence its further binding to topoisomerases and hence a specific molecular basis of action for each drug.

7.2 Summary and Conclusions

^{31}P NMR thus appears to be able to provide a convenient monitor of the phosphate ester backbone conformational changes upon binding of the intercalating drugs with the hexanucleotide. Temperature dependence studies of the uncomplexed DNA hexamer showed that there is duplex to single strand transition. The ^{31}P resonance assignment was performed using $^1\text{H} - ^{31}\text{P}$ HMBC. Titrations at various D/N ratio showed that there was systematic regular variation in signal strengths and line widths. $^{31}\text{P} - ^{31}\text{P}$ NOESY exchange clearly proves the fact that there are bound and free species in slow exchange on NMR time scale and yielded $\Delta\delta$ of the drug-DNA complex. Presence of B_{II} conformation is substantiated by observed downfield shifts of ~ 1.7 ppm in phosphorus signals at C1pG2 and C5pG6 intercalating base pair steps. The adjacent sites G2pA3 and T4pC5 are also affected. ^{31}P resonance spectra as a function of temperature shows that the drug is stabilizing the complex till 308 K and beyond this temperature, unbinding of the drug starts. T_1 studies confirm the complex formation. To the best of our knowledge, it is for the first time we are reporting ^{31}P NMR of 4'-epiadriamycin with d-(CGATCG) $_2$. The change in backbone conformation in this complex is markedly different from that reported in chapter 5 for adriamycin-d-(TGATCA) $_2$ complex and could be a signature of the drug as well as hexanucleotide sequence.

Studies on 4'-Epiadriamycin complexed with d-(CGATCG)₂ by Proton Nuclear Magnetic

Resonance Spectroscopy and Restrained Molecular Dynamics

The distinguishing feature of drug-DNA interaction studies is to know about the structural and dynamic characterization of intermolecular interactions at the atomic resolution level. The biological activities of different anthracycline based drugs depend on the minor modifications in their chemical structure and accordingly 4'-epiadriamycin (epimer of adriamycin having inversion of the stereochemistry at the 4'-position of the sugar), has been recently developed and is better tolerated due to lesser cardiotoxicity. We report here the following study done on 4'-epiadriamycin-d-(CGATCG)₂ complex (Fig. 1a-b) by proton NMR followed by restrained molecular dynamics simulations.

- 1D ¹H NMR titration studies of 4'-epiadriamycin-d-(CGATCG)₂ complex at various drug (D)/DNA duplex (N) ratios of 0.16, 0.32, 0.48, 0.64, 0.80, 0.96, 1.11, 1.27, 1.43, 1.53, 1.60, 1.75, 1.91 and 2.03 at 275, 298 and 318 K in 90% H₂O and 10% D₂O.
- 1D NMR study as a function of temperature in the range 275-328 K at D/N = 1.0, 1.5, 2.0.
- 2D NOESY at D/N = 1.0, 1.5, 2.0 using mixing time τ_m = 100, 200, 300 ms at 275 K in 90% H₂O and 10% D₂O.
- Life-time fluorescence measurement studies for 2:1 complex of 4'-epiadriamycin-d-(CGATCG)₂.
- Diffusion Ordered Spectroscopy (DOSY) experiments of 2:1 complex of 4'-epiadriamycin-d-(CGATCG)₂, uncomplexed d-(CGATCG)₂ and free 4'-epiadriamycin at 275 and 298 K.

- Restrained molecular dynamics studies on the solution structure for the complex of 4'-epiadriamycin with d-(CGATCG)₂ in drug to DNA duplex ratio of 2:1 using inter-proton distances obtained from 2D NOESY as restraints.
- Analysis of the converged structure in terms of time average of the various conformational and helical parameters as well as fluctuations and correlations among different structural parameters.

8.1 Results and Discussion

(A) NMR studies on complex of 4'-epiadriamycin-d-(CGATCG)₂

The proton NMR spectra of the complex of 4'-epiadriamycin-d-(CGATCG)₂ at various drug (D)/DNA (N) ratios, D/N = 0.16, 0.32, 0.48, 0.64, 0.80, 0.96, 1.11, 1.27, 1.43, 1.53, 1.60, 1.75, 1.91 and 2.03 at 275, 298, 318 K are shown in Fig. 2(a-j). At 275 K, the imino protons signals are sharpened and intensified. Besides, DNA is expected to be present completely in duplex state at 275 K. Higher temperatures are chosen to know that if the drug stabilizes the drug-DNA complex. Besides this, at 318 K, the exchange process is in the intermediate to fast exchange regime on NMR time scale. The assignment of drug and nucleotide protons (Table 1a-b) are done in the similar manner as for adriamycin-d-(TGATCA)₂ complex, using the standard strategies, that is, sequential NOEs (base H8/H6)_n-sugar (H1')_{n-1}, (base H8/H6)_n-sugar(H2'')_{n-1}, (base H8/H6)_n-sugar(H2')_{n-1}.

On addition of 4'-epiadriamycin to d-(CGATCG)₂, new drug proton signals are seen which increases in intensity with D/N ratios. This is evident from the resonance signals of 1'H, 7H, 5'CH₃, 6OH, 11OH, 1H, 2H and 3H protons in Fig. 3(a-k). The initially sharp NMR spectral lines of free DNA duplex broaden significantly without the appearance of a new set of NMR resonances for the bound complex. Both the nucleotide and drug protons, each having one set of resonances, shift gradually from their position in uncomplexed state with D/N ratio (Table 2a-c

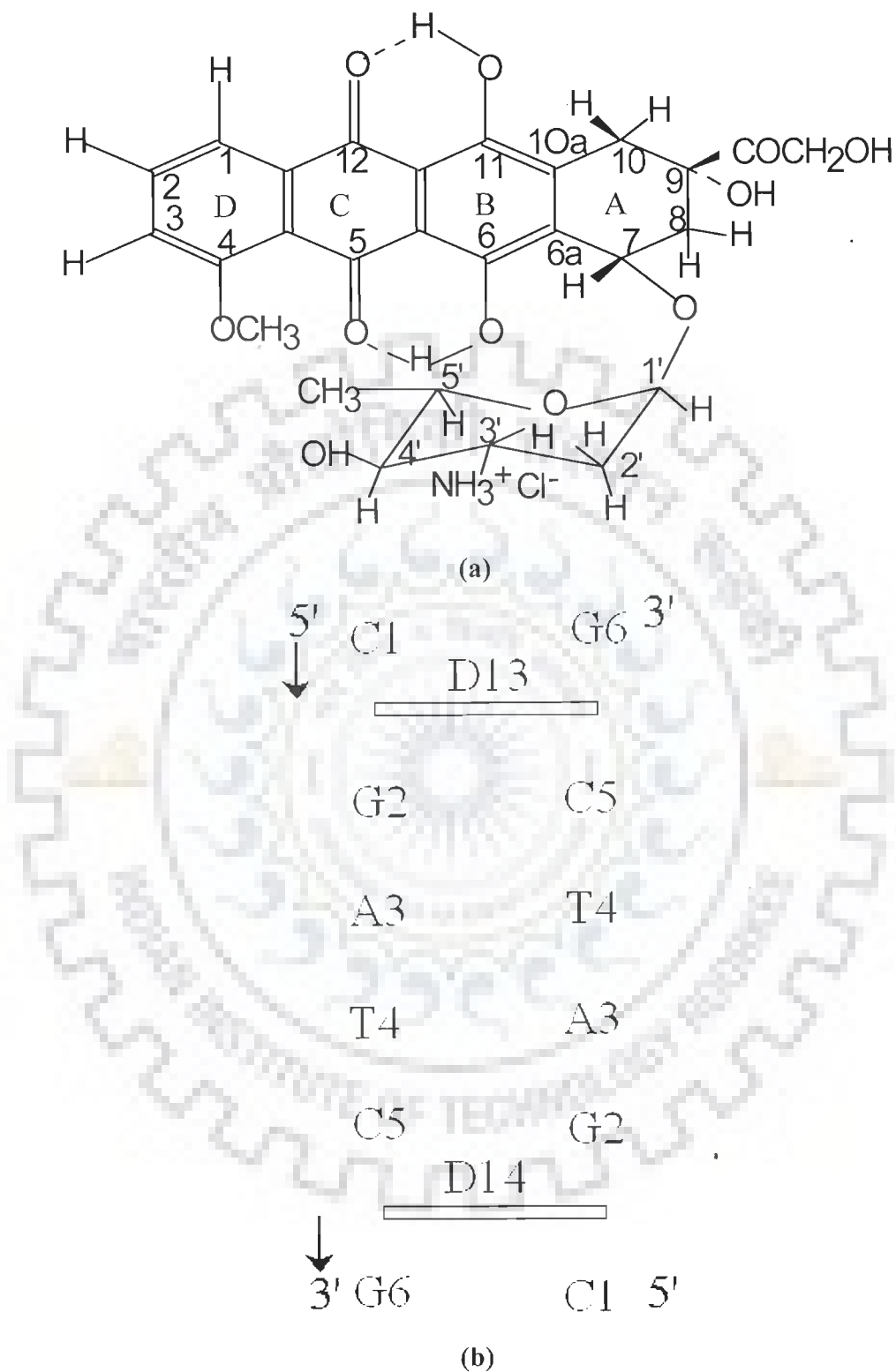
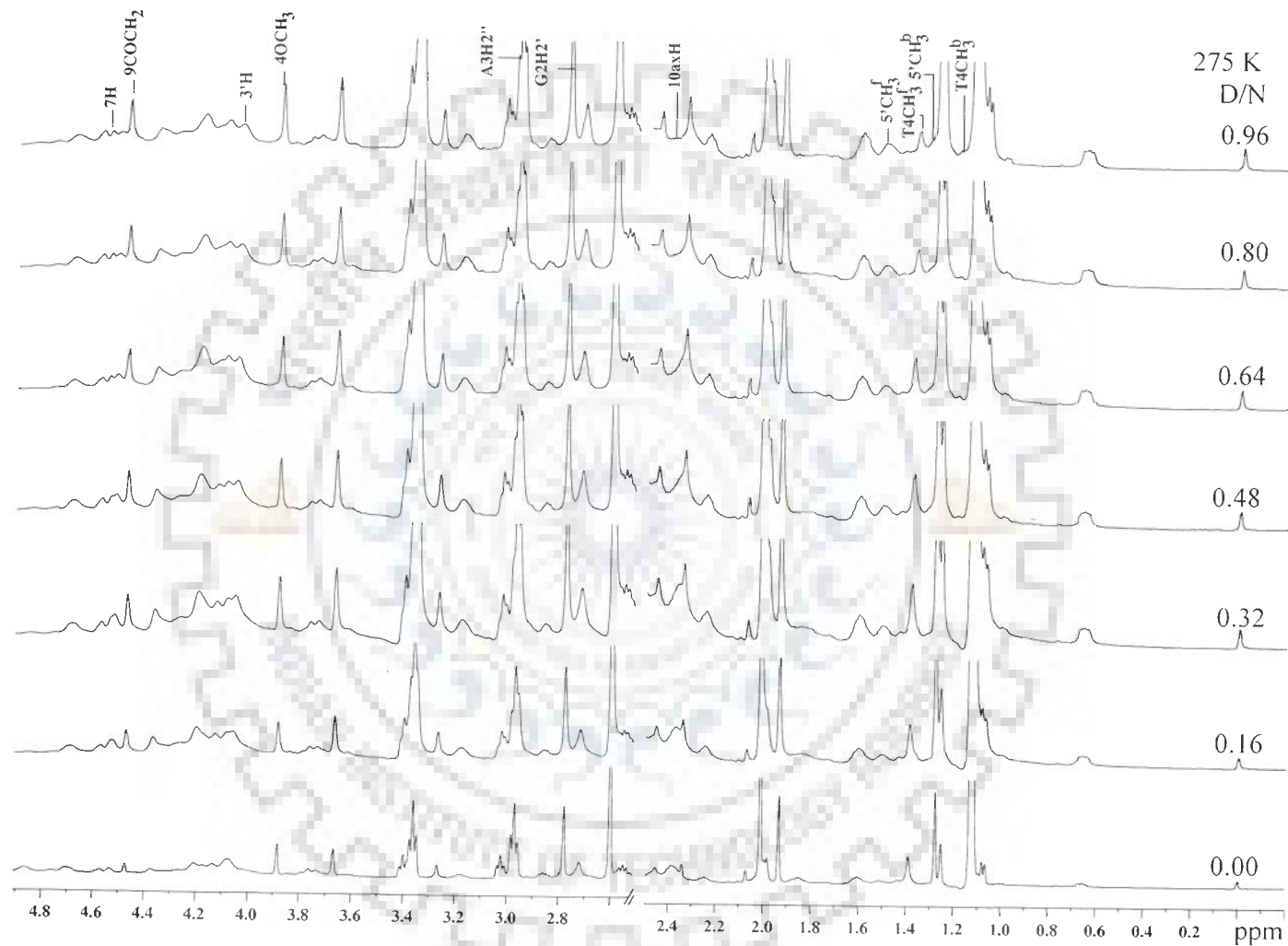
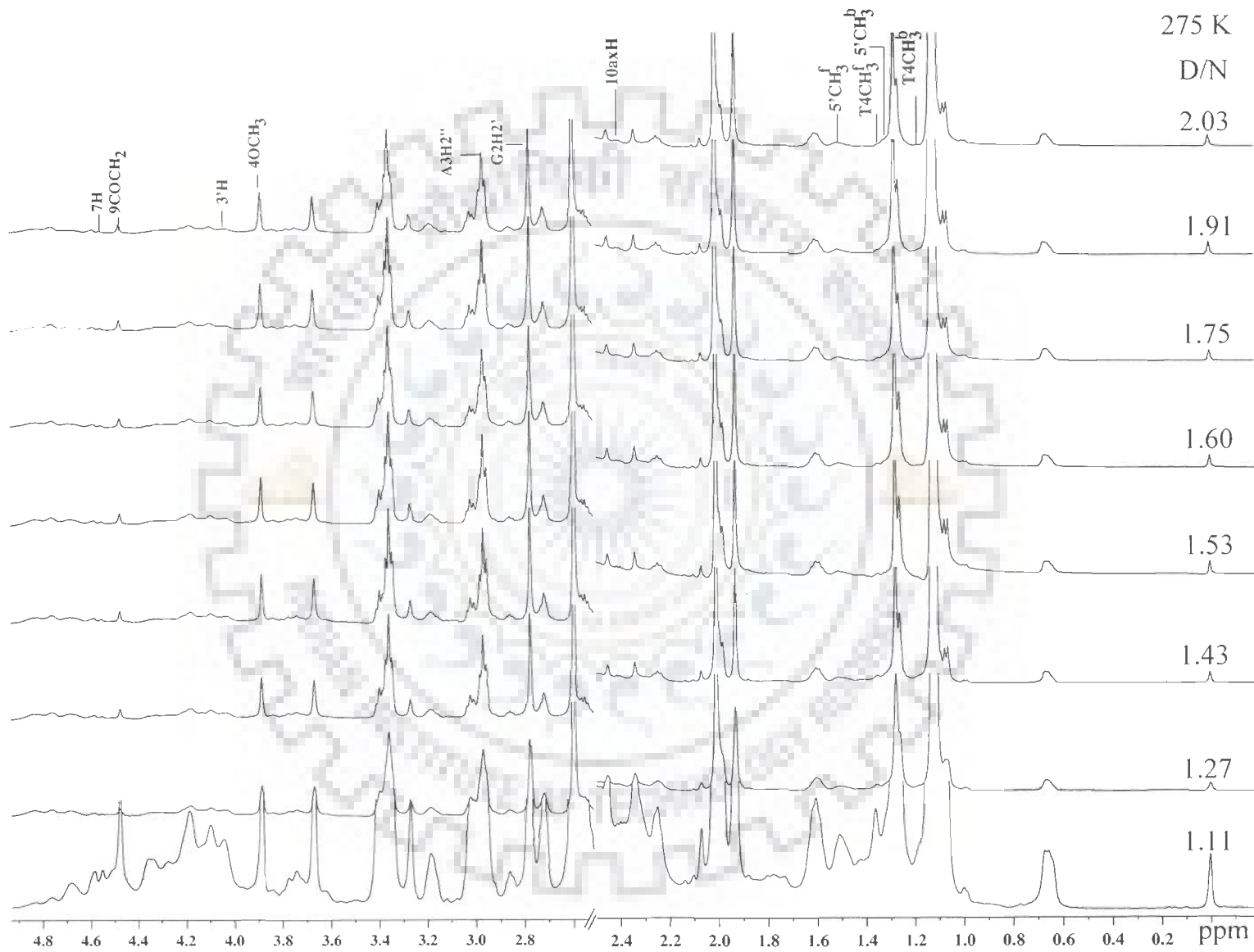


Fig.1. (a) Molecular structure of 4'-epiadriamycin (b) Schematic representation of the 2:1 4'-epiadriamycin-d-(CGATCG)₂ complex

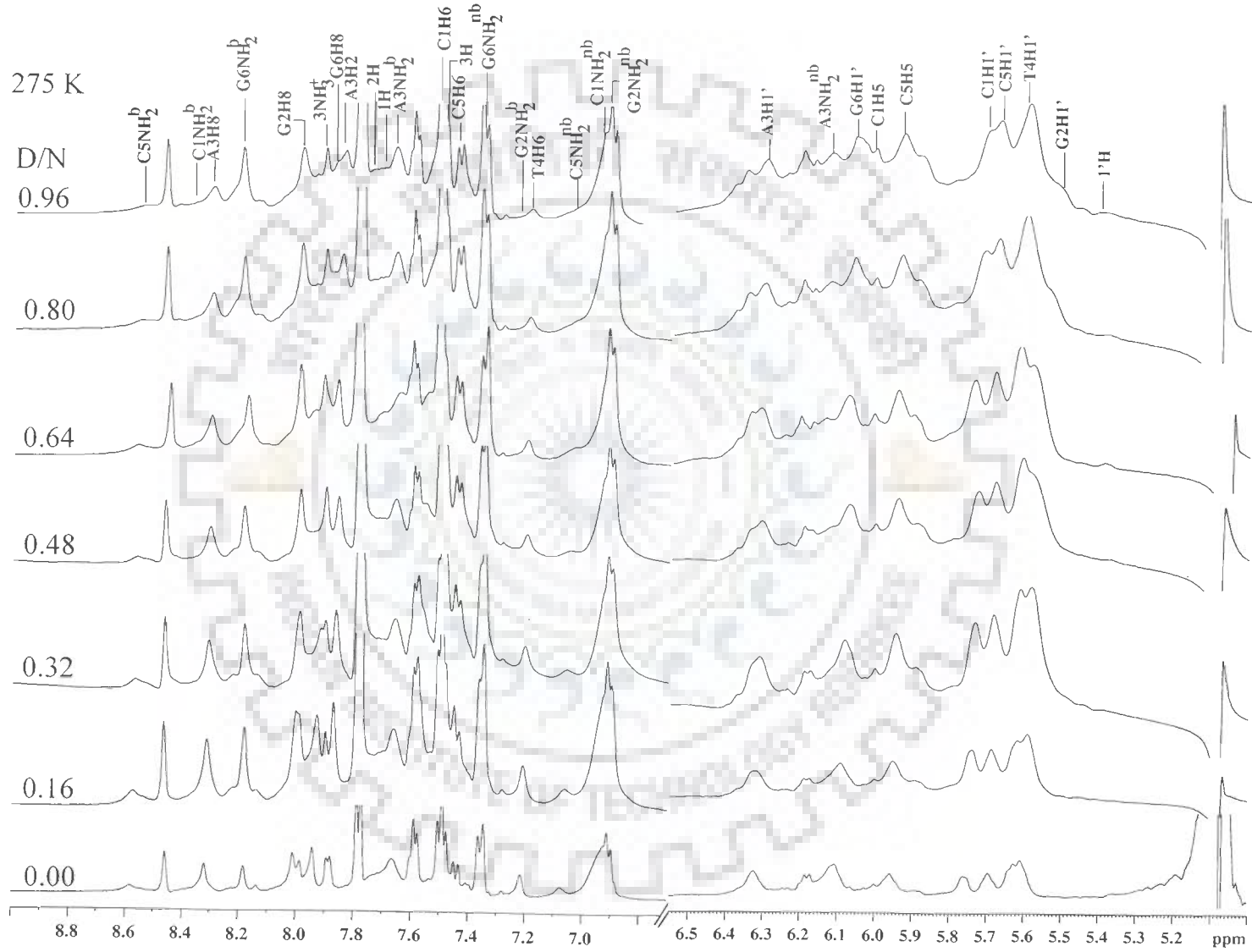


(a)

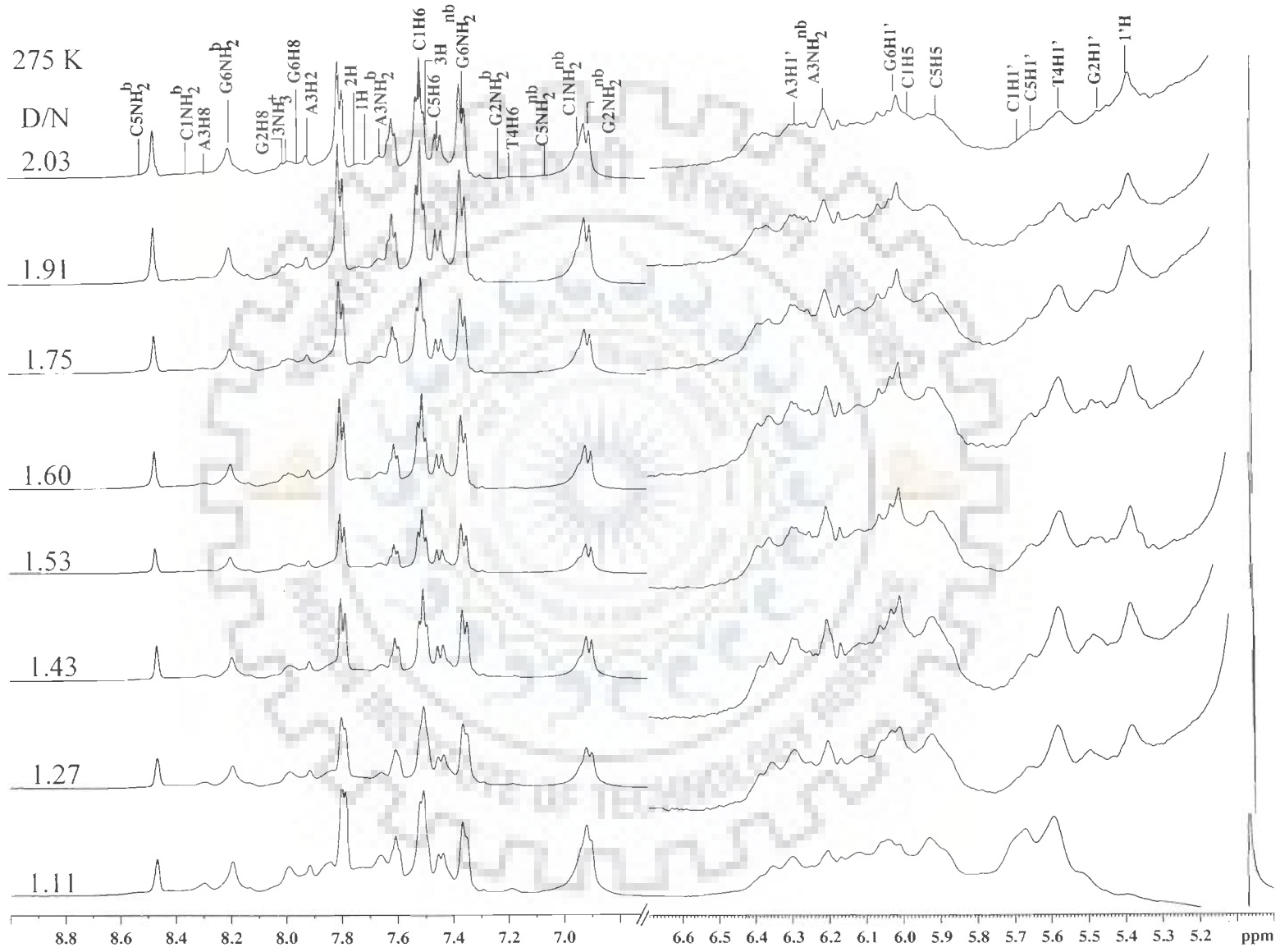
Fig. 2a-j: Proton NMR spectrum of the complex 4'-epidriamycin d-(CGATCG)₂ complex as a function of added drug (D) to DNA (N) duplex stoichiometric ratios (D/N) of 0.0, 0.16, 0.32, 0.48, 0.64, 0.80, 0.96, 1.11, 1.27, 1.43, 1.53, 1.60, 1.75, 1.91, 2.03 at 275, 298, 318 K in H₂O/D₂O.



(b)

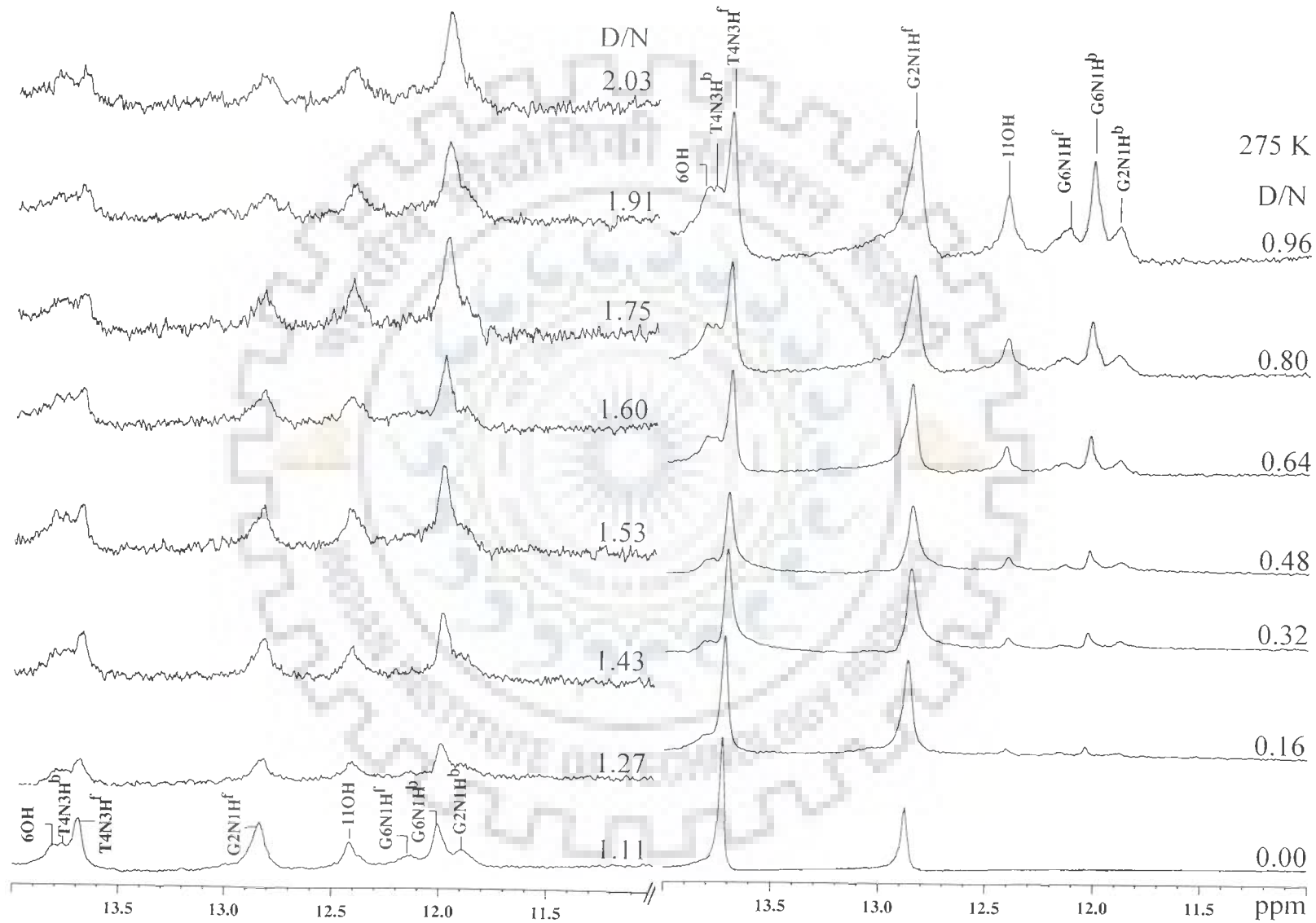


(c)

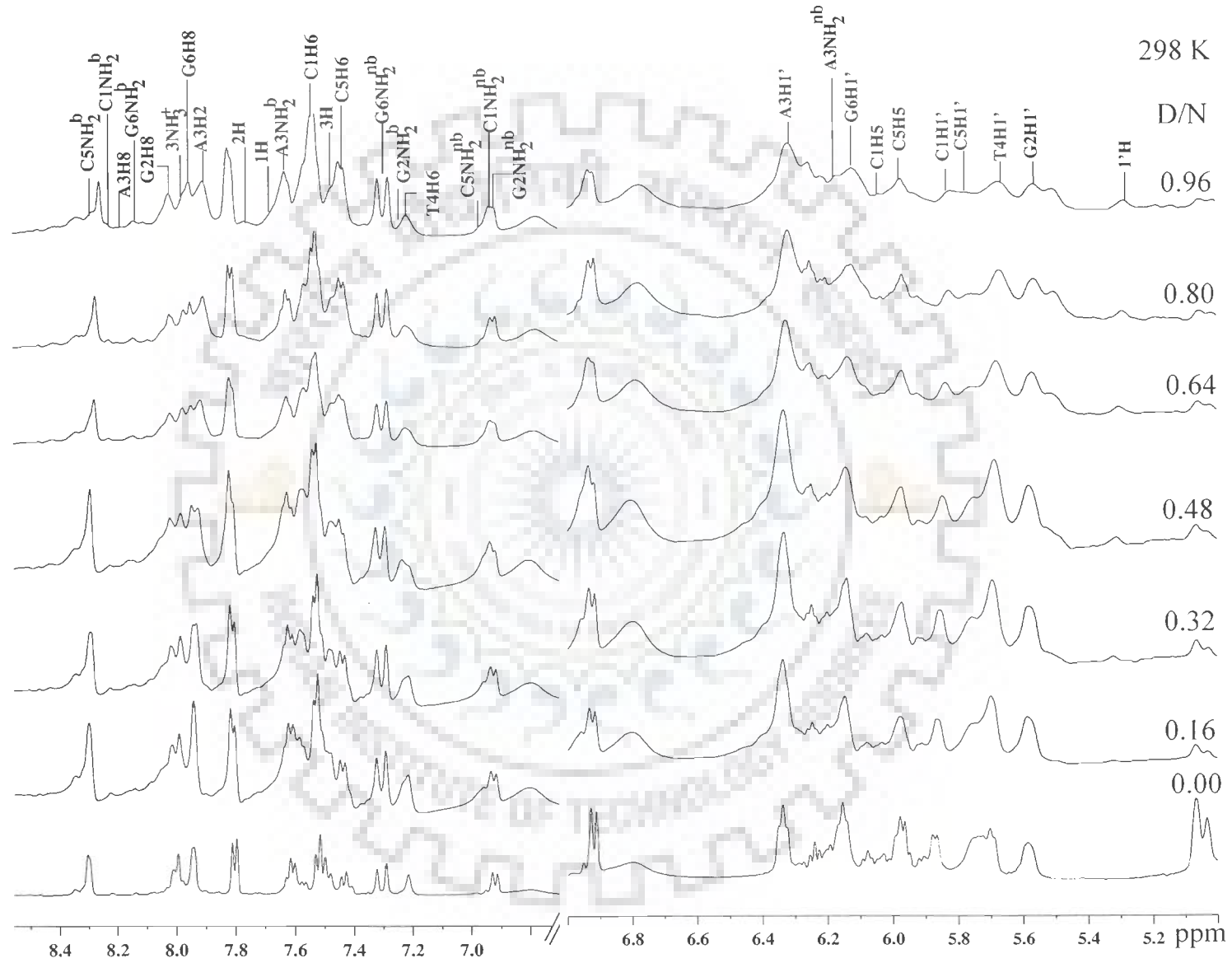


(d)

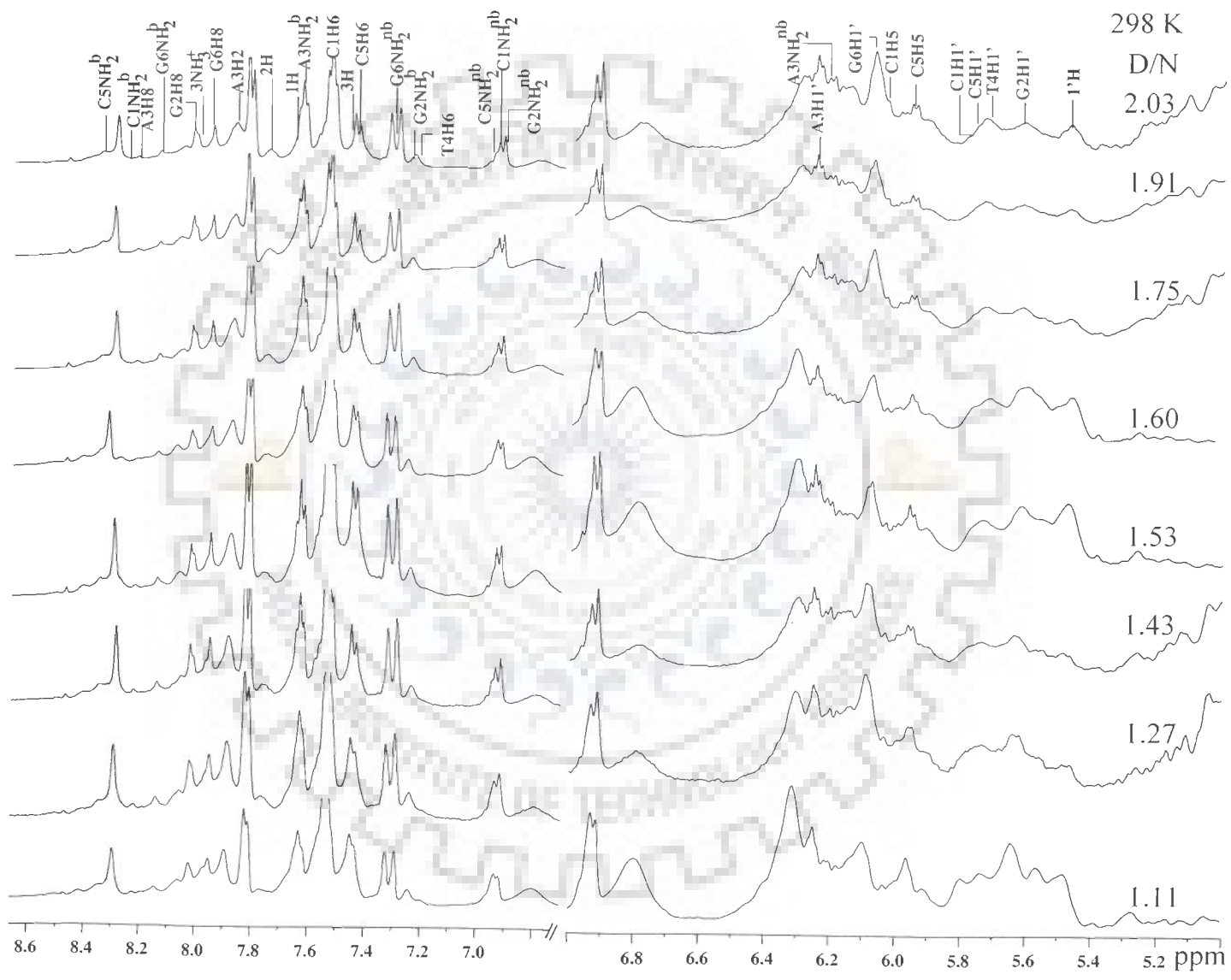
370



(e)

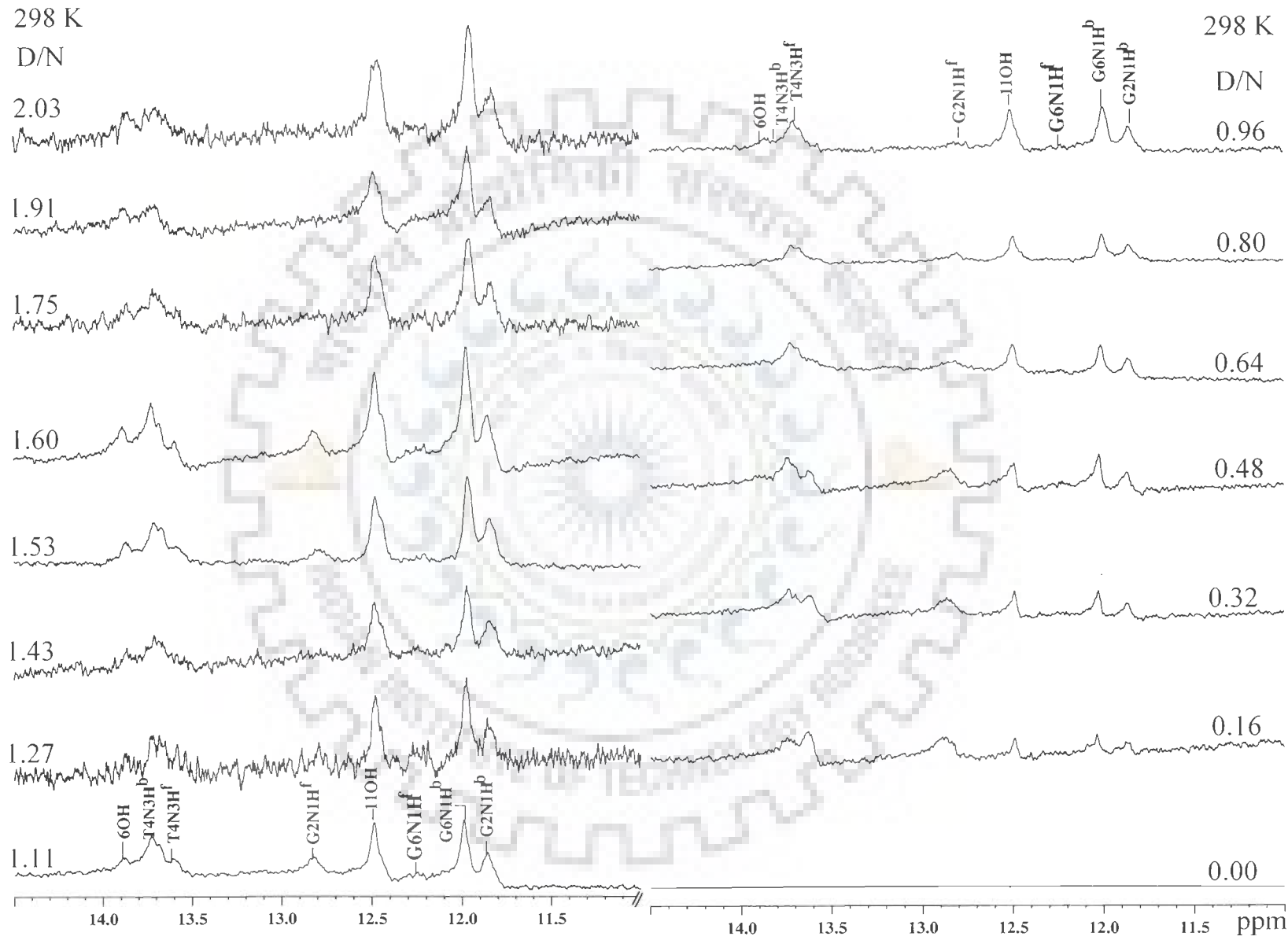


(f)

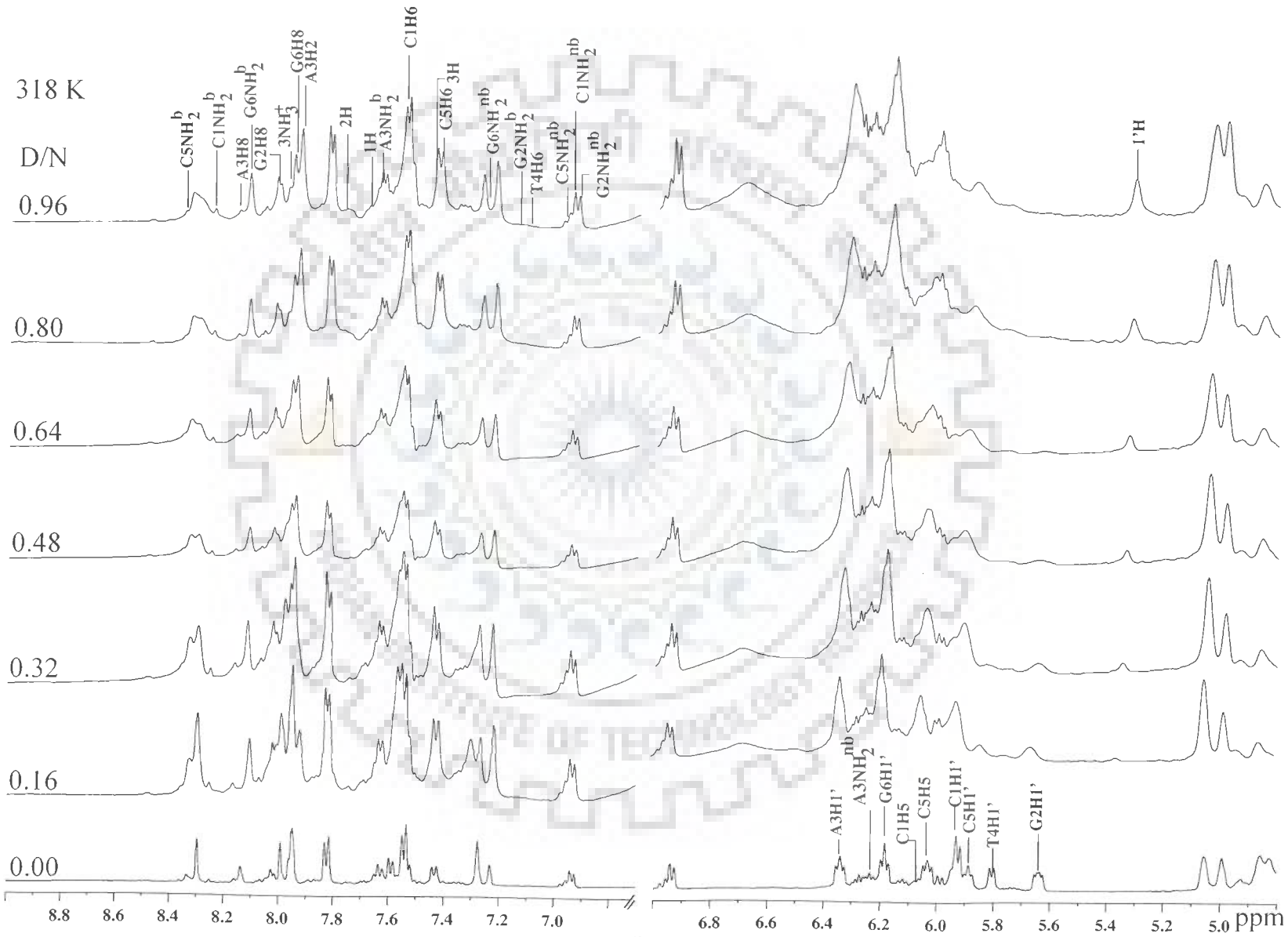


(g)

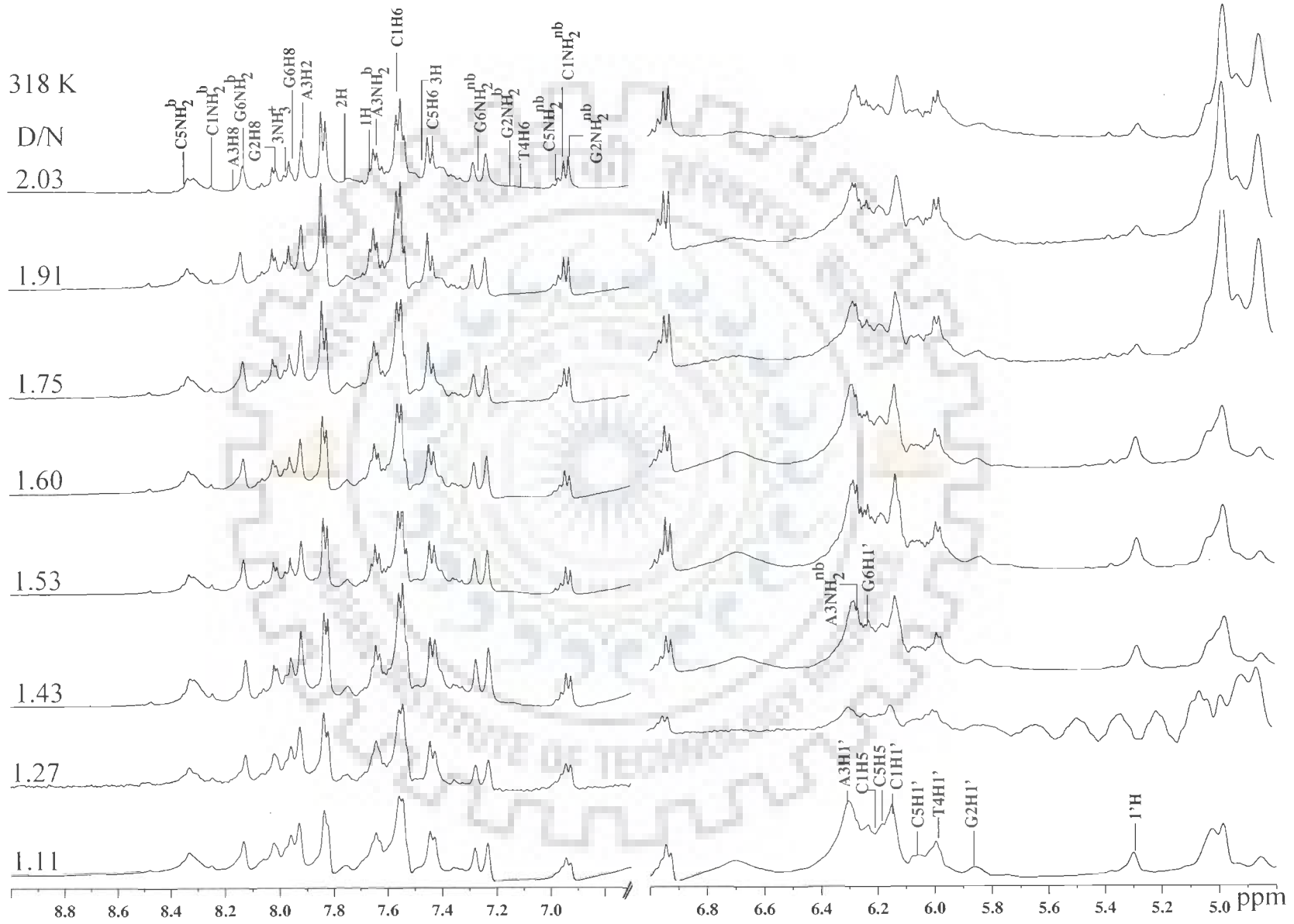
373



(h)



(i)



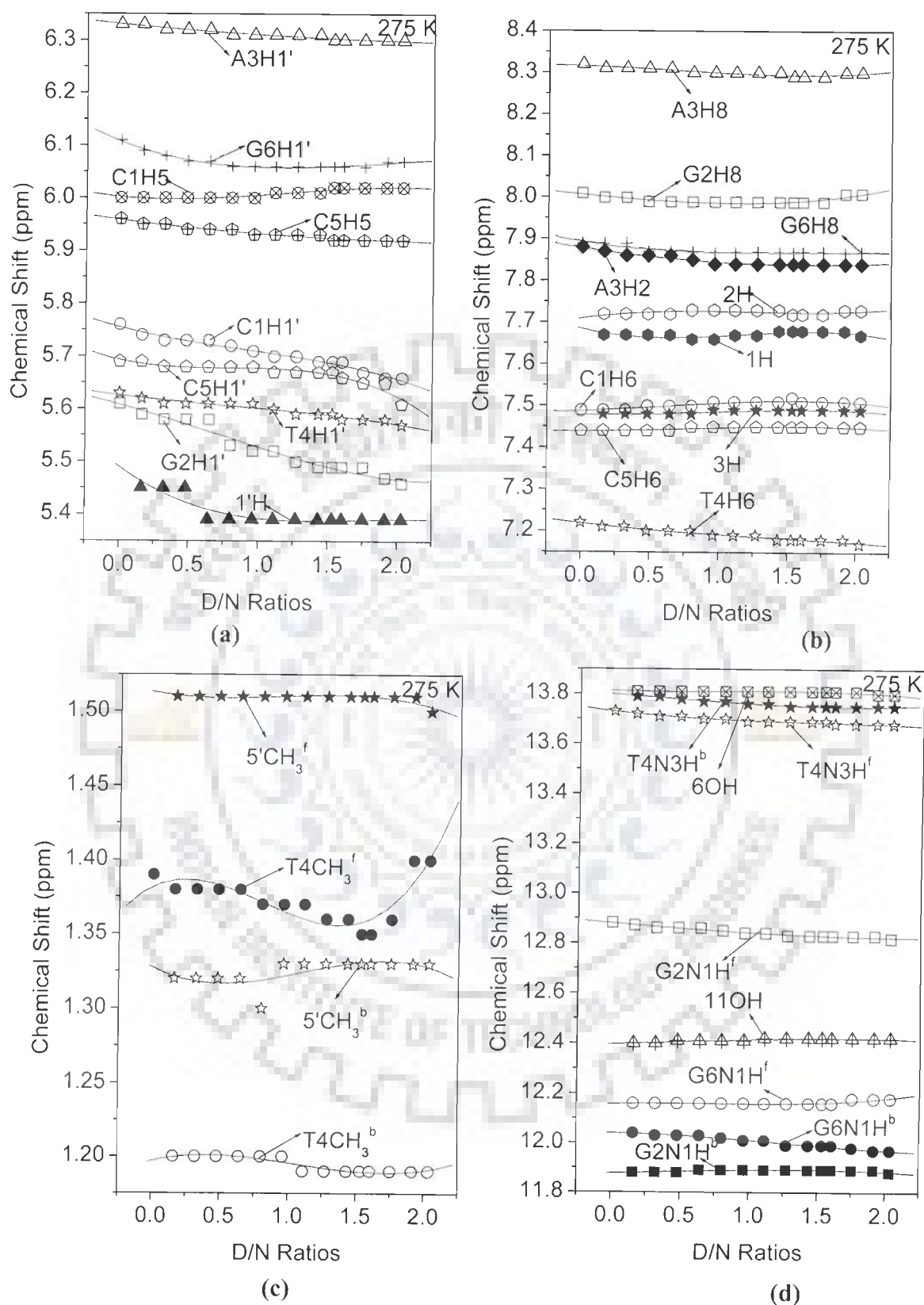
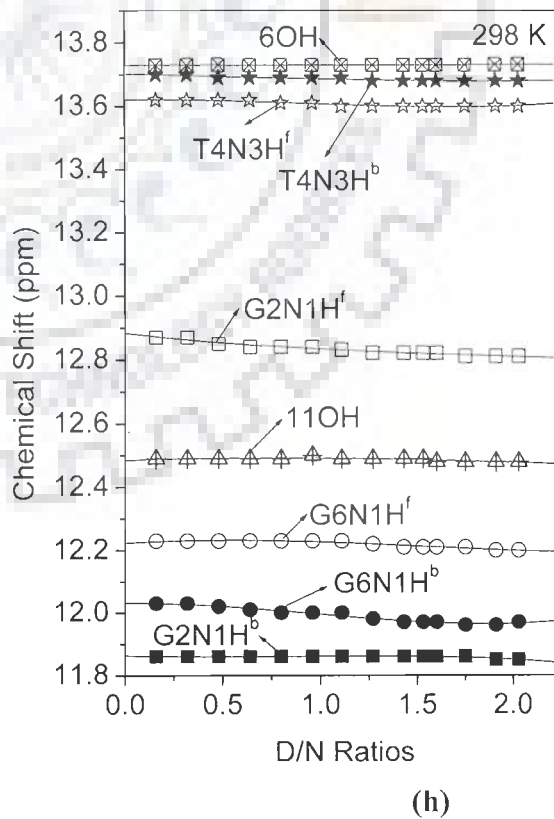
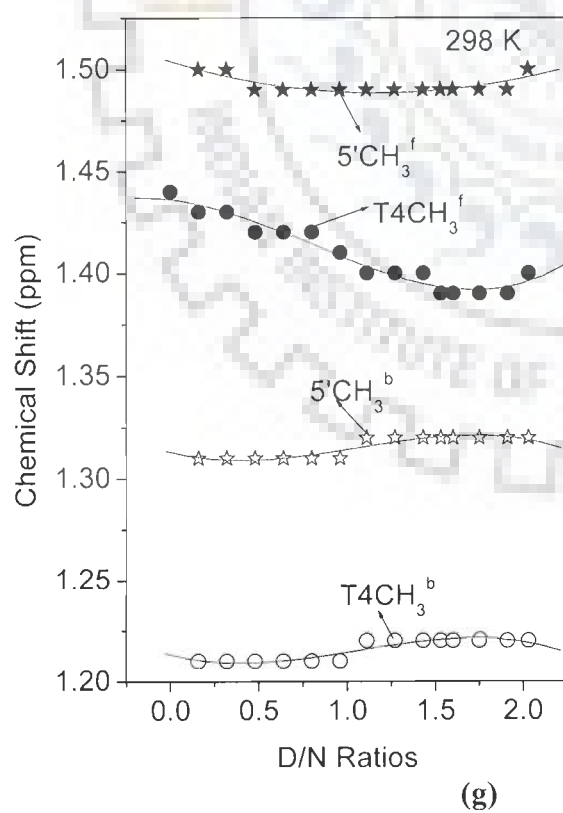
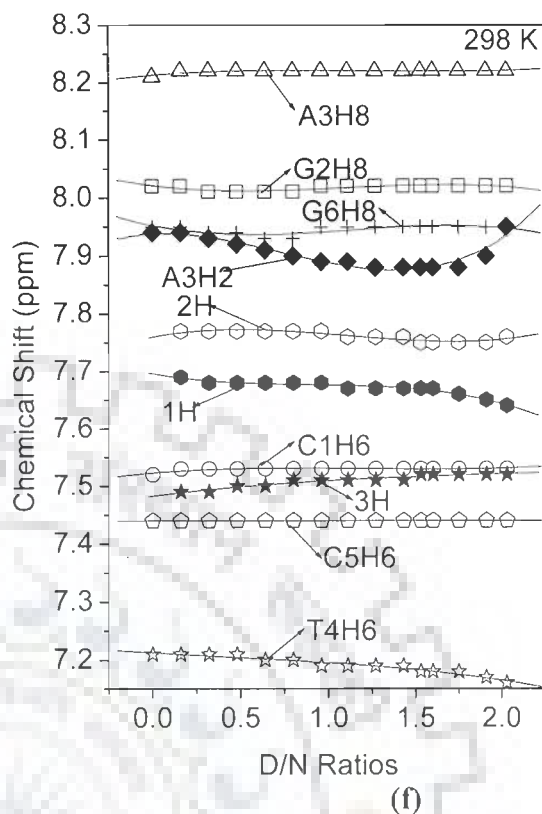
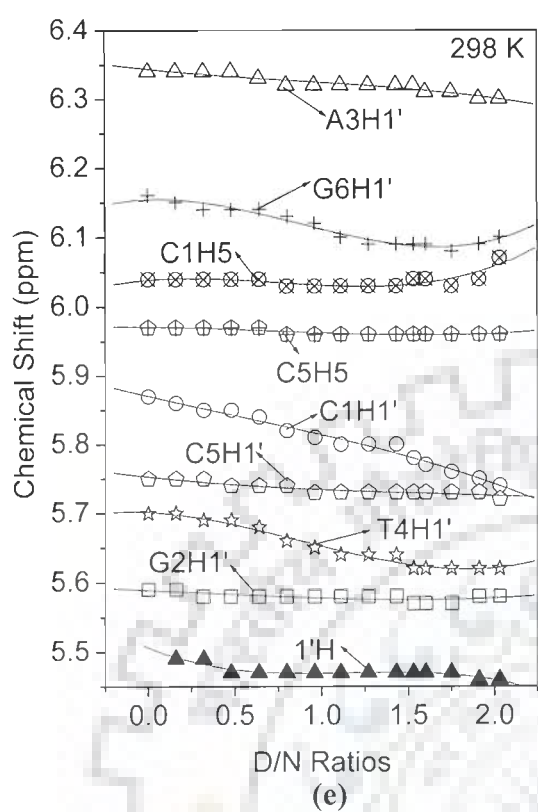
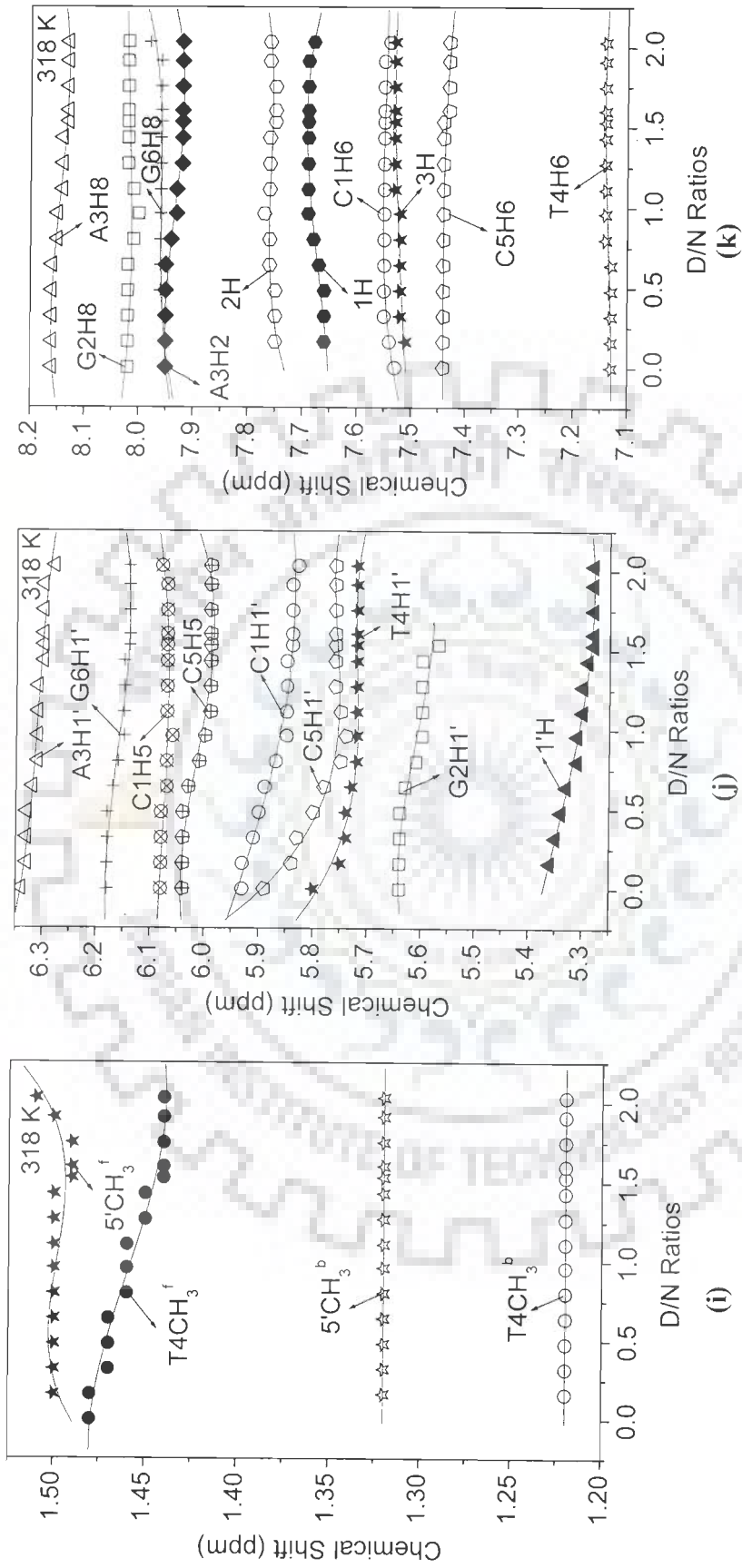


Fig. 3a-k: Chemical Shift of various protons of $d\text{-(CGATCG)}_2$ and 4'-epiadriamycin as a function of various drug to DNA ratios (D/N)





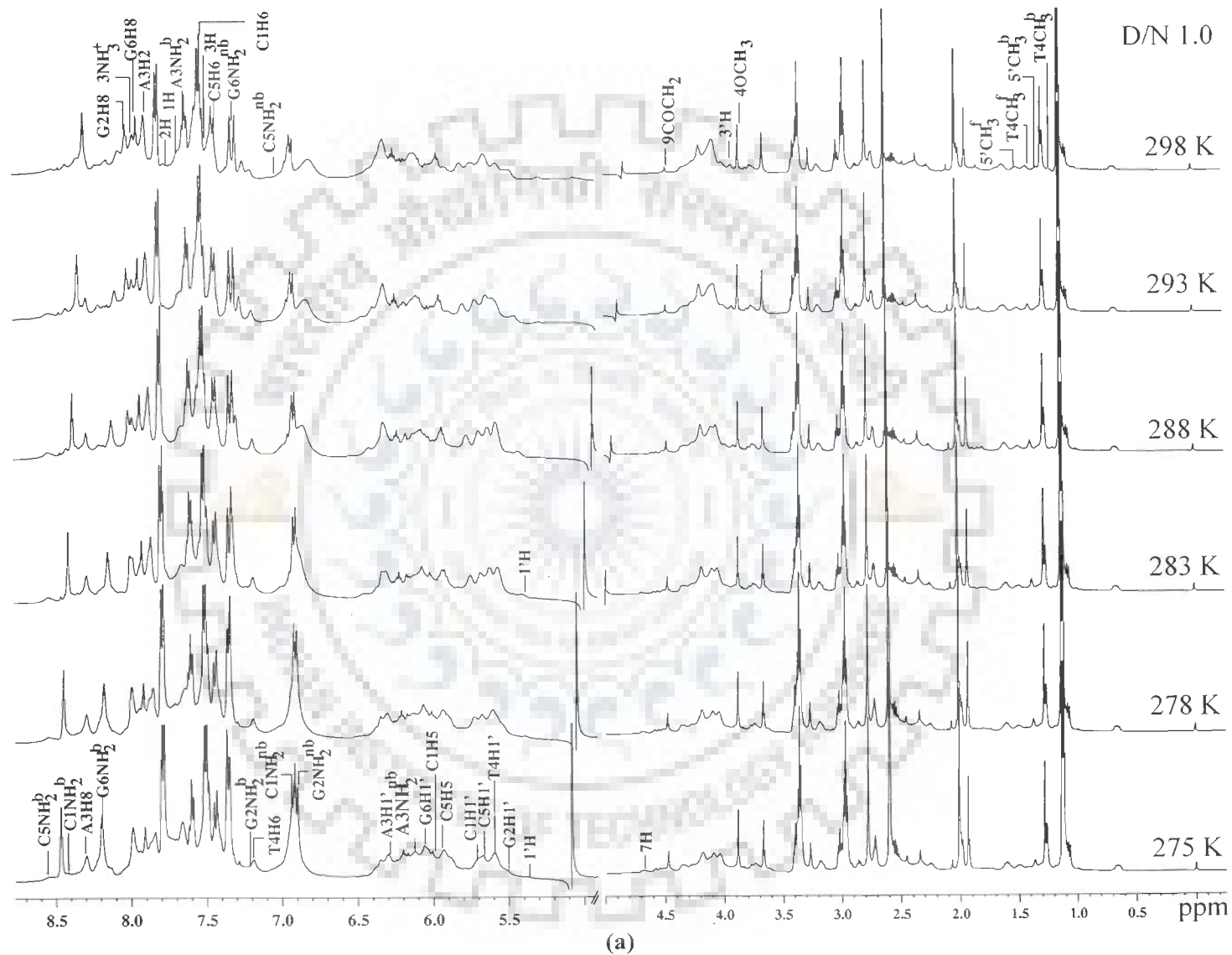
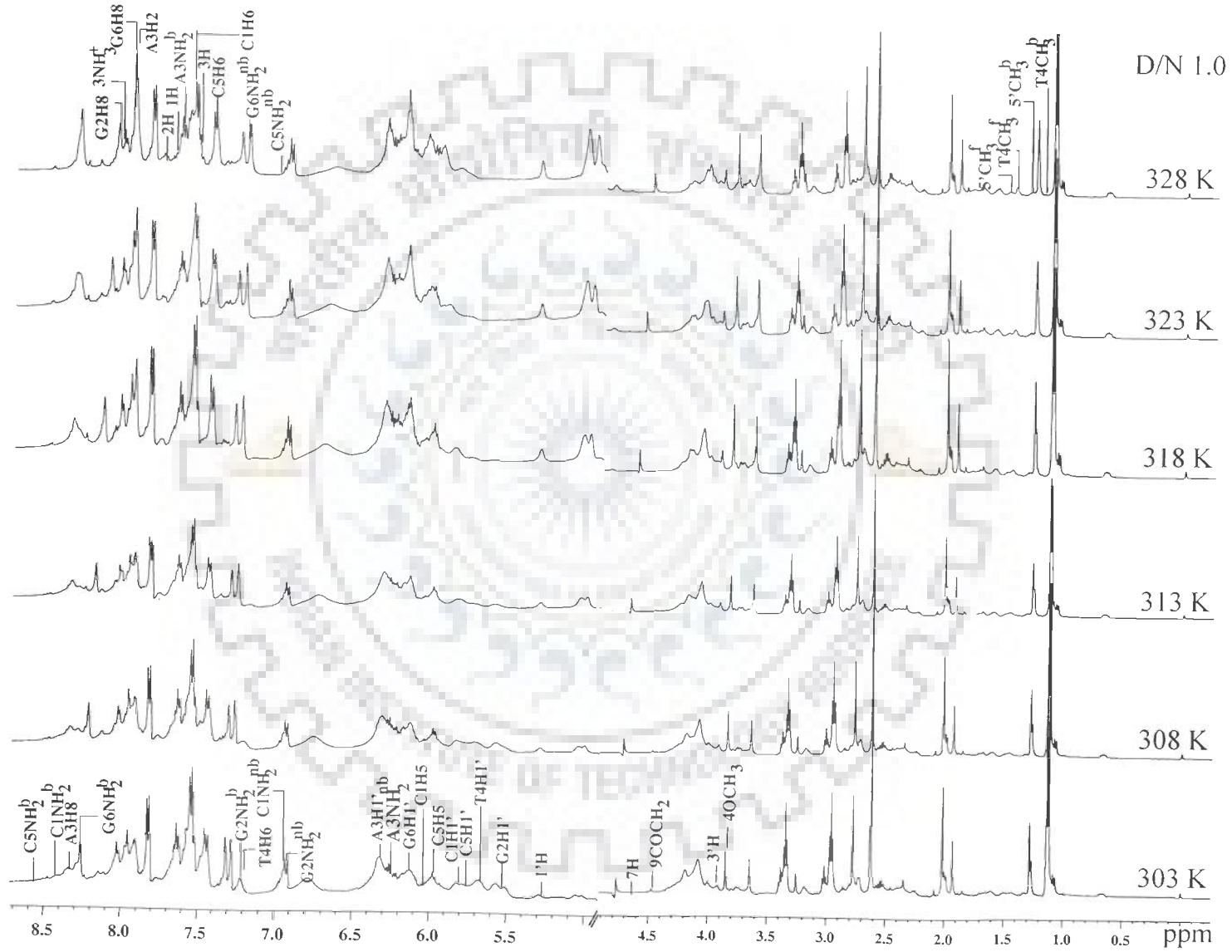
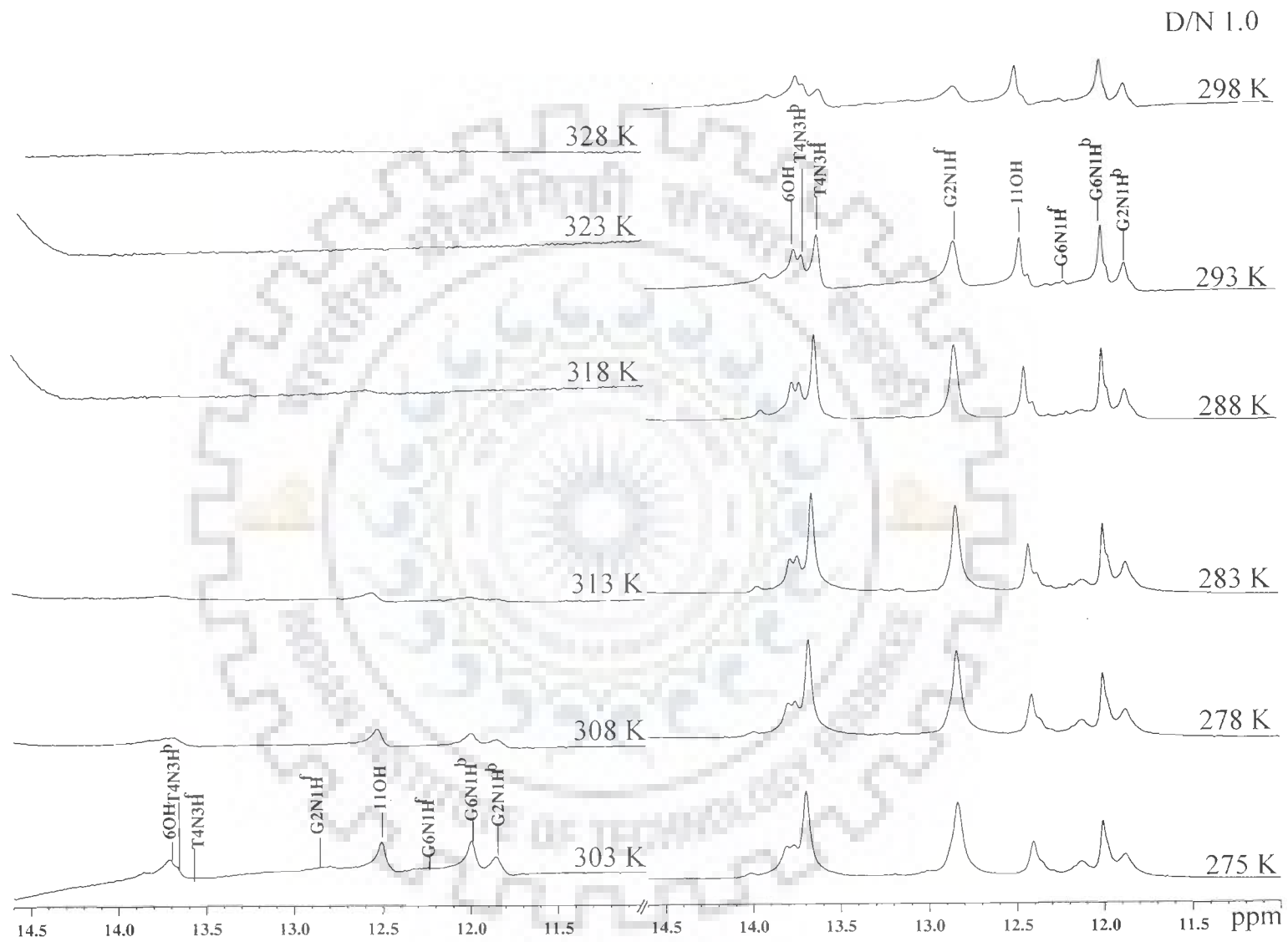


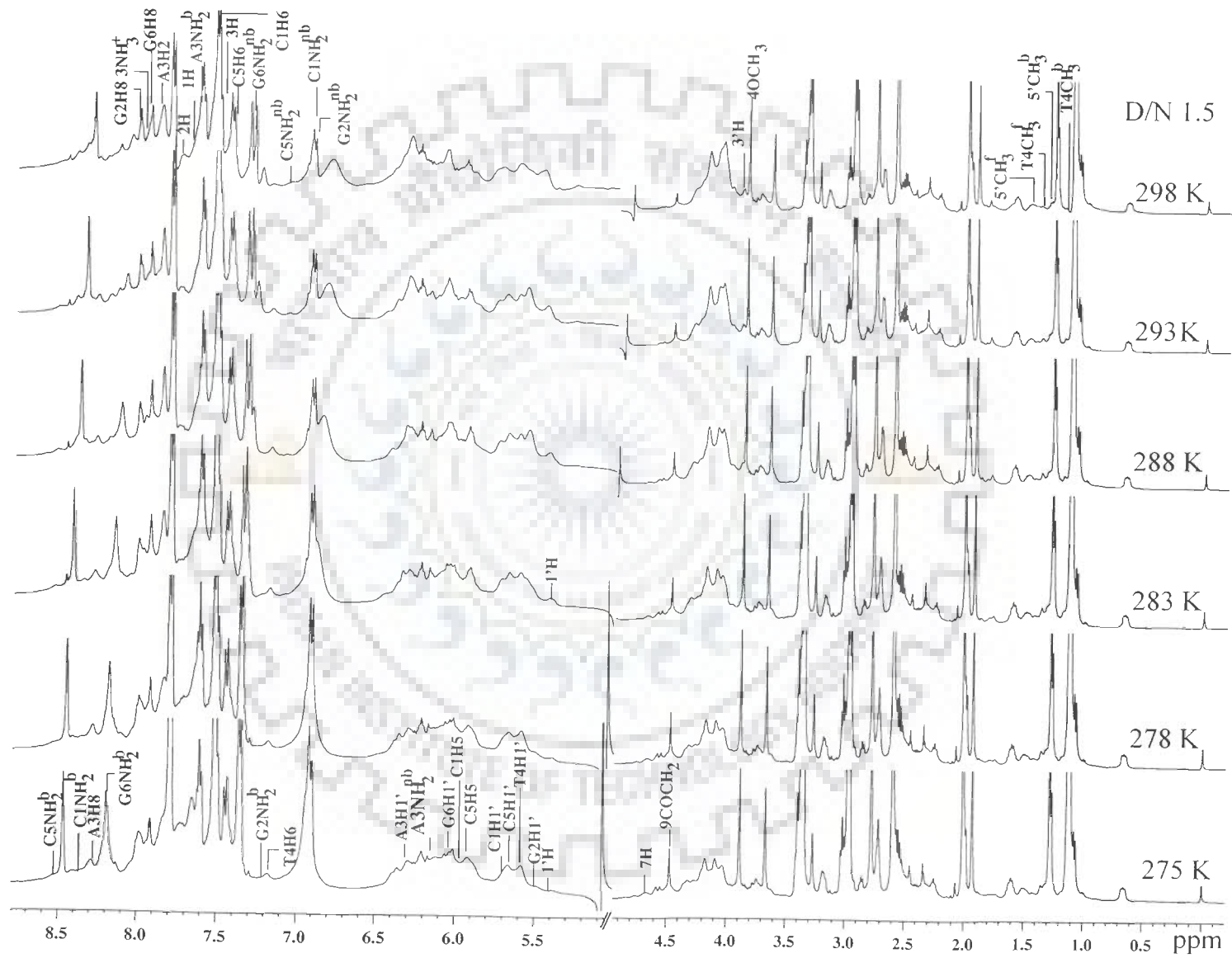
Fig. 4a-i: Proton NMR spectrum of the complex 4'-epiadriamycin d-(CGATCG)₂ complex as a function of temperature (275 – 328 K) at drug (D) to DNA (N) duplex stoichiometric ratios (D/N) of 1.0, 1.5, 2.0 in H₂O/D₂O



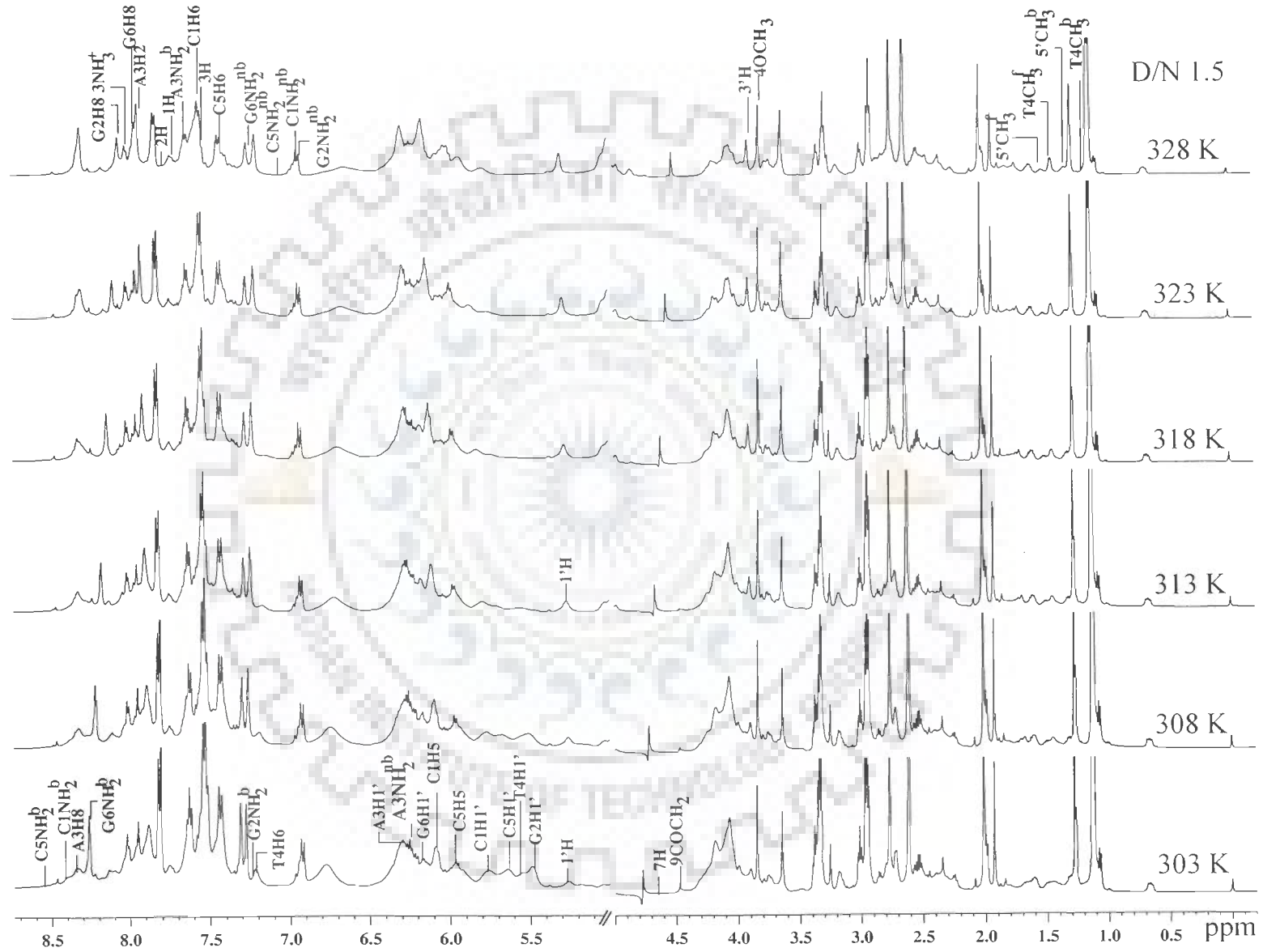
(b)



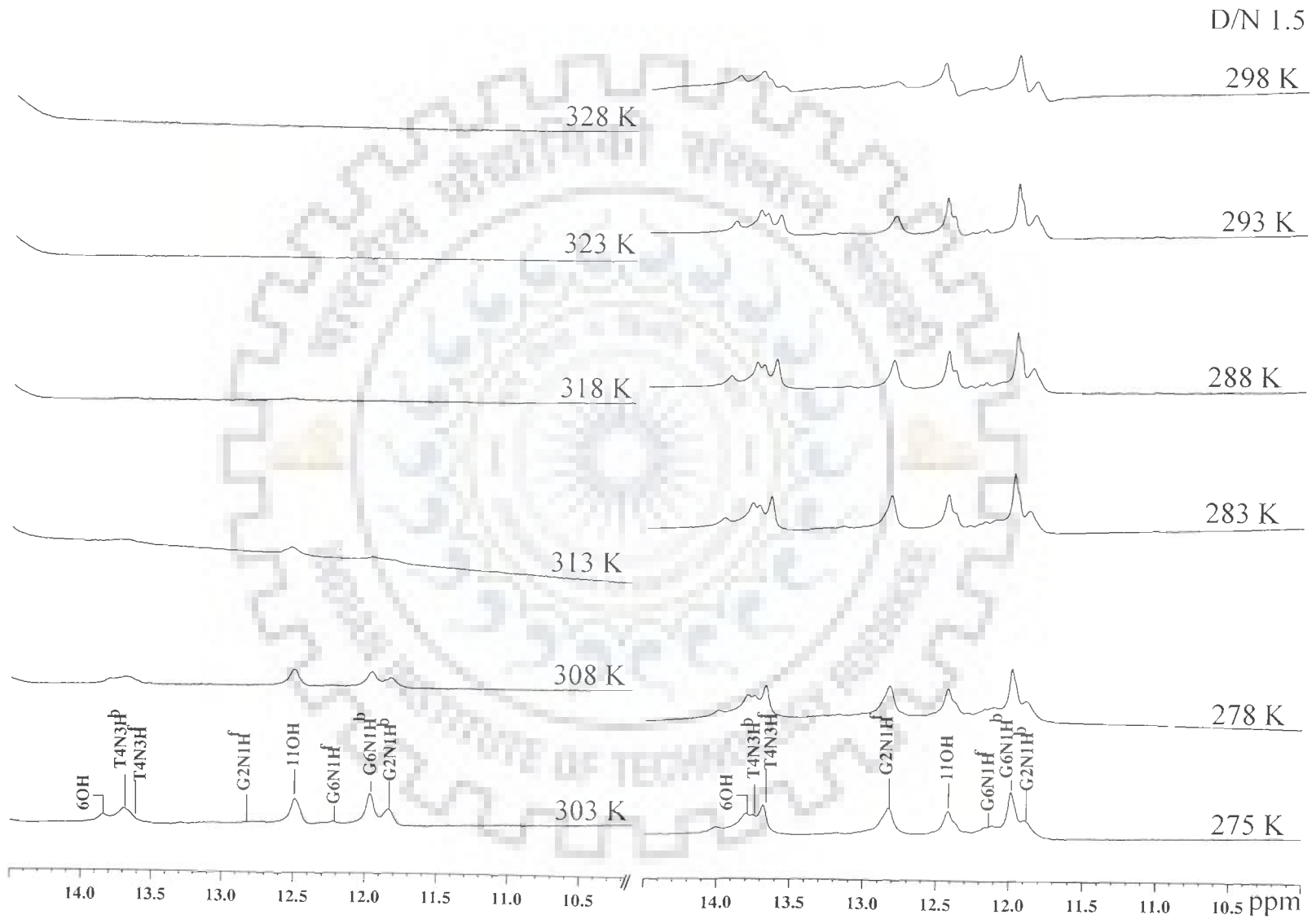
(c)



(d)

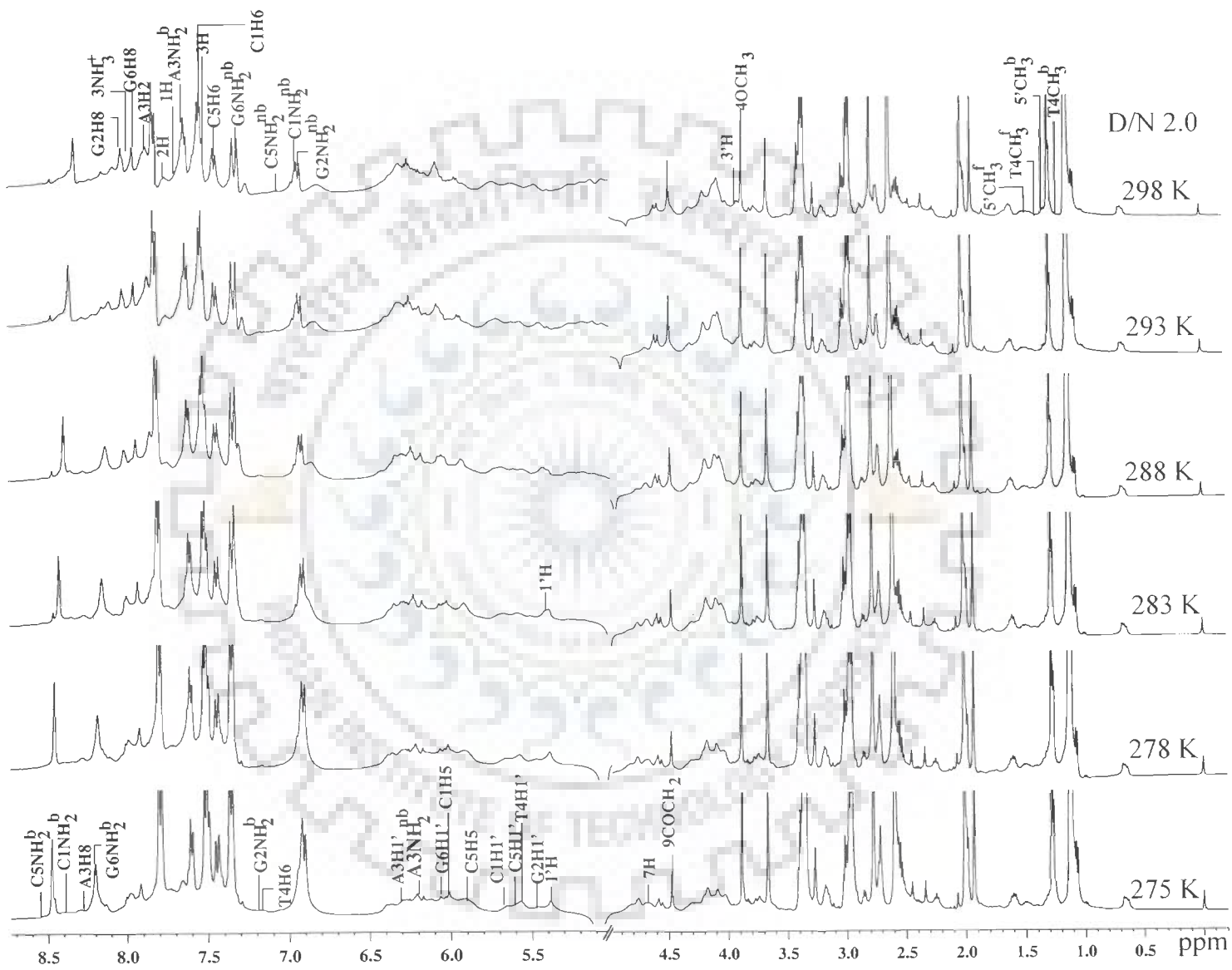


(e)

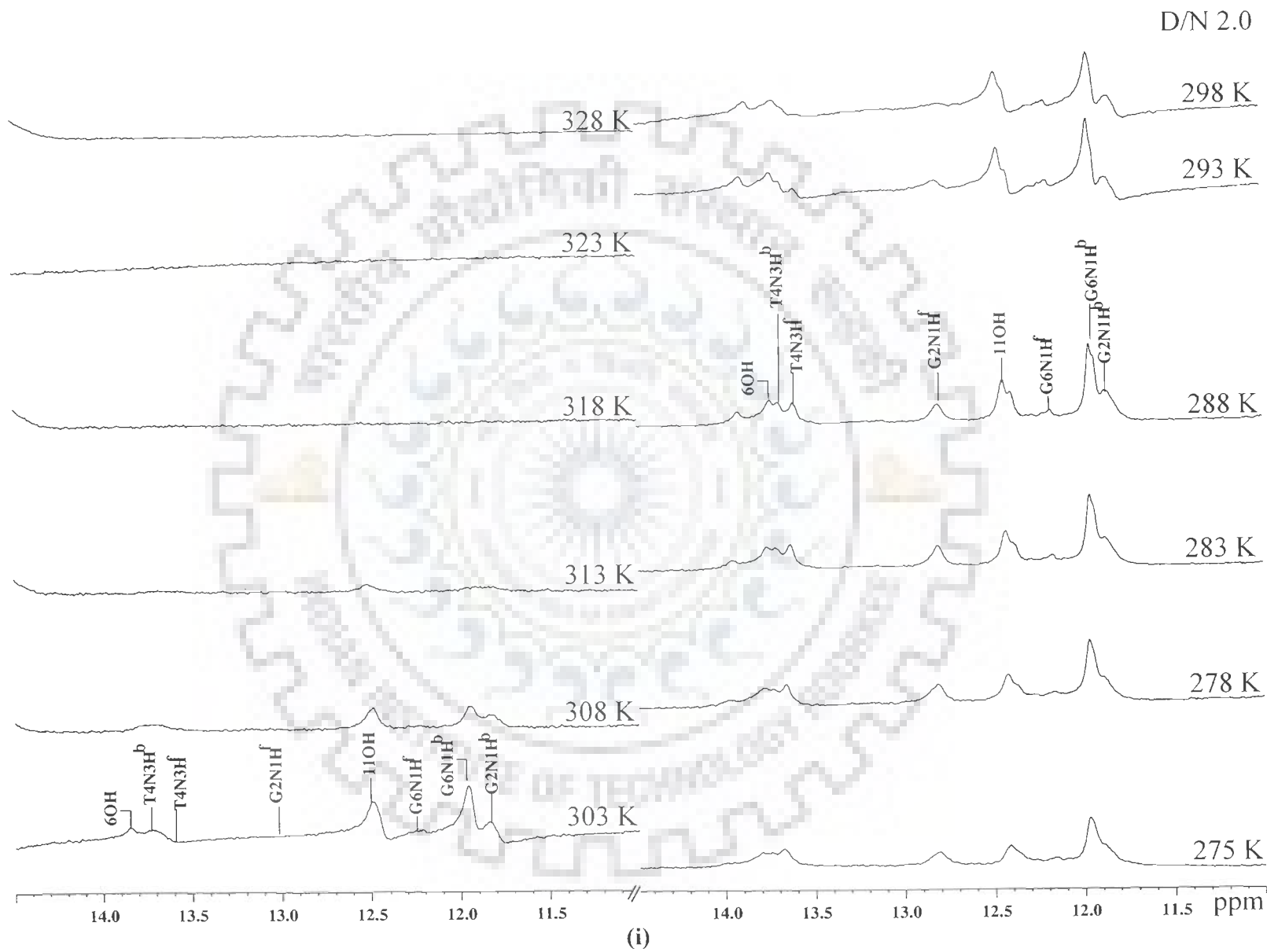


(f)

385



(g)



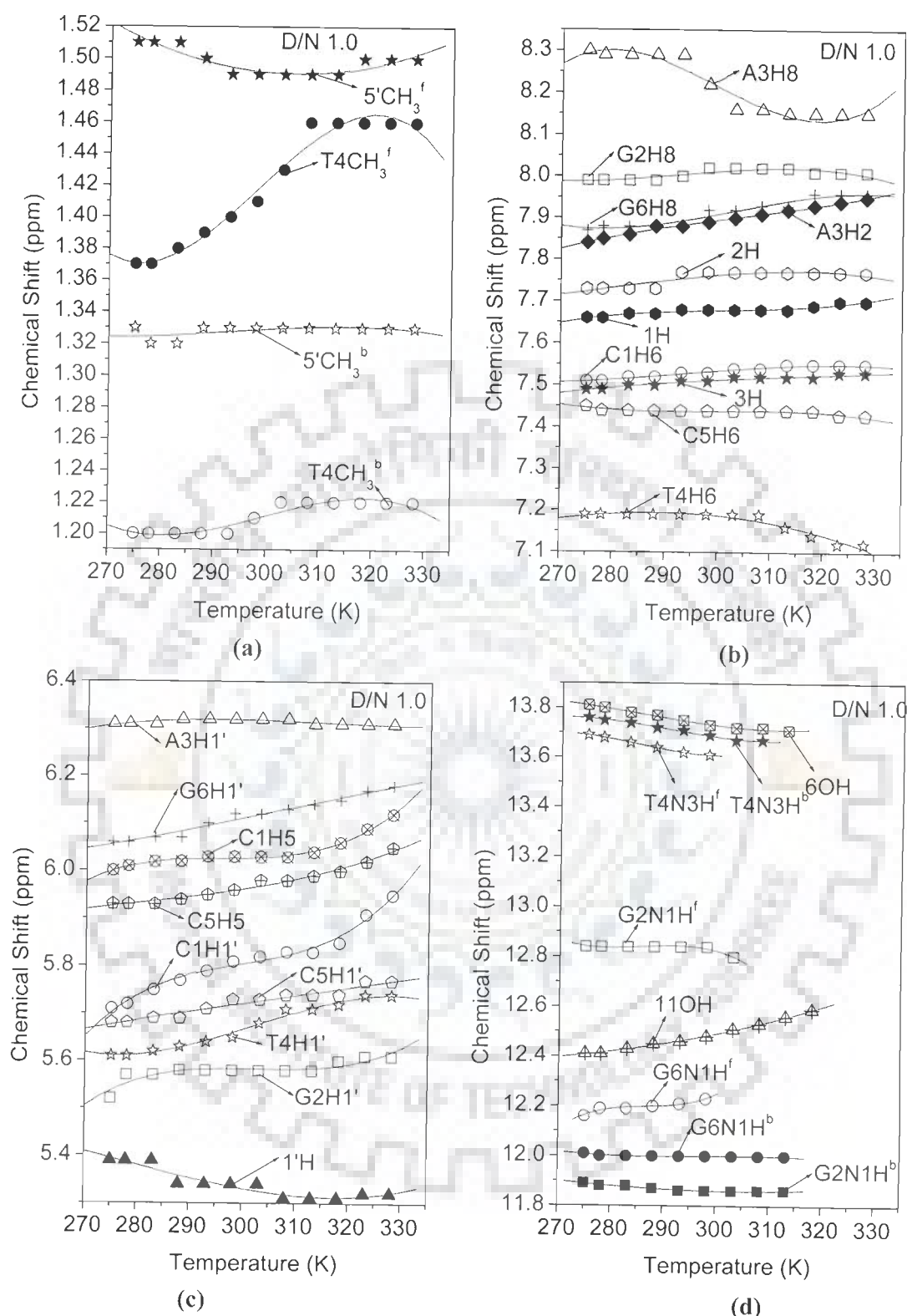
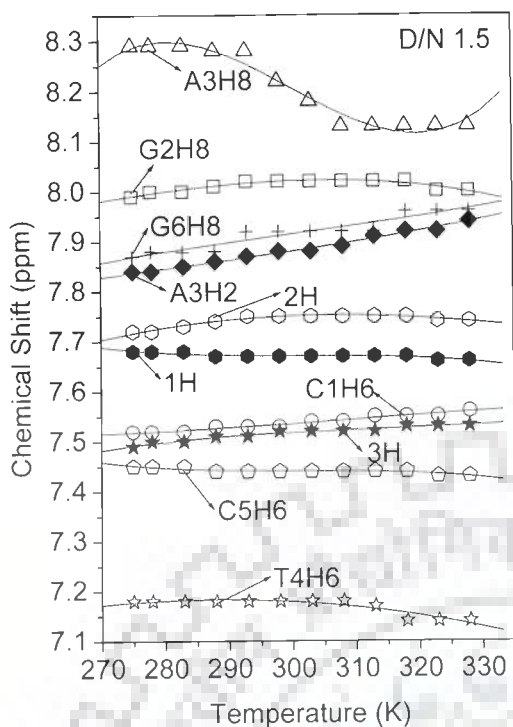
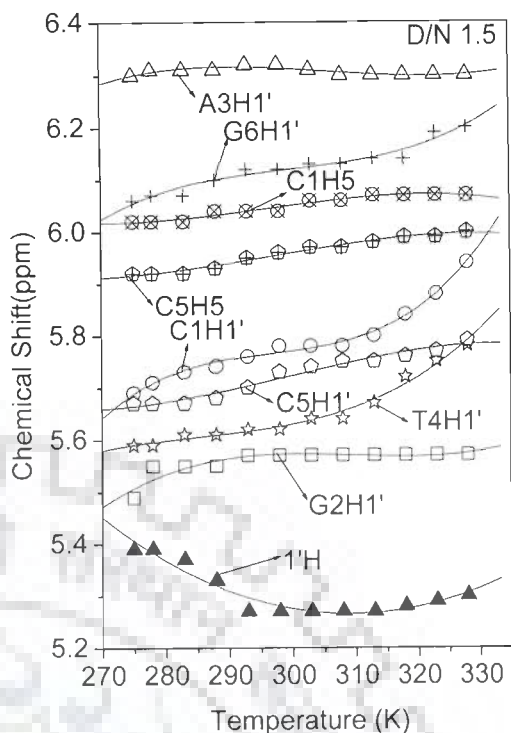


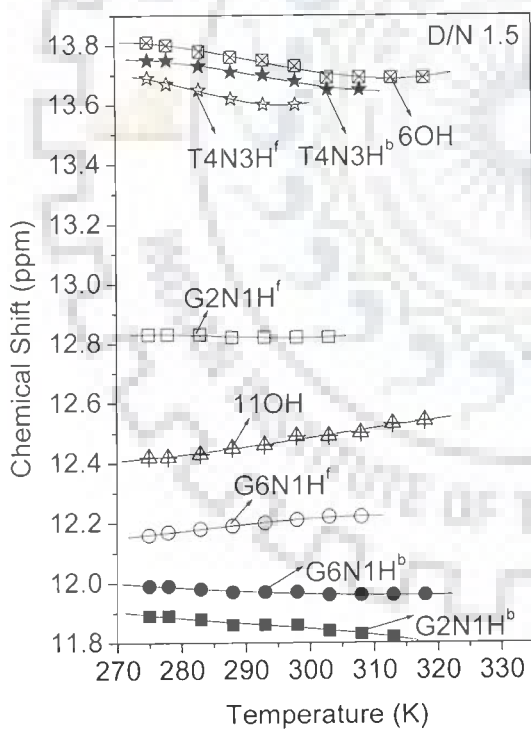
Fig. 5a-I: Chemical Shift of various protons of d-(CGATCG)₂ and 4'-epiadriamycin in 4'-epiadriamycin-d(CGATCG)₂ complex as a function of temperature (275 - 328 K) at drug (D) to DNA (N) duplex stoichiometric ratios (D/N) of 1.0, 1.5, 2.0 in H₂O/D₂O.



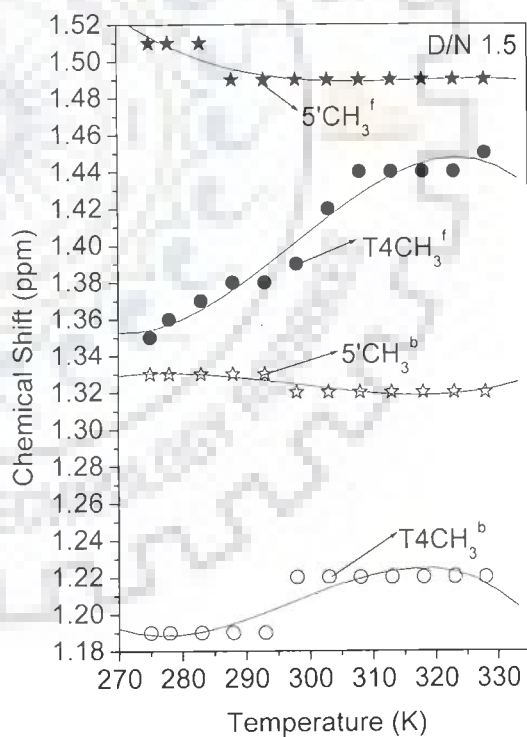
(e)



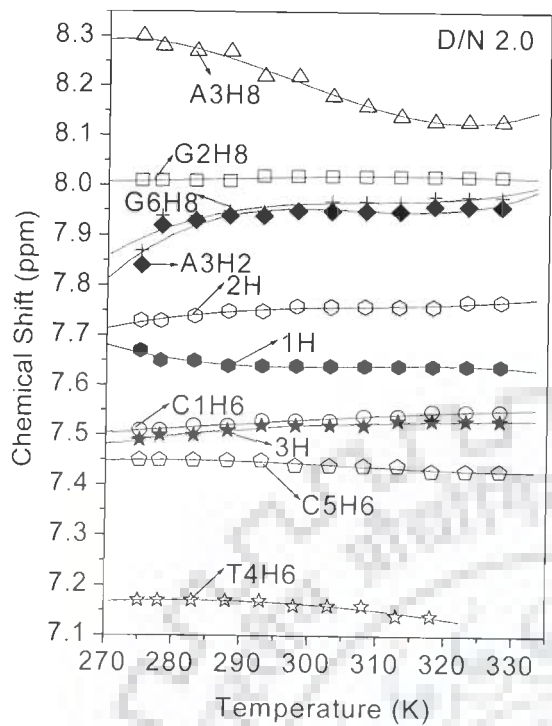
(f)



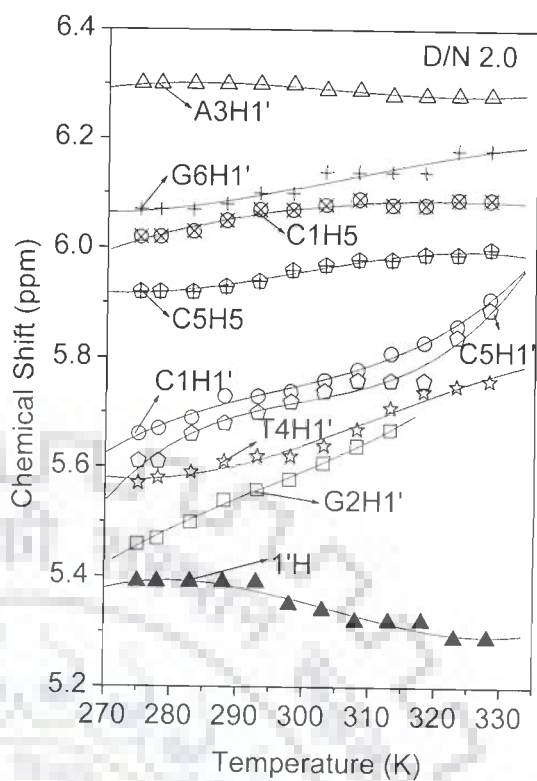
(g)



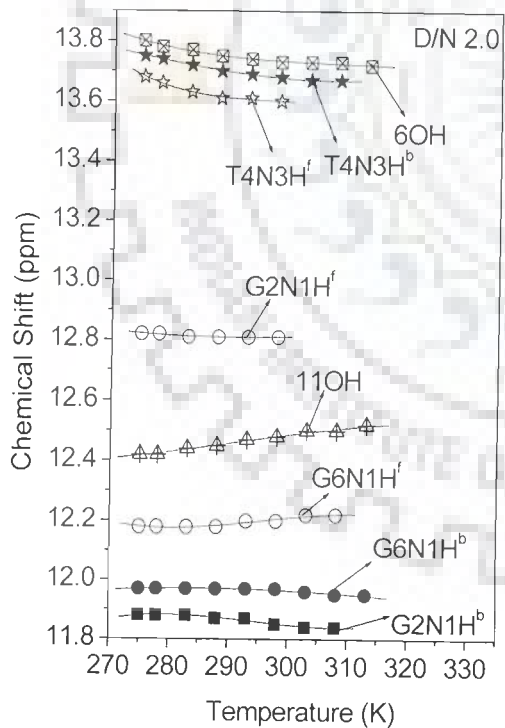
(h)



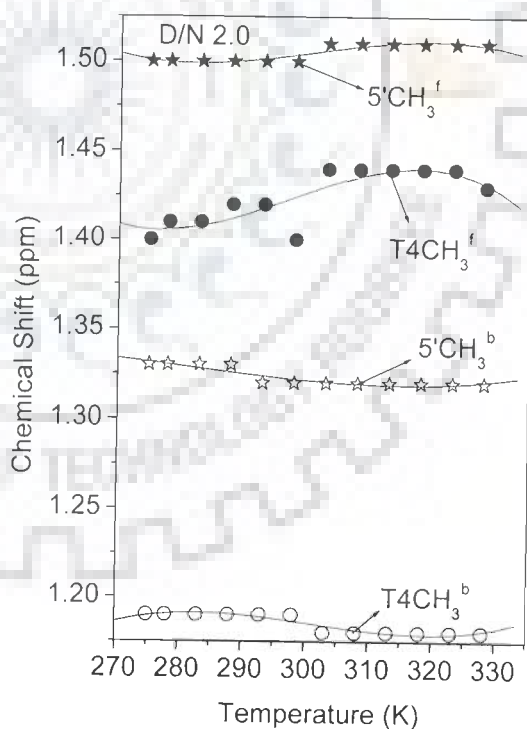
(i)



(j)



(k)



(l)

Table 1a: Chemical shift (ppm) of nucleic acid protons in uncomplexed state (δ^f) and that bound to drug (δ^b) at drug (D) to nucleic acid duplex (N) ratio D/N=1.0 at 275 K. Also shown here is the change in chemical shift on binding, that is. $\Delta\delta = \delta^b_{(D/N=1.0)} - \delta^f$ and $\Delta\delta^\# = \# \delta^b - \# \delta^f$.

Proton	C1			G2			A3			T4			C5			G6		
	δ^b	δ^f	$\Delta\delta$	δ^b	δ^f	$\Delta\delta$	δ^b	δ^f	$\Delta\delta$	δ^b	δ^f	$\Delta\delta$	δ^b	δ^f	$\Delta\delta$	δ^b	δ^f	$\Delta\delta$
H8/H6	7.51	7.69	-0.18	7.99	8.05	-0.06	8.30	8.34	-0.04	7.19	7.26	-0.07	7.45	7.51	-0.06	7.87	8.02	-0.15
H1'	5.71	5.92	-0.21	5.52	5.62	-0.10	6.31	6.37	-0.06	5.61	5.70	-0.09	5.68	5.72	-0.04	6.06	6.18	-0.12
H2'	1.82	2.02	-0.20	2.74	2.89	-0.15	2.71	2.80	-0.09	2.02	2.09	-0.07	1.95	2.06	-0.11	2.62	2.78	-0.16
H2''	2.34	2.45	-0.11	2.86	2.99	-0.13	2.99	3.08	-0.09	2.42	2.52	-0.10	2.36	2.49	-0.13	2.32	2.42	-0.10
H3'	4.66	4.80	-0.14	4.74	4.82	-0.08	5.05	5.11	-0.06	4.88	4.95	-0.07	4.84	4.91	-0.07	4.68	4.74	-0.06
H4'	4.08	4.11	-0.03	4.36	4.40	-0.04	4.51	4.53	-0.02	4.19	4.22	-0.03	4.15	4.19	-0.04	4.19	4.22	-0.03
H5'	3.78	3.77	+0.01	4.15	4.19	-0.04	4.29	4.32	-0.03	4.08	4.11	-0.03	4.08	4.11	-0.03	4.15	4.19	-0.04
H5''	3.72	3.75	-0.03	4.10	4.16	-0.06	4.19	4.22	-0.03	3.94	4.04	-0.10	3.94	4.04	-0.10	4.10	4.16	-0.06
H5/H2	6.00	6.02	-0.02	*	*	*	7.84	7.92	-0.08	*	*	*	5.93	5.98	-0.05	*	*	*
NH ₂ ^b	8.31	8.41	-0.10	7.21	7.45	-0.24	7.62	7.78	-0.16	*	*	*	8.52	8.67	-0.15	8.20	8.18	+0.02
NH ₂ ^{nb}	6.97	6.93	+0.04	6.95	6.91	+0.04	6.12	6.21	-0.09	*	*	*	7.05	7.15	-0.10	7.34	7.36	-0.02
				# δ^b	# δ^f	$\Delta\delta^\#$				# δ^b	# δ^f	$\Delta\delta^\#$				# δ^b	# δ^f	$\Delta\delta^\#$
CH ₃	*	*	*	*	*	*	*	*	*	1.20	1.37	-0.17	*	*	*	*	*	*
NH	*	*	*	11.89	12.84	-0.95	*	*	*	13.75	13.69	+0.06	*	*	*	12.01	12.16	-0.15

-ve $\Delta\delta$ indicates upfield shift
+ve $\Delta\delta$ indicates downfield shift.

Table 1b: Chemical shift (ppm) of drug protons in uncomplexed monomer a state (δ^{monomer} concentration 0.01 mM, 298 K), free (δ^f , 8.0 mM, 275 K) and that bound (δ^b) to nucleic acid duplex at drug (D) to DNA (N) ratio, D/N =1.0 at 275 K. Also shown here is the change in chemical shift, due to binding, that is, $\Delta\delta = \delta^b_{(D/N=1)} - \delta^f$ and $\Delta\delta' = \delta^b_{(D/N=1)} - \delta^{\text{monomer}}$.

Protons	$\delta^b_{(D/N=1)}$	δ^f	$\Delta\delta = \delta^b_{(D/N=1)} - \delta^f$	δ^{monomer}	$\Delta\delta' = \delta^b_{(D/N=1)} - \delta^{\text{monomer}}$
1H	7.66	7.11	+0.55	7.81	-0.15
2H	7.73	7.35	+0.38	7.85	-0.12
3H	7.49	7.08	+0.41	7.55	-0.06
7H	4.72	4.51	+0.21	4.60	+0.12
1'H	5.39	5.22	+0.17	5.46	-0.07
3'H	4.07	3.25	+0.82	3.31	+0.76
4'H	4.18	3.22	+0.96	3.13	+1.05
5'H	4.27	3.84	+0.43	4.01	+0.26
5'CH ₃	1.31	1.22	+0.09	1.33	-0.02
4OCH ₃	3.91	3.64	+0.27	3.95	-0.04
9COCH ₂	4.49	4.66	-0.17	4.86	-0.37
6 OH	13.81	12.96	+0.85	-	-
11OH	12.41	12.31	+0.10	-	-
9OH	5.08	4.96	+0.12	-	-
3NH ₃ ⁺	7.95	8.00	-0.05	-	-
4'OH	4.82	4.91	-0.09	-	-
8eqH	2.36	2.07	+0.29	2.18	+0.18
8axH	1.82	1.79	+0.03	2.13	-0.31
2'axH	1.82	1.76	+0.06	1.87	-0.05
2'eqH	2.34	2.11	+0.23	2.31	+0.03
10eqH	2.64	2.67	-0.03	3.10	-0.46
10axH	2.38	2.20	+0.18	2.92	-0.54

-ve $\Delta\delta$ indicates upfield shift

+ve $\Delta\delta$ indicates downfield shift.

Table 2a: Chemical shift (ppm) of nucleotide protons as a function of drug (D) to nucleic acid duplex (N) ratio, D/N, at 275 K. Also shown here is the change in chemical shift on binding, that is, $\Delta\delta = \delta_{(D/N=2.0)} - \delta_{(D/N=0.0)}$ equivalent to $\delta_{\text{Total}} = \delta^b_{(D/N=2.0)} - \delta^f$. -ve $\Delta\delta$ indicates upfield shift and +ve $\Delta\delta$ indicates downfield shift.

D/N Ratio	C1H1'	G2H1'	A3H1'	T4H1'	C5H1'	G6H1'	C1H6	G2H8	A3H8	T4H6	C5H6	G6H8
0.00	5.76	5.61	6.33	5.63	5.69	6.11	7.49	8.01	8.32	7.22	7.44	7.89
0.16	5.74	5.59	6.33	5.62	5.69	6.09	7.49	8.00	8.31	7.21	7.44	7.89
0.32	5.73	5.58	6.32	5.61	5.68	6.08	7.49	8.00	8.31	7.21	7.44	7.89
0.48	5.73	5.58	6.32	5.61	5.68	6.07	7.50	7.99	8.31	7.20	7.44	7.87
0.64	5.73	5.58	6.32	5.61	5.68	6.07	7.50	7.99	8.31	7.20	7.44	7.87
0.80	5.72	5.53	6.31	5.61	5.68	6.06	7.50	7.99	8.30	7.20	7.45	7.87
0.96	5.71	5.52	6.31	5.61	5.68	6.06	7.51	7.99	8.30	7.19	7.45	7.87
1.11	5.70	5.52	6.31	5.60	5.67	6.06	7.51	7.99	8.30	7.19	7.45	7.87
1.27	5.70	5.50	6.31	5.59	5.67	6.06	7.51	7.99	8.30	7.19	7.45	7.87
1.43	5.69	5.49	6.31	5.59	5.67	6.06	7.51	7.99	8.30	7.18	7.45	7.87
1.53	5.69	5.49	6.30	5.59	5.67	6.06	7.52	7.99	8.29	7.18	7.45	7.87
1.60	5.69	5.49	6.30	5.58	5.66	6.06	7.51	7.99	8.29	7.18	7.45	7.87
1.75	5.67	5.49	6.30	5.58	5.65	6.06	7.51	7.99	8.29	7.18	7.45	7.87
1.91	5.66	5.47	6.30	5.58	5.65	6.07	7.51	8.01	8.30	7.18	7.45	7.87
2.03	5.66	5.46	6.30	5.57	5.61	6.07	7.51	8.01	8.30	7.17	7.45	7.87
$\Delta\delta$	-0.10	-0.15	-0.03	-0.06	-0.08	-0.04	+0.02	+0.00	-0.02	-0.05	+0.01	-0.02

D/N Ratio	T4NH ^f	T4NH ^b	G2NH ^f	G2NH ^b	G6NH ^f	G6NH ^b	T4CH ₃ ^f	T4CH ₃ ^b	C1H5	C5H5	A3H2
0.00	13.73	-	12.88	-	-	-	1.39	-	6.00	5.96	7.88
0.16	13.72	13.79	12.87	11.88	12.16	12.04	1.38	1.20	6.00	5.95	7.87
0.32	13.71	13.79	12.86	11.88	12.16	12.03	1.38	1.20	6.00	5.95	7.86
0.48	13.71	13.78	12.86	11.88	12.16	12.03	1.38	1.20	6.00	5.94	7.86
0.64	13.70	13.77	12.86	11.89	12.16	12.03	1.38	1.20	6.00	5.94	7.86
0.80	13.70	13.77	12.85	11.89	12.16	12.02	1.37	1.20	6.00	5.94	7.85
0.96	13.69	13.76	12.84	11.89	12.16	12.01	1.37	1.20	6.00	5.93	7.84
1.11	13.69	13.76	12.84	11.89	12.16	12.01	1.37	1.19	6.01	5.93	7.84
1.27	13.69	13.75	12.83	11.89	12.16	11.99	1.36	1.19	6.01	5.93	7.84
1.43	13.69	13.75	12.83	11.89	12.16	11.99	1.36	1.19	6.01	5.93	7.84
1.53	13.69	13.75	12.83	11.89	12.16	11.99	1.35	1.19	6.02	5.92	7.84
1.60	13.68	13.75	12.83	11.89	12.16	11.99	1.35	1.19	6.02	5.92	7.84
1.75	13.68	13.75	12.83	11.89	12.18	11.98	1.36	1.19	6.02	5.92	7.84
1.91	13.68	13.75	12.83	11.89	12.18	11.97	1.40	1.19	6.02	5.92	7.84
2.03	13.68	13.75	12.82	11.88	12.18	11.97	1.40	1.19	6.02	5.92	7.84
$\Delta\delta$	-	-	-	-	-	-	-	-	+0.02	-0.04	-0.04

Table 2b: Chemical shift (ppm) of nucleotide protons as a function of drug (D) to nucleic acid duplex (N) ratio, D/N, at 298 K. Also shown here is the change in chemical shift on binding, that is, $\Delta\delta = \delta_{(D/N=2.0)} - \delta_{(D/N=0.0)}$ equivalent to $\delta_{\text{Total}} = \delta^b_{(D/N=2.0)} - \delta^f$. -ve $\Delta\delta$ indicates upfield shift and +ve $\Delta\delta$ indicates downfield shift.

D/N Ratio	C1H1'	G2H1'	A3H1'	T4H1'	C5H1'	G6H1'	C1H6	G2H8	A3H8	T4H6	C5H6	G6H8
0.00	5.87	5.59	6.34	5.70	5.75	6.16	7.52	8.02	8.21	7.21	7.44	7.95
0.16	5.86	5.59	6.34	5.70	5.75	6.15	7.53	8.02	8.22	7.21	7.44	7.95
0.32	5.85	5.58	6.34	5.69	5.75	6.14	7.53	8.01	8.22	7.21	7.44	7.94
0.48	5.85	5.58	6.34	5.69	5.74	6.14	7.53	8.01	8.22	7.21	7.44	7.94
0.64	5.84	5.58	6.33	5.68	5.74	6.14	7.53	8.01	8.22	7.20	7.44	7.93
0.80	5.82	5.58	6.32	5.66	5.74	6.13	7.53	8.01	8.22	7.20	7.44	7.93
0.96	5.81	5.58	6.32	5.65	5.73	6.12	7.53	8.02	8.22	7.19	7.44	7.95
1.11	5.80	5.58	6.32	5.64	5.73	6.10	7.53	8.02	8.22	7.19	7.44	7.95
1.27	5.80	5.58	6.32	5.64	5.73	6.09	7.53	8.02	8.22	7.19	7.44	7.95
1.43	5.80	5.58	6.32	5.64	5.73	6.09	7.53	8.02	8.22	7.19	7.44	7.95
1.53	5.78	5.57	6.32	5.62	5.73	6.09	7.53	8.02	8.22	7.18	7.44	7.95
1.60	5.77	5.57	6.31	5.62	5.73	6.09	7.53	8.02	8.22	7.18	7.44	7.95
1.75	5.76	5.57	6.31	5.62	5.73	6.08	7.53	8.02	8.22	7.18	7.44	7.95
1.91	5.75	5.58	6.30	5.62	5.73	6.09	7.53	8.02	8.22	7.17	7.44	7.95
2.03	5.74	5.58	6.30	5.62	5.72	6.10	7.53	8.02	8.22	7.16	7.44	7.95
$\Delta\delta$	-0.13	-0.01	-0.04	-0.08	-0.03	-0.06	+0.01	+0.00	+0.01	-0.05	+0.00	+0.00

D/N Ratio	T4NH ^f	T4NH ^b	G2NH ^f	G2NH ^b	G6NH ^f	G6NH ^b	T4CH ₃ ^f	T4CH ₃ ^b	C1H5	C5H5	A3H2
0.00	-	-	-	-	-	-	1.44	-	6.04	5.97	7.94
0.16	13.62	13.70	12.87	11.86	12.23	12.03	1.43	1.21	6.04	5.97	7.94
0.32	13.62	13.70	12.87	11.86	12.23	12.03	1.43	1.21	6.04	5.97	7.93
0.48	13.62	13.69	12.85	11.86	12.23	12.02	1.42	1.21	6.04	5.97	7.92
0.64	13.62	13.69	12.84	11.86	12.23	12.01	1.42	1.21	6.04	5.97	7.91
0.80	13.61	13.69	12.84	11.86	12.23	12.00	1.42	1.21	6.03	5.96	7.90
0.96	13.61	13.69	12.84	11.86	12.23	12.00	1.41	1.21	6.03	5.96	7.89
1.11	13.60	13.69	12.83	11.86	12.23	12.00	1.40	1.22	6.03	5.96	7.89
1.27	13.60	13.68	12.82	11.86	12.22	11.98	1.40	1.22	6.03	5.96	7.88
1.43	13.60	13.68	12.82	11.86	12.21	11.97	1.40	1.22	6.03	5.96	7.88
1.53	13.60	13.68	12.82	11.86	12.21	11.97	1.39	1.22	6.04	5.96	7.88
1.60	13.60	13.68	12.82	11.86	12.21	11.97	1.39	1.22	6.04	5.96	7.88
1.75	13.60	13.68	12.81	11.86	12.21	11.96	1.39	1.22	6.03	5.96	7.88
1.91	13.60	13.68	12.81	11.85	12.20	11.96	1.39	1.22	6.04	5.96	7.90
2.03	13.60	13.68	12.81	11.85	12.20	11.97	1.40	1.22	6.07	5.96	7.95
$\Delta\delta$	-	-	-	-	-	-	-	-	+0.03	-0.01	+0.01

Table 2c: Chemical shift (ppm) of nucleotide protons as a function of drug (D) to nucleic acid duplex (N) ratio, D/N, at 318 K. Also shown here is the change in chemical shift on binding, that is, $\Delta\delta = \delta_{(D/N=2.0)} - \delta_{(D/N=0.0)}$ equivalent to $\delta_{\text{Total}} = \delta^b_{(D/N=2.0)} - \delta^f$. -ve $\Delta\delta$ indicates upfield shift and +ve $\Delta\delta$ indicates downfield shift.

D/N Ratio	C1H1'	G2H1'	A3H1'	T4H1'	C5H1'	G6H1'	C1H6	G2H8	A3H8	T4H6	C5H6	G6H8
0.00	5.93	5.64	6.34	5.80	5.89	6.18	7.53	8.02	8.16	7.13	7.44	7.95
0.16	5.93	5.64	6.33	5.75	5.84	6.18	7.54	8.02	8.16	7.13	7.44	7.95
0.32	5.91	5.64	6.33	5.74	5.83	6.18	7.55	8.02	8.16	7.13	7.44	7.95
0.48	5.90	5.64	6.33	5.74	5.80	6.18	7.55	8.02	8.16	7.13	7.44	7.96
0.64	5.89	5.63	6.32	5.73	5.78	6.17	7.55	8.02	8.16	7.13	7.44	7.96
0.80	5.87	5.61	6.31	5.72	5.75	6.16	7.55	8.01	8.15	7.14	7.44	7.96
0.96	5.85	5.60	6.31	5.72	5.74	6.15	7.55	8.00	8.15	7.14	7.44	7.96
1.11	5.85	5.60	6.31	5.72	5.75	6.15	7.55	8.01	8.14	7.14	7.44	7.96
1.27	5.85	5.60	6.31	5.72	5.76	6.15	7.55	8.02	8.14	7.14	7.44	7.96
1.43	5.85	5.60	6.30	5.72	5.76	6.15	7.55	8.02	8.14	7.14	7.44	7.96
1.53	5.84	5.57	6.30	5.72	5.76	6.14	7.55	8.02	8.13	7.14	7.44	7.96
1.60	5.84	-	6.30	5.72	5.76	6.14	7.55	8.02	8.13	7.14	7.43	7.96
1.75	5.84	-	6.30	5.72	5.76	6.14	7.55	8.02	8.13	7.14	7.43	7.96
1.91	5.84	-	6.30	5.72	5.76	6.14	7.55	8.02	8.13	7.14	7.43	7.96
2.03	5.83	-	6.28	5.72	5.76	6.14	7.54	8.02	8.13	7.14	7.43	7.98
$\Delta\delta$	-0.10	-0.07	-0.06	-0.08	-0.13	-0.04	+0.01	+0.00	-0.03	+0.01	-0.01	+0.03

D/N Ratio	G6NH ^b	T4CH ₃ ^f	T4CH ₃ ^b	C1H5	C5H5	A3H2
0.00	-	1.48	-	6.08	6.04	7.95
0.16	-	1.48	1.22	6.08	6.04	7.95
0.32	-	1.47	1.22	6.08	6.04	7.95
0.48	-	1.47	1.22	6.08	6.04	7.95
0.64	-	1.47	1.22	6.07	6.03	7.95
0.80	-	1.46	1.22	6.07	6.01	7.94
0.96	-	1.46	1.22	6.06	6.00	7.93
1.11	-	1.46	1.22	6.07	5.99	7.93
1.27	-	1.45	1.22	6.07	5.99	7.92
1.43	-	1.45	1.22	6.07	5.99	7.92
1.53	11.96	1.44	1.22	6.07	5.99	7.92
1.60	-	1.44	1.22	6.07	5.99	7.92
1.75	-	1.44	1.22	6.07	5.99	7.92
1.91	-	1.44	1.22	6.07	5.99	7.92
2.03	-	1.44	1.22	6.08	5.99	7.92
$\Delta\delta$	-	-	-	+0.00	-0.05	-0.03

Table 3a: Chemical shift (ppm) of drug protons as a function of drug (D) to nucleic acid duplex (N) ratio, D/N, at 275 K. Also shown here is the maximum change in chemical shift due to binding, with respect to drug in free self associated form, δ^f , (8.0 mM, 275 K) as well as the drug in monomeric form, δ^{monomer} (0.01 mM, 298 K), δ^b of the bound form for D/N = 0.16.

D/N Ratios	3H	2H	1H	1'H	6OH	11OH	5'CH ₃ ^b	5'CH ₃ ^f
δ^{monomer}	7.55	7.85	7.81	5.46	-	-	-	1.33
δ^f	7.08	7.35	7.11	5.22	12.96	12.31	-	1.22
0.16	7.48	7.72	7.67	5.45	13.81	12.40	1.32	1.51
0.32	7.48	7.72	7.67	5.45	13.81	12.40	1.32	1.51
0.48	7.48	7.72	7.67	5.45	13.81	12.41	1.32	1.51
0.64	7.48	7.72	7.67	5.39	13.81	12.41	1.32	1.51
0.80	7.48	7.73	7.66	5.39	13.81	12.41	1.30	1.51
0.96	7.49	7.73	7.66	5.39	13.81	12.41	1.33	1.51
1.11	7.49	7.73	7.67	5.39	13.81	12.42	1.33	1.51
1.27	7.49	7.73	7.67	5.39	13.81	12.42	1.33	1.51
1.43	7.49	7.73	7.68	5.39	13.81	12.42	1.33	1.51
1.53	7.49	7.72	7.68	5.39	13.81	12.42	1.33	1.51
1.60	7.49	7.72	7.68	5.39	13.81	12.42	1.33	1.51
1.75	7.49	7.72	7.68	5.39	13.81	12.42	1.33	1.51
1.91	7.49	7.73	7.68	5.39	13.80	12.42	1.33	1.51
2.03	7.49	7.73	7.67	5.39	13.80	12.42	1.33	1.50
$\Delta\delta = \delta^b - \delta^{\text{monomer}}$	-0.07	-0.13	-0.14	-0.01	-	-	-	+0.18
$\Delta\delta' = \delta^b - \delta^f$	+0.40	+0.37	+0.56	+0.23	+0.85	+0.09	-	+0.29

-ve $\Delta\delta$ indicates upfield shift

+ve $\Delta\delta$ indicates downfield shift.

Table 3b: Chemical shift (ppm) of drug protons as a function of drug (D) to nucleic acid duplex (N) ratio, D/N, at 298 K. Also shown here is the maximum change in chemical shift due to binding, with respect to drug in free self associated form, δ^f , (8.0 mM, 298 K) as well as the drug in monomeric form, δ^{monomer} (0.01 mM, 298 K), δ^b of the bound form for D/N = 0.16.

D/N Ratios	3H	2H	1H	1'H	6OH	11OH	5'CH ₃ ^b	5'CH ₃ ^f
δ^{monomer}	7.55	7.85	7.81	5.46	-	-	-	1.33
δ^f	7.30	7.70	7.32	5.39	13.15	12.47	-	1.32
0.16	7.49	7.77	7.69	5.49	13.73	12.49	1.31	1.50
0.32	7.49	7.77	7.68	5.49	13.73	12.49	1.31	1.50
0.48	7.50	7.77	7.68	5.47	13.73	12.49	1.31	1.49
0.64	7.50	7.77	7.68	5.47	13.73	12.49	1.31	1.49
0.80	7.51	7.77	7.68	5.47	13.73	12.49	1.31	1.49
0.96	7.51	7.77	7.68	5.47	13.73	12.50	1.31	1.49
1.11	7.51	7.76	7.67	5.47	13.73	12.49	1.32	1.49
1.27	7.51	7.76	7.67	5.47	13.73	12.49	1.32	1.49
1.43	7.51	7.76	7.67	5.47	13.73	12.49	1.32	1.49
1.53	7.52	7.75	7.67	5.47	13.73	12.49	1.32	1.49
1.60	7.52	7.75	7.67	5.47	13.73	12.48	1.32	1.49
1.75	7.52	7.75	7.66	5.47	13.73	12.48	1.32	1.49
1.91	7.52	7.75	7.65	5.46	13.73	12.48	1.32	1.49
2.03	7.52	7.76	7.64	5.46	13.73	12.48	1.32	1.50
$\Delta\delta = \delta^b - \delta^{\text{monomer}}$	-0.06	-0.08	-0.12	+0.03	-	-	-	+0.17
$\Delta\delta' = \delta^b - \delta^f$	+0.19	+0.07	+0.37	+0.10	+0.58	+0.02	-	+0.18

-ve $\Delta\delta$ indicates upfield shift
+ve $\Delta\delta$ indicates downfield shift.

Table 3c: Chemical shift (ppm) of drug protons as a function of drug (D) to nucleic acid duplex (N) ratio, D/N, at 318 K. Also shown here is the maximum change in chemical shift due to binding, with respect to drug in free self associated form, δ^f , (8.0 mM, 318 K) as well as the drug in monomeric form, δ^{monomer} (0.01 mM, 298 K), δ^b of the bound form for D/N = 0.16.

D/N Ratios	3H	2H	1H	1'H	6OH	11OH	5'CH ₃ ^b	5'CH ₃ ^f
δ^{monomer}	7.55	7.85	7.81	5.46	-	-	-	1.33
δ^f	7.31	7.59	7.33	5.43	13.28	12.59	-	1.41
0.16	7.51	7.75	7.66	5.36	-	-	1.32	1.50
0.32	7.52	7.75	7.66	5.35	-	-	1.32	1.50
0.48	7.52	7.75	7.66	5.34	-	-	1.32	1.50
0.64	7.52	7.76	7.67	5.33	-	-	1.32	1.50
0.80	7.52	7.76	7.68	5.31	-	-	1.32	1.50
0.96	7.52	7.77	7.69	5.31	-	12.59	1.32	1.50
1.11	7.53	7.76	7.69	5.30	-	-	1.32	1.50
1.27	7.53	7.76	7.69	5.30	-	-	1.32	1.50
1.43	7.53	7.76	7.69	5.29	-	-	1.32	1.50
1.53	7.53	7.75	7.69	5.28	13.69	-	1.32	1.49
1.60	7.53	7.75	7.69	5.28	-	-	1.32	1.49
1.75	7.53	7.75	7.69	5.28	-	-	1.32	1.49
1.91	7.53	7.76	7.69	5.28	-	-	1.32	1.50
2.03	7.53	7.76	7.68	5.28	-	-	1.32	1.51
$\Delta\delta = \delta^b - \delta^{\text{monomer}}$	-0.04	-0.10	-0.15	-0.10	-	-	-	+0.17
$\Delta\delta' = \delta^b - \delta^f$	+0.20	+0.16	+0.33	-0.07	+0.41	-	-	+0.09

-ve $\Delta\delta$ indicates upfield shift
+ve $\Delta\delta$ indicates downfield shift.

Table 4a: Chemical shift (ppm) of nucleic acid protons in drug – DNA complex having D/N = 0.96 as a function of temperature. Also shown here is the net change in chemical shift with temperature, that is, $\Delta\delta = \delta_{(328\text{ K})} - \delta_{(275\text{ K})}$. -ve $\Delta\delta$ indicates upfield shift and +ve $\Delta\delta$ indicates downfield shift.

Temp. (K)	C1H1'	G2H1'	A3H1'	T4H1'	C5H1'	G6H1'	C1H6	G2H8	A3H8	T4H6	C5H6	G6H8
275	5.71	5.52	6.31	5.61	5.68	6.06	7.51	7.99	8.30	7.19	7.45	7.87
278	5.72	5.57	6.31	5.61	5.68	6.06	7.51	7.99	8.29	7.19	7.44	7.88
283	5.75	5.57	6.31	5.62	5.69	6.07	7.52	7.99	8.29	7.19	7.44	7.88
288	5.77	5.58	6.32	5.63	5.69	6.07	7.52	7.99	8.29	7.19	7.44	7.88
293	5.79	5.58	6.32	5.64	5.71	6.10	7.53	8.00	8.29	7.19	7.44	7.88
298	5.81	5.58	6.32	5.65	5.73	6.12	7.53	8.02	8.22	7.19	7.44	7.92
303	5.82	5.58	6.32	5.68	5.73	6.12	7.54	8.02	8.16	7.19	7.44	7.92
308	5.83	5.58	6.32	5.71	5.74	6.13	7.54	8.02	8.16	7.19	7.44	7.93
313	5.83	5.58	6.31	5.71	5.74	6.14	7.55	8.02	8.15	7.16	7.44	7.93
318	5.85	5.60	6.31	5.72	5.74	6.15	7.55	8.01	8.15	7.14	7.44	7.96
323	5.91	5.61	6.31	5.74	5.77	6.17	7.55	8.01	8.15	7.12	7.43	7.96
328	5.95	5.61	6.31	5.74	5.77	6.18	7.55	8.01	8.15	7.12	7.43	7.96
$\Delta\delta$	+0.24	+0.09	+0.00	+0.13	+0.09	+0.12	+0.04	+0.02	-0.15	-0.07	-0.02	+0.09
Temp. (K)	T4NH ^f	T4NH ^b	G2NH ^f	G2NH ^b	G6NH ^f	G6NH ^b	T4CH ₃ ^f	T4CH ₃ ^b	C1H5	C5H5	A3H2	
275	13.69	13.76	12.84	11.89	12.16	12.01	1.37	1.20	6.00	5.93	7.84	
278	13.68	13.75	12.84	11.88	12.19	12.00	1.37	1.20	6.01	5.93	7.85	
283	13.66	13.74	12.84	11.88	12.19	12.00	1.38	1.20	6.02	5.93	7.86	
288	13.64	13.72	12.84	11.87	12.20	12.00	1.39	1.20	6.02	5.94	7.88	
293	13.62	13.71	12.84	11.86	12.21	12.00	1.40	1.20	6.03	5.95	7.88	
298	13.61	13.69	12.84	11.86	12.23	12.00	1.41	1.21	6.03	5.96	7.89	
303	-	13.67	12.80	11.86	-	12.00	1.43	1.22	6.03	5.98	7.90	
308	-	13.67	-	11.86	-	12.00	1.46	1.22	6.03	5.98	7.91	
313	-	-	-	11.86	-	12.00	1.46	1.22	6.04	5.99	7.92	
318	-	-	-	-	-	-	1.46	1.22	6.06	6.00	7.93	
323	-	-	-	-	-	-	1.46	1.22	6.09	6.02	7.94	
328	-	-	-	-	-	-	1.46	1.22	6.12	6.05	7.95	
$\Delta\delta$	-0.08	-0.09	-0.04	-0.03	+0.07	-0.01	+0.09	+0.02	+0.12	+0.12	+0.11	

Table 4b: Chemical shift (ppm) of d-(CGATCG)₂ protons in drug – DNA complex having D/N = 1.53 as a function of temperature. $\Delta\delta = \delta_{(328\text{ K})} - \delta_{(275\text{ K})}$ -ve $\Delta\delta$ indicates upfield shift and +ve $\Delta\delta$ indicates downfield shift.

Temp. (K)	C1H1'	G2H1'	A3H1'	T4H1'	C5H1'	G6H1'	C1H6	G2H8	A3H8	T4H6	C5H6	G6H8
275	5.69	5.49	6.30	5.59	5.67	6.06	7.52	7.99	8.29	7.18	7.45	7.87
278	5.71	5.55	6.31	5.59	5.67	6.07	7.52	8.00	8.29	7.18	7.45	7.88
283	5.73	5.55	6.31	5.61	5.67	6.07	7.52	8.00	8.29	7.18	7.45	7.88
288	5.74	5.55	6.31	5.61	5.68	6.10	7.53	8.01	8.28	7.18	7.44	7.88
293	5.76	5.57	6.32	5.62	5.70	6.12	7.53	8.02	8.28	7.18	7.44	7.92
298	5.78	5.57	6.32	5.62	5.73	6.12	7.53	8.02	8.22	7.18	7.44	7.92
303	5.78	5.57	6.31	5.64	5.74	6.13	7.54	8.02	8.18	7.18	7.44	7.92
308	5.78	5.57	6.30	5.64	5.75	6.13	7.54	8.02	8.13	7.18	7.44	7.92
313	5.80	5.57	6.30	5.67	5.75	6.14	7.55	8.02	8.13	7.17	7.44	7.92
318	5.84	5.57	6.30	5.72	5.76	6.14	7.55	8.02	8.13	7.14	7.44	7.96
323	5.88	5.57	6.30	5.75	5.77	6.19	7.55	8.00	8.13	7.14	7.43	7.96
328	5.94	5.57	6.30	5.78	5.79	6.20	7.56	8.00	8.13	7.14	7.43	7.96
$\Delta\delta$	+0.25	+0.08	+0.00	+0.19	+0.12	+0.14	+0.04	+0.01	-0.16	-0.04	-0.02	+0.09
Temp. (K)	T4NH ^f	T4NH ^b	G2NH ^f	G2NH ^b	G6NH ^f	G6NH ^b	T4CH ₃ ^f	T4CH ₃ ^b	C1H5	C5H5	A3H2	
275	13.69	13.75	12.83	11.89	12.16	11.99	1.35	1.19	6.02	5.92	7.84	
278	13.67	13.75	12.83	11.89	12.17	11.99	1.36	1.19	6.02	5.92	7.84	
283	13.65	13.73	12.83	11.88	12.18	11.98	1.37	1.19	6.02	5.92	7.85	
288	13.62	13.71	12.82	11.86	12.19	11.97	1.38	1.19	6.04	5.93	7.86	
293	13.60	13.70	12.82	11.86	12.20	11.97	1.38	1.19	6.04	5.95	7.87	
298	13.60	13.68	12.82	11.86	12.21	11.97	1.39	1.22	6.04	5.96	7.88	
303	-	13.65	12.82	11.84	12.22	11.96	1.42	1.22	6.06	5.97	7.88	
308	-	13.65	-	11.83	12.22	11.96	1.44	1.22	6.06	5.97	7.89	
313	-	-	-	11.82	-	11.96	1.44	1.22	6.07	5.98	7.91	
318	-	-	-	-	-	11.96	1.44	1.22	6.07	5.99	7.92	
323	-	-	-	-	-	-	1.44	1.22	6.07	5.99	7.92	
328	-	-	-	-	-	-	1.45	1.22	6.07	6.00	7.94	
$\Delta\delta$	-0.09	-0.10	-0.01	-0.07	+0.06	-0.03	+0.10	+0.03	+0.05	+0.08	+0.10	

Table 4c: Chemical shift (ppm) of nucleic acid protons in drug – DNA complex having D/N = 2.03 as a function of temperature. Also shown here is the net change in chemical shift with temperature, that is, $\Delta\delta = \delta_{(328\text{ K})} - \delta_{(275\text{ K})}$. -ve $\Delta\delta$ indicates upfield shift and +ve $\Delta\delta$ indicates downfield shift.

Temp. (K)	C1H1'	G2H1'	A3H1'	T4H1'	C5H1'	G6H1'	C1H6	G2H8	A3H8	T4H6	C5H6	G6H8
275	5.66	5.46	6.30	5.57	5.61	6.07	7.51	8.01	8.30	7.17	7.45	7.87
278	5.67	5.47	6.30	5.58	5.61	6.07	7.51	8.01	8.28	7.17	7.45	7.94
283	5.69	5.50	6.30	5.59	5.66	6.07	7.52	8.01	8.27	7.17	7.45	7.94
288	5.73	5.54	6.30	5.61	5.68	6.08	7.52	8.01	8.27	7.17	7.45	7.95
293	5.73	5.56	6.30	5.62	5.70	6.10	7.53	8.02	8.22	7.17	7.45	7.95
298	5.74	5.58	6.30	5.62	5.72	6.10	7.53	8.02	8.22	7.16	7.44	7.95
303	5.76	5.61	6.29	5.64	5.74	6.14	7.53	8.02	8.18	7.16	7.44	7.97
308	5.78	5.64	6.29	5.67	5.76	6.14	7.54	8.02	8.16	7.16	7.44	7.97
313	5.81	5.67	6.28	5.71	5.76	6.14	7.54	8.02	8.14	7.14	7.44	7.97
318	5.83	-	6.28	5.74	5.76	6.14	7.55	8.02	8.13	7.14	7.43	7.98
323	5.86	-	6.28	5.75	5.84	6.18	7.55	8.02	8.13	-	7.43	7.98
328	5.91	-	6.28	5.76	5.89	6.18	7.55	8.02	8.13	-	7.43	7.98
$\Delta\delta$	+0.25	+0.21	-0.02	+0.19	+0.28	+0.11	+0.04	+0.01	-0.17	-0.03	-0.02	+0.11
Temp. (K)	T4NH ^f	T4NH ^b	G2NH ^f	G2NH ^b	G6NH ^f	G6NH ^b	T4CH ₃ ^f	T4CH ₃ ^b	C1H5	C5H5	A3H2	
275	13.68	13.75	12.82	11.88	12.18	11.97	1.40	1.19	6.02	5.92	7.84	
278	13.66	13.74	12.82	11.88	12.18	11.97	1.41	1.19	6.02	5.92	7.92	
283	13.63	13.72	12.81	11.88	12.18	11.97	1.41	1.19	6.03	5.92	7.93	
288	13.61	13.70	12.81	11.87	12.18	11.97	1.42	1.19	6.05	5.93	7.94	
293	13.61	13.69	12.81	11.87	12.20	11.97	1.42	1.19	6.07	5.94	7.94	
298	13.60	13.68	12.81	11.85	12.20	11.97	1.40	1.19	6.07	5.96	7.95	
303	-	13.67	-	11.84	12.22	11.96	1.44	1.18	6.08	5.97	7.95	
308	-	13.67	-	11.84	12.22	11.95	1.44	1.18	6.09	5.98	7.95	
313	-	-	-	-	-	11.95	1.44	1.18	6.08	5.98	7.95	
318	-	-	-	-	-	-	1.44	1.18	6.08	5.99	7.96	
323	-	-	-	-	-	-	1.44	1.18	6.09	5.99	7.96	
328	-	-	-	-	-	-	1.43	1.18	6.09	6.00	7.96	
$\Delta\delta$	-0.08	-0.08	-0.01	-0.04	+0.04	-0.02	+0.03	-0.01	+0.07	+0.08	+0.12	

Table 5: Chemical shift (ppm) of some of the drug protons in drug –DNA complex having D/N = 0.96, 1.53, 2.03 as a function of temperature. Total change in chemical shift, $\Delta\delta = \delta_{328} - \delta_{275}$. -ve $\Delta\delta$ indicates upfield shift and +ve $\Delta\delta$ indicates downfield shift.

D/N 0.96								
Temp. (K)	3H	2H	1H	1'H	6OH	11OH	5'CH ₃ ^b	5'CH ₃ ^f
275	7.49	7.73	7.66	5.39	13.81	12.41	1.33	1.51
278	7.49	7.73	7.66	5.39	13.80	12.41	1.32	1.51
283	7.50	7.73	7.67	5.39	13.78	12.43	1.32	1.51
288	7.50	7.73	7.67	5.34	13.77	12.45	1.33	1.50
293	7.51	7.77	7.68	5.34	13.75	12.46	1.33	1.49
298	7.51	7.77	7.68	5.34	13.73	12.48	1.33	1.49
303	7.52	7.77	7.68	5.34	13.72	12.51	1.33	1.49
308	7.52	7.77	7.68	5.31	13.72	12.53	1.33	1.49
313	7.52	7.77	7.68	5.31	13.71	12.56	1.33	1.49
318	7.52	7.77	7.69	5.31	-	12.59	1.33	1.50
323	7.53	7.77	7.70	5.32	-	-	1.33	1.50
328	7.53	7.77	7.70	5.32	-	-	1.33	1.50
$\Delta\delta$	+0.04	+0.04	+0.04	-0.08	-0.10	+0.18	+0.00	-0.01
D/N 1.53								
Temp. (K)	3H	2H	1H	1'H	6OH	11OH	5'CH ₃ ^b	5'CH ₃ ^f
275	7.49	7.72	7.68	5.39	13.81	12.42	1.33	1.51
278	7.50	7.72	7.68	5.39	13.80	12.42	1.33	1.51
283	7.50	7.73	7.68	5.37	13.78	12.43	1.33	1.51
288	7.51	7.74	7.67	5.33	13.76	12.45	1.33	1.49
293	7.51	7.75	7.67	5.27	13.75	12.46	1.33	1.49
298	7.52	7.75	7.67	5.27	13.73	12.49	1.32	1.49
303	7.52	7.75	7.67	5.27	13.69	12.49	1.32	1.49
308	7.52	7.75	7.67	5.27	13.69	12.50	1.32	1.49
313	7.52	7.75	7.67	5.27	13.69	12.53	1.32	1.49
318	7.53	7.75	7.67	5.28	13.69	12.54	1.32	1.49
323	7.53	7.74	7.66	5.29	-	-	1.32	1.49
328	7.53	7.74	7.66	5.30	-	-	1.32	1.49
$\Delta\delta$	+0.04	+0.02	-0.02	-0.09	-0.12	+0.12	-0.01	-0.02
D/N 2.03								
Temp. (K)	3H	2H	1H	1'H	6OH	11OH	5'CH ₃ ^b	5'CH ₃ ^f
275	7.49	7.73	7.67	5.39	13.80	12.42	1.33	1.50
278	7.50	7.73	7.65	5.39	13.78	12.42	1.33	1.50
283	7.50	7.74	7.65	5.39	13.77	12.44	1.33	1.50
288	7.51	7.75	7.64	5.39	13.75	12.45	1.33	1.50
293	7.52	7.75	7.64	5.39	13.74	12.47	1.32	1.50
298	7.52	7.76	7.64	5.35	13.73	12.48	1.32	1.50
303	7.52	7.76	7.64	5.34	13.73	12.50	1.32	1.51
308	7.52	7.76	7.64	5.32	13.73	12.50	1.32	1.51
313	7.53	7.76	7.64	5.32	13.72	12.52	1.32	1.51
318	7.53	7.76	7.64	5.32	-	-	1.32	1.51
323	7.53	7.77	7.64	5.29	-	-	1.32	1.51
328	7.53	7.77	7.64	5.29	-	-	1.32	1.51
$\Delta\delta$	+0.04	+0.04	-0.03	-0.10	-0.08	+0.10	-0.01	+0.01

and 3a-c, Fig. 3a-k). The spectra of the complex of 4'-epiadriamycin-d-(CGATCG)₂ as a function of temperatures are obtained at D/N = 1.0, 1.5 and 2.0 at the range 275 - 328 K (Fig. 4a-i). The chemical shift changes at varying temperatures are shown in Fig. 5a-l. Their values are given in Table 4a-c and 5.

Characteristic of drug-DNA complex

In uncomplexed or free d-(CGATCG)₂, T4NH and G2NH peaks appear at 13.74 and 12.95 ppm, respectively while the G6NH resonance is not seen presumably due to exchange with water solvent. On successive addition of 4'-epiadriamycin to DNA, four additional resonance peaks are observed at 11.89, 13.75, 12.16, 12.01 ppm besides the 6OH and 11OH peak at about 13.81 and 12.41 ppm. In 2D NOESY spectra (Fig. 6a) pairs of protons resonating at 12.84, 11.89; 13.69, 13.75 and 12.16, 12.01 give cross peaks with each other. Since T4NH and G2NH appear at 13.74 and 12.95 ppm in uncomplexed / d-(CGATCG)₂, the peaks at 13.75 and 11.89 ppm get assigned to T4NH and G2NH in the complex of d-(CGATCG)₂ with drug at D/N= 2.0 (designated as T4NH^b and G2NH^b). The remaining pair (12.16, 12.01 ppm), gets assigned to G6NH present in free (G6NH^f 12.16 ppm) and bound state (G6NH^b 12.01 ppm). The area under the NH peaks, confirmed that the G2NH / T4NH / G6NH indeed split into two sets of peaks. The ratio of area of T4NH^f to T4NH^b decreased from 3:1 (approximately) at D/N ratio of 1.0 to 2:1 at D/N ratio of 2.0 that is, on addition of an increasing amount of drug to DNA. It is noted that the intensity of G6NH^f peaks is significantly lesser than that of G2NH^f and T4NH^f. Also the NOE cross peak of G6NH^f and G2NH^f resonance corresponding to a distance of 3.72 Å in standard B-DNA structures is weaker in intensity than the NOE cross peak of T4NH^f and G2NH^f which also corresponds to a distance of 3.72 Å. This suggests that G6NH proton which completely exchanges with water in free d-(CGATCG)₂, is immobilized in the drug-DNA complex although it is still

fraying to some extent being the terminal base pair of DNA. Accordingly the line width of $G6NH^b$ is found to be greater than that of $G2NH^b$ and $T4NH^b$.

It is observed that the sharp $T4CH_3$ peak appearing at 1.37 ppm in $d-(CGATCG)_2$ decreases in intensity as D/N ratio increases and one new, relatively broad peak appearing at 1.20 ppm respectively start growing in intensity with D/N (Fig. 2a-b); the same is also manifested in the area plot. This peak exchange with each other and hence the peak at 1.20 ppm gets assigned to $T4CH_3$ of DNA bound to the drug molecule ($T4CH_3^b$). $T4CH_3^b$ shows all expected interproton NOE connectivities, that is, to $A3H2'$, $A3H2''$, $A3H8$, $T4H1'$, $T4H6$ (Fig. 6d-k). These NOE cross peaks are weaker in intensity than the corresponding NOEs of $T4CH_3^f$ protons resonating at 1.37 ppm respectively. The existence of two sets of $T4NH$, $G6NH$, $G2NH$, and $T4CH_3$ clearly demonstrates that the drug indeed binds to the DNA hexamer and there is a slow exchange of free and bound DNA on NMR time scale at 275 K. This is in accordance with our results of ^{31}P NMR spectra (Chapter 7) in which bound and free ^{31}P resonances showed slow exchange at this temperature.

Change in Chemical Shift due to complexation: There are two intercalative sites available for the drug. The change in chemical shift ($\Delta\delta$) of base and $H1'$ protons with ratios are gradual and small in magnitude. The $\Delta\delta$ increases with D/N ratio as more of hexamer binds to the drug and a maximum of 0.2 ppm upfield shift is observed for $C1H1'$ and $G2H1'$ protons. $T4NH$ bound imino proton is downfield shifted with respect to the corresponding imino protons in free state; the shift being 0.06 ppm, whereas $G2NH$ and $G6NH$ bound imino protons are upfield shifted and the shifts are 0.95 and 0.15 ppm respectively (Table 1a, Fig. 6a-c). Such changes may be attributed to stacking or structural changes in complexation.

1H resonance signals are observed on addition of increasing amount of drug in the temperature range 275 - 328 K at steps of 5 K (Table 4a-c, Fig. 4a-i). Till 308 K temperature, the signals are in slow exchange regime and are sufficiently broad to be followed individually

through the titration. It is observed that there is variation of chemical shift with temperature showing downfield shift of 0.25 ppm for C1H1' and 0.28 ppm for C5H1' at D/N 2.0. There is noticeable change in the drug and nucleic acid protons in the range 275-328 K. This indicates that structurally only one complex is being formed and the chemical shift at any one temperature is not an average of bound and unbound DNA / drug, the equilibrium of which is likely to shift with temperature. The area plots of T4NH, G2NH, G6NH and T4CH₃ in bound and free state also confirm that only one bound species exists in this temperature range. The gradual change with temperature in the range 275-328 K (Fig. 4a-i, 5a-l) may be due to destacking / decreased intercalation, duplex to single strand transition.

Chemical Shift of 4'-epiadriamycin in the drug-DNA complex

There is a gradual shift in drug protons on binding to DNA. The ring protons, 1H, 2H and 3H, shift upfield substantially up to 0.6 ppm with respect to the chemical shift position of drug monomer, δ^{monomer} in 2:1 drug to DNA complex at 275, 298 and 318 K (Table 3a-c). The downfield shift $\Delta\delta = \delta^{\text{b}} - \delta^{\text{f}}$ is 0.40 ppm for 3H, 0.37 ppm for 2H, 0.56 ppm for 1H, 0.23 ppm for 1'H proton and 0.85 ppm for 6OH at 275 K (Table 3a). Several protons in ring A and D of the drug experience large upfield shifts, up to 0.55 ppm. It is worth noted that there is downfield shift upto 0.96 and 0.82 ppm for 4'H and 3'H, respectively. This is due to inversion of 4'H and 4'OH in 4'-epiadriamycin in comparison to adriamycin in which these shifts are 0.29 and 0.19 ppm, respectively. This may be due to better stacking of 4'-epiadriamycin with DNA. The maximum change in chemical shift with temperature is observed for 6OH, 11OH, 1H, 2H, 3H and 1'H protons (Table 5), which are presumably close to oligomer due to stacking of 4'-epiadriamycin chromophore with base pair of DNA. These have been attributed to intercalation of drug chromophore between base pairs of DNA, which move apart to a distance of $\sim 6.8 \text{ \AA}$ on binding to drug (Nunn et al, 1991; Leonard et al, 1992; Estaintot et al, 1992) and are characteristic of stacking interaction between

aromatic/conjugated rings. The relatively smaller change in 1H and 2H protons of drug, also reported earlier (Chaires et al, 1985; Nuss et al, 1981; Philips et al, 1980; Barthwal et al, 1994; Barthwal et al, 1996), may be due to specific positioning of drug chromophore between base pairs such that the ring A partially protrudes out of base pairs resulting in much lesser overlap with adjacent base pairs and hence experiencing less ring current shifts. The base pair protons (H8, H6, H2, H5, CH₃) and deoxyribose H1' protons (being close to aromatic ring) of the intercalating base pair of DNA show ring current effect to a much lesser extent since they are destacked from the neighboring base pair in free DNA and then stacked with the conjugated aromatic rings ABCD (Fig. 1a) of 4'-epiadriamycin. The observed chemical shift at different temperatures (Fig. 5a-l) is distinctly different from that of free drug in monomer / self associated form (Barthwal et al, 1994; Barthwal et al, 1996) or free DNA (Barthwal et al, 2003). These changes in chemical shift may be due to structural alterations on binding and cannot be correlated directly to a specific structural parameter; hence not a sufficient marker of interaction. Therefore 2D NOESY data are acquired which gives inter-proton contacts and shows that the major conformer is the 2:1 molecular complex.

Conformational features of DNA and drug in the complex

The NOESY spectra of drug-DNA complex at stoichiometric D/N ratio of 1.0 have been investigated extensively at mixing time (τ_m) of 100, 200 and 300 ms. The intensities of cross peak have been estimated qualitatively as strong intense (ss), strong (s) medium (ws) and weakly intense (w) and very weak (ww) for distances of about 1.8 - 2.5, 2.5 - 3.0, 3.0 - 3.5, 3.5 - 4.0, and 4.0 - 5.0 Å, respectively from the spectra recorded at $\tau_m = 200$ ms. The inter-proton distances have also been evaluated by taking distance CH5-CH6 = 2.45 Å for $\tau_m = 200$ ms as an internal standard. The observed NOEs for (a) connectivities involving amino and imino protons of base pairs, (b) sequential connectivities (c) intranucleotide connectivities within sugar (d) intranucleotide base to sugar connectivities are given in Table 6-9.

(a) Connectivities involving amino and imino protons of base pairs: The base sequence d-(CGATCG)₂ being self-complementary is responsible for a high symmetry in the NMR spectra. The observation of NOEs (Fig. 6a-c) between the C1H2''-G6N1H^b; G2N1H^f - C5N4H₂^b; A3H2-T4NH^b; T4NH^b-A3N6H₂^b establish Watson-Crick base pairing between T1...A6, G2...C5 and A3...T4 base pairs in the duplex showing that drug is stabilizing the duplex (Table 9). The sequential connectivities among adjacent base pairs, at the terminal ends where the binding site is present, are not observed (Table 8). This clearly demonstrates that DNA duplex is intact, apparently sequential connectivities are broken between base pairs to accommodate drug chromophore as expected on binding of typical intercalator to DNA molecule.

(b) Sequential connectivities: The results in Table 8 clearly demonstrate a discontinuity in the (H6/H8)_n to (H1')_{n-1}, (H2')_{n-1}, (H2'')_{n-1}, (H3')_{n-1}, base (H6/H8)_{n-1} sequential NOE connectivities expected in right-handed B-DNA geometries at the C1pG2 and C5pG6 steps (Fig. 6d-f) by the intercalation of anthracycline ring of the drug. Intense NOE cross peaks are observed for several sequential connectivities between the steps, G2pA3, A3pT4 and T4pC5, as expected for right handed B-DNA type conformations. The intensities corresponding to these sequential NOE connectivities, (H1', H2', H2'')_{n-1} - (base H8/H6)_n are found to be in the range 2.3-4.0 Å (Table 8). Thus the drug chromophore intercalates at C1pG2 and C5pG6 steps. The cross peaks A3H8-G2H8 (5.0 Å), A3H8-T4CH₃ (3.8 Å), A3H8-T4H6 (4.8 Å) and T4H6-C5H5 (3.9 Å) have earlier been observed in the spectra of d-(CGATCG)₂ (Barthwal et al, 2003) and d-(TGATCA)₂ (Barthwal et al, 2004). These observations are indicative of good base to base stacking at these base pair steps. The stacking pattern in the base pairs adjacent to the intercalation site appears to have changed on complexation.

(c) Intranucleotide connectivities within sugar: Sugar conformation may be determined from the integrals of cross peaks in NOESY spectra (Table 6) at 275 K. Intra residue inter-

proton distances H1'-H4' and H2''-H4' distances vary significantly with P_S and χ_s , respectively hence may be used for conformational analysis. The NOE connectivity corresponding to H1'-H4' for G2 residue is weakly intense as compared to A3 and G6 residues (Table 6). This indicates that pseudo rotation phase angle for G2 residue is $\sim 162^\circ$. The observed distance from H1'-H4' NOE intensity (Table 6) increases in the order G6 < A3 < G2 and T4, C1, C5 are overlapped, hence cannot be resolved at $\tau_m = 200$ ms. Thus the pseudorotation P_S decreases as G2 > A3 > G6 so that the P_S of G6 residue is estimated as $\leq 144^\circ$. The distance H2''-H4' decreases rapidly from 3.8 Å for $P_S = 162^\circ$ to 2.3 Å for $P_S = 18^\circ$ while its variation with P_S in the range $P_S = 144^\circ$ - 180° is negligible (Wüthrich, 1986). The observed values of H2''-H4'' distance (Table 6) show that G2, A3 and G6 have distance ~ 3.8 Å, hence the fraction of N-conformer is very less in the residues. All other observed intra-sugar NOE intensities (e.g. relatively higher value of H2''-H3' and H3'-H4' distance for G2 residue) are in agreement with these estimations of P_S and χ_s and also indicate that G2 residue is closest to the B-DNA conformation. The observed intense cross peaks corresponding to H2''-H3' and H3'-H4' distances show that the S-conformer is predominant.

(d) Intranucleotide base to sugar connectivities: Among purines, H8-H1' distance increases in the following order: G2 < G6 < A3 (Table 7), which shows χ value of G2 residue is close to $\sim 105^\circ$. Among pyrimidines, H6-H1' distance increases as C1 < C5 < T4 indicating that χ value of C1 is close to $\sim 150^\circ$ (Fig. 6g-h). The H8/H6-H2'' NOE cross peaks show that the distance is least in G2 and C1 residues among the purines and pyrimidines, respectively and thus these two residues may be adopting high anti conformation. The distance increases in the order G2 < G6 < A3 and C1 < C5 < T4 among purines and pyrimidines, respectively. Strong H8/H6-H3' NOE connectivities indicate presence of mixed S and N-conformers in all the residues. Similarly intense cross peaks of base to H4', H5', H5'' protons for several residues indicate presence of N-conformer along with major S-conformer in deoxyribose.

Conformation of 4'-epiadriamycin

The intramolecular NOE connectivities within the drug molecule in the drug-DNA complex give information about the conformation of drug (Table 10). It is observed that the 7H proton is nearly equidistant to 8axH and 8eqH atoms, but since the peaks are overlapped, their distance could not be accurately measured. In daunosamine sugar, the 1'H-4'H and 1'H-5'H distances are lesser than the corresponding distance (Chapter 3) in the free drug (3.1- 4.2 Å). Thus the conformation of ring A as well as daunosamine sugar has changed due to binding. As a result the relative orientation of ring A protons with sugar protons is affected. The distance of 7H to 1'H and 3'H have increased and corresponding NOE connectivity is not observed. The distance of a 9COCH₂ proton from 1'H and 3'H proton has increased (no cross peak observed). Apparently, 9COCH₂ has moved apart from daunosamine sugar moiety. Such changes are different from the one which have been observed in X-ray crystal structure of complexes of daunomycin with d-(TGATCA)₂ (Nunn et al, 1991). It has been shown that conformation of ring A changes so that 9OH lies in close proximity to G2N2H and G2N3 atoms in order to form two hydrogen bonds. No such studies have been carried out in solution state by NMR techniques.

Intermolecular interactions

Several intermolecular contacts have been observed in the NOESY spectra (Fig. 6a-m) of major conformer and are listed in Table 11. The existence of NOESY cross peaks C1H6-1H, C1H6-2H, C1H6-3H, G6H1'-1H, C5H6-3H, C1NH₂^b-9OH, C5H6-1H, C5H6-2H, G6H1'-6OH (intense NOE cross peak) and G6H2'-11OH (weakly intense cross peak) indicates that the drug chromophore stacks with C1 and C5 residues. Since the 4OCH₃ proton is closer to C5H6 and C5H5 protons while 1H, 2H, 3H protons are close to C1H6 protons, the drug chromophore is oriented in a direction perpendicular to the long axis of C1.G6 and G2.C5 base pairs. As a result of stacking interactions, the 1'H atom of drug comes in close proximity

of G6H1' and G6H2' atoms. The daunosamine sugar is in close proximity of third base pair as 5'CH₃ shows NOE cross peaks with protons of A3 residue. We have selected some intermolecular NOE connectivities discussed above to build a model of drug-DNA complex. Several intramolecular NOE connectivities within the drug and within the DNA molecule have also been incorporated as NMR restraints. The structure obtained after restrained energy minimization followed by restrained molecular dynamics for 100 ps is shown in Fig. 7. It is observed that some of the NOEs observed between overlapping resonant peaks are possible as their corresponding distance in rMD structure is within 4.5 Å. The structure derived by rMD simulations is indeed defined by experimental NOE restraints. The comparison of the distance obtained by NMR and rMD is given in Table 12. This geometry would lead to upfield shifts in ring D and ring A protons due to anisotropic ring current effects from the adjacent base pairs. This is consistent with the observed downfield shifts of 0.03-0.21 ppm in 1'H, 7H, 10axH and 8axH protons. Ring A is seen to protrude out, somewhat towards the solvent and is consistent with the observed downfield shifts in 1H, 2H and 3H protons, being ~ 0.6 ppm. On accommodating the aromatic chromophore of drug between adjacent base pairs, the overlap geometry is considerably altered leading to shifts in their resonance positions. The base pairs however are well stacked as demonstrated by appearance of NOE cross peaks A3H8-T4CH₃ and T4H1'-C5H5.

We have derived the values of pseudorotation phase and glycosidic bond rotation in the rMD structure (Table 13a-b) and compared them with that obtained earlier in similar X-ray crystallographic structures (Mazzini et al, 1998; Frederick et al, 1990; Barthwal et al, 1994). There are no such studies on binding of 4'epiadriamycin to d-(CGATCG)₂ hexamer sequence by NMR techniques. Table 13a shows that T4 and A3 residues have pseudorotation phase angle of 126° and 107°, respectively. Similar values in the range 121-151° have been observed in complex of daunomycin and 4'-epiadriamycin with d-(TGATCA)₂ (Nunn et al,

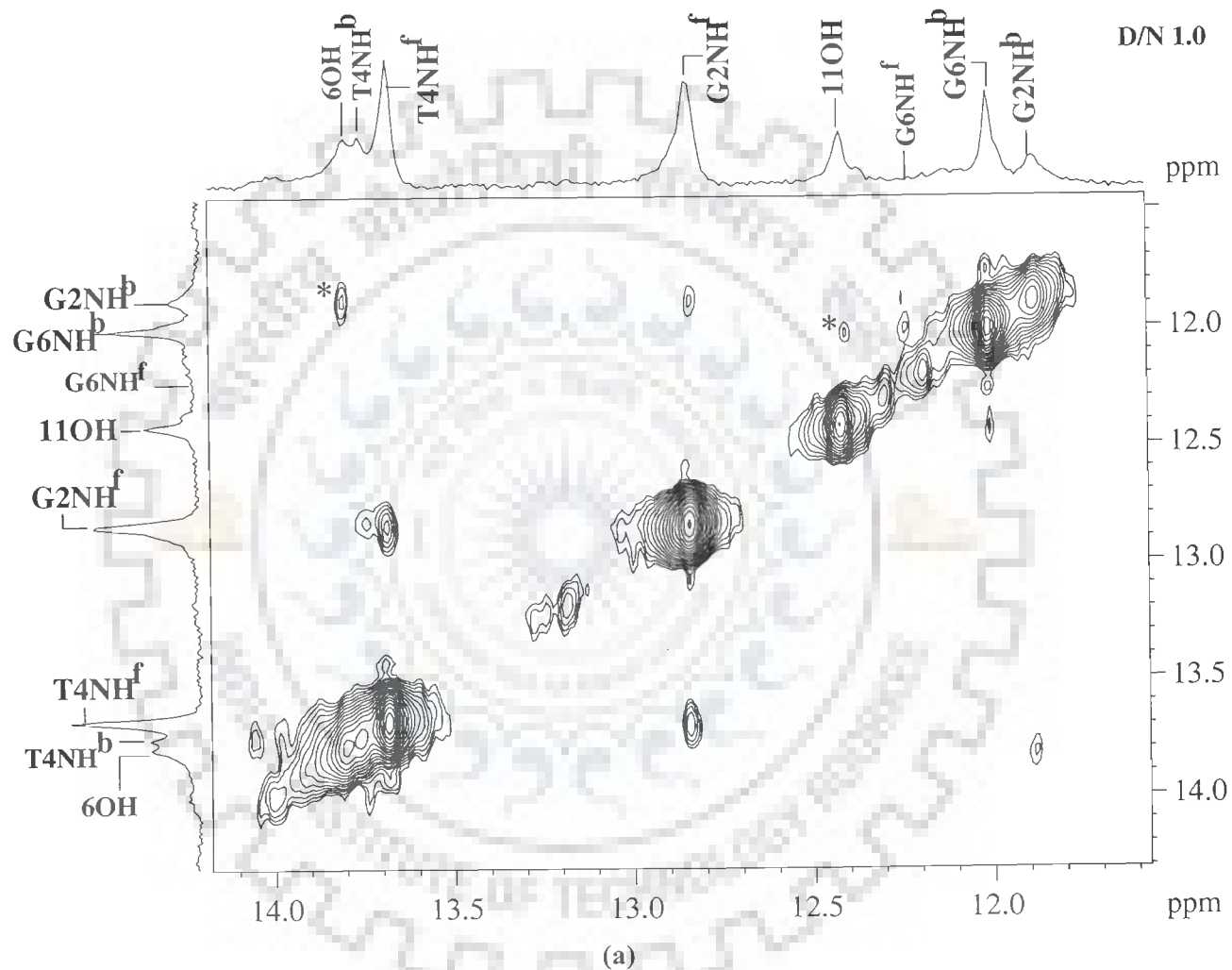
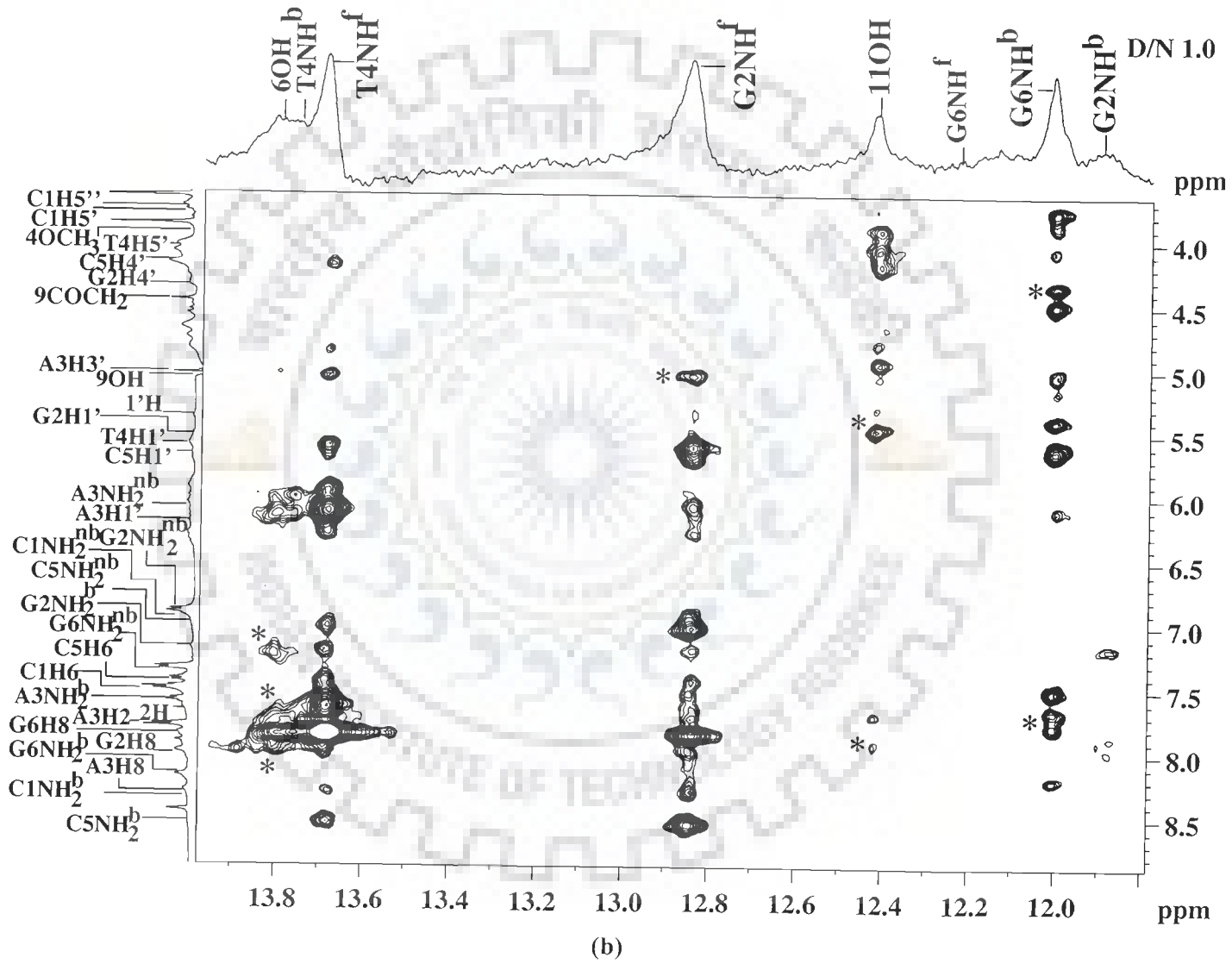
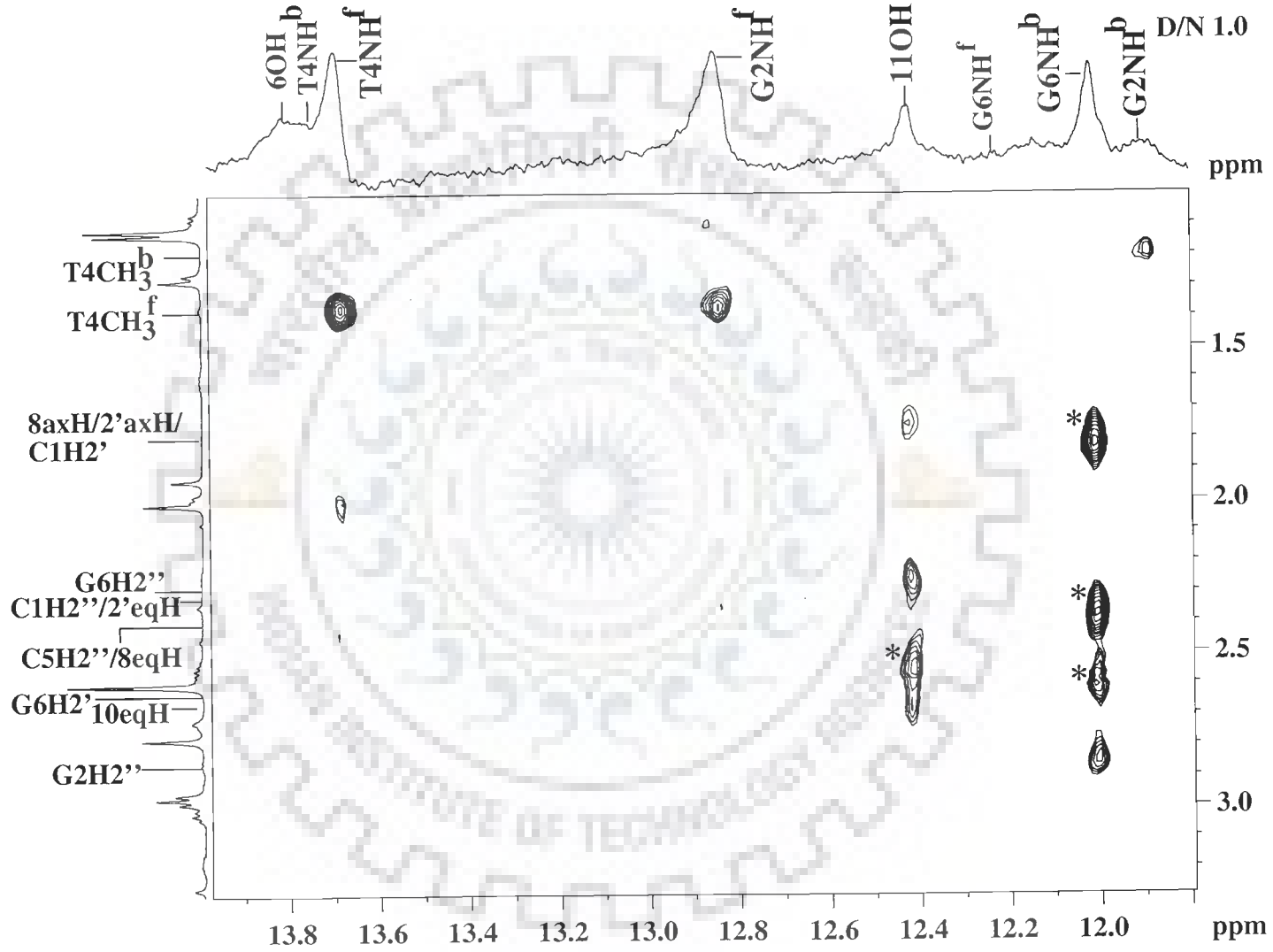
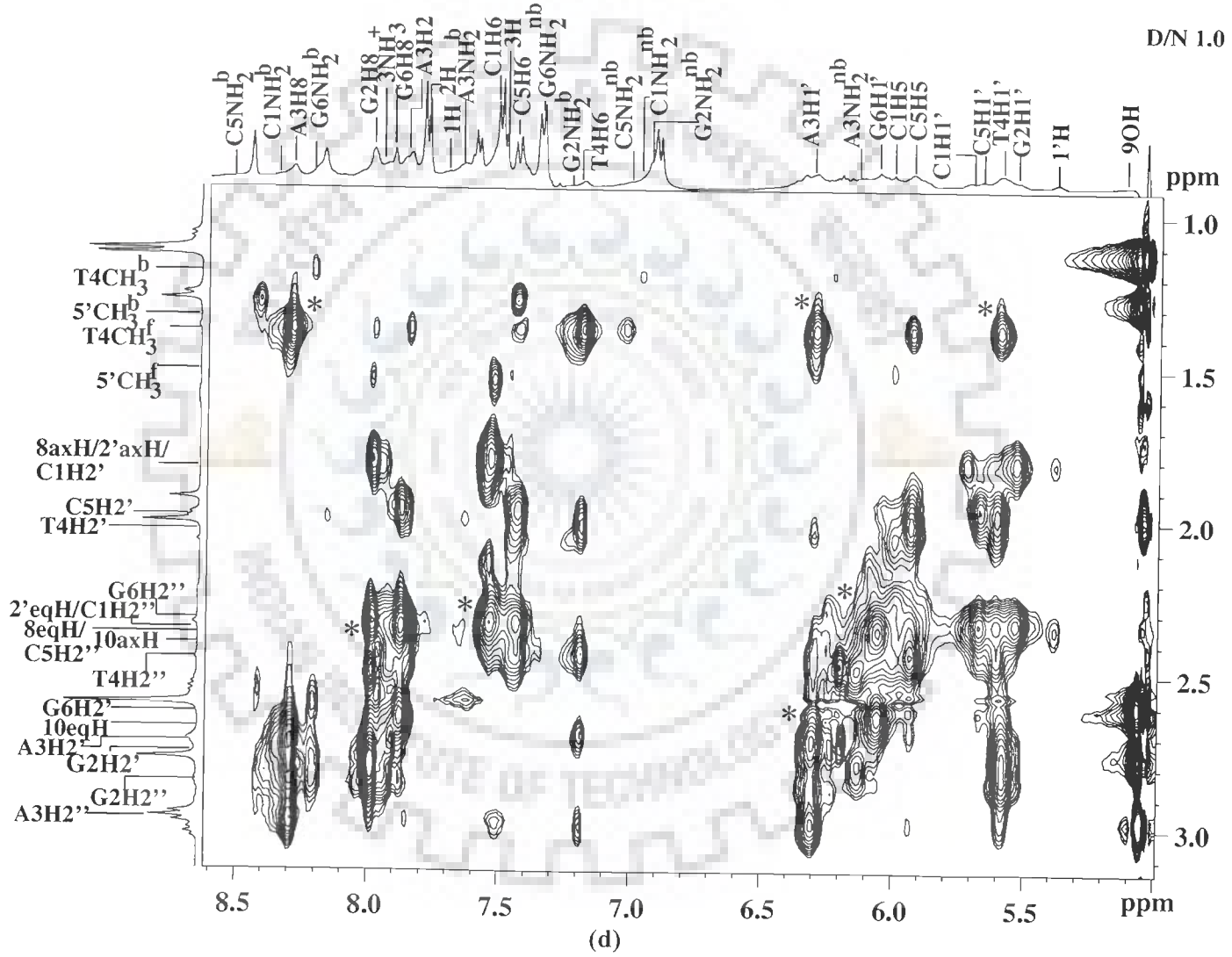


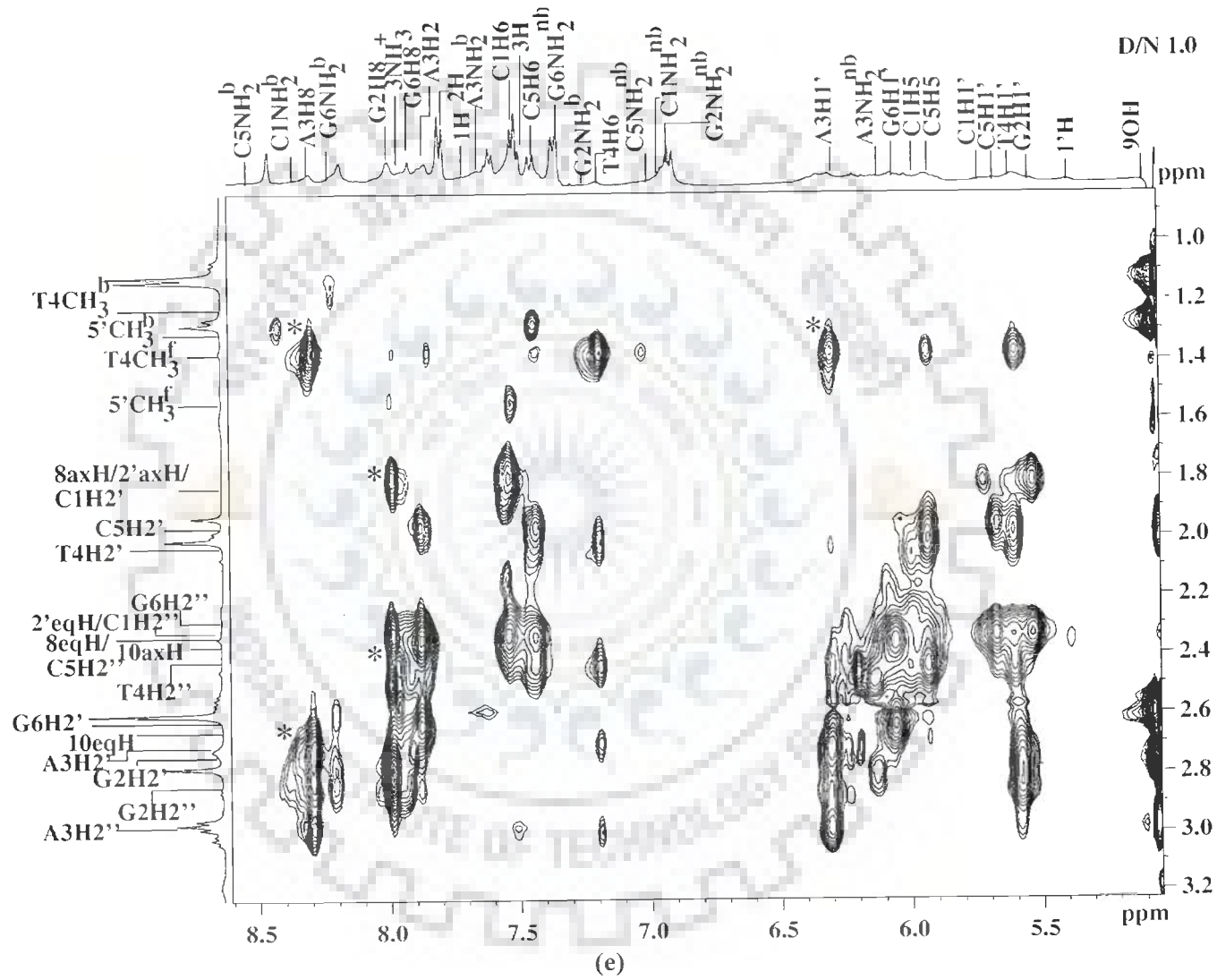
Fig. 6a-m: Expansions of various regions of 2D NOESY spectrum of 4'-epiadriamycin-d-(CGATCG)₂ complex in H₂O/D₂O and intermolecular cross peaks are shown by asterisk (*) between drug and DNA at 275 K.

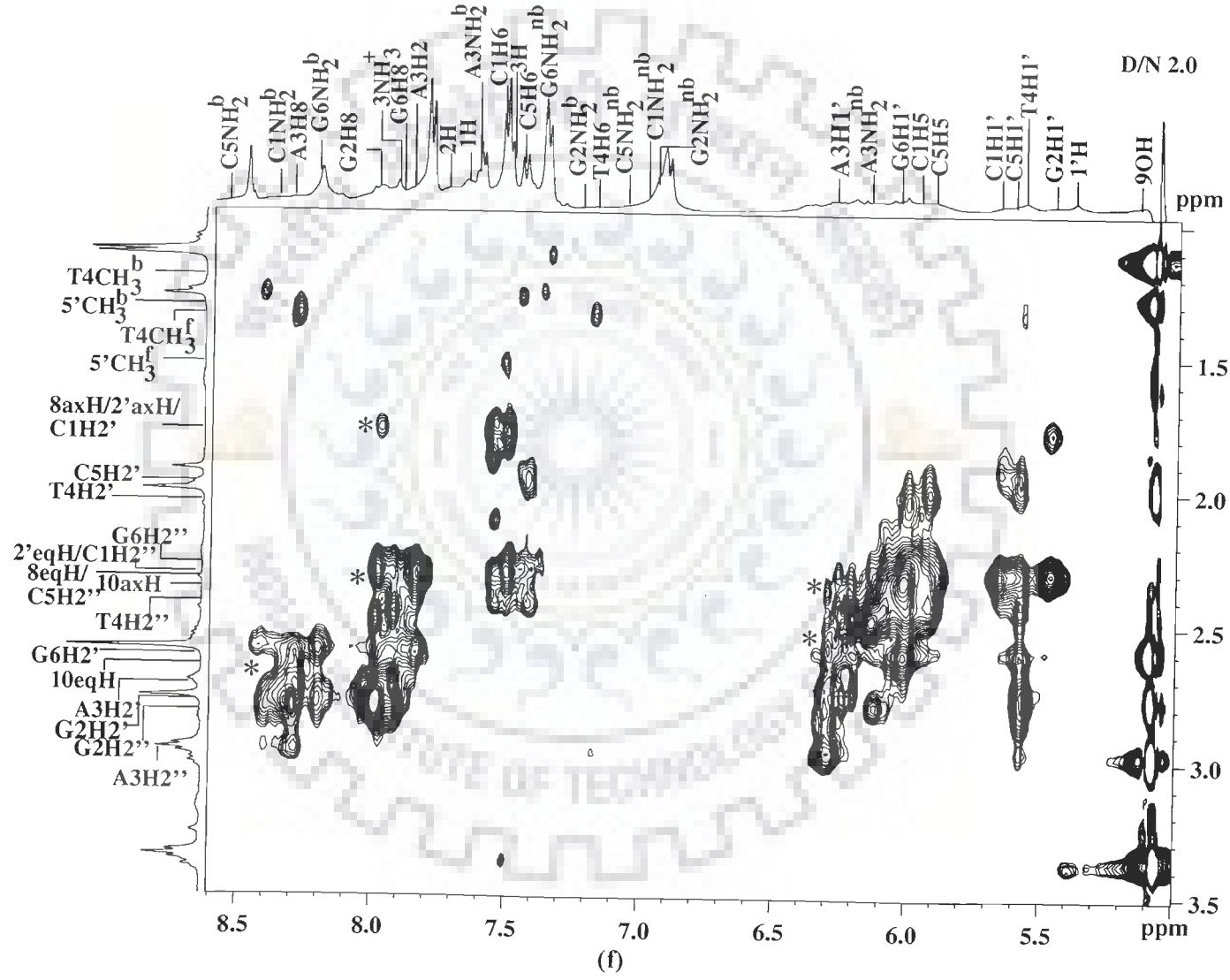


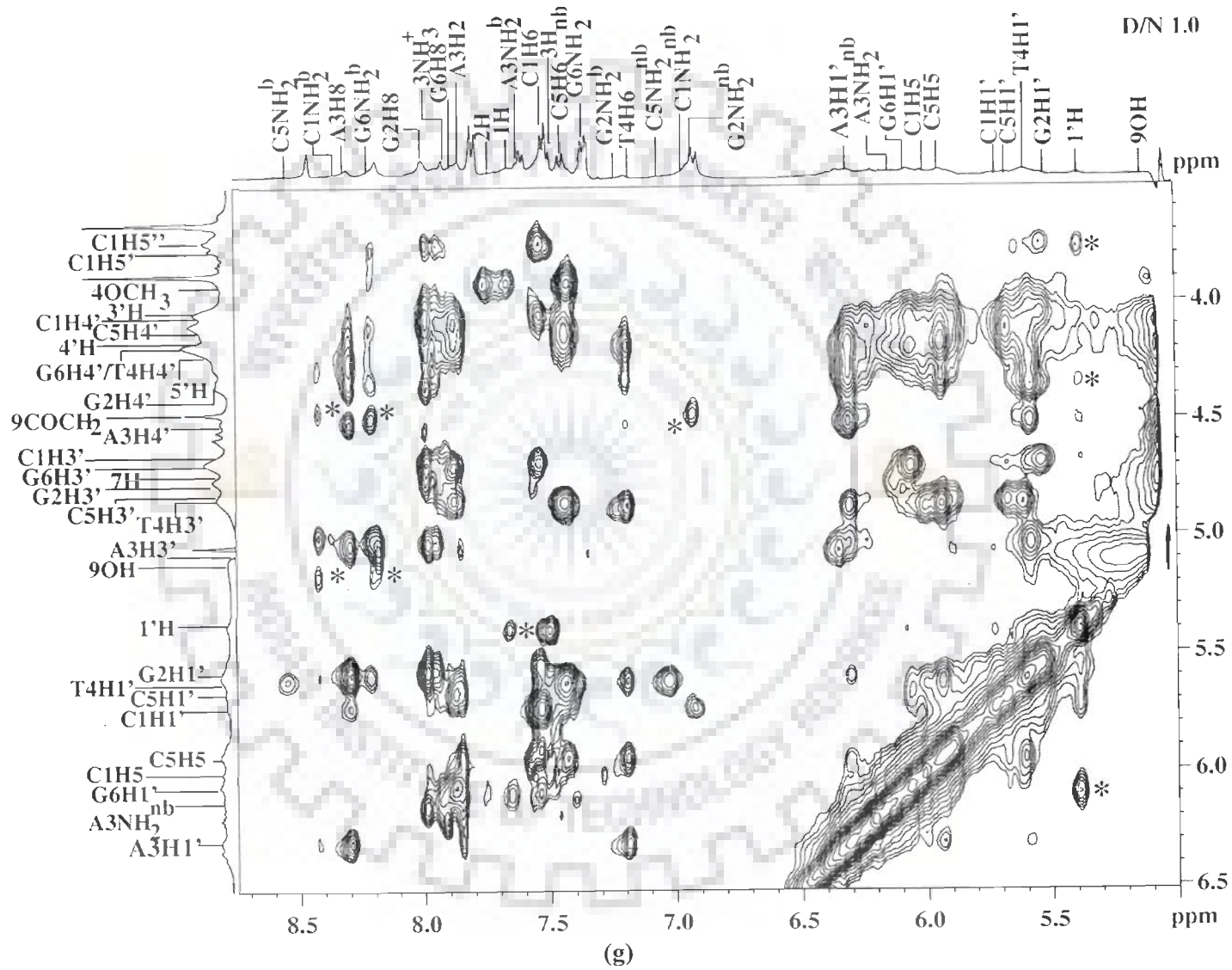


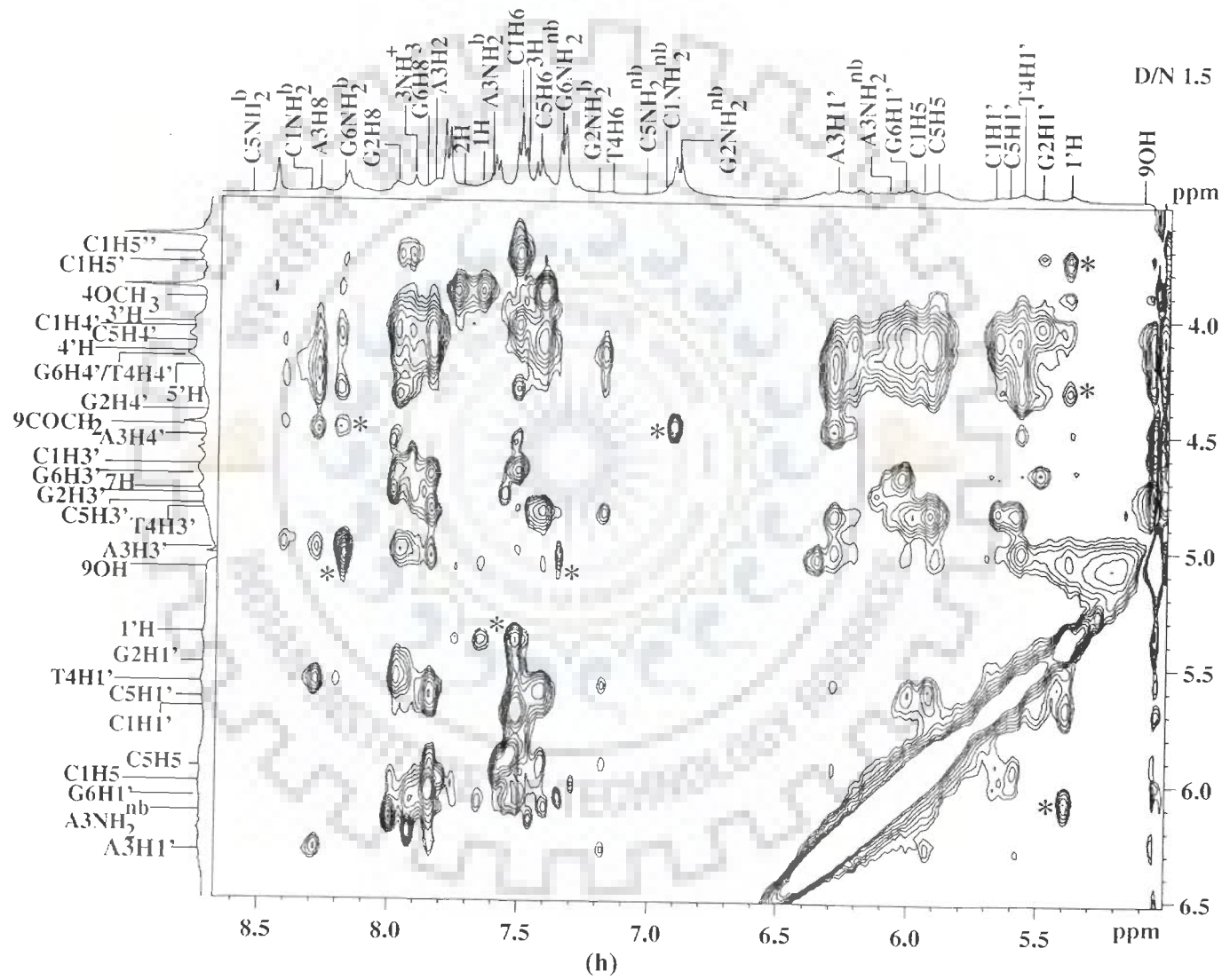
(c)

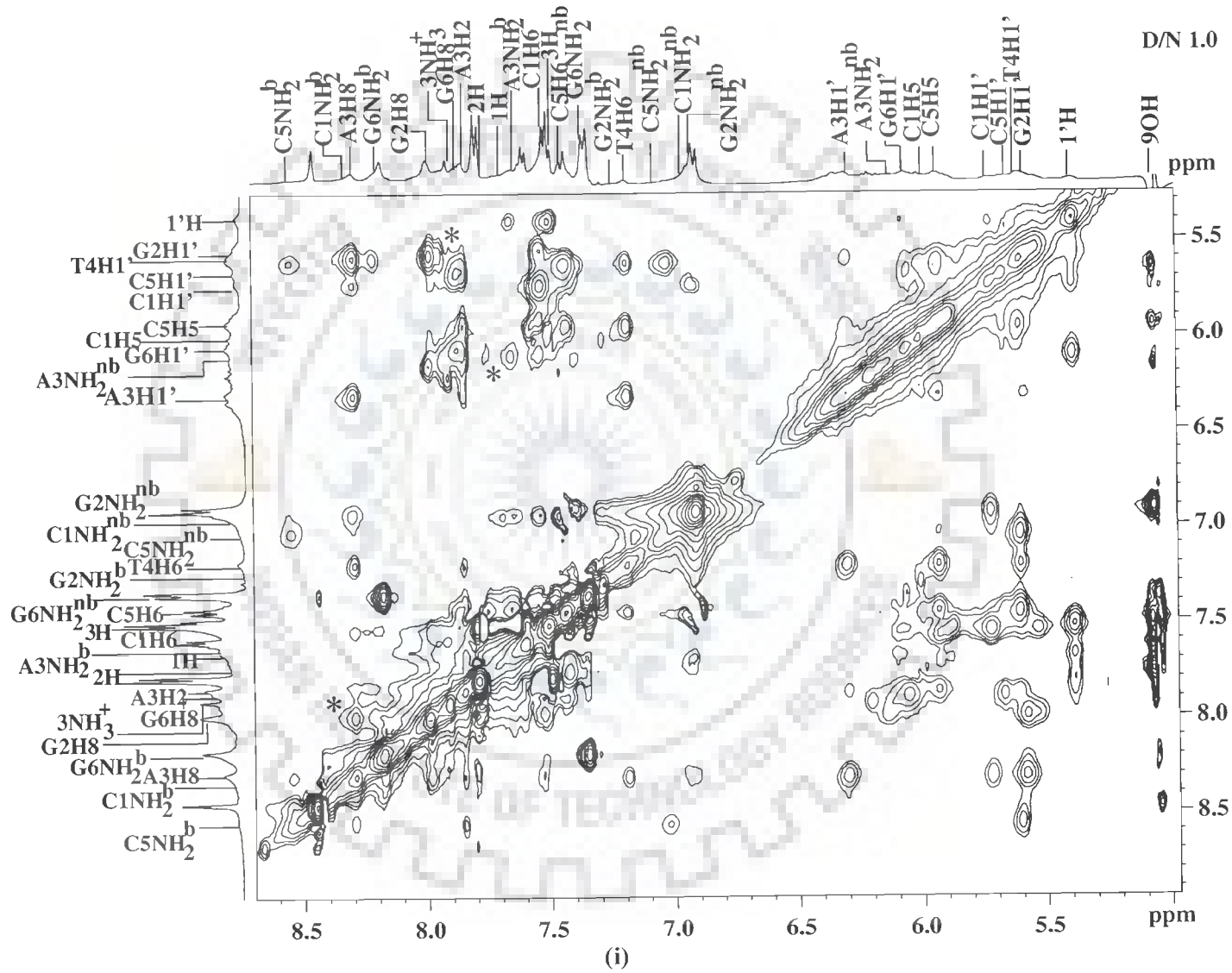


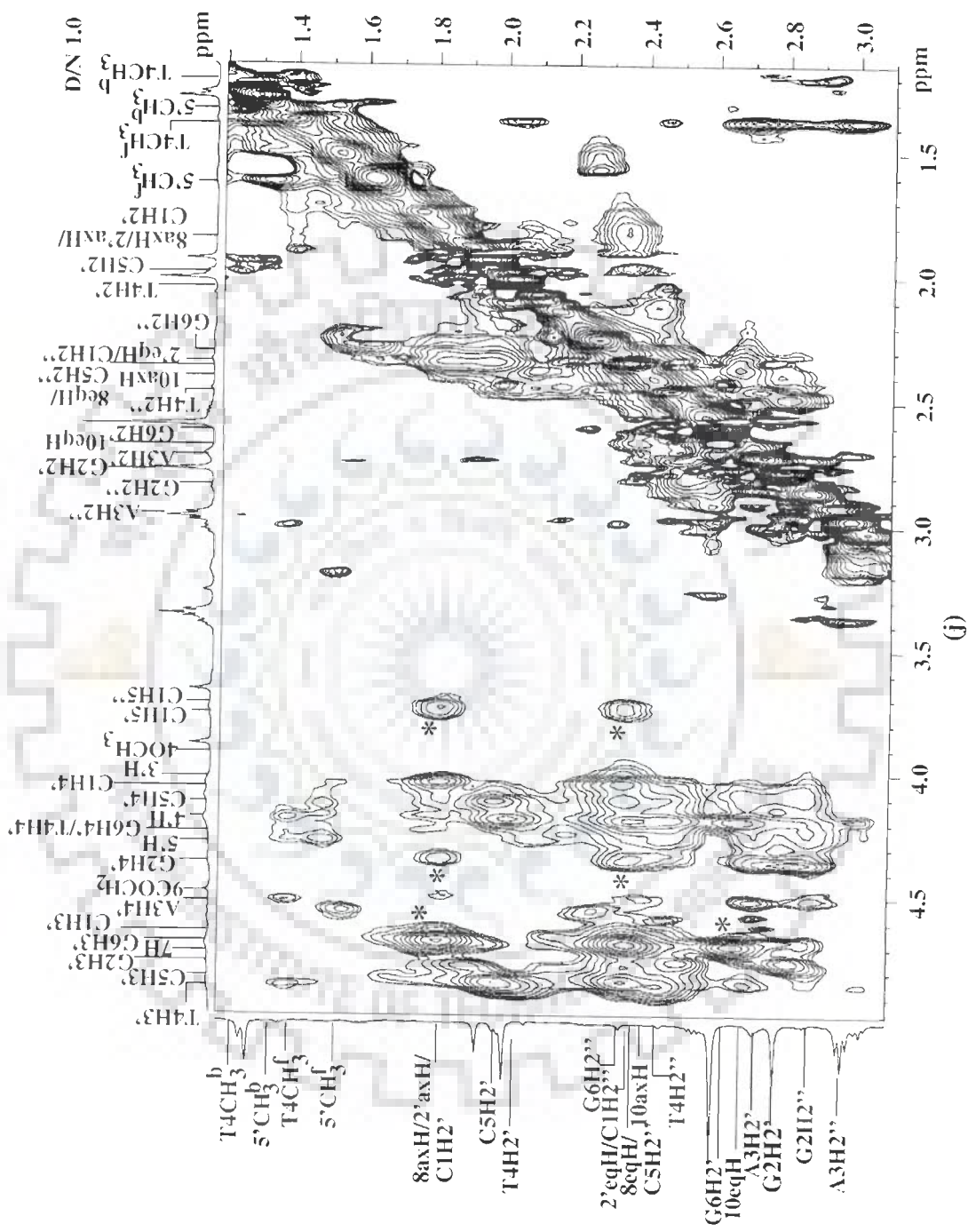


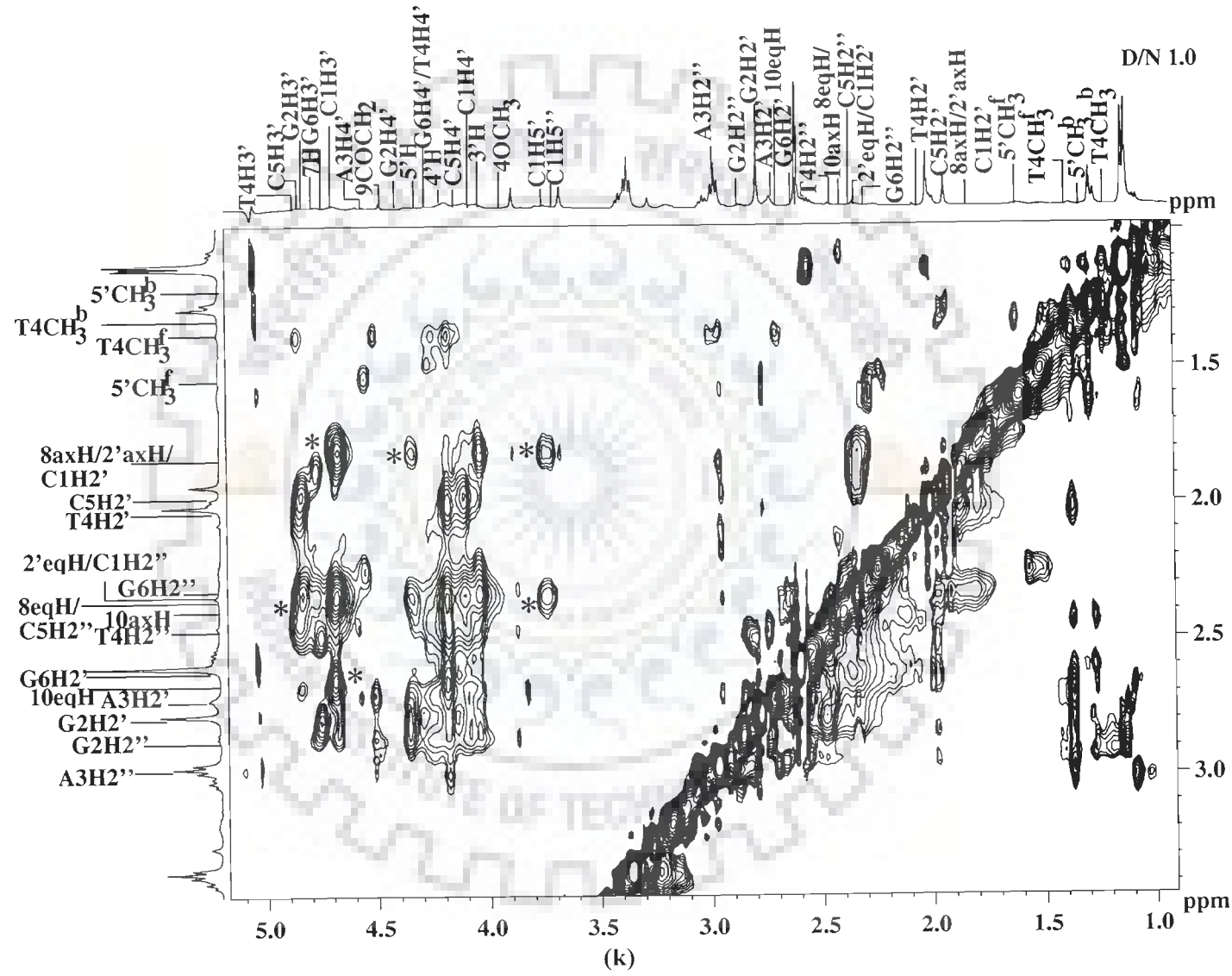


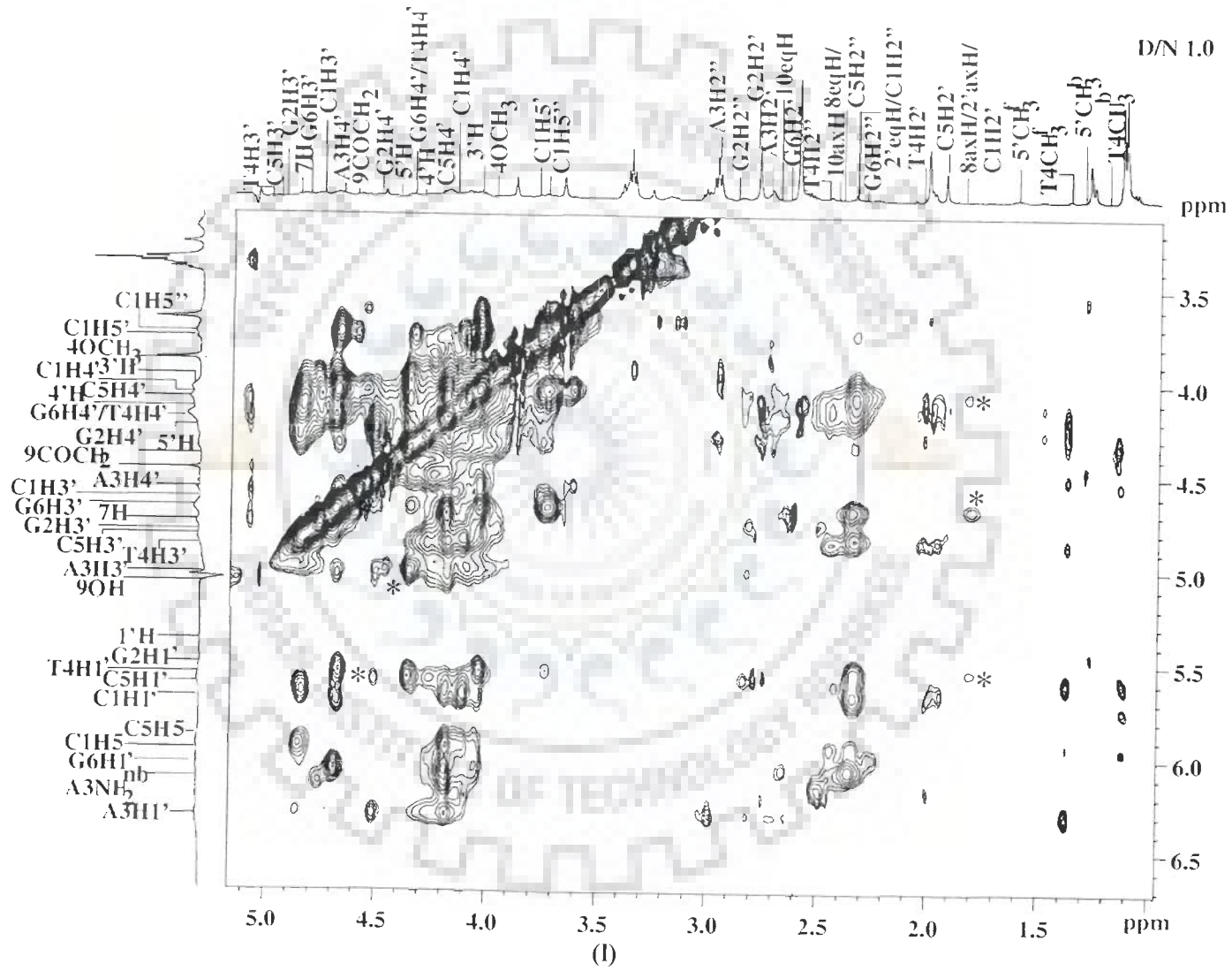












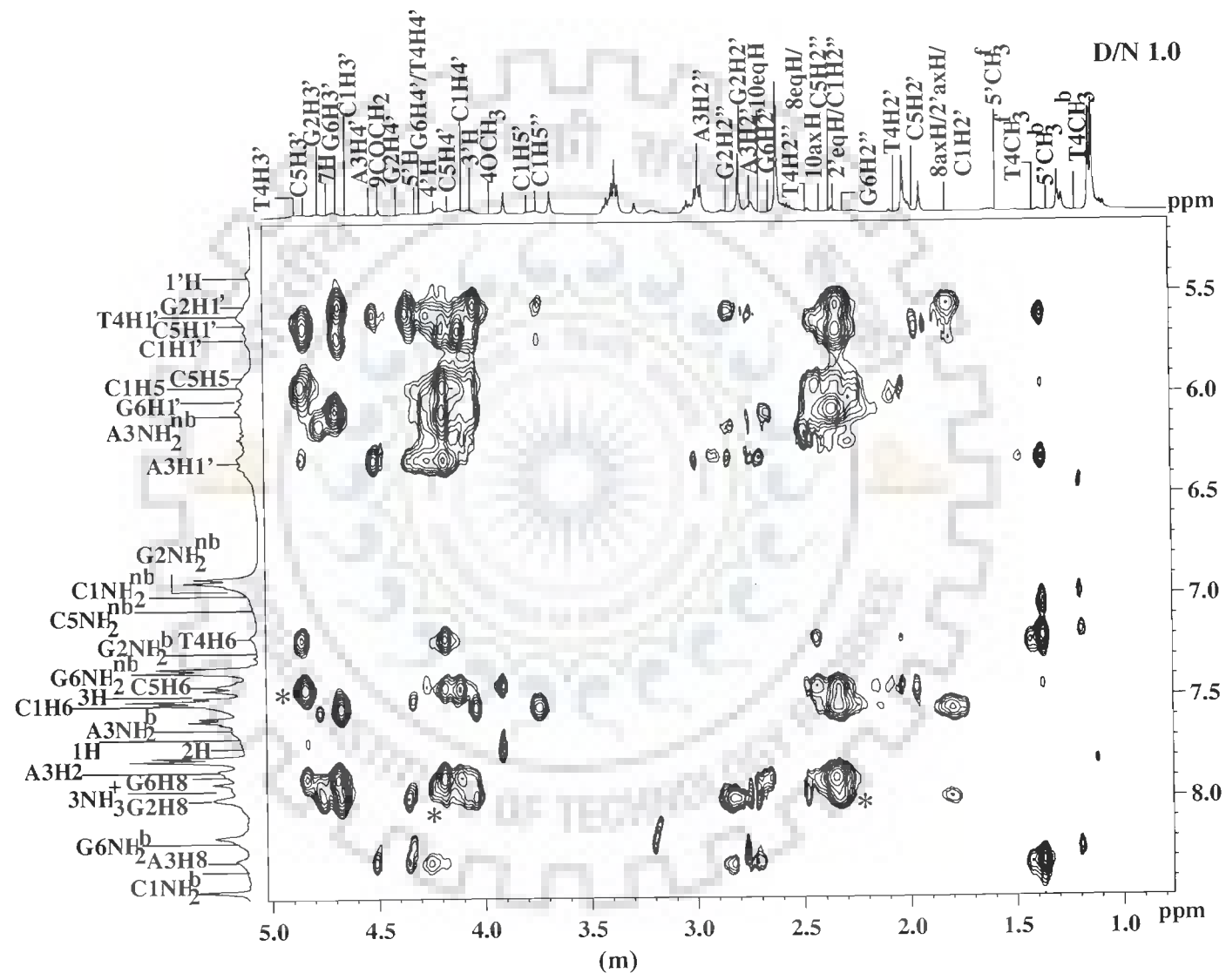


Table 6: Interproton distances (\AA) obtained from intranucleotide NOE connectivities (d_i) within sugar protons of hexanucleotide of the drug-DNA complex at $D/N = 1.0$ at 275 K estimated from NOESY spectra (Fig. 6d-m) using $C5H6-C5H5 = 2.45 \text{ \AA}$ as a standard reference. Overlap of peaks is indicated as o and – denotes absence of cross peak.

Protons	C1	G2	A3	T4	C5	G6
H1'-H2'	2.85	o	2.84	2.84	2.85	2.84
H1'-H2''	2.19	o	2.20	2.18	2.19	2.20
H1'-H3'	2.58	3.54	3.54	3.53	3.53	3.52
H1'-H4'	o	3.29	2.85	o	o	2.75
H2'-H3'	2.32	2.31	-	2.29	2.30	2.28
H2''-H3'	2.52	2.51	2.53	2.54	2.55	2.55
H2'-H4'	3.51	3.54	3.55	3.56	3.57	3.56
H2''-H4'	o	3.79	3.81	o	o	3.77
H2'-H2''	o	1.82	1.81	1.80	o	1.79
H3'-H4'	o	2.52	2.55	o	o	2.60

Table 7: Inter-proton distances (\AA) obtained from base to sugar protons of DNA in drug-DNA complex at $D/N = 1.0$ at 275 K estimated from NOESY spectra (Fig. 6d-i) using $C5H6-C5H5 = 2.45 \text{ \AA}$ as a standard reference. Overlap of peaks is indicated as 'o' and – denotes absence of cross peak.

Protons	C1	G2	A3	T4	C5	G6
H8/H6-H1'	3.48	3.78	3.89	3.67	3.55	3.80
H8/H6-H2'	2.26	2.22	2.40	2.31	2.28	2.25
H8/H6-H2''	3.40	3.31	3.58	3.62	3.42	3.34
H8/H6-H3'	4.36	4.78	4.81	4.41	4.38	4.76
H8/H6-H4'	4.85	4.82	4.80	4.86	4.87	o
H8/H6-H5'	o	o	o	o	o	o
H8/H6-H5''	o	o	o	o	o	o
H8/H6-H5	2.44	-	-		2.45	-
H8/H6-CH ₃	-	-	-	2.89	-	-

Table 8: Some of the inter residue sequential NOE cross peaks (ds) of nucleotide protons in the drug-DNA complex observed in NOESY spectra (Fig. 6a-m) of drug – DNA complex at D/N = 1.0, 1.5 and 2.0 at 275 K. The very strong (ss), strong (s), medium (ws), weak (w), very weakly (ww) intense cross peaks correspond to distances in the range ss 1.8 – 2.5 Å, s 2.5 – 3.0 Å, ws 3.0 – 3.5 Å, w 3.5 – 4.0 Å, ww 4.0 – 5.0 Å, respectively. Overlap of cross peaks is indicated as o.

Inter-residues Sequential peaks	D/N = 1.0	D/N = 1.5	D/N = 2.0
G2H8-C1H1'	-	-	-
G2H8-C1H2'/2'axH/8axH	o	o	o
G2H8-C1H2''/2'eqH	o	o	o
G2H8-C1H6	-	-	-
G2H1'-C1H6	-	-	-
G2H8-C1H3'	w	w	-
A3H8-G2H1'	s	s	ws
A3H8-G2H2'	ws	ws	w
A3H8-G2H2''	w	w	ww
A3H8- G2H8	s	s	w
T4H6-A3H1'	s	s	ww
T4H6-A3H2'	w	w	w
T4H6-A3H2''	ws	w	ww
T4H1'-A3H8	s	s	s
T4CH ₃ -A3H8	ss	ss	s
T4H6-A3H8	s	s	w
C5H6-T4H1'	ss	s	w
C5H6-T4H2''	s	s	w
C5H6-T4H2'	ss	ss	w
C5H6-T4H3'	s	ss	s
C5H5-T4H6	ws	ws	ww
C5H5- T4CH ₃	s	s	w
G6H8-C5H1'	w	w	-
G6H8-C5H2''/8eqH	o	o	o
G6H8-C5H2'	w	ww	-
G6H8-C5H3'	w	ww	-
G6H8- C5H6	ww	-	-
G6H1'-C5H6	ww	-	-

Table 9: Some of the inter-proton distances within the nucleic acid in drug-DNA complex at various D/N ratios estimated from NOESY spectra (Fig. 6a-m) at 275 K using C5H5-C5H6 = 2.45 Å as a standard reference. The corresponding distances in standard B- DNA are also shown here for reference.

	Standard B- DNA	1.0 Complex	1.5 Complex	2.0 Complex
ds peaks Distance (Å)				
G2N1H ^f - C1N4H ₂ ^b	4.0	ww	-	-
G2N2H ₂ ^b - C1H1'	4.9	-	-	-
A3H2 - G2N2H ₂ ^b	3.5	w	ww	ww
A3H2-G2N1H ^f	3.7	w	-	-
A3N6H ₂ ^b -G2N1H ^{f/b}	4.5	ww /-	-/ww	-/ww
T4N3H - A3N6H ₂ ^{nb}	4.5	s	ws	ww
T4N3H ^f -A3H2	4.0	ws	w	w
T4CH ₃ ^f - A3H8	3.8	s	ws	w
T4CH ₃ ^b - A3H8	3.8	ww	ww	ww
T4CH ₃ ^f - A3H2'	3.4	ww	-	-
T4CH ₃ ^f - A3H2''	2.9	w	ww	ww
T4CH ₃ ^f - A3H1'	3.9	s	s	s
T4CH ₃ ^b - A3H1'	3.9	-	-	ww
C5N4H ₂ ^{nb} -T4N3H ^f	5.5	w	-	-
C5N4H ₂ ^b -T4N3H ^f	3.9	ws	-	-
C5N4H ₂ ^{nb} - T4CH ₃ ^f	4.8	ws	-	-
C5N4H ₂ ^{nb} - T4CH ₃ ^b	4.8	ww	ww	-
C5N4H ₂ ^b - T4CH ₃ ^f	5.1	w	-	-
C5H6 - T4CH ₃ ^f	3.8	w	-	-
G6N1H ^b - C5N4H ₂ ^b	4.0	ww	ww	-
dps peaks				
C1N4H ₂ ^b -C5N4H ₂ ^b	2.9	ww	-	-

(contd.)

(contd.)

G2N1H ^b – G6H2 ^{''}	-	ws	w	ww
G2N2H ₂ ^b – G6N1H	4.1	-	-	-
G2N1H – G6N1H	3.4	w	ww	ww
G2N1H ^f – G6N2H ₂ ^b	4.1	ww	-	-
G2N1H ^f – G6N2H ₂ ^{nb}	5.0	-	-	-
G2N2H ₂ ^{nb} – G6N2H ₂ ^b	4.1	ww	-	-
G2N1H ^f – T4CH ₃ ^f	-	ws	-	-
A3N6H ₂ ^b – C5N4H ₂ ^b	3.6	-	-	-
A3N6H ₂ ^{nb} – C5N4H ₂ ^b	4.5	-	-	-
T4N3H ^f – T4N3H ^b	2.9	s	s	s
T4N3H ^{f/b} – G2N1H ^f	3.6	ws/ws	ws/w	w/ww
T4CH ₃ ^f – T4H6	-	ss	s	ws
T4CH ₃ ^b – T4H6	-	ww	-	-
dpi peaks				
C1N4H ₂ ^b – G6N1H ^f	2.5	-	-	ww
G2N1H ^f – C5N4H ₂ ^{nb}	4.0	ws	ww	-
G2N1H ^b – C5N4H ₂ ^b	2.5	s	ws	ww
A3H2 – T4N3H ^f	2.8	ws	w	w
A3N6H ₂ ^{nb} – T4N3H ^f	3.8	s	w	ww
A3N6H ₂ ^b – T4N3H ^f	2.5	ws	ww	ww
di peaks				
C1N4H ₂ ^{b/nb} – C1H5	2.4 / 3.5	-	-	-
C1N4H ₂ ^{b/nb} – C1H6	4.6 – 5.3 b	ww/ww	ww	-
G2N1H – G2N2H ₂ ^{b/nb}	2.3 ^b / 3.4 ^{nb}	w/ws	ww/ww	-
A3H2 – A3N6H ₂ ^{nb}	5.2	ww	ww	ww
A3H2 – A3N6H ₂ ^b	4.4	ww	ww	ww
A3N6H ₂ ^b – A3N6H ₂ ^{nb}	1.7	ss	ss	ss
A3N6H ₂ ^{b/nb} – A3H8	6.1 ^b / 4.8 ^{nb}	-	-	-
T4N3H – T4CH ₃	4.9	ws	-	-
T4CH ₃ ^f – T4H6	2.9	s	ws	ws
T4CH ₃ ^b – T4H6	-	ww	-	-
C5N4H ₂ ^{b/nb} – C5H5	3.5 ^b / 2.4 ^{nb}	-	-/ww	-
C5N4H ₂ ^{b/nb} – C5H6	5.3 ^b / 4.6 ^{nb}	-	-	-
G6N1H – G6N2H ₂ ^{b/nb}	2.3 ^b / 3.4 ^{nb}	ws/-	ww/-	ww/-

Table 10: Intensities of NOE cross peaks (di) within the drug molecule in the drug-DNA complex at D/N = 1.0, 1.5 and 2.0 at 275 K. The very strong (ss), strong (s), medium (ws), weak (w) and very weakly (ww) intense cross peaks refer to distances in the range ss 1.8 – 2.5 Å, s 2.5 – 3.0 Å, ws 3.0 – 3.5 Å, w 3.5 – 4.0 Å, ww 4 – 5 Å, respectively from the NOESY spectra, Fig. 6a-m. Overlap of peaks is indicated as o.

Protons	Uncomplexed drug	D/N = 1.0	D/N = 1.5	D/N = 2.0	Protons	Uncomplexed drug	D/N = 1.0	D/N = 1.5	D/N = 2.0
1H-2H	ss	w	ww	ww	7H-3'H	w	-	-	-
2H-3H	ss	ws	w	w	7H-5'H	w	ww	ww	ww
1'H-2' _{ax} H	ss	s	ws	ww	7H-4'H	w	-	-	-
1'H-2' _{eq} H	ss	s	ws	ww	7H-5CH ₃	ww	-	-	-
3'H-4'H	o	o	o	o	8 _{ax} H-1'H	o	o	o	o
4'H-5'H	ss	s	s	s	8 _{ax} H-3'H	o	o	o	o
3'H-2' _{ax} H	s	o	o	o	8 _{ax} H-4'H	o	o	o	o
3'H-2' _{eq} H	s	o	o	o	8 _{ax} H-5'H	o	o	o	o
2' _{ax} H-2' _{eq} H	o	ss	ss	ss	8 _{ax} H-5'CH ₃	o	-	-	-
5'H-5'CH ₃	s	-	ww	-	8 _{eq} H-1'H	o	o	o	o
7H-8 _{ax} H	ss	o	o	o	8 _{eq} H-3'H	o	o	o	o
7H-8 _{eq} H	ss	o	o	o	8 _{eq} H-4'H	o	o	o	o
8 _{ax} H-8 _{eq} H	o	ss	ss	ss	8 _{eq} H-5'H	o	o	o	o
10 _{ax} H-10 _{eq} H	ss	ss	ss	ss	8 _{eq} H-5'CH ₃	o	-	-	-
Within Ring D Protons					9COCH ₂ -3'H	ww	-	-	-
2H-4OCH ₃	ws	ws	ws	ws	9COCH ₂ -1'H	ww	-	ww	ww
1H-4OCH ₃	w	w	w	w	9COCH ₂ -5'H	ww	ww	ww	ww
3H-4OCH ₃	ss	s	s	s	Within Ring A Protons				
Within Sugar Protons					10 _{ax} H-8 _{ax} H	ws	w	w	ww
1'H-3'H	ws	ws	ws	ws	10 _{ax} H-8 _{eq} H	ws	ww	ww	-
1'H-4'H	ws	ws	ws	ws	10 _{eq} H-8 _{ax} H	ws	ww	-	-
1'H-5'H	ww	-	-	w	10 _{eq} H-8 _{eq} H	ws	w	ww	ww
1'H-5CH ₃	ww	-	-	-	10 _{eq} H-9COCH ₂	w	w	ww	-
3'H-5'H	o	o	o	o	10 _{ax} H-9COCH ₂	w	ww	-	-
3'H-5'CH ₃	ss	ww	ww	ww	8 _{ax} H-9COCH ₂	w	ww	-	-
4'H-2' _{ax} H	o	o	o	o	8 _{eq} H-9COCH ₂	ws	ww	ww	ww
4'H-2' _{eq} H	o	o	o	o	11OH-10 _{eq} H	w	ww	-	-
4'H-5'CH ₃	o	-	-	-	11OH-9OH	ww	ww	-	-
Ring A with sugar Protons					11OH-9COCH ₂	ww	-	ww	-
7H-1'H	s	-	-	-					

Table 11: Relative intensities of intermolecular NOE connectivities between d-(CGATCG)₂ and 4'-epiadriamycin molecule in the drug-DNA complex at drug to DNA ratio D/N =1.0, 1.5 and 2.0 from NOESY spectra (Fig. 6a-m) at 275 K. The very strong (ss), strong (s), medium (ws) and weakly (w) intense cross peaks correspond to distance of ss 1.8 – 2.5 Å, s 2.5 – 3.0 Å, ws 3.0 – 3.5 Å, w 3.5 – 4.0 Å, ww 4 – 5 Å. Overlap of peaks is indicated as o and '-' indicates absence of peak due to broadening.

S. No.	Intermolecular Cross peak	D/N 1.0	D/N 1.5	D/N 2.0	S.No.	Intermolecular Cross peak	D/N 1.0	D/N 1.5	D/N 2.0
1.	A3H8-5'CH ₃ ^b	ww	ww	ww	26.	G2H4'-10axH	w	w	w
2.	A3H1'-5'CH ₃ ^b	ww	ww	ww	27.	G2H4'- 2'axH/8axH/C1H2'	o	o	o
3.	T4H1'-5'CH ₃ ^b	ww	ww	ww	28.	C1H5''/C1H5'-10axH	s	ws	w
4.	G2H8-10axH	ww	ww	ww	29.	G6H3'- 2'axH/8axH/C1H2'	o	o	o
5.	C1H6-10axH	ww	ww	ww	30.	G2N1H ^b -6OH	ws	ww	ww
6.	G6H1'-10axH	w	w	w	31.	G6N1H ^b -11OH	ww	ww	ww
7.	G6H1'-10eqH	w	w	w	32.	G6H1'-6OH	ws	w	-
8.	A3H8-3'H	ww	ww	ww	33.	G6H2'-11OH	ww	ww	-
9.	G6NH ₂ ^b -9COCH ₂	ws	ws	ws	34.	C1H4'/C5H5'/T4H5' -11OH	ww	ww	-
10.	A3H8-5'H	ww	ww	ww	35.	G2H5'/G6H5'/C5H4' -11OH	ww	ww	-
11.	G2NH ₂ ^{nb} - 9COCH ₂	ws	ws	ws	36.	G6N1H ^b - 2'axH/8axH/C1H2'	o	o	o
12.	C1NH ₂ ^b -9OH	ws	w	w	37.	G6N1H ^b - C5H2''/8eqH	ww	ww	ww
13.	G6NH ₂ ^b -9OH	ws	ws	w	38.	G6N1H ^b -10eqH	ww	-	-
14.	G6H8-9OH	w	w	w	39.	G6N1H ^b -9COCH ₂	ww	ww	ww
15.	G2H8-9OH	ws	ws	w	40.	C5H3'-3H	ww	ww	w
16.	G6NH ₂ ^{nb} -9OH	ww	ww	ww	41.	A3H2-5'H	ww	-	-
17.	C1H5''/C1H5'- 1'H	w	ww	ww	42.	C1H2''/2'eqH-3NH ₃ ⁺	o	o	o
18.	G2H4'-1'H	ww	w	w	43.	G2H1'- 2'axH/8axH/C1H2'	o	o	o
19.	A3NH ₂ ^{nb} -1'H	w	ws	ws	44.	G2H4'-9OH	ww	ww	ww
20.	G6H1'-9OH	ww	ww	ww	45.	G2H1'-9COCH ₂	ww	-	-
21.	C1H6-1'H	w	w	ww	46.	G2NH ₂ ^b -6OH	ws	w	-
22.	G6H1'-1H	w	ww	ww	47.	G6H8-6OH	ws	w	ww
23.	A3H8-3NH ₃ ⁺	w	ww	-	48.	G2H1'-11OH	ww	ww	ww
24.	T4H1'-3NH ₃ ⁺	w	ww	ww	49.	G2H8-11OH	ws	-	-
25.	G6H3'-10eqH	w	w	w					

Table 12: Inter-proton distances (Å) obtained from intermolecular NOE connectivities between hexanucleotide and the drug molecule in the drug–DNA complex from NOESY spectra (Fig. 6a–m) at 275 K. (Distances are taken for rMD model from intramolecular and intermolecular peaks of drug and DNA).

S.No.	Intermolecular Cross peak	Distance obtained from rMD	
		Experimental Distance(Å)	Observed Distance(Å)
1.	G2H8-10axH	4.34	4.36
2.	G6NH ₂ ^{nb} -9OH	4.96	4.94
3.	G2H4'-10axH	3.74	3.75
4.	G2N1H ^b -6OH	3.59	3.61
5.	G6N1H ^b -11OH	4.44	4.43
6.	G6H1'-6OH	3.08	3.06
7.	G6N1H ^b -C5H2''/8eqH	4.87	4.88
8.	G6N1H ^b -10eqH	4.98	5.00
9.	G2H1'-9COCH ₂	4.26	4.27
10.	G2NH ₂ ^b -6OH	3.32	3.70
11.	G6H8-6OH	3.86	3.86
12.	G2H1'-11OH	4.73	4.74
13.	G2H8-11OH	3.33	3.35

Table 13a: Comparison of deoxyribose conformation (pseudorotation°)

	Present Work		CGA+ mor ^a	CGA+ adm ^b	CGA+ dnm ^c	CpG+ dnm ^d
	NMR	rMD				
C1	153-162	-139	120, 143	158	160	153
G2	180	130	95,136	141	142	135
A3	153-162	107	77, 73	129	131	
T4	144	126	92, 130	124	122	
C5	153-162	143	137, 119	151	141	
G6	162	185	147, 142	161	165	

^aCGATCG + morpholinodoxorubicin (Mazzini et al., 1998); ^bCGATCG + adriamycin (Frederick et al., 1990); ^cCGATCG + daunomycin (Frederick et al., 1990); ^dCpG + daunomycin (Barthwal et al., 1994)

Table 13b: Comparison of glycosidic bond rotation (°)

		Present Work		CGA+mor ^a	CGA+ adm ^b
		NMR	rMD		
C1	High anti	-150	180	-	148
G2	Anti	-105	-108	-131, -92	-90
A3	Anti	-105 to -120	-136	-148, -146	-130
T4	Anti	-105 to -120	-118	-141, -123	-113
C5	High anti	-90	-86	-105, -112	-90
G6	High anti	-90	-82	-104, -110	-90

^aCGATCG + morpholinodoxorubicin (Mazzini et al., 1998); ^bCGATCG + adriamycin (Frederick et al., 1990)

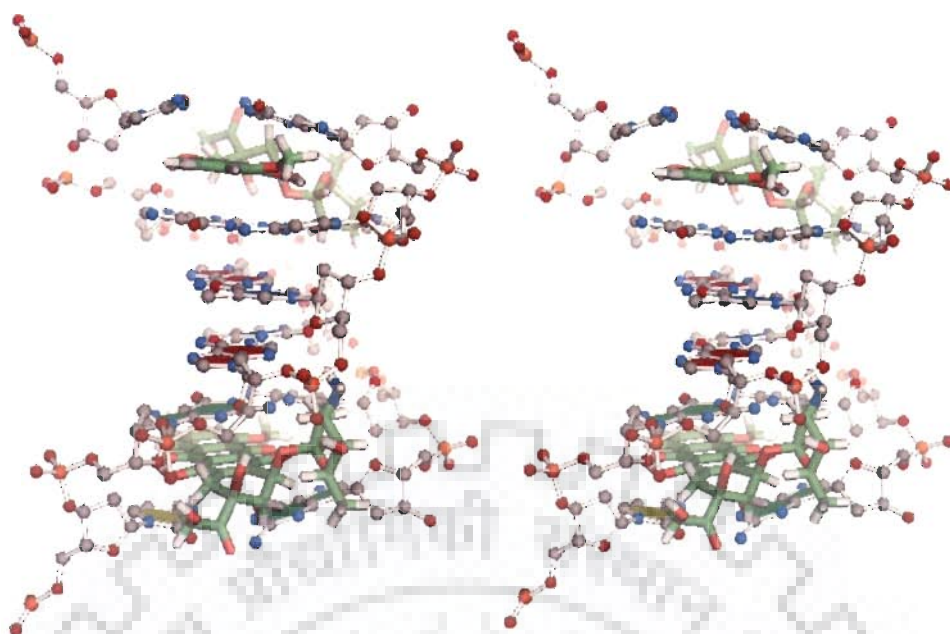


Fig. 7: The stereoview of final rMD structure of d-(CGATCG)₂-4'-epiadriamycin derived from the NOE data.

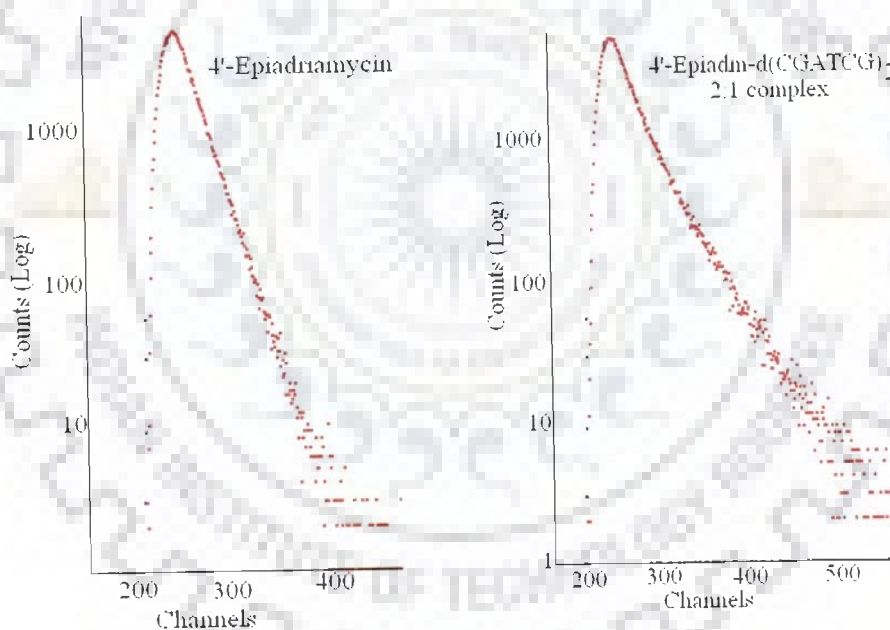


Fig. 8: Fluorescence lifetime decay measurement profile of 4'-epiadriamycin and 2:1 4'-epiadriamycin-d-(CGATCG)₂ complex.

Table 14: Lifetimes parameters of 4'-epiadriamycin fluorescence and its 2:1 complex with d-(CGATCG)₂ in water at 298 K.

samples	Lifetime decay (ns)	Amplitude	Lifetime decay (ns)	Amplitude
	τ_1	B_1	τ_2	B_2
4'-Epiadriamycin	0.83	0.06	2.19	0.03
d-(CGATCG) ₂ -4'-Epiadriamycin 2:1 complex	0.71	0.01	1.08	0.08

1991; Leonard et al, 1992; Estaintot et al, 1992) for T1, A3 and T4 residues. It may be noted that our NMR results indicate that deoxyribose sugar is a mixture of S- and N- conformers in dynamic equilibrium. The S-conformer exists as the predominant form having pseudorotation P_S in the range 135-162°. Thus these results show the feasibility and relevance of NMR studies of 4'-epiadriamycin bound to d-(CGATCG)₂. Some of the features such as NOE connectivities A3H1'-5'CH₃ and G6H1'/A6H1'-1'H are common to complexes with d-(CGATCG)₂. But various other detailed structural features appear to be unique to the drug-DNA complex studied. This reflects on drug-specific or DNA sequence specific interactions at molecular level and is relevant to differences in molecular basis of their action.

(B) TCSPC Analysis: Time-resolved fluorescence measurements

Time resolved fluorescence decays were obtained by the Time-Correlated Single-Photon Counting method on the Spectrofluorimeter (model FluoroLog-TCSPC, make HORIBA Jobin Yvon Spex). All conditions are same as for adriamycin-d-(TGATCA)₂ complex. The fluorescence decay curve profile of free drug is expected to be monoexponential but it is biexponential with two lifetimes and two amplitudes. The lifetime of free 4'-epiadriamycin is found to be $\tau_1 = 0.83$ ns, $\tau_2 = 2.19$ and amplitude is $B_1 = 0.06$, $B_2 = 0.03$. This shows that there may be presence of two conformers of the drug or the aggregation of the drug molecule. On the formation of d-(CGATCG)₂ - 4'-epiadriamycin 2:1 complex, $\tau_1' = 0.71$ ns, $\tau_2' = 1.08$ ns; $B_1' = 0.01$ and $B_2' = 0.08$. In the present study the smaller B_1' and higher B_1 lifetime components represent the intercalated and free form of the drug respectively. The τ_1 value ($\tau_1' = 0.71$ ns) of the complex is less than that of τ value ($\tau_1 = 0.83$ ns) of free 4'-epiadriamycin, showing that there is shortening of the decay time of 4'-epiadriamycin due to intercalation (Table 14, Fig. 8). This indicates the complexation of the DNA base with the drug and is due to electron transfer from the d-(CGATCG)₂ to 4'-Epiadriamycin. The $\tau_2' = 1.08$ ns component may reflect the other

conformations of unprivileged structures. Thus there is clear indication that 4'-epiadriamycin is intercalating in the d-(CGATCG)₂ hexamer sequence and forming the complex.

(C) Diffusion Ordered Spectroscopy (DOSY) studies on 4'-epiadriamycin-d-(CGATCG)₂ complex

DOSY spectra of 4'-epiadriamycin-d-(CGATCG)₂ complex of 2:1 D/N ratio is compared with that of 4'-epiadriamycin (Fig. 22a in chapter 4) and d-(CGATCG)₂ alone at 275 (Fig. 9a) and 298 K (Fig. 9b). On complex formation, the diffusion coefficient value decreases of the drug resonances in the complex in comparison to that in the drug alone. The corresponding values of the drug resonances in complex and the drug alone are 0.27×10^{-11} and 1.84×10^{-11} m²/s, respectively and that of d-(CGATCG)₂ in the complex and alone hexamer are 2.61×10^{-10} and 6.30×10^{-10} m²/s, respectively at 275 K. This is because of the interaction of the drug with DNA which slower the rate of diffusion, same is found with d-(CGATCG)₂ alone. However, at 298 K, the diffusion coefficient value for the same hexamer signal for complexed and uncomplexed DNA are 2.25×10^{-10} and 1.38×10^{-10} m²/s, respectively, while that for bound and free drug resonance, the values are 5.11×10^{-10} and 1.53×10^{-10} m²/s, respectively. The diffusion coefficient values have been increased on comparing the complexed and the uncomplexed form. This may be due to the fact that the drug starts uncomplexing with increase in temperature. One set of peak is due to averaging of the diffusion coefficients. The exchange is slower at 275 K in comparison to that obtained at 298 K on the diffusion time scale.

(D) Restrained Molecular Dynamics Studies

The nucleotides are labelled from C1 base paired to G12 with C1 to G6 in the 5' to 3' direction on strand 1 and from C7 to G12 on strand 2. The 4'-epiadriamycin molecules are numbered D13 and D14 and the atomic numbering scheme for the molecule is shown in Fig. 1a and schematic representation of drug-DNA complex is shown in Fig. 1b. The protocol for

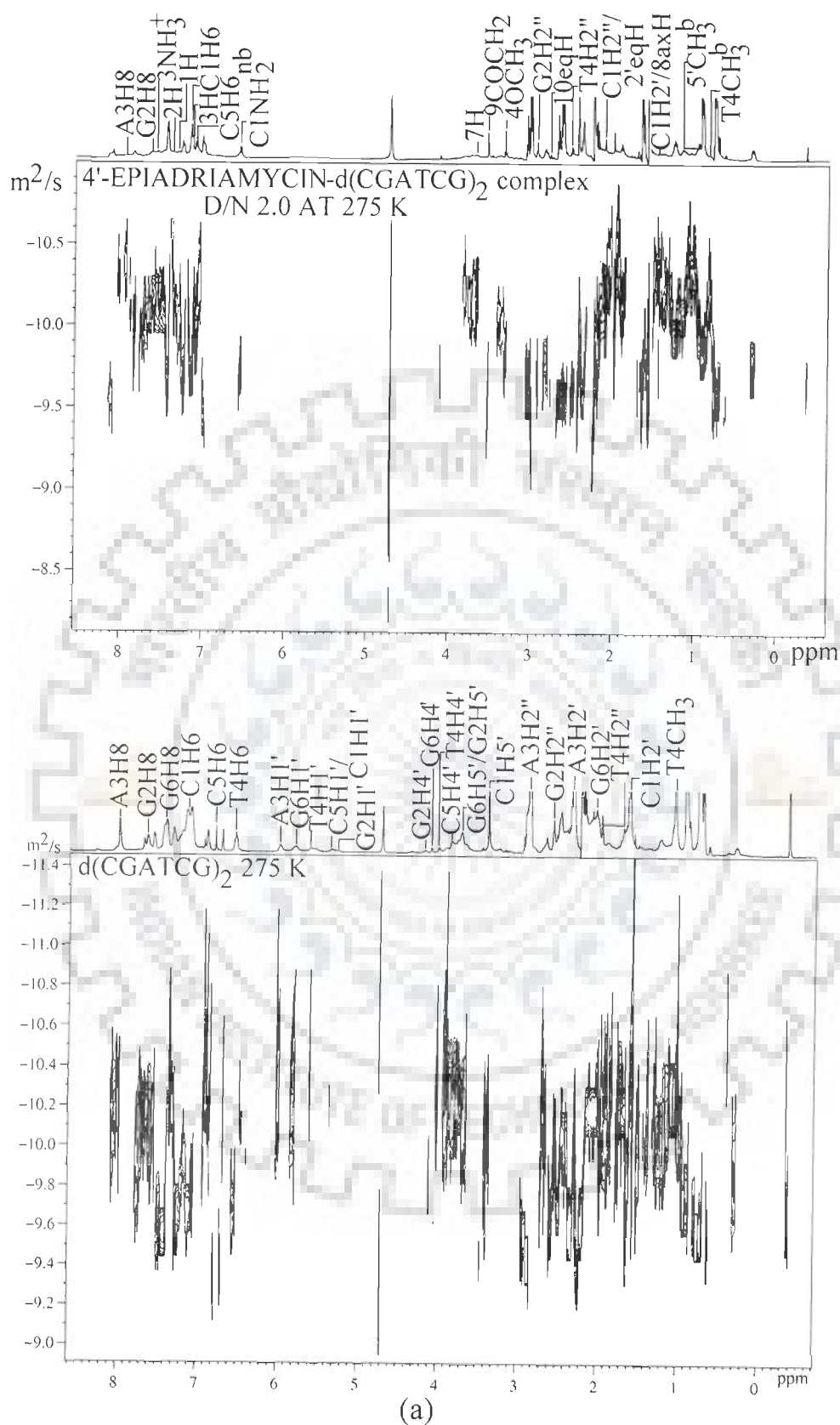
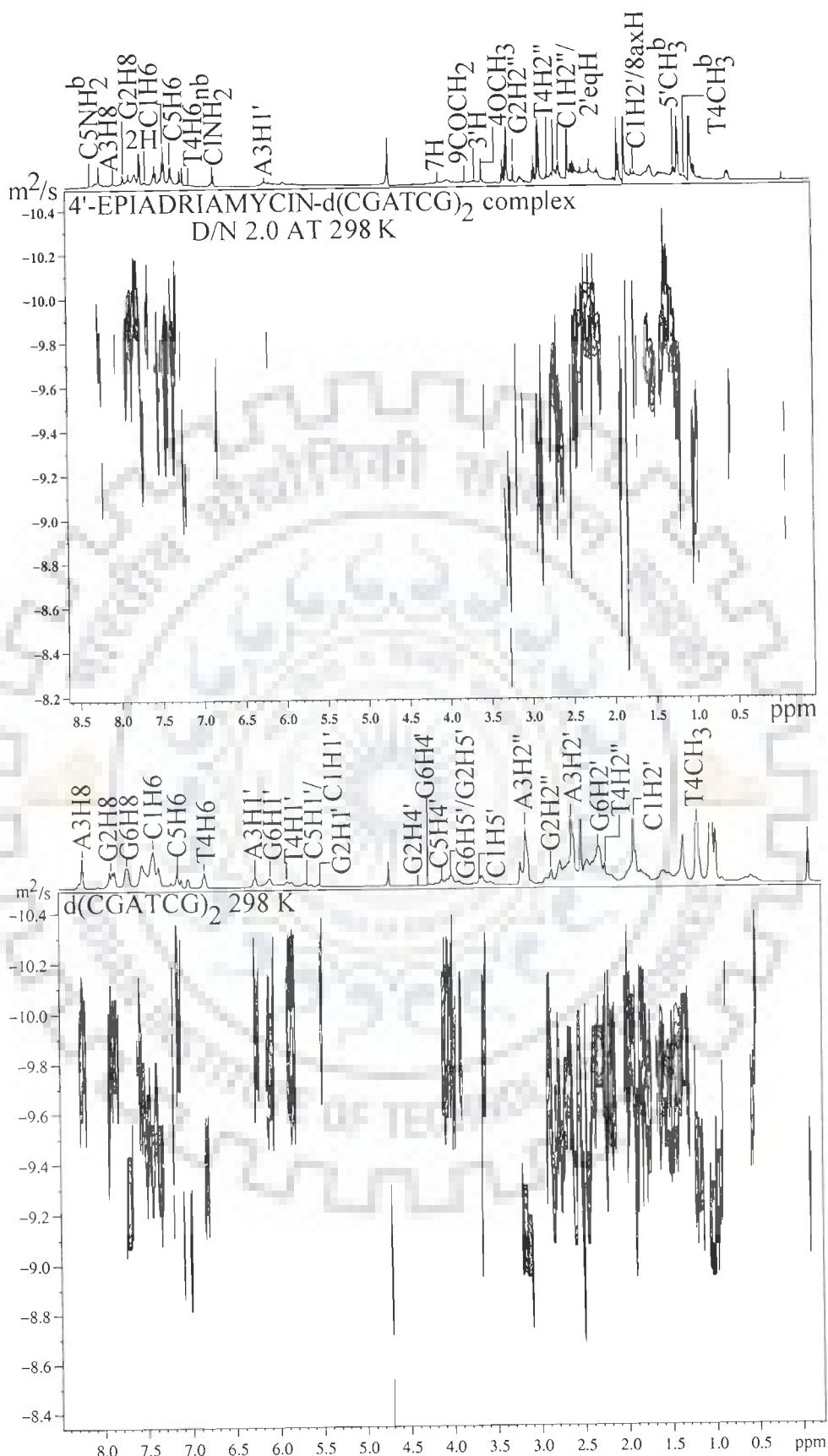


Fig. 9: DOSY Spectra of 4'-epiadriamycin-d(CGATCG)₂ complex and d(CGATCG)₂ at (a) 275 and (b) 298 K in D₂O.



(b)

building the structure and strategy for rMD simulation is similar to that for the adriamycin-d-(TGATCA)₂ complex. Best-fit refined structure showing all atoms is given in Fig. 10 (Side view and front view). The drug-DNA complex is stabilized via close contacts which involve specific hydrogen bonding and van der Waal's interactions (Table 15). The various superimposed structures obtained by restrained molecular dynamics simulations are shown in Fig. 11. The root mean square deviation between the rMD structure and the starting structure is quite large but among various final structures is very low. This is an indication that convergence has been achieved. Table 16 indicates an assessment of refined structure in terms of energetics and distance deviation from the target distance. The total energy of the final structure is 146 Kcal mol⁻¹, which is lower than the initial B-DNA structure. Table 17 shows the pair wise as well as residue wise root mean square deviations (RMSD) of the complex. The starting structure was chosen as reference and the value of target RMSD is chosen to be 0.0. It may be noted that distance deviation reached a minimum of 0.8 Å from an initial average deviation of 0.0 Å.

Conformation of DNA

All helical parameters, backbone torsional angles and sugar conformations of the resulting rMD structures were thoroughly analyzed with the program CURVES, version 5.1 (Lavery et al., 1996; Lavery et al., 1989). The plots of helicoidal parameters (global unless specified otherwise) are made as a function of residue position in the duplex, along with that for the classical structures of A-DNA and B-DNA and are shown in Fig. 12(a-b).

Among the base pair axis parameters, the x-displacement (dx) and y-displacement (dy) are found to vary to a large extent for all base pairs. The base pairs are inclined at an angle (η) up to 6°, the inclination being larger at 5' end. The tip angle fluctuates along the base sequence. The variation in shear, stretch, stagger, and buckle is fairly large for the CG base pair at both the ends. The propeller twist at either ends are negative and large, indicating that the ends are not having

fraying effects. The inter-base parameters shift (D_x) and slide (D_y), vary in the range -0.16 to $+0.07$ Å. The rise per residue (D_z) is 3.25 Å at A3pT4 base pair step while that at C1pG2 and C5pG6 base pair step increases up to 6.3 Å to accommodate drug chromophore. The intercalation results in large amount of tilt ($\tau = 2.21^\circ$ to -0.75°) in base pairs. The roll angle (ρ) varies from $+10^\circ$ to -3° . Positive roll opens the angle between the base pairs towards the minor groove; as a result a wider minor groove and bending towards major groove causing a curvature in the helix occurs. The large positive roll at C5pG6 ($+10^\circ$), step indicates reduced base stacking at C5pG6 end. This is due to the fact that intercalating anthracycline ring chromophore is oriented approximately perpendicular to the base pair axis in the helix, as found in the crystal structures of the complexes. The A3pT4 base pair step show negative value of the roll (-3°). The propeller twist is in the range from -6 to 29° out of which the terminals are having negative value as the drug is intercalating at the terminal ends. The local inter base parameters also show positive roll angle at both the ends of the helix and negative roll in the centre. The twist (Ω) varies in the range 30.1 - 40.0° . The twist angle values at the intercalation steps indicate that there is unwinding of DNA at these steps. Also there is unwinding of DNA at the steps adjacent to the intercalation steps. The width and depth of major groove is found to be 12.48 and 4.53 Å while the corresponding values for minor groove are 6.05 and 5.00 Å respectively. Thus, the minor groove is wider perhaps to allow proximity of daunosamine sugar moiety.

The backbone torsional angles values (Table 18) along with the values for canonical B-DNA and A-DNA are plotted in Fig. 13. The torsional angles α , β and γ adopt gauche⁻, trans and gauche⁺ conformations, respectively. The torsional angle ζ , however, deviates from the normal gauche⁻ conformation and adopts a trans conformation for the G2 and C5 bases. This is due to the opening of base pairs at these sites. This is accompanied by a corresponding deviation in torsional angle ϵ for G2 and C5 bases to a lower negative value of 91° and 100° , respectively, as

compared to a value to 155° found in B-DNA structures. The torsional angle, δ as well as pseudorotation phase angle P , is deviated from the normal range around C2' endo conformation. The glycosidic bond rotation, χ , of the DNA molecule measuring rotation of base around sugar varies along base sequence. The χ angles are as follows: C1, 180° ; G2, -108° ; A3, -136° ; T4, -118° ; C5, -86° ; G6, -82° . On C1pG2 side of the backbone, the 2'-deoxyguanine residue on the 5'-end site changes the glycosyl angle from an anti (-98° in B-DNA) to a low anti value (-108°). At the same time by adjusting ϵ angle from a near trans (155° in B-DNA) to a lower value (-91°), it allows the adjacent bases to separate from 3.4 to 6.3 Å.

On the C1pG2 side, both nucleotide units maintain the glycosyl angle at trans (180° , -108°). But the ϵ value is changed from 155° to a near gauche (-91°) conformation in the G2 residue, it is possible to separate the neighboring G2 and C1 bases to a distance of ~ 6.3 Å. This can be achieved by coupling it with the rotation of the phosphodiester linkage from a normal gauche-, gauche- conformation to a trans, gauche-, as observed in X-ray crystallography (Wang et al., 1987; Frederick et al., 1990; Moore et al., 1989; Williams et al., 1990) and NMR (Mazzini et al., 1998) structures of similar complexes. The change in phosphodiester linkage gets reflected in the backbone torsional angles ϵ , ζ , α and β . A correlation between these torsional angles has been found on the basis of a number of B-DNA crystal structures, which have shown that two conformational states are usually observed in B-DNA, namely B_I and B_{II} . The B_I state is characterized by torsional angles α , -62° ; β , 176° ; γ , 48° ; δ , 128° ; ϵ , -176° ; ζ , -95° ; and χ , -102° to -119° ; while the B_{II} state is characterized by α , -62° ; β , 176° ; γ , 48° ; δ , 144° ; ϵ , -114° ; ζ , -174° ; and χ , -89° . Our results (Table 18) show that both G2 and C5 residues tend to adopt B_{II} conformation. The A3 and T4 residues remain in the more stable B_I state. It has been reported earlier that the idealized g-g- conformation of phosphodiester bond from 5' to 3' direction

changes g-g- – tg- – g-g- – g-g- – tg- (where t and g- stand for trans and gauche-, respectively) in X-ray crystallographic (Nunn et al., 1991) and NMR structures (Mazzini et al., 1998) in hexamer sequences d-CGATCG and d-CGTACG on binding to similar drugs. The trans, gauche-conformation in G2pT3 or G2pA3 step in X-ray structure (Frederick et al., 1990; Nunn et al., 1991) is associated with change in β angle of T4/A3 residue (adjacent to intercalating bases) to $120^\circ - 138^\circ$. Further in these complexes, pseudorotation $P = 105^\circ$ for T4 residue or δ angle of $72^\circ - 92^\circ$ for A3 and T4 residues have been reported. The corresponding δ or P for T4 residue in our case is $117^\circ - 126^\circ$.

We have also looked into correlation between different torsional angles during the course of rMD run. It is observed that the variations in ζ and ε (Fig. 14) are coupled. The torsional angle ε deviates from the normal value of 155° to values in the range -91° to -100° whenever ζ angle adopts trans conformation for G2 and C5 residues. Thus, the conformational states having torsional angles, δ , 126° ; ε , -91° ; ζ , 169° ; χ , -108° ; and δ , 137° ; ε , -100° ; ζ , -174° ; χ , -86° ; for G2 and C5 residues, respectively (Table 18) are indeed the most populated conformations and are close to the characteristic value of δ , 144° ; ε , -114° ; ζ , 174° ; and χ , -89° ; for B_{II} conformation of DNA.

It was observed that at the intercalation site C5pG6 the phosphorus is in B_I conformation and the phosphorus directly lying on the opposite strand has B_{II} conformation. Further at the site adjacent to intercalation site, that is, G6pA7 phosphorus is in B_{II} conformation and the corresponding phosphorus in opposite strand is in B_I conformation. Intercalation of daunomycin induces and stabilizes a distinct pattern of phosphates of the DNA backbone. There appears to be a possibility to directly influence the DNA backbone through complexation, hence leads to a redirection of

intercalation caused structural changes to the backbone, as proposed in literature (Trieb et al., 2004).

Conformation of 4'-Epiadriamycin

The bond distance and angles in the 4'-epiadriamycin molecule are within the limits of accepted values. In the aglycon part of the molecule, the B and D rings are most aromatic with an averaged C-C distance of 1.40 Å. The distance between O5 and O6 atoms and between O11 and O12 atoms are 1.75 and 1.88 Å, respectively; they presumably form intra-molecular hydrogen bonds. The aromatic part of the aglycon is quite planar with rms distance of 0.80 Å for the least squares plane calculated from all the atoms of rings B, C, and D without the exocyclic atom. The methyl group in the 4-methoxy side chain is also in plane with a deviation of 0.78 Å. The orientation of methoxy group is such that the methyl group is pointed away from O5 atoms and protrudes into the solvent region. The torsional angles of the 4'-epiadriamycin molecule in the complex (Table 19) are different from that of daunomycin in the free state (Neidle et al., 1977) and in the same/similar bound complexes (Moore et al., 1989; Frederick et al., 1990). In ring A, the torsional angles around C19-C20 (5-8°) and C20-C7 (28-35°) bonds are negligible while that around C8-C9 (45-50°) and C9-C10 bonds are (-13 – -16°) in magnitude. Thus, practically all atoms except C9 atom are out of the plane containing other atoms and aromatic rings B, C, and D. The C9 atom is displaced by 0.89 Å in same direction as the amino sugar relative to the plane of aglycon molecule as a consequence of which 9OH can no longer form intramolecular hydrogen bond with 7H atom. The torsional angles corresponding to O-glycosyl linkage, C20-C7-O7-C1' and C7-O7-C1'-C2', are lower (-137°, 168°) than the corresponding angles in the pyridine salt of daunomycin molecule (Chaires et al., 1982) in the free state (-114°, 167°). The amino sugar is in a chair conformation with all the side chains pointing away from the aglycon.

The torsional angle around C1'-C2' bond (39°) is shorter than the expected gauche value in the six membered ring.

4'-Epiadriamycin-d-(CGATCG)₂ Interactions

A view showing the stacking interactions is shown in Fig. 15. There are significant deviations from 2-fold symmetry relating the backbone of the B-DNA molecules. The G2.C11 base pair is translated towards minor groove by ~ 1.3 Å and tilted with respect to A3.T10 base pair. The A3.T10 base pair is translated along long axis of the base pair by about 1Å with respect to next base pair along 5'-3' direction.

The drug is positioned with respect to DNA molecule (Fig. 16a-b) such that the hydroxyl oxygen atom of 9OH in ring A is within the hydrogen bonding distance of N3 and N2 atoms of guanine base G2. However, there is existence of weak hydrogen bonding. The distance between O9 and G2N3 atom is 3.93 Å and varies in the range 3.5 - 4.7 Å in 100 structures saved at equal intervals during 100 ps rMD simulations. The distance of O9 from G2N2 atom is 4.01 Å and varies in the range 4.0 - 4.5 Å so that this hydrogen bond is rather weak. O7 atom of 4'-epiadriamycin which links the chromophore and amino sugar, is close to N2 of G2 residue with the separation of 3.0 Å while O9 is far from O4' of G2 (4.2 Å). The distance of O7 atom from O9 atom of 9OH hydroxyl group in ring A is 2.87 Å so that there is possibility of intramolecular hydrogen bond between O7 and 9OH. Apparently in order to have hydrogen bond of O9 with G2N3, the ring conformation is altered in a specific way which moves O7 atom away (Wang et al., 1987). This hydrogen bonding interaction is likely to be sensitive to conformation of ring A. The distance between O13 and O2 of C1 in our structure is 5.11 Å so that bridging of O13 to O2 of C1 through water may not be possible. Further the distance between O4 and O-1P of G6 is 8.97 Å. However the distance between O5 and C5N1 is 3.24 Å. A hydrogen bond involving O4 and O5 atoms with phosphate groups of G6 are possible through two water molecules acting as

bridges between them. In our rMD structures these N–H...O distances from C5O2, C5O4', and T4O2 atoms are 3.61, 3.98, and 4.76 Å, respectively. We have therefore looked into these contacts throughout the course of simulations. It is found that the distance of NH₃⁺ from C5O2, C5O4', and T4O2 are in the range 3.5 - 4.3, 3.8 - 4.3, and 3.9 - 5.0 Å, respectively. At the other intercalation site, the distance of NH₃⁺ from C11O2, C11O4', and T10O2 are in the range 4.2 - 4.9, 4.5 - 5.1 and 4.6 - 5.1 Å, respectively. If we consider 3.5 Å as the cut off distance for hydrogen bond then NH₃⁺ moiety is able to make at the most two hydrogen bonds. The distance of NH₃⁺ from O4' of T4 / T10 and N3 of A3 / A9 are in the range 5.0 - 6.5 and 4.5 - 5.0 Å, respectively, so that there are no contacts through hydrogen bonds between these groups of atoms, as seen in some X-ray crystal structures (Wang et al., 1987; Moore et al., 1989; Nunn et al., 1991).

An interesting feature of daunomycin / adriamycin / 4'-epiadriamycin is its flexibility of O-glycosidic bond rotation C7-O7-C1'-C2'. Throughout the course of simulations, we find that the O-glycosidic angle C7-O7-C1'-C2' remains within a narrow range of angles, 165°-180°, and stabilizes at 168°. In uncomplexed daunomycin and its analogues it is found to be 162–168° (Neidle et al., 1977; Von Dreele et al., 1977; Anguilli et al., 1971; Courseille et al., 1979) while in the X-ray crystal structure of adriamycin complexed with d-CGATCG it is 148° and in some complexes, e.g., 4'-epiadriamycin complexed with d-TGATCA and daunomycin with d-CGATCG it is 132° - 137° (d'Estaintot et al., 1992; Lipscomb et al., 1994). In most other crystal structures, it is 145° - 161° (Leonard et al., 1992; Moore et al., 1989; Williams et al., 1990). The molecular dynamics simulations have however shown (Trieb et al., 2004) that a much lower dihedral angle, 57° - 61°, is also accessible. In the first conformation centered at 159°, the nitrogen of the ammonium group is at a distance of 5.5, 5.1, and 3.2 Å from C5O4', T4O2, and T4O4', respectively, while in the second centered at 137°, the corresponding distances are 3.2,

3.0, and >6 Å, respectively. In the third conformation centered at 59° , the distance of nitrogen of NH_3^+ from G6O4' and G6O5' are 3.4 and 3.0 Å, respectively. The energy barrier between 137° and 159° conformations is 0.3- 0.7 kcalmol⁻¹ and that between 137° and 59° conformations is 1.4 kcalmol⁻¹. Apparently in our case, the first and second substrates were kinetically readily accessible. The observed distance of nitrogen of NH_3^+ from C5O4'/C11O4', T4O2/T10O2, and T4O4'/T10O4' is in the range 3.1 - 5.1 Å and that from G2O4' and G2O5' is in the range of 9 - 12 Å.

During the course of simulations, it is observed that hydrogen atom of 6OH group of ring B of 4'-epiadriamycin points towards O5 atom (that is away from O7 atom) in 98 out of 100 structures while hydrogen of 11OH points towards O12 and is away from C10 position. Apparently 6OH...5O hydrogen bond is only stabilized in the drug-DNA complex. This is similar to the existence of both hydrogen bonds in the uncomplexed daunomycin, adriamycin, and 4'-epiadriamycin [unpublished] investigated by us. The position of H atom of 6OH remains fixed and is not correlated to O-glycosidic bond rotation C7-O7-C1'-C2' which while varying in the range 165° - 180° , positions the daunosamine sugar moiety close to 6OH in different orientations. The stabilization of 6OH...5O hydrogen bond thus ensures a fixed position of hydrogen atom of 6OH which has been found to be close to C5H1' (distance 3.24 Å) of DNA (Table 15). Besides this, several other contacts O5-C5H1', O6-C5H1', O5-C5H2', 4OCH₃-C5H2', 6OH-C5H1', having distances within 4.0 - 5.0 Å, establish the involvement of 4OCH₃, O5, O6, and 6OH atoms in stabilizing the drug-DNA complex. Some of the contacts, also observed earlier (Wang et al., 1987), e.g., 10axH with C1O2; 10eqH with G2N3; 3'H with G2N2; 2'axH with C5O2, have an important role in binding.

4'-Epiadriamycin drug differs from daunomycin by a hydroxyl group attached at C14 position, that is, presence of 9COCH₂OH group as compared to 9COCH₃ group in daunomycin and

Table 15: Close contacts (Å) between drug and DNA molecule

Van der Waal's contacts			H-Bond contacts		
S.No.	Protons	Distance	S.No.	Protons	Distance
1	G2NH ₂ ^b -6O	2.07	1	C1N1-11O	2.94
2	G2C6-C11a	2.78	2	C1N3-12CO	2.82
3	G2C4-C11	2.72	3	G2N7-12CO	2.73
4	G2NH ₂ ^{nb} -O7	2.11	4	G2N7-11OH	2.41
5	G2N3-C10a	2.62	5	G2N9-11O	2.86
6	A3P-14OH	1.71	6	G2NH ₂ ^b -6O	2.07
7	T4P-4'OH	1.72	7	G2NH ₂ ^{nb} -O7	2.11
8	G6NH ₂ ^b -8axH	1.63	8	A3P-14OH	1.72
9	G6C6-C5	2.66	9	T4P-4'OH	1.73
10	G6C5-5CO	2.58	10	C5N3-5CO	2.54
11	G6C2-C6	2.76	11	C5O2-6OH	2.37
			12	G6N7-5CO	2.68
			13	G6N9-6O	2.88
			14	G6N3-6O	2.74

Table 16: Energy terms (Kcal mol⁻¹) for starting model and final rMD structure.

Energies (Kcal mol ⁻¹)	d-(CGATCG) ₂ -4'-Epiadriamycin complex	
	Initial	Final
Total	1218	146
Bond	91	98
Angle	556	560
Dihedral	-46	-55
Van der Waal	138	179
Repulsion	2119	2179
Dispersive	-1981	-2000
Electrostatic	541	434
Restraint	203	189

Table 17: Summary of experimental restraints and statistical analysis of final structure generated by restrained molecular dynamics (rMD)

Parameters	No. of distance restraints
Intra residue	172
Inter residue	62
Total NOE violations	31
Average pairwise RMSD	Initial = 0.0; Final = 0.76
Average residue wise RMSD	C1 = 0.058, G2 = 0.078, A3 = 0.047, T4 = 0.053, C5 = 0.055, G6 = 0.083
Minor groove	Width = 7.22 Å; Depth = 4.85 Å
Major groove	Width = 13.09 Å; Depth = 1.95 Å

Table 18: Backbone torsional angles ($^{\circ}$), pseudorotation phase angle ($^{\circ}$) and glycosidic bond rotation ($^{\circ}$) of the final structure

Residues	α	β	γ	δ	ϵ	ζ	χ	P
C1	-	-	51	153	-107	-49	180	-139
G2	-56	149	53	126	-91	169	-108	130
A3	-63	109	57	99	-176	-81	-136	107
T4	-59	170	56	117	-164	-80	-118	126
C5	-67	161	49	137	-100	174	-86	143
G6	-70	163	50	149	-	-	-82	185
C7	-	-	51	153	-107	-49	180	-139
G8	-56	149	53	126	-91	169	-108	130
A9	-63	109	57	99	-176	-81	-136	107
T10	-59	170	56	117	-164	-80	-118	126
C11	-67	161	49	137	-100	174	-86	143
G12	-70	163	50	149	-	-	-82	185

Table 19: Selected torsional angles ($^{\circ}$) of the 4'-epiadriamycin in the complex and their comparison with similar structures available in literature. ^aTGATCA + daunomycin (Nunn et al., 1991); ^bTGTACA + daunomycin (Nunn et al., 1991); ^cTGATCA + 4'-epiadriamycin (Estaintot et al., 1992), ^dTGTACA + 4'-epiadriamycin (Leonard et al., 1992); ^edaunomycin (Neidle et al., 1977).

TORSIONAL ANGLES	Present Work CGA + 4'-epi	TGA + dnm ^a	TGT + dnm ^b	TGA + 4'-epi ^c	TGT + 4'-epi ^d	dnm ^e
RING A						
C20-C7-C8-C9	-58	-56	-40	-45	-50	-48
C7-C8-C9-C10	50	66	55	68	63	58
C8-C9-C10-C19	-15	-35	-44	-60	-42	-38
C9-C10-C19-C20	-14	-2	27	33	14	14
C10-C19-C20-C7	5	10	-11	-8	-1	-5
C19-C20-C7-C8	30	18	14	13	18	20
GLYCOSYL						
C8-C7-O7-C1'	96	129	120	96	95	125
C20-C7-O7-C1'	-137	-115	-125	-139	-142	-114
C7-O7-C1'-O5'	-64	-115	-105	-102	-81	-68
C7-O7-C1'-C2'	168	127	137	132	159	167
AMINO SUGAR						
O5'-C1'-C2'-C3'	39	-49	-60	-31	-53	-54
C1'-C2'-C3'-C4'	-57	50	49	41	52	56
C2'-C3'-C4'-C5'	16	-20	-17	-53	54	-61
C3'-C4'-C5'-O5'	44	-16	-5	61	57	61
C4'-C5'-O5'-C1'	-67	19	-9	-55	-59	-59
C5'-O5'-C1'-C2'	24	17	42	36	57	57

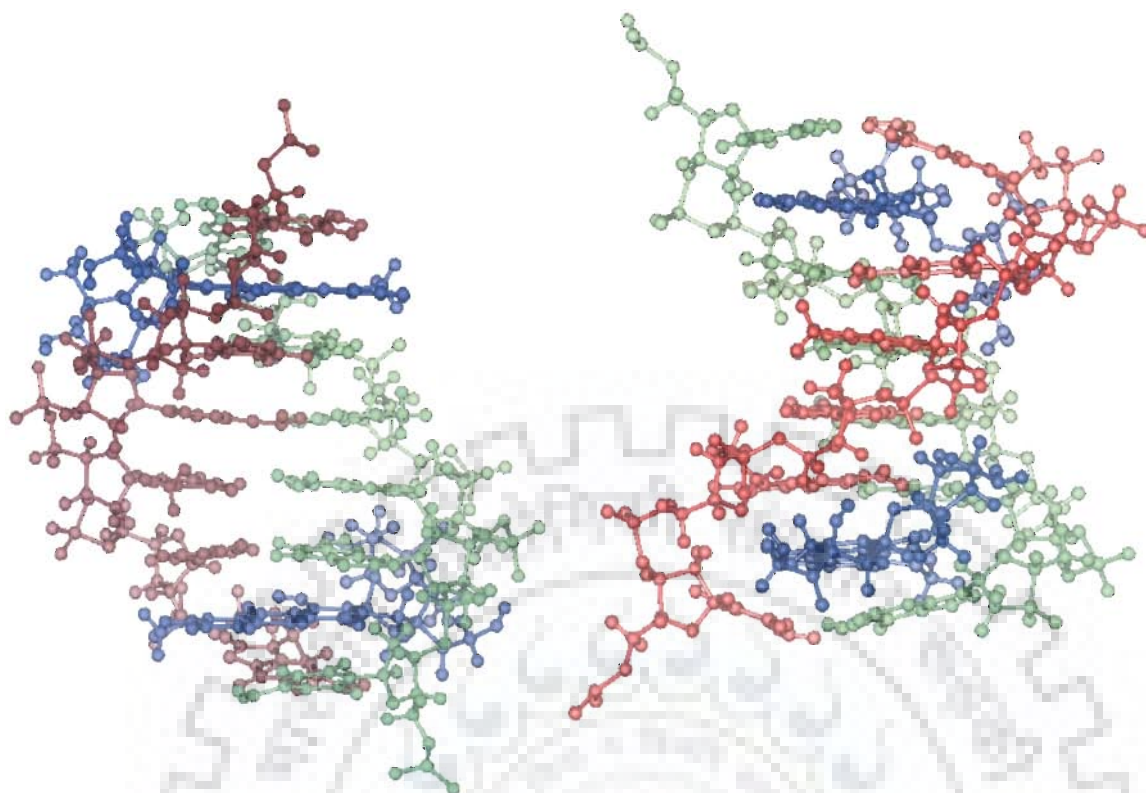


Fig.10: Side view and front view of the final structure of d-(CGATCG)₂-4'-epiadriamycin obtained by restrained molecular dynamics simulations.

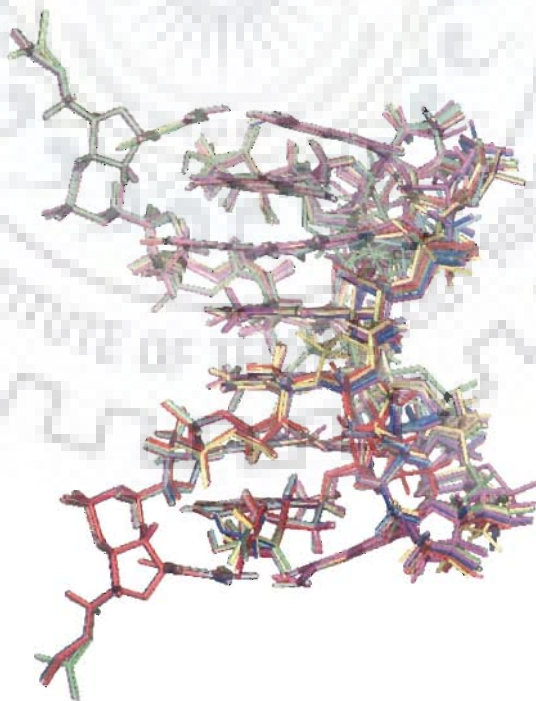
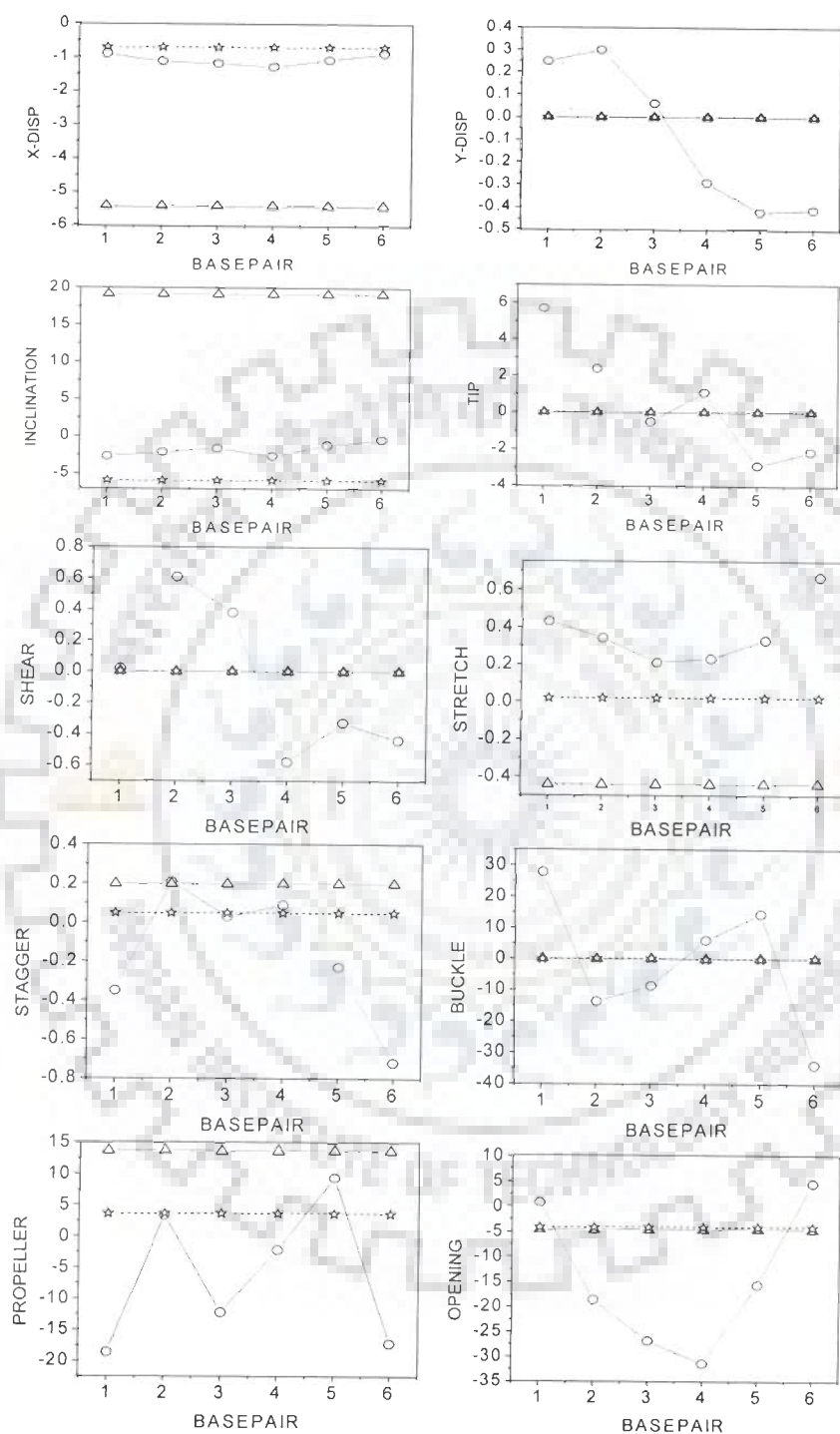
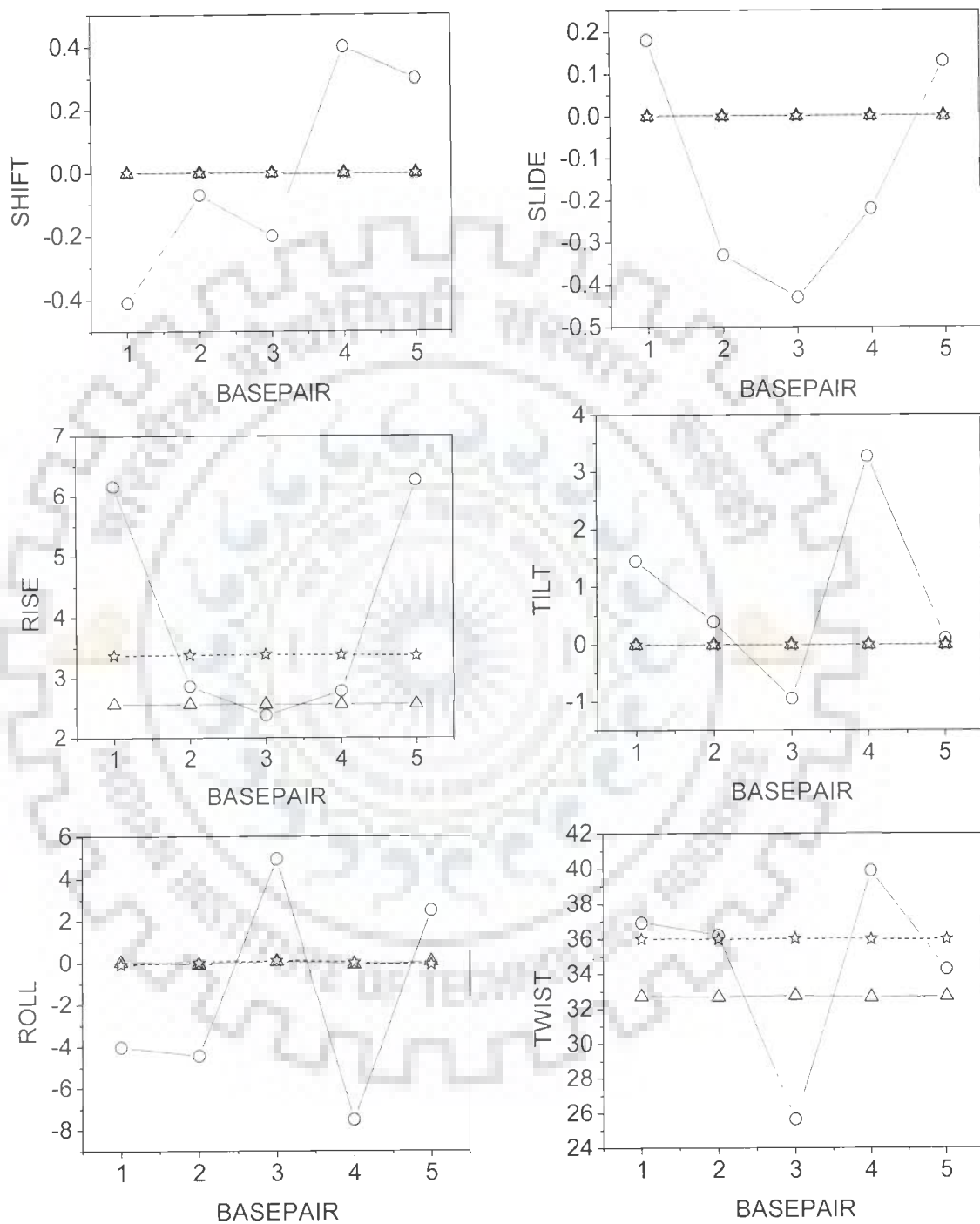


Fig. 11: Superimposed structures of d-(CGATCG)₂-4'-epiadriamycin obtained by restrained molecular dynamics simulations.



(a)

Fig.12: (a) and (b) Helical parameters for d-(CGATCG)₂ complexed with 4'-epiadriamycin calculated for structure obtained by restrained molecular dynamics simulations (○) and that for standard A-DNA (△), B-DNA (☆).



(b)

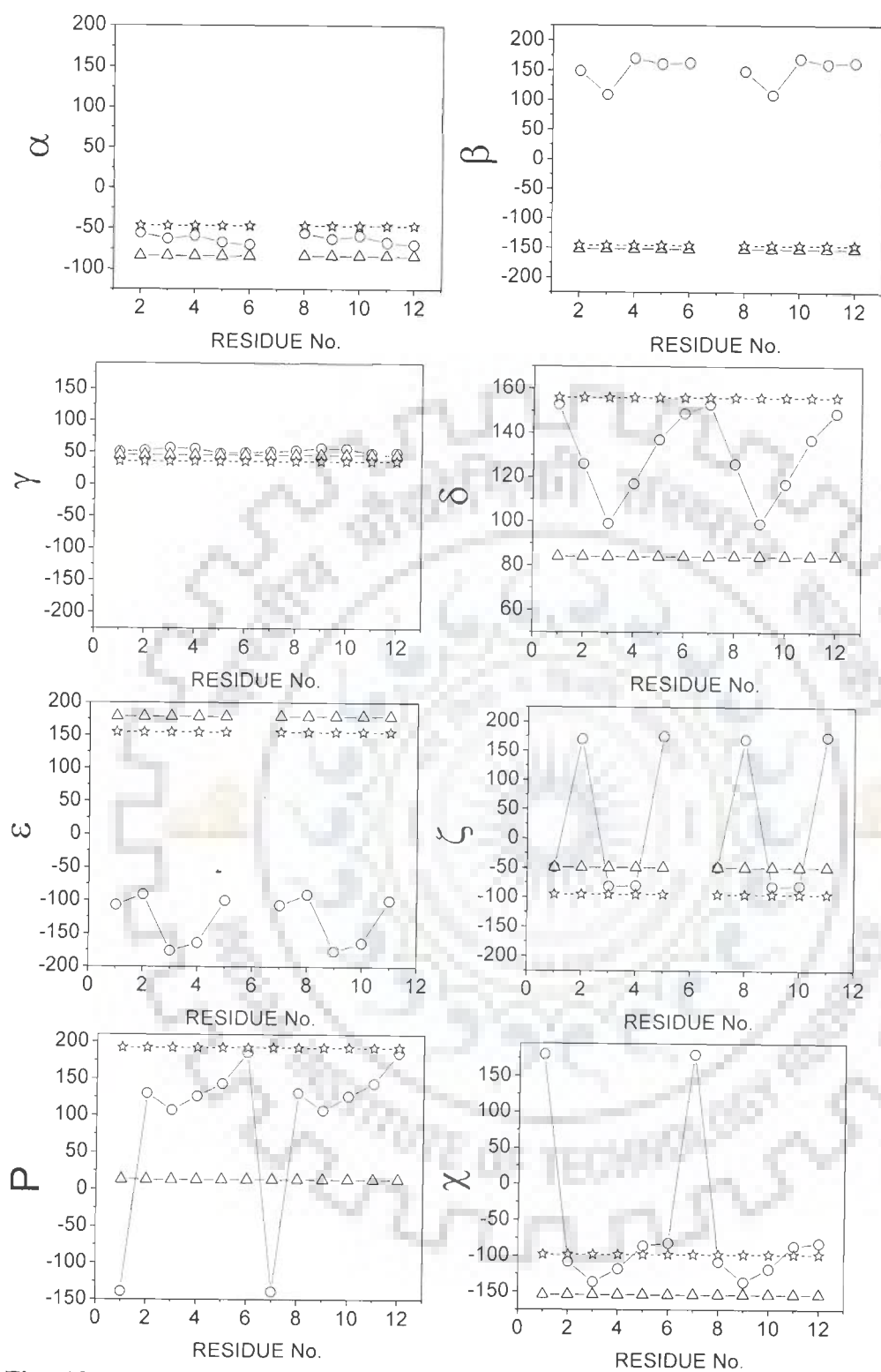


Fig. 13: Backbone torsional angles for d-(CGATCG)₂ complexed with 4'-epidriamycin calculated for structure obtained by restrained molecular dynamics simulations (○) and that for standard A-DNA (△), B-DNA (☆).

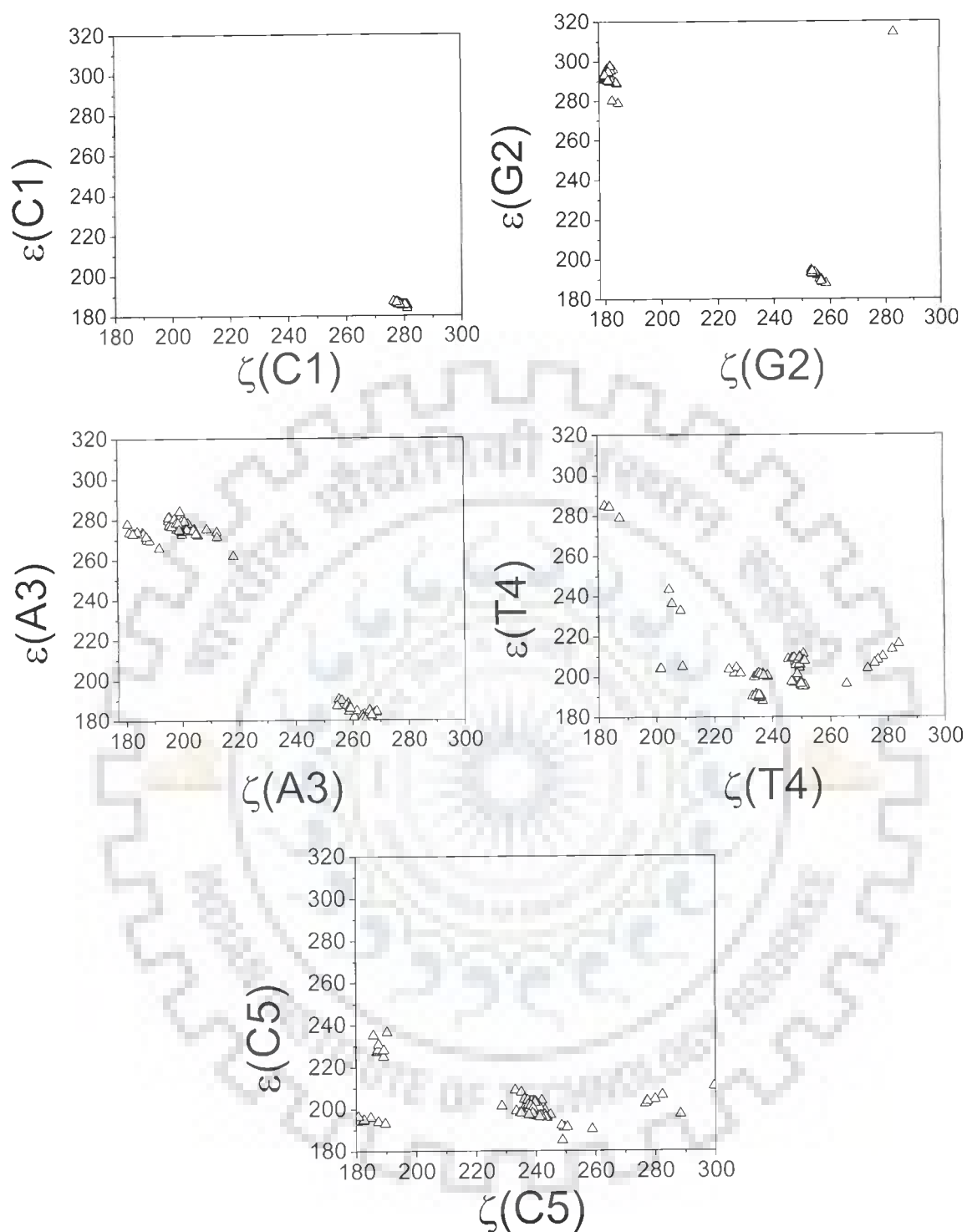


Fig. 14: Correlation between ϵ and ζ torsional angles in the structure obtained after 100 ps rMD run of d-(CGATCG)₂ complexed with 4'-epiadriamycin.

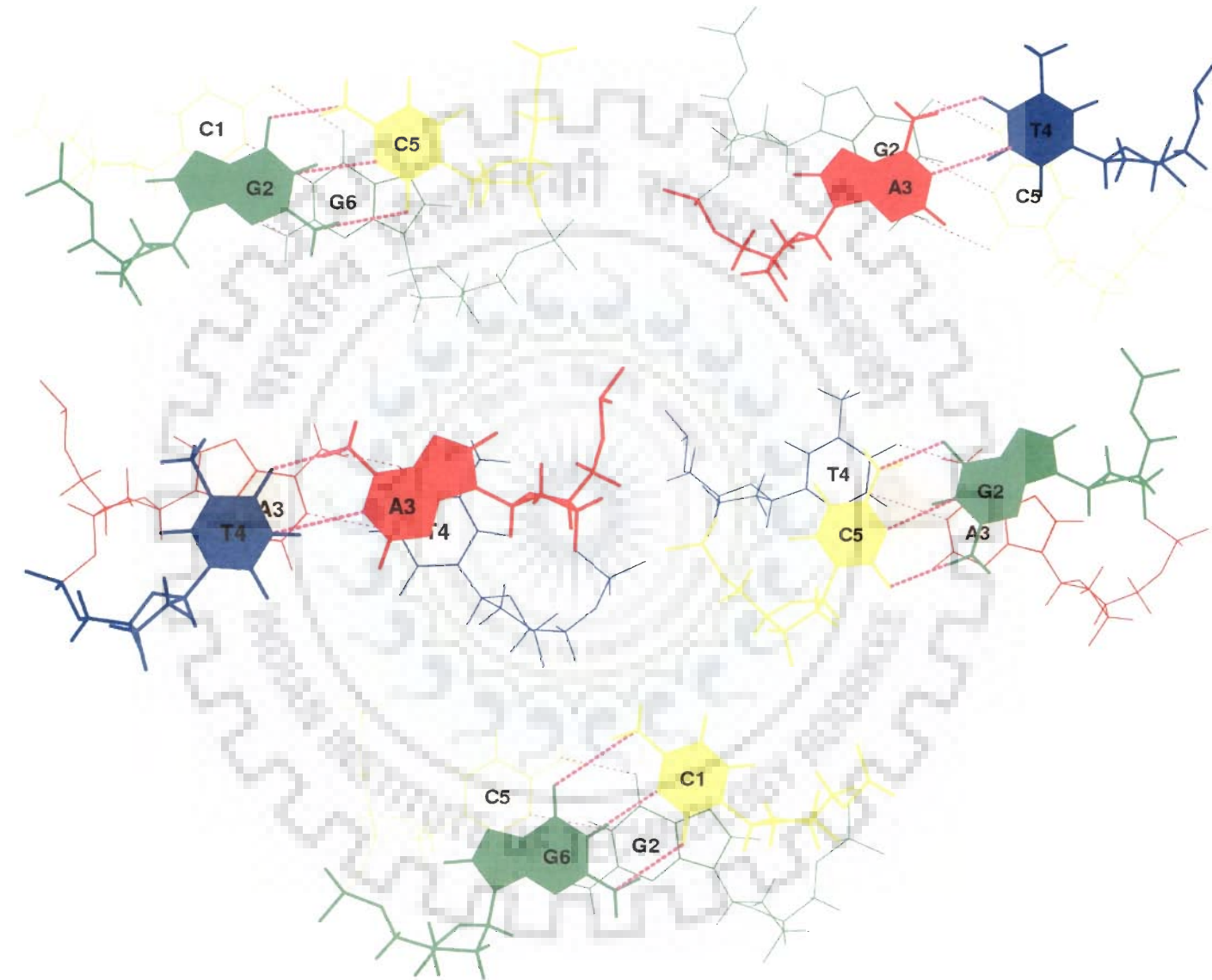


Fig.15: Overlap of base pairs at different base pair steps in d-(CGATCG)₂-4'-epiadriamycin complex showing stacking interactions.

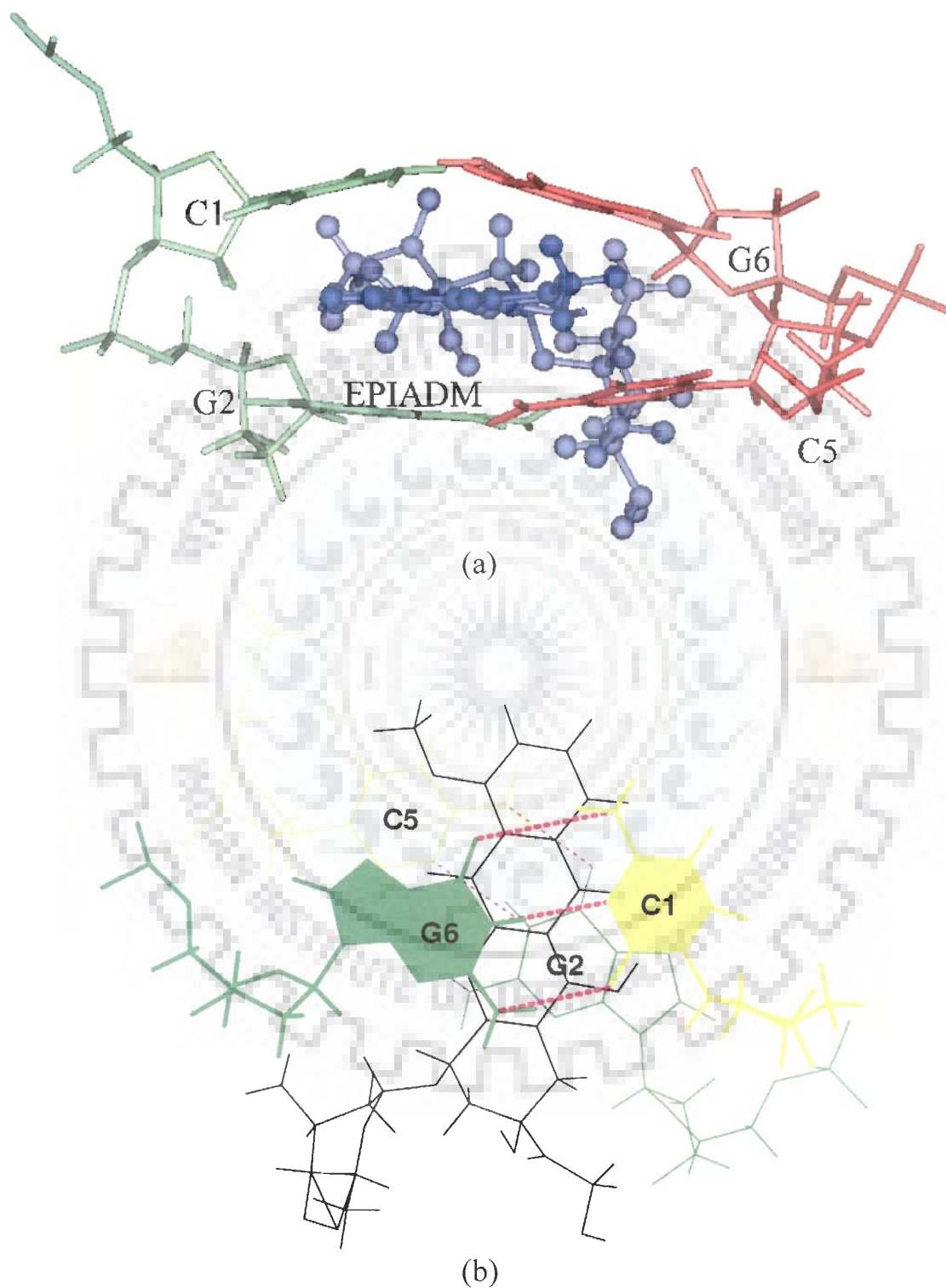


Fig.16: Drug-DNA stacking interaction in the intercalation site showing the orientation of the 4'-epiadriamycin with respect to base pairs (a) front view (b) top view.

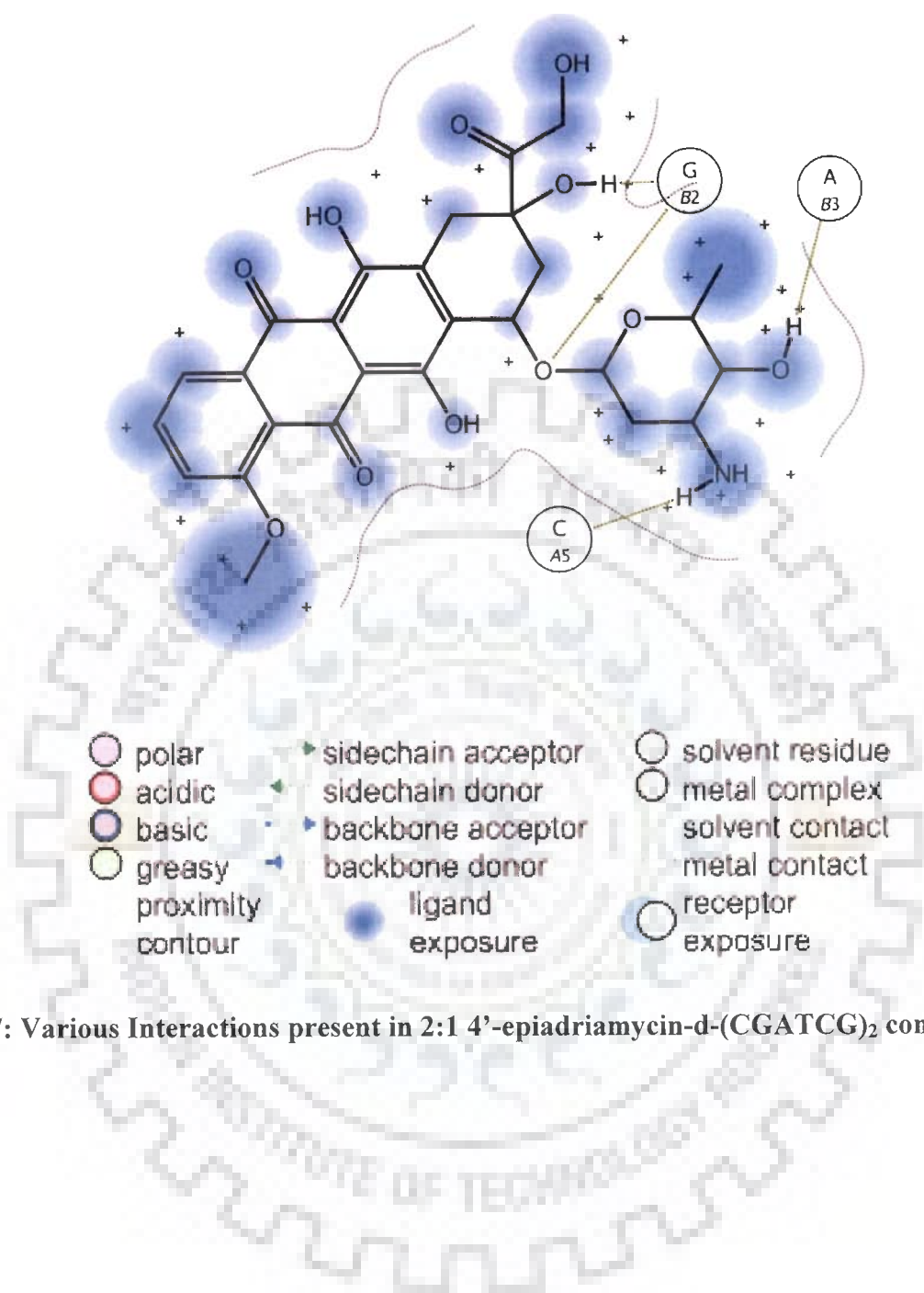


Fig. 17: Various Interactions present in 2:1 4'-epiadriamycin-d-(CGATCG)₂ complex.

inversion of 4'OH at the daunosamine sugar moiety. In the rMD structure of the complex, it is observed that the hydroxyl group makes short van der Waal's contact with A3H5' (3.01 Å) and A3H4' (4.89 Å). Its distance from G2O3' and G2 phosphorus atom is 4.66 and 3.98 Å (Table 15), respectively. This group has been implicated in binding to phosphate through water bridge in X-ray crystal structure of adriamycin with d-CGATCG (Frederick et al., 1990). Thus we find that 5O, 4OCH₃, 6OH and O7 groups are involved in drug-DNA interactions (Fig. 17). This may require existence of 6OH...5O and 11OH...12O hydrogen bond. Involvement of NH₃⁺ group in interaction is related to conformation of O-glycosidic bond. The binding to DNA through 9CO13, 9OH, and 9CH₂OH groups depends upon ring A conformation. Presence of 11OH...12O hydrogen bond may not be critical for binding and atoms of position 1, 2, 3, 12, and 11 are not involved in drug-DNA interactions.

8.2 Summary and Conclusions

Large upfield shifts are observed in C1H1', G2H1', G2NH, G6NH and G6H2' protons on binding of drug to DNA hexamer sequence. The 1H, 2H, 3H, 7H protons of the drug are shifted downfield up to 0.6 ppm while the sugar protons 3'H, 4'H and 6OH are shifted downfield up to 0.9 ppm in the complex. Sequential nOe (nuclear Overhauser effect) connectivities between C1pG2 and C5pG6 steps are not observed as the drug chromophore intercalates at these base pair steps. Presence of several other intermolecular nOes, that is, G2H8-7H, G6H8-6OH and C5H6-4OCH₃ corroborate the same. The daunosamine sugar protons are in close proximity of third base pair. B_I and B_{II} transition has been detected at these base pair steps. The observed sequence dependant variations in DNA occur presumably to allow intercalation of the drug chromophore. The conformation of the drug also changes in order to have interaction with G2 base. Our studies establish the role of 9OH, C13O13, NH₃⁺, 7O, 4OCH₃ groups in binding to DNA. The observed

NOEs and short interproton distances in the solution structure of the complex confirm that the anthraquinone ring intercalates between CG base pairs excluding 3 base pairs adjacent to it. Besides this, life time measurement study has been done to show that there is shortening of decay time on complex formation. The DOSY spectral analysis also show that the rate of diffusion decreases due to the binding of drug to DNA hexamer. The present study is the first rMD study on the solution structure of 4'-epiadriamycin with d-(CGATCG)₂ hexamer. The rMD simulations of 4'-epiadriamycin- d-(CGATCG)₂ complex based on intermolecular and intramolecular NOEs have led to a detailed conformational analysis. The intercalation of drug chromophore at d-CpG steps is stabilized by stacking interactions while several other hydrogen bonds and van der Waal's interactions involving O5, 6OH, and NH₃⁺ moiety of daunosamine sugar, and rings A protons stabilize the drug-DNA complex. The O9 atom is involved in hydrogen bond formation with G2N3 and G2N2H while O7 atom has close contact with G2N2 atom. The O-glycosidic bond C6a-C7-O7-C1' is stabilized around 137°. The conformation of O-glycosidic bond and ring A is related to cleavage of C7-O7 bond and subsequent production of free radicals which are responsible for cardiotoxicity. Therefore, any substitution in ring A or daunosamine sugar will effect the binding (and hence anti cancer action) as well as cell toxicity. These findings can provide leads for designing drugs of higher potency, reduced cell toxicity, and decreased resistance to tumor cell lines and hence find potential medical applications.

References

1. Adams A., Guss J.M. and Collyer C.A. Crystal structure of the topoisomerase II poison 9-amino-[N-(2-dimethylamino)ethyl]acridine-4-carboxamide bound to the DNA hexanucleotide d(CGATCG)₂. *Biochemistry*, 1999, 38, 9221.
2. Adel A. L., Dorr R. T. and Liddil J. D. The effect of anticancer drug sequence in experimental combination chemotherapy. *Cancer Invest.* 1993, 11, 15-24.
3. Alberts D. S., Salmon S. E., Surit E. A., Chen H. S. G., Moon T. E. and Meyskens F. L. Combination chemotherapy (CRX) in vitro with the human – tumor stem-cell assay. *Proc Am Assoc Cancer Res.* 1981, 23, 153.
4. Altona C. and Sundaralignam M. Conformational analysis of the sugar ring in nucleosides and nucleotides. A new description using the concept of pseudorotation. *J. Am. Chem. Soc.*, 1972, 94, 8205.
5. Anderson, J. E., Ptashne, M., & Harrison, S.C. Structure of the bacteriophage 434 repressor-operator complex. *Nature*, 1987, 326, 846-852.
6. Andreoni, A. Colasanti, G. and Roberti, G. Excited singlet state properties of anthracenedione photosensitizers. *J. Photochem. Photobiol. B: Biology*, 1992, 14, 319-328.
7. Anguilli R., Foresti E., Rivi di S.L., Isaacs N.W., Kennard O., Mothewell W.D.S., Wampler D.L. and Arcamone F. Structure of daunomycin: X-ray analysis of N-Br-acetyl daunomycin solvate. *Nature (London), New Biol.*, 1971, 234, 78.
8. Arcamone F. and Penco S. In “Anthracyclines and anthracediones based anticancer agents”. (Eds. Lown J.W.), Elsevier, New York, 1988.
9. Arcamone F. Doxorubicin: In “Anticancer Antibiotics”. Academic Press, New York, 1981.

10. Arora S.K. Molecular structure, absolute stereochemistry, and interactions of nogalamycin, a DNA-binding anthracycline antitumor antibiotic. *J. Amer. Chem. Soc.*, 1983, 105, 1328.
11. Bacolla A., Gellibolian R., Shimizu M., Amirhaeri S., Kang S., Ohshima K., Larson J.E., Harvey S.C., Stollar B.D. and Wells R.D. Flexible DNA: Genetically unstable CTG.CAG and CGG.CCG from human hereditary neuromuscular disease genes. *J. Biol. Chem.*, 1997, 272, 16783.
12. Barthwal R., Awasthi P., Monica, Kaur M., Sharma U., Srivastava N., Barthwal S.K. and Govil G. Structure of DNA sequence d-TGATCA by two-dimensional Nuclear Magnetic Resonance Spectroscopy and Restrained Molecular Dynamics. *J. Struct. Biol.*, 2004, 148, 34-50.
13. Barthwal R., Mujeeb A. and Govil G. Interaction of daunomycin with deoxydinucleotide d-CpG by two dimensional proton magnetic resonance techniques. *Arch. Biochem. Biophys.*, 1994, 313, 189.
14. Barthwal, R., Monica, Awasthi, P., Srivastava, N. Sharma, U., Kaur, M., Govil, G. J. *Biomol. Struct. Dyn.*, 2003, 2, 407-418.
15. Barthwal, R., Mujeeb, A., Srivastava, N., Sharma, U. A proton nuclear magnetic resonance investigation of the conformation of daunomycin. *Chemico-Biol. Interactions*, 1996, 100, 125-139.
16. Barthwal, R., Sharma, U., Srivastava, N., Monica, Awasthi, P., Kaur, M., Barthwal, S.K. and Govil, G. Structure of daunomycin complexed to d-(TGATCA) by two-dimensional Nuclear Magnetic Resonance Spectroscopy. *Eur. J. Med. Chem.*, 2006, 41, 27-39.
17. Barthwal, R., Srivastava, N., Sharma, U., Govil, G.) A 500 MHz proton NMR study of the conformation of adriamycin. *J. Mol. Struct.*, 1994, 327, 201-220.

18. Becke A.D., Perspective on "Density functional thermochemistry. III. The role of exact exchange. *J Chem Phys.* 1993, 98, 5648-5652.
19. Bertucat G., Lavery R. and Prévost C.A. A model for parallel triple helix formation by RecA: Single-strand association with a homologous duplex via the minor groove. *J. Biomol. Struct. Dyn.*, 1998, 16, 535.
20. Bertucat, G., Lavery R. and Prévost, C. A model for parallel triple helix formation by RecA: Single-strand association with a homologous duplex via the minor groove, *J. Biomol. Struct. Dyn.*, 1998, 16, 535-546.
21. Beutal B.L. and Gold L. In vitro evolution of intrinsically bent DNA. *J. Mol. Biol.*, 1992, 228, 803.
22. Bhattacharyya D. and Bansal M. Groove width and depth of B-DNA structures depend on local variations in slide. *J. Biomol. Struct. Dyn.*, 1992, 10, 213.
23. Bodenhausen G., Freeman R. and Turner D.L. Suppression of artifacts in two-dimensional spectroscopy. *J. Magn. Reson.*, 1977, 27, 511.
24. Breslauer, K. J. Extracting Thermodynamics Data from Equilibrium Melting Curves for Oligonucleotide Order-Disorder Transitions. *Methods in Enzymology*, 1987, 259, 221-242.
25. Calendi E., Di Marco A., Reggiani M., Scarpinato B. and Valentini L. On physico-chemical interactions between daunomycin and nucleic acids. *Biochem. Biophys. Acta.*, 1965, 103, 25.
26. Callandine, C. R. Mechanics of sequence-dependent stacking of bases in B-DNA. *J.Mol. Biol.* 1982, 161, 343-352.
27. Celda V., Widmer H., Leupin W., Chazin W., Denny A. and Wuthrich K. Conformational studies of d-(AAAAATTTTT)₂ using constraints from nuclear overhauser effects and from quantitative analysis of the cross peak fine structures in

- two-dimensional ^1H Nuclear Magnetic Resonance spectra. *Biochemistry*, 1989, 28, 1462.
28. Chaires J.B. Daunomycin inhibits the B \rightarrow Z transition in poly d-(G-C). *Nucleic Acids Research*, 1983, 11, 8485.
 29. Chaires J.B. Thermodynamics of the daunomycin-DNA interaction: Ionic strength dependence of the enthalpy and entropy. *Biopolymers*, 1985a, 24, 403.
 30. Chaires J.B., Dattagupta N. and Crothers D.M. *Biochemistry*. Self-association of daunomycin. *Biochemistry*, 1982, 21, 3927.
 31. Chaires J.B., Dattagupta N. and Crothers D.M. Kinetics of the daunomycin-DNA interaction. *Biochemistry*, 1985, 24, 260.
 32. Chaires J.B., Dattagupta N. and Crothers D.M. Studies on interaction of anthracycline antibiotics and deoxyribonucleic acid: Equilibrium binding studies on interaction of daunomycin with deoxyribonucleic acid. *Biochemistry*, 1982a, 21, 3933.
 33. Chaires J.B., Fox K.R., Herrera J.E., Britt M. and Waring M.J. Site and sequence specificity of the daunomycin-DNA interaction. *Biochemistry*, 1987, 26, 8227.
 34. Chaires J.B., Herrera J.E. and Waring M.J. Preferential binding of daunomycin to 5'A/TCG and 5'A/TGC sequences revealed by footprinting titration experiments. *Biochemistry*, 1990, 29, 6145.
 35. Chastain P.D. and Sinden R.R. CTG repeats associated with human genetic disease are inherently flexible. *J. Mol. Biol.*, 1998, 275, 405.
 36. Chen C.W., Knop R.H. and Cohen J.S. Adriamycin inhibit the B to Z transition of poly (dGm⁵dC). *Poly (dGm⁵dC)*. *Biochemistry*, 1983, 22, 5468.
 37. Chen H. and Patel D.J. Solution structure of a quiniomycin bisintercalator DNA complex. *J. Mol. Biol.*, 1995, 246, 164.

38. Chen K.X., Gresh N. and Pullman B. A theoretical investigation on the sequence selective binding of daunomycin to double-stranded polynucleotides. *J. Biomol. Struct. Dyn.*, 1985, 3, 445.
39. Chen K.X., Gresh N. and Pullman B. A theoretical investigation on the sequence selective binding of adriamycin to double-stranded polynucleotides. *Nucleic Acids Research*, 1986, 14, 2251.
40. Cheung S., Arndt K. and Lu P. Correlation of Lac-Operator Imino proton exchange kinetics with its Function. *Proc. Natl. Acad. Sci., U.S.A.*, 1984, 81, 3665.
41. Chuprina V.P., Lipanov A.A., Fedoroff O.Y., Kim S.G., Kintanar A. and Reid B.R. Sequence effects on local DNA topology. *Proc. Natl. Acad. Sci., U.S.A.*, 1991, 88, 9087.
42. Cieplak P., Rao S.N., Grootenhuis P.D.J. and Kollman P.A. Free energy calculation on base specificity of drug-DNA interactions: Application to daunomycin and acridine intercalation into DNA. *Biopolymers*, 1990, 29, 717.
43. Cirilli M., Bachechi F. and Ughetto G. Interactions between morpholinyl anthracyclines and DNA. The crystal structure of a morpholino doxorubicin bound to d-(CGTACG). *J. Mol. Biol.*, 1992, 230, 878.
44. Courseille C., Busetta B., Geoffre S. and Hospital M. Complex daunomycin-butanol. *Acta Cryst.*, 1979, B35, 764.
45. Dagleish D.G., Fey G. and Kersten W. Circular dichroism studies of complexes of the antibiotics daunomycin, nogalamycin, chromomycin and mithramycin with DNA. *Biopolymers*, 1974, 13, 1757.
46. Davies D.B., Eaton R.J., Baranovsky S.F. and Veselkov A.N. NMR investigation of the complexation of daunomycin with deoxytetranucleotides of different base sequence in aqueous solution. *J. Biomol. Struct. Dyn.*, 2000, 17, 887.

47. Davies D. B., Veselkov D. A., Djimant L. N. and Veselkov A. N. Hetero-association of caeffine and aromatic drugs and their competitive binding with DNA oligomer. *Eur. Biophys. J.*, 2001, 30, 354-356.
48. Derome A.E. In "Modern NMR techniques for chemistry research". Volume 6, Pergamon Press, Oxford U.K. 1987.
49. Di Marco A., Arcamone F. and Zunino F. In "Antibiotics". (Eds. Corcoran J.W. and Hahn I.E.) Springer-Verlag, Berlin, 1974,101.
50. Dickerson R.E., Bansal M., Calladine C.R., Diekmann, S., Hunter W.N., Kennard O., Kitzing von E., Lavery R., Nelson H.C.M., Olson W.K., Saenger W., Shakked Z., Sklenar H., Soumpasis D.M, Tung C.S., Wang A.H.J. and Zhurkin V.B. Definitions and Nomenclature of Nucleic Acid Structure Parameters. *J. Mol. Biol.*, 1989, 208, 787.
51. Dickerson R. E. Base sequence and helix structure variation in B and A DNA. *J. Mol. Biol.* 1983, 166, 419-441.
52. Donlan M.E. and Lu P. Transcriptional enhancer related DNA sequences: Anomalous ¹H NMR NOE crosspeaks. *Nucleic Acids Research*, 1992, 20, 525.
53. Dornberger U., Flemming J. and Fritzsche H. Structure determination and analysis of helix parameters in the DNA decamer d-(CATGGCCATG)₂ comparison of results from NMR and crystallography. *J. Mol. Biol.*, 1998, 284, 1453.
54. Ed: Labauowski J, Andzeln J Density functional methods in chemistry, Springer – verlag, New york. 1991.
55. Evstigneev M.P., Khomich V.V., and Davies D.B. Complexation of anthracycline drugs with DNA in the presence of caffeine. *Eur. Biophys. J.*, 2006b, 36, 1.
56. Evstigneev M.P., Khomich V.V., and Davies D.B. Self-Association of Daunomycin Antibiotic in Various Buffer Solutions. *Russ. J. Phys. Chem.*, 2006a, 80, 741.

57. Favier A., Blackledge M., Simorre J.P., Crouzy S., Dabouis V., Gueiffer A., Dominique M. and Debouzy J.C. Solution structure of 2-(pyrido[1,2-e]purin-4-yl)amino-ethanol intercalated in the DNA duplex d-(CGATCG)₂. *Biochemistry*, 2001, 40, 8717.
58. Feigon J., Wright J. M., Leupin W., Denny W.A. and Kearns D.R. Use of two-dimensional NMR in the study of double-stranded decamer. *J. Amer. Soc.*, 1982, 104, 5540.
59. Frechet D., Chen D. M., Kan L.S. and Tso P.O.P. Nuclear overhauser effect as a tool for the complete assignment of non-exchangable proton resonance in short deoxyribonucleic acid helices. *Biochemistry*, 1983, 22, 5194.
60. Frederick C.A., Williams L.D., Ughetto G., Van der Marel G.A., Van Boom J.H., Rich A. and Wang A.H.J. Structural comparison of anticancer drug-DNA complexes: Adriamycin and daunomycin. *Biochemistry*, 1990, 29, 2538.
61. Fritzsche H., Triebel H., Chaires J.B., Dattagupta N. and Crothers D.M. Studies on interaction of anthracycline antibiotics and deoxyribonucleic acid geometry of intercalation of iremycin and daunomycin. *Biochemistry*, 1982, 21, 3940.
62. Gabbay E.J., Grier D., Fingerie R.E., Reimer R., Levy R., Pearce S.W. and Wilson W.D. Interaction specificity of the anthracyclines with deoxyribonucleic acid. *Biochemistry*, 1976, 15, 2062.
63. Gao Y.G. and Wang A.H.J. Crystal structures of four morpholino-doxorubicin anticancer drugs complexed with d-(CGTACG) and d-(CGATCG): Implications in drug-DNA crosslink. *J. Biomol. Struct. Dyn.*, 1995, 13, 103.
64. Giessner-Prettre C. and Pullman B. On the atomic or local contributions to chemical shifts due to the anisotropy the diamagnetic susceptibility of the aromatic side chain of

- amino acids and of the porphyrin ring. *Biochem. Biophys. Res. Commun.*, 1976, 15, 2277.
65. Gochin M. Zon G. and James. T.L. Two dimensional COSY and two dimensional NOE spectroscopy of d(AC)₄, d(GT)₄: Extraction of structural constraints. *Biochemistry*. 1990, 29, 11161.
 66. Goodsell D.S., Kopka M.L., Cascio D. and Dickerson R.E. Crystal structure of CATGGCCATG and its implication for A tract bending models. *Proc. Natl. Acad. Sci., USA.*, 1993, 90, 2930.
 67. Gorenstein, D. G. ³¹P NMR of DNA Spectroscopic methods for analysis of DNA. *Methods in Enzymology*, 1992, 211, 254.
 68. Gorenstein, D. G. ³¹P NMR of DNA Spectroscopic methods for analysis of DNA. *Methods in Enzymology*, 1992, 211, 254-285.
 69. Gorenstein, D. G., in "Phosphorus-31 NMR: Principles and Applications" (D. G Gorenstein ed.) p.7. Academic Press, Orlando, Florida, 1984.
 70. Gorenstein, D. G., Kar, D. *Biochem. Biophys. Res. Commun.* 1975, 65, 1073.
 71. Gorenstein D. G., Luxon B. A., and Findlay J. B., *Biochim Biophys. Acta*, 1977, 475, 184.
 72. Gorenstein D.G., Lai K. ³¹P NMR Spectra of Ethidium, Quinacrine, and Daunomycin Complexes with Poly (adenylic acid). Poly (uridylic acid) RNA Duplex and Calf Thymus DNA. *Biochemistry*, 1989, 28, 2804-2812.
 73. Gorin A.A., Zhurkin V.B. and Olson W.K. B-DNA twisting correlates with base-pair morphology. *J. Mol. Biol.*, 1995, 247, 34.
 74. Graves D.E. and Krugh T.R. Adriamycin and daunorubicin bind in a cooperative manner to deoxyribonucleic acid. *Biochemistry*, 1983, 22, 3941.

75. Gronenborn A. M. and Clore G.M. Investigation of the solution structure of short nucleic acid fragments by means of nuclear overhauser enhancements measurements. *Prog. NMR Spec.*, 1985, 17, 1.
76. Grzeskowiak K. Sequence dependent structural changes in B-DNA. *Chem. Biol.*, 1996, 3, 785.
77. Grzeskowiak, K., Yanagi, K., Prive, G.G. and Dickerson, R.E. The structure of B-helical C-G-A-T-C-G-A-T-C-G and comparison with C-C- A-A-C-G-T-T-G-G. The effect of base pair reversals, *J. Biol. Chem.*, 1991, 266, 8861-8883.
78. Guano F., Pourquier P., Tinelli S., Binaschi M., Bigioni M., Animati F., Manzini S., Zunino F., Kohlhagen G., Pommier Y. and Capranico G. Topoisomerase Poisoning Activity of Novel Disaccharide Anthracyclines. *Molecular Pharmacology*, 1999, 56, 77.
79. Gunther U. L., Ludwig C. and Ruterjans H. NMRLAB-Advanced NMR data processing in MATLAB. *J. Magn. Reson.*, 2000, 145, 201.
80. Hare D.H., Wemmer D.E., Chou S.H., Drobny G. and Reid B.R. Assignment of the non-exchangable proton resonances of d-(CGCGAATTCGCG)₂ using two-dimensional methods. *J. Mol. Biol.*, 1983, 171, 319.
81. Holbrook S.R., Wang A.H.J., Rich A. and Kim S.H. Local mobility of nucleic acids as determined from crystallographic data III daunomycin-DNA complex. *J. Mol. Biol.*, 1988, 199, 349.
82. Hosur R.V., Govil G. and Miles H.T. application of two-dimensional NMR spectroscopy in the determination of solution conformations of nucleic acids. *Magn. Reson. Chem.*, 1988, 26, 927.

83. Hosur R.V., Ravikumar M., Roy K.B., Tan-Zu-Kun, Miles H.T. and Govil G. In "Magnetic resonance in biology and medicine". (Eds. Govil G., Khetrpal C.L. and Saran A.) Tata Mcgraw Hill, New Delhi, 1985, 305.
84. Hosur, R.V., Ravikumar M., Chary K.V.R., Sheth A., Govil G., Tan-Zu-Kunn and Miles H.T. solution structure of d-GAATTCGCAATTC by 2D NMR: A new approach to determination of sugar geometries in DNA segments. FEBS Letts., 1986, 205, 71.
85. Hu G.G., Shui X., Leng F., Priebe W., Chaires J.B. and Williams L.D. Structure of DNA-bisdaunomycin complex. Biochemistry, 1997, 36, 5940.
86. Hunter C.A. Sequence-dependent DNA Structure: The role of base stacking interactions. J. Mol. Biol., 1993, 230, 1025.
87. Igarashi J. and Sunagawa M. Structural analysis by NMR of antitumor drug-DNA complexes: 9-aminoanthracycline (SM-5887). Bioorganic & Medicinal Chemistry Letters, 1995, 5, 2923.
88. Islam S.A., Neidle S., Gandecha B.M., Partridge M., Patterson L.H. and Brown J.R. Comparative computer graphics and solution studies of the DNA interaction of substituted anthraquinones based on doxorubicin and mitoxantrone. J. Med. Chem., 1985, 28, 857.
89. Jain, M., Barthwal, S.K., Barthwal, R., Govil, G. Arch. Biochem. Biophys., 2005, 439, 12-24.
90. Jeener J. Paper presented at the AMPERE International summer school, Borsko, Polje, Yugoslavia, 1971.
91. Jones M.B., Hollstein U. and Allen F.S. Site specificity of binding of antitumor antibiotics to DNA. Biopolymers, 1987, 26, 121.

92. Jones R. L., Wilson W.D. Effect of Intercalating Ligands on the ^{31}P Chemical Shift of DNA. *J. Am. Chem. Soc.* 1980, 102, 7778-7779.
93. Kabsch W., Sander S. and Trifonov E.N. The helical twist angle of B-DNA. *Nucleic Acids Research*, 1982, 10, 1097.
94. Keeler J. and Neuhaus D. Comparison and evaluation of methods for two-dimensional NMR spectra with absorption mode line shape. *J. Magn. Reson.*, 1985, 63, 454.
95. Kemler I., Schreiber E., Muller M.M., Matthias P. and Schaffner W. Octamer transcription factors bind to two different sequence motifs of the immunoglobulin heavy chain promoter. *EMBOJ.*, 1989, 8, 2001.
96. Khetrapal, C.L., Kunwar, A.C., Tracey, A.S. and Diehl P.; Nuclear Magnetic Resonance Studies in Lyotropic Liquid Crystals, *NMR: Basic Principles and Progress*, 9, 1975, Berlin-Heidelberg-New York, Springer.
97. Kleyer D. L., Koch T. H., *J. Am. Chem. Soc.*, 1983, 105, 2504.
98. Kohn W., Sham L. *J. Phys. Rev.* 1965, 140, 1133. see also: Kohn W., Becke A.D., Parr R.G. *J. Phys. Chem.* 1996, 100, 12974.
99. Kosikov, K.M., Gorin, A.A., Zhurkin, V.B., Olson, W.K. DNA stretching and compression: Large-scale simulations of double helical structures, *J. Mol. Biol.*, 1999, 26, 1301-1326.
100. Kotovych, J. W. Lown, J and P. K. Tong, High field ^1H and ^{31}P NMR studies on the binding of the anticancer agent mitoxantrone to $d-(\text{CpGpApTpCpG})_2$, *J. Biomol. Struct. Dyn.*, 1986, 4, 111-125.
101. Kumar R., Hosur R.V., Chary K.V.R., Sheth A., Govil G., Kunn T.Z. and Miles H.T. Solution structure of $d\text{-GAATTCGAATTC}$ by 2D NMR: A new approach to determination of sugar geometries in DNA segments. *FEBS Letts.*, 1986, 205, 71.

102. Lam S. L. and Au-Yeung S.C.F. Sequence specific local structural variations in solution structures of d(CGXXCG)₂ and d(CAXXTG)₂ self complementary deoxyribonucleic acids. *J. Mol. Biol.*, 1998, 266, 745.
103. Lancelot G. and Paquet F. In: G.A. Webb, Editor, *Annual Reports on NMR Spectroscopy*, Elsevier Science Ltd. 2003 pp. 170.
104. Langlois d'Estaintot B., Gallois B., Brown T. and Hunter W.N. The molecular structure of a 4-epiadriamycin complex with d-(TGATCA) at 1.7 Å resolution: Comparison with the structure of 4'-Epiadriamycin d-(TGTACA) and d-(CGATCG) Complexes. *Nucleic Acids Research*, 1992, 20, 3561.
105. Lavery R. and Sklenar H. CURVES 5.1. Helical analysis of irregular nucleic Acids. Laboratory of Theoretical Biology. CNRS, Paris, 1996.
106. Lavery R. and Sklenar H. The definition of generalized helicoidal parameters and of axis curvature for irregular nucleic acids. *J. Biomol. Struct. Dyn.*, 1988, 6, 63.
107. Lavery R. and Sklenar J. Defining the Structure of Irregular Nucleic Acids: Conventions and Principles. *J. Biomol. Struct. Dyn.*, 1989, 6, 655.
108. Lee C., Yang W., Parr R.G. *Phys. Rev B.* 1988, 37, 785.
109. Leonard G.A., Brown T., Hunter W.N. Anthracycline binding to DNA. High-resolution structure of d-(TGTACA) complexed with 4'-epiadriamycin, *Eur. J. Biochem.* 1992, 204, 69.
110. Leonard G.A., Hambley T.W., Mc Auley Hecht K., Brown T. and Hunter W.N. Anthracycline-DNA interactions at unfavourable base pair triplet binding sites: Structures of d-(CGGCCG)/daunomycin and d-(TGGCCA)/adriamycin complexes. *Acta Cryst.*, 1993, D49, 458.
111. Lerman L.S. Structural considerations in the interaction of DNA with acridines. *J. Mol. Biol.*, 1961, 3, 18.

112. Levy, G. C., Eijchart, A., Marchetti, P. S. Effect of Intercalated Ethidium on DNA Conformational Dynamics. A Reevaluation by ^{31}P and ^{13}C NMR Studies. *J. Magn. Reson.* 1984, 57, 130-135.
113. Lipscomb L.A., Peek M.E., Zhou F.X., Berrand J.A., Van Derveer D. and Williams L. D. Water ring structure at DNA interfaces: Hydration and dynamics of DNA-anthracycline complexes. *Biochemistry*, 1994, 33, 3649.
114. Lown J.W., Sim S.K., Majumdar K.C. and Chang R.Y. Strand scission of DNA by bound adriamycin and daunorubicin in the presence of reducing agents. *Biochem. Biophys. Res. Commun.*, 1977, 76, 705.
115. Lyubchenko Y.L., Shlyakhtenko L., Appella S.E. and Harrington R.E. CA runs increase DNA flexibility in the complex of λ cro protein with the O_R3 site. *Biochemistry*, 1993, 32, 4121.
116. Malatesta V., Penco S., Sacchi N., Valentini L., Vigevani A., Arcamone F., *Can. J. Chem.*, 1984, 62, 2845.
117. Manfait M., Alix A.J.P., Jeannesson P., Jardillier J.C. and Heophanides T. Interaction of adriamycin with DNA as studied by resonance Raman spectroscopy. *Nucleic Acids Research*, 1982, 10, 3803.
118. Maple J.R, Thacher T.S., Dinur U. and Hagler A.T. Biosym forcefield research results in new techniques for the extraction of inter and intra molecular forces. *Chemical Design Automation News*, 1990, 5, 5.
119. Maple J.R., Dinur U. and Hagler T. Derivation of force field for molecular mechanics and dynamics from ab-initio energy surfaces. *Proc. Natl. Acad. Sci., U.S.A.*, 1988, 85, 5350.
120. Marek R., Seckarova P., Hulova D., Marek J., Dostal J. & Sklenar V. *J. Nat. Prod.*, 2003, 66, 481-486.

121. Marion D. and Wuthrich K. Application of phase sensitive two-dimensional correlated spectroscopy (COSY) for measurement of ^1H - ^1H spin coupling constant in proteins. *Biochem. Biophys. Res. Comm.*, 1983, 113, 967.
122. Mark S. Searle, Jon G. Hall, William A. Denny, L.P.G. Wakelin. NMR Studies of the Interaction of the Antibiotic Nogalamycin with the Hexadeoxyribonucleotide Duplex $d(5'-\text{GCATGC})_2$. *Biochemistry*, 1988, 27, 4340-4349.
123. Mazzini S., Mondelli R. and Ragg E. Structure and dynamics of intercalation complexes of anthracyclines with $d(\text{CGATCG})_2$. 2D- ^1H and ^{31}P NMR investigations. *J. Chem. Soc., Perkin Trans.*, 1998, 2, 1983.
124. Mazzini, S., Bellucci, M. C. and Mondelli, R. Mode of binding of the cytotoxic alkaloid Berberine with the double helix oligonucleotide $d(\text{AAGAATTCTT})_2$. *Bioorganic and Medicinal Chemistry*, 2003, 11, 505-514.
125. Mazzini, S., Bellucci, M.C., Dallavalle, S., Fraternali, F. and Mondelli, R. Mode of binding of camptothecins to double helix oligonucleotides. *Org. Biomol. Chem.*, 2004, 2, 505-513.
126. Mc Ateer K. and Kennedy M.A. NMR evidence for base dynamics at all TpA steps in DNA. *J. Biomol. Struct. Dyn.*, 2000, 17, 1001.
127. Messori L., Temperini C., Piccioli F., Animati F., Di Bugno and Orioli P. Solution chemistry and DNA binding properties of MEN 10755, a novel disaccharide analogue of doxorubicin. *Bioorganic & Medicinal Chemistry*, 2001, 9, 1815.
128. Miller K.J. and Newlin D.D. Interactions of molecules with nucleic acids VI. Computer design of chromophoric intercalating agents. *Biopolymers*, 1982, 21, 633.
129. Mondelli R., Ragg E. and Fronza G. Conformational analysis of N-acetyl daunomycin in solution. A transient H nuclear overhauser effect study of the glycosidic linkage geometry. *J. Chem. Soc., Perkin Trans.*, 1987, II, 27.

130. Mondelli R., Ragg E., Fronza G. and Arnone A. Nuclear magnetic resonance conformational study of daunomycin and related antitumor antibiotics in solution. The conformation of ring A. *J. Chem. Soc., Perkin Trans.*, 1987, II, 15.
131. Moore M.H., Hunter W.N., Langlois d'Estaintot B. and Kennard O. DNA-drug interactions. The crystal structure of d-(CGATCG) complexed with daunomycin. *J. Mol. Biol.*, 1989, 206, 693.
132. Mujeeb A., Kerwin S.M., Kenyon G.L. and James T.L. Solution structure of conserved DNA sequence from the HIV-I genome: Restrained molecular dynamics simulation with distance and torsion angle restraints derived from two-dimensional NMR spectra. *Biochemistry*, 1993, 32, 13419.
133. Nakata Y. and Hopfinger A.J. An extended conformational analysis of doxorubicin. *FEBS Letts.*, 1980, 95, 583.
134. Nakata Y. and Hopfinger A.J. Predicted mode of intercalation of doxorubicin with dinucleotide dimers. *Biochem. Biophys. Res. Commun.*, 1980a, 95, 583.
135. Neidle S. and Taylor G.L. Nucleic acid binding drugs. Some conformational properties of the anticancer drug daunomycin and several of its derivatives. *FEBS Letts.*, 1979, 107, 348.
136. Neidle S. and Taylor G.L. Nucleic acid binding drugs: Part IV. The crystal structure of the anti cancer agent daunomycin. *Biochim. Biophys. Acta.*, 1977, 479, 450.
137. Neidle S., Sanderson M.R. and Waring M.J.. In "Molecular aspects of anticancer drug action" . Mac Millan, London, 1983.
138. Neuman J.M., Cavailles J.A., Herve M., Dinh S.T., Langlois d'Estaintot B., Huynh Dinh T. and Igolen J. 500 MHz ^1H NMR study of the interaction of daunomycin with B and Z helices of d-(CGm⁵CGCG). *FEBS Letts.*, 1985, 182, 360.

139. Norwood T., Tillett M. and Lian L.Y. Influence of cross-correlation between the chemical shift anisotropies of pairs of nuclei on multiple-quantum relaxation rates in macromolecules. *Chem. Phys. Letts.*, 1999, 300, 429.
140. Nunn C.M., Meervelt L.V., Zhang S., Moore M.H. and Kennard O. DNA-drug interactions. The crystal structures of d-(TGTACA) and d-(TGATCA) complexed with daunomycin. *J. Mol. Biol.*, 1991, 222, 167.
141. Nuss M.E., James T.L., Apple M.A. and Kollman P.A. A NMR study of the interaction of daunomycin with dinucleotides and dinucleoside phosphates. *Biochim. Biophys. Acta.*, 1980, 609, 136.
142. Nuss M.E., Marsh F.J. and Kollman P.A. Theoretical studies of drug-DNA interactions. Empirical Energy Function calculations on the interaction of ethidium, 9-aminoacridine, and proflavin cations with base-paired dinucleotides GpC and CpG. *Biochemistry*, 1979, 14, 825.
143. Odefey C., Westendorf J., Diechmann T. and Oschkinat H. Two dimensional nuclear magnetic resonance studies of an intercalation complex between the novel semisynthetic anthracycline 3'-deamino-3'-(2-methoxy-4-morpholinyl)-doxorubicin and the hexanucleotide duplex d-(CGTACG). *Chem. Biol. Interact*, 1992, 85, 117.
144. Olson W.K. and Lü X.J. 3DNA version 1.4.1, A 3-dimensional Nucleic acid Structure analysis and rebuilding software package. Department of Chemistry, Rutgers University, NJ, 2001.
145. Ott, J. and Eckstein, F. *Biochemistry*, 1985, 24, 2530.
146. Pachter J.A., Huang C.H., Du Vernay V.H., Prestayko A.W. and Crooke S.T. Viscometric and fluorometric studies of deoxyribonucleic acid interactions of several new anthracyclines. *Biochemistry*, 1982, 21, 1541.

147. Paciucci P.A., Cuttner J., Gottlieb A., Davies R.B., Martelo O. and Molland F. Sequential mitoxantrone, daunorubicin and cytosine arabinoside for patients with newly diagnosed acute myelocytic leukemia. *Am. J. Haematol.*, 1997, 56, 214.
148. Pan S. and Bachur N. R., *Mol. Pharmacol.*, 1980, 17, 95.
149. Parr R.G., Yang W., *Density Functional Theory Of Atoms And Molecules*, Oxford University Press. 1989.
150. Patel D.J. and Canuel L.L. Anthracycline antitumour antibiotics. Nucleic acid interactions. Structural aspects of the daunomycin, poly(dA-dT) complex in solution. *Eur. J. Biochem.*, 1978, 90, 247.
151. Patel D.J. Helix-coil transition of the dG-dC-dG-dC self-complementary duplex and complex formation with daunomycin in solution. *Biopolymers*, 1979, 18, 553.
152. Patel D.J., Kozlowski S.A. and Rice J.A. Hydrogen bonding, overlap geometry, and sequence specificity in anthracycline antitumour antibiotic. DNA complexes in solution. *Proc. Natl. Acad. Sci., U.S.A.*, 1981, 78, 3333.
153. Patel, D. J. and Canuel, L. L. Ethidium bromide-(dC-dG-dC-dG)₂ complex in solution: intercalation and sequence specificity of drug binding at the tetranucleotide duplex level. *Proc. Natl. Acad. Sci. USA*, 1976, 73, 3343-3347.
154. Patel, D. J. Peptide antibiotic dinucleotide interactions. Nuclear Magnetic Resonance investigations of complex formation between actinomycin D and d-pGpC in aqueous solution. *Biochemistry*, 1974, 13, 2388-2395.
155. Patel, D. Helix-coil transition of the dG-dC-dG-dC self-complementary duplex and complex formation with daunomycin in solution. *J., Acc. Chem. Res.* 1979, 12, 118.
156. Patel, D. J., Kozlowski, S. A., Nordheim, A. and Rich, A. Right handed and left handed DNA: Studies of B- and Z-DNA by proton nuclear Overhauser effect and P NMR. *Proc. Natl. Acad. Sci. USA*, 1982, 79, 1413-1417.

157. Patel, D. J., Kozlowski, S.A. and Rice J. A. Hydrogen bonding, overlap geometry, and sequence specificity in anthracycline antitumor antibiotic: DNA complexes in solution. *Proc. Natl. Acad. Sci. USA*, 1981, 78, 3333–3337.
158. Phillips D.R. and Roberts G.C.K. Proton nuclear magnetic resonance study of the self- complementary hexanucleotide d-(pTpA)₃ and its interaction with daunomycin. *Biochemistry*, 1980, 19, 4795.
159. Piantini U., Sorensen O.W. and Ernst R.R. Multiple quantum filters for elucidating NMR networks. *J. Am. Chem. Soc.*, 1982, 104, 6800.
160. Pigram W.J., Fuller W. and Hamilton L.D. Stereochemistry of intercalation: Interaction of daunomycin with DNA. *Nature New Biol.*, 1972, 235, 17.
161. Pilch D.S., Yu C., Makhey D., Lavoie E.J., Srinivasan A.R., Olson W.K., Saucers R.R., Brealauer K.J., Geacintov N.E. and Liu L.F. Minor groove-directed and intercalative ligand DNA interactions in the poisoning of DNA topoisomerase I by protoberberine analogs. *Biochemistry*, 1997, 36, 12542.
162. Pindur U., Haber M. and Sattler K. Antitumour active drug as intercalators of deoxyribonucleic acid. *Journal of Chemical Education*, 1993, 70, 263.
163. Piosik J., Zdunek M. and Kapuscinski J. The modulation by xanthines of the DNA-damaging effect of polycyclic aromatic agents. Part II. The stacking complexes of caffeine with doxorubicin and mitoxantrone. *Biochem Pharma.* 2002, 63, 635-646.
164. Plumbridge T.W. and Brown J.R. Spectrophotometric and fluorescence polarization studies of the binding of ethidium, daunomycin and mepacrine to DNA and to Poly (I.C). *Biochim. Biophys. Acta.*, 1977, 479, 441.
165. Pohle W., Flemming J. and Bohl M. Adriamycin binding to DNA phosphates as evidenced by spectroscopic and quantum-chemical results. *Studia Biophysica*, 1987, 122, 223.

166. Pohle W., Flemming J., Bohl M. and Bohlig H. Subsidiary hydrogen bonding of intercalated anthraquinonic anticancer drugs to DNA phosphate. *Biophysical Chem.*, 1990, 35, 213.
167. Quigley G.J., Wang A.H. J., Ughetto G., Van der Marel G., Van Boom J.H. and Rich A. Molecular structure of an anticancer drug-DNA complex: Daunomycin plus d-(CpGpTpApCpG). *Proc. Natl. Acad. Sci., USA.* 1980, 77, 7204.
168. Radha P.K., Madan A., Nibedita R. and Hosur R.V. Solution structure of the combined segment of Myb cognate DNA sequence by 2D NMR, spectral simulation, restrained energy minimization, and distance geometry calculations. *Biochemistry*, 1995, 34, 5913.
169. Ragg E., Mondelli R., Battistini C., Garbesi A. and Colonna F.P. ³¹P NMR study of daunorubicin-d-(CGTACG) complex in solution: Evidence of the intercalation sites. *FEBS Letts.*, 1988, 236, 231.
170. Rajeshwari, M. R. Tryptophan Intercalation in G, C containing Polynucleotides: Z to B conversion of Poly [d(G-5MC)] in low salt induced by a tetrapeptide. *J. Biomol. Struct. & Dyn.*, 1996, 14, 25-30.
171. Rameta D.P., Mudd C.P., Berger R.L. and Breslauer K.J. Thermodynamics characterization of daunomycin-DNA interactions: Microcalorimetric measurements of daunomycin-DNA binding enthalpies. *Biochemistry*, 1991, 30, 9799.
172. Redfield A.G., Kunj S. and Ralph E.K. Quadrature fourier NMR detection, simple multiplex for dual detection and discussion. *J. Magn. Reson.*, 1975, 19, 116.
173. Reid B.R., Baukes K., Flynn P. and Nerdal W. NMR distance measurement in DNA duplex: Sugar and bases have the same correlation times. *Biochemistry*, 1989, 28, 10001.

174. Roberts G.C.K. Applications of NMR in drug discovery. *Drug Discovery Today*, 2000, 5, 230.
175. Roberts G.C.K. NMR spectroscopy in structure-based drug design. *Curr. Opin. Biotechnol.*, 1999, 10, 42.
176. Robinson H., Priebe W., Chaires J.B. and Wang A.H.J. Binding of two novel bisdaunorubicins to DNA studied by NMR spectroscopy. *Biochemistry*, 1997, 36, 8663.
177. Roche C. J., Berkowitz D., Sulikowski G.A., Danishefsky S.J. and Crothers D.M. Binding affinity and site selectivity of daunomycin analogues. *Biochemistry*, 1994, 33, 936.
178. Rohs R., Bloch I., Sklenar H. And Shakked Z. Molecular flexibility in ab initio drug docking to DNA: binding-site and binding-mode transitions in all-atom Monte Carlo simulations. *Nucleic Acids Research*, 2005, 33, 7048.
179. Saenger, W. *Principles of Nucleic Acid Structure*, Springer-Verlag, New York. 1984.
180. Saminadin P., Dautant A., Mondon M., d'Estaintot B.L., Courseille C. and Precigoux G. Release of the cyano moiety in the crystal structure of N-cyanomethyl-N-(2-methoxy ethyl)-daunomycin complexed with d-(CGATCG). *Eur. J. Biochem.*, 2000, 267, 457.
181. Sarai A. and Takeda Y. Lambda repressor recognizes the approximately 2-fold symmetric half-operator sequences asymmetrically *Proc. Natl. Acad. Sci., U.S.A.*, 1989, 86, 6513.
182. Scheek R.M., Russo N., Boelens R., Kaptein R. and Van Boom J.H. Sequential resonance assignments in DNA ¹H NMR spectra by two-dimensional NOE spectroscopy. *J. Amer. Chem. Soc.*, 1983, 105, 2914.

183. Schmitz U., Sethson I., Egan, W.M. and James T.L. Solution structure of a DNA octamer containing the pribnov box via restrained molecular dynamics simulations with distance and torsion angles derived from two-dimensional nuclear magnetic resonance spectral fitting. *J. Mol. Biol.*, 1992, 227, 510.
184. Schroeder, S.A., Roongta, V., Fu, J. M., Jones, C. R. and Gorenstein, D. G. Sequence-dependent variations in the ^{31}P NMR spectra and backbone torsional angles of wild-type and mutant Lac operator fragments. *Biochemistry*, 1989, 28, 8292–8303.
185. Schultz S.C., Shields G.C. and Steitz T.A. Crystal structure of a CAP-DNA complex: the DNA is bent by 90 degree. *Science*, 1991, 253, 1001.
186. Shafer R.H. Spectroscopic studies of the interaction of daunomycin with transfer RNA. *Biochem. Pharmacol.*, 1977, 26, 1729.
187. Singh M.P., Joseph, T., Kumar S., Bathini, Y. and Lown, J.W. Synthesis and Sequence –Specific DNA binding of a Topoisomerase Inhibitory Analog of Hoechst 33258 designed for altered base and sequence recognition. *Chem. Res. Toxicol.* 1992, 5, 597-607.
188. Skorobogaty A., White R.J., Phillips D.R and Reiss J.A. The 5'-CA DNA-sequence preference of daunomycin. *FEBS Letts.*, 1988, 227, 103.
189. States D.J., Haberkorn R.A. and Reuben D.J. A two-dimensional overhauser experiment with pure absorption phase in four quadrants. *J. Magn. Reson.*, 1982. 48, 286.
190. Sundaralingam M. *Biopolymers*, 1969, 7, 821.
191. Tewey K.M., Rowe T.C., Yang L., Hallingan B.D. and Liu L.F. Adriamycin induced DNA damage mediated by mammalian DNA topoisomerase II. *Science*, 1984, 226, 466.

192. Traganos F., Kapuscinski J. and Darzynkiewicz Z. Caffeine modulate the effects of DNA-intercalating drug in vitro: a flow cytometric and spectrophotometric analysis of caffeine interaction with novatrone, doxorubicin, ellipticine and doxorubicin analogue AD198. *Cancer Res.* 1991, 51, 3682-3689.
193. Trieb M., Rauch C., Wellenzohn, B., Wibowo F., Loerting T., Mayer E. and Liedl K. R. Daunomycin intercalation stabilizes distinct backbone conformations of DNA. *J. Biomol. Struct. Dyn.*, 2004, 21, 713.
194. Trifonov E.N. and Brendal V. GNOMIC—A Dictionary of Genetic Codes. Vch Verlagsgesellschaft Weinheim, Germany, 1986.
195. Trifonov E.N. Curved DNA. *CRC Crit. Rev. Biochem.*, 1985, 19, 89.
196. Trist H. and Phillips D.R. In vitro transcription analysis of the role of flanking sequence on the DNA sequence specificity of adriamycin. *Nucleic Acids Research*, 1989, 17, 3673.
197. Tsai C.C., Jain S.C. and Sobell H.M. Visualization of drug-nucleic acid interactions at atomic resolution I. Structure of an ethidium/dinucleoside monophosphate crystalline complex, ethidium: 5-iodouridylyl (3-5) adenosine. *J. Mol. Biol.*, 1977, 114, 301.
198. Tsou K.C. and Yip K.F. Effect of deoxyribonuclease on adriamycin-polynucleotide complexes. *Cancer Res.*, 1976, 36, 3367.
199. Von Dreele R.B. and Einck J.J. The crystal and molecular structure of carminomycin I hydrochloride monohydrate. *Acta. Cryst.*, B 33, 1977, 3283.
200. Wang A.H.J, Gao Y.G, Liaw Y.C. and Li Y.K. Formaldehyde cross-links daunorubicin and DNA efficiently: HPLC and X-ray diffraction studies. *Biochemistry*, 1991, 30, 3812.

201. Wang A.H.J., Ughetto G., Quigley G.J. and Rich A. Interactions between an anthracycline antibiotic and DNA: Molecular structure of daunomycin complexed to d-(CpGpTpApCpG) at 1.2 Å resolution. *Biochemistry*, 1987, 26, 1152.
202. Waring M. Variation of the supercoils in closed circular DNA by binding of antibiotics and drugs: Evidence for molecular models involving intercalation. *J. Mol. Biol.*, 1970, 54, 247.
203. Williams L.D., Egli M., Ughetto G., van der Maerl G.A., van Boom J.H., Quigley G.J., Wang A.H.J. and Rich A. *J. Mol. Biol.*, 1990, 215, 313.
204. Williams L.D., Frederick C.A., Ughetto G. and Rich A. Ternary interactions of spermine with DNA: 4'-epiadrinamycin and other DNA: Anthracycline complexes. *Nucleic Acids Research*, 1990, 18, 5533.
205. Wilson, W. D. and Jones, R. L. Interaction of actinomycin D, ethidium quinacrine daunorubicin, and tetralysine with DNA: ³¹P NMR chemical shift and relaxation investigation. *Nucleic Acids. Res.* 1982, 10, 1399-1410.
206. Winger, R.H., Liedl, K.R., Rudisser, S., Pichler, A., Hallbrucker, A., Mayer, E. DNA's B_I → B_{II} conformer substate dynamics Is coupled with water migration, *J. Phys. Chem. B.* 1998, 102, 8934-8940.
207. Wuthrich K. In "NMR of proteins and nucleic acids". John Wiley, New York, 1986.
208. Xodo L.E., Manzini G., Ruggiero J. and Quadrifoglio F. On the interaction of daunomycin with synthetic alternating DNAs: Sequence specificity and polyelectrolytes effects on the intercalation equilibrium. *Biopolymers*, 1988, 27, 1839.
209. Yang X.L., Robinson H., Gao Y.G. and Wang A.H.J. Binding of macrocyclic bisacridine and ametantrone to CGTACG involves similar unusual intercalation platforms. *Biochemistry*, 2000, 39, 10950.

210. Zhurkin V.B., Ulyanov N.B., Gorin A.A. and Jernigan R.L. Static and statistical bending of DNA evaluated by Monte Carlo simulations. *Proc. Natl. Acad. Sci., U.S.A.*, 1991, 88, 7046.
211. Zunino F., Gambetta R. and Di Marco A. Effects of the stereochemical configuration on the interaction of some daunomycin derivatives with DNA. *Biochem. Biophys. Res. Commun.*, 1976, 69, 744.
212. Zunino F., Gambetta R., Di Marco A. and Zaccara A. Interaction of daunomycin and its derivatives with DNA. *Biochim. Biophys. Acta.*, 1972, 277, 489.

